



**Combining fusidic acid with metal ions
as a potential reformulation for the
treatment of bacterial keratitis**

by

Hannah Marie Boostrom



Presented in part fulfilment of the requirements for the degree of

Doctor of Philosophy

School of Pharmacy and Pharmaceutical Sciences

Cardiff University

Nov-2019

Summary

Fusidic acid is a protein synthesis inhibitor commonly used to treat Gram-positive infections caused by pathogens such as *Staphylococcus aureus*. Gram-negative bacteria are intrinsically resistant due to their low permeability outer membrane and efflux pumps. UK optometrists are licenced to prescribe fusidic acid for the treatment of bacterial eye infections. However, 45 % cases of bacterial keratitis – a severe, sight-threatening corneal infection – are caused by Gram-negative organisms. As some metal ions have been found to enhance the activity and extend the spectrum of established antimicrobial drugs, this work sought to investigate the efficacy of combining metal ions with fusidic acid as a potential reformulation strategy to repurpose fusidic acid as a broad spectrum, first line treatment for bacterial keratitis. The presence of Al^{3+} , Cu^{2+} or Fe^{2+} ions was found to increase the activity of the fusidic acid sodium salt, sodium fusidate, against a selection of multi-drug resistant Gram-negative *Escherichia coli*, *Klebsiella pneumoniae* and *Pseudomonas aeruginosa* isolates, without reducing anti-*S. aureus* efficacy. *P. aeruginosa* was particularly susceptible to sodium fusidate with Al^{3+} . There was no apparent link between the carriage of multi-drug resistance determinants and susceptibility to the combinations. With no evidence of spontaneous complexation, the mechanism of action against *E. coli* was determined to be reduced fusidate solubility enabling increased membrane access combined with the independent antimicrobial activity of metal ions. Proliferation of human corneal epithelial cells was less inhibited by Al^{3+} , Cu^{2+} or Fe^{2+} than the Gram-negative reference strains, suggesting clinical selectivity. Unfortunately, the combinations were inactive against Gram-negatives in a novel rationalised simulated tear fluid, likely due to protein binding of both agents. However, future formulation optimisation may overcome this issue. Finally, the discovery of Al^{3+} and sodium fusidate activity against *P. aeruginosa* has prompted further research into the combined mechanism of action in this important opportunistic pathogen.

Table of contents

Summary.....	i
Table of contents	ii
List of figures.....	xvii
List of tables.....	xxv
Abbreviations	xxviii
Publications and presentations	xxx
Acknowledgements.....	xxxii

Chapter 1: Introduction..... 1

1.1 Overview 2

1.2 Bacterial keratitis..... 2

1.2.1 Prevalence and predisposing factors 3

1.2.2 Symptoms, pathology and progression 4

1.2.3 Diagnosis..... 6

1.2.4 Causative organisms..... 8

1.2.5 Treatment strategy and limitations 10

1.2.6 Antimicrobial resistance 11

1.3 Fusidic acid..... 16

1.3.1 Discovery and introduction 16

1.3.2 Current clinical use..... 21

1.3.3 Mechanism of action 22

1.3.4	Limitations in bacterial keratitis	24
1.4	Antimicrobial development, drug repurposing and co-formulation	27
1.4.1	Standard drug development	27
1.4.2	The failing antimicrobial pipeline.....	29
1.4.3	Co-formulation to extend antimicrobial spectrum	33
1.4.3.1	Synergy or potentiation between antimicrobial agents	34
1.4.3.2	Prevention of antimicrobial degradation	34
1.4.3.3	Increasing antimicrobial access to its target.....	35
1.4.4	Desirable mechanisms of agents for co-formulation with fusidic acid	36
1.4.4.1	Membrane permeabilisation	36
1.4.4.2	Efflux inhibition	37
1.4.5	Metals as antimicrobial adjuvants.....	37
1.4.5.1	Nanoparticles.....	38
1.4.5.2	Metal complexation.....	39
1.4.5.3	Free metal ions.....	40
1.5	Hypothesis and aims	41
 Chapter 2: General methodology.....		43
2.1	Test agent stock solution preparation and storage	44
2.2	Sources, storage and maintenance of bacterial strains	45
2.2.1	Source of strains.....	45
2.2.2	Preparation of initial glycerol stocks	45

2.2.3	Maintenance of stocks and cultures	46
2.3	Enumeration of bacteria	46
2.4	Determination of minimum inhibitory and minimum bactericidal concentrations by microdilution.....	47
2.5	The chequerboard assay	49
2.6	Fusidic acid quantification by RP-HPLC	53
2.6.1	Separation method 1	53
2.6.2	Separation method 2	53
2.7	Determination of FA solubility	54
2.8	Measurement of solution pH	54
2.9	Statistical analysis	55

Chapter 3: Optimisation of the microdilution and chequerboard assays..... 57

3.1	Introduction.....	58
3.1.1	Aims and objectives	59
3.2	Methods.....	59
3.2.1	Selection of bacteriological medium.....	59
3.2.2	Effect of low concentration ethanol on bacterial growth	61
3.2.3	Metal ion MIC ₉₀ s, MBCs and concentration range selection	61

3.2.4	The effects of sodium sulphate and sodium chloride on bacterial growth and sodium fusidate activity.....	62
3.3	Results	63
3.3.1	Bacteriological medium selection	63
3.3.2	Effect of low concentration ethanol.....	64
3.3.3	The instability of Fe ²⁺ in aqueous solution.....	66
3.3.4	Metal ion MIC ₉₀ s, MBCs and concentration range selection.....	67
3.3.5	Effects of sodium sulphate alone on bacterial growth	68
3.3.6	Sodium fusidate activity in the presence of sodium sulphate	69
3.3.7	Effect of sodium chloride on bacterial growth and the activity of sodium fusidate	71
3.4	Conclusions	71

Chapter 4: Antimicrobial activity of sodium fusidate combined with metal ions..... 73

4.1	Introduction	74
4.1.1	Metal ions of interest for combining with sodium fusidate	74
4.1.1.1	Aluminium.....	75
4.1.1.2	Cobalt.....	76
4.1.1.3	Copper.....	77
4.1.1.4	Iron	78
4.1.1.5	Manganese.....	79
4.1.1.6	Nickel.....	80

4.1.1.7 Palladium	80
4.1.1.8 Zinc	81
4.1.2 Selection of methods for assessment of antimicrobial activity	82
4.1.3 Aims and objectives	83
4.2 Methods.....	84
4.2.1 Bacteriostatic and bactericidal activity of sodium fusidate combined with metal salts	84
4.2.2 Biocidal capability of sodium fusidate combined with copper(II) sulphate against <i>E. coli</i>	85
4.2.3 Effect of sodium fusidate on kill kinetics of copper(II) sulphate against <i>E. coli</i>	86
4.3 Results	86
4.3.1 Combined bacteriostatic activity of sodium fusidate and metal ions	86
4.3.1.1 FIC ₉₀ Is between metal ions and sodium fusidate.....	86
4.3.1.2 Metal ion and sodium fusidate isobolograms	87
4.3.1.3 Effect of sub-MIC ₉₀ metal ion concentrations on sodium fusidate MIC ₉₀	89
4.3.2 Effect of the counter-ion on bacteriostatic activity of sodium fusidate combined with copper(II).....	90
4.3.2.1 Copper(II) salt and sodium fusidate FIC ₉₀ Is	90
4.3.2.2 Isobologram analysis for sodium fusidate and copper(II) salts	91
4.3.3 Investigations into bactericidal activity of sodium fusidate combined with copper(II) sulphate	93
4.3.3.1 Combined MBCs of metal ions and sodium fusidate	93
4.3.3.2 Biocidal capability of sodium fusidate combined with copper(II) sulphate against <i>E. coli</i>	94

4.3.3.3 <i>E. coli</i> kill-time kinetics of combined copper(II) sulphate and sodium fusidate	95
4.4 Discussion.....	96
4.4.1 Links between antimicrobial mechanisms of metal ions and their effect on sodium fusidate activity.....	96
4.4.1.1 Metal ions antagonistic and suppressive to sodium fusidate anti- <i>E. coli</i> activity.....	96
4.4.1.2 Metal ions eliciting neither an antagonistic nor synergistic effect when combined with sodium fusidate against <i>E. coli</i>	97
4.4.1.3 Metal ions that synergise with sodium fusidate against <i>E. coli</i>	99
4.4.2 Effect of the copper(II) salt counter-ion on anti- <i>E. coli</i> activity in combination with sodium fusidate	100
4.4.3 Anti- <i>E. coli</i> biocidal activity of copper(II) sulphate and sodium fusidate ...	101
4.4.3.1 Effect of sodium fusidate on the biocidal activity of copper(II) sulphate	101
4.4.3.2 Effects of different solvents on biocidal activity of copper(II) sulphate combined with sodium fusidate	102
4.5 Conclusions	103

Chapter 5: Sodium fusidate solution chemistry and effect on anti-*E. coli* activity 105

5.1 Introduction.....	106
5.1.1 Spontaneous complexation between metal ions and antimicrobials	106
5.1.2 Potential effects of metal ion-mediated pH reduction	108
5.1.2.1 Bacterial response to pH stress.....	108

5.1.2.2 Sodium fusidate solubility at reduced pH.....	109
5.1.3 Aims and objectives	110
5.2 Methods.....	111
5.2.1 Investigations into interactions between fusidate and copper(II) ions	111
5.2.1.1 Ultraviolet-visible light (UV-Vis) spectrophotometric analysis	111
5.2.1.2 Isothermal titration calorimetry (ITC).....	111
5.2.2 Relationship between broth pH and sodium fusidate anti- <i>E. coli</i> activity, with and without metal ions.....	113
5.2.2.1 Metal sulphate pH measurements	113
5.2.2.2 Anti- <i>E. coli</i> activity of sodium fusidate in pH adjusted broth.....	113
5.2.2.3 Copper(II) in combination with sodium fusidate at neutral pH.....	113
5.2.3 The effect of broth pH on sodium fusidate solubility, with and without metal ions	114
5.2.3.1 Preliminary test for pH-induced precipitation of sodium fusidate in nutrient broth	114
5.2.3.2 Assessment of sodium fusidate stability at reduced pH.....	115
5.2.3.3 Solubility of sodium fusidate at reduced pH and with metal ions	115
5.2.4 Modelling correlations between sodium fusidate solubility and anti- <i>E. coli</i> activity	116
5.2.5 Quantification of sodium fusidate associated with <i>E. coli</i> cells.....	117
5.3 Results	118
5.3.1 Investigations into interactions between fusidate and copper(II) ions.....	118
5.3.1.1 UV-Vis spectrophotometric analysis of sodium fusidate and copper(II)	118

5.3.1.2 Effect of pH on the interaction between fusidate and copper(II) by ITC	120
5.3.2 Relationship between pH and sodium fusidate activity against <i>E. coli</i>	123
5.3.2.1 Metal sulphate pH in nutrient broth and inhibition of <i>E. coli</i>	123
5.3.2.2 Relationship between broth pH and inhibition of <i>E. coli</i> by sodium fusidate	124
5.3.2.3 Copper(II) in combination with sodium fusidate at neutral pH	126
5.3.3 Sodium fusidate solubility and anti- <i>E. coli</i> activity	127
5.3.3.1 Preliminary confirmation of pH-induced precipitation of sodium fusidate in nutrient broth.....	127
5.3.3.2 Assessment of sodium fusidate stability at reduced pH	129
5.3.3.3 Sodium fusidate solubility in pH adjusted nutrient broth and correlation with anti- <i>E. coli</i> activity	132
5.3.3.3.1 Sodium fusidate solubility in pH adjusted broth	132
5.3.3.3.2 Relationship between sodium fusidate solubility and anti- <i>E. coli</i> activity in pH adjusted nutrient broth.....	137
5.3.3.4 Sodium fusidate solubility in nutrient broth with metal sulphates and correlation with anti- <i>E. coli</i> activity.....	138
5.3.3.4.1 Solubility of sodium fusidate with metal sulphates in nutrient broth	138
5.3.3.4.2 Predictability of anti- <i>E. coli</i> activity of sodium fusidate based on solubility in nutrient broth with metal sulphates	140
5.3.3.5 Predictability of anti- <i>E. coli</i> activity of sodium fusidate based on solubility in with other copper(II) salts and in other broths.....	147
5.3.3.5.1 Copper(II) D-gluconate in nutrient broth at native and neutral pH	147
5.3.3.5.2 Copper(II) sulphate in LB and cation adjusted Müller-Hinton broth	149

5.3.4	Association of sodium fusidate with <i>E. coli</i> cells	150
5.4	Discussion	152
5.4.1	Precipitation (and not complexation) of sodium fusidate in the presence of copper(II) ions	152
5.4.2	Relationship between broth pH and sodium fusidate solubility	152
5.4.3	Predicting anti- <i>E. coli</i> activity of sodium fusidate based on its solubility ...	154
5.4.3.1	Metal sulphates in nutrient broth	154
5.4.3.1.1	Sodium fusidate with synergistic aluminium, copper(II) or iron(II)	154
5.4.3.1.2	Sodium fusidate with indifferent cobalt(II), nickel(II) or palladium(II)	155
5.4.3.1.3	Sodium fusidate with antagonistic manganese(II) or zinc(II) ...	156
5.4.3.2	Copper(II) D-gluconate in nutrient broth at native and neutral pH	157
5.4.3.3	Copper(II) sulphate in LB and cation adjusted Müller-Hinton broth ..	157
5.4.4	Association of sodium fusidate with <i>E. coli</i> cells in the presence of metal ions or reduced pH.....	158
5.5	Conclusions	159

Chapter 6: Activity of sodium fusidate and metal ion combinations against Gram-negative multi-drug resistant isolates 161

6.1	Introduction.....	162
6.1.1	Aim and objectives	163

6.2	Methods	164
6.2.1	Sources and maintenance of bacterial strains	164
6.2.2	Susceptibility testing	164
6.2.3	Data analysis	165
6.3	Results	166
6.3.1	Metal ion activity against Gram-negative MDR isolates	166
6.3.2	Activity of sodium fusidate combined with metal ions against Gram-negative MDR isolates	169
6.3.3	The effect of metal ions on sodium fusidate MIC ₉₀ S	171
6.4	Discussion.....	175
6.4.1	Activity of metal ions alone	175
6.4.2	Combined activity of sodium fusidate and metal ions.....	178
6.5	Conclusions	180

Chapter 7: Effect of sodium fusidate and metal ions on human corneal epithelial cell survival and proliferation..... 181

7.1	Introduction	182
7.1.1	Aim and objectives.....	183
7.2	Methods	184
7.2.1	Cell line and standard culture conditions	184
7.2.2	Preparation, storage and recovery of frozen cell stocks.....	185

7.2.3	Combined LDH and MTT assay procedure.....	185
7.2.4	Test concentrations and combinations.....	188
7.2.5	Data processing	189
7.2.5.1	Cytotoxicity.....	189
7.2.5.2	Cell proliferation	189
7.2.5.3	EC ₅₀ , IC ₅₀ and IC ₉₀ calculation	190
7.3	Results	190
7.3.1	Inhibitory and cytotoxic effects of sodium fusidate, aluminium, copper and iron ions alone on corneal epithelial cells.....	190
7.3.2	Effects of sodium fusidate combined with metal ions on the proliferation of corneal epithelial cells	192
7.3.3	Comparison of antimicrobial activity versus corneal epithelial cell proliferation in the presence of sodium fusidate and metal ion combinations.....	194
7.3.3.1	Inhibition profiles	194
7.3.3.2	Selectivity indices.....	198
7.4	Discussion	199
7.4.1	Human corneal epithelial cell proliferation in the presence of sodium fusidate, metal ions and sodium fusidate combined with metal ions	199
7.4.2	Comparison of human corneal epithelial cell and bacterial inhibition by sodium fusidate combined with metal ions.....	200
7.5	Conclusions.....	201

Chapter 8: Anti-Gram-negative activity and solubility of sodium fusidate combined with metal ions in a novel simulated tear fluid203

8.1	Introduction	204
8.1.1	Aim and objectives.....	205
8.2	Methods	207
8.2.1	Development of a novel simulated tear fluid formulation	207
8.2.1.1	Collation of published data	207
8.2.1.2	Design and optimisation of a novel STF	207
8.2.1.2.1	Materials.....	208
8.2.1.2.2	Initial assessment of bacterial growth	208
8.2.1.2.3	Formulation refinement to mimic physiological pH.....	208
8.2.2	Optimisation of an antimicrobial assay in novel simulated tear fluid.....	209
8.2.3	Antimicrobial activity of sodium fusidate in novel simulated tear fluid, with and without metal ions	209
8.2.4	Solubility of sodium fusidate in novel simulated tear fluid, with and without metal ions	211
8.2.4.1	Sodium fusidate solubility in novel STF	211
8.2.4.2	pH of metal sulphates in novel STF.....	211
8.3	Results	212
8.3.1	Development of a novel simulated tear fluid formulation for bacterial studies	212
8.3.1.1	Collation of published data	212

8.4.4 Solubility of sodium fusidate in novel simulated tear fluid and 50 % nutrient broth comparator	235
8.5 Conclusions	236
Chapter 9: General discussion.....	237
9.1 Reflections on findings and context.....	238
9.2 Limitations in application of this work	240
9.3 Future directions.....	243
9.3.1 Further research	243
9.3.1.1 Mechanism of action.....	243
9.3.1.2 Formulation.....	245
9.3.1.3 Efficacy and toxicity	246
9.3.2 Additional and alternative clinical applications.....	247
9.4 Closing remarks.....	248
References.....	249
Appendices.....	299
Appendix A: Personal and environmental safety.....	300
Appendix B: Calibration curves for quantification of fusidate by RP-HPLC	301

Appendix C: Optimisation of assay parameters for study of sodium fusidate association with <i>E. coli</i> cells	304
C(i): Verification of bacterial pellet processing and sodium fusidate extraction....	304
C(ii): Selection of RP-HPLC method for quantification of fusidate	305
Appendix D: Isothermal titration calorimetry (ITC) performance validation and additional replicates	307
D(i): EDTA-CaCl ₂ performance validation standard	307
D(ii): Additional experimental ITC replicates	308
Appendix E: Co-optimisation of LDH and MTT assays	311
E(i): Pilot investigations	311
E(ii): MTT optimisation	314
E(iii): LDH optimisation	318
E(iv): Seeding density selection	320
E(v): Combined assay procedure	321
Appendix F: Concentrations of lipids and trace elements in STF formulations and human tears	322

List of figures

Figure 1.1 - Examples of bacterial keratitis presentation from the literature	5
Figure 1.2 – The 2D and 3D structures of fusidic acid and cholesterol	17
Figure 1.3 - Formulations of fusidic acid and sodium fusidate produced by LEO Pharma	21
Figure 1.4 - Schematic of prokaryote protein synthesis and mechanism of fusidic acid inhibition	23
Figure 1.5 - Structure of the cell envelope in Gram-negative and Gram-positive bacteria	24
Figure 1.6 - Schematic representation of the superstructure and transportation mechanism of the <i>E. coli</i> AcrAB-TolC efflux pump, based on images in Wang <i>et al</i> , 2017 ^[153]	26
Figure 1.7 - Illustration of the classical drug development pipeline from target identification to regulatory approval, constructed based on data from Rang, 2006 ^[167]	28
Figure 1.8 –Duration between antimicrobial discovery and development of clinical resistance (from Brooks & Brooks, 2014 ^[187]).....	31
Figure 1.9 - Number of new systemic antibiotics approved by the FDA during each 5 year period since 1980 (from Ventola, 2015 ^[169])	32
Figure 1.10 – Comparison of <i>de novo</i> drug discovery timeline to that for drug repurposing (based on Ashburn & Thor, 2004 ^[164])	33
Figure 2.1 – The dilution and plating steps in the Miles & Misra method ^[280]	47
Figure 2.2 - Illustration of typical chequerboard assay set-up	50
Figure 2.3 - Selection of wells from hypothetical chequerboard results for FIC ₉₀ calculation	51
Figure 2.4 – Schematic representation of isobolograms produced by synergistic, additive, antagonistic and suppressive antimicrobial combinations	52

Figure 3.1 - <i>E. coli</i> NCTC 10418 growth heatmaps in the presence of sodium fusidate and copper(II) sulphate combinations in three media: cation adjusted Müller-Hinton broth (CAMHB), Miller's lysogeny broth (LB) and nutrient broth No. 1 (NB)	64
Figure 3.2 - Inhibition of <i>S. aureus</i> NCTC 12973 by ethanol concentrations equivalent to those present in sodium fusidate test dilutions	65
Figure 3.3 - Inhibition of <i>E. coli</i> NCTC 12973 by ethanol concentrations equivalent to those present in sodium fusidate test dilutions	65
Figure 3.4 - Wells containing iron(II) sulphate in sterile nutrient broth after incubation for 18±2 h at 35 °C and 120 rpm illustrating precipitation and colour change indicative of generation of heterogenous iron species.....	67
Figure 3.5 - Inhibitory effect of sodium sulphate on the growth <i>E. coli</i> NCTC 10418 and <i>S. aureus</i> NCTC 12973 in nutrient broth after incubation for 18±2 h.....	69
Figure 3.6 - Difference in inhibition of <i>S. aureus</i> NCTC 12973 by sodium fusidate in the presence of sodium sulphate compared to sodium fusidate alone	69
Figure 3.7 - Difference in inhibition of <i>E. coli</i> NCTC 10418 in the presence of sulphate and sodium fusidate compared to sodium fusidate alone.....	70
Figure 4.1 – Cyclical production of hydroxyl radicals <i>via</i> the Fenton reaction ^[336]	79
Figure 4.2 - Combined metal and sodium fusidate MIC _{90s} against <i>E. coli</i> NCTC 10418	88
Figure 4.3 - Combined metal and sodium fusidate MIC _{90s} against <i>S. aureus</i> NCTC 12973.....	89
Figure 4.4 – Sodium fusidate MIC ₉₀ fold reduction in the presence of 25 or 12.5 % metal ion MIC _{90s}	90
Figure 4.5 – Combined MIC _{90s} of sodium fusidate and copper(II) salts against <i>E. coli</i> NCTC 10418.....	91
Figure 4.6 - Combined MIC _{90s} of sodium fusidate and copper(II) salts against <i>S. aureus</i> NCTC 12973.....	92
Figure 4.7 - Concentrations of copper(II) sulphate required to kill <i>E. coli</i> NCTC 10418 in the presence of sodium fusidate after 6 h exposure in a range of solvents.....	94

Figure 4.8 - Percentage of log ₁₀ <i>E. coli</i> NCTC 10418 killed by copper(II)sulphate with or without sodium fusidate in HPLC grade water at 20 °C	95
Figure 4.9 - Known antimicrobial targets or mechanisms of metal ions and their ranked co-operativity with sodium fusidate against <i>E. coli</i> NCTC 10418	100
Figure 5.1 - Example of ITC output data for an exothermic complexation reaction between silver ions and the antimicrobial cefuroxime	107
Figure 5.2 – Absorbance spectra of 200 µM sodium fusidate titrated with increasing concentrations of copper(II) sulphate in aqueous solution	119
Figure 5.3 - UV-Vis extinction curves illustrating pH-dependent changes in sodium fusidate precipitation on mixing with copper(II) salts	120
Figure 5.4 – ITC thermograms of sodium fusidate with copper(II) sulphate (A), copper(II) D-gluconate at native pH (B), copper(II) gluconate at pH 6.12 (C) and sodium D-gluconate (D).....	121
Figure 5.5 - ITC thermogram of sodium fusidate with dilute sulphuric acid.....	123
Figure 5.6 - Relationship between pH of metal sulphates in nutrient broth and inhibition of <i>E. coli</i> NCTC 10418.....	124
Figure 5.7 - Relationship between pH of metal sulphates in nutrient broth and inhibition of <i>E. coli</i> NCTC 10418 by 20 µM (6.25 % MIC ₉₀) sodium fusidate	125
Figure 5.8 - Inhibition of <i>E.coli</i> NCTC 10418 by 20 µM sodium fusidate in the presence of copper(II) D-gluconate at unadjusted and neutral pH.....	126
Figure 5.9 - Combined MIC ₉₀ s of sodium fusidate and copper(II) D-gluconate at unadjusted native pH and neutral pH 7.2 against <i>E. coli</i> NCTC 10418.....	127
Figure 5.10 - Inhibition of <i>S. aureus</i> NCTC 12973 by sodium fusidate remaining after removal of large aggregates by filtration	128
Figure 5.11 – Alignment of data for <i>S. aureus</i> NCTC 12973 inhibition by sodium fusidate after exclusion of large aggregates induced by lowered pH to unadjusted control	129
Figure 5.12 - Alignment of raw sodium fusidate 18 h stability chromatograms (lower panel) with published, annotated example from Byrne <i>et al.</i> , 2015 ^[288] (upper panel)	130

Figure 5.13 - Example stability-indicating RP-HPLC overlay chromatograms produced by 2.5 mM sodium fusidate before and after incubation for 18 h at 35 °C	131
Figure 5.14 - Concentration of sodium fusidate remaining in solution after equilibration in pH adjusted nutrient broths for 1.5±0.5 h at 20 °C.....	132
Figure 5.15 - Percentage of different initial sodium fusidate concentrations remaining in solution after 1-2 h equilibration at 20 °C in nutrient broth at a range of pHs	133
Figure 5.16 - Concentration of sodium fusidate remaining in solution after equilibration in pH adjusted nutrient broth for 18±2 h at 35 °C and 120 rpm	134
Figure 5.17 - Percentage of different initial sodium fusidate concentrations remaining in solution after 18±2 h equilibration at 35 °C in nutrient broth at a range of pHs	135
Figure 5.18 - Comparison of sodium fusidate solubility in pH adjusted nutrient broth after 1.5±0.5 h at 20 °C and 18±2 h at 35 °C.....	136
Figure 5.19 - Linear (A), exponential (B) and polynomial (C) modelling of the relationship between sodium fusidate solubility and its impact on growth of <i>E. coli</i> NCTC 10418.	137
Figure 5.20 - Solubility of 1280 µM sodium fusidate in nutrient broth with metal sulphates after incubation for 1.5±0.5 h at 20 °C (blue) or 18±2 h at 35 °C (red)	139
Figure 5.21 - Comparison of solubility of 1280 µM sodium fusidate in pH adjusted nutrient broth (open circles) and nutrient broth with metal sulphates (labelled closed circles) after equilibration for 18±2 h at 35 °C	140
Figure 5.22 - Comparison of observed inhibition with two methods of predicting inhibition of <i>E. coli</i> NCTC 10418 by 20 µM sodium fusidate in the presence of aluminium as sulphate in nutrient broth	141
Figure 5.23 - Comparison of observed inhibition with two methods of predicting inhibition of <i>E. coli</i> NCTC 10418 by 20 µM sodium fusidate in the presence of cobalt(II) sulphate in nutrient broth.....	142
Figure 5.24 - Comparison of observed inhibition with two methods of predicting inhibition of <i>E. coli</i> NCTC 10418 by 20 µM sodium fusidate in the presence of copper(II) sulphate in nutrient broth.....	142
Figure 5.25 - Comparison of observed inhibition with two methods of predicting inhibition of <i>E. coli</i> NCTC 10418 by 20 µM sodium fusidate in the presence of iron(II) sulphate in nutrient broth.....	143

Figure 5.26 - Comparison of observed inhibition with two methods of predicting inhibition of <i>E. coli</i> NCTC 10418 by 20 µM sodium fusidate in the presence of manganese(II) sulphate in nutrient broth.....	144
Figure 5.27 - Comparison of observed inhibition with two methods of predicting inhibition of <i>E. coli</i> NCTC 10418 by 20 µM sodium fusidate in the presence of nickel(II) sulphate in nutrient broth	144
Figure 5.28 - Comparison of observed inhibition with two methods of predicting inhibition of <i>E. coli</i> NCTC 10418 by 20 µM sodium fusidate in the presence of palladium(II) sulphate in nutrient broth.....	145
Figure 5.29 - Comparison of observed inhibition with two methods of predicting inhibition of <i>E. coli</i> NCTC 10418 by 20 µM sodium fusidate in the presence of zinc(II) sulphate in nutrient broth	145
Figure 5.30 - Comparison of observed inhibition with two methods of predicting inhibition of <i>E. coli</i> NCTC 10418 by 20 µM sodium fusidate in the presence of copper(II) D-gluconate in nutrient broth at unadjusted native pH	147
Figure 5.31 - Comparison of observed inhibition with two methods of predicting inhibition of <i>E. coli</i> NCTC 10418 by 20 µM sodium fusidate in the presence of copper(II) D-gluconate in nutrient broth adjusted to pH 7.2.....	148
Figure 5.32 - Comparison of observed inhibition with two methods of predicting inhibition of <i>E. coli</i> NCTC 10418 by 20 µM sodium fusidate in the presence of copper(II) sulphate in Miller's lysogeny broth	149
Figure 5.33 - Comparison of observed inhibition with two methods of predicting inhibition of <i>E. coli</i> NCTC 10418 by 20 µM sodium fusidate in the presence of copper(II) sulphate in cation adjusted Müller-Hinton broth.....	150
Figure 5.34 – Sodium fusidate per million <i>E. coli</i> NCTC 10418 cells recovered from bacterial pellet after exposure to 160 µM in nutrient broth in the presence of metal ions or reduced pH for 30 min at 35 °C and 120 rpm.....	151
Figure 6.1 – AUCs of metal ion-normalised bacterial growth with sodium fusidate in the presence of metal ions	170
Figure 6.2 – Fold reduction in sodium fusidate MIC ₉₀ when in the presence of metal ions	174

Figure 7.1 - Layout of 96 well plates for LDH and MTT assays	186
Figure 7.2 - Sodium fusidate-induced cytotoxicity and growth inhibition of human corneal epithelial cells after 18±2 h incubation at 37 °C in 5 % CO ₂	191
Figure 7.3 – Metal ion-induced growth inhibition of human corneal epithelial cells after 18±2 h incubation at 37 °C in 5 % CO ₂	192
Figure 7.4 - Inhibition of human corneal epithelial cell growth by sodium fusidate combined with 0.625 mM metal ions after 18±2 h incubation at 37 °C in 5 % CO ₂	193
Figure 7.5 - Comparison of growth inhibition of human corneal epithelial cells and bacterial reference strains <i>E. coli</i> NCTC 10418, <i>K. pneumoniae</i> NCTC 9633 and <i>P. aeruginosa</i> NCTC 13359 by sodium fusidate alone	194
Figure 7.6 – Comparison of growth inhibition of human corneal epithelial cells and bacterial reference strains <i>E. coli</i> NCTC 10418, <i>K. pneumoniae</i> NCTC 9633 and <i>P. aeruginosa</i> NCTC 13359 by aluminium ions alone (A) and sodium fusidate in the presence of 0.625 mM aluminium ions (B)	195
Figure 7.7 - Comparison of growth inhibition of human corneal epithelial cells and bacterial reference strains <i>E. coli</i> NCTC 10418, <i>K. pneumoniae</i> NCTC 9633 and <i>P. aeruginosa</i> NCTC 13359 by copper(II) ions alone (A) and sodium fusidate in the presence of 0.625 mM copper(II) ions (B)	196
Figure 7.8 - Comparison of growth inhibition of human corneal epithelial cells and bacterial reference strains <i>E. coli</i> NCTC 10418, <i>K. pneumoniae</i> NCTC 9633 and <i>P. aeruginosa</i> NCTC 13359 by iron ions alone (A) and sodium fusidate in the presence of 0.625 mM iron ions (B).....	197
Figure 8.1 - Scale diagram of the tear film structure	206
Figure 8.2 – The <i>in vivo</i> pH of human tear fluid and its variation in response to air exposure	218
Figure 8.3 - Mean absorbance of STF formulations and nutrient broth at 595 nm over 60 h incubation at 35 °C.....	220
Figure 8.4 - Growth of <i>E. coli</i> NCTC 10418 in STF formulations and nutrient broth as determined by absorbance at 595 nm over 60 h incubation at 35 °C	221
Figure 8.5 - Change in pH of novel STF before, during and after incubation at 37 °C with 5 % CO ₂	222

Figure 8.6 - Photograph of novel STF after overnight incubation at 37 °C and 5 % CO ₂	223
Figure 8.7 - Growth of <i>E. coli</i> NCTC 10418 after 24 h at 37 °C and 5 % CO ₂ in novel STF compared to various dilutions of nutrient broth.....	224
Figure 8.8 - Bacterial growth curves in novel STF and 50 % nutrient broth comparator over 28 h at 37 °C and 5 % CO ₂	225
Figure 8.9 – Activity of sodium fusidate and metal sulphates against <i>E. coli</i> , <i>K. pneumoniae</i> and <i>P. aeruginosa</i> reference strains in novel STF and 50 % nutrient broth	226
Figure 8.10 - Solubility of 1280 µM sodium fusidate in novel STF or 50 % nutrient broth with or without metal sulphates after 4 h at 37 °C and 5 % CO ₂	228
Figure 8.11 - Solubility of 1280 µM sodium fusidate sodium salt compared to pH of metal sulphates in novel STF and 50 % NB after 4 h at 37 °C and 5 % CO ₂	229
Figure 10.1 - Example chromatogram for fusidate resolved by RP-HPLC separation method 1 ^[287]	301
Figure 10.2 - Example chromatogram for fusidate resolved by RP-HPLC separation method 2 ^[288]	301
Figure 10.3 - Calibration curve for fusidate quantification by RP-HPLC separation method 1 ^[287]	302
Figure 10.4 - Calibration curve for fusidate quantification by RP-HPLC separation method 2 ^[288]	303
Figure 10.5 - Example chromatograms for fusidate in bacterial lysate resolved by RP- HPLC separation method 1 and separation method 2	306
Figure 10.6 – Example of EDTA-CaCl ₂ ITC performance validation data	307
Figure 10.7 –ITC thermograms of sodium fusidate with copper(II) sulphate.....	308
Figure 10.8 –ITC thermogram of sodium fusidate with copper(II) D-gluconate at native pH.....	309
Figure 10.9 –ITC thermogram of sodium fusidate with copper(II) gluconate at pH 6.12	309

Figure 10.10 –ITC thermograms of sodium fusidate with sodium D-gluconate	310
Figure 10.11 - ITC thermogram of sodium fusidate with dilute sulphuric acid	310
Figure 10.12 – Maximal LDH release from HCE-2 after 18 or 42 h	313
Figure 10.13 - Absorbance of MTT formazan produced by HCE-2 seeded at 12,500 cells per well over time after solubilisation in DMSO at 540 nm	314
Figure 10.14 - Absorbance at a variety of wavelengths of formazan produced by HCE-2 after exposure to 1 mg mL ⁻¹ MTT for 2 h and correlations with seeding density	317
Figure 10.15 – LDH activity from HCE-2 with and without mixing on addition of assay reagents and correlations with seeding density	319
Figure 10.16 – Comparison of optimised LDH and MTT assay results and linear relationships between HCE-2 seeding density and absorbance.....	320

List of tables

Table 1.1 – Summary of variation in contribution of the four most commonly reported predisposing factors to initiation of microbial keratitis by country (%)	4
Table 1.2 – Variation in percentage of bacterial keratitis cases caused by Gram-positive and Gram-negative organisms summarised from 24 observational studies.....	9
Table 1.3 - Summary of fluoroquinolone and cephalosporin resistance identified in bacterial keratitis isolates	13
Table 2.1 - Mobile phase gradient for HPLC method 2	54
Table 3.1 - Composition of bacteriological media.....	60
Table 3.2 – MIC ₉₀ and MBC of antimicrobial metal sulphates against <i>E. coli</i> NCTC 10418 and <i>S. aureus</i> NCTC 12973 after 18±2 h incubation in nutrient broth at 35 °C and 120 rpm	67
Table 4.1 – Summary of known antimicrobial targets and mechanisms of metal ions selected for investigation in combination with sodium fusidate	75
Table 4.2 - FIC _{90I} for antimicrobial metal ions in combination with sodium fusidate against <i>E. coli</i> NCTC 10418 and <i>S. aureus</i> NCTC 12973, in order of anti- <i>E. coli</i> efficacy	87
Table 4.3 - FIC _{90I} for copper(II) salts in combination with sodium fusidate against <i>E. coli</i> NCTC 10418 and <i>S. aureus</i> NCTC 12973	91
Table 4.4 – Area under the isobologram curves for copper(II) salts combined with sodium fusidate against <i>E. coli</i> NCTC 10418.....	92
Table 4.5 – Area under the isobologram curves for copper(II) salts combined with sodium fusidate against <i>S. aureus</i> NCTC 12973.....	93
Table 4.6 - MCKC of copper(II) sulphate against <i>E. coli</i> NCTC 10418 after 6 h room temperature incubation in a range of solvents.....	94
Table 5.1 – The pH of each initial individual solution used in ITC experiments and an equilibrated mixture at the same final ratio.....	122
Table 5.2 - Correlation slopes and R ² values for relationship between initial sodium fusidate concentration and concentration in solution after equilibrium at 20 °C for 1.5±0.5 h in pH adjusted nutrient broth	132

Table 5.3 - Correlation slopes and R ² values for relationship between initial sodium fusidate concentration and concentration in solution after equilibrium at 35 °C for 18±2 h in pH adjusted nutrient broth	134
Table 5.4 - Difference between observed <i>E. coli</i> NCTC 10418 inhibition by 20 µM sodium fusidate in the presence of metal sulphates and that predicted by model (i)	146
Table 5.5 - Difference between observed <i>E. coli</i> NCTC 10418 inhibition by 20 µM sodium fusidate in the presence of metal sulphates and that predicted by model (ii)	146
Table 5.6 - Comparison of sodium fusidate recovered from <i>E. coli</i> NCTC 1014 to its activity and solubility under the same conditions, ordered by mass recovered	151
Table 6.1 – Multi-drug resistant Gram-negative isolates provided by Prof Walsh laboratories	164
Table 6.2 – MIC ₉₀ s and MBCs (in parentheses) of metal ions against MDR bacterial isolates and their reference strains (mM).....	167
Table 6.3 – Sodium fusidate MIC ₉₀ s (µM) and FIC ₉₀ s (in parentheses) with metal ions	172
Table 7.1 – Mammalian cell proliferation inhibition data from the literature	182
Table 7.2 – Concentration range of each agent tested alone for cytotoxicity and proliferation effects on HCE-2.....	188
Table 7.3 – Mean sodium fusidate IC ₅₀ s and IC ₉₀ s against human corneal epithelial cells, with and without 0.625 mM metal ions.....	193
Table 7.4 – Sodium fusidate selectivity indices against human corneal epithelial cells and Gram-negative reference strains, with and without metal ions	198
Table 8.1 - Published simulated tear fluid formulations included in the analysis	212
Table 8.2 - Concentrations of electrolytes, metabolites and proteins employed in published simulated tear fluid formulations.....	213
Table 8.3 - Concentrations of electrolytes and metabolites measured in human tears	215
Table 8.4 – Concentrations of proteins measured in human tears	216
Table 8.5 - Reported pH of eight simulated tear fluid formulations.....	217

Table 8.6 - Rationalised concentrations of novel STF components	219
Table 8.7 - Effect of bicarbonate concentration and phosphate protonation state on STF pH in normal air at room temperature.....	222
Table 8.8 - Composition of optimised novel STF.....	223
Table 8.9 - pH of novel STF and 50 % NB with and without 625 μ M metal ions after 4 h at 37 °C and 5 % CO ₂	228
Table 10.1 - Control inhibition zone diameters produced by sodium fusidate against <i>S. aureus</i> NCTC 12973 on nutrient broth.....	305
Table 10.2 - Zones of inhibition of <i>S. aureus</i> NCTC 12973 on nutrient broth produced by lysate of <i>E. coli</i> NCTC 10418 exposed to sodium fusidate.....	305
Table 10.3 - Combinations of optimisation test conditions	315
Table 10.4 - R ² values for linear relationship between cell seeding density and absorbance of MTT formazan in DMSO produced by HCE-2 exposed to 0.5 or 1.0 mg mL ⁻¹ MTT with or without mixing of DMSO on addition	316
Table 10.5 - Published cell seeding densities used in MTT assay	320
Table 10.6 - Timepoints and tasks for the combined LDH and MTT assay procedure	321
Table 10.7 - Concentrations of lipids in eleven published simulated tear fluid formulations	322
Table 10.8 - Concentrations of trace elements in eleven published simulated tear fluid formulations.....	322
Table 10.9 - Concentrations of trace elements measured in human tears.....	323

Abbreviations

°C	degrees Celsius
µcal	microcalories
µg	micrograms
µL	microlitres
µM	micromolar
µm	microns
µmol	micromoles
2D	two-dimensional
3D	three-dimensional
ACN	acetonitrile
ADP	adenosine diphosphate
ATCC	American Type Culture Collection
ATP	adenosine triphosphate
AU	absorbance units
AUC	area under the curve
BPE	bovine pituitary extract
BSA	bovine serum albumin
BSAC	British Society for Antimicrobial Chemotherapy
CAMHB	cation-adjusted Müller-Hinton broth
CFU	colony forming units
CI	confidence interval
CLSI	Clinical Laboratory Standards Institute (formerly NCCLS)
cm	centimetres
CoNS	coagulase-negative <i>Staphylococcus/Staphylococci</i>
DMSO	dimethyl sulfoxide
DNA	deoxyribonucleic acid
EC	effective concentration
ECOFF	epidemiological cut-off value
EDTA	ethylenediaminetetraacetic acid
EF-G	elongation factor G
EF-Tu	elongation factor Tu
EGF	epidermal growth factor
ESBL	extended-spectrum β-lactamase
EtOH	ethanol
EUCAST	European Committee on Antimicrobial Sensitivity Testing
FA	fusidic acid
FDA	United States Food and Drug Administration

FIC	fractional inhibitory concentration
FICI	fractional inhibitory concentration index
FNa	sodium fusidate
g	grams
GDP	guanosine diphosphate
GN	Gram-negative
GP	Gram-positive
GTP	guanosine triphosphate
h	hours
HCE-2	human corneal epithelial cells [50.B1] ATCC® CRL-11135
HPLC	high performance liquid chromatography
IC	inhibitory concentration
IM	inner membrane
ITC	isothermal titration calorimetry
kcal	kilocalories
kg	kilograms
KSFM	keratinocyte serum-free medium
L	litres
LB	Miller's lysogeny broth
LD	lethal dose
LDH	lactate dehydrogenase
LLB	Lennox lysogeny broth
LOD	limit of detection
LOQ	limit of quantification
LPS	lipopolysaccharide
M	molar
MAP	muco-aqueous pool
mAU	milli-absorbance units
MBC	minimum bactericidal concentration
MCKC	minimum complete-kill concentration
MDR	multi-drug resistant/resistance
MeOH	methanol
mg	milligrams
MHB	Müller-Hinton broth
MIC	minimum inhibitory concentration
min	minutes
mL	millilitres
mM	millimolar
mm	millimetres

mmol	millimoles
MOPS	3-(N-morpholino)propanesulfonic acid
mRNA	messenger ribonucleic acid
MRSA	methicillin-resistant <i>Staphylococcus aureus</i>
MSSA	methicillin-sensitive <i>Staphylococcus aureus</i>
MTT	3-(4,5-dimethylthiazol-2-yl)-2,5-diphenyltetrazolium bromide
NA	nutrient agar
NB	nutrient broth
NCCLS	National Committee for Clinical Laboratory Standards (now CLSI)
NCTC	National Collection of Type Cultures
NDM-1	New Delhi metallo- β -lactamase 1
ng	nanograms
nM	nanomolar
nm	nanometres
nmol	nanomoles
OD	optical density
OM	outer membrane
PBS	phosphate buffered saline
PCR	polymerase chain reaction
PES	polyethersulfone
pg	picograms
PMF	proton motive force
RNA	ribonucleic acid
RP-HPLC	reversed-phase high performance liquid chromatography
rpm	revolutions per minute
rRNA	ribosomal ribonucleic acid
s	seconds
SCV	small colony variant
SD	standard deviation
SI	selectivity index
STF	simulated tear fluid
tRNA	transfer ribonucleic acid
UV	ultraviolet
UV-Vis	ultraviolet-visible light
v	volume
w	weight
WHO	World Health Organisation
x g	times gravity

Publications and presentations

Publications in preparation

Antimicrobial activity of metal ions against Gram-negative bacteria. Target journal: *Antimicrobial Agents and Chemotherapy* (planned submission Jan-2020)

MICs and sub-MIC effects of metal sulphates against reference strains and multi-drug resistant isolates of *Escherichia coli*, *Klebsiella pneumoniae* and *Pseudomonas aeruginosa*. The data will add to the limited published metal ion MICs and suggests metal ion resistance is not inherently co-localised with multi-drug resistance genes.

Synergistic activity of antimicrobial metal ions and sodium fusidate against Gram-negative bacteria. Target: *Journal of Antimicrobial Chemotherapy* (planned Mar-2020)

The efficacy of metal ions combined with sodium fusidate against multi-drug resistant *E. coli*, *K. pneumoniae* and *P. aeruginosa*. The sensitisation of these important pathogens to an anti-Staphylococcal agent is unexpected and suggests novel combination treatment with potential clinical relevance.

A rationally-designed artificial simulated tear fluid formulation for the study of bacterial eye infections. Target journal: *Nature Methods* (planned May-2020)

A modified simulated tear fluid formulation optimised to accurately reflect human mucocaqueous pool composition and support growth of common ocular pathogens, enabling study of bacterial behaviour in *in situ*-like conditions.

Oral presentations delivered

Anti-Staphylococcal agent sodium fusidate becomes active against *Escherichia coli* at reduced pH. *CITER Annual Scientific Meeting*, 18-Sep-2018
(awarded prize for Best Oral Presentation)

Towards the repurposing of existing topical antimicrobials by reformulation.
LSRNW 5th Annual Drug Discovery Congress, 11-Sep-2018

New tricks performed by old drugs: Activity of the anti-staphylococcal agent sodium fusidate against *Escherichia coli* when combined with transition metal ions. *CITER Annual Scientific Meeting*, 18-Sep-2017

Combining metal ions with fusidic acid to treat bacterial keratitis.
Speaking of Science, 04-May-2017

Acknowledgements

Firstly, I would like to sincerely thank my supervisors for their guidance and support throughout this journey: Dr Charles Heard and Prof Les Baillie. Thank you for the initial opportunity to pursue this Ph.D., your advice and encouragement to bring my ideas to life, your understanding through tough times and, most recently, your time and helpful feedback on the preparation of this thesis. In addition, I would like to thank Dr Claire Simons for her support and encouragement as my advisor. I am grateful to all three members of my supervisory team for helping me in many different ways at different times, together providing everything I needed to be able to complete this huge task.

My thanks also go to those who have provided vital training and resources: Anna Fuller and Dr David Cole for training in ITC and use of the equipment; Dr Jon Tyrrell and Dr Kirsty Sands for the donation of resistant isolates and provision of genotyping data, respectively; and Dr Barbora Červinková Hroch for training in HPLC. I am also grateful to the Life Sciences Research Network Wales (LSRNW) for the funding and the School of Pharmacy and Pharmaceutical Sciences support staff for enabling this Ph.D. project.

Thank you to my dear friends, new and old, and everyone in Office 2.62 for the kindness and support that has helped me through. Melissa, Hélène, Shayda, Helen, Barbora and Amal: I am so grateful to have had each of you with me on this ride. Ray, Di, Sam and Gill: thank you for always being there even while far away. And thank you to all my family for never doubting me: my mum & step-dad, Alison & Scott; my dad & step-mum, Martin & Corinne; my sister & brother-in-law, Emily & Scott; and my brothers Ryan & Nick.

Finally, my unending thanks go to my wonderful husband, Ian, who put his own career on hold for me to pursue this degree. Words cannot adequately express how much your sacrifice, encouragement, constant patience and unwavering confidence mean to me. I will be forever grateful to you for making this a reality. Thank you for being here and doing this with me. I love you.

In honour of my Nan,
Frances Phyllis Fitzgerald
(13-Jul-1929 to 04-Feb-2009),
and her lessons in grace, generosity
and believing the best of people,
including yourself.

In honour of my Grandma,
Margaret Olive Bundy
(07-Jun-1930 to 17-Mar-2019),
and her lessons in strength, resilience
and the importance of productivity,
never idle hands.

"But then science is nothing but a series of questions that lead to more questions, which is just as well, or it wouldn't be much of a career path, would it?" - Terry Pratchett & Steve Baxter, The Long Earth

Chapter 1: Introduction



1.1 Overview

Antimicrobial agents are regularly relied upon to prevent and treat bacterial infections, which would have been incapacitating or fatal not too many years ago. However, the diversity and rapid evolution of pathogenic organisms can limit the effectiveness of antimicrobial drugs and necessitates the continuous development of new anti-infective strategies. By exploiting the potential for co-administration of agents to enhance the activity of previously approved antimicrobials, new therapeutic formulations with wider spectrums of activity may be developed and made available for human use in a shorter time frame than a completely novel drug could be. Such potential has already been demonstrated in the literature, and preliminary investigations at Cardiff University's School of Pharmacy and Pharmaceutical Sciences have identified a promising combination of fusidic acid (FA) and ionic metals. This combination will form the basis of the present thesis which aims to understand the possible mechanisms and spectrum of activity of FA metal ion mixtures and assess their potential for clinical application in bacterial keratitis.

1.2 Bacterial keratitis

Keratitis is a serious sight-threatening inflammation of the cornea, usually occurring in response to infection. In most cases, keratitis is instigated by damage to the corneal epithelium due to traumatic injury, surgery, or, more commonly, abrasion such as that experienced during contact lens wear^[1]. This allows pathogenic microbes to infiltrate the cornea, initiate infection and cause ulceration. While less common, keratitis can also be caused by microorganisms that are able to cross the intact corneal epithelial barrier^[2]. Infectious keratitis can be bacterial, fungal, viral or protozoan and even polymicrobial. Prognosis, severity and treatment vary between causative organism and predisposing or concomitant factors. The focus of this work employing the antibacterial agent FA is bacterial keratitis.

1.2.1 Prevalence and predisposing factors

Incidence of microbial keratitis in industrialised and cooler regions is lower than in tropical or developing countries. For example, rates of all-cause keratitis in temperate Minnesota during the late 1980s was 11 per 100,000 people per year^[3] whereas in the early 1990s 113 and 799 per 100,000 per year were reported in South India and Nepal, respectively. Based on the available incidence figures for these developing countries, the WHO estimates a burden of 1.5 to 2 million cases per year in Africa and Asia alone^[4].

Incidence has significantly increased over time in industrialised countries due to widespread contact lens use^[5]. There was a 435 % increase in annual cases between the 1950s and late 1980s in the Minnesota population^[3] and by the late 1990s, incidence in northern California was 27.6 per 100,000 per year. However, from 2005 to 2015 in Queensland, Australia, microbial keratitis cases were less common at 6.6 per 100,000 people per year^[6]. Rates for bacterial keratitis alone are not accurately known as these population-based studies do not differentiate between infective agent. However, it is understood that bacterial pathogens predominate in industrialised, temperate regions, whereas fungi and parasites are more common in tropical and developing areas^[1].

Even in regions with the highest prevalence, total incidence of microbial keratitis is substantially lower than most other ocular infections. For example, a conservative estimate for conjunctivitis caused solely by bacterial infection is >3,000 per 100,000 people per year in Denmark^[7]. However, complications in conjunctivitis are extremely rare^[8] whereas even with effective treatment and excellent care, serious, vision-impairing complications occur in at least 5 % of bacterial keratitis cases^[9].

Predisposing factors also vary by geographical region and population. Contact lens use is the most important risk for the development of bacterial keratitis in industrialised areas^{[1],[10]}. This includes both day-time vision-correction or cosmetic lenses and overnight corneal-shaping orthokeratological lenses^[10]. The risk is further compounded by poor lens hygiene, use during swimming or showering and long duration of wear due to increased likelihood of biofilm formation, contamination by environmental organisms or slowed clearing of potential pathogens, respectively^[1]. In particular, extended wear of lenses increases chances of establishment of infection as the lens protects any microbes between it and the ocular surface from the sweeping action of blinking, allowing them to adhere^[2]. In a study of keratitis in Taiwanese children – a population with a high prevalence of myopia – 34 % of cases were associated with soft contact lens wear and a further 19 % with orthokeratology^[10].

Conversely, traumatic injury is the most common cause of microbial keratitis in developing countries where agricultural occupations predominate^{[11],[12]}. Table 1.1 summarises rates of the most commonly reported predisposing factors identified in seven different studies of microbial keratitis. Industrialised countries see ≤20 % cases caused by traumatic injury^{[10],[13]–[15]}, whereas more than 45 % were related to trauma in an agricultural region of India^[12].

Table 1.1 – Summary of variation in contribution of the four most commonly reported predisposing factors to initiation of microbial keratitis by country (%)

	Hong Kong ^[16] *	Taiwan ^[10] (paediatric)	Australia ^[17]	USA ^[13] *	India ^[12] #	France ^[14] #	Switzerland ^[15] #
Contact lens use	51.9	52.9	33.7	43.0	2.0	50.3	36.5
Ocular surgery	5.1	4.4	NR	34.0	22.0	4.0	5.9
Ocular trauma	12.6	16.2	36.4	13.0	46.6	15.0	20.0
Ocular surface disease	33.2	10.3	6.0	44.0	12.5	21.3	8.2

Values do not total 100 % per country due to inclusion of other factors not summarised here.

* Hong Kong and USA studies assigned patients to multiple categories.

Numbers from India, France and Switzerland are for bacterial keratitis only.

NR: not reported

Ocular surgery such as corneal transplant is also an important keratitis risk factor, along with pre-existing ocular surface disease. Both these conditions alter the normal structure and function of the corneal epithelium. Frequency of surgery-related keratitis varies by region whereas ocular surface disease appears to be the sole identified predisposing factor for approximately 10-20 % of keratitis cases globally.

1.2.2 Symptoms, pathology and progression

Bacterial keratitis presents as a combination of decreased visual acuity^{[1],[18],[19]}, photophobia^{[1],[18]} and pain^{[1],[18],[19]}, often with redness of the eye^{[1],[18],[19]} and discharge^[18]. The discomfort experienced is usually a foreign body sensation rather than the gritty feeling common to other eye infections such as conjunctivitis^[18]. However, not all symptoms are present in all patients^[19]. On closer physical examination the affected eye can be found to exhibit corneal ulceration or stromal abscess with or without a hypopyon or localised oedema^[20]. Presentation and progression can, but does not always, vary depending on the causative organism. Figure 1.1 illustrates various presentations and stages of keratitis caused by a variety of bacteria.

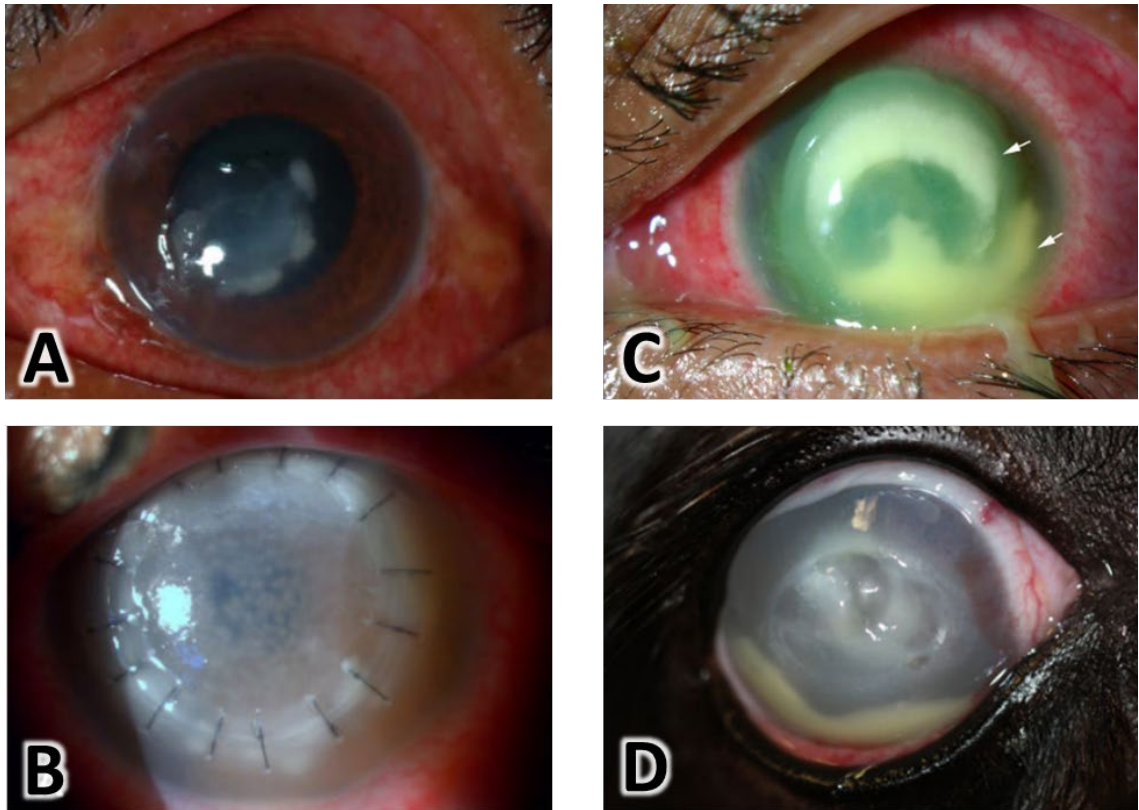


Figure 1.1 - Examples of bacterial keratitis presentation from the literature

- A: *Streptococcus pneumoniae* (Gram-positive) with an early uneven corneal infiltrate^[21];
- B: *Klebsiella pneumoniae* (Gram-negative) diffuse growth in a corneal graft^[22];
- C: *Pseudomonas aeruginosa* (Gram-negative) severe presentation illustrating large corneal infiltrate (top arrow) and hypopyon (bottom arrow)^[1];
- D: An unidentified Gram-negative in canine ulcerative keratitis nearing corneal perforation^[23].

The infection starts with colonisation of an epithelial abrasion or defect by a microbial pathogen^[24]. Once adhered, the organisms are able to migrate into the corneal stroma and trigger an inflammatory response. Figure 1.1A depicts an early uneven corneal infiltrate at the beginning of infection. This leads to ulceration (Figure 1.1C) and corneal degradation (Figure 1.1D) which can result in perforation and loss of the eye^[1]. The rapidity and severity of progression varies by organism^[24]. Fungal infections tend to advance more quickly than those of Gram-positive (GP) bacteria. However, keratitis caused by Gram-negative (GN) bacteria – and *Pseudomonas aeruginosa* in particular – can cause extensive inflammation, progress rapidly and result complete corneal destruction within as little as 24-48 h^{[20],[24]}.

Bacteria are not only capable of melting the cornea by digesting collagen^[25], they can also secrete agents which actively inhibit cell migration and therefore prevent healing of the epithelium^[26]. Examples of organisms that have been shown to produce migration inhibitors include the GP *Staphylococcus aureus* and GNs *Serratia marcescens* and *P. aeruginosa*^[26]. *P. aeruginosa* also produces multiple virulence factors which increase the severity of disease. These include a glycocalyx coating which provides protection

from phagocytosis, proteases which degrade the extracellular tissue structures and cause mammalian cell lysis, and exotoxins which destroy immunoglobulins, inhibit mammalian protein synthesis and induce apoptosis^[19]. In addition, triggering of the immune response and ulceration contributes further to corneal damage, slowing healing and increasing chances of perforation^[1]. If the infection goes uncontrolled, bacteria can also spread into the internal eye and cause endophthalmitis which even further complicates treatment and increases likelihood of resulting in enucleation^[27]. Finally, while re-epithelialisation is indicative of successful treatment, the healed cornea frequently remains scarred which causes permanent reduction in visual acuity^{[28],[29]}.

1.2.3 Diagnosis

Rapid and accurate diagnosis is essential to providing appropriate treatment in all types of microbial keratitis. Visualisation of the size, depth, location and shape of corneal infiltrates can be assessed using a slit lamp^{[1],[18]}. These features, as well as the general condition of the surrounding eye tissues, may give indication to the cause of infection^[1]. However, visual features vary widely and even highly trained corneal specialists are only able to distinguish bacterial from fungal aetiology 66 % of the time^[21]. Alternatively, experienced practitioners can also use *in vivo* confocal microscopy to identify fungal or *Acanthamoeba* infections. However, bacterial cells are too small to be visualised *via* confocal microscopy and equipment availability and expertise is not widespread^[1].

Corneal scrape for microscopy and culture is the gold standard for diagnosis of microbial keratitis^{[1],[18],[30]}. Multiple corneal scrapes are performed using a needle or blade in order to recover and identify the causative organism(s). Each scrape is immediately used either to smear slides for staining and microscopy or to inoculate one of a variety of microbiological media. The smears and inoculations must be performed “patient-side” and, while the materials will be delivered to a laboratory for processing and interpretation, the required media and sampling skills need to be available to the consulted healthcare professional^{[1],[30]}. Gram and Giemsa staining on receipt of the prepared slides can enable early indicative diagnosis of infective agent and, therefore, most appropriate initial treatment. However, the reliability of Gram stain results is directly linked to organism density in the smear which may be too low in scrapes from the early stages of disease or due to poor scraping and/or smearing technique^[30]. The received cultures are incubated for at least 1-2 weeks as certain bacteria and other causers of microbial keratitis can be extremely slow growing in the laboratory^[30]. Finally, antimicrobial

sensitivity testing is carried out on the recovered isolates in order to confirm drug selection and guide modification of the treatment regimen where necessary.

Even with careful collection and processing, frequency of successful recovery of the infecting organism from a corneal scrape can be as low as 30-50 %^{[31]–[33]}. Highest reported rates of positive microbial culture are only 65-85 %^{[15],[34],[35]}. Lack of understanding of the cause of infection and the antimicrobial sensitivity profile can severely limit the healthcare provider's ability to administer efficacious treatment. Alternative sample collection methods have been trialled in an attempt to increase the uptake and reliability of corneal culture. As an alternative to the healthcare professional undertaking multiple corneal scrapes and inoculating the required media patient-side, a single-use brush-like "ESwab" has been tested^[36]. The ESwab is used to sample the corneal ulcer just once and placed in specialised transport medium which both maintains microbial viability and preserves nucleic acids for polymerase chain reaction (PCR) analysis. The ESwab sample is shipped directly to the microbiology laboratory for culturing and analysis. While the culture positive rate was no greater than the traditional method, the ESwab was found to minimise inadvertent growth of contaminants and be more cost-effective than the traditional scrape method. Another modified sample collection method is a corneal impression membrane^[37]. A circular piece of sterile polytetrafluoroethylene (PTFE) membrane is carefully placed on the infected cornea for 5 s to adsorb present microbes onto its hydrophilic surface. Similarly to the ESwab, the membrane is then immersed in transport medium and sent to the laboratory for processing. The authors found a significant increase in organism recovery with an impression membrane compared to using a surgical blade.

However, regardless of the increased performance and convenience of these modified sample collection methods, the long turnaround time for culture and sensitivity testing can cause a severely detrimental delay to the initiation of effective treatment. Nevertheless, knowledge of antimicrobial susceptibility profiles is essential to management of the infection in the context of ever-increasing and evolving resistance in both bacterial and fungal pathogens. In order to address the need for both faster and more reliable confirmation of the causative organism, a number of PCR protocols have already been developed, with results often available within 24 h^{[1],[30]}. Unlike microbial culture, these tests require only very small amounts of DNA to be recovered from a corneal sample and do not rely on the successful collection of viable organisms in order to obtain results. However, access to facilities and equipment necessary to carry out such tests and analyse results currently remains sparse. Construction of rapid diagnostic panels have also been suggested, such as a dot hybridisation assay^[38]. In this method, bacterial DNA from corneal sampling is amplified by PCR, labelled with a UV-sensitive

marker and applied to a membrane embedded with organism-specific complimentary DNA probes. On exposure to UV light, positive dots become coloured indicating presence of the sought DNA and identifying the infecting organism. Such an assay may be more easily modified into a patient-side version than more comprehensive PCR analysis. This technique could theoretically also include known resistance genes in order to provide indicative antimicrobial susceptibility data. However, isolation and culture of the organism and determination of the minimum inhibitory concentration (MIC) of specific agents is likely to still be required in parallel, as bacteria and other pathogens often evolve novel resistance mechanisms which could otherwise go undetected. In addition, for many antimicrobials, resistance is rarely absolute and topical antimicrobial application can often surpass the MICs of organisms considered clinically resistant.

1.2.4 Causative organisms

A meta-analysis compiling bacterial causes of ocular infection demonstrated that the percentage of bacterial keratitis cases attributable to each species varied substantially by country^[27]. The proportion of GN isolates reported in each study varied from <10 to >60 %. However, in 10 of 11 studies, *P. aeruginosa* was the most frequent GN isolate (in the report from the 11th country the percentage of infections caused by *P. aeruginosa* was equal to another GN organism, *Escherichia coli*, both accounting for 20 %). Table 1.2 demonstrates a similarly wide variety in the ratio of GP:GN organisms isolated from bacterial keratitis both by country and reporting period in 24 additional observational studies from the literature.

GP bacteria most often isolated from bacterial keratitis tend to be Staphylococcal and Streptococcal species, however, distribution varies by region^[27]. The two most frequently isolated causative organisms in a 1996 Southern Californian study were *Staphylococcus epidermidis* (GP, a coagulase-negative *Staphylococcus* (CoNS)) and *P. aeruginosa* (GN), with isolation rates of 51.4 and 16.2 %, respectively^[39]. Only a few years later in Northern California, *S. aureus* (GP) and CoNS accounted for 27.6 and 24.1 % of keratitis cases, respectively. In Florida around the same time, *S. aureus* was the most frequently found GP bacterium, isolated in 19.4 % of cases^[40], and 25.2 % of cases were also caused by *S. aureus* in the Pittsburgh study^[41]. Outside the USA, the two most common bacterial keratitis isolates have been reported as *S. epidermidis* (32.5 %) and *Streptococcus pneumoniae* (GP, 13.9 %) in a Central Indian study^[12], *S. pneumoniae* (45.0 %) and *P. aeruginosa* (23.8 %) in South India, *S. epidermidis* (32.0 %) and *S. aureus* (21.3 %) in Switzerland^[15], *P. aeruginosa* (49.4 %) and *S. aureus* (14.8 %) in

East Kent, and *S. aureus*, *S. epidermidis*, *E. coli* and *P. aeruginosa* all at 22.4 % in South Eastern Nigeria. While CoNS also accounted for the highest proportion of bacterial keratitis cases in a French study (32.8 %), the second most commonly isolated organism was the GP anaerobe, *Propionibacterium acnes* (10.1 %)^[14]. Interestingly, *P. acnes*, was also found in 11.1 % of the Taiwanese paediatric cases during 2008-2012^[10] and 7.2 % isolates during 15 years in St Louis^[13] but does not appear to have been reported elsewhere. This wide variation in bacterial species isolated from keratitis cases is found throughout the literature, differing both by region and over time^{[33],[42]-[50]}.

Table 1.2 – Variation in percentage of bacterial keratitis cases caused by Gram-positive and Gram-negative organisms summarised from 24 observational studies

Location	Reporting period	Percentage of bacterial keratitis isolates	
		Gram-positive	Gram-negative
Vancouver, BC, Canada ^[34]	2006-2008	85.8	14.2
Vancouver, BC, Canada ^[34]	2009-2011	72.0	28.0
St Louis, Missouri, USA ^[13]	1999-2013	58.8	41.2
Pittsburgh, Pennsylvania, USA ^[41]	1993-2012	53.7	46.3
Southern Florida, USA ^[40]	1990-1998	49.0	51.0
São Paulo, Brazil ^[32]	1975-2007	71.6	28.4
Glasgow, UK ^[51]	1995-1998	84.0	16.0
Glasgow, UK ^[51]	2004-2007	67.0	33.0
London, UK ^[45]	1994-1999	54.7	45.3
East Kent, UK ^[52]	1999-2008	38.9	61.1
Lausanne, Switzerland ^[15]	1997-1998	76.0	24.0
Izmir, Turkey ^[44]	1990-2005	88.6	11.4
Mansoura Egypt ^[31]	2013-2015	61.8	38.2
Riyadh, Saudi Arabia ^[43]	2001-2002	79.1	20.9
Hyderabad, Pakistan ^[53]	2011-2012	65.0	35.0
Hyderabad, India ^[12]	1991-2001	82.1	17.9
Hyderabad, India ^[42]	2007-2010	75.1	24.9
Hyderabad, India ^[42]	2011-2014	85.5	14.5
Shanghai, China ^[54]	2005-2010	51.9	48.1
Taiwan ^[50]	1992-1996	49.1	50.9
Taiwan ^[50]	1997-2001	32.5	77.5
Taiwan ^[55]	2003-2007	46.2	53.8
Taiwan ^[55]	2008-2012	54.8	45.2
Taiwan ^[10] (paediatric cases only)	1998-2002	36.0	64.0
Taiwan ^[10] (paediatric cases only)	2008-2012	52.9	47.1
Adelaide, Australia ^[46]	1998-2003	70.1	29.9
Sydney, Australia ^[17]	2001-2003	71.3	28.7
Sydney, Australia ^[47]	2016	83.4	16.6
Christchurch, New Zealand ^[48]	1997-2001	71.6	28.4
Wellington, New Zealand ^[49]	2001-2005	82.5	17.5

However, it is clear that regardless of the local ratio of GP:GN isolates, GN bacteria are consistently more common in contact lens-related keratitis than that of any other cause^{[10],[15],[16]}. In a French investigation into the predisposing factors of bacterial keratitis, 30.5 % of contact lens-related cases were found to be caused by GN organisms

while GNs caused only 16.4 % of cases overall^[14]. Perhaps more dramatically, the study from Florida found 50 % of bacterial corneal isolates from all cases to be GN whereas 93 % of contact lens users were infected with GN organisms^[40]. In another study comparing isolates from patients with various predisposing factors, authors found that 43 % of contact lens users' infections were caused by GN species whereas only 25 % of isolates from non-contact lens users were GN^[15]. The ratio of GN to GP isolates has also been shown to increase within a population over time, approximately in line with contact lens use^{[52],[56],[57]}. In addition, *P. aeruginosa* is the most commonly isolated GN bacterium in multiple studies of infectious keratitis^{[10],[13],[15],[27],[33],[39],[40]} and is strongly correlated with both prior contact lens use and poor visual outcome^{[2],[10],[13],[16],[17],[58]}. In a four year investigation in Central Saudi Arabia, 91.4 % of isolates were GP with only 6.0 % cases caused by *P. aeruginosa*. The authors suggested this relatively low rate of *P. aeruginosa* may be due to the rarity of contact lens use in the country's dry climate^[59]. Interestingly, however, despite 29.4 % of cases being contact lens-associated, no *P. aeruginosa* was found in a New Zealand North Island study^[49], further illustrating the differences in isolates recovered worldwide. Other GN organisms such as *S. marcescens*, *K. pneumoniae*, *E. coli* and *Moraxella* species are also found in many studies, again with frequencies varying by location^{[27],[34],[39],[53],[57],[60]–[62]}.

1.2.5 Treatment strategy and limitations

Initial treatment of all microbial keratitis cases must be aggressive to give the best chances of slowing progression and limiting further damage to the eye^[20]. First line drugs are applied hourly for 5-7 days. Since less than 5 % of a dose applied to the ocular surface is retained in the cornea^[63], very frequent administration is required in order to ensure continuously high enough concentrations to rapidly reduce microbial numbers. In the absence of laboratory results, broad-spectrum empirical treatment is initiated based on the presumptive diagnosis of a bacterial, yeast or filamentary fungal infection^{[20],[39]}.

The current treatment strategy still in use in the UK is well summarised by Ong & Corbett, 2015^[1]. For bacterial keratitis, a fluoroquinolone, such as moxifloxacin 0.5 % or levofloxacin 0.5 %, is usually selected as the first line treatment. In severe cases, this is combined with a cephalosporin, for example cefuroxime 5 % or ceftazidime 5 %. Fluoroquinolones are inhibitors of DNA replication with good activity against most GN and GP aerobic bacteria^[64], however, anaerobic organisms are more susceptible to some fluoroquinolone agents (e.g. moxifloxacin) than others (e.g. levofloxacin)^{[39],[65]}. Cephalosporins are β -lactams which work by preventing cell wall peptidoglycan cross-

linking^[66]. Although cephalosporins are effective against both aerobic and anaerobic GP and GN isolates, GP isolates tend to be most sensitive to the first generation cephalosporins (e.g. cefuroxime) which have less activity against GN organisms while, conversely, GNs are more susceptible to third generation (e.g. ceftazidime) which are less active against GPs^[66]. In addition, development and spread of antimicrobial resistance varies over time and by geographical region. Therefore, the exact agent or combination used initially will be informed by the healthcare provider's current knowledge of potential ocular pathogens circulating locally and their resistance profiles. The course of infection is usually closely monitored, allowing therapy to be reviewed and modified based on clinical response as well as laboratory results once available^[67].

However, empirical treatment does not always aid resolution^[39] and use of ineffective agents can significantly extend the time taken for the cornea to heal once appropriate therapy is started^[5]. Success of empirical treatment is also limited by the inevitable development and spread of antimicrobial resistance. Resistance to the cephalosporins and fluoroquinolones commonly used in keratitis has already been repeatedly observed^{[24],[40],[67]–[69]}

1.2.6 Antimicrobial resistance

Continually increasing antimicrobial resistance poses a significant challenge to effectively managing and treating bacterial keratitis^[70]. Where there is high incidence of resistance, empirical treatment cannot be relied upon to consistently slow or halt the infection and, in resistant cases, may not provide any clinical benefit. In addition, not only is the spectrum of bacteria capable of causing keratitis and their respective innate capacities to tolerate certain antimicrobials wide, the tendency to develop and harbour resistance also varies between species and changes over time. It is therefore evermore necessary to determine the antimicrobial susceptibility profile of corneal isolates, not only to direct treatment of the individual patient but also to understand and track local resistance patterns and inform future first line treatment^{[14],[70]}.

Bacteria can be resistant to antimicrobials by intrinsic and acquired mechanisms. Intrinsic resistance describes a universal phenotypic, metabolic or genetic feature of the bacterial species which renders the organism tolerant to an antimicrobial. For example, *S. marcescens* is intrinsically resistant to polymyxin B due to the innate structure of the lipopolysaccharides (LPS) of their outer membrane^[71]. Acquired resistance occurs with genetic changes which enable the bacterium to produce a modified version of or

alternative to the antimicrobial target, different to the archetypal members of its species. These changes can either be as a result of mutations in the original gene on the chromosome or by gaining additional genes harboured on a plasmid. Plasmids are small, circular, non-essential, extra-chromosomal DNAs which often encode for multiple drug resistance genes and can be transferred between bacterial species. In addition to like-for-like substitutions for the antimicrobial target, plasmids may also enable resistance by encoding enzymes which can inactivate the antimicrobial, efflux operons which allow the bacterium to pump the antimicrobial out of the cell or alternative uptake porins which prevent the antimicrobial entering the cell. For example, β -lactamase is a plasmid-encoded enzyme which cleaves and inactivates β -lactam antimicrobials (penicillins)^[72]. Intrinsic resistance limits the spectrum of use of individual antimicrobial drugs at the time of their introduction and throughout their lifecycle. On the other hand, both chromosomally acquired and plasmid-borne resistance develops in bacterial populations in response to exposure to an antimicrobial. This resistance emerges and spreads over time, gradually decreasing the drug's usefulness.

While the development of resistance could be limited by comprehensive antimicrobial stewardship, geographical and economical differences in drug availability, commonplace international travel and, in particular, variations in clinical and agricultural use policies combine to thwart such efforts^[73]. Some studies have reported no increase in antimicrobial resistance and retention of high rates of susceptibility in bacterial keratitis isolates (comparison between 1998-2002 and 2008-2012 in Taiwan^[10], comparison between 2006-2008 and 2009-2011 in Vancouver^[34], over eleven years up to 2015 in Queensland^[6] and over 15 years up to 2013 in Central India^[13]). However, there is evidence of increasing resistance to fluoroquinolones in both GP and GN bacteria and the spread of extended-spectrum β -lactamases (ESBLs) threatens the effectiveness of cephalosporins. Table 1.3 illustrates the variety in fluoroquinolone and cephalosporin resistance levels in bacterial keratitis isolates globally over 35 years as snapshots from individual studies.

Table 1.3 - Summary of fluoroquinolone and cephalosporin resistance identified in bacterial keratitis isolates

Location	Reporting period	Organism(s)	Fluoroquinolones % resistant				Cephalosporins % resistant			
			MXF	CIP	OFX		CEF	CAZ		
San Francisco, California, USA ^[74]	1996-2015	MSSA	8.5	7.7	-		0.0	-		
		MRSA	90.5	92.0	-		-	-		
		<i>S. pneumoniae</i>	0.0	-	0.0		-	-		
		MSCoNS	33.3	16.1	0.0		0.0	-		
		MRCoNS	87.1	81.3	0.0		83.0	-		
		<i>Pseudomonas</i> sp.	3.4	1.9	-		-	-	1.9	
		<i>Serratia</i> sp	0.0	0.0	-		-	-	0.0	
		<i>Moraxella</i> sp	0.0	0.0	-		-	-	0.0	
Dallas, Texas, USA ^[75]	2000-2004	CoNS	CIP/LVX							
		<i>S. aureus</i>	33.3							
		<i>P. aeruginosa</i>	15.4				-			
Miami, Florida, USA ^[76]	1985-1987	<i>P. aeruginosa</i>	OFX	CIP	TVA					
			9.4	0.0	0.0	-				
Miami, Florida, USA ^[76]	1995-1999	<i>P. aeruginosa</i>	OFX	CIP	TVA					
			9.4	4.7	4.7	-				
Miami, Florida, USA ^[77]	1990-2001	<i>S. pneumoniae</i>	LVX	OFX	CIP					
			0.0	46.0	36.0	-				
Glasgow, UK ^[51]	1995-1998	All GN	CIP			CXM	LEX			
		All GP	0			4	61			
Glasgow, UK ^[51]	2004-2007	All GN	CIP			CXM	LEX			
		All GP	5			61	7			
Glasgow, UK ^[51]	2004-2007	All GN	CIP			CXM	LEX			
		All GP	0			63	51			
Glasgow, UK ^[51]	2004-2007	All GN	CIP			CXM	LEX			
		All GP	7			9	8			
Aba, Nigeria ^[78]	2005-2006	<i>S. aureus</i>	OFX	CIP	LEX					
		<i>S. epidermidis</i>	80	20	20					
		<i>S. pneumoniae</i>	70	80	20					
		<i>E. coli</i>	20	90	20					
		<i>K. pneumoniae</i>	80	60	50					
		<i>P. aeruginosa</i>	30	20	55					
Mansoura, Egypt ^[31]	2013-2015	<i>S. aureus</i>	CIP	OFX	GAT	MXF	CTX			
		<i>S. epidermidis</i>	23.8	19.0	4.8	28.6	19.0			
		<i>Streptococcus</i> sp.	25.0	12.5	0.0	27.5	12.5			
		<i>P. aeruginosa</i>	40.0	20.0	0.0	20.0	0.0			
		<i>K. pneumoniae</i>	16.7	25.0	25.0	16.7	33.3			
		<i>P. aeruginosa</i>	20.0	20.0	0.0	0.0	40.0			
Irbid, Jordan ^[79]	2005-2009	All GN	CIP				CEC	CFM	CEF	CTX
		All GP	22.3				55.6	74.0	68.8	55.6
Irbid, Jordan ^[79]	2005-2009	All GN	CIP				CEC	CFM	CEF	CTX
		All GP	22.0				42.2	68.9	34.3	15.7
Riyadh, Saudi Arabia ^[43]	2001-2002	<i>S. pneumoniae</i>	OFX			CFZ	CRO	CAZ		
		<i>S. aureus</i>	0.0			38.5	0.0	-		
		CoNS	0.0			33.3	-	-		
		<i>P. aeruginosa</i>	0.0			72.4	-	-		
Hyderabad, Pakistan ^[53]	2011-2012	All isolates (35 % GN)	OFX	CIP	NOR	CFZ				
			21.3	26.3	27.5	20.0				
Coimbatore, India ^[80]	2002	CoNS	CIP		OFX	CFZ	CTX			
			40.0		31.4	51.4	51.4			
Hyderabad, India ^[81]	2005-2008	All GP cocci	CIP	OFX	MXF	GAT	-			
			24.4	30.0	28.6	5.1				

Table 1.3 continued overleaf.

Table 1.3 continued - Summary of fluoroquinolone and cephalosporin resistance identified in bacterial keratitis isolates

Location	Reporting period	Organism(s)	Fluoroquinolones % resistant				Cephalosporins % resistant		
			CIP	OFX	GAT	MXF	CEF	CAZ	CFZ
Hyderabad, India ^[42]	2007-2010	<i>S. pneumoniae</i>	5.5	1.3	5.9	0.0	0.0		
		<i>S. aureus</i>	48.1	30.0	7.7	36.8	3.8		
		<i>P. aeruginosa</i>	4.1	4.0	2.0	4.7	-		
Hyderabad, India ^[42]	2011-2014	<i>S. pneumoniae</i>	3.3	0.8	2.4	1.9	0.8		
		<i>S. aureus</i>	46.1	29.4	17.4	42.0	6.8		
		<i>P. aeruginosa</i>	10.9	9.1	8.5	13.4	-		
Trichy, India ^[62]	2005-2012	<i>S. epidermidis</i>	29.6	6.2	30.4	19.5			
		<i>S. aureus</i>	23.4	2.1	26.6	17.0	-		
		<i>S. pneumoniae</i>	24.3	5.0	13.5	13.6			
		<i>P. aeruginosa</i>	17.1	7.2	7.9	23.2			
Shanghai, China ^[82]	2005-2010	All GN	0.0	9.1	18.2		FEP 9.1	CAZ 18.2	CFZ 36.4
		All GP	10.8	13.2	18.4		6.9	6.9	13.8
Taiwan ^[33]	1994-2005	All GN		CIP 1.2			CAZ 2.7	CFZ 80.0	
		All GP		-			-	15.4	
Taiwan ^[55]	2003-2012	All GN		CIP 6.3			CAZ 9.1		
Adelaide, Australia ^[46]	1998-2003	CoNS		CIP 0.0			CEF 35.0		
Queensland, Australia ^[6]	2005-2015	All GN		unspecified 1.5			1 st gen 29.5	3 rd gen 2.0	
		All GP		5.7			18.7	5.9	
Sydney, Australia ^[83]	1998-2002	<i>S. aureus</i>		CIP 16.7			CEF 0.0	CAZ -	
		CoNS		6.3			21.7	-	
		<i>P. aeruginosa</i>		0.0			-	0.0	
Sydney, Australia ^[84]	2002-2003	CoNS		CIP 10.0			CEF 0.0		
		<i>P. aeruginosa</i>		0.0			100.0		
		<i>S. aureus</i>		0.0			0.0		
Sydney, Australia ^[47]	2016	<i>S. aureus</i>		OFX/CIP 7			CEF 7		
		CoNS		9			9		
		<i>S. pneumoniae</i>		40			0		
		<i>P. aeruginosa</i>		7			-		
Brisbane, Australia ^[58]	1999-2004	CoNS		CIP 6			CEF 34	CAZ/CTX -	
		<i>S. aureus</i>		5			5	-	
		<i>S. pneumoniae</i>		0			0	-	
		<i>P. aeruginosa</i>		0			-	0	
Auckland, New Zealand ^[85]	2013-2014	All GN		CIP 0.0			CFZ 0.0	CXM 66.6	CAZ 0.0
		All GP		1.2			0.0	-	0.0

MSSA: methicillin-sensitive *S. aureus*, MRSA: methicillin-resistant *S. aureus*,

MSCoNS: methicillin-sensitive CoNS, MRCoNS: methicillin-resistant CoNS

CIP: ciprofloxacin, GAT: gatifloxacin, LVX: levofloxacin, MXF: moxifloxacin, NOR: norfloxacin,

OFX: ofloxacin, TVA: trovafloxacin; CEC: cefaclor, CEF: cefalotin (cephalothin), CFZ: cefazolin,

FEP: cefepime, CFM: cefixime, CTX: cefotaxime (cephotaxime), CAZ: ceftazidime,

CRO: ceftriaxone, CXM: cefuroxime, LEX: cephalixin

- : not reported

Fluoroquinolone resistance in *S. aureus* keratitis isolates was found to have increased from 11 % in 1990 to 28 % in 1998 in South Florida^[40], however, *P. aeruginosa* remained susceptible over the same period. In Pittsburgh, overall GP resistance to ciprofloxacin and ofloxacin increased from 19.1 to 41.1 and 15.0 to 35.7 %, respectively, from 1993 to 1997 while GN fluoroquinolone resistance remained constant at no more than 6 % throughout the study period^[56]. At around the same time, *P. aeruginosa* resistance to ciprofloxacin emerged in Hyderabad, India, increasing from 0 % in 1992 to 20 % in 1997^[69]. Later, and nearly 600 miles South in Coimbatore, *P. aeruginosa* resistance to moxifloxacin dramatically increased over two years, from 19 % in 2007 to 52 % in 2009^[86]. Elsewhere in South India, fluoroquinolone resistance in both methicillin-susceptible *S. aureus* (MSSA) and *Enterobacteriaceae* was found to rise between 2004 and 2010^[86]. Methicillin-resistant *S. aureus* (MRSA) ocular isolates with high levels of resistance to fluoroquinolones conferred by multiple mechanisms were found in Japan in 2003 and 2004^[87] and emergence of ciprofloxacin resistance was identified in Melbourne, Australia with rates increasing from 0 % in 2000 to 6.6 % in 2014^[88].

Cephalosporin resistance has also risen. *S. aureus* resistance to cefazolin was found to have increased from 23 to 40 % in North Carolina from 1997 to 2004 while *P. aeruginosa* remained susceptible to ceftazidime over the same period^[89]. GN resistance to cefuroxime dramatically increased in Glasgow from 4 % in 1995-1998 to 63 % in 2004-2007^[51]. While it was already high in Oxford, it also increased between 1999-2004 and 2004-2009 from 87.3 to 96.2 %^[90]. GN resistance to ceftazidime emerged from 2000 to 2015 in Toronto, with rates increasing to 20 %^[35]. Interestingly, decreasing GN cefuroxime resistance was identified in Manchester with overall rates changing from 51.8 % in 2004-2006 to 38.6 % in 2013-2015^[91]. However, the proportion of GN infections caused by *P. aeruginosa* (which is intrinsically resistant to cefuroxime) decreased between these periods which may explain this shift. While most studies do not identify the mechanism of resistance, ESBL production is increasingly common in resistant GN organisms and likely to be present in many clinical settings. Between 7 and 16 % of GN organisms isolated from ocular infections from Sep-2008 to Aug-2009 in Tirunelveli, South India produced at least one ESBL^[92]. Of these, 53, 44 and 2 % of *E. coli*, *K. pneumoniae* and *P. aeruginosa* isolates, respectively, were ESBL producers. At the same institute between 2011 and 2014, 17 % of all GN ocular isolates produced ESBLs, including 17, 8 and 38 % of *E. coli*, *K. pneumoniae* and *P. aeruginosa* isolates, respectively^[93]. Often due to co-localisation of other virulence factors, ESBL-producing and multi-drug resistant (MDR) GN organisms can cause particularly severe corneal disease with swifter progression, greater risk of corneal perforation and increased likelihood of surgical intervention^{[94],[95]}.

While development of antimicrobial resistance cannot be circumvented, the availability of additional treatment options may aid the preservation of current fluoroquinolone and cephalosporin activity in bacterial keratitis. Fusidic acid (FA) is an old drug which can be effective in treating Staphylococcal keratitis^[96]. More than 97 % of ocular MRSA isolates remain susceptible to FA despite resistance to other agents according to a study from 2005-2015 in Hong Kong^[97]. Furthermore, addition of corticosteroids to bacterial keratitis treatment regimens for the control of inflammation has been shown to reduce scarring^[1] and FA is known to exert moderate anti-inflammatory activity^[98].

1.3 Fusidic acid

1.3.1 Discovery and introduction

FA is a natural product and true antibiotic produced by the fungus *Fusidium coccineum*. The isolation was first reported in the early 1960's by Godfredsen *et al* of LEO Pharmaceutical Products, Denmark. The initial method of harvest required 120 h growth of the fungus at 24 °C in deep culture fermenters, the antibiotic being extracted directly from the growth medium after clarification^[99].

In its free acid form, FA is only sparingly soluble in water, however, the sodium salt, sodium fusidate (FNa) is considered soluble at concentrations up to 50 mg mL⁻¹. The structure was elucidated in 1964 and confirmed to be steroidal but with an unusual chair-boat-chair conformation^[100]. Figure 1.2 illustrates the three-dimensional structure of FA compared to cholesterol.

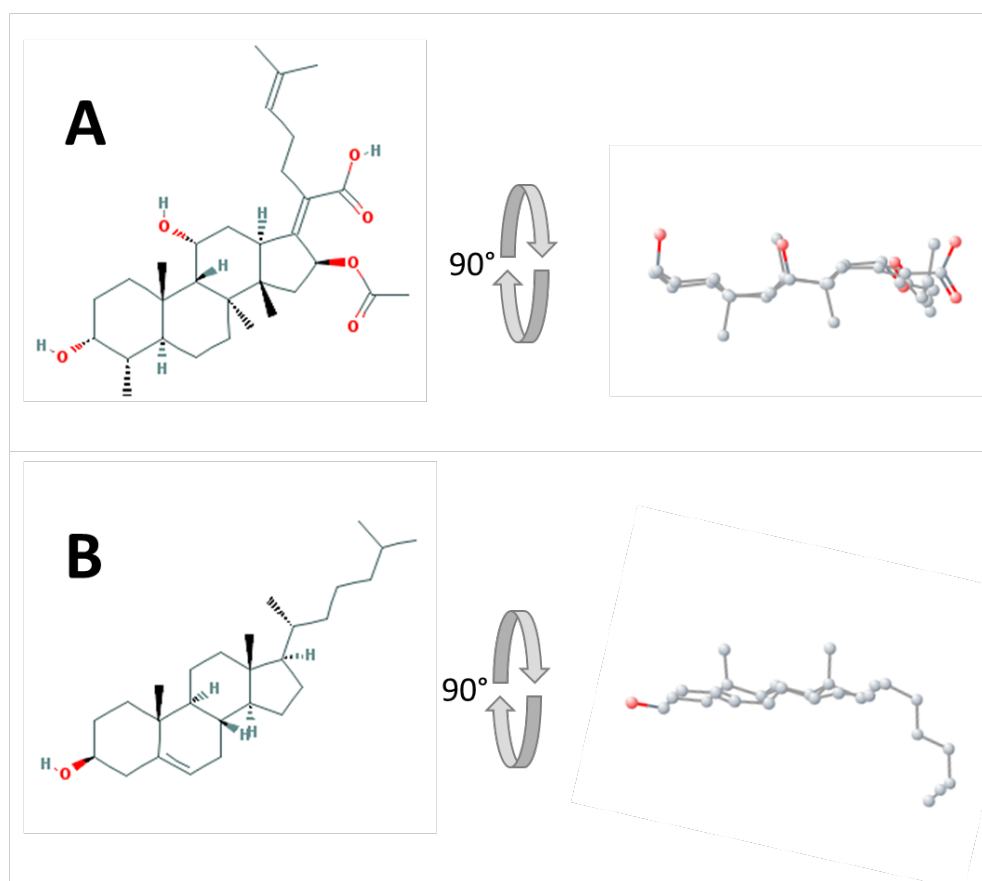


Figure 1.2 – The 2D and 3D structures of fusidic acid and cholesterol

A: fusidic acid 2D diagram and its 3D structure rotated along the steroid core axis by 90° revealing the boat-chair-boat conformation;
 B: cholesterol, a typical steroid with boat-boat-boat arrangement.

Early reports confirmed FNa to be bacteriostatic against a number of GP organisms. Strains of *S. aureus* exhibited the most consistent susceptibility and required lower concentrations to be inhibited than other GP species, with MICs in the range of 0.03 to 0.5 $\mu\text{g mL}^{-1}$ and the majority being 0.25 $\mu\text{g mL}^{-1}$ or less^{[101],[102]}. Bactericidal activity was also found against *S. aureus* with 0.5 $\mu\text{g mL}^{-1}$ killing 90 % of cells after 15 h^[101] and, where variation in minimum bactericidal concentration (MBC) was found, it fell within a range of 2 to 4 times that of the MIC^[102]. The first investigation into clinical isolates in 1962 found only 4 of 200 penicillin resistant strains of *S. aureus* were also resistant to inhibition of growth by up to 1 $\mu\text{g mL}^{-1}$ FNa^[103]. FNa was also tested and shown to be active against *Corynebacterium diphtheriae* (the causative agent of diphtheria) and *Clostridium tetani* (tetanus)^[99].

The initial *in vivo* investigations of FNa indicated an LD₅₀ of 0.2 g kg⁻¹ in mice and the drug proved to be well tolerated in rats inducing no pathological changes after oral administration of 0.4 g kg⁻¹ for 6 months^[99]. Soon afterwards, testing in human volunteers confirmed FNa to be antimicrobially active in the serum after administration of 20 mg kg⁻¹

orally every 6 h, despite significant albumin and γ -globulin binding^[103]. Trials in patients began almost immediately, and the developmental timeline was as follows:

1962 In a controlled clinical trial in *S. aureus* burn infections, a higher proportion of wounds were cleared of infection by FNa (17/18) than with the methicillin comparator (10/15) or no-treatment control (1/18). However, post-treatment, resistant isolates were obtained from half the patients who received FNa, and these were also found as either colonisers or causes of infection in other patients on the same ward^[104]. Conversely, in a case series from the same time, FNa was shown to be effective as monotherapy in the treatment of *S. aureus* gastroenteritis, upper respiratory tract infection, pneumonia and chronic osteomyelitis, with only one osteomyelitis isolate developing resistance to FA^[103].

When used topically to clear intranasal *S. aureus* carriage, FNa out-performed the standard chlorhexidine treatment (68/77 patients), but strains isolated after re-establishment of carriage showed resistance to FA^[103].

A single case report of particular interest was the successful treatment of septicaemia caused by *Staphylococcus pyogenes*. The patient's infection had been largely unresponsive to a range of antimicrobials given both alone and in combination over the course of more than 4 months but was cleared by FNa^[105].

1963 In a case series of 8 patients with extensive post-operative wound infections and osteomyelitis, FNa treatment combined with penicillin resulted in complete healing and sterilisation of the lesion site within 12 days in 5 cases^[102]. Furthermore, favourable outcome was obtained for all but one patient and no induction of resistance was detected. Rapidity of healing was such the authors suggested FA may have a direct role in accelerating healing, independent of the antimicrobial activity. In another study, 5 days of oral FNa given to nurses with skin and soft tissue infections caused by *S. aureus* resistant to penicillin, streptomycin, tetracyclines and sulphonamides was very well tolerated^[106]. Treatment resulted in cure in 13 of 16 cases, the final three recovering after an additional course required due to severity or complications.

1967 FA was found to be well tolerated and effective in the treatment of children with a range of staphylococcal infections at 30 mg kg⁻¹ ^[107].

1971 Oral FA 250 mg once daily in patients with chronic psoriasis (6 months to 5 years) was associated with definitive improvement in 12 out of 13^[108]. However, the

author noted the possible influence of the placebo effect due to the role of emotional factors in psoriasis.

- 1984 Oral FNa was shown to be non-inferior to the standard alternatives vancomycin and metronidazole in the treatment of *Clostridium difficile* antibiotic-associated colitis^[109].
- 1987 FA 1 % viscous eye drops were shown to be safe and effective for the treatment of external eye infections in two clinical trials, with success rates of 85 and 93 %^{[110],[111]}. Both trials also reported lower rates of resistance to FA than to the comparator(s) in the causative strains, possibly the reason for increased cure.
- 1989 In the first trial of FA in staphylococcal keratitis, 1 % suspension was found to be safe and effective, with open-label administration resulting in evidence of healing within 21 days for 85 % of patients^[96].
- 1990 A Belgian study of *S. aureus* blood isolate susceptibility found 11.3 % to be resistant to oxacillin *in vitro*. However, for all but two isolates, the MBC of FA was 1 to 2 mg L⁻¹ which is well within the maintainable blood concentration during administration, indicating FNa to be of potential use in MRSA bacteraemia^[112].
- 1994 First trial of FNa in the treatment of lepromatous leprosy was conducted. Dosing regimens of either 500 mg per day for 8 weeks or 750 mg per day for 4 weeks followed by 4 weeks 500 mg per day both showed slow but clinically relevant improvement during the course of the study. However, no cure was seen during the eight week treatment period^[113].
- 2004 In a double-blind randomised controlled trial for the treatment of initial episodes of *C. difficile*-associated diarrhoea, FA was found to be an adequate alternative to metronidazole with no significant differences in reduction of toxin or clearance of bacterial load^[114].
- 2005 FA viscous eye drops were approved for supply by optometrists in the UK^[115].
- 2010 FA was assessed *in vitro* for potential use in the treatment of common sexually transmitted bacterial infections where resistance to standard antimicrobials is rising. Of 35 *Neisseria gonorrhoeae* and ten *Chlamydia trachomatis* isolates tested all were sensitive to FA with MICs $\leq 2 \mu\text{g mL}^{-1}$ ^[116].
- 2011 First reports from FA pharmacokinetic and clinical trials of a revised oral dosing regimen were published in preparation for licensing in the USA. The phase I trial confirmed the inclusion of a loading dose designed to optimise

pharmacodynamics was well tolerated and achieved the desired stable plasma concentrations^[117].

Subsequent clinical trial of the loading-dose initiated regimen in patients with acute bacterial skin and skin structure infections proved comparable to linezolid, the standard of care treatment^[118]. The modified dosing regimen was 1500 mg twice per day on day 1, followed by 600 mg twice per day for 10 to 14 days.

2015 With significant rise in frequency in incidence of MDR *Acinetobacter baumannii* infection, synergy between colistin and FA was investigated *in vitro* as a potential treatment^[119]. FA not only prevented the emergence of colistin resistance, which was readily selected for with colistin alone, but synergy between 1 mg mL⁻¹ FA and 0.06 mg mL⁻¹ colistin was identified on checkerboard testing.

Use of topical FA in the care of clean dermatologic procedures was retrospectively studied in comparison to petrolatum^[120]. No significant differences were found in either the outcome or patient satisfaction between the two methods, indicating prophylactic topical FA is no more beneficial than non-antimicrobial wound care in such cases and therefore not recommended for use.

2016 A randomised trial of combined oral FA and rifampicin uncovered a previously undetected interaction^[121]. FA plasma concentrations were significantly lowered in the presence of rifampicin and declined over time as treatment continued. The effect was thought to be due to rifampicin induction of cytochrome P450 3A4 which increased metabolism and clearance of FA.

2018 Oral FA was successfully used to clear MRSA from cystic fibrosis patients as part of a combined multi-drug and hygiene eradication protocol^[122].

Knowledge regarding FA has been built slowly since its introduction, and in a manner quite different to methods used to satisfy modern standardised regulatory requirements. However, the accumulated data and experience has shown it to be a valuable drug, particularly in combination with other antibiotics for the treatment of serious MRSA infections^[123]. In addition, information is being rapidly expanded by recent investigations and ongoing clinical trials to license FA in the USA.^{[124]–[126]}

1.3.2 Current clinical use

In the UK, both FA and FNa are available in a range of formulations in line with its various applications in staphylococcal infections. LEO Pharma, Berkshire, UK, are still the primary manufacturer of FA and FNa preparations in the UK. However, as the drug is off-patent, a number of generic versions are also available. Bacterial conjunctivitis, most commonly caused by *S. aureus*, is treated with 1 % viscous eye drops (Figure 1.3A). Skin infections, including impetigo, erythrasma, contact dermatitis and infected cuts caused by susceptible *S. aureus* can respond to 2 % cream or ointment (Figure 1.3B and C). For more serious skin infection, topical use is often administered in combination with systemic therapy. Oral FA is formulated as either 50 mg mL⁻¹ suspension or 250 mg tablets (Figure 1.3D and Figure 1.3E). Oral administration is indicated in osteomyelitis, pneumonia, septicaemia and wound infections involving susceptible strains of *S. aureus*, including MRSA. Intravenous formulation is also available for use if oral therapy is inappropriate, such as in patients with reduced gastrointestinal absorption or lacking ability to swallow (Figure 1.3F).

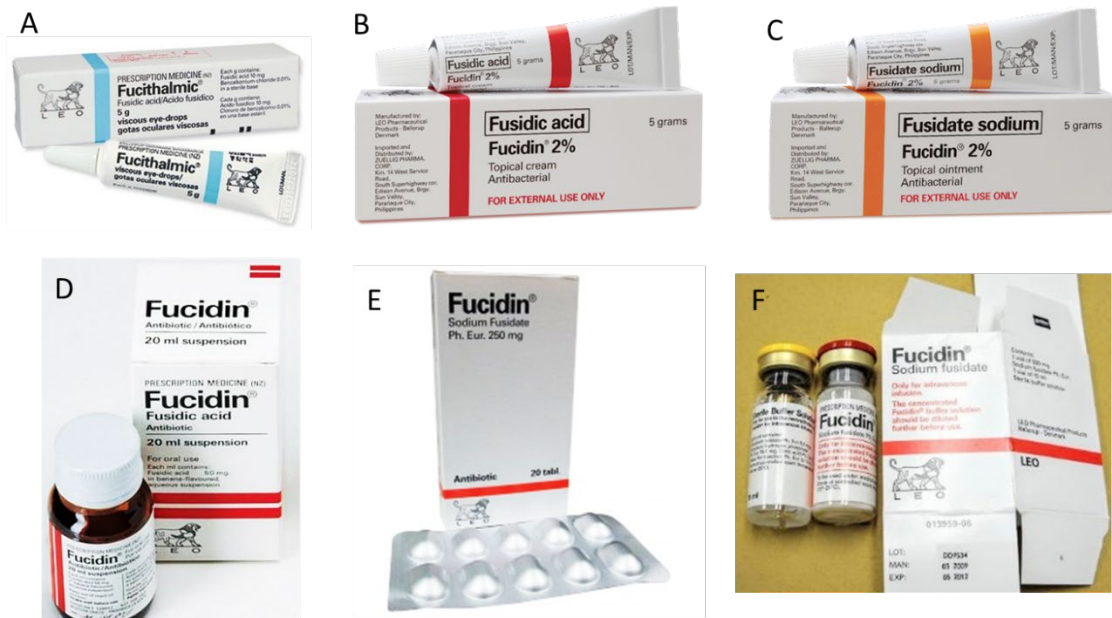


Figure 1.3 - Formulations of fusidic acid and sodium fusidate produced by LEO Pharma

A: Fucithalmic, 1 % fusidic acid viscous eyedrops. B: Fucidin cream, 2 % fusidic acid.

C: Fucidin ointment, 2 % sodium fusidate. D: Fucidin oral suspension, 50 mg mL⁻¹ fusidic acid.

E: Fucidin tablets, 250 mg sodium fusidate. F: Fucidin for intravenous injection, 50 mg mL⁻¹ sodium fusidate when mixed with 10 mL buffer solution.

1.3.3 Mechanism of action

FA is a protein synthesis inhibitor, exerting its effect by halting the progression of peptide elongation at the tRNA translocation step. After initiation, the normal process of protein synthesis proceeds as elongation factor Tu (EF-Tu), complexed with GTP, activates a tRNA carrying the amino acid to be next joined to the growing peptide chain (Figure 1.4, box 1). The EF-Tu consumes GTP to assist with the docking of the aminoacyl-tRNA into the acceptor site (A site) of the ribosome and alignment of the tRNA anti-codon to the mRNA (Figure 1.4, box 2). A transpeptidation reaction between the newly arrived amino acid and C-terminal end of the developing peptide is catalysed by peptidyl transferase within the ribosome, transferring the growing chain onto the A site tRNA (Figure 1.4, box 3)^[127]. Once transpeptidation has occurred, translocation begins with the tRNA in the A site shifting within the 50S subunit towards the peptidyl (P) site while the now deacylated tRNA in the P site shifts towards the exit (E) site (Figure 1.4, box 4)^{[128],[129]}. This produces a substantial rotation of the 50S relative to the 30S subunit^{[130],[131]}. Elongation factor G (EF-G), activated by another GTP, then catalyses a conformational change in the 30S subunit, allowing the mRNA to move through the ribosome and the associated tRNAs and peptide chain to complete their shift to their destination sites (Figure 1.4, box 5)^{[132],[133]}. This process consumes the GTP complexed to EF-G, dissociating GDP from the elongation factor and allowing EF-G to dissociate from the ribosome^[134]. The deacylated-tRNA at the E site is simultaneously released (Figure 1.4, box 6a)^{[135],[136]}.

FA interrupts protein synthesis by interfering with the translocation step by binding EF-G at the point of the EF-G•GTP complex docking onto the ribosome and inducing the conformational change (Figure 1.4, box 6b). GTP is consumed but FA stabilises the EF-G•GTP•ribosome complex, preventing the dissociation of GDP and consequently locking EF-G in place. This ultimately means the ribosome remains in the distorted translocation conformation, preventing a new aminoacyl-tRNA from docking into the A site to continue adding to the growing peptide (Figure 1.4, box 7)^{[132],[137]–[139]}.

As the interference of FA halts protein synthesis, its classification is bacteriostatic. The agent does not outright kill the bacterium and, if the FA concentration is reduced or the drug removed after initial exposure, bacterial cells can recover. However, after 8-15 h in the presence of FA, a high proportion of susceptible *S. aureus* will die due to lack of ability to produce new proteins in order to continue to maintain their cellular structures and functions^{[101],[103],[140]}.

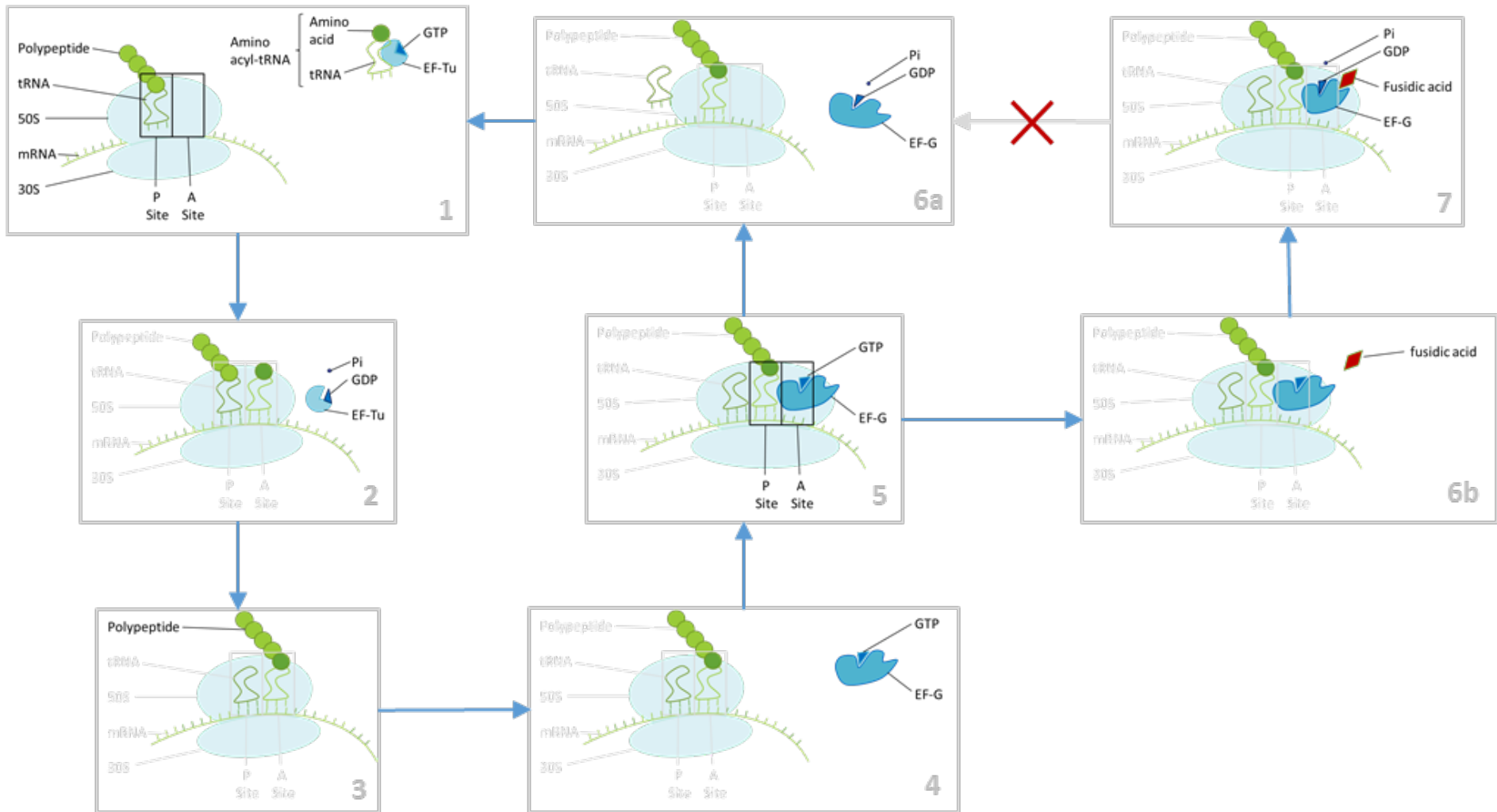


Figure 1.4 - Schematic of prokaryote protein synthesis and mechanism of fusidic acid inhibition

The normal process of protein synthesis cycles through steps 1 to 6a. However, fusidic acid is able to halt protein synthesis by binding to elongation factor G (EF-G) while it is on the ribosome, preventing dissociation.

1.3.4 Limitations in bacterial keratitis

As a clinically significant proportion of bacterial keratitis cases in the UK and worldwide are caused by GN bacteria, empirical treatment must be effective against a wide spectrum of organisms. FA alone is not clinically effective against GN infections and, therefore, is generally not used in the emergency treatment of keratitis. However, lack of efficacy is not due to a lack of the EF-G target. In fact, many investigations into FA mechanism of action have been carried out using the protein synthesis machinery isolated from the model GN organism *E. coli*^{[127],[128],[130],[133],[136]–[139]}. Intrinsic GN resistance occurs because, while FA can readily cross the single phospholipid membrane of GP bacteria, the LPS-containing outer membrane (OM) of GN organisms poses a considerably greater barrier to large and lipophilic drugs^{[141],[142]}. At the same time, GNs possess highly effective multi-drug efflux pumps which contribute to their extensive antimicrobial resistance by exporting any toxic molecules that do manage to enter the cell^{[141]–[145]}.

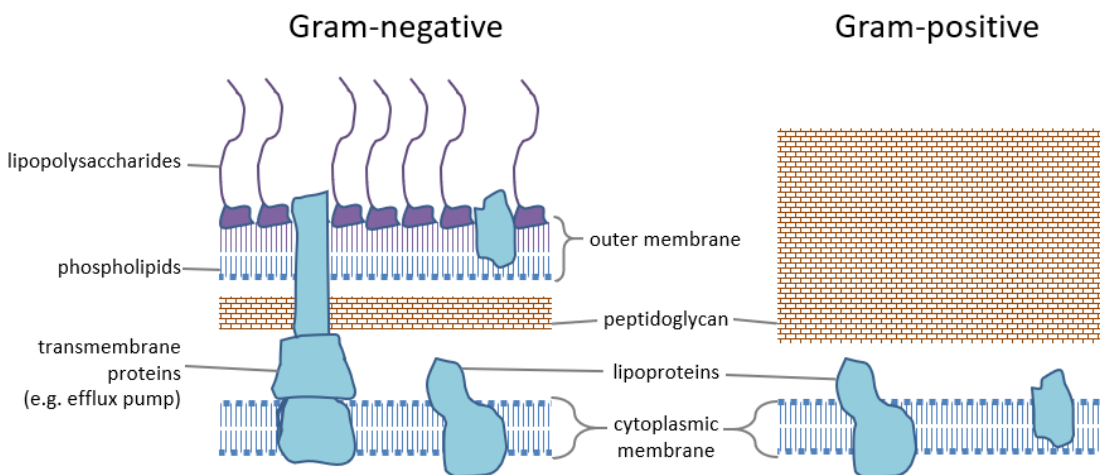


Figure 1.5 - Structure of the cell envelope in Gram-negative and Gram-positive bacteria

Gram-negative organisms have a phospholipid inner cytoplasmic membrane, 7-8 nm layer of peptidoglycan and an outer membrane composed of a phospholipid inner leaflet and lipopolysaccharide-containing outer leaflet. Gram-positive organisms also exhibit a phospholipid cytoplasmic membrane but have no outer membrane and a much thicker 20-80 nm peptidoglycan cell wall. Illustration not to scale.

Figure 1.5 illustrates the comparative structures of the GN and GP cell envelope. As peptidoglycan is a porous lattice-like structure, the only barrier to the cell interior in GP organisms is the single phospholipid cytoplasmic membrane. Lipophilic compounds and the lipophilic portion of amphiphilic compounds readily associate with phospholipid membranes such as those encasing the bacterial cytoplasm^[146]. This allows lipophilic and amphiphilic drugs to passively diffuse through to the internal surface of the

membrane and consequently access their intracellular targets. However, by comparison, cross-linking between the core regions of long LPS molecules and the consequent reduction in membrane fluidity substantially limits diffusion of lipophilic molecules through the asymmetrical GN OM^{[144],[147]}. For example, the rate of steroid probe diffusion through the OM is only 1/100th of that through a standard phospholipid bilayer^[148]. Therefore, to gain access to the GN cell interior, a drug molecule must first pass through the OM either *via* specific porin channels if hydrophilic^[149] or by very slow diffusion if hydrophobic^[147], then traverse the periplasmic space and finally make it through the cytoplasmic membrane.

To further protect themselves, GN bacteria also employ efflux pumps to remove any harmful agents that manage to reach the periplasm or cytosol before they can accumulate and cause damage. In *E. coli*, periplasmic FA is expelled by the resistance nodulation division (RND) superfamily efflux pump, AcrAB-TolC^{[150],[151]}. This multi-drug efflux pump is composed of six AcrA, three AcrB and three TolC proteins which together span both membranes and the periplasm^{[151]–[154]} (Figure 1.6A). The TolC trimer forms an outer membrane protein (OMP) with an internal channel leading to the extracellular space. Three AcrBs form an inner membrane proton antiporter which protrudes into the periplasm and is responsible for recognition and movement of the efflux pump substrates. The hexamer of AcrA forms a funnel-like periplasmic membrane fusion protein between AcrB and TolC. On contact with a recognised substrate, the structure of a pore in AcrB changes from a resting loose “L” shape (Figure 1.6B) to the tight “T” state by employing H⁺ influx energy (Figure 1.6C). This structural shift scoops the toxic agent into the AcrB transport pore which subsequently cycles to an open “O” state. Through this series of dramatic conformational changes, the offending molecule is shunted through and out of AcrB and into the AcrA funnel. At the same time, the T and O conformations in AcrB modify the shape of AcrA which, in turn, pulls the TolC channel open like an iris, allowing the drug to pass directly into the extracellular space (Figure 1.6C). Once the substrate is expelled the efflux pump returns to the resting confirmation (Figure 1.6B)^[153]. An additional subunit, AcrZ, is frequently found in association with the intracellular face of AcrB and its presence, while non-essential to efflux pump function, increases the spectrum of transported substrates^[155].

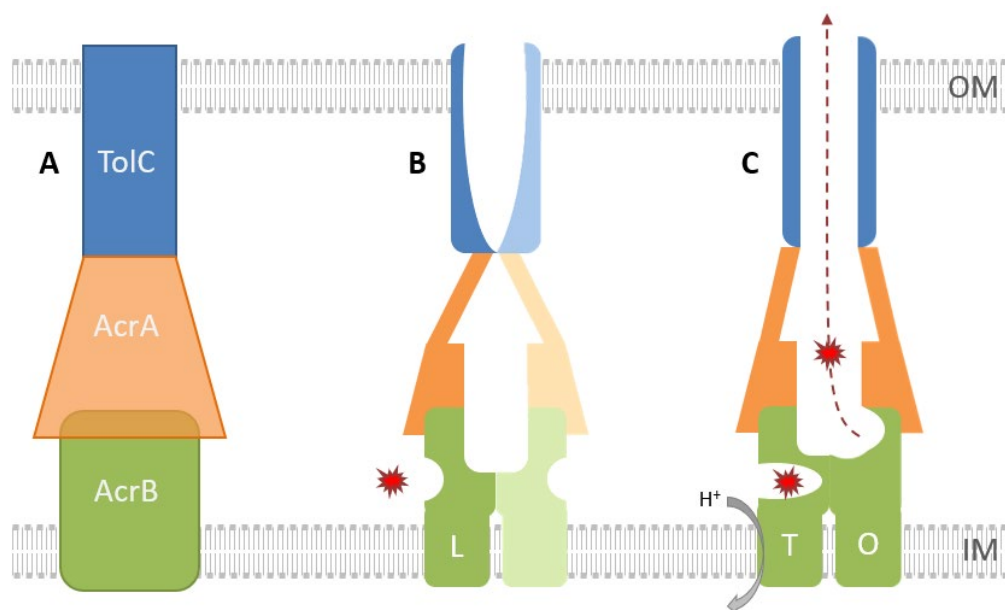


Figure 1.6 - Schematic representation of the superstructure and transportation mechanism of the *E. coli* AcrAB-TolC efflux pump, based on images in Wang *et al*, 2017^[153]

A: The tripartite AcrAB-TolC structure composed of the TolC outer membrane protein, AcrB inner membrane antiporter and AcrA periplasmic membrane fusion protein.

B: Closed, resting conformation of AcrAB-TolC with the AcrB pore in the L position.

C: Active transport by AcrAB-TolC. The AcrB pore receives the substrate as it changes to the T conformation under proton motive force. This structural shift induces conformational change in AcrA which pulls the TolC channel open. AcrB then cycles into the O confirmation, expelling the substrate through the AcrA-TolC channel and out of the cell.

Other than FA, *E. coli* AcrAB-TolC, is known to be responsible for the efflux of many toxic and harmful substances. Substrates include a wide range of antimicrobials such as β -lactams, macrolides and rifampicin as well as tetracyclines and chloramphenicol when complexed with AcrZ^{[142],[155]–[157]}. In addition, AcrAB-TolC also effluxes detergents, cationic dyes, bile salts, fatty acids and solvents^{[142],[157]–[159]}. While the proteins specifically isolated from *E. coli* have been heavily studied, identical AcrAB-TolC is also produced by other *Enterobacteriaceae* such as *K. pneumoniae* and *Salmonella* spp^[142]. Homologous RND family efflux pumps are likewise found throughout GN bacteria, for example: MexAB-OprM and AdelJK are responsible for expulsion of FA in *P. aeruginosa*^[143] and *A. baumannii*, respectively^[160].

Despite these intrinsic phenotypic resistance mechanisms, FA is an attractive option for potential reformulation in order to extend antimicrobial spectrum for three key reasons: 1) EF-G is a ubiquitous target in GP and GN bacterial causes of keratitis^[161]; 2) although genetic FA resistance can develop, rates in *S. aureus* appear to remain relatively stable during topical and ocular use^{[91],[162]}; and, 3) UK optometrists are already licensed to prescribe FA for acute conjunctivitis^{[115],[163]}. Co-formulation with an appropriate agent to overcome intrinsic FA resistance in GN organisms could provide a more effective

empirical option for keratitis, enabling a wide range of healthcare professionals to provide rapid and efficient treatment. Using an antimicrobial with a well-established safety profile can also minimise the need for extensive pre-clinical studies, clinical trials and *de novo* licensing.

1.4 Antimicrobial development, drug repurposing and co-formulation

1.4.1 Standard drug development

Novel drugs take 10-17 years to make it from initial discovery in the laboratory to an approved medication available for use^[164], currently at the cost of approximately \$489 million (not including post regulatory Phase IV observational studies or marketing costs)^{[165],[166]}. In addition, the rate of failure of drug development projects at each stage is such that less than one new medication is successfully brought to market for every 40 projects initiated^[167] (Figure 1.7).

After identification of a therapeutic concept, the standard drug development process begins by investigating potential drug targets. Approximately 60 % of initiated drug discovery projects successfully find an appropriate target. Large libraries of 100,000 or more compounds are screened for interaction with the target, usually utilising *in silico* modelling. This process takes 6 to 12 months and results in a substantially smaller library of around 100 to 1,000 compounds that may be suitable drug candidates. The next step is lead optimisation during which the selected compounds are tested for their *in vitro* interactions and efficacy at the target. In most cases, promising candidates go through multiple rounds of chemical modification in order to hone their specificity and activity. Seventy-five per cent of drug discovery projects which begin lead optimisation successfully produce about 3 optimised molecules for use in pre-clinical testing. However, 60 % of projects fail during pre-clinical testing, which is the first time the drug is investigated *in vivo*. Issues that derail the development process at this stage include lack of distribution to the target tissue (unsatisfactory pharmacodynamics), poor pharmacokinetic profile resulting in rapid elimination, or toxicity due to drug interactions with tissues, cells or receptors other than the intended target.

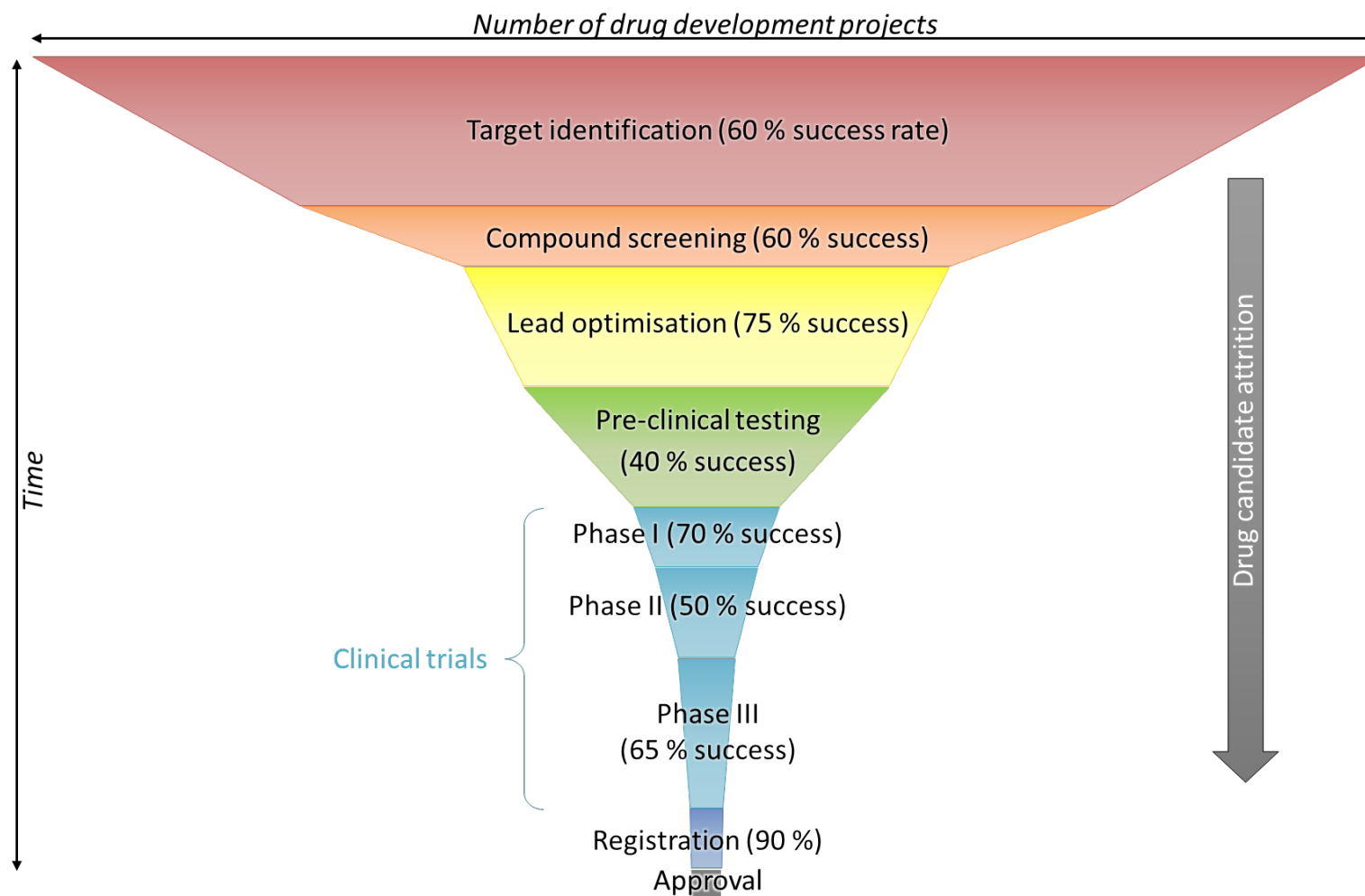


Figure 1.7 - Illustration of the classical drug development pipeline from target identification to regulatory approval, constructed based on data from Rang, 2006^[167]

The width of each trapezoid at the bottom compared to the top represents the proportion of projects estimated to successfully complete that step. Height of the trapezoid is proportionate to mean duration to complete the step. Less than one of every 40 drug development projects successfully brings a medication to market.

The largest expense in the drug development process are clinical trials. Clinical trials are stratified into four main phases, each involving greater numbers of subjects and closer to real-world situations than the last. Phase I trials are carried out in a small number of carefully selected healthy volunteers. First in man testing is performed to confirm the safety of the drug and formulation. This consists of an initial single small dose, followed by repeat dosing of incrementally larger amounts if results continue to be favourable. Pharmacodynamic and pharmacokinetic investigations are also performed during Phase I in order to inform development of suitable dosing regimens.

The primary aim of Phase II trials is to confirm efficacy of the new drug in a select group of patients suffering from the target disease. These tests are generally carried out in a larger number of subjects and over a longer duration than Phase I, depending on the indication. Only 50 % of Phase II trials successfully confirm efficacy and tolerability of investigative new drugs in patients. However, if the outcome is positive, Phase III trials can be initiated. These studies recruit large numbers of patients with less strict inclusion criteria, resulting in a sample population which much more closely resembles the target population. Phase III trials are often double-blinded, where neither the patient nor the healthcare professional know whether the novel drug or a comparator (or sometimes a placebo) is being administered. Approximately 65 % of Phase III clinical trials yield results that sufficiently support the efficacy and safety of the tested agent. The new drug must be shown to meet strict criteria in order to be granted regulatory approval for marketing and use by the geographically appropriate body (e.g. the MHRA in the UK or the FDA in the USA)^{[166],[168]}. Finally, Phase IV post-marketing observational studies are carried out in order to monitor safety in the wider population and inform regime modifications or potential contra-indications in sub-populations not included in the earlier phases. While these regulatory requirements do greatly contribute to the overall quality of available medications, complex application processes, differences between requirements in different countries, changes in regulatory rules and long approval times all extend the duration from novel drug discovery to clinical use^[169].

1.4.2 The failing antimicrobial pipeline

While this pipeline is very similar for drug development regardless of the therapeutic area, the long and expensive process is particularly detrimental in antimicrobial development. In the early days of antibiotics, lack of extensive regulatory control and approval allowed rapid development and introduction of novel agents^{[170],[171]}. Alexander Fleming initially reported the discovery of penicillin in 1929^[172], but it was introduced into

clinical use within 3 years of successful purification and demonstration of its activity *in vivo* by Chain *et al*^[173]. Other antimicrobials were developed and put into use during the early years of penicillin, including streptomycin, chloramphenicol and doxycycline all before 1950^[174]. In the United States, the infection-related death rate between 1937 and 1953 dropped by 8.2% per year^[175] – a nearly 3-fold decrease over 15 years. This gave rise to the golden age of antibiotics, where introduction of novel agents kept pace with and even surpassed the development of resistance. However, resistance was acknowledged as a potential problem soon after penicillin's discovery^{[176]–[178]} and Fleming was famously quoted in the *New York Times* on 26-Jun-1945, observing the dangers of poor antimicrobial stewardship:

“The greatest possibility of evil in self-medication is the use of too small doses so that instead of clearing up infection, the microbes are educated to resist penicillin and a host of penicillin-fast organisms is bred out which can be passed to other individuals and from them to others until they reach someone who gets a septicaemia or a pneumonia which penicillin cannot save.”

Now, 80 years after the discovery of penicillin, the widespread and often inappropriate use of antimicrobials in humans, companion animals and agriculture has produced increasingly resistant bacterial strains worldwide^{[174],[179],[180]}. There are already many examples of extremely resistant pathogens. These include, but are by no means limited to, carbapenemase-producing *Enterobacteriaceae*^[181], MDR hospital-acquired *A. baumannii*^[182], and *Mycobacterium tuberculosis* resistant to all available antibiotics^[183]. The rate of increase in antimicrobial resistance is such that it has been declared a global health emergency and new drugs or treatment strategies are desperately needed^[184]. However, while resistance is the primary driver of this need, it also severely reduces the attractiveness of antimicrobial development as a pharmaceutical company investment.

Exactly when and how resistance to a particular antimicrobial will occur cannot yet be adequately predicted^{[185],[186]}. Figure 1.8 illustrates the variety in time elapsed between discovery and identification of clinical resistance for a selection of antimicrobials, which ranges from 5 to 60 years^[187]. *In vitro* studies have been used to assess induction of resistance in an effort to predict the likely timeframes and mechanisms involved but fail to mimic occurrence of resistance *in vivo* or in clinical situations^[188]. This is because the complex combinations of selective pressures bacteria experience in real life – transferring from host to environment to carrier and to host – are quite different and highly variable compared to the carefully controlled laboratory environment^[185]. Large and

complex computational models are currently required in order to address this issue^[186]. Until then, unlike drugs for chronic medical conditions, antimicrobials do not have an indefinite, or even defined, usable life and are highly likely to become obsolete^[189]. In addition, novel antimicrobials are often reserved as treatments of last resort in order to limit development of resistance and are only administered for short periods at a time, which both reduce sales^[189].

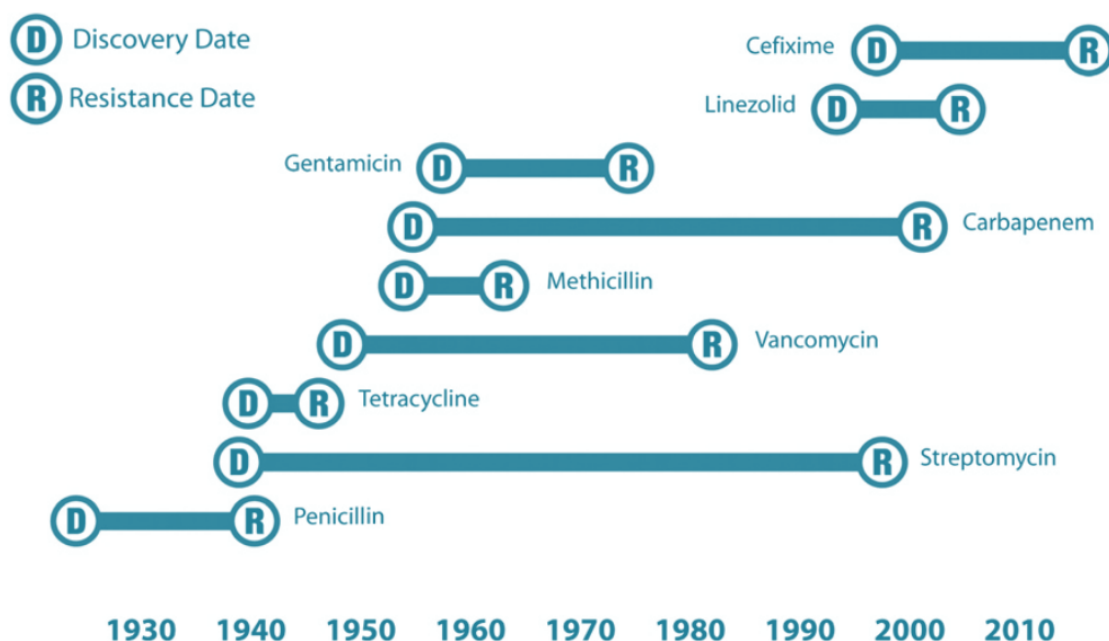


Figure 1.8 –Duration between antimicrobial discovery and development of clinical resistance (from Brooks & Brooks, 2014^[187])

The useable lifetime of antimicrobial agents varies considerably with between 5 and 60 years passing between their discovery and the development of resistance.

All these factors combine to make the development of novel antimicrobials unattractive to pharmaceutical companies as the investment to bring such a drug to market far outweighs the potential return^{[190],[191]}. The pharmaceutical industry has consequently largely abandoned the antimicrobial market since the 1990s and this has resulted in an almost empty pipeline^[192]. Figure 1.9 shows the decline in antimicrobial approvals in the USA from 1980 to 2014. The FDA has approved six new antimicrobial drugs since 2015, however, all are additions to current classes, including two cephalosporins and two glycopeptides^[192]. The USA and many European countries have recently introduced market entry reward schemes which employ monetary incentives to stimulate pharmaceutical development of antimicrobial drugs^{[191],[193],[194]}. However, due partly to the limited value of funding available, there is concern that the structure of these schemes may result in support being awarded for drugs reliant on only a small number

of mechanisms of action, leaving the market still vulnerable to the spread of unpredictable novel resistance mechanisms^[195].

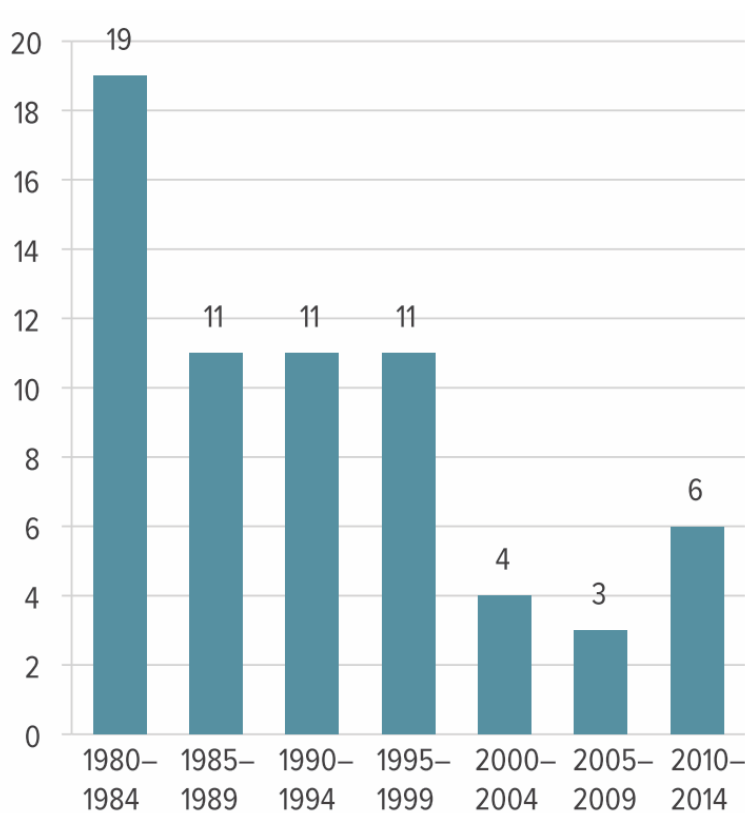


Figure 1.9 - Number of new systemic antibiotics approved by the FDA during each 5 year period since 1980 (from Ventola, 2015^[169])

The number of new antibiotics developed and approved has decreased steadily over the past three decades (although four new drugs were approved in 2014), leaving fewer options to treat resistant bacteria.

To help refill the empty pipeline and negate a large proportion of the development time and monetary investment, the repurposing of existing drugs is being taken up as an alternative route of antimicrobial discovery^{[196]-[199]}. The principle is to discover or recover activity of already licensed or well characterised agents. This circumvents the often lengthy lead identification and optimisation processes and reduces the need for, or number of, costly pre-clinical toxicology and early Phase I studies. In addition, previously established safety data can aid the development and licensing processes. Repurposing of an existing agent can consequently take as little as 4 years (Figure 1.10). Reviving and reinstating old antimicrobials in this way is, therefore, a viable option to help fill the current gap in the novel antimicrobial drug pipeline^{[200],[201]}.

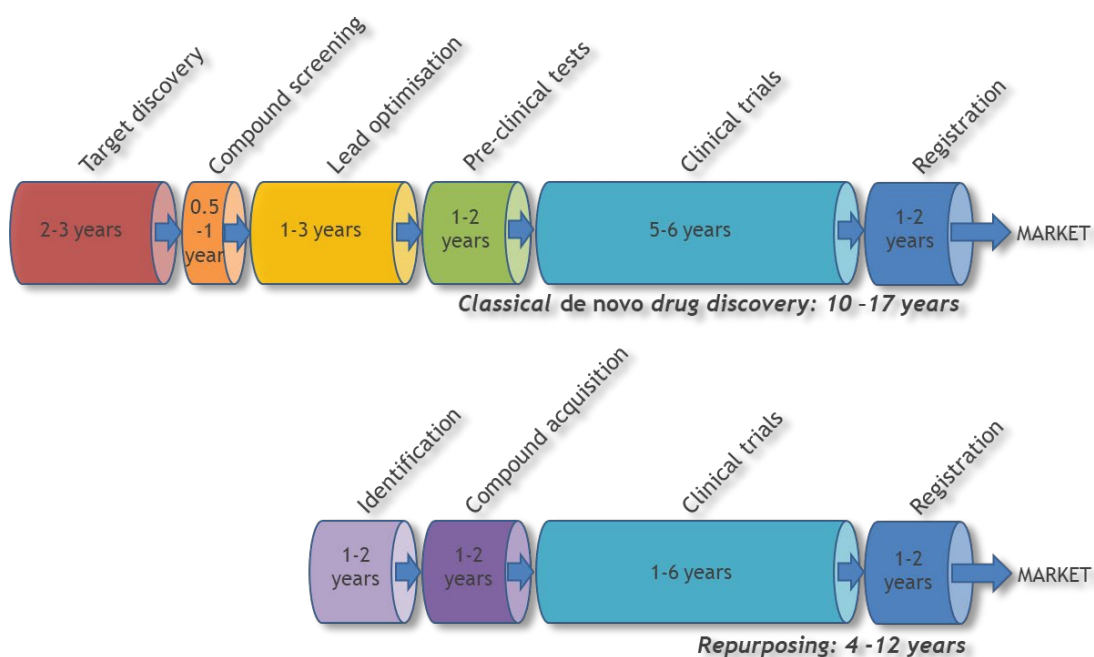


Figure 1.10 – Comparison of *de novo* drug discovery timeline to that for drug repurposing (based on Ashburn & Thor, 2004^[164])

After identification of a therapeutic concept, *de novo* drug discovery takes 10-17 years, up to 9 years of which is dedicated to identifying the potential drug target, screening or designing molecules, optimisation to create a lead drug candidate and *in vivo* pre-clinical investigations. In contrast, drug repurposing begins by identifying a novel property of an existing therapeutic followed by legally acquiring the compound, which usually take up to 4 years combined. Agents discovered by either route are subsequently assessed through clinical trials before being registered for regulatory approval. However, depending on the similarity between the original and novel application and the quality of data previously generated, repurposed drugs may require relatively short clinical investigations to confirm efficacy in the new indication.

1.4.3 Co-formulation to extend antimicrobial spectrum

Co-administration – the administration of more than one antimicrobial drug concomitantly – has long been used to increase efficacy. Co-formulation can be used to combine fixed dosages of two or more antimicrobials in one preparation for easier co-administration. Combining antimicrobial agents can have multiple advantages over monotherapy. When combined, antimicrobial drugs can be more efficacious while used at standard dosages, thereby reducing chances of toxicity compared to using high-dose monotherapy to enhance efficacy; co-administration yields greater treatment success rates than monotherapy against infections clinically resistant to either of the individual agents; and, in particular, synergistic drug pairs can reduce the induction of resistance^{[187],[202]–[204]}. However, co-administration of two or more antimicrobial drugs is not the only method to enhance activity. Adjuvants – often agents without antimicrobial activity in their own right – can be combined with antimicrobials in order to recover, extend or enhance activity of

the drug. There are three principal types of antimicrobial adjuvants: 1) an adjuvant that prevents the degradation or modification of the antimicrobial, 2) an adjuvant that increases intracellular entry or retention of the antimicrobial, or 3) an adjuvant that inhibits repair or alternative pathways which would allow tolerance to the antimicrobial^[202].

1.4.3.1 Synergy or potentiation between antimicrobial agents

Trimethoprim and sulphamethoxazole was first established as an excellent synergistic combination for the treatment of *N. gonorrhoeae* infection (gonorrhoea) in 1967^[205] and an effective option for hospital-acquired urinary tract infection in 1969^[206]. The synergistic activity of trimethoprim and sulphonamide antimicrobials had previously been documented *in vitro*^[207]. These agents are specific to two sequential enzymes in the bacterial folic acid biosynthesis pathway, a pathway which is essential to DNA replication and therefore growth. While each drug can be effective against a range of organisms when administered alone, the combination overcomes resistance to a single agent already present and induces significantly less additional resistance compared to single-agent exposure. This combination has since been produced as a single formulation and continues to be successfully used in the treatment of urinary tract infections.

Synergy between the fluoroquinolone levofloxacin and vancomycin or teicoplanin (both peptidoglycan synthesis inhibitors) has also been found *in vitro* against *S. pneumoniae* (GP)^[208]. However, the combined activity of levofloxacin with either rifampicin (an RNA synthesis inhibitor) or FA was indifferent against the same panel of organisms.

The use of phage (bacterial viruses) in combination with established antimicrobials has gained traction over the last 10 years^[209]. While synergy has been identified in some pairings, others appear to antagonise each other. However, studies using successful pairs have indicated reduced rates of resistance induction to both the antimicrobial and the bacteriophage *in vitro* and good efficacy *in vivo*.

1.4.3.2 Prevention of antimicrobial degradation

An excellent example of activity recovery is the story of clavulanic acid. In 1976, a novel β -lactam was isolated from *Streptomyces clavuligerus* but, rather than having direct antimicrobial properties, was found to be a β -lactamase inhibitor^[210]. Shortly after discovery, clavulanic acid was tested *in vitro* in combination with various penicillins and restoration of activity against β -lactamase-producing strains was identified^{[211],[212]}. Within six years of discovery, trials of clavulanic acid combined with amoxicillin in patients with

complicated^[213] and urinary tract^[214] infections caused by β -lactamase producers were completed and confirmed excellent tolerability and favourable outcome. The combination was licensed by GlaxoSmithKline as Augmentin and is still on the market today.

Following the same principle, a number of combination formulations of carbapenem (another class of β -lactams with broader spectrum but increasing resistance) or cephalosporin and ESBL-inhibitor are now also available^[202]. These include imipenem-relebactam and meropenem-vaborbactam which recover carbapenem activity against non-susceptible *Enterobacteriaceae* and *P. aeruginosa*^[215], and ceftazidime–avibactam and ceftolozane–tazobactam which both have potent activity against clinical MDR ESBL-producing isolates of *E. coli*, *K. pneumoniae* and *P. aeruginosa*^[216].

1.4.3.3 Increasing antimicrobial access to its target

Low molecular weight antimicrobial peptides are produced as part of the innate immune systems of most lifeforms and many structural analogues and peptides of novel design have been shown to exhibit antimicrobial activity in their own right^[217]. In addition, these synthetic and semi-synthetic antimicrobial peptides can synergise with a variety of traditional antimicrobial drugs both *in vitro* and *in vivo*. Colistin is an old antimicrobial peptide which has been revived for last-line treatment of MDR GN infections, often in combination with a carbapenem^[218]. Novel antimicrobial peptides are also in development specifically for their ability to synergise with other agents. For example, one novel antimicrobial peptide has been shown to eradicate 99.9 % of *S. aureus* from a mouse wound infection model after a single dose when combined with levofloxacin^[219]. Oligo-acyl-lysyls (OAKs) also mimic host antimicrobial peptides and synergise with rifampicin *in vitro*^[220]. In the presence of 5 $\mu\text{g mL}^{-1}$ OAK, the MIC of rifampicin against *E. coli* reduced from 8 $\mu\text{g mL}^{-1}$ to 0.004 $\mu\text{g mL}^{-1}$. However, similarly to other antimicrobial peptides, preliminary toxicology and pharmacokinetic investigations in mice have shown OAKs are not well absorbed after oral administration. Nevertheless, subcutaneous injection of OAKs 1 h after oral rifampicin doubled survival of *K. pneumoniae* infected-mice compared to rifampicin alone^[220]. However, not all peptide and drug combinations produce predictable synergy based on the currently understood mechanisms of action. For example, membrane permeabilising agents are known to enhance fluoroquinolone activity against GN organisms but one study found no evidence of increased ciprofloxacin activity *in vitro* when combined with any of a variety well-characterised antimicrobial peptides known to disrupt the OM^[221].

Natural products have also been investigated as potentiators of antimicrobial drugs. Eugenol, the major component of clove oil, has been shown to synergise with a broad

spectrum of antimicrobials against GN bacteria *in vitro* by disrupting the OM^[222]. A number of plant extract compounds have also been found to synergise with various antimicrobials to prevent and eradicate biofilms, possibly by disrupting the extracellular matrix which is usually impenetrable to most antimicrobials^[223]. Combinations of antimicrobials and enzymes are also under investigation for the same purpose of combating biofilms^[224].

1.4.4 Desirable mechanisms of agents for co-formulation with fusidic acid

Since low OM permeability and efflux are the intrinsic resistance determinants in GN bacteria, agents which target one or both of these phenotypes may be useful for co-formulation with FA.

1.4.4.1 Membrane permeabilisation

Membrane permeabilisation is a promising potential option to extend the spectrum of classically anti-GP lipophilic drugs to cover GN organisms. Polymyxin B nonapeptide has long been known to sensitise *E. coli* to hydrophobic antimicrobials and synergises with FA^[225]. Other small synthetic cationic peptides that can permeabilise the OM also synergise with hydrophobic drugs against GN bacteria^{[226],[227]}. In particular, colistin has been shown to strongly enhance the activity of FA against MDR *A. baumannii*, as previously mentioned in Section 1.3.1^[119]. Another novel antimicrobial peptide, SPR741, has been shown to synergise with several hydrophobic antimicrobials including FA against *E. coli*, *K. pneumoniae* and *A. baumannii* reference strains, and is currently in clinical development^{[228],[229]}. These are potentially promising agents for co-formulation with FA. However, polymyxins are currently reserved as last-line antibiotics for otherwise resistant GN infections and their use may therefore need to be limited in order to delay induction of resistance as far as possible. High-throughput screening methods have even been developed and successfully employed to test and identify a wide variety of agents capable of permeabilising the *E. coli* cellular envelope^[230]. One peptide unrelated to the polymyxins identified *via* this method was able to reduce the FA MIC from 500 to 16 µg mL⁻¹.

Sodium hexametaphosphate, a phosphate polymer and metal chelator, is another agent which sensitises GN organisms to FA and other hydrophobic drugs in a synergistic manner^[231]. Other metal chelators are also known to increase OM permeability by scavenging the Mg²⁺ and Ca²⁺ responsible for LPS cross-linking, increasing membrane

fluidity and consequently enhancing cellular uptake of hydrophobic agents^[232]. Unfortunately, systemic administration of metal chelators is known to cause retinal damage due to local depletion of Cu and Zn^[233] and sodium hexametaphosphate specifically is an ocular irritant^[234]. However, identification of additional agents that can selectively destabilise bacterial OMs could provide a suitable option for coadministration with FA.

1.4.4.2 Efflux inhibition

A variety of AcrAB-TolC efflux pump inhibitors have been discovered and investigated *in vitro*^{[142],[235]}. However, the ability of each inhibitor to recover the activity of an otherwise effluxed antimicrobial varies, which is thought to depend on the individual ArcB binding site of each agent^[142]. There have been no reports of efflux inhibitors combined with FA. In addition, high concentrations of these inhibitors are generally needed in order to achieve adequate AcrAB-TolC inactivation. However, if inhibition comparable to the deletion of the *acrAB* locus could be achieved, *E. coli* sensitivity to FA would potentially be increased by more than 100-fold^[150]. Despite the challenges presented by efflux over-expression, the search for effective inhibitors goes on. Recent investigations have identified novel metabolites from *Actinomyces* spp. capable of sensitising GN bacteria to classically GP antibiotics such as rifampicin and linezolid by competing for efflux^[236].

1.4.5 **Metals as antimicrobial adjuvants**

Many metals are essential micronutrients to biological processes in all life forms^[237]. Iron, for example, is an important element for the correct structure and activity of multiple enzymes. Most bacteria gather iron by producing molecules known as siderophores (from the Greek for “iron bearer”) which are excreted, chelate extracellular Fe³⁺ and are then internalised as an Fe-complex by dedicated receptors^[238]. The removal of iron from the intracellular siderophore as Fe²⁺ is catalysed by specific enzymes and carefully controlled to prevent release of free, reactive iron ions. Nevertheless, when bacteria are exposed to high concentrations of iron or other metal ions, homeostasis systems can become saturated leaving cells vulnerable to the detrimental effects of these reactive ions.

Throughout history, metals and their solutions have been naturally selected as a means to prevent and treat infections, even prior to understanding of the cause. Copper and silver vessels were used in ancient Egypt (2000 BC) and ancient Greece (400 BC) to

keep safe drinking water^{[239],[240]}. This principle was also adopted by early American pioneers who placed copper or silver coins in water barrels^[241]. Ancient medical applications of metals have included copper oxide and malachite for skin conditions by the Aztecs and silver plates to aid wound healing by Macedonians^{[239],[240]}. Possibly the first published evidence of medical silver nitrate use is in a Roman pharmacopoeia dated 69 BC^[240]. By the nineteenth century, anti-infectious metal use was widely documented, including such applications as copper salts for rabies prophylaxis and the treatment of infected ulcers^[242], silver sutures to reduce “muco-purulent secretion” and promote healing in the repair of vaginal tears postpartum^[243] and mercury(II) chloride as a disinfection agent after exposure to faecal matter from patients with cholera and typhoid^[244]. Bordeaux Mixture, a combination of copper sulphate and calcium hydroxide (lime), was discovered in the late nineteenth century and commercialised as a fungicide for grape vine mildew^[245]. The use of metals to control microbial growth has been continued to modern times. Comparatively recent discoveries such as the Bordeaux Mixture see ongoing commercial success while metallic copper touch surfaces have been shown to positively contribute to infection control in healthcare settings^{[246],[247]}.

Metal ions can be well tolerated in humans and are present in a variety of drugs in clinical use, particularly as anticancer agents^[248]. They have also been employed in vaccine formulation in order to enhance efficacy^[249]. Over the past 15-20 years, the use of metals either as nanoparticles, free ions or to form complexes has been investigated as a means to increased activity of antimicrobial drugs.

1.4.5.1 Nanoparticles

A variety of metal and metal-based nanoparticles have been found to be active against many microbial species and some exhibit synergy with established antimicrobial drugs^[250]. Addition of ZnO nanoparticles at subinhibitory concentrations can enhance the activity of ciprofloxacin against clinical isolates of both *S. aureus* and *E. coli*^[251]. However, the authors found that the same nanoparticle concentration had no effect on, or was even detrimental to, the antimicrobial activity of a wide variety of other drugs tested. Ag⁺ nanoparticles have also been shown to synergise with several antimicrobials, most notably with colistin against a resistant *E. coli* strain and penicillin against a resistant *S. aureus* strain^[252]. In another investigation, MDR isolates of *E. coli* and *K. pneumoniae* were re-sensitised to cephalosporins, ciprofloxacin and gentamicin by Ag⁺ nanoparticles^[253]. However, there are concerns over the environmental impact of nanoparticles^[254], including the induction of antimicrobial resistance gene transfer between bacterial species when released into the environment^[255].

1.4.5.2 Metal complexation

Metal complexes of antimicrobials can be synthesised by chemical manipulation processes or may occur in aqueous, biological or other environments spontaneously. Metal-fluoroquinolone complexes have been investigated extensively^[256]. Magnesium, as well as the antimicrobial metal ions Mn^{2+} , Zn^{2+} , Fe^{3+} and Al^{3+} , were originally reported to reduce the activity of fluoroquinolones in a concentration-dependent manner due to spontaneous metal-drug binding in aqueous solutions^{[257],[258]}. However, Co^{2+} , Ni^{2+} , Cu^{2+} and even Zn^{2+} complexes of ciprofloxacin exhibit very similar *in vitro* antimicrobial activities to the standard sodium salt against a wide range of bacterial species and strains^[259]. Pd^{2+} and Pt^{2+} complexes of ciprofloxacin, levofloxacin, ofloxacin, sparfloxacin, and gatifloxacin have also been shown to retain antimicrobial activity against *M. tuberculosis*^[260]. Many other combinations of metals and fluoroquinolone have been synthesised^{[261]–[263]}. In addition, most metal cations were found to enhance rather than reduce fluoroquinolone solubility when buffered to a range of physiologically relevant pHs^[264], therefore indicating that the early reports of determinantal metal interaction may have been due to the specific artificial experimental conditions.

A Cu-tobramycin complex has been shown to have equal anti-*P. aeruginosa* activity to tobramycin^[265]. However, the complex exhibited enhanced anti-inflammatory effects *in vitro* compared to the parent drug, giving an important advantage for the potential treatment of pulmonary infection in cystic fibrosis patients^[265]. Pd^{2+} complexes of anti-tuberculosis drugs capreomycin, kanamycin and ofloxacin have also been generated and found to be slightly more active than the parent compounds against intracellular *M. tuberculosis in vitro*^[266].

A silver salt of FA, silver fusidate, has been investigated and found to have similar antimicrobial activity per mg as FNa^[267]. However, as the molecular mass of silver is approximately 5 times that of sodium, the molar activity of silver fusidate is actually slightly greater than FNa, likely due to the additional antimicrobial activity of dissociated Ag^+ ions.

The mechanism of action of most metal-antimicrobial complexes appear to be the same as the parent antimicrobial. Where enhanced activity is seen, this is thought to be due to either the dissociation of the complex affording the additional antimicrobial effect of free metal ions or due to alterations in uptake of the complex compared to the free drug.

1.4.5.3 Free metal ions

While metal-drug complexation essentially leads to a novel chemical entity, co-formulation of free metal ions and antimicrobial drug may enhance activity by combining mechanisms of action as a two (or more) pronged attack. Many metal ions exhibit antimicrobial activity, but only a few have been investigated as potential adjuvants. The presence of Ag^+ ions has been shown to synergise with bactericidal antimicrobials against *E. coli*, greatly increasing the activity of otherwise sub-lethal concentrations of gentamicin, ampicillin and ofloxacin^[268]. Studies in a mouse model of urinary tract infection also confirmed the gentamicin and Ag^+ ion combination to be effective at killing bacteria *in vivo*. Another study found that Ag^+ , and to a lesser extent Cu^{2+} , was able to enhance the activity of gentamicin against *E. coli*, whereas Fe^{2+} , Co^{2+} , Zn^{2+} and Ni^{2+} were not^[269]. Ag^+ was found to allow gentamicin to bypass one of the steps in its usual uptake mechanism and accumulate intracellularly more rapidly. Tobramycin, another aminoglycoside, has also been shown to be potentiated by Ag^+ ions against *P. aeruginosa* biofilms^[270]. In addition, Cu^{2+} ions have been found to inactivate the important ESBL New Delhi metallo- β -lactamase 1 (NDM-1)^[271]. When combined with carbapenems *in vitro*, Cu^{2+} ions synergised against an NDM-1-producing strain of *E. coli*, recovering the activity of the antimicrobial.

While systemic administration of most metal ions is inadvisable due to toxicity as well as poor distribution, topical application is less likely to suffer these challenges. Issues with absorption and distribution are largely overcome when an antimicrobial is applied directly to the site of infection. In addition, generalised toxicity becomes far less likely and any risk of localised problems can be weighed against the benefits of treatment^[187].

Metal ions can both disrupt bacterial membranes and denature proteins^[272], potentially synergising with FA by targeting both the impermeable OM and active efflux pumps. In addition, topical administration to the eye is likely to avert the systemic toxicity common to oral or other exposure routes. Repurposing of FA as a GN antimicrobial could be effectively achieved by co-formulation with metal ions and is yet to be explored. Therefore, this work sought to investigate the combined *in vitro* antimicrobial activity of FA and metal ions as a potential treatment bacterial keratitis.

1.5 Hypothesis and aims

It was hypothesised that one or more antimicrobial metal ion(s) would enhance the activity of FA against GN bacteria without reducing anti-GP efficacy. In addition, the combination would exhibit low toxicity against mammalian cells and good activity in a simulated tear fluid mimicking the ocular environment.

The primary aims of the work presented in this thesis were:

- 1) To identify metal ion(s) which increase FA activity against GN organisms without decreasing its anti-GP efficacy.
- 2) To determine whether the key mode of combined activity is *via* spontaneous complexation, action against dual antimicrobial targets or another mechanism.
- 3) To investigate whether activity of combination(s) extends to multiple GN species and resistant isolates.
- 4) To characterise toxicity of combination(s) against human corneal epithelial cells.
- 5) To assess antimicrobial activity of combination(s) in a simulated tear fluid.

Chapter 2: General methodology



The methods presented here outline procedures used for experimentation reported in multiple Chapters and the materials listed were used throughout this thesis. Specific method details are described within the relevant chapter. Appropriate personal and environmental safety procedures were followed, and precautions taken throughout the work, as detailed in Appendix A.

2.1 Test agent stock solution preparation and storage

Stock solutions of metal salts were prepared in HPLC-grade water (Fisher Scientific, Loughborough, UK) and filter sterilised (0.22 μm PES). Aluminium sulphate hydrate ($\text{Al}_2(\text{SO}_4)_3 \cdot \text{H}_2\text{O}$), cobalt(II) sulphate heptahydrate ($\text{CoSO}_4 \cdot 7\text{H}_2\text{O}$), copper(II) sulphate anhydrous (CuSO_4), manganese(II) sulphate monohydrate ($\text{MnSO}_4 \cdot \text{H}_2\text{O}$), iron(II) sulphate heptahydrate ($\text{FeSO}_4 \cdot 7\text{H}_2\text{O}$), nickel(II) sulphate hexahydrate ($\text{NiSO}_4 \cdot 6\text{H}_2\text{O}$), zinc(II) sulphate heptahydrate ($\text{ZnSO}_4 \cdot 7\text{H}_2\text{O}$), copper(II) D-gluconate (Cu D-glu), copper(II) chloride anhydrous (CuCl_2), copper(II) nitrate hemipentahydrate ($\text{Cu}(\text{NO}_3)_2 \cdot 2.5\text{H}_2\text{O}$), sodium D-gluconate (Na D-glu) and sodium chloride (NaCl) were purchased from Sigma Aldrich (Gillingham, UK). Palladium(II) sulphate dihydrate ($\text{PdSO}_4 \cdot 2\text{H}_2\text{O}$) and sodium sulphate anhydrous (Na_2SO_4) were from Fisher Scientific (Loughborough, UK). For $\text{Al}_2(\text{SO}_4)_3$, CoSO_4 , CuSO_4 , MnSO_4 , NiSO_4 , ZnSO_4 , CuCl_2 , $\text{Cu}(\text{NO}_3)_2$, and Cu D-glu the final concentration of metal ions was adjusted to 400 mM and the solutions stored at room temperature for up to one month. As PdSO_4 is not soluble in aqueous solution, a 40 mM stock was prepared in 160 mM NaCl (affording a 1:4 molar ratio of Pd^{2+} and Cl^-) to enable the formation of water-soluble sodium tetrachloropalladate complexes. A volume of NaCl stock solution without PdSO_4 was reserved for use as a control for the effects of NaCl at concentrations equivalent to those present in PdSO_4 tests. PdSO_4 and NaCl stock solutions were kept at room temperature for no more than two weeks. Due to instability in aqueous solution (see Section 3.3.3), fresh 400 mM FeSO_4 solution was prepared and used within 30 min for each experiment. Na_2SO_4 stock solution was prepared at a concentration of 400 mM for use as a control for the effects of sulphate.

Sodium fusidate (fusidic acid sodium salt, FNa) was purchased from Sigma Aldrich (Gillingham, UK) and HPLC-grade absolute ethanol (EtOH) from Fisher Scientific (Loughborough, UK). A 51.2 mM FNa stock solution was prepared in 50 % v/v EtOH ^[273] by first dissolving the appropriate mass of FNa in absolute EtOH followed by dilution with HPLC-grade water. The resulting solution was filter sterilised through 0.22 μm PES and

stored for up to a month at room temperature as solubility is reduced at cooler temperatures.

2.2 Sources, storage and maintenance of bacterial strains

2.2.1 Source of strains

Escherichia coli, National Collection of Type Cultures (NCTC) strain reference 10418, *Staphylococcus aureus* NCTC 12973 *Klebsiella pneumoniae* NCTC 9633 and *Pseudomonas aeruginosa* NCTC 13359 were obtained from glycerol stocks produced from NCTC sourced samples (Salisbury, England) and frozen at -80 °C.

E. coli NCTC 10418 and *S. aureus* NCTC 12973 were chosen for the initial testing as both are well-characterised representatives of GN and GP organisms, respectively. In addition, both strains exhibit wild-type susceptibility to fusidic acid and were the British Society of Antimicrobial Chemotherapy (BSAC) recommended control strains for determining antimicrobial susceptibility at the time of the initial work^{[274]–[276]}. *K. pneumoniae* NCTC 9633 and *P. aeruginosa* NCTC 13359 (also known in the American Type Culture Collection (ATCC) as ATCC 13883 and ATCC 15542, respectively) were selected as reference strains during testing of multi-drug resistant (MDR) plasmid-harboring isolates (Chapter 6) as both are type strains exhibiting wild-type susceptibilities^{[277],[278]}. The MDR isolates of *E. coli*, *K. pneumoniae* and *P. aeruginosa* were provided by the School of Medicine on agar plates.

2.2.2 Preparation of initial glycerol stocks

A 10 µL inoculation loop of frozen glycerol stock or three to five morphologically identical colonies from MDR culture plates was transferred to sterile, room temperature phosphate buffered saline (PBS, 10 mM, pH 7.4, Fisher Scientific, Loughborough, UK), and vortexed for 20 s. The resulting bacterial suspension was streaked onto nutrient agar (NA) plates prepared from nutrient agar powder (Thermo Scientific Oxoid, Basingstoke, UK) per the manufacturer's instructions and incubated at 37 °C for 18-24 h. Plates were checked visually for uncontaminated growth. Three to five morphologically identical colonies were

suspended in 20 mL prepared and autoclaved nutrient broth No. 1 (NB, Thermo Scientific Oxoid, Basingstoke, UK) and incubated for 18±2 h at 37 °C and 120 rpm. The bacterial culture was mixed with an equal volume sterile 20 % v/v glycerol (Sigma Aldrich, Gillingham, UK) and stored in 1 mL aliquots at -80 °C. Stock viability and purity was confirmed after three days by inoculating NB with three random samples of each organism followed by subculture on NA.

2.2.3 Maintenance of stocks and cultures

Frozen glycerol stocks were maintained following the seed lot method^[279]. For each organism, twelve of the originally prepared glycerol stocks were reserved as the seed lot and the remainder used as working lot. As the supply of working lot reached depletion, a new batch of working lot was produced from one of the seed lot stocks. In order to replenish the frozen working lot, NB was inoculated with one rapidly thawed seed lot glycerol stock and incubated at 37 °C and 120 rpm for 18±2 h. The bacterial culture was mixed with an equal volume sterile 20 % v/v glycerol and 1 mL aliquots frozen at -80 °C as the new working stock. In this way, each glycerol stock used for experimentation was a minimal number of passages from the original NCTC isolate, avoiding any large genetic variation which may occur with repeated culture.

Working agar cultures of each organism were produced once monthly by reviving one rapidly thawed working lot glycerol stock in nutrient broth incubated at 37 °C and 120 rpm for 18±2 h. Disposable inoculation loops were used to streak 10 µL bacterial culture onto NA plates. Plates were incubated at 37 °C for 18-24 h and the resulting working cultures stored agar side up at 4 °C for a maximum of 6 weeks.

2.3 Enumeration of bacteria

Bacteria were enumerated as colony forming units (CFU). CFU counts were performed using the Miles & Misra method^[280], as summarised in Figure 2.1. Briefly, serial 10-fold dilutions of a bacterial suspension were performed in PBS and 10 µL aliquots plated onto NA in triplicate. After drying for 10-15 min at room temperature, the plates were incubated at 37 °C for 18-24 h. The mean number colonies in the least dilute suspension where

discrete colonies could be counted was used to calculate the CFU mL⁻¹ in the original bacterial suspension using the following formula:

$$s = (\bar{n} \times 10^{-d}) \times 100$$

Where s = CFU mL⁻¹ in the original bacterial suspension, \bar{n} = mean discrete CFU per 10 μ L aliquot and d = dilution number.

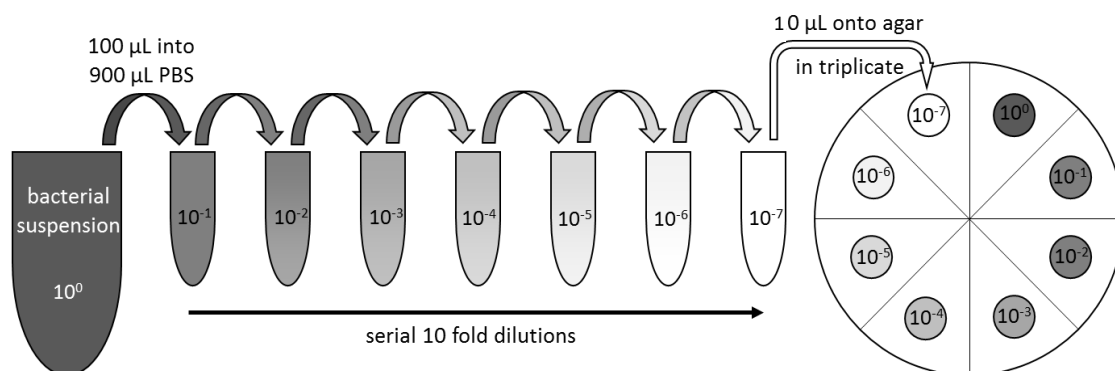


Figure 2.1 – The dilution and plating steps in the Miles & Misra method^[280]

Up to seven 10-fold serial dilutions were performed in PBS and 10 μ L of the each of the suspensions of interest dropped on nutrient agar in triplicate. Plates were allowed to dry at room temperature for 10-15 min then incubated at 37 °C for 18-24 h.

The number of dilutions in the series was varied depending on the nature of the investigation. For example, for confirmatory enumeration of a $5 \pm 3 \times 10^5$ CFU mL⁻¹ inoculum only three dilutions were performed and the 10⁻² and 10⁻³ plated whereas seven dilutions were performed and plated for kill-time assays.

2.4 Determination of minimum inhibitory and minimum bactericidal concentrations by microdilution

Microdilution was selected as the most appropriate method to ascertain single agent antimicrobial activities^[281]. Firstly, unlike agar diffusion-based methods (disc diffusion or well diffusion), microdilution enables determination of the minimum inhibitory concentrations (MICs) of agents. Secondly, by employing 96-well plates, microdilution is comparatively high-throughput testing, requiring less set-up time and fewer resources compared to the more traditional macrodilution method. Finally, while agar dilution can also be used for accurate and very high-throughput MIC determination, the employment

of a microplate reader enables precise quantification of growth inhibition in each well of the microdilution assay. This allows analysis of effects of sub-MIC agent concentrations on bacterial growth, which is particularly useful in assessment of metal ions since many are micronutrients.

The method used was based on that published by the Clinical and Laboratory Standards Institute (CLSI)^[282], with modifications as directed by the checkerboard assay optimisation (see Chapter 3). Three to five colonies from working agar cultures were used to inoculate fresh NA plates and incubated at 37 °C overnight. Serial dilutions of test agents were performed using 100 µL sterile filtered (0.22 µm) HPLC-grade water per well in sterile un-coated flat-bottomed 96 well plates (Corning Costar, New York, USA). At least one agent-free control well (HPLC-grade water only) was included on each plate. Bacteria were picked from the overnight growth and suspended in 3 mL sterile HPLC-grade water. HPLC-grade water was used in place of the usual PBS to prevent the formation of insoluble metal phosphate precipitates. The optical density (OD) of the bacterial suspension at 625 nm was adjusted to approximately 1×10^8 CFU mL⁻¹ for the particular organism using a Jenway 6305 spectrophotometer and semi-micro polystyrene cuvettes giving a 1 cm path length, based on OD : CFU mL⁻¹ calibration curves constructed previously. The resulting suspension was diluted 1/100 in double strength NB, of which, 100 µL was used to inoculate each well to a final concentration of $5 \pm 3 \times 10^5$ CFU mL⁻¹ ^[282]. Double strength NB was employed so that the final 1:1 mixture of test agent in aqueous solution and bacterial inoculum would be in standard concentration NB. Immediately after inoculation, a separate designated control well was used to perform a drop count in order to confirm the initial number of CFU mL⁻¹ in each test plate. A 10 µL aliquot from the inoculum control well was serially diluted in PBS, of which 10 µL aliquots were plated onto NA and incubated overnight at 37 °C. Blank 96 well plates, each with identical agent dilutions to a test plate, were also prepared using sterile double strength NB. Blank plates enabled baseline correction against any colouration caused by the test agents over the concentrations used. All test and blank plates were wrapped in plastic to reduce evaporation and incubated for 18±2 h at 35 °C and 120 rpm.

Providing the drop count results confirmed the inoculum to be within the accepted range, a Tecan Infinite F200 PRO spectrophotometric microplate reader was used to measure the absorbance in each well of the test and blank plates at 595 nm (wavelength filter accuracy ±10 nm^[283]) with 5 flashes from a single central beam. Plates were read in triplicate with each read being preceded by 30 s orbital shaking at an amplitude of 6 mm. Shaking and read repetition was used for two reasons: 1) to minimise the impact of any precipitate on final values as multiple reads allowed averaging of dense and less dense

areas (this occurred infrequently and was borne from necessity for a small number of wells in certain chequerboards (see Chapter 3)), and 2) to enable erroneous single read data to be removed before further processing, e.g. bubbles or dust particles located in the transmittance path during one of the three reads.

Absorbance data was used to calculate baseline-corrected well-by-well percentage growth inhibition as follows. The mean absorbance reads for the test plate were background corrected for growth medium, 96 well plate material and test agent absorbance by subtracting blank plate read values of corresponding wells. Percentage bacterial growth inhibition in each test condition of the 96 well plate was calculated using background-corrected absorbance values (cA) as:

$$\text{percentage inhibition} = \left(1 - \frac{cA_{\text{test well}}}{cA_{\text{control well}}}\right) \times 100$$

Where $cA_{\text{test well}}$ = the mean background-corrected absorbance value for a particular test well, and $cA_{\text{control well}}$ = the mean background-corrected absorbance value for the agent free control well, representative of 100 % (maximal) growth.

Minimum bactericidal concentrations (MBCs) were also determined by plating 20 μL aliquots from wells with ≥ 90 % inhibition (as calculated using the above formula) onto NA and checking for growth of viable organisms after 18-24 h incubation at 37 °C.

All experiments were performed in triplicate using three independent bacterial suspensions. The MIC_{90} of each test agent was determined as the lowest concentration needed to produce a mean of at least 90 % growth inhibition and the MBC as the lowest concentration to result in no growth on agar in any replicate.

2.5 The chequerboard assay

The chequerboard assay enables evaluation of the combined antimicrobial efficacy of two agents by determining the fractional inhibitory concentration index (FICI) as a measure of synergy or antagonism^[284]. This assay was employed to assess the bacteriostatic activity of FNa combined with a range of metal salts. All tests were carried out in sterile un-coated flat-bottomed 96 well plates. Chequerboard assays were prepared using two-fold serial dilutions of the two test agents on opposing axes, as illustrated for FNa and metal sulphate in Figure 2.2. The highest concentration of FNa

and metal salt were both four times their respective MIC₉₀ for the organism being tested (as determined by preliminary microdilution data and within agent solubility limits) in order to enable detection of and differentiation between any antagonistic and suppressive combinations^[201]. Dilutions of all agents were prepared in sterile filtered HPLC-grade water, mixed in the 96 well plate and allowed to stand for 60±15 min before inoculation. Single agent, positive and sterility controls were also included.

As described for the microdilution assay (Section 2.4), 96 well plates were set up in pairs. One of each pair of prepared plates was inoculated to a final concentration of $5 \pm 3 \times 10^5$ CFU mL⁻¹ and the inoculum confirmed by drop count on NA. The other plate of each pair was set up as a blank by adding sterile double strength NB. Plates were incubated, wrapped in plastic, for 18±2 h at 35 °C and 120 rpm. After confirmation of initial inoculum, absorbance at 595 nm was measured using a Tecan Infinite F200 PRO microplate reader. Reads were carried out in triplicate, each after 30 s orbital shaking and the data used to calculate well-by-well baseline-corrected percentage growth inhibition. Minimum bactericidal concentrations (MBCs) of the combinations were also determined by plating aliquots from wells with ≥90 % inhibition onto NA and checking for growth of viable organisms after 18-24 h incubation at 37 °C. Each chequerboard assay was performed in triplicate using an independent bacterial suspension for each replicate.

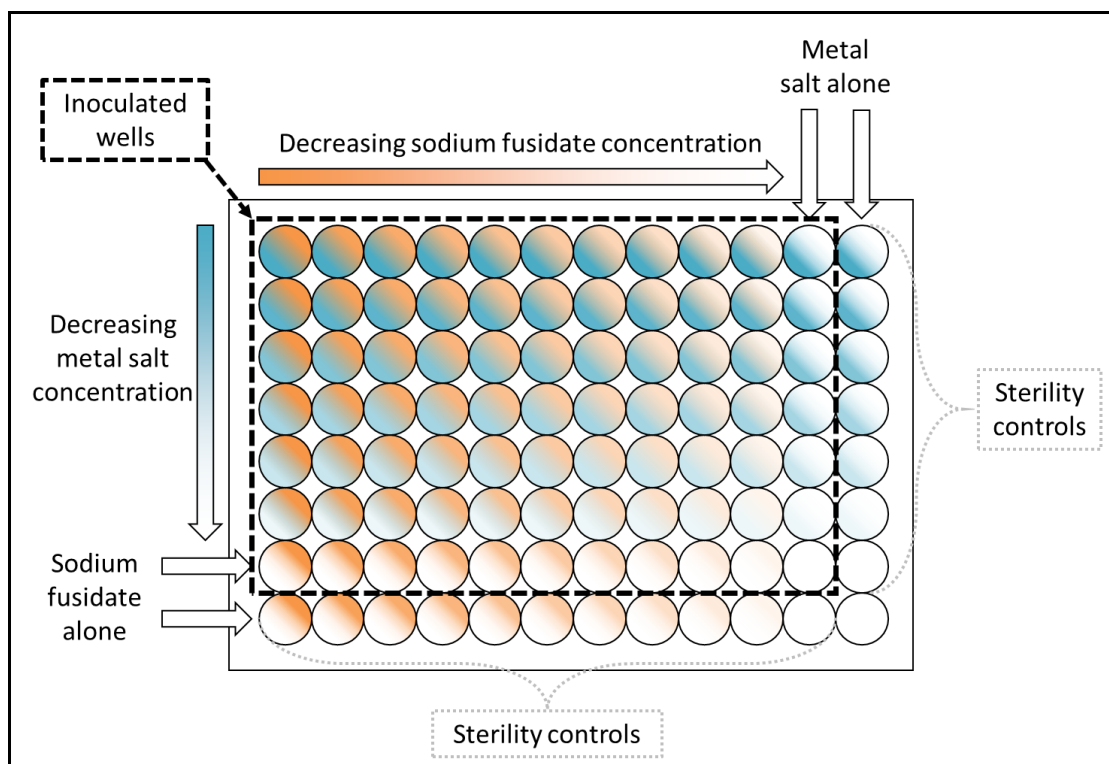


Figure 2.2 - Illustration of typical chequerboard assay set-up

Sodium fusidate is shown in orange and metal salt in cyan, with greater colour intensity representing higher concentration. Nutrient broth without the test organism was added to sterility control wells in order to verify the reagents employed were free from contamination.

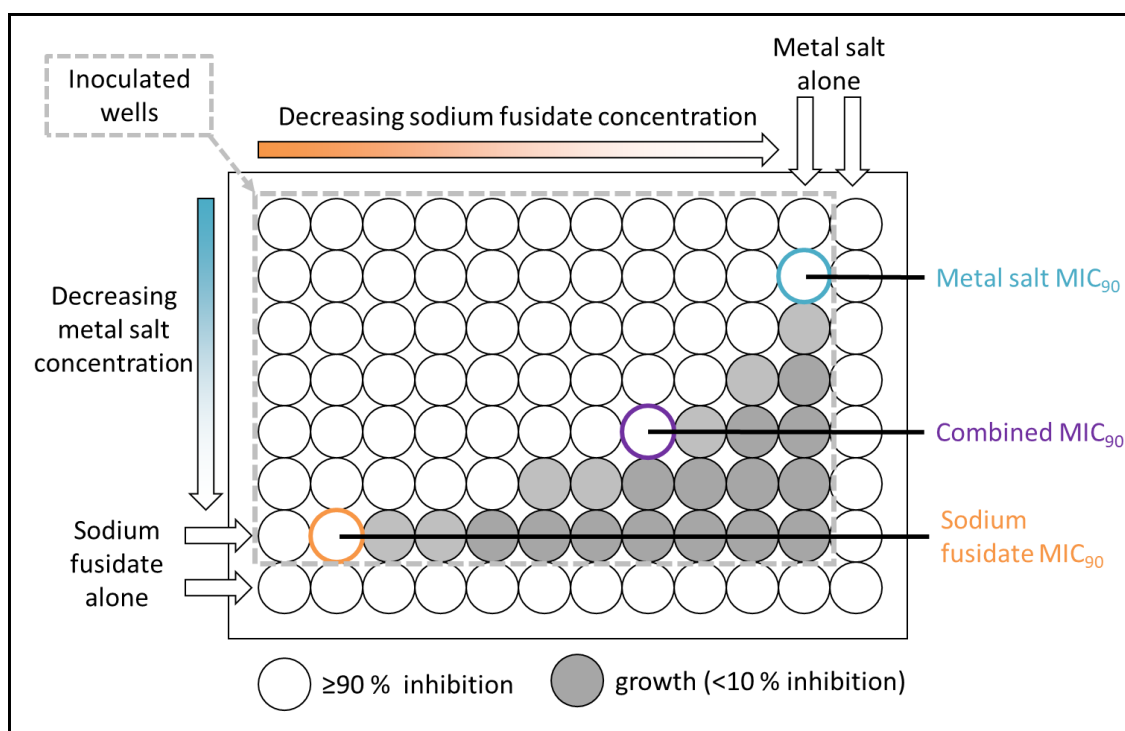


Figure 2.3 - Selection of wells from hypothetical chequerboard results for FIC_{90I} calculation

Shaded wells represent bacterial growth inhibited by <10 %. Metal salt MIC₉₀ well is highlighted in cyan, sodium fusidate in orange and the combined MIC₉₀ in purple.

The mean lowest FIC_{90I} (fractional 90 % inhibitory concentration index)^[285] for each chequerboard triplicate was used to determine whether a synergistic (FICI ≤0.5) or antagonistic (FICI >4.0) interaction occurred between the test agents^[286] and quantify the extent. The FIC_{90I} was calculated for each replicate as follows:

$$FIC_{90I} = FIC_{90}(A) + FIC_{90}(B)$$

Where:

$$FIC_{90}(A) = \frac{MIC_{90}(A) \text{ in combination}}{MIC_{90}(A) \text{ alone}} \quad \text{and} \quad FIC_{90}(B) = \frac{MIC_{90}(B) \text{ in combination}}{MIC_{90}(B) \text{ alone}}$$

FIC_{90S} (fractional 90 % inhibitory concentrations) were calculated from three individual wells within each replicate: 1) the MIC₉₀ of the metal salt alone, 2) the MIC₉₀ of FNa alone, and 3) the well where the combined lowest concentration of the two agents produced ≥90 % inhibition, as illustrated in Figure 2.3. This method provides a calculated FIC_{90I} closer to the true value than other approaches, while also accounting for any day-to-day variation in MIC₉₀^[221].

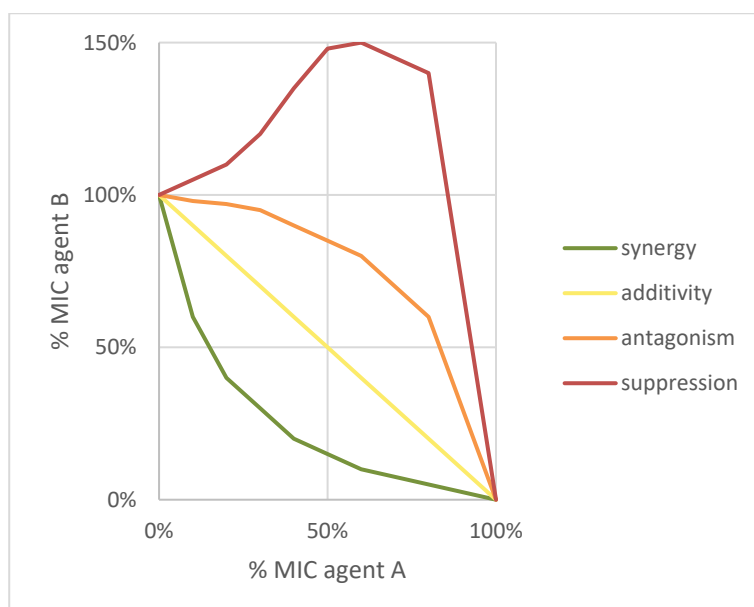


Figure 2.4 – Schematic representation of isobolograms produced by synergistic, additive, antagonistic and suppressive antimicrobial combinations

Based on summaries provided in Cottarel & Wierzbowski, 2007^[202] and Bollenbach, 2015^[201].

Interactions were also assessed graphically by constructing isobolograms – plots of the concentration of one agent required to produce inhibition when in combination with another agent. In the example in Figure 2.4 the agent concentrations have been converted to % of their respective MICs. This data transformation was used when comparing agents with different MIC₉₀s to facilitate visual comparison on the same graph. The shape of the isobologram indicates the nature of the interaction. No interaction results in additive effects and a straight line between MICs^{[201],[202],[284]}. Synergy and antagonism between agents produce inward and outward bows between the MICs, respectively^{[201],[202],[284]}. Suppression, an extreme form of antagonism, is defined as the presence of one agent increasing the MIC of the other and results in the plot forming a peak which exceeds at least one of the agent's MIC^[201]. The use of isobologram plots aided distinction between antagonistic and suppressive combinations for which there is no standard using the FICI.

Further data were extracted and analysed from checkerboard results in line with the nature of specific investigations, the details of which are provided in the chapters that follow.

2.6 Fusidic acid quantification by RP-HPLC

Two reversed phase high performance liquid chromatography (RP-HPLC) methods were employed to determine the concentration of fusidate. While separation method 1 performed well for most applications and was employed for the majority of assays, peaks were insufficiently resolved when components from bacterial cells were present (see Appendix C). Therefore, a substantially longer, gradient elution method – separation method 2 – was used for the analysis of such samples.

For both methods, the HPLC system was composed of a G1379B Degasser, G1311A QuatPump, G1313A ALS autosampler and G1314A VWD UV detector, all from Agilent, and fitted with a 5 µm Gemini-NX C18 4.6 x 250 mm column as the stationary phase. Agilent ChemStation for LC systems (revision B.04.02 SP1) was used for system control and data visualisation and processing. Calibration curves were constructed for both methods (see Appendix B).

Acetonitrile (ACN), >98 %, HPLC-grade water, gradient grade methanol (MeOH) and glacial acetic acid were purchased from Fisher Scientific (Loughborough, UK). Phosphoric acid (H₃PO₄), >85 % in water, was from Sigma Aldrich (Gillingham, UK). All chemicals were used as received.

2.6.1 Separation method 1

Separation method 1 was based on that reported by Curbete & Salgado^[287], employing an isocratic mobile phase of 72:28 v/v ACN : 1 % aqueous acetic acid, injection volume of 20 µL and flow rate of 1 mL min⁻¹. The detection wavelength was optimised to 235 nm (see Section 5.3.1.1) and the analysis run time was 10 min per sample.

2.6.2 Separation method 2

Separation method 2 was a gradient method with a 60 min analysis run time, based on that reported by Byrne *et al*^[288]. This was employed when method 1 yielded insufficient peak resolution, for example: due to additional, overlapping peaks produced by high concentrations of bacterial cell components.

Mobile phase A was 16:21:21:42 v/v/v/v MeOH : 10 g L⁻¹ H₃PO₄ : H₂O : ACN and mobile phase B was 24:5:5:66 v/v/v/v MeOH : 10 g L⁻¹ H₃PO₄ : H₂O : ACN. The gradient is described in Table 2.1. The flow rate was 0.7 mL min⁻¹ and injection volume 50 µL with a detection wavelength also of 235 nm.

Table 2.1 - Mobile phase gradient for HPLC method 2

Time (min)	% A	% B
START	95	5
20.00	95	5
45.00	0	100
50.00	95	5
60.00	STOP	-

2.7 Determination of FA solubility

Solubility of FNa at various concentrations was determined in 1 mL volumes of the solute of interest in sterile 2 mL centrifuge tubes. After equilibration duration and temperature suitable to the investigation, solutions were centrifuged in a Heraeus Fresco 17 (Fisher Scientific, Loughborough, UK) at 17,000 x g (13,300 rpm) for 20 min to pellet any non-solubilised particles. Five hundred microliters of clear supernatant were carefully pipetted from each tube immediately after centrifugation and transferred to a prepared brown glass HPLC vial. When equilibration was performed in an incubator (35 or 37 °C), the centrifuge was pre-warmed and maintained at the appropriate temperature throughout and supernatant samples were mixed with 500 µL EtOH to prevent precipitation of fusidate while at room temperature. Supernatant samples were analysed using RP-HPLC separation method 1 and resulting peak areas were converted to fusidate concentration using the inverted linear regression equation (Appendix B), correcting for additional dilution with EtOH where necessary.

2.8 Measurement of solution pH

Unless otherwise specified, all pH measurements were made using an HI-99165 pH meter fitted with an FC242D amplified electrode, accuracy ±0.2 pH units (Hanna Instruments, Leighton Buzzard, UK). Two-point calibration of the instrument was performed no more than 20 min prior to each batch of readings. The read accuracy was

checked using standard pH 4.01 and pH 7.01 buffers (Fisher Scientific, Loughborough, UK) between every 6-8 measurements.

2.9 Statistical analysis

Data was assumed to be normally distributed for the purposes of statistical analysis and a p value of ≤ 0.05 was considered significant. All statistical analyses were carried out using Microsoft Office Excel 365 software, version 1902 (Microsoft Corporation, Redmond, Washington, USA). Statistical tests were selected based on the specific nature of each inquiry and data set, the details of which are provided within each Chapter.

Chapter 3: Optimisation of the microdilution and chequerboard assays

3.1 Introduction

Standardised microdilution assays against non-fastidious bacteria are carried out in the rich medium cation-adjusted Müller-Hinton broth (CAMHB)^[282]. Consistent employment of CAMHB enables valuable, reproducible and directly comparable antimicrobial susceptibility testing to be performed across multiple laboratories and countries^[289]. However, such standardisation may not always be helpful when searching for novel topical agents or combinations^[290]. The nutritional environment of CAMHB is tailored to support rapid bacterial growth. While this is an advantage for standard diagnostic susceptibility testing, it does not reflect the conditions during infection. In fact, antimicrobial susceptibility testing in media mimicking tissue fluid has illustrated marked changes in the minimal inhibitory concentrations compared to CAMHB. For example, azithromycin was found to be highly active against *A. baumannii* in the mammalian culture medium RPMI, while the same strains are classified as resistant in CAMHB^[291]. In addition, the same authors found that both the susceptibility of *A. baumannii* to azithromycin and synergy of azithromycin with minocycline observed in RPMI *in vitro* was replicated in a mouse model of pneumonia^[291]. Conversely, a range of both GN and GP uropathogens exhibited similar fluoroquinolone minimum inhibitory concentrations (MICs) when grown in synthetic urine as in CAMHB^[292]. It appears that these variations are, at least in part, linked to bacterial growth rate, with slower growth corresponding to increased susceptibility^[293]. This is likely to be compounded by concomitant stressors and antimicrobial solution chemistry. However, while these factors complicate *in vitro* determination of the clinical effectiveness of antimicrobial agents, they may not be as problematic when considered during drug discovery or development. In particular, the increasing number and sophistication of options for topical formulations enable greater manipulation and control of the delivered agent(s) to answer specific developmental questions. For example, a co-polymer of α -cyclodextrin and chitosan has been used to solubilise the antifungal agent econazole, increasing the concentration delivered to the cornea by more than 600 times^[294], while semi-synthetic vesicles have been developed to adhere and deliver encapsulated drugs to specific tissues^[295]. Hence, once the mechanism of action of an antimicrobial has been understood in a particular artificial environment, formulation chemistry can be used to modulate the delivery and efficacy *in situ*. The focus of this initial optimisation work was therefore to determine conditions that enabled the most sensitive detection of potential synergy between FNa and metal ions against GN bacteria. Since preliminary results from prior work carried out in our

laboratory (not shown) indicated potential enhancement of FNa activity against *E. coli* NCTC 10418 in the presence of CuSO₄, this organism and agent combination was employed for optimisation.

3.1.1 Aims and objectives

Aim: to optimise the chequerboard assay for use in the study of the combined antimicrobial activity of FNa and metal ions, with a focus on GN-bacteria.

Objectives:

- 1) To select an appropriate bacteriological medium for detection of antimicrobial interactions between FNa and Cu²⁺ against *E. coli* NCTC 10418.
- 2) To determine the MIC₉₀ of FNa against *E. coli* NCTC 10418 and *S. aureus* NCTC 12973 and thereby select appropriate concentration ranges for use in chequerboard assays.
- 3) To determine the MIC₉₀ and MBCs of eight metal sulphates against *E. coli* NCTC 10418 and *S. aureus* NCTC 12973 and select appropriate concentration ranges for use in chequerboard assays.
- 4) To determine the impact of EtOH, sulphate counterion and NaCl, at concentrations equivalent to those present in FNa and metal ion dilutions, respectively, on the growth of *E. coli* NCTC 10418 and *S. aureus* NCTC 12973.

3.2 Methods

3.2.1 Selection of bacteriological medium

An initial pilot investigation to identify indicative MICs and appropriate concentration ranges for FNa and CuSO₄ was conducted using the standard bacteriological medium for antimicrobial testing: CAMHB^[282]. Müller-Hinton broth (MHB) powder (Sigma Aldrich, Gillingham, UK) was prepared in deionised water and sterilised by autoclaving per the manufacturer's instructions. Stock solutions of 7.5 g L⁻¹ CaCl₂·2H₂O and 10 g L⁻¹

MgCl₂•6H₂O were prepared in deionised water and filter sterilised. After autoclaved MHB had cooled to room temperature, stock solutions were used to adjust the concentration of Ca²⁺ and Mg²⁺ cations to 20-25 and 10-12.5 mg L⁻¹, respectively^[282]. Serial two-fold dilutions of FNa and CuSO₄ were prepared in CAMHB in a sterile un-coated flat-bottomed 96 well plate. The plate was inoculated with *E. coli* NCTC 10418 suspended in CAMHB to a final concentration of 5±3 × 10⁵ CFU mL⁻¹ and incubated for 18±2 h at 35 °C and 120 rpm. After incubation, plates were inspected visually to determine the indicative MIC of each agent and select prospective concentration ranges for use.

To compare bacteriological media, chequerboard assays were set up generally following the method described in Chapter 2, page 49. FNa and CuSO₄ dilutions were performed in HPLC-grade water then transferred to six sterile un-coated flat-bottomed 96 well plates. *E. coli* NCTC 10418 suspended in double strength CAMHB (with 40-50 and 20-25 mg L⁻¹ Ca²⁺ and Mg²⁺, respectively), Miller's lysogeny broth (LB, Fisher Scientific, Loughborough, UK), or NB was used to inoculate three of the prepared plates with 5±3 × 10⁵ CFU mL⁻¹. Sterile double-strength CAMHB, LB or NB was added to the remaining three plates as blanks. The final formulation of each bacteriological medium is detailed in Table 3.1.

Table 3.1 - Composition of bacteriological media

Medium name	Ingredients (g L⁻¹)
Cation adjusted Müller-Hinton broth (CAMHB) ^[282]	Beef infusion solids, 2.0 Casein hydrolysate, 17.5 Starch, 1.5 Ca ²⁺ , 20-25 mg L ⁻¹ Mg ²⁺ , 10-12.5 mg L ⁻¹
Miller's lysogeny broth (LB) ^[296]	Tryptone, 10. Yeast extract, 5.0 NaCl, 10.0
Nutrient broth No. 1 (NB) ^[297]	Lab-Lemco beef extract, 1.0 Peptone, 5.0 Yeast extract, 2.0 NaCl, 5.0

All 96 well plates were incubated for 18±2 h at 35 °C and 120 rpm, wrapped in plastic to reduce evaporation. Absorbance at 595 nm in all wells was measured and background corrected % inhibition calculated as previously described in Chapter 2, page 49. The experiment was performed in triplicate using an independent bacterial suspension for each replicate. The number of wells resulting in precipitation of higher concentration agents, lowest achievable MIC₉₀s and mean standard deviation (SD) % inhibition in each well (as a measure of reproducibility between replicates) were assessed in order to select an appropriate broth for ongoing use.

3.2.2 Effect of low concentration ethanol on bacterial growth

Due to limited solubility in aqueous solution, standard laboratory practice is to prepare an initial FNa stock solution in EtOH^[273]. However, EtOH can denature proteins and therefore disrupt bacterial growth^[298]. The effect of low concentrations of EtOH on growth of *S. aureus* NCTC 12973 and *E. coli* NCTC 10418 in the chosen bacteriological medium was therefore investigated. This was performed using EtOH concentrations equivalent to those present in dilutions of a 51.2 mM FNa stock solution in 50 % v/v EtOH.

The concentration range of FNa for use with *S. aureus* NCTC 12973 in the chosen broth was optimised by first testing the range selected for *E. coli* NCTC 10418 and then further extending the two-fold dilutions. Once the FNa concentration range was determined for both organisms, dilution series of equivalent concentrations of EtOH were prepared in 96 well plates and inoculated with $5 \pm 3 \times 10^5$ CFU mL⁻¹ of *E. coli* NCTC 10418 or *S. aureus* NCTC 12973. Percentage inhibition was determined after incubation for 18 ± 2 h at 35 °C and 120 rpm as for other investigations. The 95 % confidence intervals (95 % CI) were calculated for each EtOH concentration to determine whether there was a statistically significant difference in inhibition compared to the EtOH-free control ($p \leq 0.05$).

3.2.3 Metal ion MIC₉₀s, MBCs and concentration range selection

The MIC₉₀ and MBC of the sulphates of Al³⁺, Co²⁺, Cu²⁺, Fe²⁺, Mn²⁺, Ni²⁺, Pd²⁺ and Zn²⁺ against *E. coli* NCTC 10418 and *S. aureus* NCTC 12973 was determined using the microdilution method described in Section 2.4. Stock solutions of metal sulphates were prepared and stored as described in Section 2.1. All metal ions were initially tested using two-fold dilutions from a maximum concentration of 10 mM. This concentration range was selected based on experience with Cu²⁺ during initial chequerboard optimisation (Section 3.3.1). If the MIC₉₀ could not be identified in this range, a lower or higher starting concentration was selected as appropriate and the assay repeated. Each experiment was carried out in triplicate. The MIC₉₀s were used to select the concentration range of each metal to be used for chequerboard testing as a highest concentration of two or four times the MIC₉₀ followed by five two-fold dilutions. Where the MIC₉₀ varied between organisms, the *E. coli* MIC₉₀ was used as a basis for range calculation because of the focus on anti-GN efficacy.

3.2.4 The effects of sodium sulphate and sodium chloride on bacterial growth and sodium fusidate activity

It was important to validate that any modulation of microbiological activity was due to the metal ions, and not the sulphate counterion. Therefore, once the chequerboard concentration ranges were selected, the effect of sulphate was investigated using sodium sulphate (Na_2SO_4). Na_2SO_4 was selected as concentrations of Na^+ up to 850 mM and 2.3 M have been found to be non-inhibitory to the growth of *E. coli* and *S. aureus*, respectively^[299]. The microdilution assay was used to determine % inhibition of *E. coli* NCTC 10418 and *S. aureus* NCTC 12973 produced by Na_2SO_4 at concentrations equivalent to sulphate present in the highest selected metal sulphate concentration ranges, in triplicate. In addition, the microdilution assay using NaCl was also carried out in triplicate in order to assess the effect of NaCl equivalent to concentrations present in Pd^{2+} solutions. The 95 % CIs were calculated for each Na_2SO_4 and NaCl concentration to determine whether there was a statistically significant difference compared to the control ($p \leq 0.05$).

Finally, the effect of sulphate and NaCl on activity of FNa against *E. coli* NCTC 10418 and *S. aureus* NCTC 12973 was assessed by chequerboard assay, as described in Chapter 2, Section 2.5. The highest concentration of FNa tested against *E. coli* and *S. aureus* was 1280 and 10 μM , respectively, whereas both organisms were exposed to a maximum of 10 mM Na_2SO_4 or 5 mM NaCl. FNa MIC_{90} and MBC values with and without the various concentrations of Na_2SO_4 or NaCl were compared. The absolute difference between % inhibition caused by combinations of FNa and sodium salt and the same concentration of FNa alone was calculated in the presence of each Na_2SO_4 or NaCl concentration in three separate replicates. Absolute inhibition differences of $\pm < 5\%$ were considered negligible. The 95 % CIs were used to determine whether differences in inhibition of $\pm \geq 5\%$ were statistically significant ($p \leq 0.05$).

3.3 Results

3.3.1 Bacteriological medium selection

Initial MICs of 5 mM CuSO₄ and 1280 µM FNa against *E. coli* NCTC 10418 were visually determined from the pilot investigation in CAMHB. However, precipitation of FNa in CAMHB was apparent in wells containing >1280 µM of the drug. Concentration ranges of 0.156 to 5 mM CuSO₄ and 2.5 to 1280 µM FNa were therefore selected for chequerboard bacteriological medium optimisation.

Broth comparison chequerboard results analysed using the microplate reader are presented as mean % inhibition heatmaps in

Figure 3.1. Precipitation of FNa was apparent in high concentration wells in all broths tested, as indicated by pink shading, and these wells were excluded from the analysis. The MIC₉₀ of FNa against *E. coli* NCTC 10418 in CAMHB was found to be >1280 µM on spectrophotometric assessment which was greater than that visually determined in the pilot test. A concentration of 1280 µM FNa produced a mean 86.0 % inhibition. Since precipitation of FNa was observed in the pilot test with concentrations of >1280 µM and the MIC₉₀ fell within this range, CAMHB was rejected as an option suitable for chequerboard analysis of FNa and metal salt combinations against GN organisms. FNa MIC₉₀s in LB and NB were 80 and 320 µM, respectively, and no precipitation of FNa alone was detected in these broths at concentrations up to and including 1280 µM. Precipitation in both LB and NB was apparent at the highest combined concentrations of the agents tested. However, concentrations of FNa and CuSO₄ involved in precipitation were several times higher than the respective and combined MIC₉₀s.

The MIC₉₀ of CuSO₄ alone against *E. coli* NCTC 10418 was found to be at least 8 times higher in LB than NB, at >5 and 1.25 mM, respectively. The mean of the SDs for all analysed wells were quite similar at 0.93 % with LB and 1.11 % with NB, indicating similar inter-replicate reproducibility with both broths. However, NB was selected based on the lower CuSO₄ MIC₉₀ and consequent reduced requirement for resources.

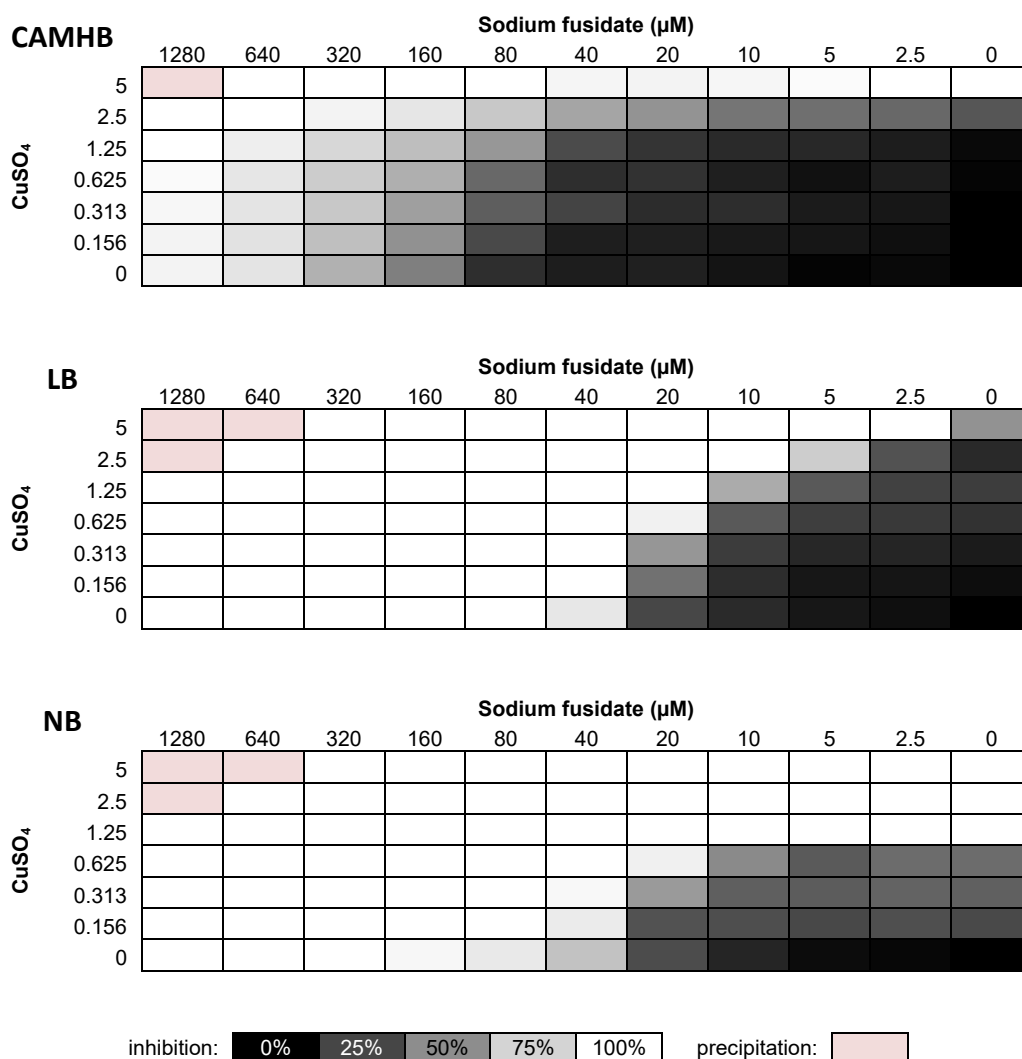


Figure 3.1 - *E. coli* NCTC 10418 growth heatmaps in the presence of sodium fusidate and copper(II) sulphate combinations in three media: cation adjusted Müller-Hinton broth (CAMHB), Miller's lysogeny broth (LB) and nutrient broth No. 1 (NB)

Colour density of shading corresponds to percentage inhibition in each well, as indicated in the key. Pink wells indicate presence of precipitation.

(n = 3)

3.3.2 Effect of low concentration ethanol

The MIC₉₀ of FNa against *S. aureus* NCTC 12973 in NB was found to be 312.5 nM. As the purpose of chequerboard testing against *S. aureus* was to confirm absence of adverse effects of the presence of metals on the activity of FNa (to which *S. aureus* is already sensitive), the FNa concentration range selected was 19.5 nM to 10 μM to allow detection of both decreased and increased inhibition. The FNa concentration range for *E. coli* was maintained at 2.5 to 1280 μM , as determined above.

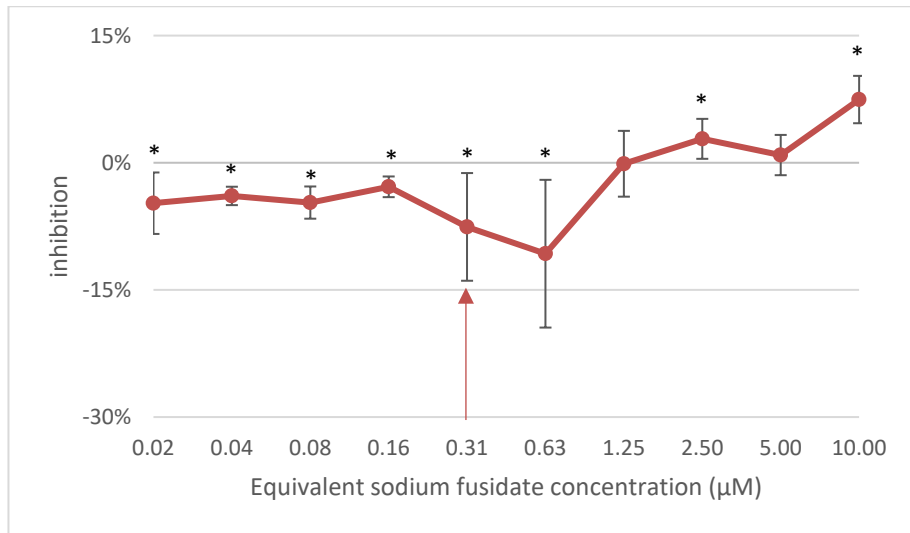


Figure 3.2 - Inhibition of *S. aureus* NCTC 12973 by ethanol concentrations equivalent to those present in sodium fusidate test dilutions

Arrow indicates sodium fusidate MIC₉₀.
(n = 3, error bars = 95 % CI, * = p ≤ 0.05)

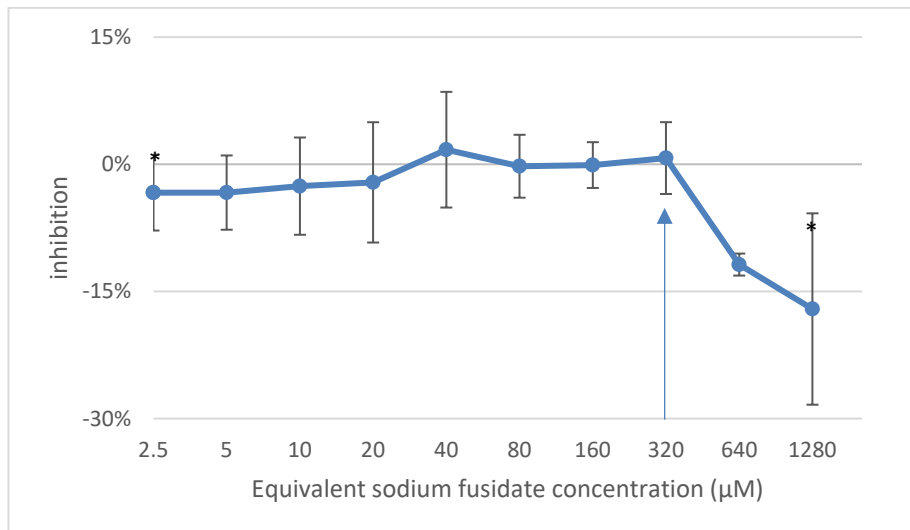


Figure 3.3 - Inhibition of *E. coli* NCTC 12973 by ethanol concentrations equivalent to those present in sodium fusidate test dilutions

Arrow indicates sodium fusidate MIC₉₀.
(n = 3, error bars = 95 % CI, * = p ≤ 0.05)

Inhibition of *S. aureus* NCTC 12973 and *E. coli* NCTC 10418 by EtOH in NB at concentrations relevant to the corresponding FNa test ranges is presented in Figure 3.2 and Figure 3.3, respectively. The equivalent FNa concentration is shown on the x axis for ease of interpretation of the impact of EtOH in direct relation to the chequerboard FNa concentration range. For reference, dilution of a 51.2 mM stock solution of FNa in 50 % v/v EtOH equates to 1.25 % EtOH being present with 1280 μM FNa, 0.00980 % with 10 μM and 0.000305 % with 0.313 μM.

The 95 % CIs indicated small but significant enhancement of *S. aureus* growth in the presence of EtOH concentrations equivalent to those present with 0.625 μM FNa and below, illustrated by negative inhibition values ranging from -10.7 to -2.8 % ($p < 0.05$, Figure 3.2). However, since the *S. aureus* MIC₉₀ of FNa falls within this range (0.313 μM), the small growth-enhancing effect of low concentration EtOH alone appears to be overcome by the much larger inhibitory effects of FNa. *S. aureus* growth was inhibited by EtOH equivalent to 2.5 and 10 μM FNa dilutions by 2.8 and 7.5 %, respectively ($p < 0.05$). However, inhibition by FNa at these concentrations of 4- and 32-times the MIC₉₀, respectively, was already determined to be >95 %.

There was no significant impact on growth of *E. coli* in NB in the presence of EtOH concentrations equivalent to those present with 5 to 640 μM FNa, inclusive ($p > 0.05$, Figure 3.3). Interestingly, when exposed to EtOH alone at concentrations equal to those present in the lowest and highest FNa dilutions tested (2.5 and 1280 μM), the calculated inhibition of *E. coli* was significantly different from the control, at -4.6 and -11.8 % ($p < 0.05$), respectively, indicating increased cell density compared to the EtOH-free control. However, since 2.5 and >95 % *E. coli* inhibition was already confirmed in the presence of 2.5 and 1280 μM FNa, respectively (

Figure 3.1 in Section 3.3.1), this phenomenon with EtOH alone appears to have a negligible impact on the interpretation of the effects of FNa.

3.3.3 The instability of Fe²⁺ in aqueous solution

On initial preparation, stock solutions of FeSO₄ in sterile HPLC-grade water were pale green in colour, due to the presence of Fe²⁺ ions. However, over time in aqueous solution and after incubation for 18±2 h in bacteriological media, an orange-brown colour and precipitate developed. Figure 3.4 illustrates the concentration-dependent colour change and precipitation after incubation in nutrient broth.

Iron ions are well known for their ability to be readily oxidised or reduced between Fe²⁺ and Fe³⁺ and to exist as multiple species of both divalent and trivalent ions in aqueous solution, including bacteriological media. For example, after 24 h incubation in LB, Fe²⁺ precipitates as Fe₃O₄ and Fe³⁺ as Fe(OH)_{2.7}Cl_{0.3}^[300]. However, while it is unknown whether these insoluble products are responsible for or involved in the antimicrobial activity of iron, concentrations at which they appear to form in NB (≥ 2.5 mM) are bactericidal to both *E. coli* and *S. aureus*.

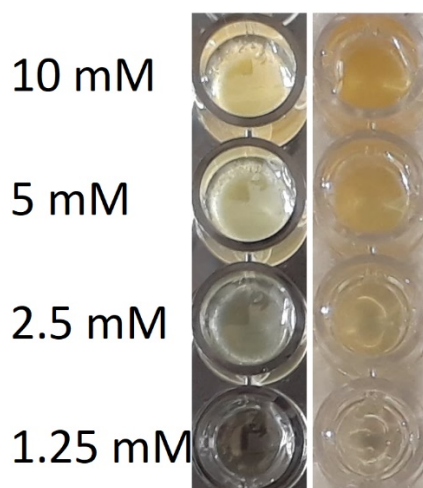


Figure 3.4 - Wells containing iron(II) sulphate in sterile nutrient broth after incubation for 18±2 h at 35 °C and 120 rpm illustrating precipitation and colour change indicative of generation of heterogenous iron species

Precipitate (cloudiness) and colour change (orange-brown, Fe³⁺) developed during incubation of ≥2.5 mM iron(II) sulphate in nutrient broth. No precipitation or colour change occurred with ≤1.25 mM. Left image is photographed over a black background to enhance visualisation of the precipitate and right over a white background for visualisation of the colour change.

3.3.4 Metal ion MIC₉₀s, MBCs and concentration range selection

The MIC₉₀ and MBC of each metal ion against *E. coli* NCTC 10418 and *S. aureus* NCTC 12973 are displayed in Table 3.2. In all cases, the MIC₉₀ against the two organisms fell within one two-fold dilution of each other. Where determined, the MBCs were also similar, except Al³⁺ which killed *E. coli* at 2.5 mM while *S. aureus* was able to survive in the presence of at least 10 mM. There was no significant difference between growth of *E. coli* NCTC 10418 or *S. aureus* NCTC 12973 in the presence of NaCl concentrations equal to those found in Pd²⁺ dilutions and the controls (*p* >0.05).

Table 3.2 – MIC₉₀ and MBC of antimicrobial metal sulphates against *E. coli* NCTC 10418 and *S. aureus* NCTC 12973 after 18±2 h incubation in nutrient broth at 35 °C and 120 rpm

	<i>E. coli</i> NCTC 10418		<i>S. aureus</i> NCTC 12973	
	MIC ₉₀ (mM)	MBC (mM)	MIC ₉₀ (mM)	MBC (mM)
Aluminium as sulphate	2.5	2.5	2.5	>10
Cobalt(II) sulphate	0.156	0.313	0.156	0.625
Copper(II) sulphate	1.25	2.5	2.5	2.5
Iron* sulphate	2.5	2.5	2.5	2.5
Manganese(II) sulphate	2.5	>10	1.25	>10
Nickel(II) sulphate	0.625	1.25	0.313	2.5
Palladium(II) sulphate	0.625	1.25	1.25	1.25
Zinc(II) sulphate	0.313	0.625	0.156	>0.625

*Colour change on mixing and incubation with broth indicates heterogeneous iron species are generated (see Figure 3.4 in Section 3.3.3)

In combination with values from the literature, the determined MIC₉₀s illustrated effect of growth medium on the antimicrobial activity of metal ions. For example, the lowest reported MICs of Co²⁺ are 1 mM in LB against *E. coli*^[301] and 3 mM in tryptone soy broth (TSB) against *S. aureus*^[302], both >6 times the MIC₉₀ determined in NB (Table 3.2). The Zn²⁺ MIC₉₀s in NB were also many times lower than the reported MICs in richer growth media of 3.73 in CAMHB against *E. coli*^[303] and 5 mM in TSB against *S. aureus*^[302]. Conversely, the MIC₉₀s of Pd²⁺ in NB were higher than reported values in minimal media of 0.015 against *E. coli* and 0.2 mM against *S. aureus*^[304] while the reported MICs in LB were only approximately two to four times those found in NB at 2.82 and 2.24 mM, respectively^[305]. Interestingly, Al³⁺ MIC against *E. coli* has been reported to be only one two-fold dilution higher than that found in NB at 5 mM in Lennox LB^[300] and very similar to in NB at 2 mM in a mineral salts medium^[306]. However, reported Cu²⁺ MICs against *E. coli* were 1 mM in minimal medium^[306], 4^[301] or 5^[271] mM in LB, 10 mM in MHB^[307] and 12 mM on brain heart infusion (BHI) agar^[308]. Overall, metal ion MIC values in NB are lower than in rich bacteriological media such as LB or MHB, but higher than those in minimal media, indicating that lower nutrient content increases metal ion susceptibility. These differences reflect previously reported data comparing antimicrobial activity and growth medium composition^{[309],[310]}.

Based on MIC₉₀ results in NB, concentration ranges for use in chequerboards were selected as follows: 0.3125 to 10 mM Al³⁺, 19.5 to 625 µM Co²⁺, 0.156 to 5 mM Cu²⁺, 0.313 to 10 mM Fe²⁺, 0.313 to 10 mM Mn²⁺, 0.781 to 2.5 mM Ni²⁺, 0.391 to 1.25 mM Pd²⁺, and 19.5 to 625 µM Zn²⁺.

3.3.5 Effects of sodium sulphate alone on bacterial growth

Na₂SO₄ concentrations of 0.313 to 10 mM were selected for investigation (Figure 3.5). There was no significant difference between growth of *E. coli* NCTC 10418 in the presence of any concentration of Na₂SO₄ tested ($p > 0.05$) except 2.5 mM. At this concentration Na₂SO₄ inhibited *E. coli* growth by 1.9 % which, while small, was statistically significant ($p \leq 0.05$). *S. aureus* NCTC 12973 was not affected by the presence of 0.313 to 1.25 mM Na₂SO₄, inclusive ($p > 0.05$), however, 2.5, 5 and 10 mM inhibited 6.9, 9.8 and 19.7 % of growth, respectively ($p \leq 0.05$). Consequently, the determined MIC₉₀s of 2.5 mM Al³⁺, Cu²⁺ and Fe^{2+/3+} could have been influenced by the additional inhibition caused by 3.75, 2.5 and 2.5 mM sulphate, respectively. However, the MIC₉₀ of these metal sulphates inhibited *S. aureus* growth by 100 ± 0 , 97.4 ± 4.1 and

100 ± 0 % (95 % CI), respectively. Therefore, normalisation to inhibition caused by the presence of 2.5 to 5 mM Na₂SO₄ still results in >90 % attributable to the metal ions.

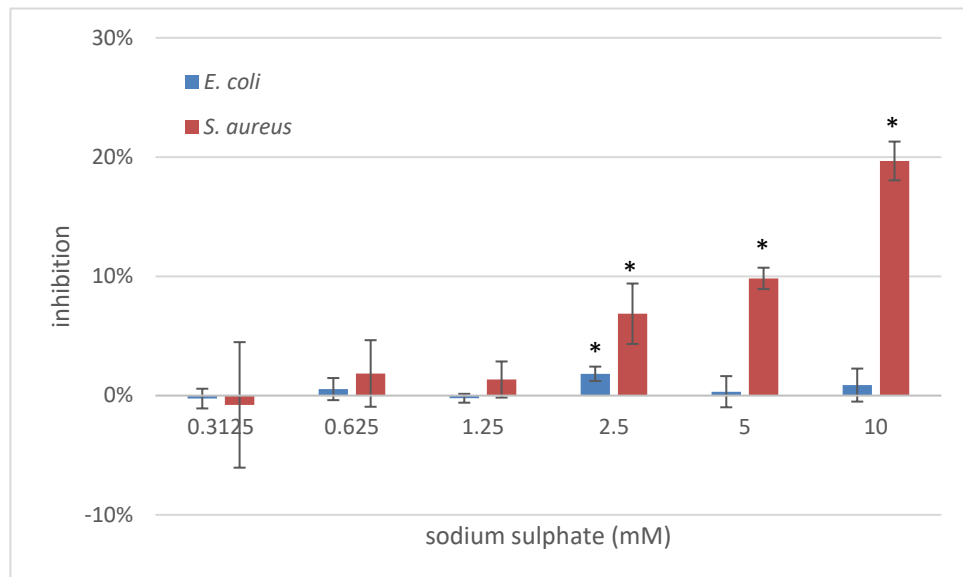


Figure 3.5 - Inhibitory effect of sodium sulphate on the growth *E. coli* NCTC 10418 and *S. aureus* NCTC 12973 in nutrient broth after incubation for 18±2 h
(n = 3, error bars = 95 % CI, * = p<0.05)

3.3.6 Sodium fusidate activity in the presence of sodium sulphate

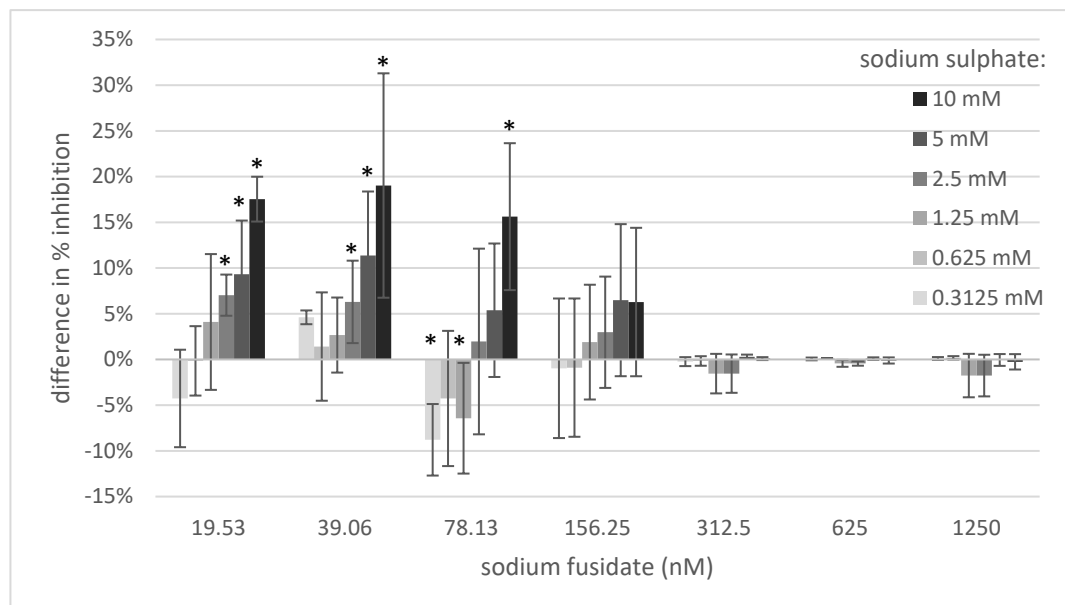


Figure 3.6 - Difference in inhibition of *S. aureus* NCTC 12973 by sodium fusidate in the presence of sodium sulphate compared to sodium fusidate alone
Sodium fusidate concentrations up to 4 x MIC₉₀ are shown.
(n = 3, error bars = 95 % CI, * = difference ±5 % and p<0.05)

The MIC₉₀ and MBC of FNa against *S. aureus* NCTC 12973 were not affected by the presence of any concentration of Na₂SO₄ tested. However, statistically significant differences in the inhibition produced by sub-MIC₉₀ concentrations of FNa with and without Na₂SO₄ were identified ($p \leq 0.05$, Figure 3.6). Inhibition by 78.1 nM FNa (0.25 x MIC₉₀) was reduced by 8.8 and 6.4 % when combined with 0.313 and 1.25 mM Na₂SO₄, respectively, whereas it was increased by 15.6 % by 10 mM. The inhibition produced by 39.1 and 19.5 nM FNa was also increased by 6.3 and 7.0, 11.4 and 9.3, and 19.0 and 17.5 % in the presence of 2.5, 5 and 10 mM Na₂SO₄, respectively.

The MIC₉₀ against *E. coli* NCTC 10418 was also unaffected in the presence of ≤ 1.25 mM Na₂SO₄. With 2.5, 5 and 10 mM Na₂SO₄ the FNa MIC₉₀ against *E. coli* was reduced by one two-fold dilution to 160 μ M, however, only in the presence of 10 mM was the inhibition ≥ 5 % and statistically different to that produced by FNa alone ($p < 0.05$, Figure 3.7). Na₂SO₄ at 10 mM also significantly increased the antimicrobial activity of 80, 40, 20 and 10 μ M FNa by 7.5, 12.9, 18.2 and 5.9 %, respectively ($p < 0.05$), and at 5 and 2.5 mM added 6.3 and 6.6 % to growth inhibition by 20 μ M FNa ($p < 0.05$). The MBC of FNa against *E. coli* was above the tested concentration range >1280 μ M and therefore not assessed.

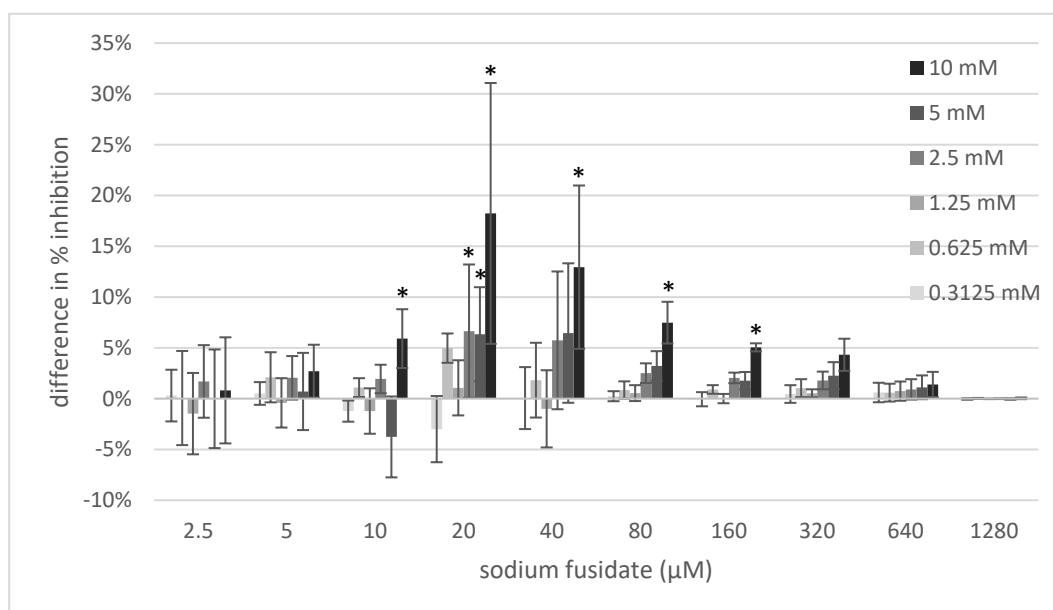


Figure 3.7 - Difference in inhibition of *E. coli* NCTC 10418 in the presence of sulphate and sodium fusidate compared to sodium fusidate alone
(n = 3, error bars = 95 % CI, * = difference $\pm \geq 5$ % and $p \leq 0.05$)

The inhibitory effects of sulphate combined with FNa against *S. aureus* NCTC 12973 and *E. coli* NCTC 10418 were found to occur at concentrations at or above those present with the MIC₉₀ of metal ions. Sulphate-normalised % inhibition of metal ions at MIC₉₀ was

still ≥ 90 %. Therefore, this activity was considered to have no impact on the interpretation of chequerboard results.

3.3.7 Effect of sodium chloride on bacterial growth and the activity of sodium fusidate

NaCl at concentrations present in Pd²⁺ dilutions were found to have little effect on the interpretation of results. No significant differences in growth of either *E. coli* NCTC 10418 or *S. aureus* NCTC 12973 were found between any NaCl concentration tested and agent-free controls. Significant differences of ≥ 5 % in growth inhibition between FNa alone and in the presence of NaCl were detected against both organisms. *E. coli* NCTC 10418 was inhibited by an additional 5.7 % by 40 μ M FNa when combined with 2.5 mM NaCl. However, this NaCl concentration was equivalent to that present with 0.625 Pd²⁺ which caused >98 % growth inhibition, therefore indicating no interference with determination of the *E. coli* MIC₉₀. When 78.1 and 39.1 nM FNa were each combined with 5 mM NaCl against *S. aureus* NCTC 12973, growth inhibition was increased by 11.6 and 16.6 %, respectively. This NaCl concentration was equivalent to that present with 1.25 mM Pd²⁺, the *S. aureus* MIC₉₀ and, more notably, MBC, therefore being unlikely to have any impact on interpretation.

3.4 Conclusions

NB was found to be the most appropriate medium for conducting chequerboards of FNa and metal salts against GN bacteria and was therefore employed for all microdilution-based assays against all organisms. Selection was based on lower *E. coli* NCTC 10418 MIC₉₀ of CuSO₄ compared to LB and CAMHB, reproducibility between replicates and lack of FNa precipitation at critical concentrations.

Low concentration EtOH in NB was found to exhibit some small but significant impacts on the growth of both *S. aureus* NCTC 12973 and *E. coli* NCTC 10418. In particular, the growth of *S. aureus* was enhanced by EtOH concentrations equivalent to those present in sub-MIC₉₀ FNa dilutions by up to 4.8 %. However, these effects appeared to have a negligible influence on the antimicrobial performance of FNa and the interpretation of MIC₉₀ values, therefore, FNa dilutions prepared from 51.2 mM stock solution in 50 % v/v

EtOH were determined to be suitable for use in microdilution and chequerboard assays without further adjustment.

The chequerboard and microdilution assays were therefore successfully optimised for the study of the antimicrobial activity of metal ions, FNa and both combined. The finalised microdilution and chequerboard methods presented in Chapter 2, Sections 2.4 and 2.5, respectively.

Chapter 4: Antimicrobial activity of
 **sodium fusidate combined**
with metal ions

4.1 Introduction

As previously discussed in Chapter 1, FNa inhibits bacterial growth by targeting the prokaryotic elongation factor EF-G and preventing protein synthesis. While GN organisms do not lack the EF-G target, they are intrinsically resistant to FNa due to a combination of a low permeability OM and multi-drug efflux pumps. Formulations of FA and FNa are already licensed for and frequently used in the treatment of conjunctivitis. Repurposing FNa for use in both GP and GN keratitis is therefore an attractive drug development option as the safety and efficacy in ocular use is already established. Metal ions are well known to exhibit a range of antimicrobial and chemical properties. One or more antimicrobial mechanism of metal ions may exert a co-operative effect to overcome intrinsic FNa resistance and render GN organisms susceptible to its protein synthesis inhibitory effects. Metal ions were therefore selected for investigation into extending the antimicrobial spectrum of FNa by co-formulation.

4.1.1 Metal ions of interest for combining with sodium fusidate

Metal ions exert their antimicrobial effect by targeting multiple bacterial structures and systems. These include damaging proteins by displacing native ions, disrupting iron-sulphur (Fe-S) clusters or binding and denaturing polypeptides; damaging membranes by attacking embedded proteins, peroxidising lipids or altering crosslinking and fluidity; damaging nucleic acids by binding amino acid residues or causing strand breaks; interfering with ribosomal function by ion displacement or structural damage; and generalised oxidative stress *via* the generation of reactive oxygen species (ROS) or saturation of ROS management systems^[272]. The specific mechanisms of metal ion antimicrobial activity have taken many years to elucidate and some metals are better understood than others. As discussed in Section 1.4.4, increased OM permeabilisation and inhibition of efflux are likely to be effective strategies to overcome intrinsic FNa tolerance in GN bacteria. However, other features, such as induction of oxidative stress or the ability to synchronously interfere with protein synthesis, may also help increase drug activity.

Inclusion criteria for elemental metal ion selection in this work was essentially based on whether their established antimicrobial mechanisms had the potential to produce a co-

operative effect with FNa. Consequently, the following 8 metal ions were selected: Al³⁺, Co²⁺, Cu²⁺, Fe²⁺, Mn²⁺, Ni²⁺, Pd²⁺ and Zn²⁺. The unique combinations of each metal ion's targets are detailed in Sections 4.1.1.1 to 4.1.1.8 below and summarised in Table 4.1. Overlap between antimicrobial mechanisms was chosen to support potential identification of metal ion targets necessary or detrimental to effective combination with FNa.

Table 4.1 – Summary of known antimicrobial targets and mechanisms of metal ions selected for investigation in combination with sodium fusidate

Metal	Known antimicrobial targets and mechanisms					
	oxidative stress	DNA	RNA	ribosomes	intracellular proteins	membranes
Al ³⁺						✓
Co ²⁺	✓		✓	✓	✓	
Cu ²⁺	✓				✓	✓
Fe ²⁺	✓	✓			✓	✓
Mn ²⁺		✓		✓	✓	
Ni ²⁺	✓		✓		✓	
Pd ²⁺	✓	✓			✓	✓
Zn ²⁺	✓		✓		✓	✓

4.1.1.1 Aluminium

Al³⁺ is believed to be non-essential to biological systems and is not spontaneously taken up into bacterial cells^{[300],[311],[312]}. However, Al³⁺ ions are able to exert an antimicrobial effect by damaging external cell structures: trivalent Al³⁺ can outcompete both Ca²⁺ and Mg²⁺ for phosphate functional groups leading to misfolding of membrane proteins and disruption of lipopolysaccharide (LPS) and phospholipid organisation in GN bacteria^{[300],[313],[314]}. This may also lead to alterations in transmembrane potential^[315] as well as acceleration of lipid peroxidation in the presence of reactive iron^[316]. Al³⁺ is also thought to be able to hijack Fe³⁺ uptake systems, compromising Fe homeostasis and limiting production of essential Fe-containing enzymes^[237]. At sub-bactericidal concentrations, the presence of Al³⁺ specifically induces GN membrane stress reporter genes^[300] as well as enhanced expression of flagellin^[317] and an enzyme involved in the production of modified, cation-resistant lipid A^{[318],[319]}.

Al³⁺ is also toxic to GP bacteria *via* similar mechanisms as occur in GNs, causing damage to membrane proteins and phospholipids^[320]. However, the GP bactericidal effect of Al³⁺-containing solutions is not as rapid or dramatic as against GN organisms^[321]. This may be because Al³⁺ readily adsorbs onto carboxyl and phosphate sites of the exposed GP cell wall peptidoglycan^[322], thereby reducing the local concentration freely able to access and damage the membrane components. The overall antimicrobial mechanism of Al³⁺

follows a similar pattern in both GN and GP organisms: damage initially decreases function and stability of the cell membrane(s) inhibiting active growth and this, if too extensive for rapid repair, results in increased permeability, consequent leakage of intracellular material and cell death.

Al³⁺ may be able to enhance FNa anti-GN activity by producing both increased intracellular access through destabilised OM and decreased efflux pump function due to cell surface protein damage and disruption of the required IM PMF.

4.1.1.2 Cobalt

Co²⁺ is an essential nutrient required for the proper function of cobalamin-dependent enzymes^[161]. As such, bacteria exhibit specific uptake and homeostasis mechanisms to acquire and manage intracellular Co²⁺. However, excess Co²⁺ can interfere with essential cellular processes, including the assembly and stability of Fe-S cluster- and haem-containing proteins, Fe²⁺ uptake and normal redox status disturbance^{[323]–[326]}. In *E. coli*, Co²⁺ is acquired *via* the major cobalt importer CorA^[323], cobalamin uptake^[327] or as a citrate-coupled complex by replacing the preferred Mg²⁺^[328]. When present in excess, Co²⁺ can also out-compete Fe²⁺ and Ni²⁺ uptake *via* FeoB and NikA, respectively^[324]. Exposure to increased Co²⁺ induces the expression of the Co²⁺ and Ni²⁺ efflux encoding gene *rcnA* *via* RcnR^[329] while *feoB* and *nikA* expression is stopped^[324]. If these measures fail to adequately reduce intracellular Co²⁺ levels, the assembly of Fe-S enzymes is compromised. In the presence of excess Co²⁺, scaffold proteins, responsible for transient assembly of Fe-S clusters and transfer to the target protein, can erroneously replace approximately half of Fe²⁺ in the immature Fe-S assemblies with Co²⁺^[323]. These inactive mixed Co-Fe-S clusters are then transferred to the target enzymes resulting in an inoperative product^[323]. Processes dependent upon Fe-S proteins include gene regulation, tRNA turnover, DNA maintenance and, crucially, respiration^[324]. In order to limit the impact on overall cell function, the expression of Fe-S biogenesis genes is increased in response to Co²⁺ exposure, presumably to compensate for the proportion of miss-assembled enzymes in essential pathways, and non-essential Fe-S-dependent pathways and proteins are downregulated^[324]. However, Co²⁺ can also disrupt complete and fully-functional Fe-S proteins by displacing Fe^[323]. This is further confounded by the reduction of intracellular Fe²⁺ *via* Co²⁺-induced reversal of Fur repression and consequent ferrichrome reductase (*fhuF*) expression^[330], preventing Fe-S cluster recovery.

While Co²⁺ plays no role in the generation of reactive oxygen species inside bacteria^[331] and appears to inhibit Fe²⁺-H₂O₂-mediated lipid peroxidation^[332], it can indirectly produce

oxidative stress. Glutathione (GSH), an antioxidant, is able to chelate intracellular Co^{2+} . Strangely, the $\text{GSH}\cdot\text{Co}^{2+}$ complex acts as a pro-oxidant, catalysing the formation of $\cdot\text{OH}$ and singlet oxygen from H_2O_2 via a Fenton-type reaction^[325]. These reactive oxygen species can cleave DNA. In addition, Co^{2+} has been found to inhibit *E. coli* protein synthesis^[333] by direct interference with ribosomal subunit assembly^[334] which may be due lack of differentiation between Co^{2+} and Zn^{2+} when either ion is present in excess^[335]. Finally, Co^{2+} can also inhibit RNA synthesis in *E. coli*^[333].

Co^{2+} is an interesting option for combination with FNa due potential synergy between each agent's mechanism of protein synthesis inhibition. Furthermore, disruption of Fe-S cluster-dependent enzymes and pathways or additional oxidative stress may further limit survivability when in combination with protein synthesis inhibition.

4.1.1.3 Copper

Cu^{2+} is also an essential micronutrient utilised as a cofactor in many bacterial enzymes including cytochrome oxidases and oxygenases^{[161],[336]}. Homeostasis in *E. coli* is primarily governed by two chromosomal operons: *cue* (copper efflux) and *cus* (copper sensing)^[337]. CueR regulates expression of Cu management genes by binding to the promoter of *copA* (a P-type ATPase which exports Cu^+ to the periplasm^[338]) and *cueO* (a periplasmic oxygen-dependent multi-copper oxidase which oxidises Cu^+ to the less damaging Cu^{2+}) in the presence of elevated intracellular Cu^+ . (Any free ions in the cytoplasm are the more reactive Cu^+ due to the reducing intracellular environment^[339].) However, these systems can become overwhelmed in the presence of excess extracellular Cu^{2+} , leading to toxicity. The first and most deleterious effect of Cu^{2+} overload appears to be the disruption of Fe-S clusters in dehydratases^[340]. Dehydratases are essential to the branched chain amino acid biosynthesis pathway required for growth, as well as various other metabolic functions. Cu^+ displaces Fe^{2+} from the Fe-S cluster, leading to enzyme dysfunction and degradation. Dehydratases appear to be particularly susceptible to Cu^+ attack due to the exposed nature of their Fe-S clusters whereas the function of enzymes with occluded clusters is not affected^[340]. Cu^{2+} has also been found to interfere with the biosynthesis of haem by inhibiting an Fe-S cluster-containing decarboxylase of one of the porphyrins upstream of Fe^{2+} incorporation. This results in loss of the enzymes catalase and peroxidase which in turn decreases ROS defences^[341]. This is interesting, since the generation of intracellular ROS was long disputed as a direct mechanism of Cu^+ toxicity. It appears that Fe^{2+} released from damaged Fe-S clusters may initiate ROS production^[340], while abrogation of detoxifying enzymes exacerbates the situation. As with other metal ions, the majority of free intracellular Cu^+ is sequestered by GSH^[340]. While the GSH pool within cells is very large and unlikely to become

saturated by Cu^+ , even when exposed to toxic concentrations^[342], reduced reserves may have a knock-on effect on the ability of the cell to manage its redox homeostasis. This is likely to result in increased susceptibility to ROS generated by released Fe^{2+} in the same way that exposure to combined Cu^{2+} and H_2O_2 was found to produce high levels of intracellular $\cdot\text{OH}$ radicals in *E. coli*^[343]. Therefore, oxidative stress can play a role in Cu^{2+} toxicity, but it is mediated *via* the accumulative effects of other mechanisms rather than direct redox cycling. However, almost all unbound copper ions are found in the periplasm^[339] and here they can damage both membranes by causing lipid peroxidation *via* a cyclical redox reaction^{[332],[336]} and interfere with the structure and function of periplasmic and membrane proteins^[342].

The propensity of Cu^{2+} to readily bind to antimicrobial drugs has long been employed for the detection and differentiation of sulphonamides^[344]. A number of these complexes have been shown to retain their antimicrobial activity *in vitro*^{[345],[346]}. Cu^{2+} , along with a number of other divalent cations, has also been shown to spontaneously form complexes with a variety of cephalosporins, however, none have been found with increased activity^{[347]–[349]}. Conversely, the Cu-complex of the fluoroquinolone ciprofloxacin is equally active as the parent drug^{[259],[350],[351]}, whereas Cu-enrofloxacin has been shown to be about twice as effective as equivalent ionic mixtures or free enrofloxacin alone^[352].

The combination of permeability-altering membrane damage and disruption of essential metabolic pathways caused by Cu^{2+} may enhance FNa activity by increasing entry into the cell while decreasing growth capacity. In addition, disruption of membrane and periplasmic proteins may damage AcrAB-TolC, reducing or preventing efflux. Alternatively, complex formation may enhance activity by preventing efflux or enabling direct delivery of Cu^{2+} into the cytoplasm.

4.1.1.4 Iron

Iron is the most abundantly available and biologically utilised metal on Earth, essential to all forms of life^[353]. Its importance is such that all animals flood their exposed mucosal surfaces with Fe-sequestering proteins to limit the availability of Fe to potential pathogens, a function known as “nutritional immunity”^[353]. Interestingly, some bacteria express receptors capable of obtaining Fe^{2+} *via* siderophores and other Fe-bound proteins that are produced by other organisms in order to overcome Fe-limited conditions^[354]. Despite the necessity and extensive measures to overcome any scarcity of Fe, exposure to high concentrations can be very damaging to bacterial cells.

ROS generation and the resulting oxidative stress is believed to be the primary mechanism of Fe toxicity. All homeostatic processes are geared to utilising gathered Fe while preventing any uncontrolled reactivity. However, free ions accumulated during overload readily react with endogenous respiration products H_2O_2 and O_2^- in a cyclical manner^{[336],[355]} (Figure 4.1). Fe^{2+} reduces H_2O_2 to produce OH^- and highly reactive and damaging $\bullet\text{OH}$. The resulting Fe^{3+} is then readily reduced back to Fe^{2+} by O_2^- , perpetuating the cycle. Excess $\bullet\text{OH}$ reacts with biological macromolecules, primarily damaging DNA and proteins^[300]. In addition, Fe^{2+} and Fe^{3+} can directly catalyse the oxidation of proteins^[300] and membrane lipid peroxidation^{[332],[336]}.

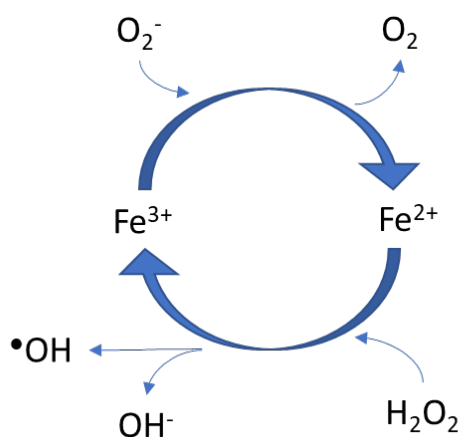


Figure 4.1 – Cyclical production of hydroxyl radicals *via* the Fenton reaction^[336]
 Fe^{3+} is reduced by O_2^- to Fe^{2+} . Fe^{2+} reduces H_2O_2 to OH^- and highly reactive $\bullet\text{OH}$, oxidising to Fe^{3+} in the process.

The combination of membrane and protein damage may be advantageous to FNa activity by facilitating entry into the cell and reducing efflux, respectively. In addition, considerable oxidative stress may limit bacterial resources for induced AcrAB-TolC expression while, *vice versa*, stalling of protein synthesis would prevent replenishment of damaged proteins and free radical scavengers.

4.1.1.5 Manganese

While Mn^{2+} is also a micronutrient, it too can cause damage to an array of bacterial systems when present in excess. Extracellular Mn^{2+} outcompetes Mg^{2+} for uptake when at a high relative concentration ratio^[328] and, when the internal concentration ratio shifts, Mn^{2+} displaces Mg^{2+} at multiple intracellular locations including enzymatic active sites and structural positions in ribosomal RNA (rRNA) folding^[356]. It can also cause errors during DNA replication by displacing Mg^{2+} at the DNA polymerase I active site, reducing

nucleotide alignment fidelity^{[357],[358]}. Since the homeostasis of Mn^{2+} and Fe^{2+} are linked (primarily *via* the Fur operon), excess Mn^{2+} inhibits the synthesis of haem and Fe-S clusters by inducing the depletion of intracellular Fe^{2+} and out-competing available Fe^{2+} for inclusion in these structures^{[359],[360]}. The consequent inactivation of key enzymes results in disruption of both the TCA (Krebs) cycle and electron transport chain – the two pathways for ATP generation^[360]. In addition, Mn^{2+} stress is inhibitory to *E. coli* cell division, producing a filamentous morphology void of septation due to downregulation of penicillin binding protein 3 (PBP3) expression^[361].

Any of these modes of toxicity could potentially synergise with FNa activity, however, Mn^{2+} -induced ribosomal misfolding coupled with protein synthesis stalling by FNa could be particularly effective at inhibiting bacterial growth.

4.1.1.6 Nickel

Ni^{2+} is another essential micronutrient required structurally or catalytically for the correct function of multiple enzymes^{[161],[337]}. However, when in excess, Ni^{2+} can displace Zn^{2+} from its binding sites in enzymes and metalloproteins. For example, the structurally essential Zn^{2+} of *E. coli* fructose-1,6-bisphosphate aldolase is readily replaced by surplus Ni^{2+} , abolishing enzymatic activity^[362]. This enzyme is essential for utilisation of glucose and fructose as an energy source and, therefore, its disruption is thought to be a key mechanism of Ni^{2+} toxicity in limited carbon-source environments. GSH-associated ROS generation occurs with Ni^{2+} in the same way as with Co^{2+} ^[336]. In addition, and unlike Co^{2+} , Ni^{2+} enhances Fe^{2+} -mediated lipid peroxidation^[332], however, this does not appear to be sufficient to damage membranes under standard laboratory growth conditions without iron supplementation^[363]. Ni^{2+} is able to denature proteins by catalysing spontaneous disulphide bond formation^[331] and can also reduce RNA synthesis^[333]. This combination of antimicrobial mechanisms could work to prevent FNa efflux by denaturing AcrAB-TolC components while reducing mRNA available for transcription, limiting energy utilisation and overloading the cells with oxidative stress.

4.1.1.7 Palladium

In response to the success of the Pt-based anticancer agent cisplatin and the similarity between Pt^{2+} and Pd^{2+} coordination chemistry, a wide variety of Pd-complexes have been studied for their anticancer^{[364]–[367]}, antimicrobial^{[368]–[371]} and antiviral^[372] efficacies. Pd readily forms complexes with ligands containing N, S, P and/or O co-ordination sites. In many cases, such complexation has been found to increase the biological activity of the parent molecule. For example, the antimicrobial activity of a variety of quinolones

was increased approximately 5-fold against a number of bacterial species including *E. coli* and *P. aeruginosa* by complexation with Pd^[373]. Complexation with Pd has also been shown to dramatically increase the efficacy of tetracycline against TetA efflux-mediated resistant *E. coli*^[374] indicating that the complex retains antimicrobial activity but resists efflux. Pd also spontaneously binds β -lactams^[375], fluoroquinolones^{[376],[377]} and cephalosporins^{[378],[379]}, but these properties are employed in drug quantification assays and the complexes have not been tested for antimicrobial activity.

Pd²⁺ ions have been less extensively investigated as antimicrobial agents. However, at 500 mg L⁻¹ Pd²⁺ can completely eradicate 7 day old biofilms of *A. baumannii*, *K. pneumoniae* and *E. faecalis*^[380] and the same investigators found Pd²⁺ to be more active against planktonic bacterial cells than the more popularly investigated metal ions, Ag⁺ and Cu²⁺. In addition, unlike their Pt²⁺ counterparts, Pd²⁺ ions have been demonstrated to not be genotoxic to either *E. coli* cells or human peripheral lymphocytes^[381]. Pd nanoparticles also exhibited antimicrobial properties, possibly *via* membrane damage and ROS generation^[382]. However, Pd²⁺ ions appear to be more bactericidal in water suspension than nanoparticles at equimolar concentrations^[383]. While this data is interesting, the precise mechanism of Pd²⁺ antimicrobial activity has not been fully investigated. PdCl₄ has been shown to irreversibly inactivate some enzymes by binding to critically positioned sulphhydryl groups and/or cystine and other amino acid residues^{[384],[385]}. Pd²⁺ is also known to increase the production of hydroxyl radicals in the presence of Fe²⁺, but cannot catalyse the Fenton reaction alone^[386], and Pd²⁺-induced membrane damage has been indicated in one environmental GN species^[387]. Finally, Pd²⁺ has been found to have high affinity to bind the phosphate backbone of DNA where it can generate damaging •OH.

Pd²⁺ has potential to work well with FNa against *E. coli* by either forming a novel complex which resists AcrAB-TolC efflux or by causing synergistic membrane, enzyme or DNA damage.

4.1.1.8 Zinc

Ionic zinc only occurs as Zn²⁺. Similar to Al³⁺, Zn²⁺ causes membrane damage in *E. coli* and induces membrane stress responses, increased flagellum production and upregulation of genes involved in processing and modification of LPS lipid A^{[388]–[394]} as well as proteins required for anchoring LPS to peptidoglycan^[395]. This damage results in increased membrane permeability^[396] which could facilitate greater internalisation of FNa. Zn²⁺ overload inhibits essential Fe-S cluster biosynthesis by preventing assembly proteins binding Fe²⁺ ^[397]. In addition, the presence of excess Zn²⁺ inhibits detoxification

of ROS by replacing Fe²⁺ in the haem clusters of catalases, inactivating the enzymatic activity^[331]. Like Co²⁺ and Ni²⁺, Zn²⁺ has also been shown to inhibit RNA synthesis in *E. coli*^[333]. However, Zn²⁺ is also a bacterial micronutrient therefore its specific homeostatic mechanisms must be overcome by exposure to concentrations in excess of that which the cell can manage. Nevertheless, the combination of increased membrane permeability and decreased RNA levels is promising for combination with FNa. These mechanisms could overcome the normally limited FNa access through the OM and contribute to the antibiotic's protein synthesis inhibition by reducing the amount of mRNA available for translation. Furthermore, Zn²⁺ has been shown to reduce expression of *E. coli* virulence factors^{[396],[398]} which would be particularly advantageous in the treatment and clearing of infection.

4.1.2 Selection of methods for assessment of antimicrobial activity

Antibacterial substances can be considered in three categories based on the combination of their overarching mode of action and application: biocidal agents for external and environmental use, bactericidal drugs, and bacteriostatic drugs. Fast-acting biocidal agents rapidly kill bacteria and other organisms. Biocides are important in applications such as surface disinfection in healthcare settings but are unsuitable for systemic or prolonged topical use in humans and other animals. The maximum in-use contact time for such formulations is generally 1 min or less, during which a 3 log₁₀ reduction must occur in order for a disinfectant to be considered effective^[399]. Bactericidal antimicrobial drugs can be administered to humans and other animals and kill actively growing bacteria while causing minimal damage to the infected host. These are often used for severe or systemic infections and in immunocompromised patients^[400]. Finally, bacteriostatic agents effectively aid eradication of a localised microbial infection by preventing further growth of the causative organisms, allowing the previously inundated immune system to regain control.

As biocides are potentially used against metabolically inactive organisms on surfaces, their mechanism of action often involves causing physically disruptive damage to the cellular structure such as breaking open cell membranes^[401]. Conversely, bacteriostatic and bactericidal agents tend to target and halt microorganism-specific metabolic processes, preventing their growth or cell maintenance^[400]. Therefore, information on the bacteriostatic and bactericidal efficacy of metal ion and FNa combinations must be determined in order to assess their potential as novel topical antimicrobial formulations. Various assays can be utilised in order to assess the capability of agents or combinations

to act in these ways. Additional consideration with regards to assessment of whether the presence of either agent enhances or reduces the activity of the other must also be made.

As previously discussed in Chapter 3, the chequerboard assay was selected and optimised for the assessment of combined bacteriostatic efficacy of metal ions and FNa. This method can also be used to detect changes in efficacy of bactericidal antimicrobials. The effects of different metal counter-ions on the bacteriostatic activity of a representative metal ion in combination with FNa was also investigated using this method. A qualitative suspension test was used to initially assess whether biocidal activity was exerted by the combination of FNa and a representative metal ion. The suspension test was carried out in a range of solvents in order to investigate the effects of their variation on biocidal efficacy results. Finally, a kill kinetics assay was used to detect differences in speed of bacterial killing over time between a representative combination and each agent alone.

4.1.3 Aims and objectives

Aims: to identify metal ions which can enhance the antimicrobial activity of FNa and characterise whether the relationship(s) *in vitro* are bacteriostatic, bactericidal or biocidal, with particular interest in anti-GN efficacy.

Objectives:

- 1) To identify metal ions exhibiting bacteriostatic synergy in combination with FNa against *E. coli* and *S. aureus* reference strains.
- 2) To determine whether the counter-ion influences the combined bacteriostatic activity of a representative metal ion (Cu^{2+}) synergistic with FNa.
- 3) To investigate whether bacteriostatic synergy against *E. coli* correlates with biocidal activity of a representative metal ion (Cu^{2+}) and FNa.
- 4) To investigate whether the presence of FNa effects the *E. coli* kill kinetics of a biocidal metal ion (Cu^{2+}), representative of metals that synergise with FNa.

4.2 Methods

4.2.1 Bacteriostatic and bactericidal activity of sodium fusidate combined with metal salts

The chequerboard assay, as described in Chapter 2, Section 2.5, was used to test the activity of FNa against *E. coli* NCTC 10418 and *S. aureus* NCTC 12973 in combination with the following metal salts: $\text{Al}_2(\text{SO}_4)_3$, CoSO_4 , CuSO_4 , FeSO_4 , MnSO_4 , NiSO_4 , PdSO_4 , ZnSO_4 , CuCl_2 , $\text{Cu}(\text{NO}_3)_2$, and Cu D-glu. The highest concentration of FNa tested against *E. coli* and *S. aureus* was 1280 and 10 μM , respectively. Concentration ranges for the metal sulphates were selected as described in Section 3.3.4, page 67. CuCl_2 , $\text{Cu}(\text{NO}_3)_2$, and Cu D-glu were used at the same concentrations as determined for CuSO_4 . Percentage inhibition, $\text{MIC}_{90\text{s}}$, MBCs and $\text{FIC}_{90\text{I}}$ s were calculated as previously described (Sections 2.4 and 2.5).

The activity profiles of each metal sulphate and FNa combination were visually compared by plotting isobolograms of the concentration of FNa required to produce $\geq 90\%$ inhibition against each metal concentration, both converted to a percentage of their respective MIC_{90} . FNa and metal sulphate $\text{FIC}_{90\text{I}}$ s were assessed for synergy and antagonism. Finally, the concentration of FNa needed to produce $\geq 90\%$ growth inhibition in the presence of metal sulphates at 25 and 12.5 % of their respective $\text{MIC}_{90\text{s}}$ was determined from the chequerboard data and the fold reduction of FNa MIC_{90} calculated. Statistical significance of FNa MIC_{90} changes were ascertained using the 95 % CI ($p \leq 0.05$).

Comparison between activities of the different Cu(II) salts combined with FNa was performed in order to assess the effects of the different counter-ions. $\text{FIC}_{90\text{I}}$ s were calculated and compared. In addition, isobolograms of the concentration of FNa required to produce $\geq 90\%$ inhibition plotted against each metal concentration were constructed and the area under the curve (AUC) calculated to numerically compare the combined activity. Statistical significance of differences between AUCs with each Cu(II) salt was determined using the 95 % CI ($p \leq 0.05$).

4.2.2 Biocidal capability of sodium fusidate combined with copper(II) sulphate against *E. coli*

Biocidal capability of FNa and CuSO₄ was qualitatively investigated in a range of solvents against *E. coli* NCTC 10418 in order to determine whether the combination was able to enhance killing in the absence of bacteriological medium. The following solvent solutions were tested: PBS, HPLC grade water, 10 % v/v dimethyl sulphoxide (DMSO, Fisher Scientific, Loughborough, UK) in HPLC grade water and 10 % v/v MeOH in HPLC grade water. Prepared solvent solutions were sterilised by filtration (0.22 µm). Stock solutions of CuSO₄ and FNa were prepared in each solvent with one exception: CuSO₄ in sterile deionised water was used as a stock solution for tests in PBS to prevent formation and precipitation of insoluble copper phosphates^[402]. While PBS was included as an experimental solvent in order to investigate whether this interaction had any effect on antimicrobial activity with FNa, the possibility of precipitation prior to exposure was avoided.

All tests were carried out in sterile un-coated round-bottomed 96 well plates. For each agent, serial 10-fold dilutions were made using the test solvent solution. Final well concentrations of CuSO₄ ranged from 0.01 µM to 100 mM and FNa concentrations from 1 µM to 10 mM. CuSO₄ and FNa dilutions were added to the 96 well plate with their concentration gradients on opposing axes, as for the chequerboard assay, and mixed by gentle pipetting. Prepared plates were allowed to stand at 20 °C for 15-20 min and then inoculated with a suspension of *E. coli* NCTC 10418 in the test solvent solution to a final concentration of $5 \pm 3 \times 10^5$ CFU mL⁻¹. After inoculation, the plates were wrapped in laboratory film to reduce evaporation and left on a benchtop at 20 °C in a temperature controlled room for 6 h. Bacterial survival was determined qualitatively by plating a triplicate of 20 µL aliquots from every well onto NA and checking for growth of viable organisms after 18-24 h incubation at 37 °C. Resulting growth was categorised as present or absent.

The concentration of CuSO₄ required to produce complete killing in combination with each concentration of FNa was determined. In order to differentiate from the minimum bactericidal concentration (MBC) as determined by the microdilution or chequerboard assays in bacteriological growth medium, this 6 h 20 °C biocidal concentration was named the minimum complete-kill concentration (MCKC). The MCKC of CuSO₄ combined with FNa was plotted against FNa concentration and the 95 % CIs used to determine statistically significant differences ($p \leq 0.05$).

4.2.3 Effect of sodium fusidate on kill kinetics of copper(II) sulphate against *E. coli*

Kill-time assays were performed to investigate whether the presence of FNa had any impact on *E. coli* NCTC 10418 bactericidal kinetics by CuSO₄. Test solutions investigated were 1 mM FNa, 1 mM CuSO₄, 1 mM FNa + 1 mM CuSO₄, 2 mM FNa, 2 mM CuSO₄ and 2 mM FNa + 2 mM CuSO₄. Bacteria were suspended in sterile HPLC grade water and added to the test solutions and agent-free control to achieve an initial concentration of $1 \pm 5 \times 10^7$ CFU mL⁻¹. CFU counts were performed using the Miles & Misra method^[280] (see Section 2.3, page 46) immediately following inoculation and after 10 min, 30 min, 1 h, 2 h, 6 h and 24 h exposure at 20 °C in a temperature controlled room. The log₁₀ reduction was calculated for each replicate at each time point by subtracting the post-exposure log₁₀ CFU mL⁻¹ from the initial log₁₀ CFU mL⁻¹. Bacterial survival in the presence of FNa was compared to that in the paired agent-free controls using the 95 % CIs and statistically significant differences identified ($p \leq 0.05$). The log₁₀ reduction values for CuSO₄ alone and FNa + CuSO₄ were normalised to their paired agent-free and FNa alone controls, respectively. Statistically significant differences between CuSO₄ alone and in combination with FNa at each time point were assessed by comparing 95 % CIs ($p \leq 0.05$).

4.3 Results

4.3.1 Combined bacteriostatic activity of sodium fusidate and metal ions

The MIC_{90S} of FNa against *E. coli* NCTC 10418 and *S. aureus* NCTC 12973 were confirmed to be 320 µM and 312.5 nM, respectively, as previously determined during chequerboard optimisation (see Sections 3.3.1 and 3.3.2, pages 63 and 64).

4.3.1.1 FIC₉₀Is between metal ions and sodium fusidate

The FIC₉₀Is for Al³⁺, Fe²⁺ and Cu²⁺ with FNa against *E. coli* NCTC 10418 were found to be 0.229, 0.375 and 0.425, respectively, indicating synergy (Table 4.2). Conversely, Zn²⁺ and Mn²⁺ were antagonistic to FNa activity against *E. coli*, with FIC₉₀Is of 4.250 and 10.125, respectively. Interestingly, FIC₉₀Is for all five of these metal ions combined with

FNa against *S. aureus* fell within the indifference range, demonstrating little impact on anti-*S. aureus* FNa activity by their presence. Pd²⁺, however, strongly antagonised FNa against *S. aureus*, with an FIC₉₀I of 48.125, but did not affect *E. coli* susceptibility. Finally, Co²⁺ and Ni²⁺ exhibited neither FNa synergy nor antagonism against either organism.

Table 4.2 - FIC₉₀I for antimicrobial metal ions in combination with sodium fusidate against *E. coli* NCTC 10418 and *S. aureus* NCTC 12973, in order of anti-*E. coli* efficacy

	FIC ₉₀ I	
	<i>E. coli</i> NCTC 10418	<i>S. aureus</i> NCTC 12973
Aluminium sulphate	0.229 [§]	0.833
Iron(II) sulphate	0.375 [§]	1.250
Copper(II) sulphate	0.425 [§]	0.875
Cobalt(II) sulphate	0.594	1.250
Nickel(II) sulphate	0.628	0.525
Palladium(II) sulphate	1.250	48.125 [#]
Zinc(II) sulphate	4.250 [#]	1.500
Manganese(II) sulphate	10.125 [#]	0.725

green [§] = synergy (FICI ≤ 0.5), red [#] = antagonism (FICI > 4.0), grey = indifference (n = 3)

4.3.1.2 Metal ion and sodium fusidate isobolograms

Isobolograms for *E. coli* NCTC 10418 and *S. aureus* NCTC 12973 are shown in Figure 4.2 and Figure 4.3, respectively. None of the metal ion MIC₉₀s were increased by the presence of any concentration of FNa against either organism.

The *E. coli* isobologram (Figure 4.2) demonstrated that FNa activity was suppressed by Zn²⁺ and Mn²⁺, as indicated by the peaked shape of the curves. The presence of each concentration of Zn²⁺ and Mn²⁺ investigated increased the FNa MIC₉₀ to more than twice the MIC₉₀ of FA when alone. The isobolograms for Al³⁺, Cu²⁺ and Fe²⁺ illustrated synergy with FNa, as indicated by the FIC₉₀Is. Interestingly, the curve for Ni²⁺ also suggested a moderate synergy which may be reflected by the FIC₉₀I of 0.628. At 50 % its MIC₉₀, Pd²⁺ appeared to be purely additive to FNa activity, while antagonism occurred at some of the lower concentrations which also aligns with its FIC₉₀I of 1.250 (since an FICI of 1 is absolute additivity). Conversely, Co²⁺ appeared to exhibit synergy at 50 % its MIC₉₀ but antagonism at all lower concentrations, despite an FIC₉₀I of 0.594.

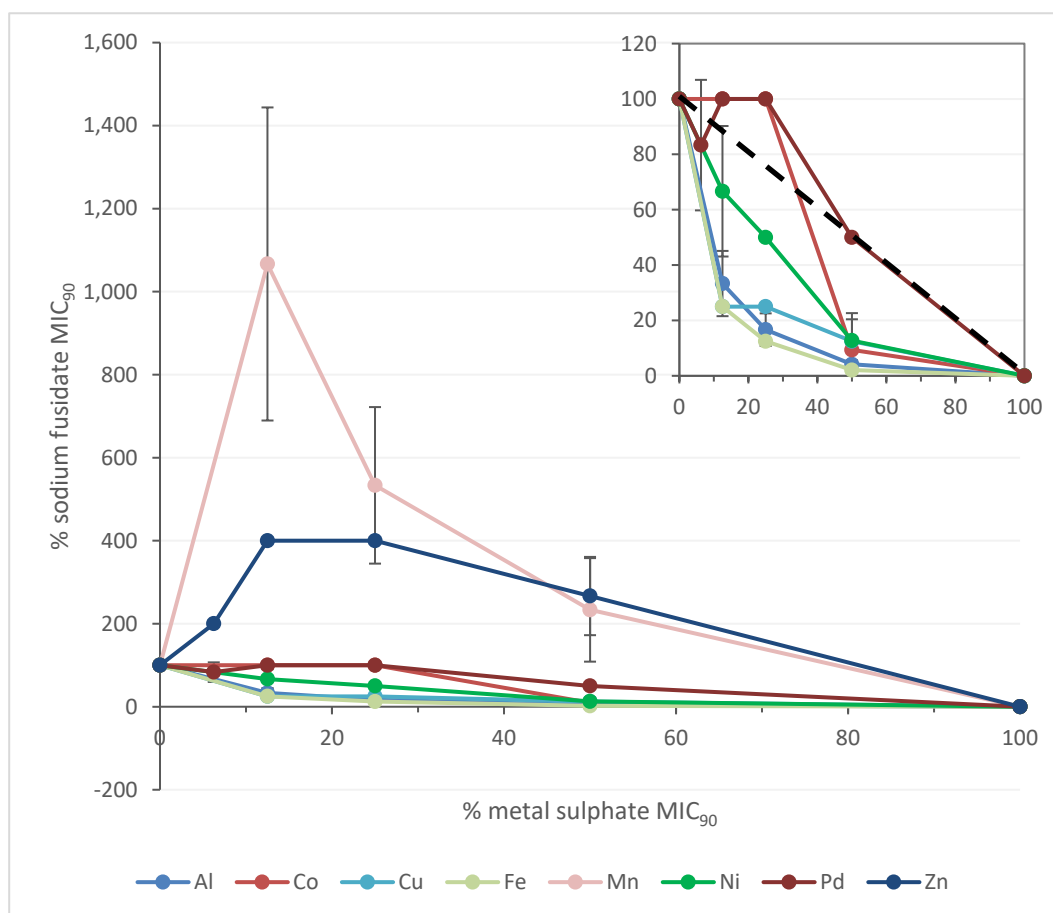


Figure 4.2 - Combined metal and sodium fusidate MIC₉₀s against *E. coli* NCTC 10418

Data is presented as % individual agent MIC₉₀ to allow visual comparison between metals. Each point illustrates mean % sodium fusidate MIC₉₀ required in combination with set metal concentration to produce 90 % inhibition. Insert is for clearer visualisation of otherwise obscured activity profiles. The dashed black line represents the line of additivity.
(n = 3, error bars = SD)

Figure 4.3 illustrates that the Pd²⁺ antagonism of FNa against *S. aureus* indicated by the FIC₉₀I of 48.125 was also suppression. The isobolograms of FNa with Al³⁺, Mn²⁺ and Ni²⁺ closely followed the line of additivity while FIC₉₀I of 0.833, 0.725 and 0.525, respectively, would suggest more difference between them. Similarly, the curve for Fe²⁺ illustrated synergy with FNa at 50 and 25 % the metal MIC₉₀ while Cu²⁺ was synergistic only at 50 % MIC₉₀ but their FIC₉₀I of 1.250 and 0.875, respectively, could suggest the inverse. However, Co²⁺ and Zn²⁺ curves indicated antagonism to FNa which FIC₉₀I of 1.250 and 1.500, respectively, also hinted.

While FICI cut-offs can be used to differentiate synergy, antagonism and indifference, the isobologram curves provide useful additional detail. This enables identification of suppressive combinations and information on particular concentrations of one agent which can enhance or antagonise the antimicrobial, activity of another.

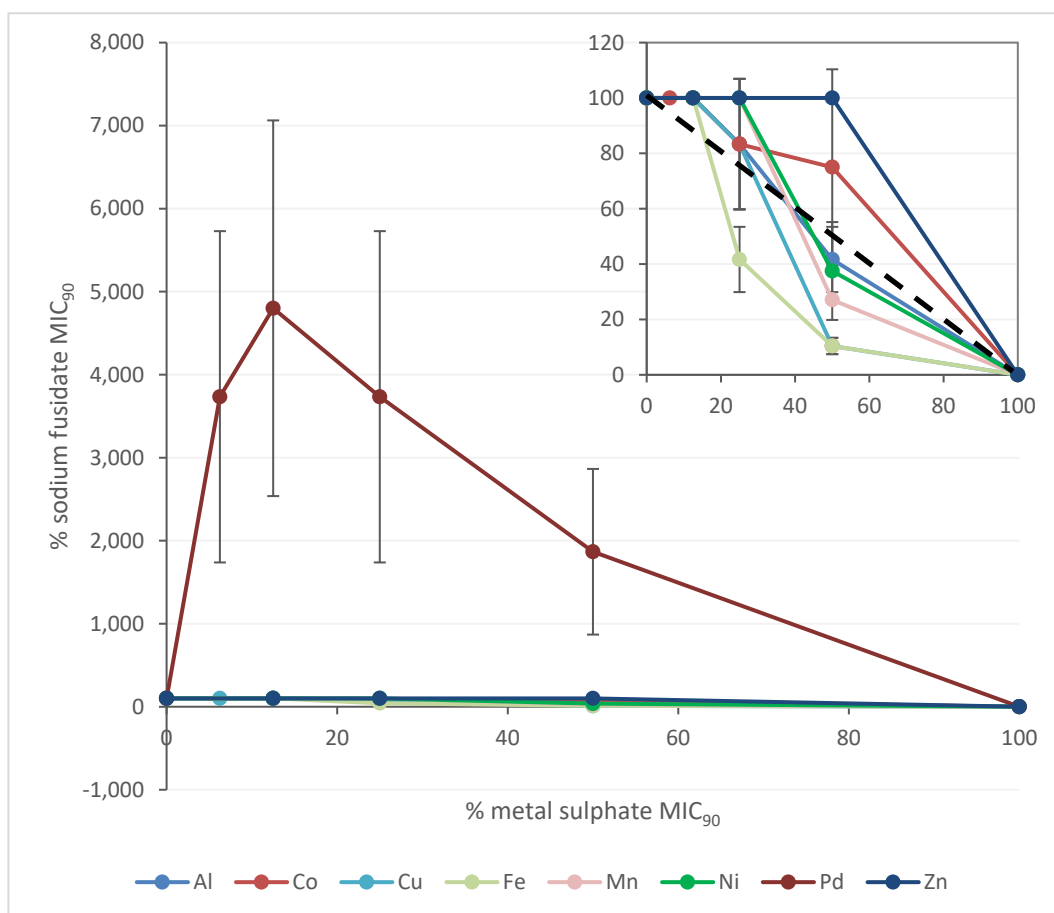


Figure 4.3 - Combined metal and sodium fusidate MIC₉₀s against *S. aureus* NCTC 12973
 Data is presented as % individual agent MIC₉₀ to allow visual comparison between metals. Each point illustrates mean % sodium fusidate MIC₉₀ required in combination with set metal concentration to produce 90 % inhibition. Insert is for clearer visualisation of otherwise obscured activity profiles. The dashed black line represents the line of additivity.
 (n = 3, error bars = SD)

4.3.1.3 Effect of sub-MIC₉₀ metal ion concentrations on sodium fusidate MIC₉₀

Figure 4.4 summarises fold reduction in FNa MIC₉₀ against *E. coli* NCTC 10418 and *S. aureus* NCTC 12973 in the presence of 25 and 12.5 % of each metal ion MIC₉₀. No statistically significant change in the MIC₉₀ of FNa against *S. aureus* was found when combined with either concentration of Al³⁺, Co²⁺, Cu²⁺, Mn²⁺, Ni²⁺ or Zn²⁺ ($p > 0.05$). There was also no significant change with 12.5 % the Fe²⁺ MIC₉₀ ($p > 0.05$) but, as observed on the isobologram (Figure 4.3), with 25 % Fe²⁺ MIC₉₀ the concentration of FNa required to produce ≥ 90 % inhibition decreased by a mean 2.67-fold ($p \leq 0.05$). The presence of Pd²⁺ at 25 and 12.5 % its MIC₉₀ produced a 0.04- and 0.03-fold reduction (equal to 25- and 33.3- fold increases, respectively) in FNa MIC₉₀ against *S. aureus* ($p \leq 0.05$), further illustrating the suppressive interaction.

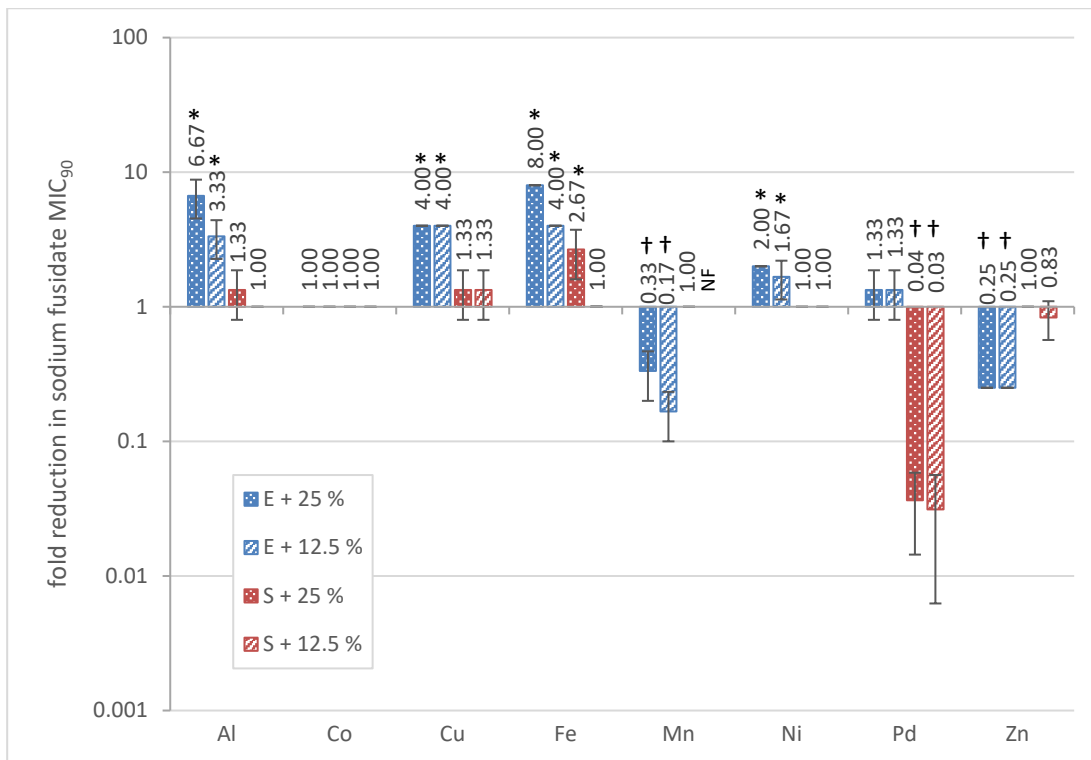


Figure 4.4 – Sodium fusidate MIC₉₀ fold reduction in the presence of 25 or 12.5 % metal ion MIC₉₀s

E + 25 % = *E. coli* NCTC 10418 in the presence of 25 % metal ion MIC₉₀

E + 12.5 % = *E. coli* NCTC 10418 in the presence of 12.5 % metal ion MIC₉₀

S + 25 % = *S. aureus* NCTC 12973 in the presence of 25 % metal ion MIC₉₀

S + 1.25 % = *S. aureus* NCTC 12973 in the presence of 12.5 % metal ion MIC₉₀

* = reduction in sodium fusidate MIC₉₀, † = increase in sodium fusidate MIC₉₀ ($p \leq 0.05$ for both)

NF = not found. (n = 3, error bars = 95 % CI, y axis is log₁₀ scale)

Only Co²⁺ and Pd²⁺ failed to exhibit statistically significant effect on FNa MIC₉₀ against *E. coli* ($p > 0.05$). Fold reductions of FNa MIC₉₀ in the presence of Al³⁺, Cu²⁺ and Fe²⁺ at 25 and 12.5 % the metal MIC₉₀ all fell within the ranges 4.0 to 8.0 and 3.3 to 4.0, respectively ($p \leq 0.05$). Ni²⁺ decreased the FNa MIC₉₀ to a lesser degree, by 2.0- and 1.67-fold when present at 25 and 12.5 % its MIC₉₀ ($p \leq 0.05$). Both Mn²⁺ and Zn²⁺ had the opposite effect, increasing the MIC₉₀ by between 3- to 6-fold at both concentrations investigated ($p \leq 0.05$).

4.3.2 Effect of the counter-ion on bacteriostatic activity of sodium fusidate combined with copper(II)

4.3.2.1 Copper(II) salt and sodium fusidate FIC₉₀ls

The MIC₉₀ and MBC of Cu²⁺ against each organism did not vary with counter-ion. When assessed by FIC₉₀l, the anion also had no effect on the antimicrobial interaction between

Cu²⁺ and FNa against either *E. coli* NCTC 10418 or *S. aureus* NCTC 12973 (Table 4.3). While there was some variation in FIC_{90I} values, all indicated synergy against *E. coli* and an indifferent effect against *S. aureus*.

Table 4.3 - FIC_{90I} for copper(II) salts in combination with sodium fusidate against *E. coli* NCTC 10418 and *S. aureus* NCTC 12973

	FIC _{90I}	
	<i>E. coli</i> NCTC 10418	<i>S. aureus</i> NCTC 12973
Copper(II) sulphate	0.375 [§]	1.250
Copper(II) chloride	0.375 [§]	0.563
Copper(II) D-gluconate	0.375 [§]	0.708
Copper(II) nitrate	0.458 [§]	0.917

green[§] = synergy (FICI ≤ 0.5), red[#] = antagonism (FICI > 4.0), grey = indifference (n = 3)

4.3.2.2 Isobologram analysis for sodium fusidate and copper(II) salts

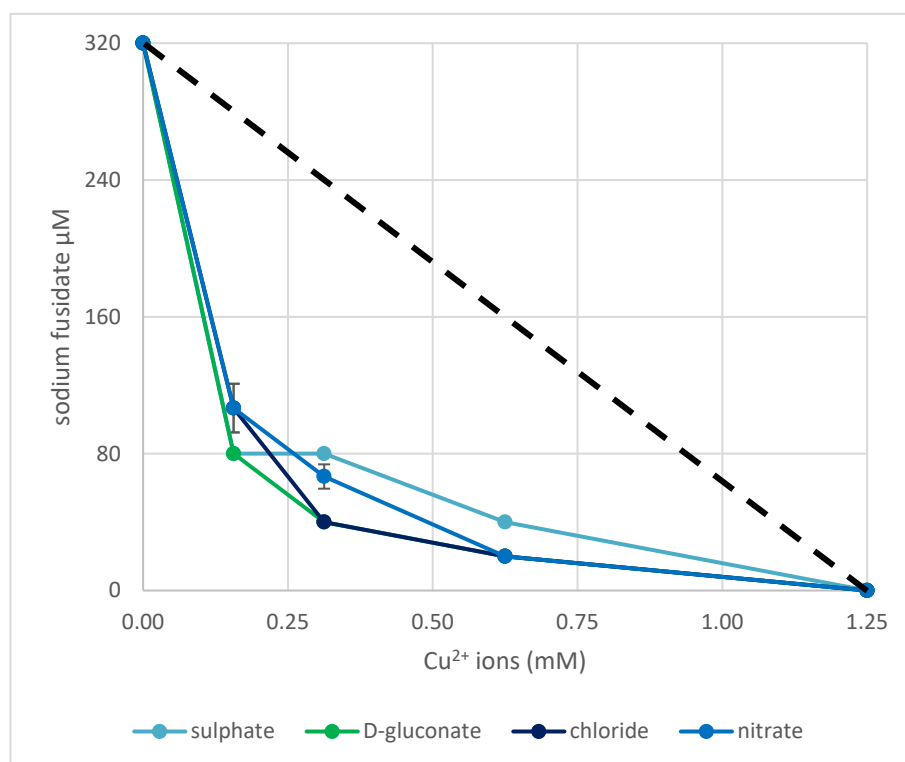


Figure 4.5 – Combined MIC_{90s} of sodium fusidate and copper(II) salts against *E. coli* NCTC 10418

The dashed black line represents the line of additivity.
(n = 3, error bars = SD)

Table 4.4 – Area under the isobologram curves for copper(II) salts combined with sodium fusidate against *E. coli* NCTC 10418

Salt	AUC (95 % CI)
D-gluconate	56.25 (56.25 – 56.25)
chloride	60.42 (53.75 – 67.08)
nitrate	66.67 (56.53 – 76.81)
sulphate	75.00 (75.00 – 75.00)

The isobolograms for all copper(II) salts tested with FNa were indicative of synergy against *E. coli* NCTC 10418 (Figure 4.5). However, comparison of AUCs illustrated some significant differences between total efficacy of the copper(II) salts (

Table 4.4). FNa with Cu D-glu and CuCl₂ produced isobologram AUCs of 56.25 and 60.42, respectively, both of which were significantly smaller than 75.0 with CuSO₄ ($p \leq 0.05$) indicating greater antimicrobial efficacy. The AUC for Cu D-glu was also significantly smaller ($p \leq 0.05$) than that with Cu(NO₃)₂ which fell between CuCl₂ and CuSO₄ at 66.67.

Table 4.4 lists the copper(II) salts in approximate order of efficacy in combination with FNa against *E. coli*.

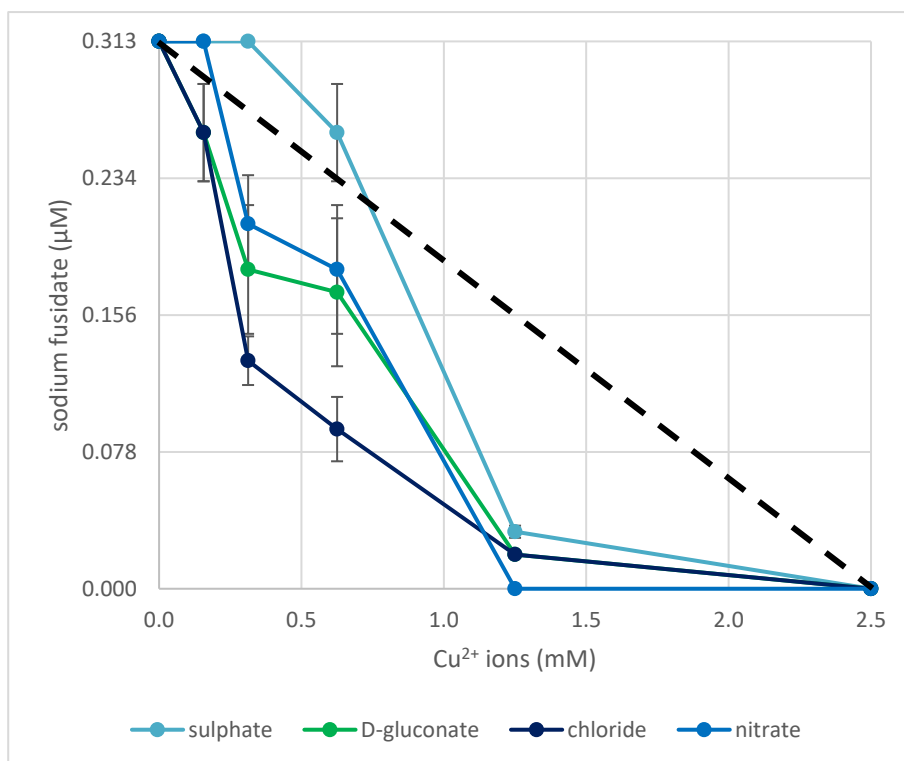


Figure 4.6 - Combined MIC_{90s} of sodium fusidate and copper(II) salts against *S. aureus* NCTC 12973

The dashed black line represents the line of additivity.
(n = 3, error bars = SD)

Table 4.5 – Area under the isobologram curves for copper(II) salts combined with sodium fusidate against *S. aureus* NCTC 12973

Salt	AUC (95 % CI)
chloride	0.189 (0.110 – 0.268)
nitrate	0.267 (0.117 – 0.416)
D-gluconate	0.287 (0.112 – 0.462)
sulphate	0.421 (0.328 – 0.514)

Figure 4.6 illustrates that both CuCl₂ and Cu D-glu synergise with FNa against *S. aureus* NCTC 12973 on isobologram assessment. The curve with Cu(NO₃)₂ also fell primarily below the line of additivity suggesting possible synergy while CuSO₄ is least active.

Table 4.5 lists the copper(II) salts in approximate order of efficacy in combination with FNa against *S. aureus*. As against *E. coli*, FNa combined with CuSO₄ produced the largest AUC against *S. aureus* indicating it was the least active of the copper(II) salts tested. CuCl₂ produced the most *S. aureus* inhibition in combination with FNa with an AUC significantly smaller than CuSO₄ ($p \leq 0.05$). Cu(NO₃)₂ and Cu D-glu fell between CuCl₂ and CuSO₄ and were not significantly different to one another or either of the extremes ($p > 0.05$). The combined antimicrobial activity of metal salts and FNa therefore appears to be slightly affected by different counter-ions.

4.3.3 Investigations into bactericidal activity of sodium fusidate combined with copper(II) sulphate

4.3.3.1 Combined MBCs of metal ions and sodium fusidate

For all metal ions tested, the MBC against *E. coli* NCTC 10418 and *S. aureus* NCTC 12973 was not modulated by the presence of any concentration of FNa. Similarly, the FNa MBC against *S. aureus* NCTC 12973 remained the same in the presence of most metals. The exceptions were Pd²⁺, which increased the FNa MBC to 10 µM when present at 39.1 µM and to >10 µM at ≥78.1 µM, and Ni²⁺, which decreased the FNa MBC by one two-fold dilution when at ≥625 µM. Although the MBC of FNa alone against *E. coli* NCTC 10418 could not be determined, Al³⁺ and Fe²⁺ both produced a combined MBC of 625 µM metal ions and 320 µM FNa. No other metals lowered the FNa MBC to within the detectable range.

4.3.3.2 Biocidal capability of sodium fusidate combined with copper(II) sulphate against *E. coli*

The 6 h minimum complete-kill concentration (MCKC) of CuSO₄ alone against *E. coli* NCTC 10418 showed a high level of variability between solvents, ranging from 0.83 μM in 10 % MeOH to 23.3 mM in PBS (Table 4.6) with a statistically significant difference between all solvents ($p \leq 0.05$). None of the agent-free solvents or any concentration of FNa tested alone was biocidal in any of the solvents over the same exposure period.

Table 4.6 - MCKC of copper(II) sulphate against *E. coli* NCTC 10418 after 6 h room temperature incubation in a range of solvents

Solvent	CuSO ₄ MCKC (μM ± SD)
10 % MeOH	0.833 ± 0.236
HPLC grade water	2.33 ± 1.89
10 % DMSO	350.00 ± 212.13
PBS	23,333.33 ± 18856.18

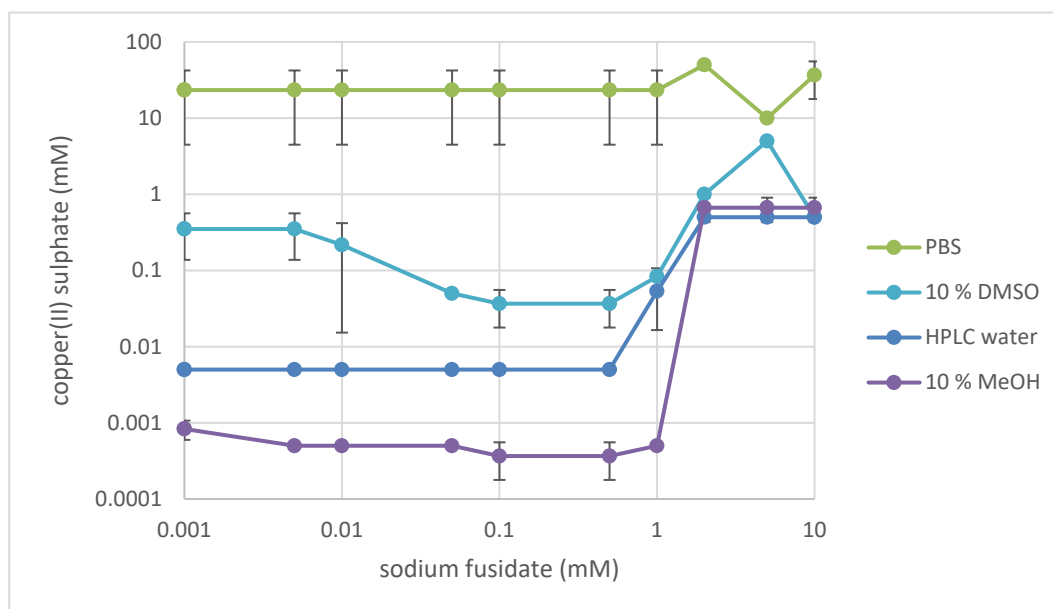


Figure 4.7 - Concentrations of copper(II) sulphate required to kill *E. coli* NCTC 10418 in the presence of sodium fusidate after 6 h exposure in a range of solvents (n = 3, error bars = SD)

The MCKC of CuSO₄ in the presence of a range of FNa concentrations is presented in Figure 4.7. Regardless of solvent, the concentration of CuSO₄ needed for biocidal activity in combination with 10 mM FNa was higher than with ≤1 mM FNa, however, the difference was not statistically significant in PBS. In 10 % DMSO there appeared to be a pattern of decreasing CuSO₄ MCKC as FNa concentration increased from 1 μM to 100 μM, followed by an increase with FNa from 100 μM to 5 mM. A similar but less pronounced trend was also suggested in 10 % MeOH, whereas CuSO₄ MCKCs in HPLC

grade water and PBS remained constant in the presence of ≤ 0.5 and ≤ 1 mM FNa, respectively.

4.3.3.3 *E. coli* kill-time kinetics of combined copper(II) sulphate and sodium fusidate

There was no significant difference between *E. coli* NCTC 10418 survival in 1 or 2 mM FNa and the paired agent-free controls at each time point ($p > 0.05$). Mean \log_{10} reduction across all controls and time points was 0.28, ranging from -0.28 to 1.38, whereas \log_{10} of the initial CFU concentration was 6.90 (range 6.34 to 7.46).

Complete killing was achieved by all CuSO_4 -containing solutions within 4 h (Figure 4.8). After 10 min, 30 min and 1 h exposure, there was no significant difference between proportion of *E. coli* killed by CuSO_4 alone or in the presence of FNa at the same concentration ($p > 0.05$). However, there were some differences in efficacy of the different concentrations. After 30 min and 1 h exposure, 1 mM CuSO_4 alone killed 61.9 and 63.2 % *E. coli* cells whereas 2 mM killed only 35.2 and 48.0 %, respectively ($p \leq 0.05$). The mean \log_{10} reduction at 10 min was also greater with 1 mM than 2 mM CuSO_4 , however, this difference was not significant. When combined with equimolar FNa, 2 mM CuSO_4 killed only 22.2 % *E. coli* after 30 min but 1 mM killed 56.5 % ($p \leq 0.05$). In addition, 49.2 % *E. coli* was killed after 2 h exposure to 2 mM FNa combined with 2 mM CuSO_4 which demonstrated significantly reduced biocidal efficacy compared to 74.9 % produced by the same concentration of CuSO_4 alone.

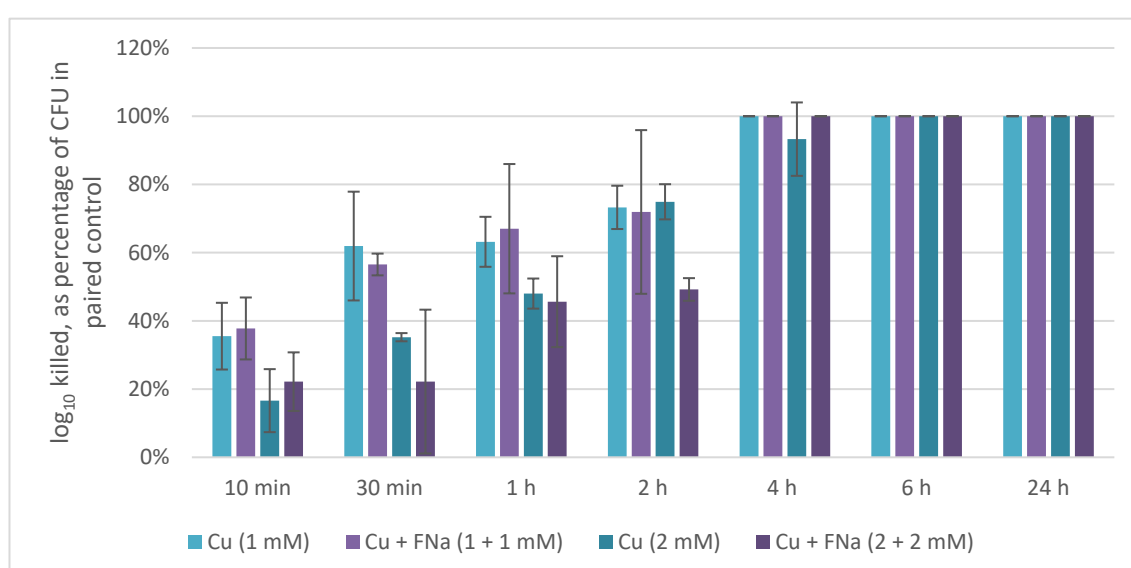


Figure 4.8 - Percentage of \log_{10} *E. coli* NCTC 10418 killed by copper(II)sulphate with or without sodium fusidate in HPLC grade water at 20 °C

Individual replicate values were normalised to their paired metal-free controls.

(n = 3, error bars = 95 % CI)

4.4 Discussion

4.4.1 Links between antimicrobial mechanisms of metal ions and their effect on sodium fusidate activity

Not all antimicrobially active metal ions tested had the same effect on bacteriostatic efficacy when combined with FNa. Since metal ions exert their activity *via* different routes, variability in FNa-combined activity profile could be due to the differences in individual metal ion modes of action.

4.4.1.1 Metal ions antagonistic and suppressive to sodium fusidate anti-*E. coli* activity

Based on known antimicrobial mechanisms (as detailed in Section 4.1.1), it appears that metal ions which reduce FNa activity against *E. coli* may be capable of enhancing efflux. Mn²⁺ suppressed the activity of FNa against *E. coli* producing an FIC_{90l} of 10.125 (Table 4.2, page 87) and increased the concentration of FNa required to inhibit growth when present at any of the sub-MIC₉₀ concentrations tested (Figure 4.2, page 88). Conversely, Mn²⁺ had very little effect on the activity of FNa against *S. aureus* (Figure 4.3, page 89). While there are no reports on the specific effects of Mn²⁺ on efflux activity, exposure to sub-inhibitory concentrations is known to upregulate many cellular processes in *E. coli* including electron transport, ribosomal turnover, cell division and membrane biogenesis^[360]. On the other hand, effects on *S. aureus* are strictly limited to downregulation of Mn²⁺ uptake and upregulation of Mn²⁺ efflux^[403] affording effective homeostasis. Mn²⁺ is a micronutrient which is known to be utilised by *E. coli* in direct detoxification of ROS^[337], and as a co-factor to both superoxide dismutase which detoxifies oxygen radicals^[161] and the penicillin binding protein complex which catalyses the final peptidoglycan cross-linking step in cell wall assembly^[404]. It is also required as a co-factor in ubiquinone-8 (Q8) biosynthesis^{[404],[405]}. Q8 is the substrate for all three respiratory cytochrome complexes (ubiquinone oxidases) in the *E. coli* electron transport chain^[406] which produces the inner membrane PMF^[407]. PMF is not only utilised in ATP production but also many membrane functions including powering AcrB, the substrate recognition and extrusion subunit of the FNa efflux pump^{[142],[408]}. The presence of Mn²⁺ may, therefore, also enable increased AcrAB-TolC activity due to the upregulated electron transport activity. A wide variety of metabolites have also been shown to increase expression of AcrAB-TolC^[409], therefore, enhancement of any of the many

metabolic pathways Mn^{2+} induces may further contribute to increased FNa efflux while enhancing bacterial growth.

Zn^{2+} was also suppressive to anti-*E. coli* activity of FNa with an FIC_{90} of 4.250 (Table 4.2, page 87). Like Mn^{2+} , Zn^{2+} is also a co-factor for Q8 biosynthesis^{[404],[405]} which may increase AcrAB-TolC activity. In addition, Zn^{2+} induces expression of MdtABC-TolC, another RND efflux pump^[388]. MdtABC-TolC can export Zn^{2+} as well as a range of antimicrobial compounds, bile salts and surfactants^[151]. There is also evidence that FNa can be an MdtABC-TolC substrate^[410]. The expression of MdtABC-TolC is usually at a much lower level than AcrAB-TolC with the latter being responsible for the bulk of FNa efflux^[410]. However, induction of MdtABC-TolC expression by Zn^{2+} may be substantial enough to contribute to FNa tolerance. In addition, the ability of Zn^{2+} to interfere with translation by targeting RNA and ribosomes may trigger increased transcription and ribosomal production or turnover. This could contribute to lowered FNa susceptibility by increasing translation and releasing FNa from stalled ribosomes. Sub-MIC Zn^{2+} has also been shown to elicit a heterogeneous response in *E. coli* populations, resulting in stalled growth or death of some cells while others already expressing Zn^{2+} exporters continue to reproduce^[411]. This may explain why Zn^{2+} was not found to be as effective an FNa suppressant as Mn^{2+} in these experiments despite additional mechanisms which may afford tolerance. Finally, Zn^{2+} neither enhanced nor reduced FNa activity against *S. aureus* when at sub-MIC₉₀ concentrations, which aligns with the less complex homeostasis mechanisms present in GP organisms^[412].

4.4.1.2 Metal ions eliciting neither an antagonistic nor synergistic effect when combined with sodium fusidate against *E. coli*

Pd^{2+} did not suppress or enhance anti-*E. coli* FNa activity (Figure 4.2, page 88). There was evidence of antagonism at lower Pd^{2+} concentrations on the isobologram while at 50 % the MIC₉₀, the combined activity with FNa was strictly additive. It is likely that on exposure to lower concentrations the induced stress response in *E. coli* can compensate for any Pd^{2+} -related damage leaving only the inhibitory effects of FNa to be observed. Furthermore, the additivity of inhibition caused by 50 % Pd^{2+} MIC₉₀ and FNa indicates there is unlikely to be any interaction or cross-over between the two agents' mechanisms of anti-*E. coli* activity. Conversely, Pd^{2+} was very suppressive to the activity of FNa against *S. aureus*, producing an FIC_{90} of 48.125 (Table 4.2, page 87 and Figure 4.3, page 89). There is a possibility that Pd^{2+} can induce an undiscovered metabolic pathway or cellular process able to afford high-level resistance to FNa in *S. aureus*. However, the observed bacterial growth was enhanced to such an extent and the mechanism of FNa activity is well enough understood that it seems unlikely the suppression was due to the

biochemical activity of Pd²⁺ alone. A more plausible explanation may be due to a combination of Pd²⁺ properties. Firstly, the presence of the metal ions and induction of stress responses increases the growth rate of *S. aureus*. Secondly, since Pd²⁺ is well known to form complexes at N, S, P and/or O co-ordination sites, Pd²⁺ may spontaneously co-ordinate fusidate, forming complexes unable to diffuse through the bacterial membrane and effectively concealing FNa from the bacterial cells. Concentration combinations of 2:1, 1:1 and 1:2 FNa : Pd²⁺ were particularly ineffective, which may be indicative of binding ratios. Alternatively, Pd²⁺ may bind to the exposed peptidoglycan of the GP cells, possibly trapping FNa to prevent its access to the cell. The latter scenario may be more likely since no antagonistic or suppressive effects were observed against *E. coli* with its shielded cell wall.

The combination of FNa and Co²⁺ was neither synergistic nor antagonistic against *E. coli* with an FIC₉₀ of 0.594 (Table 4.2, page 87). However, the isobologram suggested a biphasic activity (Figure 4.2, page 88). The highest sub-MIC₉₀ Co²⁺ concentration lowered the FNa MIC₉₀ while 25 % Co²⁺ MIC₉₀ and below had no effect on the concentration of FNa required to produce inhibition. This may be explained by the bacterium's ability to maintain both FNa efflux and Co²⁺ homeostasis in the presence of the lower Co²⁺ concentrations but not at 50 % MIC₉₀. At this concentration, the combined requirements for FNa and Co²⁺ efflux likely overwhelms ATP production capacity and available reserves, compounded by the effects of Co²⁺ on the normal aerobic electron transport chain respiration^[326], the function of Fe-containing enzymes^[323] and ROS generation^[325], along with FNa inhibition of protein synthesis. *S. aureus* displayed less sensitivity to the addition of Co²⁺ at 50 % MIC₉₀ (Figure 4.3, page 89), possibly because of its lack of FNa efflux pump allowing sole defensive investment in Co²⁺ removal. However, sub-MIC₉₀ Co²⁺ concentrations tested did moderately reduce the FNa MIC₉₀. The most likely explanation is the competition for ATP and other resources between ribosome turnover and Co²⁺ homeostasis.

Ni²⁺ was neither antagonistic nor synergistic to FNa activity against either organism, with FIC₉₀s of 0.628 for *E. coli* and 0.525 for *S. aureus* (Table 4.2, page 87). Nonetheless, the isobologram did reveal some enhancement of activity against *E. coli* compared to the line of absolute additivity (Figure 4.2, page 88). Both Co²⁺ and Ni²⁺ exert their antimicrobial activity *via* protein disruption, DNA damage, transcription inhibition and ROS generation. Both are also managed by the same metal homeostasis systems and effluxed by RcnA. However, although Co²⁺ also interferes with ribosome assembly while Ni²⁺ does not, Ni²⁺ has been shown to produce ROS inside *E. coli* cells at a significantly higher rate than Co²⁺ ^[331]. Increased oxidative stress may explain the greater impact on FNa MIC₉₀ in the presence of more sub-MIC₉₀ Ni²⁺ concentrations compared to Co²⁺.

4.4.1.3 Metal ions that synergise with sodium fusidate against *E. coli*

Cu^{2+} , Fe^{2+} and Al^{3+} all synergised with FNa against *E. coli* with $\text{FIC}_{90\text{Is}}$ of 0.425, 0.375 and 0.229, respectively (Table 4.2, page 87). All three also target the lipids of bacterial membranes. This suggests that membrane damage and the resulting permeability changes enhances FNa activity against GN organisms, as hypothesised. In addition, Cu^{2+} , Fe^{2+} and Al^{3+} can all cause protein damage. While there are no reports of membrane-specific protein damage by Cu^{2+} or Fe^{2+} , if these ions can injure intracellular proteins, they can presumably do the same to membrane proteins *via* the same mechanisms. Such protein damage may contribute to membrane disorganisation or efflux pump inhibition.

However, Pd^{2+} and Zn^{2+} also cause membrane and protein damage and did not synergise with FNa against *E. coli*. The binding chemistry of Pd^{2+} may explain its lack of synergistic activity with FNa. Once Pd^{2+} injures the OM and accesses the periplasmic space, it may be adsorbed onto the cell wall peptidoglycan, as hypothesised for *S. aureus*. This could mean FNa can more readily access the periplasm and migrate through the IM, resulting in the additive effect of the combination observed against *E. coli*. Al^{3+} is also known to be adsorbed onto peptidoglycan and exhibited similar antimicrobial efficacy to Pd^{2+} when combined with FNa at equivalent concentrations. However, insufficient data was generated to draw an adequate comparison between equimolar Al^{3+} and Pd^{2+} due to the differences in $\text{MIC}_{90\text{s}}$ and consequent concentration ranges utilised experimentally. Zn^{2+} , on the other hand, suppressed FNa activity against *E. coli* despite being known to cause damage to membrane lipids. The possible mechanisms of FNa activity suppression by Zn^{2+} have already been discussed (Section 4.4.1.1) and their impact is clearly sufficient to overcome the presumably detrimental membrane damage.

Both Cu^{2+} and Fe^{2+} are also known to generate ROS, as discussed in Sections 4.1.1.3 and 4.1.1.4, which puts considerable stress on the bacterial cell. However, Al^{3+} is not known to do the same, but synergises more strongly with FNa than either Cu^{2+} or Fe^{2+} . The combined efficacy of FNa and metal ions is clearly more complex than the sum of their antimicrobial mechanisms.

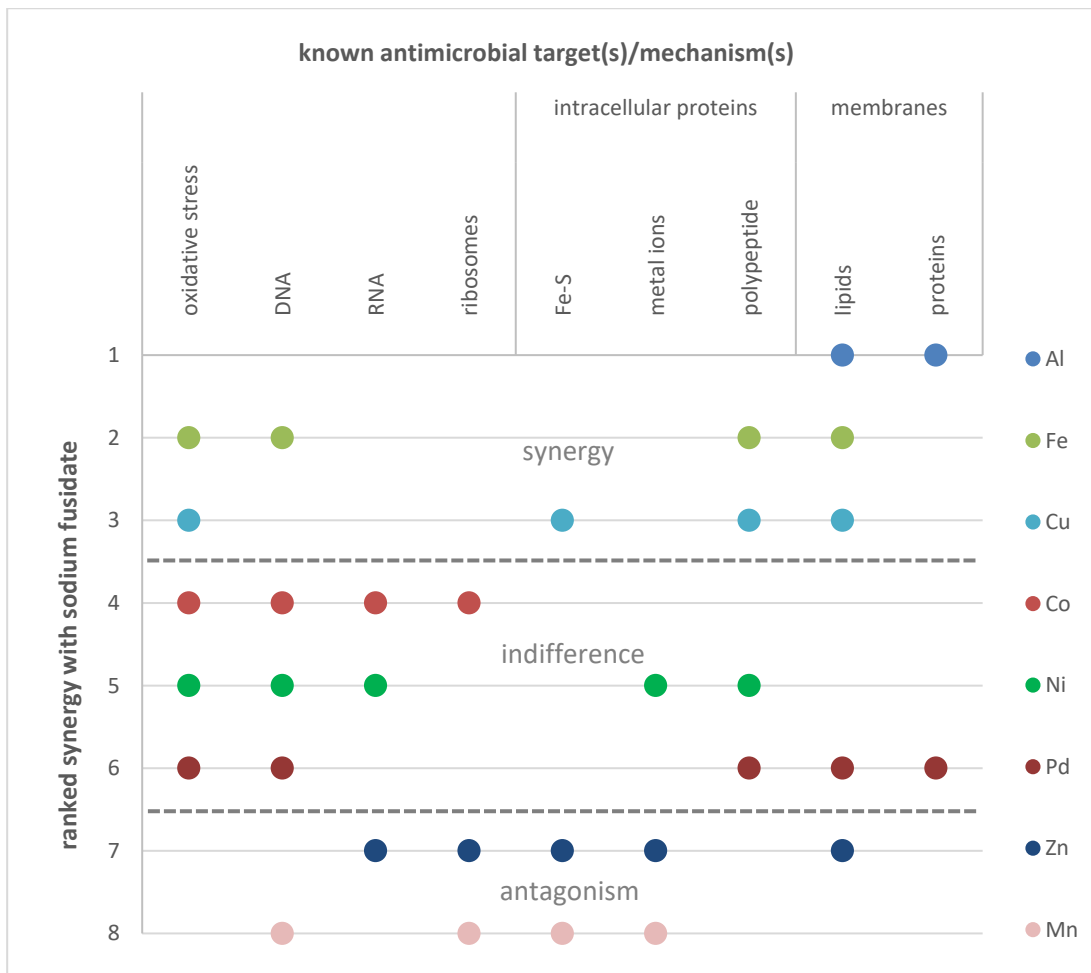


Figure 4.9 - Known antimicrobial targets or mechanisms of metal ions and their ranked co-operativity with sodium fusidate against *E. coli* NCTC 10418

Figure 4.9 was constructed to illustrate the lack of clear correlation between known metal ion mechanisms and their ability to enhance FNa activity against *E. coli*. It appears that membrane damage, possibly to both lipids and proteins, is likely to contribute to the combined activity but cannot solely explain the interactions. As already indicated, antimicrobial metal ion mechanisms are complex and multi-faceted. In addition to the specific targets and processes discussed, generalised stressors can influence bacterial responses to metal ions. Reduced pH is one such stressor which may be particularly relevant with the limited buffering of NB used in these experiments.

4.4.2 Effect of the copper(II) salt counter-ion on anti-*E. coli* activity in combination with sodium fusidate

In combination with FNa, Cu D-glu was more effective against *E. coli* than $\text{Cu}(\text{NO}_3)_2$ or CuSO_4 (Figure 4.5, page 91). This may be because *E. coli* can utilise gluconate as a

carbon source by switching on the Entner-Doudoroff pathway^[413]. It has been long established that antimicrobial activity tends to be most potent during the log phase of bacterial growth, where cells are growing and dividing at their maximum rate^{[414],[415]}. Somewhat paradoxically, the increased metabolic activity afforded by the addition of gluconate may therefore result in greater FNa-mediated inhibition of *E. coli* growth. Alternatively, differences in pH of the Cu²⁺ salts in NB may influence the antimicrobial effect by exerting various degrees of concomitant acidic stress.

CuSO₄ was the least efficacious of the four salts tested against *S. aureus* when combined with FNa (Figure 4.6, page 92). As observed during chequerboard optimisation (see Chapter 3, Section 3.3.5), *S. aureus* exhibited some sensitivity to high concentrations of Na₂SO₄. In an inverse manner to the hypothesised effects of gluconate on *E. coli* growth, concurrent growth inhibition by another agent could reduce FNa efficacy. On the other hand, this may be another manifestation of the differences in pH produced by the Cu(II) salts in NB. If CuSO₄ is the least acidic Cu(II) salt in NB it will exert less acid stress than the other salts. This could result in less growth inhibition overall by eliminating or reducing the impact of acid stress on the combined antimicrobial activity. In addition, GP tolerance of acidic environments is generally greater than GN which may explain the differences in susceptibility patterns between species.

4.4.3 Anti-*E. coli* biocidal activity of copper(II) sulphate and sodium fusidate

No bactericidal synergy was found with Cu²⁺ and FNa against either *E. coli* or *S. aureus* by chequerboard assay. However, the biocidal efficacy against *E. coli* was investigated in order to explore the effects of FNa and various solvents on Cu²⁺ activity.

4.4.3.1 Effect of sodium fusidate on the biocidal activity of copper(II) sulphate

The observed degree of *E. coli* killing by combined 1 mM FNa and 1 mM Cu²⁺ at each timepoint was no greater than that by the same concentration of Cu²⁺ alone (Figure 4.8, page 95). This indicates that the biocidal activity of the 1 mM combination in room temperature water was due solely to the activity of Cu²⁺ and there was no modulation by the presence of FNa. This is to be expected since the bacteriostatic effects of FNa are only observed against growing organisms while bacteria suspended in water are likely to have a very slow or inactive metabolism. Interestingly, 2 mM Cu²⁺ alone was not as effective as 1 mM after 30 min or 1 h ($p < 0.05$). The higher Cu²⁺ concentration may be

less injurious at first because it is likely to induce a more rapid upregulation of homeostatic mechanisms in response to the greater initial influx of Cu^{2+} into the cell. However, by 2 h, the cells become just as overwhelmed as those with a slower response on exposure to 1 mM ($p > 0.05$). Interestingly, after 2 h exposure, 2 mM FNa and 2 mM Cu^{2+} was significantly less effective than 2 mM Cu^{2+} alone ($p < 0.05$), indicating a protective effect of FNa. This may be through membrane stabilisation. FNa is known to readily incorporate into lipid bilayers^{[416]–[418]} and at the higher concentration of 2 mM, FNa inclusion could be sufficient to protect membrane integrity and reduce disruption by Cu^{2+} .

4.4.3.2 Effects of different solvents on biocidal activity of copper(II) sulphate combined with sodium fusidate

Despite differences between the tested solvents, the 6 h exposure biocidal activity of Cu^{2+} against *E. coli* was also modulated by higher concentrations of FNa in all but one (Figure 4.7, page 94). Only in PBS was there no effect of FNa concentration on the amount of Cu^{2+} required to kill *E. coli* ($p > 0.05$). This was likely due to the relative ineffectiveness of Cu^{2+} in PBS, presumably because of phosphate binding producing an antimicrobially inactive precipitate.

Compared to water, Cu^{2+} was more effective at killing *E. coli* in 10 % MeOH and less effective in 10 % DMSO ($p < 0.05$). Increased Cu^{2+} efficacy in 10 % MeOH is likely due to the effect of MeOH on the *E. coli* OM. MeOH and other alcohols are known to increase the fluidity of phospholipid membranes^{[419],[420]}. Increased fluidity results in increased permeability and would therefore facilitate Cu^{2+} entry to the periplasm. The addition of ≤ 1 mM FNa had no impact on Cu^{2+} activity in 10 % MeOH ($p > 0.05$), whereas > 1 mM reduced Cu^{2+} efficacy ($p < 0.05$). This again implies a membrane stabilising effect induced by FNa at higher concentrations. DMSO is also known to penetrate and stabilise phospholipid bilayers^{[421]–[423]}. This characteristic, in contrast to the destabilising effect of MeOH, likely explains the decreased sensitivity of *E. coli* to Cu^{2+} in 10 % DMSO compared to 10 % MeOH. FNa concentrations of > 1 mM appeared to have a similar membrane stabilising effect in 10 % DMSO to those observed in water or 10 % MeOH, necessitating higher Cu^{2+} to kill *E. coli* than with lower FNa concentrations. However, the presence of 0.05 to 1 mM FNa resulted in reduced Cu^{2+} tolerance compared to < 0.05 or > 1 mM FNa in 10 % DMSO. While unexpected, this may be an artefact of interaction between DMSO and FNa within the membranes resulting in less stabilisation and more Cu^{2+} access. These observations highlight the complexities and dependency of antimicrobial activity on the solvent or growth medium.

4.5 Conclusions

The major conclusions drawn from the work in this Chapter can be summarised as follows:

- 1) Al^{3+} , Fe^{2+} and Cu^{2+} exhibit bacteriostatic synergy in combination with FNa against *E. coli* NCTC 10418, an organism intrinsically resistant to FNa.
- 2) None of the eight metal ions tested synergised with FNa against FNa-sensitive *S. aureus* NCTC 12973.
- 3) No bactericidal or biocidal synergy was detected against either *E. coli* NCTC 10418 or *S. aureus* NCTC 12973.
- 4) The counter-ion may impact bacteriostatic synergy between metal salts and FNa against *E. coli* NCTC 10418 due to impact on pH or bacterial utilisation.
- 5) The mechanism of anti-*E. coli* synergy with FNa appears to involve metal ion-mediated membrane damage; however, the role of other factors such as pH require further examination.

Chapter 5: Sodium fusidate solution

chemistry and effect on anti-
***E. coli* activity**

5.1 Introduction

As discussed in Chapter 4, the mechanism of the antimicrobial synergy discovered between FNa and the metal ions Al^{3+} , Fe^{2+} and Cu^{2+} is unclear. We have already established that metal ions exhibit multiple antimicrobial mechanisms independently (Chapter 4) but can also form complexes that sometimes increase the activity of antimicrobial agents (Chapter 1). In addition, metal ions can lower the pH of aqueous solutions which may cause pH stress in bacteria, affect the solvation of FNa or both. In this Chapter, the role of chemistry-based factors in the anti-*E. coli* activity of FNa and metal ion combinations are explored.

5.1.1 Spontaneous complexation between metal ions and antimicrobials

Al^{3+} has well known and extensive binding properties and is used commercially as a mordant in fixing dyes to fabrics and binds to organic molecules such as polyphenolics^[424]. Al^{3+} readily coordinates O-donor sites^[425] and has been found to form complexes with the cephalosporin cefodizime^[426] and the fluoroquinolones ciprofloxacin and norfloxacin^[427], all without altering their antimicrobial efficacy. In fact, Al^{3+} complexes of ciprofloxacin and norfloxacin were shown to be much more soluble than the parent drugs, a characteristic advantageous to systemic administration^[428]. Coordination complexes of Cu^{2+} have been much more thoroughly explored than those of Al^{3+} . In particular, Cu^{2+} spontaneously complexes several antimicrobial drugs in aqueous solution at room or physiological temperatures, including streptomycin^[429], cycloserine and novobiocin^[430], ciprofloxacin^{[259],[350],[351]} and a variety of cephalosporins^[347]. Many of these complexes were also found to have at least equal activity to the parent drug when tested against a diverse panel of GP and GN bacteria^{[259],[350],[351],[429],[430]}. However, the efficacy of cephalosporins against both GP and GN organisms was reduced by Cu^{2+} complexation^[347], presumably due to structural changes resulting in lower affinity for the PBP binding site. The same workers found that Fe-cephalosporin complexes also spontaneously formed in aqueous solution, but with similar antimicrobial results^[347]. Fe^{2+} also spontaneously complexes ciprofloxacin in room temperature water-EtOH mixture^[431]. Other Fe^{2+} complexes of antimicrobials have been generated and studied for their efficacy; however, synthesis was carried out in organic solvents or dry alcohols^{[426],[431]}, presumably to maintain the preferred Fe species.

The observed synergy between FNa and Al^{3+} , Cu^{2+} and Fe^{2+} could be due to similar spontaneous formation of coordination complexes. Such a complex may be more active than the parent *via* several mechanisms. For example, complexation may modify drug solubility which could enhance membrane passage by creating a system with increased thermodynamic activity. It may also modulate transport of the parent drug, if relatively weak, the complex may dissociate intracellularly, delivering the toxic metal to vulnerable macromolecules. Conversely, a strong complex may resist efflux due to its modified structure or shielded features normally recognised by AcrB. The mechanism may also be a combination of all of these, and other scenarios.

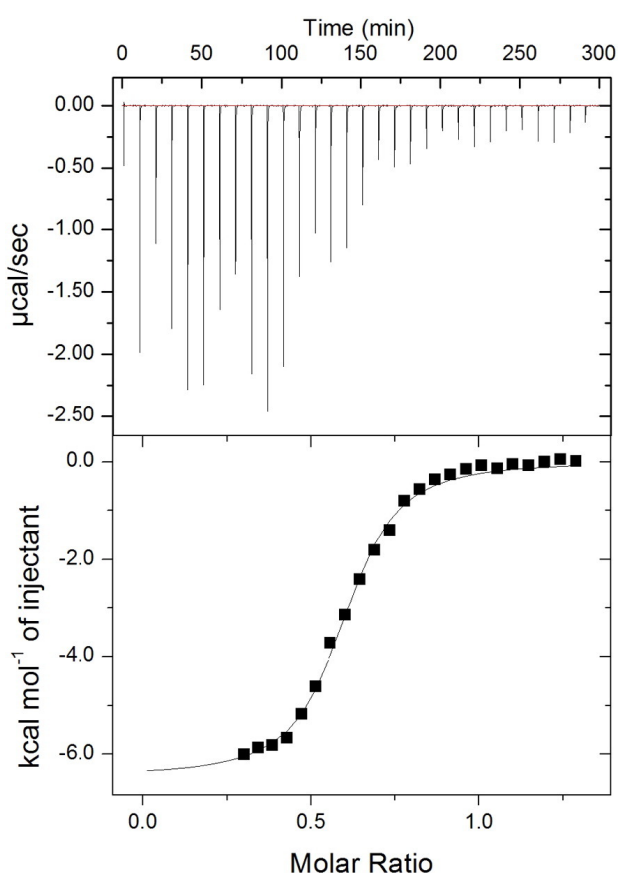


Figure 5.1 - Example of ITC output data for an exothermic complexation reaction between silver ions and the antimicrobial cefuroxime

The upper panel shows the enthalpy change at each injection over time and the lower panel shows the integrated enthalpy curve points normalized per mole of injectant as a function of molar ratio. Image from Möhler *et al*, 2017^[432].

Investigations into interactions between metal ions and FNa were therefore required in order to determine whether spontaneous complexation may play a role in their combined antimicrobial activity. Cu^{2+} was selected over the other two synergistic metal ions since it exhibits lower reactivity with metal surfaces (such as those found in delicate isothermal calorimetry equipment) compared to Al^{3+} and superior aqueous stability compared to

Fe²⁺. Initially, ultraviolet-visible light (UV-Vis) spectrophotometry was used to collect the absorption spectra of aqueous mixtures of CuSO₄ and FNa in order to detect shifts indicative of spontaneous complex formation^[433]. Isothermal titration calorimetry (ITC) was then employed to investigate whether a complexation reaction between FNa and Cu²⁺ occurred on mixing. ITC can be used to identify and characterise molecular interactions by measuring the enthalpy change as heat liberated or absorbed on binding^{[434]–[436]}. The technique has many applications and has been employed in the biochemical sciences to characterise interactions such as potential drug ligand-receptor binding properties^[437] and enzyme kinetics^{[438],[439]}. Figure 5.1 illustrates the ITC results from a typical exothermic complexation interaction^[432].

5.1.2 Potential effects of metal ion-mediated pH reduction

5.1.2.1 Bacterial response to pH stress

A feature common to many metal ions is that they are innately acidic. The reduction in pH when metal ions are in aqueous solution can give rise to pH stress and potentially death in a microbe. Multiple acid tolerance or acid resistance (AR) systems are employed by bacteria to respond to various combinations and degrees of acid stress conditions, many of which have been extensively studied in *E. coli*. At very low pH (≤ 2.5), bacterial growth ceases and one or more of four AR systems (AR1-4) is expressed, depending on the exposure conditions and preceding environment^{[440],[441]}. While AR1 is not well characterised, key components of AR2, AR3 and AR4 are amino acid decarboxylases which consume intracellular protons by employing them to convert glutamate, arginine and lysine to glutamine, agmatine and cadaverine, respectively; along with a corresponding amino acid-amine antiporter^{[440]–[442]}. However, even small fluctuations in external pH rapidly alter the periplasmic pH to similar values, indicating that the OM is permeable to protons^{[441],[442]}. Whether this OM permeability is due to movement through ion channels, directly through the bilayer or a combination is yet to be determined. Low pH can produce ionic changes in proteins and cause them to unfold by protonating amino acid residues and causing them to repel one another^[442]. Since the pH in the periplasm is effectively contiguous with the external environment, *E. coli* relies on chaperone proteins HdeA and HdeB to survive and recover from pH stress. HdeA and HdeB interact with acid-damaged proteins to prevent their aggregation and deliver them to other periplasmic chaperones responsible for refolding once the pH has returned to neutral^[442]. When initially exposed to moderately low external pH (down to pH 5), the cytoplasmic pH also drops but then rapidly recovers^{[441],[442]}. The rapidity of this equilibration indicates

it is likely due to the buffering capacity of the cytosol or conformational switching of ion transporters rather than slower a transcriptional response^{[441],[442]}. The IM also has lower permeability to protons compared to the OM due to the presence of cyclopropane fatty acids. *E. coli* upregulates expression of cyclopropane fatty acid synthase in response to acid stress, increasing the IM cyclopropane fatty acid content to minimise acid-mediated damage^[442].

Alterations in IM composition could presumably change its permeability to FNa. In addition, damage to the periplasmic portion of AcrAB-TolC would reduce the efficacy of FNa efflux.

5.1.2.2 Sodium fusidate solubility at reduced pH

In addition to the direct effects on the bacterial cell, lowered pH is likely to affect the solubility of FNa. FA is a weak acid with a pK_a of 5.35^[443]. This means that as solution pH is lowered to below 5.35, the dissociation equilibration favours a higher proportion of protonated fusidate increasing its thermodynamic activity, as described by the Henderson-Hasselbalch equation^{[444],[445]}. Fully protonated fusidate (which is undissociated FA) is non-polar and therefore insoluble in polar solvents such as water and bacteriological media which leads to precipitation. However, non-polar molecules are lipophilic and FA has been shown to solubilise in membrane lipids as efficiently as bile salts^[446]. Therefore, lowered pH could effectively drive fully protonated FA into, and consequently across, the bacterial OM. Interestingly, free fatty acids that are fully protonated in moderately reduced external pH (e.g. octanoic acid (C8) with a pK_a of 4.89) have been found to exert intracellular pH stress by permeating membranes and deprotonating in response to the neutral pH inside the cell^[447]. Fully protonated FA may well exhibit the same behaviour.

Most of this chapter therefore focusses on investigations into the pH of metal salts in bacteriological media, the solubility of FNa in these environments and whether a relationship between FNa solubility and anti-*E. coli* activity can be characterised mathematically. Finally, the association of fusidate with *E. coli* cells under a selection of representative exposure conditions is measured directly.

5.1.3 Aims and objectives

Aims: to investigate the complexation and physical chemistry of synergistic metal ion and FNa mixtures and characterise the role of these interactions in the combined anti-GN efficacy.

Objectives:

- 1) To determine whether a representative metal ion (Cu^{2+}) spontaneously complexes FNa in aqueous solution.
- 2) To investigate the impact of pH on the anti-*E. coli* activity of FNa, with and without metal ions.
- 3) To characterise the relationship between FNa solubility and its anti-*E. coli* activity, with and without metal ions.
- 4) To investigate the effect of reduced solubility on association of FNa with *E. coli* cells.

5.2 Methods

5.2.1 Investigations into interactions between fusidate and copper(II) ions

5.2.1.1 Ultraviolet-visible light (UV-Vis) spectrophotometric analysis

Stock solutions of 400 μM FNa and 1 mM CuSO_4 were prepared separately in HPLC-grade water. The full scanning range of the Agilent Cary 60 UV-Vis spectrophotometer was employed (190-1100 nm), performed at a scan rate of 200 nm min^{-1} and intervals of 0.15 nm. A standard quartz cuvette with a 1 cm path length was first filled with a 1 in 2 dilution of the FNa stock solution (final concentration 200 μM) to a total volume of 3500 μL and the absorbance spectrum measured. An aliquot of 100 μL was removed from the cuvette and replaced with 50 μL 400 μM FNa solution and 50 μL 1 mM CuSO_4 solution, and the cuvette inverted several times before the spectrum was read. This process was repeated to titrate with increasing CuSO_4 concentration, while maintaining 200 μM FNa. Collected spectra were used to produce extinction curves by correcting against absorbance of FNa alone and assessed graphically to determine wavelength ranges of interest.

The effect of pH on extinction curve absorbance shift was also investigated. As an alternative to the use of a buffering agent, due to the limitations presented in Sections 5.2.1.2 and 5.3.1.2, putative complex formation with Cu D-glu at both native and near-neutral pH was also assessed by UV-Vis spectrophotometry. A separate Cu D-glu 2 mM stock solution aliquot was adjusted to pH 7.3 by addition of NaOH flakes (Fisher Scientific, Loughborough, UK). Mixtures of 100 μM FNa with 1 mM Cu D-glu were prepared using the pH adjusted and a pH unadjusted stock solution. A mixture of 100 μM FNa with pH unadjusted 1 mM CuSO_4 was also prepared. The 200-600 nm UV-Vis absorbance spectrum of each of the mixtures and 100 μM FNa alone was measured as described above. FNa extinction curves were determined for each mixture and compared graphically.

5.2.1.2 Isothermal titration calorimetry (ITC)

ITC was performed using an iTC₂₀₀ Microcalorimeter (MicroCal, Northampton, MA, USA). Data generated was imported into the MicroCal Origin software for analysis. Prior to use the instrument performance was validated using a standardised protocol for the reaction

between ethylenediaminetetraacetic acid (EDTA) and calcium chloride (CaCl_2), as provided by the manufacturer (see Appendix D).

Cu^{2+} is known to form complexes and otherwise adversely interact with components of many common buffering solutions^[448]. 3-(N-morpholino)propanesulfonic acid (MOPS), a buffer not complexed by metal ions^{[448],[449]}, was therefore selected for the preparation of CuSO_4 and FNa solutions. However, lack of FNa solubility in ≥ 10 mM MOPS prohibited the use of this buffer altogether (see Section 5.3.1.2 of Results). Attempts were subsequently made to adjust the pH of an un-buffered aqueous solution of 1 mM FNa to match the unadjusted pH of un-buffered aqueous 10 mM CuSO_4 and *vice versa* using dropwise addition of 1 M HCl or 1 M NaOH (Fisher Scientific, Loughborough, UK) without success. Finally, since similar antimicrobial synergy with other Cu^{2+} salts in combination with FNa had been observed (see Chapter 4, Section 4.3.2, page 90), pH adjustment of un-buffered aqueous solutions of CuCl_2 , $\text{Cu}(\text{NO}_3)_2$ and Cu D-glu was also attempted.

To investigate the nature of the possible interaction between Cu^{2+} and FNa, ITC was performed against 1 mM FNa with a variety of injectants: 10 mM CuSO_4 , 10 mM Cu D-glu (pH unadjusted), 10 mM Cu D-glu (increased pH), 10 mM sodium D-gluconate (Na_2 D-glu) and dilute sulphuric acid (H_2SO_4 , Fisher Scientific, Loughborough, UK). Cu D-glu was used as an alternative Cu^{2+} source since it was found to be amenable to pH adjustment (see Section 5.3.1.1 of Results). Na_2 D-glu was tested to determine any interaction between FNa and D-gluconate. H_2SO_4 was used in an attempt to investigate the effect of reduced pH without Cu^{2+} ions. All solutions were prepared in 1 % v/v EtOH which was selected to maintain FNa dissolution.

The ITC run parameters were based on those used in the performance validation assay: 25 °C cell temperature, injection interval of 150 s, and 20 injections with initial injection of 0.4 μL over 0.8 s and subsequent injections of 2 μL over 4 s. However, a slower stirring speed of 100 rpm was employed to prevent frothing of the FNa solution observed at higher speeds used in preliminary runs. The reference cell was filled with 1 % v/v EtOH.

All test solutions were prepared approximately 24 h in advance of the ITC experiments to ensure equilibration at the time of use. Shortly after the initiation of each ITC run, the pH of aliquots of the same solutions used was measured and a mixture of the pair was prepared at the final ratio and same concentrations as produced by the ITC. The pH of each mixture was measured after equilibration at room temperature for 12-24 h. Each complete test – ITC run and pH measurements – was performed in duplicate or triplicate.

5.2.2 Relationship between broth pH and sodium fusidate anti-*E. coli* activity, with and without metal ions

5.2.2.1 Metal sulphate pH measurements

The pH of 1 mL samples of metal sulphates in NB were measured after 18±2 h incubation at 35 °C and 120 rpm, mimicking the antimicrobial test conditions. The metal sulphate broth solutions were prepared in triplicate at concentrations equal to those previously investigated for antimicrobial activity. The pH measurements were used in combination with previously generated *E. coli* inhibition data (Chapter 4) to probe the relationships between pH and activity.

5.2.2.2 Anti-*E. coli* activity of sodium fusidate in pH adjusted broth

The pH of 100 mL volumes of NB was adjusted to between 4.2 and 7.0 at 0.2±0.05 unit increments by drop-wise addition of 0.5 M H₂SO₄ and filter sterilised. The pH-adjusted broths were then used to perform a modified chequerboard assay in order to assess the activity of FNa at different pHs but without the presence of additional metal ions. Two-fold dilutions of FNa were prepared in each pH adjusted broth and 100 µL aliquots of each series transferred to one row of a flat-bottomed 96 well plate. Solutions were thoroughly mixed between dilution steps and before transfer to the 96 well plate in order to ensure any precipitate present was suspended as evenly as possible. A 1 × 10⁸ CFU mL⁻¹ suspension of *E. coli* NCTC 10418, prepared as previously described (see Section 2.4), was diluted 1/100 into an aliquot of pH-adjusted broth and rapidly used to inoculate the corresponding row of the prepared 96 well plate with 100 µL aliquots. This process was repeated for each pH adjusted broth. After incubation at 35 °C and 120 rpm for 18±2 h, absorbance in each well was used to calculate the % inhibition. The experiment was performed in triplicate.

5.2.2.3 Copper(II) in combination with sodium fusidate at neutral pH

In order to probe whether the activity of FNa in combination with Cu²⁺ (as a representative synergistic metal) was primarily due to the pH change produced by the metal salt, chequerboard assays were carried out using a range of Cu²⁺ concentrations all adjusted to neutral pH. Cu D-glu was used in this experiment because all but the lowest concentrations of CuSO₄ required were previously found to precipitate in aqueous solution if the pH was raised above ~5.5 (see Section 5.3.1.2). Since in previous chequerboard experiments Cu D-glu was found to be slightly more effective than CuSO₄

when in combination with FNa (see Section 4.3.2), the unadjusted Cu D-glu chequerboard results were used as a comparator.

Serial two-fold dilutions of Cu D-glu were prepared in NB and the pH of each adjusted to pH 7.2±0.1 using 1 M NaOH. The pH-adjusted Cu D-glu broth solutions were filter sterilised and used to prepare serial dilutions of FNa in a 96 well plate in chequerboard format. As for the pH adjusted broth chequerboard described in Section 5.2.2.2, bacterial suspensions were prepared in each pH-adjusted Cu D-glu broth dilution and used to inoculate all wells with $5\pm3 \times 10^5$ CFU mL⁻¹ *E. coli* NCTC 10418. Plates were incubated at 35 °C and 120 rpm for 18±2 h and the absorbance in each well used to calculate % inhibition. The experiment was performed in triplicate.

As described for the comparisons between different copper(II) salts in Chapter 4 (page 4.2.184), isobolograms of the concentration of FNa required to produce ≥90 % inhibition plotted against each Cu²⁺ concentration were constructed and the AUC calculated to compare the combined activity. Statistically significant differences between AUCs with pH-adjusted Cu D-glu and the unadjusted comparator were determined using 95 % CIs ($p \leq 0.05$).

5.2.3 The effect of broth pH on sodium fusidate solubility, with and without metal ions

5.2.3.1 Preliminary test for pH-induced precipitation of sodium fusidate in nutrient broth

In order to determine whether lowered pH may be associated with increased aggregation and precipitation of FNa under antimicrobial test conditions, solutions of 2.56 mM FNa were prepared in aliquots of standard NB (pH 7.2±0.2) or NB which had been adjusted to pH 5.0 using 1 M H₂SO₄. After equilibration at room temperature for 1 h, syringe filters (0.22 µm PES) were used to remove any large aggregates and the resulting solution re-adjusted to pH 7.2 by drop-wise addition of 1 M NaOH. One solution of FNa in unadjusted NB was also filtered to determine the presence of similarly sized precipitate in standard broth and another used as an un-filtered, unadjusted control.

Two-fold dilutions of the final FNa broth solutions were carried out in standard NB in flat-bottomed 96 well microtiter plates. Plates were inoculated with *S. aureus* NCTC 12973 to a final concentration of $5\pm3 \times 10^5$ CFU mL⁻¹ and incubated at 35 °C and 120 rpm for 18±2 h. As described for similar assays, the absorbance of the resulting growth was

measured at 595 nm using a Tecan Infinite PRO microtiter plate reader and the % inhibition in each well calculated. The mean % inhibition from three biological replicates was plotted against the dilution number. An estimation of the FNa concentration in the pH adjusted broth was made by shifting the resulting curve to fit that of the control. The 95 % CIs were used to determine statistically significant differences ($p \leq 0.05$).

5.2.3.2 Assessment of sodium fusidate stability at reduced pH

Solutions of 2.5 mM FNa were prepared in 3 mL aliquots of standard NB (native pH 7.2 ± 0.2), NB which had been adjusted to pH 5.0 using H_2SO_4 , NB with $625 \mu M ZnSO_4$ or 2.5 mM $CuSO_4$ in duplicate. One of each pair was prepared for immediate HPLC analysis: one drop of NaOH was added to acidic solutions (pH 5 NB and NB with $CuSO_4$) in order to dissolve precipitated FNa and an equal volume of water was added to the others (standard NB and NB with $ZnSO_4$). Solutions were transferred to individual HPLC autosampler vials. The other of each pair was incubated at $35 \text{ }^\circ C$ and 120 rpm for 18 ± 2 h and the same neutralisation and control steps were performed. All samples were analysed by RP-HPLC separation method 2 (Section 2.6.2) which was specifically developed for the assessment of fusidic acid stability^[288]. Chromatograms of 0 h and post-incubation samples were compared and differences in degradation products identified.

5.2.3.3 Solubility of sodium fusidate at reduced pH and with metal ions

The pH of seven 100 mL volumes of NB was lowered to between approximately 4.4 and 6.8 at intervals of 0.4 ± 0.05 units using dropwise addition of 1 mM H_2SO_4 . Serial two-fold dilutions of FNa stock solution were performed in each pH adjusted broth and unadjusted nutrient broth control to produce concentrations from 2.5 to 1,280 μM , the same range as used in *E. coli* checkerboard assays. In triplicate, separate 1 mL aliquots were equilibrated at room temperature ($20 \text{ }^\circ C$) for 1.5 ± 0.5 h and at $35 \text{ }^\circ C$ and 120 rpm for 18 ± 2 h to represent point of inoculation and end of incubation, respectively. Post-equilibration processing was as described in Section 2.7, as appropriate for the incubation temperature. Additional triplicate 1 mL samples of each test broth and control were equilibrated under the same conditions in order to verify the pH. FNa solubility was determined after 1.5 ± 0.5 h at $20 \text{ }^\circ C$ and 18 ± 2 h at $35 \text{ }^\circ C$ and 95 % CIs used to determine statistically significant differences ($p \leq 0.05$).

To investigate FNa solubility in NB with metal sulphates, serial two-fold dilutions of metal sulphates were made in HPLC-grade water and mixed 1:1 with 2560 μM FNa (2.5 % v/v EtOH) in double concentration NB. The resulting mixtures contained 1280 μM FNa and

metal sulphate at concentrations of one two-fold dilution above the MIC₉₀, the MIC₉₀ and the next three lower concentrations used in *E. coli* checkerboard assays. As for pH adjusted broth experiments, two triplicate sets of aliquots were equilibrated at 20 °C for 1.5±0.5 h and at 35 °C and 120 rpm for 18±2 h for HPLC analysis and pH verification.

FNa solubility in NB with Cu D-glu at unadjusted native pH and at pH 7.2 was also investigated. Serial two-fold dilutions of Cu D-glu were performed in standard NB in duplicate. The pH of one set of dilutions was adjusted to pH 7.2±0.1 using 1 M NaOH and filter sterilised. FNa was added to each of the pH adjusted and unadjusted dilutions to a final concentration of 1280 µM and two sets of triplicate aliquots were incubated at 35 °C and 120 rpm for 18±2 h for HPLC analysis and pH verification.

Finally, the effect of different broths on FNa solubility in the presence of CuSO₄ was assessed. Serial two-fold dilutions of CuSO₄ prepared in HPLC-grade water were mixed with 2560 µM FNa in double concentration LB or CAMHB and aliquots incubated at 35 °C and 120 rpm for 18±2 h.

All solutions for quantification of dissolved FNa were processed as described in Section 2.7, and analysed by HPLC separation method 1 (Section 2.6.2).

5.2.4 Modelling correlations between sodium fusidate solubility and anti-*E. coli* activity

Microsoft® Excel® (MSO Professional Plus 2016, Microsoft Corporation, WA, USA) was used to detect and characterise correlations between FNa solubility after 18±2 h at 35 °C and activity against *E. coli* NCTC 10418 in pH adjusted broth. Data for 1280 µM solubility and 20 µM activity were fitted to exponential, polynomial and linear equations and the strongest correlation determined.

The selected equation was applied to solubility data for 1280 µM FNa in the presence of metal sulphates in order to predict inhibition of *E. coli* by 20 µM FNa under the same conditions. A modified model, accounting for the inhibitory effect of each metal concentration alone, was also applied by adding the paired value recorded within the same replicate to the previously predicted inhibition. The predictive accuracy of each model was assessed using the 95 % CIs to determine statistically significant differences between observed and predicted data points ($p \leq 0.05$) and by calculating the absolute difference in mean observed vs mean predicted inhibition at each metal concentration.

The accuracy of both models at predicting *E. coli* inhibition in the presence of Cu D-glu, with and without pH adjustment, and in LB or CAMHB was assessed in the same way.

5.2.5 Quantification of sodium fusidate associated with *E. coli* cells

A simple method, based on that of Lemire *et al.* (2011)^[450], was employed to determine the amount of FNa associated with *E. coli* cells after exposure in the presence of metal ions or reduced pH.

E. coli NCTC 10418 was grown overnight on NA. Four separate 40 mL volumes of standard NB were inoculated using disposable plastic loops touched to three to five morphologically identical colonies and incubated at 35 °C and 120 rpm for 18 to 24 h. The grown cultures were centrifuged in a Heraeus Megafuge 8R centrifuge (Thermo Scientific, Osterode am Harz, Germany) for 20 min at 3260 x *g* (4500 rpm) at room temperature. Meanwhile, 25 mL volumes of each exposure broth were prepared: NB with 312.5 µM CuSO₄, NB with 625 µM MnSO₄, NB adjusted to pH 6.0±0.2 and standard NB at native pH as a control. The adjustment of NB to pH 6 was achieved by dropwise addition of 1 M H₂SO₄ followed by filter sterilisation (0.22 µm) before use. Other exposure broths were prepared aseptically throughout. FNa stock solution was added to each exposure broth to a final concentration of 160 µM.

The supernatants of the four centrifuged *E. coli* cultures were decanted and each bacterial pellet resuspended in 10 mL of one of the exposure broths. Resuspended viable bacteria were immediately enumerated using the Miles & Misra^[280] drop counting technique, as described in Section 2.3, and incubated at 35 °C and 120 rpm for 30 min. Separate sterile 10 mL volumes of each exposure broth were incubated in the same way. Samples of the remaining exposure broths were taken for quantification of FNa initial concentration by HPLC.

After the 30 min exposure period, viable bacteria were again enumerated by drop count. Both the exposed *E. coli* and uninoculated exposure broth controls were centrifuged for 20 min at 3260 x *g* and 4 °C (pre-cooled). This temperature was selected in order to halt or reduce any further bacterial replication. Supernatants were carefully decanted. The bacterial pellets were thoroughly resuspended in 1 mL water and a third drop count performed. One mL water was also used to thoroughly rinse the bottom of each bacteria-free control tube in order to dissolve or suspend any FNa present. The resuspensions and controls were mixed 1:1 with EtOH in 2 mL centrifuge tubes, sealed to prevent evaporation and incubated at room temperature for 30-45 min in order to kill bacteria and

fully dissolve FNa (see Appendix C). Syringe filters (0.22 μm) were used to prepare each mixture for HPLC. FNa was quantified using RP-HPLC separation method 2 (Section 2.6.2). The experiment was carried out in triplicate.

HPLC and drop count data were used to calculate mean FNa in pg per 10^6 *E. coli* cells. Results were normalised to FNa precipitated in the same broth conditions without bacteria present. The 95 % CIs were used to determine statistically significant differences ($p \leq 0.05$).

5.3 Results

5.3.1 Investigations into interactions between fusidate and copper(II) ions

5.3.1.1 UV-Vis spectrophotometric analysis of sodium fusidate and copper(II)

The FNa-normalised absorbance spectra of 200 μM FNa titrated with increasing concentrations of CuSO_4 in aqueous solution are presented in Figure 5.2. Absorbance in the ranges of approximately 205 to 215 nm and 250 to 270 nm were found to increase with increased CuSO_4 concentration, whereas absorbance between approximately 235 and 240 nm decreased.

Extinction spectra were produced for 100 μM FNa mixed with 1 mM either pH-unadjusted CuSO_4 , pH-unadjusted Cu D-glu or Cu D-glu adjusted to neutral pH (Figure 5.3). The mixture containing pH-unadjusted Cu D-glu produced the highest peak at approximately 250 nm. The native pH of 2 mM Cu D-glu was the lowest of the three Cu^{2+} salt solutions at 4.9. Conversely, no discernible peak was produced by pH 7.3 Cu D-glu combined with FNa. The peak from pH 5.4 CuSO_4 was not as large as that with pH unadjusted pH 4.9 Cu D-glu. This indicated that the observed absorbance shifts were likely due to FNa precipitation as pH was lowered, rather than spontaneous formation of a Cu-fusidate complex.

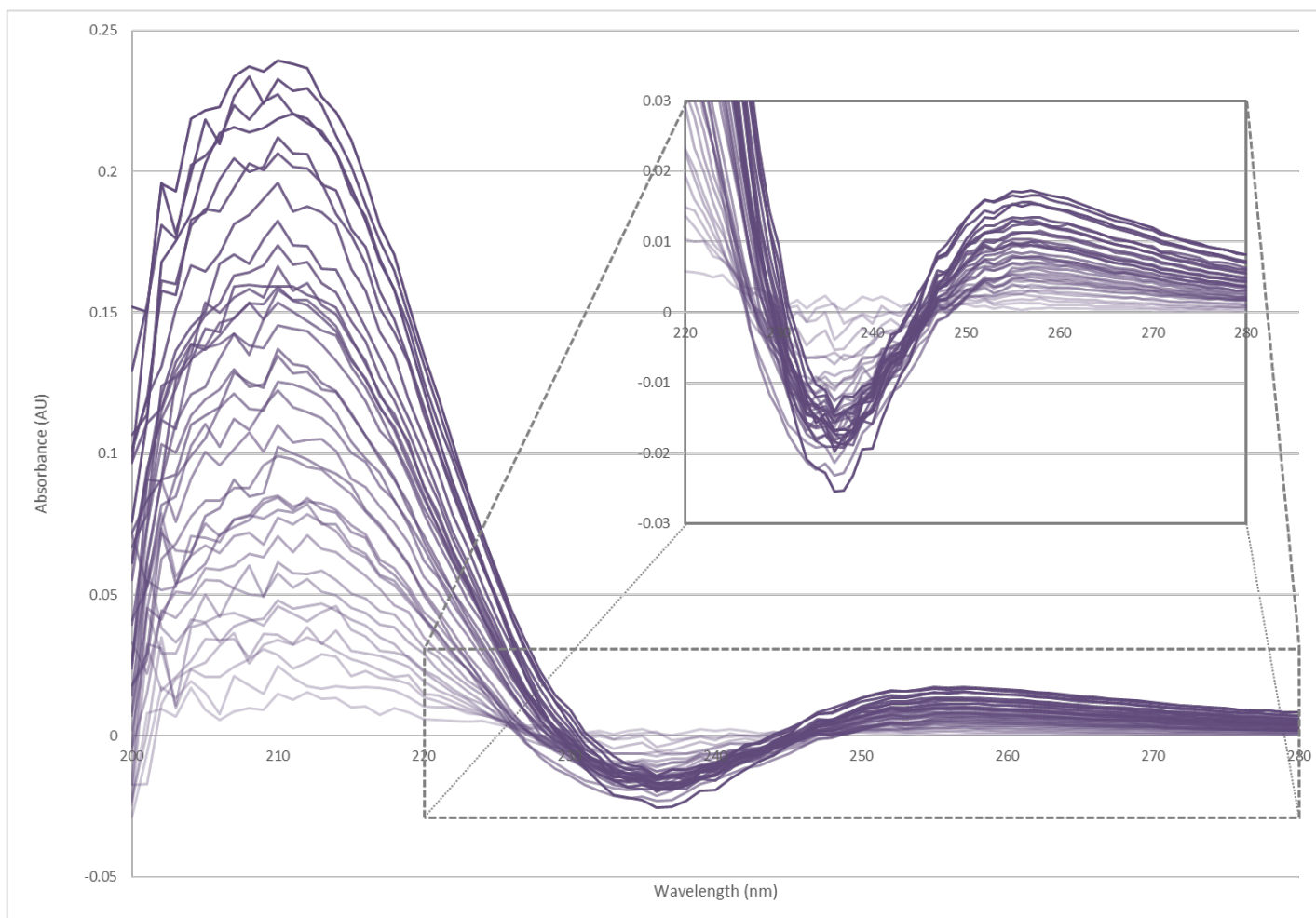


Figure 5.2 – Absorbance spectra of 200 μM sodium fusidate titrated with increasing concentrations of copper(II) sulphate in aqueous solution
 Darker colour = greater copper(II) sulphate concentration (range = 15-600 μM). Spectra are normalised to 200 μM sodium fusidate absorbance.
 Insert included for visualisation of otherwise obscured area of interest.

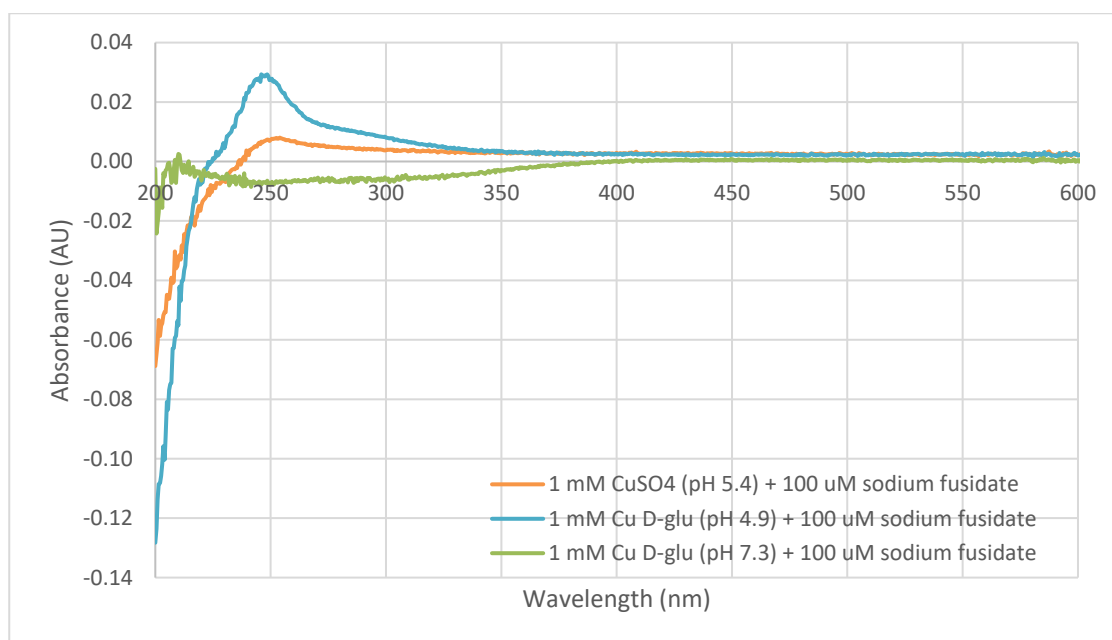


Figure 5.3 - UV-Vis extinction curves illustrating pH-dependent changes in sodium fusidate precipitation on mixing with copper(II) salts

Quoted pH is that of the 2 mM copper(II) salt solution prior to mixing. Neutral pH results in very little absorbance shift when the two agents are mixed resulting in no detectable extinction spectrum peak. (n = 3)

5.3.1.2 Effect of pH on the interaction between fusidate and copper(II) by ITC

ITC instrument performance was successfully validated using the EDTA-CaCl₂ standard prior to each set of experiments (see Appendix D). ITC experimentation is generally performed in buffered solutions in order to ensure pH matching between the injectant and receiving sample. If the pH is not closely matched, the resulting enthalpy of mixing can interfere with detection of molecular interactions. However, it was not possible to carry out buffered ITC experimentation with FNa and Cu²⁺ ions due to solubility limitations. FNa was found to be insoluble in ≥10 mM aqueous MOPS. Dissolution of up to 4.5 mM FNa was achieved with a combination of 10 mM MOPS and 40 % EtOH, however, CuSO₄ was insoluble in this buffer-alcohol mixture. In lieu of identification of an effective buffer, adjustment of aqueous solutions of FNa and Cu²⁺ salts to the same pH was investigated. Addition of HCl to 1 mM FNa in 1 % v/v EtOH generated a white precipitate at pH ~5.8. When the pH of 10 mM CuSO₄ was increased using NaOH, a dense, bright blue precipitate formed at pH ~5.2. Similar precipitation was seen on attempted pH increase of CuCl₂ and Cu(NO₃)₂ solutions. However, the pH of up to 96 mM Cu D-glu was successfully raised to over 8.5 with no visually detectable precipitation indicating this salt was alone in remaining dissolved at increased pH. Cu D-glu was therefore employed to investigate the interactions between FNa and Cu²⁺ in aqueous solution at equal pH. The results presented here comprise of one representative run per test condition (Figure 5.4 and Figure 5.5). Other replicates can be found in Appendix D.

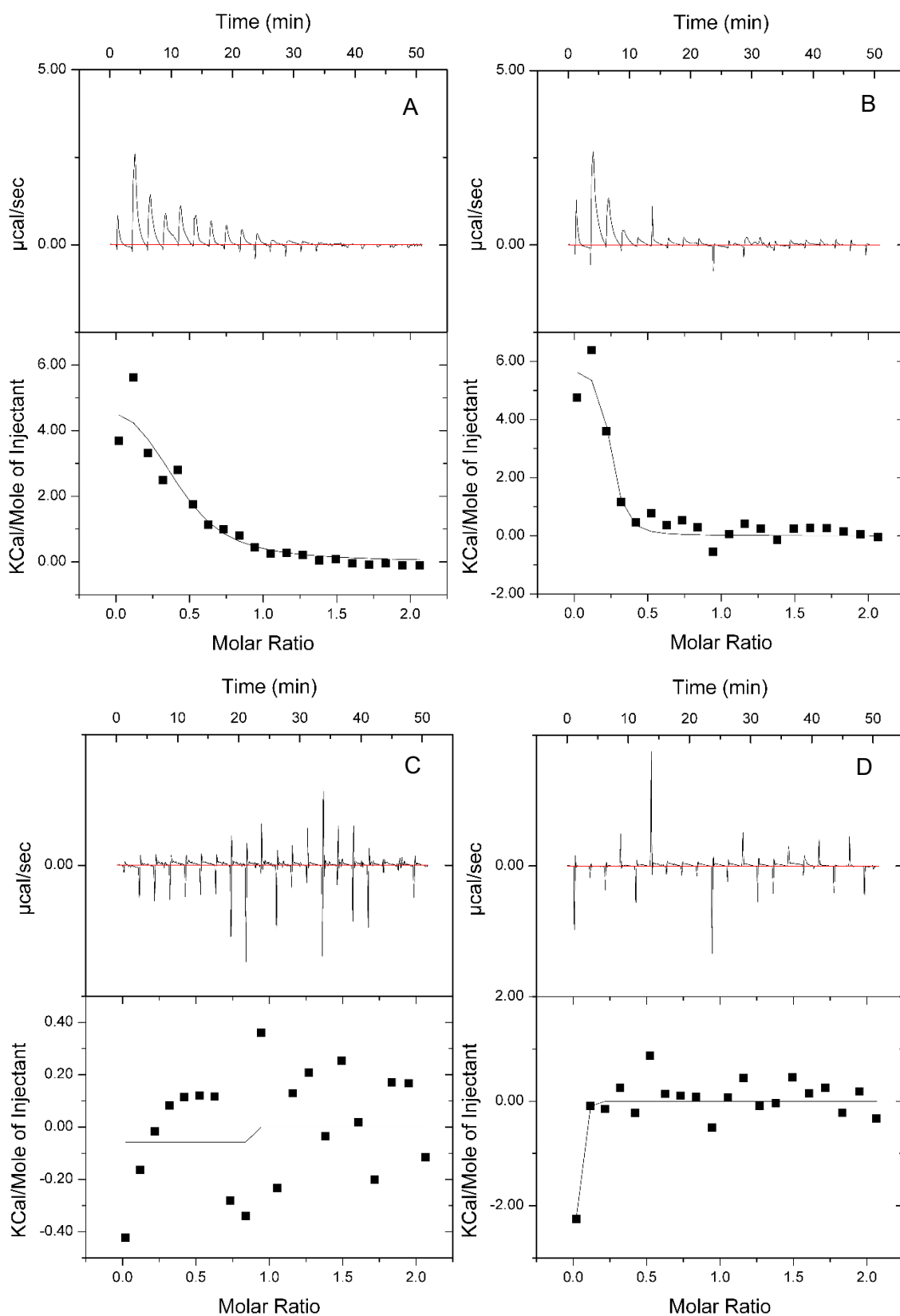


Figure 5.4 – ITC thermograms of sodium fusidate with copper(II) sulphate (A), copper(II) D-gluconate at native pH (B), copper(II) gluconate at pH 6.12 (C) and sodium D-gluconate (D)

The upper panels show enthalpy change at each injection over time and the lower panels show the integrated enthalpy curve points normalized per mole of injectant as a function of molar ratio. Note difference between scale in A/B and C/D.

Table 5.1 – The pH of each initial individual solution used in ITC experiments and an equilibrated mixture at the same final ratio

Injectant	Initial pH		Equilibrated mixture pH
	Injectant	Sodium fusidate aliquot	
CuSO ₄	4.77	6.42	5.77
Cu D-glu (native pH)	4.46	6.53	5.10
Cu D-glu (adjusted)	6.12	6.39	6.55
Na ₂ D-glu	6.43	6.34	6.67
H ₂ SO ₄	4.75	6.33	6.43

The enthalpy change peaks (Figure 5.4, upper panels) on interaction between FNa and both CuSO₄ (A) and Cu D-glu (B) at their native pHs were too wide for quantitative data interpretation. However, qualitative assessment of the tailing shape along with width of these peaks was indicative of precipitation. The pH of the test solutions are listed in Table 5.1. The reaction with Cu D-glu (Figure 5.4B) reached completion after fewer injections than with CuSO₄ (Figure 5.4A). In addition, the Cu D-glu injectant solution was a lower pH than CuSO₄ (Table 5.1). Combined, these facts indicated a pH-related precipitation of FNa, since the lower initial pH Cu D-glu would have lowered the pH of the receiving FNa solution more rapidly than CuSO₄. Indeed, the pH of the final mixture of FNa and Cu D-glu was lower than FNa and CuSO₄ at 5.10 compared to 5.77, respectively. Precipitation of FNa in a pH-dependent manner was further supported by the lack of net enthalpy change when Cu D-glu adjusted to pH 6.12 (Figure 5.4C) or Na₂ D-glu (Figure 5.4D, native pH equal to that of the FNa solution) was titrated against FNa. These results illustrated no interaction between Cu²⁺, the D-gluconate ion or Na⁺ and FNa.

A dilute H₂SO₄ solution of pH 4.75, equal to the test solution of CuSO₄ ±0.02 units, was also titrated against FNa in an attempt to confirm the effect of reduced pH without metal ions. However, addition of diluted H₂SO₄ to FNa resulted no significant pH change. The equilibrated mixture at their final test concentrations was very similar to the native pH of the original FNa solution at pH 6.43 (Table 5.1). As would therefore be expected, there was also no net enthalpy change during ITC with the same concentration of H₂SO₄ (Figure 5.5).

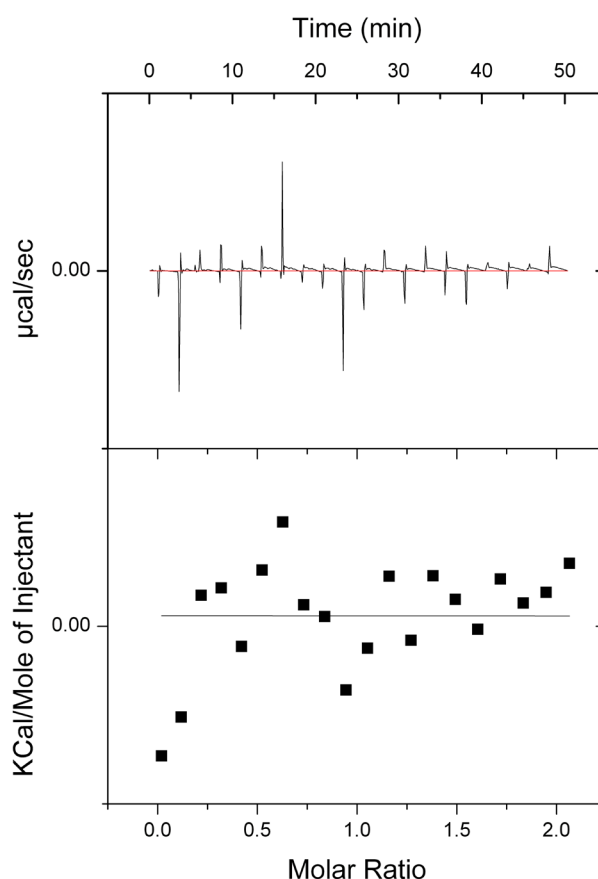


Figure 5.5 - ITC thermogram of sodium fusidate with dilute sulphuric acid

The upper panel shows enthalpy change at each injection over time and the lower panel shows the integrated enthalpy curve points normalized per mole of injectant as a function of molar ratio.

5.3.2 Relationship between pH and sodium fusidate activity against *E. coli*

5.3.2.1 Metal sulphate pH in nutrient broth and inhibition of *E. coli*

Since Cu^{2+} -related pH change was identified as a modulator of FNa solubility, the inhibition of *E. coli* NCTC 10418 by metal sulphates alone was first plotted against the pH of the same metal sulphate and concentration in NB after 18 ± 2 h incubation at 35°C (Figure 5.6). The pH of NB was also adjusted using dropwise addition of 1 M H_2SO_4 to determine pH effect without added metal ions.

Where the pH of a metal sulphate in broth was <6.0 , *E. coli* inhibition was $>90\%$ for all metals tested. With pH adjustment using sulphuric acid alone, this degree of inhibition was only seen at pH ~ 4.4 ; inhibition at ~ 4.6 and 4.8 was 26.7 and 8.5% , respectively, and $\leq 5.0\%$ at pH ~ 5.0 and above. For data points corresponding to metal sulphate concentrations below the MIC_{90} , there was an apparent trend between pH and inhibition by Al^{3+} , Co^{2+} , Cu^{2+} , Fe^{2+} , Ni^{2+} & Pd^{2+} . At their lowest concentrations, the pH of Al^{3+} , Fe^{2+} and Ni^{2+} were >6.75 in nutrient broth and growth of *E. coli* was not inhibited by their

presence. Conversely, Cu^{2+} and Pd^{2+} inhibited growth at every concentration tested, despite their lowest concentrations having minimal impact on broth pH. Co^{2+} , Mn^{2+} and Zn^{2+} had very little effect on broth pH at any concentration tested, their respective MIC_{90} s being pH 7.02, 7.08 and 7.13.

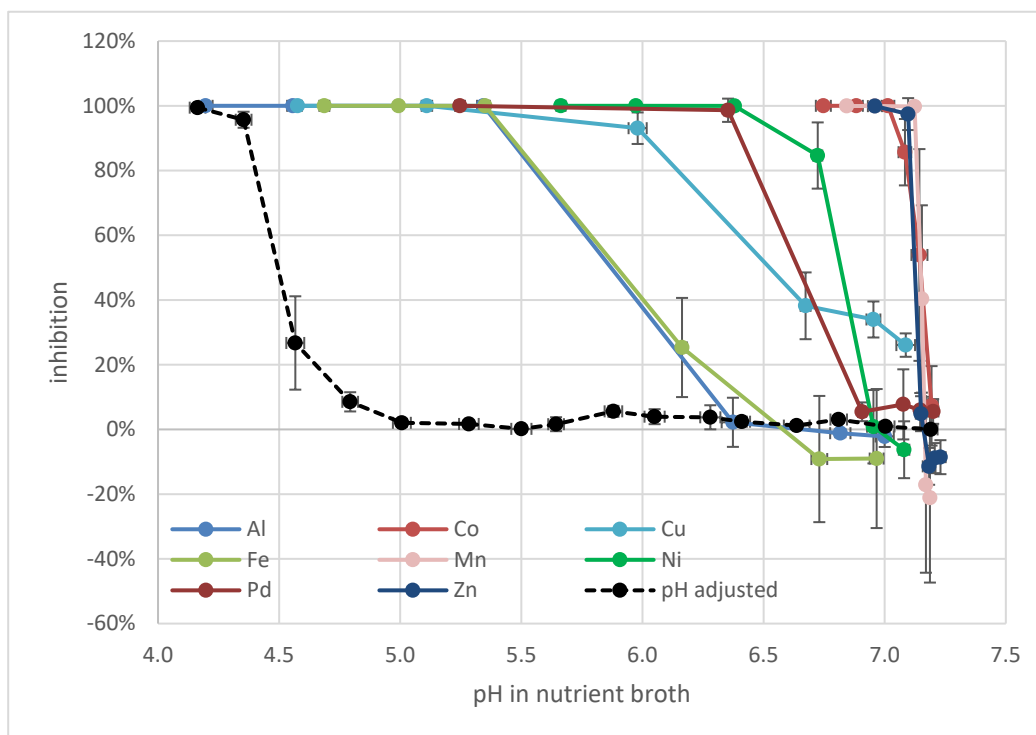


Figure 5.6 - Relationship between pH of metal sulphates in nutrient broth and inhibition of *E. coli* NCTC 10418

(n = 3, vertical error bars = SD, horizontal error bars = SD + pH electrode accuracy)

5.3.2.2 Relationship between broth pH and inhibition of *E. coli* by sodium fusidate

There was no significant difference between the recorded pH of any metal sulphate in NB with or without FNa. A sub-inhibitory FNa concentration of 20 μM (6.25 % MIC_{90}) was selected for representative comparison of the combined effects of metal sulphate, pH and antibiotic and to investigate whether pH alone may dictate the anti-*E. coli* efficacy of FNa. Figure 5.7 illustrates inhibition of *E. coli* by 20 μM FNa in the presence of metal sulphates or in pH adjusted NB, plotted against pH.

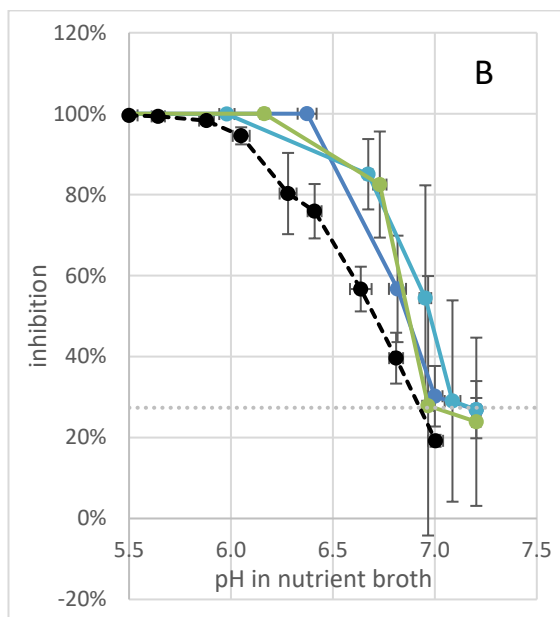
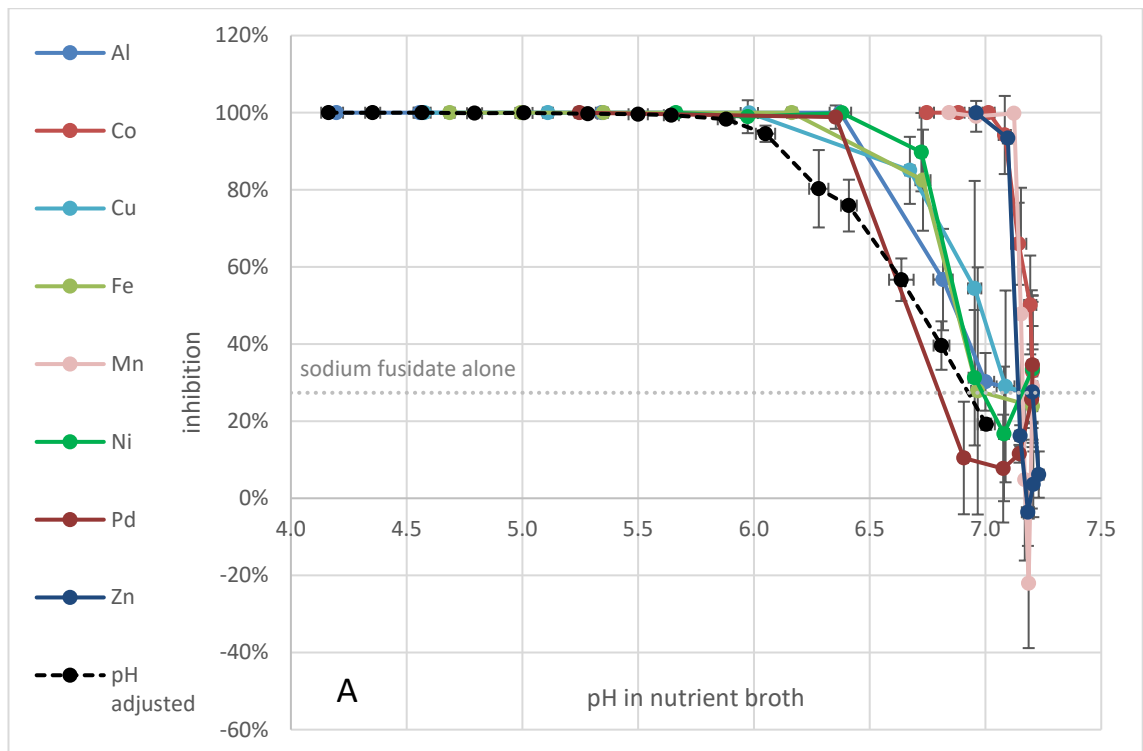


Figure 5.7 - Relationship between pH of metal sulphates in nutrient broth and inhibition of *E. coli* NCTC 10418 by 20 μ M (6.25 % MIC₉₀) sodium fusidate

A: all metal sulphates tested.

B: only metal sulphates found to synergise with sodium fusidate.

Concentrations of metal sulphates are two-fold dilutions. Broth pH was adjusted by dropwise addition of 0.5 M sulphuric acid until target pH \pm 0.15 was achieved. Dotted line denotes degree of inhibition by sodium fusidate alone.

(n = 3, error bars = SD)

Sulphates that were suppressive to FNa activity, Zn²⁺ and Mn²⁺, produced a pH change of \leq 0.25 units, and did not exhibit any correlation between pH and inhibition of *E. coli* (Figure 5.7A). Combinations of FNa with Co²⁺, Ni²⁺ or Pd²⁺ were determined as antimicrobially indifferent – neither synergistic nor antagonistic/suppressive. Despite lowering the pH to <6.5 at their most antimicrobially active concentrations, lower concentrations of both Ni²⁺ and Pd²⁺ enhanced bacterial growth when combined with FNa compared to FNa alone. However, while Co²⁺ had little effect on broth pH at any

concentration tested, its antimicrobial activity in combination with FNa was consistently higher than the effects of the equivalent metal-free pH-adjusted broth.

Inhibition vs pH data for only the metal sulphates that were found to synergise with FNa are shown in Figure 5.7B. A trend was apparent between pH and the activity of Al^{3+} , Cu^{2+} and Fe^{2+} in combination with FNa. Where similar pH was produced by the metal dilutions, there was no significant difference between their combined activity with 20 μM FNa ($p \geq 0.05$). However, FNa with metal ions generally produced 10-20 % additional inhibition compared to FNa in NB adjusted to the same pH using H_2SO_4 . Similar patterns were observed for the metals and pH-adjusted broths at all sub-inhibitory concentrations of FNa tested.

5.3.2.3 Copper(II) in combination with sodium fusidate at neutral pH

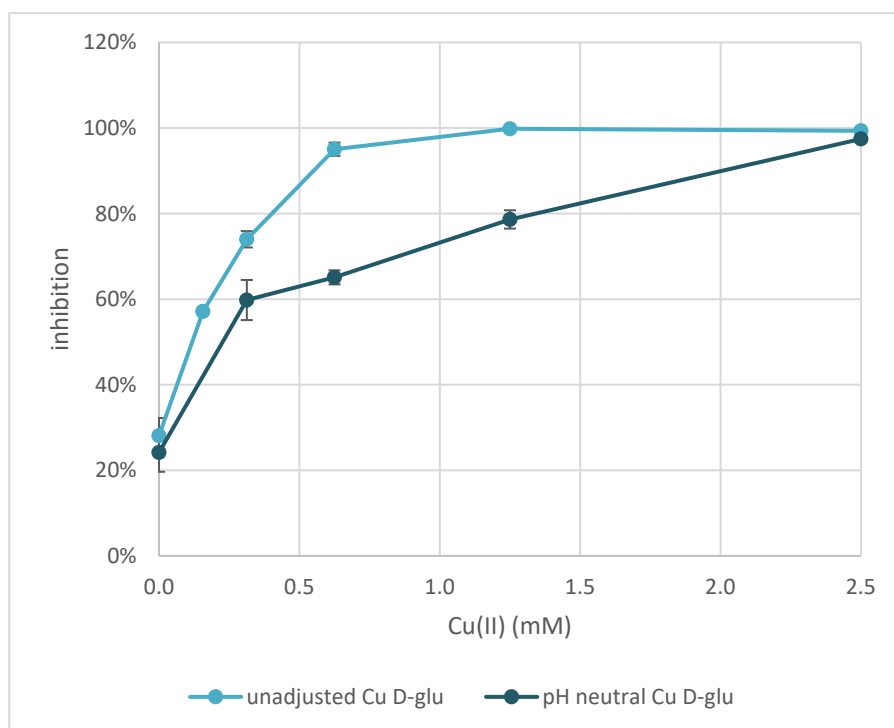


Figure 5.8 - Inhibition of *E. coli* NCTC 10418 by 20 μM sodium fusidate in the presence of copper(II) D-gluconate at unadjusted and neutral pH
(n = 3, error bars = SD)

Next, the effect of Cu^{2+} ions combined with FNa at neutral pH was assessed to determine whether neutralisation of metal acidity negated enhancement of FNa activity. Figure 5.8 illustrates the inhibition of *E. coli* NCTC 10418 by 20 μM FNa and a range of Cu D-glu concentrations with (dark blue) and without (turquoise) pH adjustment to 7.2 ± 0.1 . Without pH adjustment, the MIC_{90} of Cu D-glu with 20 μM FNa was 625 μM , however,

when the pH was adjusted to ~7.2 the MIC₉₀ increased 4-fold to 2.5 mM. The Cu D-glu MBC also increased from 1.25 mM at native pH to 10 mM at pH 7.2. Furthermore, increasing of pH to neutral significantly reduced the percentage inhibition produced by all <2.5 mM concentrations Cu D-glu in combination with 20 µM FNa ($p \leq 0.05$).

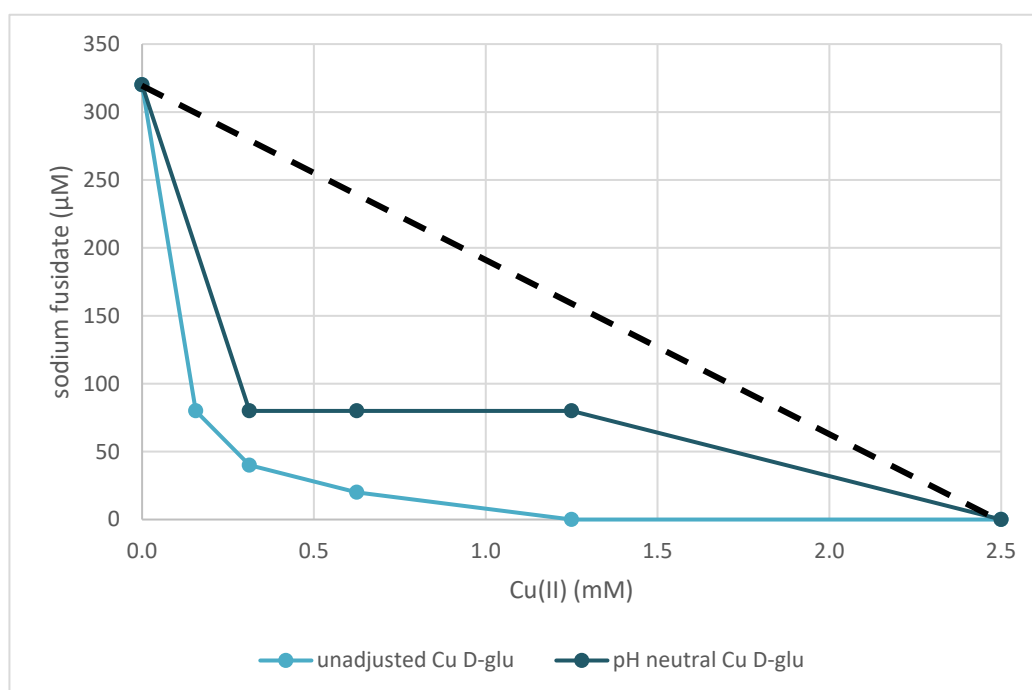


Figure 5.9 - Combined MIC₉₀s of sodium fusidate and copper(II) D-gluconate at unadjusted native pH and neutral pH 7.2 against *E. coli* NCTC 10418
The dashed black line represents the line of additivity.
(n = 3, error bars = SD)

Comparison of the isobolograms for FNa with unadjusted and pH 7.2 Cu D-glu further illustrated reduced antimicrobial activity of the neutralised solutions (Figure 5.9). Statistically significant differences in isobologram AUCs were found: 56.25 ± 0 with pH-unadjusted and 187.50 ± 0 with pH 7.2 Cu D-glu ($p < 0.05$).

5.3.3 Sodium fusidate solubility and anti-*E. coli* activity

5.3.3.1 Preliminary confirmation of pH-induced precipitation of sodium fusidate in nutrient broth

FNa-sensitive *S. aureus* NCTC 12973 was used to detect changes in FNa concentration after filtration of precipitate generated at pH 5.0. No significant difference was found between the inhibition of *S. aureus* caused by dilutions of filtered and unfiltered 2.56 mM

FNa prepared in standard NB at native pH ($p > 0.05$, Figure 5.10). This indicates there was little aggregation of FNa in NB at pH 7.2 and any aggregates present must have been $< 0.22 \mu\text{m}$. However, from dilution number 12 to 17, there was significant difference between the effect of dilutions prepared from filtered pH 5.0 FNa broth solution returned to pH 7.2 and the unadjusted control. Reduced inhibition of *S. aureus* by the filtered pH 5.0 solution indicates that filtration of the low-pH solution through a $0.22 \mu\text{m}$ membrane lowered the FNa concentration by removing large aggregates. This was also supported cloudiness observed in the pH 5.0 broth on addition of 2.56 mM FNa and clarity after filtration.

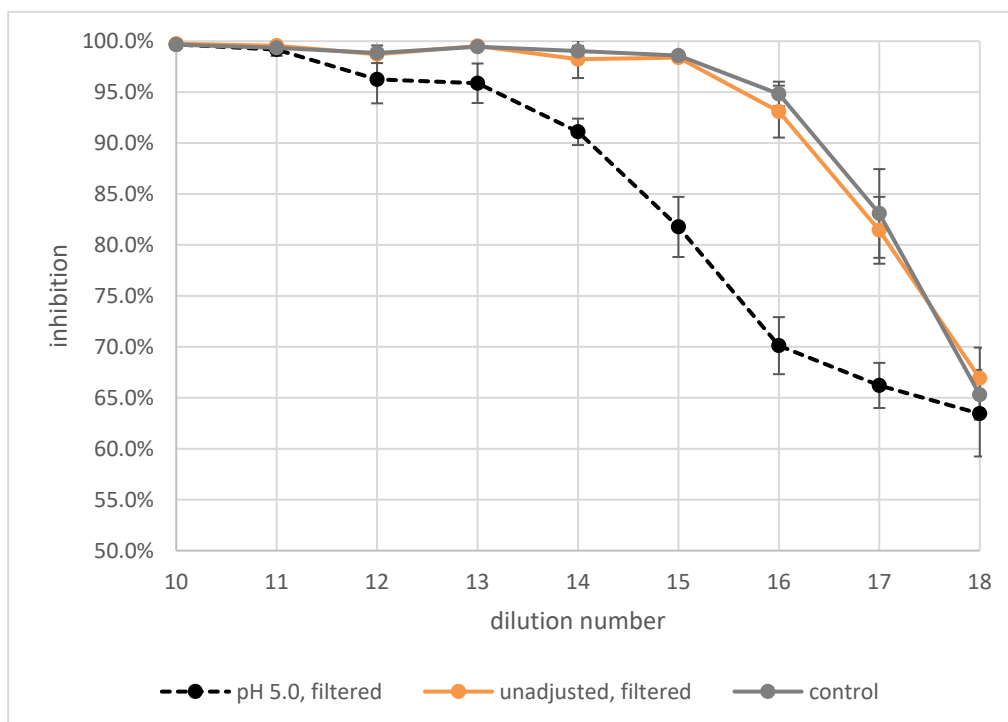


Figure 5.10 - Inhibition of *S. aureus* NCTC 12973 by sodium fusidate remaining after removal of large aggregates by filtration

Dilution number 15 equates to 78.125 nM sodium fusidate in unadjusted filtered broth and the control. The pH 5.0 broth was adjusted back to 7.2 after filtration of aggregates.
($n = 3$, error bars = 95 % CI)

The pH 5.0 inhibition plot was aligned with the activity of known FNa concentration against *S. aureus* by shifting the data by two dilutions (Figure 5.11). There was no significant difference between activity of known concentrations of 39.1, 19.5 or 9.8 nM FNa and that of the FNa present in the aligned filtered pH 5.0 broth ($p < 0.05$). As the shift of two two-fold dilutions equated to a four-fold difference in concentration, this implies that approximately 75 % of the FNa originally added to the pH 5.0 broth was removed by filtration, likely having formed aggregates of $\geq 0.22 \mu\text{m}$.

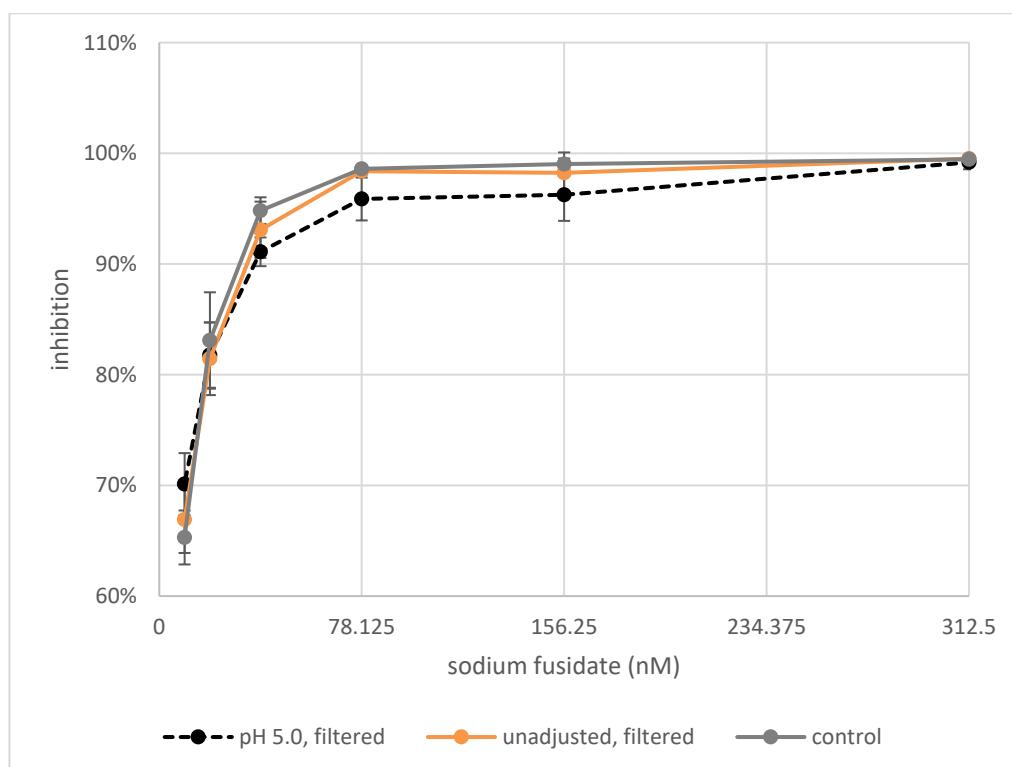


Figure 5.11 – Alignment of data for *S. aureus* NCTC 12973 inhibition by sodium fusidate after exclusion of large aggregates induced by lowered pH to unadjusted control
 Shifting the data for inhibition caused by sodium fusidate remaining in filtered pH 5.0 broth by two dilutions and comparison to controls allowed for estimation of sodium fusidate concentration.
 (n = 3, error bars = 95 % CI)

5.3.3.2 Assessment of sodium fusidate stability at reduced pH

To first assess whether phenomenon of pH-related FNa activity may be due to degradation of the drug into products more active against GN bacteria, a stability-indicating RP-HPLC method (separation method 2) was used to determine whether acid hydrolysis of FNa may occur under reduced pH conditions. Chromatograms for FNa in broth and in 50 % EtOH after 18 h incubation at 35 °C were aligned with the example provided by Byrne *et al.*, 2015^[288], the authors of the RP-HPLC method (Figure 5.12). Retention times observed were not identical to those reported due to differences in employed column length and material, however, the majority of fusidate breakdown products could be presumptively detected. (Assignment of fusidate peak had been previously verified during calibration curve construction, see Appendix B.)

Figure 5.13 displays example overlaid FNa chromatograms generated immediately after mixing and after 18 h incubation at 35 °C. The y axis upper bounds are limited to 100 mAU in order to allow visualisation of the smaller degradation product peaks. In standard NB, some FNa degradation occurred over the 18 h incubation period, as illustrated by the increased peak areas for 11-didehydrofusidic acid at approximately 25 and 16-

epideacetylfulvic acid at 30 min (Figure 5.13A). A similar degree and pattern of degradation was observed with 625 μM ZnSO_4 (Figure 5.13C). Conversely, lowered pH reduced this degradation, with or without the presence of antimicrobial metal ions. Figure 5.13B and D illustrate reduced FNa degradation in NB adjusted to pH 5.0 using H_2SO_4 and NB with 2.5 mM CuSO_4 (producing pH 5.11), respectively, compared to the unadjusted control, A. The results therefore suggest lowered pH may have a protective, stabilising effect on FNa in some conditions and, at least, does not induce hydrolysis or otherwise increase degradation.

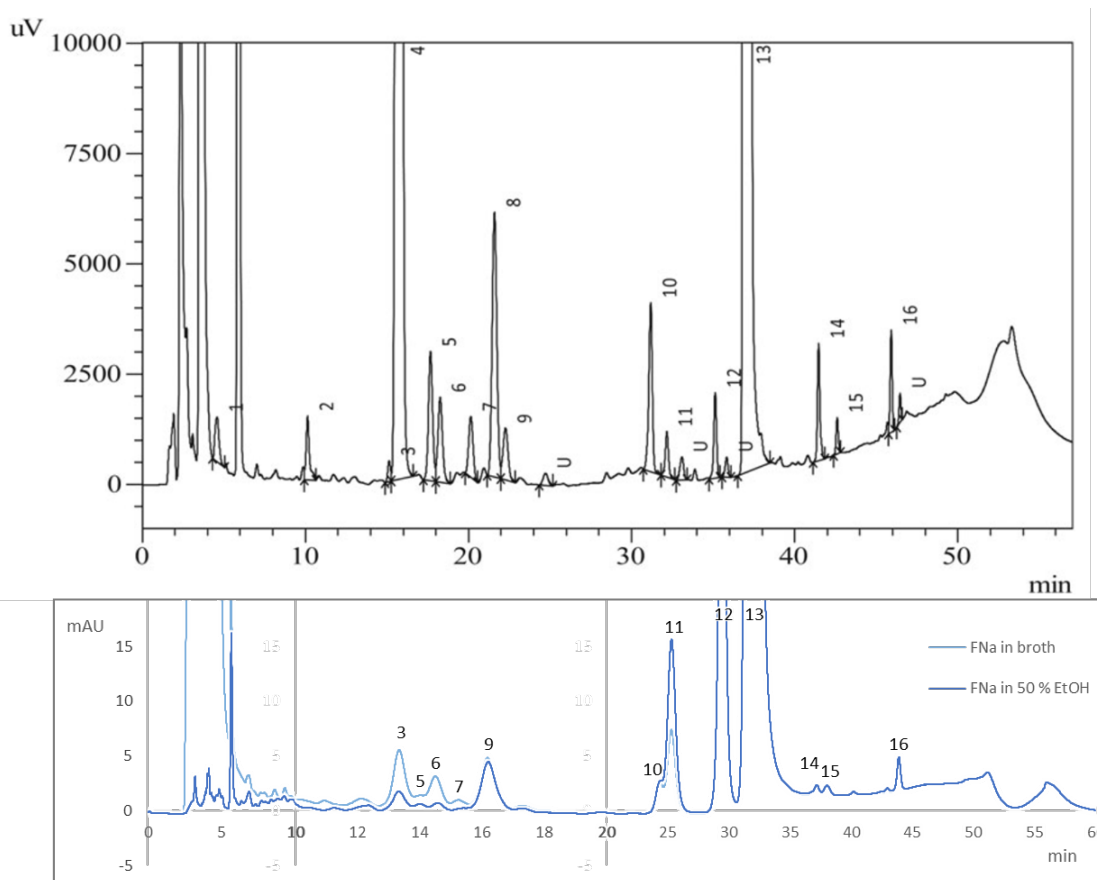


Figure 5.12 - Alignment of raw sodium fusidate 18 h stability chromatograms (lower panel) with published, annotated example from Byrne *et al.*, 2015^[288] (upper panel)

Peak identification, as given in Byrne *et al.*, 2015^[288]: 1. Betamethasone. 2. 24,25-Dihydro-24,25-dihydroxyfusidic acid. 3. 24,25-Dihydro-24,25-dihydroxyfusidic acid 21,25-lactone. 4. Betamethasone-17-valerate. 5. (24*R*)-24,25-dihydro-24,25-dihydroxyfusidic acid-21,24-lactone. 6. 26-Hydroxyfusidic acid. 7. (24*S*)-24,25-dihydro-24,25-dihydroxyfusidic acid-21,24-lactone. 8. Betamethasone-21-valerate. 9. 26-Oxofusidic acid. 10. 3-Didehydrofusidic acid. 11. 11-Didehydrofusidic acid. 12. 16-Epideacetylfulvic acid. 13. Fusidic acid. 14. 16-epideacetylfulvic acid-21,16-lactone. 15. Deacetylfulvic acid-21,16-lactone. 16. 11-Deoxyfusidic acid. U, unknown impurity. While quantification of derivatives was not the aim of this work, their presence and relative abundance could be compared.

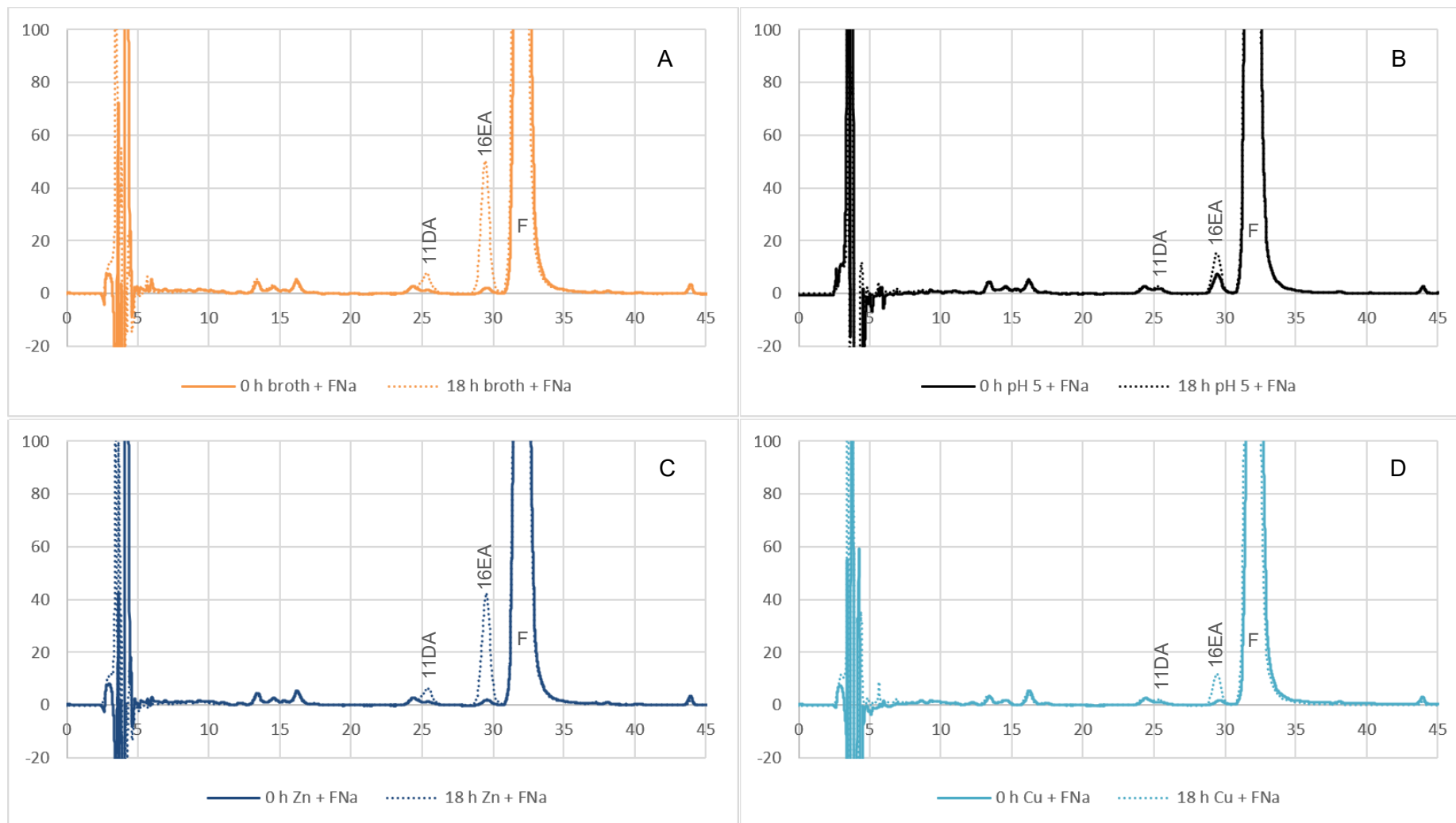


Figure 5.13 - Example stability-indicating RP-HPLC overlay chromatograms produced by 2.5 mM sodium fusidate before and after incubation for 18 h at 35 °C
 A: standard nutrient broth; B: nutrient broth adjusted to pH 5 using sulphuric acid; C: nutrient broth with 625 μM zinc(II) sulphate (pH 6.96); D: nutrient broth with 2.5 mM copper(II) sulphate (pH 5.11). Peak annotation: 11DA = 11-didehydrofusidic acid, 16EA = 16-epideacetylfusidic acid, F = fusidate.

5.3.3.3 Sodium fusidate solubility in pH adjusted nutrient broth and correlation with anti-*E. coli* activity

5.3.3.3.1 Sodium fusidate solubility in pH adjusted broth

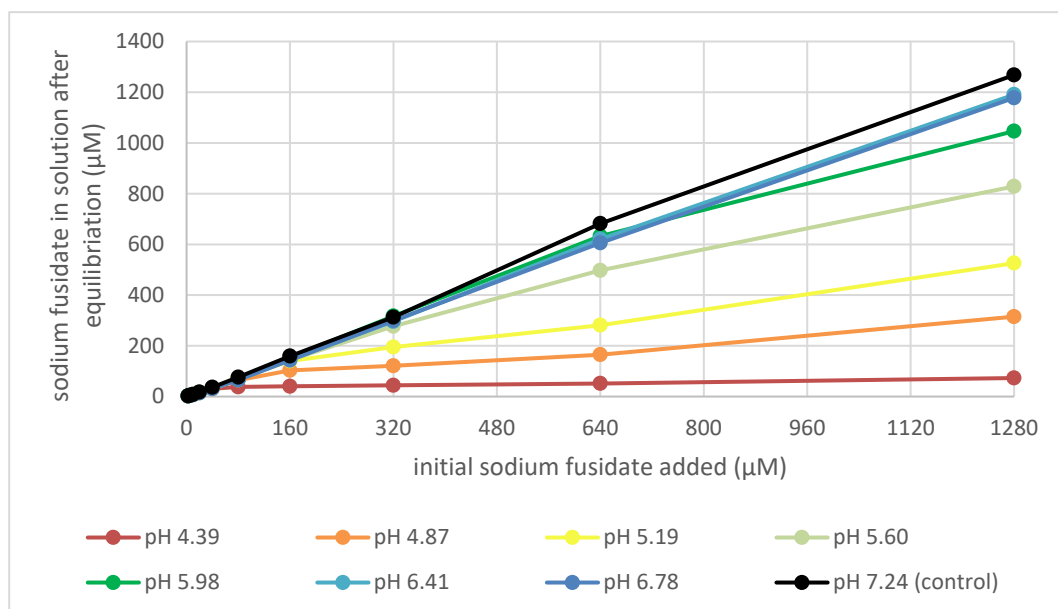


Figure 5.14 - Concentration of sodium fusidate remaining in solution after equilibration in pH adjusted nutrient broths for 1.5 ± 0.5 h at 20°C (n = 3, error bars = SD)

Table 5.2 - Correlation slopes and R^2 values for relationship between initial sodium fusidate concentration and concentration in solution after equilibrium at 20°C for 1.5 ± 0.5 h in pH adjusted nutrient broth

Broth pH	Initial : post-equilibrium sodium fusidate correlation slope (4 d.p.)	Initial : post-equilibrium sodium fusidate R^2 (4 d.p.)
4.39	0.0360	0.8533
4.87	0.2174	0.9635
5.19	0.3859	0.9790
5.60	0.6522	0.9873
5.98	0.8358	0.9889
6.41	0.9409	0.9994
6.78	0.9301	0.9997
7.24 (control)	0.9968	0.9999

The solubility of FNa in NB adjusted to different pHs was investigated in order to assess whether this correlated with enhanced anti-*E. coli* activity. Figure 5.14 illustrates the relationship between FNa remaining in solution after equilibrium for 1.5 ± 0.5 h at 20°C and initial FNa concentration at each broth pH, as determined by RP-HPLC. The correlations between initially added FNa and that remaining in solution at each pH tested are listed in Table 5.2. At pH 4.87 and above, the correlations between initial and post

equilibration FNa concentrations were very strong ($R^2 > 0.96$). The FNa saturation point in NB did not appear to be met at pH 4.87 and above using any of the concentrations tested. Due to the stock solution preparation method, EtOH was present in proportion to FNa concentration (1.25 % v/v with 1280 μM) which likely effected solubility, however, this was identical to the composition of dilutions used in all antimicrobial testing and therefore directly representative of conditions at the point of inoculation.

At pH 4.39, the correlation between initial FNa concentration and that remaining in solution was markedly reduced compared to higher pHs, with an R^2 of 0.85 compared to >0.96 . The concentration in solution after equilibration was only 28.7, 35.3, 38.3, 41.8, 49.3 and 71.1 μM when 40, 80, 160, 320, 640 and 1280 μM FNa had initially been added, respectively. A strong correlation with EtOH concentration in the respective dilution was also found ($R^2 = 0.98$), suggesting that the EtOH-free solubility of FNa in pH 4.4 broth at 20 °C was below the 28.7 μM observed when 0.039 % v/v EtOH was present.

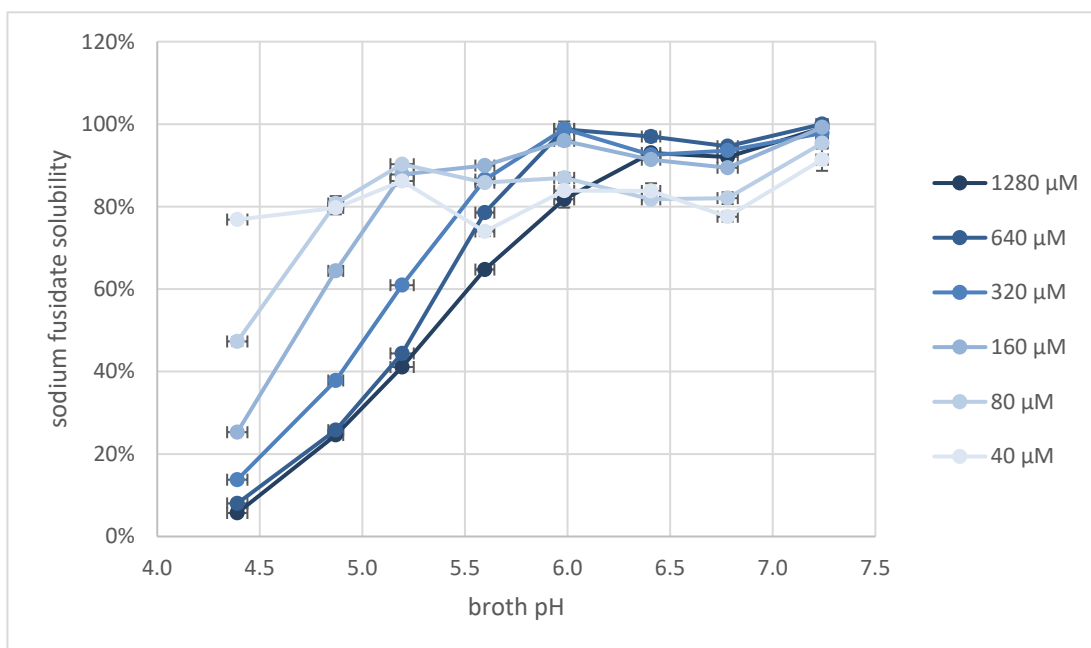


Figure 5.15 - Percentage of different initial sodium fusidate concentrations remaining in solution after 1-2 h equilibration at 20 °C in nutrient broth at a range of pHs
(n = 3, vertical error bars = SD, horizontal error bars = SD + pH electrode accuracy)

The nature of the relationship between FNa remaining in solution and NB pH varied depending on the initial FNa (and EtOH) added (Figure 5.15). With 1280 μM , (1.25 % v/v EtOH) there was a possibly sigmoid-like correlation between pH and FNa remaining in solution, with a linear portion between pH 4.8 and 6.0 ($R^2 = 1.00$) and maximal solubility apparently reached at pH 6.4 where there was no significant difference between FNa in solution at pH 6.8 ($p > 0.05$). There was a similar pattern in correlation between pH and

FNa remaining in solution after addition of 640 (0.625) and 320 μM (0.313 % v/v EtOH). Both exhibited linear relationships between pH 4.8 and 6.0 ($R^2 = 0.99$ and 0.98 , respectively) where maximal solubility was reached. With 160 and 80 μM FNa (0.156 and 0.078 % v/v EtOH, respectively), maximal solubility was reached at pH 5.2 after a possible linear relationship from pH 4.4. There was no apparent correlation between pH and FNa remaining in solution when only 40 μM (0.039 % v/v EtOH) was initially added, with between 26.7 and 34.3 μM detected at all pHs tested. In addition, solubility of 1280 μM FNa in pH 4.87 and 5.19 broths was 24.6 and 41.1 %, respectively, which, given the trend of decreasing solubility with increasing initial FNa concentration, directly supports the estimated 75 % precipitation of 2560 μM in pH 5.0 broth observed in Section 5.3.3.1.

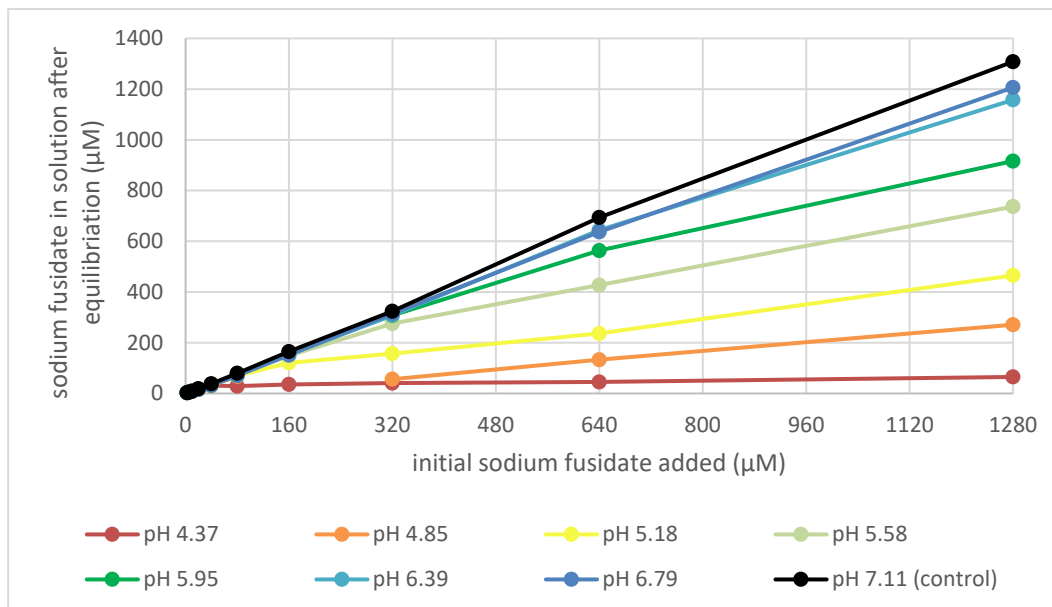


Figure 5.16 - Concentration of sodium fusidate remaining in solution after equilibration in pH adjusted nutrient broth for 18 ± 2 h at 35°C and 120 rpm
(n = 3, error bars = SD)

Table 5.3 - Correlation slopes and R^2 values for relationship between initial sodium fusidate concentration and concentration in solution after equilibrium at 35°C for 18 ± 2 h in pH adjusted nutrient broth

Broth pH	Initial : post-equilibrium sodium fusidate correlation slope (4 d.p.)	Initial : post-equilibrium sodium fusidate R^2 (4 d.p.)
4.37	0.0256	0.9890
4.85	0.1914	0.9620
5.18	0.3264	0.9875
5.58	0.5615	0.9843
5.95	0.7113	0.9842
6.39	0.9273	0.9973
6.79	0.9689	0.9992
7.11 (control)	1.0043	1.0000

Figure 5.16 illustrates the relationships between FNa remaining in solution after 18 ± 2 h at 35°C and initial FNa concentration, which were similar to those observed at 20°C (Figure 5.14). The correlation slopes and R^2 s between initially added FNa and that remaining in solution at each pH tested are listed in Table 5.3. The correlation between initial and post-equilibration FNa concentration was very strong for every pH, with $R^2 > 0.98$ for all but pH 4.8 which was 0.96. As with 1.5 ± 0.5 h equilibration at 20°C (Table 5.2), an equally strong correlation ($R^2 = 0.99$) was found between FNa remaining in solution after 18 ± 2 h equilibration in pH 4.4 broth at 35°C and EtOH concentration in the respective dilution.

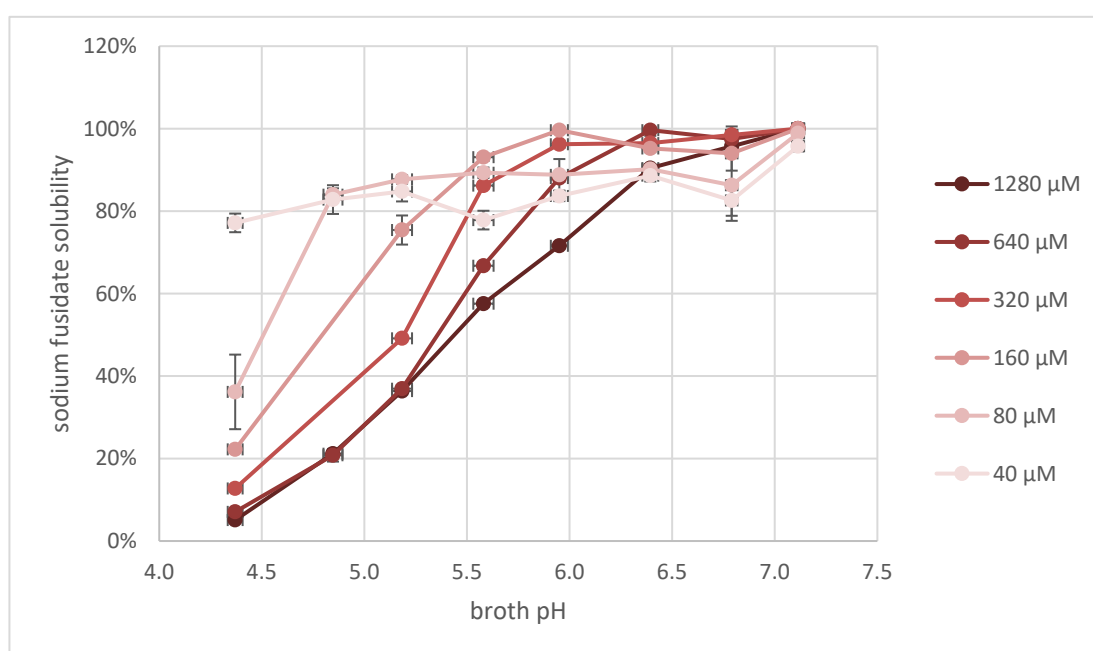


Figure 5.17 - Percentage of different initial sodium fusidate concentrations remaining in solution after 18 ± 2 h equilibration at 35°C in nutrient broth at a range of pHs
($n = 3$, vertical error bars = SD, horizontal error bars = SD + pH electrode accuracy)

As found at 20°C , the relationship between pH and FNa remaining in solution after equilibration at 35°C varied depending on the initial amount of FNa added (Figure 5.17). Sigmoidal correlations were apparent with 1280 (1.25 %), 640 (0.625 %) and 320 μM (0.313 % v/v EtOH) FNa. However, the pH range of the linear portions differed between initially added FNa (and EtOH) concentration, being from pH 4.8 to 6.4 ($R^2 = 1.00$), 4.8 to 6.0 ($R^2 = 1.00$) and 4.8 to 5.6 ($R^2 = 1.00$) with 1280, 640 and 320 μM , respectively. Maximal solubility with 640 and 320 μM FNa (0.625 and 0.313 % v/v EtOH) was reached at pH 6.4 and 6.0, respectively. With 1280 μM FNa (1.25 % v/v EtOH), the saturation point did not appear to be met and, although the concentration increment decreased beyond pH 6.4, there were significant differences in dissolved FNa at pH 6.4, 6.8 and

the pH 7.1 control ($p \leq 0.05$). Similar solubility patterns for 160, 80 and 40 μM FNa to those observed after 1.5 ± 0.5 h at 20 °C were found after equilibration at 35 °C.

The reduced differences detected in FNa solubility at lower initial concentrations maybe due to limitations in the ability of the processing method to remove undissolved drug from solution when there is high thermodynamic activity and low total concentration, rather than actual differences in solubility between starting concentrations. At low concentrations where aggregates do not form the duration of the fully protonated state is too short to result in any precipitation of FNa, consequently preventing removal of any undissolved fraction despite its presence. As such, an initial FNa concentration of 1280 μM was used in all subsequent testing.

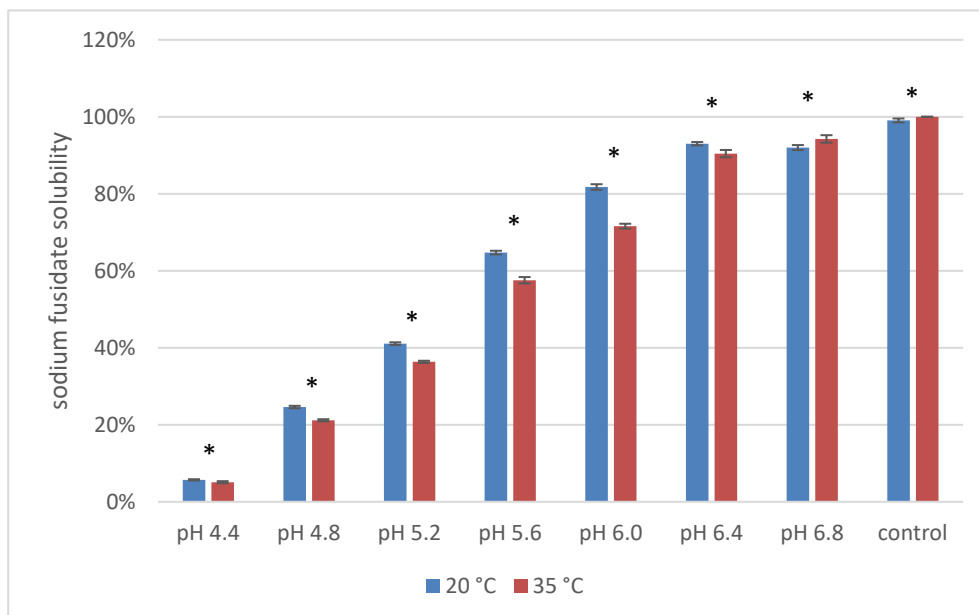


Figure 5.18 - Comparison of sodium fusidate solubility in pH adjusted nutrient broth after 1.5 ± 0.5 h at 20 °C and 18 ± 2 h at 35 °C
($n = 3$, error bars = 95 % CI, * = $p < 0.05$)

There were small but statistically significant ($p < 0.05$) differences between FNa solubility after equilibration 1.5 ± 0.5 h at 20 °C and 18 ± 2 h at 35 °C in pH adjusted nutrient broth (Figure 5.18). At pH 6.8 and below, apparent FNa solubility was lower after incubation at 35 °C for 18 h than 1.5 ± 0.5 h at room temperature. In order to more closely represent conditions in microbiological assays, data for 35 °C solubility was selected for use in all further analyses.

5.3.3.3.2 Relationship between sodium fusidate solubility and anti-*E. coli* activity in pH adjusted nutrient broth

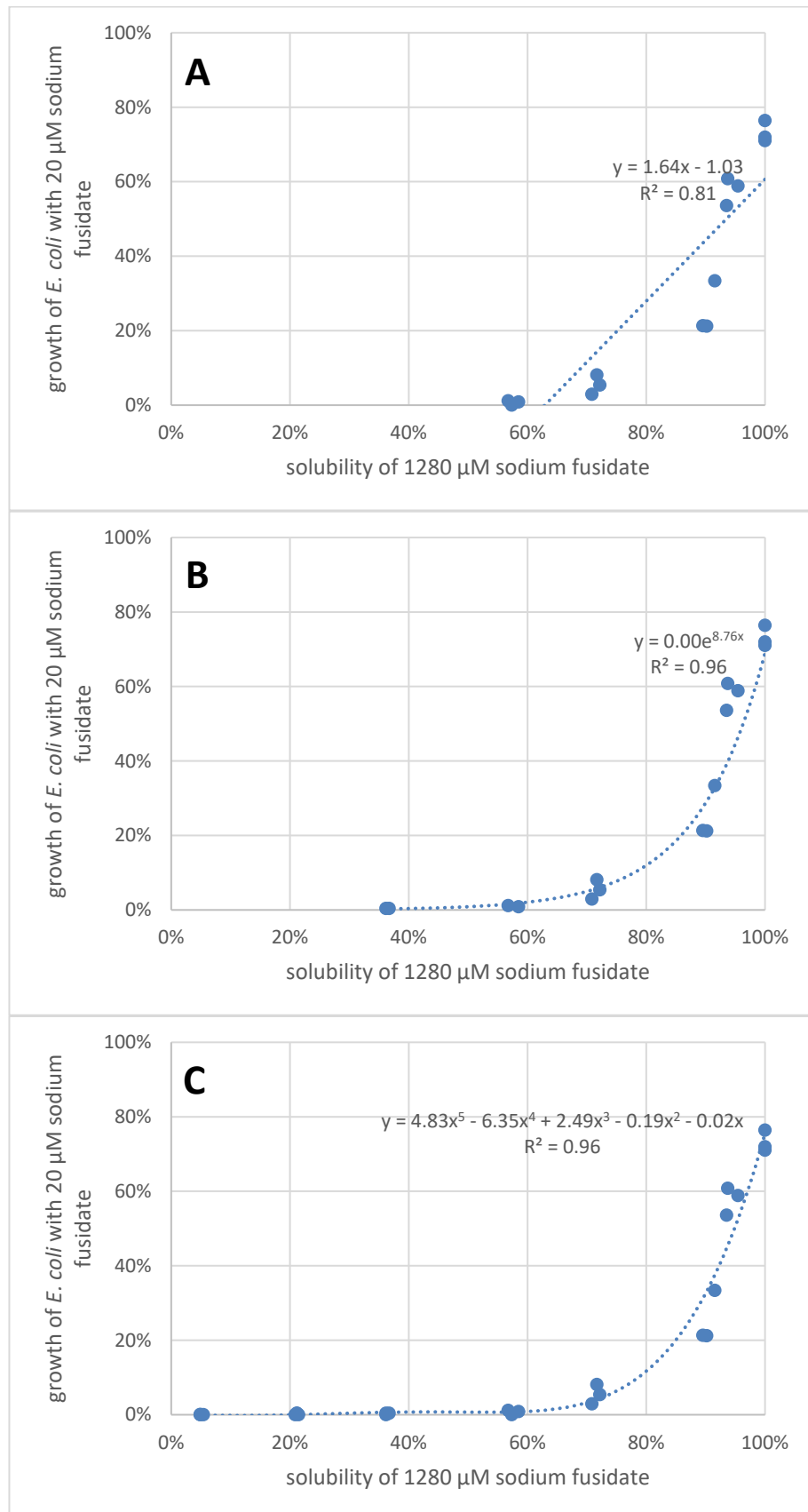


Figure 5.19 - Linear (A), exponential (B) and polynomial (C) modelling of the relationship between sodium fusidate solubility and its impact on growth of *E. coli* NCTC 10418

Data for solubility of 1280 µM FNa after equilibration for 18±2 h at 35 °C was selected for further correlation investigations as, in addition to being representative of microbiological test conditions, this initial concentration yielded the widest and most well distributed range of values over the investigated pH range, thereby enhancing the sensitivity of potential trend detection. After an initial analysis (not shown), *E. coli* data was inverted from % inhibition to % maximal growth in order to more effectively utilise Excel® trendline functions. Growth in the presence of 20 µM was selected for modelling as the variation in FNa activity across broth pH similarly exhibited a wide variation.

Figure 5.19 illustrates the three mathematical descriptions for the relationship between FNa solubility and its effect of *E. coli* growth. While removal of data points corresponding to solubility below 55 % from the analysis achieved an R² of 0.809, a linear correlation was not observed (Figure 5.19A). A strong correlation was identified as an exponential plot, with R² = 0.963 (Figure 5.19B), however, data points corresponding to no bacterial growth could not be included due to limitations in Excel® exponential fitting function. The use of this formula in relationship modelling would therefore be limited to solubilities of ≥36 % which correspond to >0 % maximal growth and would not be able to predict 100 % inhibition. However, the relationship was similarly well described by a fifth order polynomial equation (R² = 0.967, Figure 5.19C) which allowed inclusion of all data points in the fitting calculations. The following formula, derived from the polynomial curve in Figure 5.19C, was therefore used as the basis for modelling the relationship between inhibition of *E. coli* growth by 20 µM FNa and solubility of 1280 µM FNa:

$$A = 1 - ((4.83 \times S^5) - (6.35 \times S^4) + (2.49 \times S^3) - (0.19 \times S^2) - (0.02 \times S^1))$$

Where *A*: activity of 20 µM FNa as % inhibition of *E. coli* NCTC 10418, and *S*: % solubility of 1280 µM FNa.

5.3.3.4 Sodium fusidate solubility in nutrient broth with metal sulphates and correlation with anti-*E. coli* activity

5.3.3.4.1 Solubility of sodium fusidate with metal sulphates in nutrient broth

Percentage solubility of 1280 µM FNa in NB with metal sulphates after 1.5±0.5 h at 20 °C and 18±2 h at 35 °C are shown in Figure 5.20. In the presence of the two suppressive metals, Mn²⁺ and Zn²⁺, FNa exhibited more than 95 % solubility regardless of the metal concentration or the incubation temperature and duration. However, FNa solubility in NB in the presence of the other metals was dependent both on metal concentration and

incubation conditions. In particular, the solubility of FNa with Fe^{2+} reduced dramatically after incubation at 35 °C, consistent with the pH reduction and precipitation observed previously. Since differences in FNa solubility between equilibration conditions occurred and replicating the microbiological incubation environment was important to building a predictive model, FNa solubility data for 18 ± 2 h at 35 °C was selected for further use.

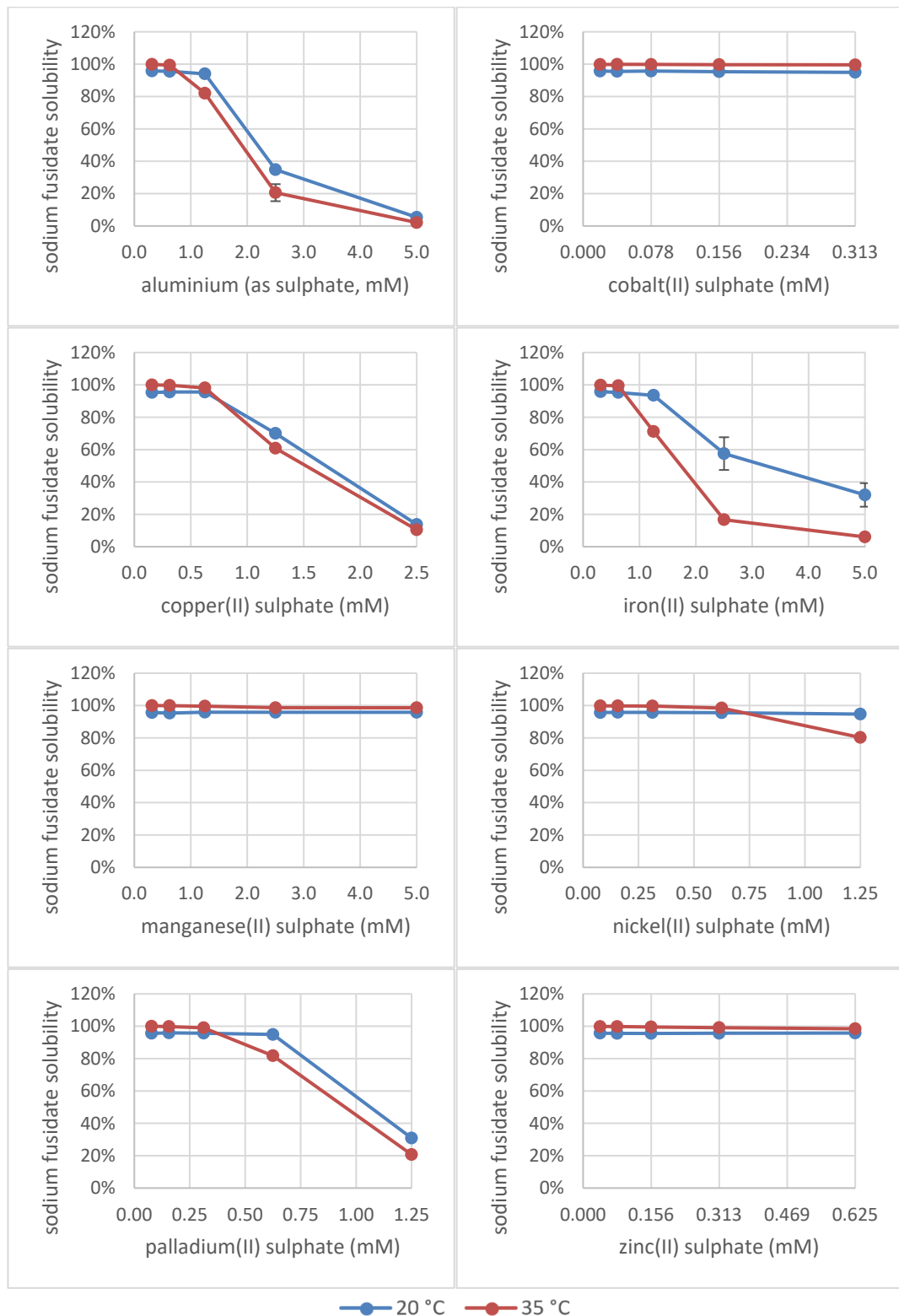


Figure 5.20 - Solubility of 1280 µM sodium fusidate in nutrient broth with metal sulphates after incubation for 1.5 ± 0.5 h at 20 °C (blue) or 18 ± 2 h at 35 °C (red)

(n = 3, error bars = SD)

In order to assess whether the effect on solubility was a direct function of broth pH change induced by the metal sulphate, the % 1280 μM FNa remaining in solution in the presence of the highest metal concentration tested was plotted against the pH for each equilibration condition. Data for 1280 μM FNa solubility in metal-free pH adjusted nutrient broth was included in the same graphs in order to assess whether solubility in the presence of metal sulphates aligned with the previously observed correlation with broth pH (Figure 5.21). FNa solubility in NB in the presence of other metal sulphates conformed well to the data for pH adjusted broth without metals.

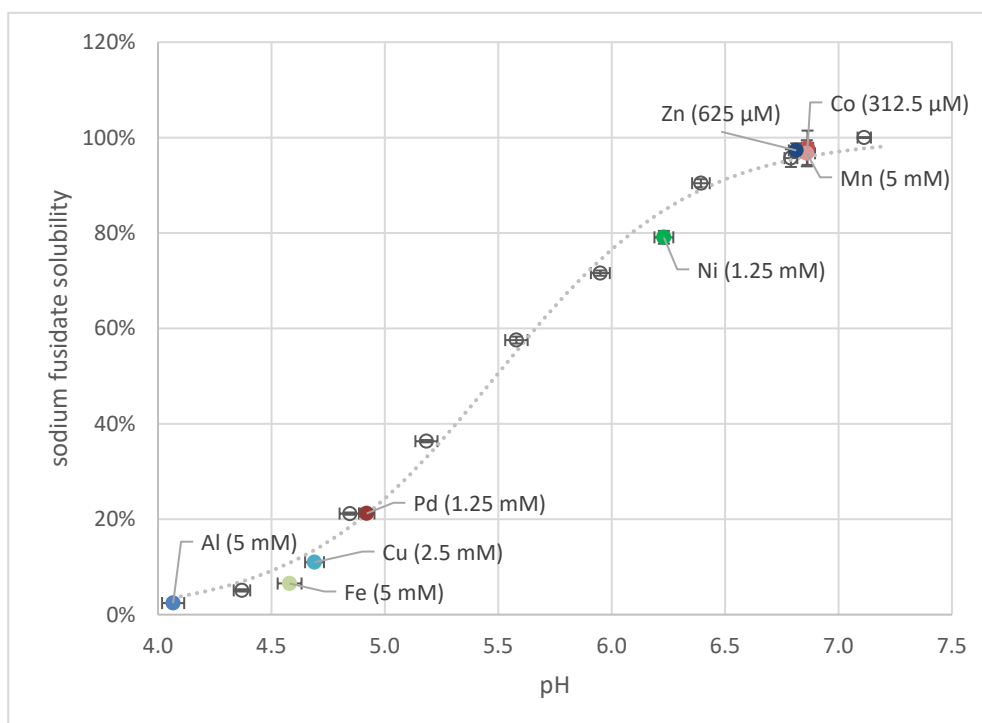


Figure 5.21 - Comparison of solubility of 1280 μM sodium fusidate in pH adjusted nutrient broth (open circles) and nutrient broth with metal sulphates (labelled closed circles) after equilibration for 18 \pm 2 h at 35 $^{\circ}\text{C}$

(n = 3, vertical error bars = SD, horizontal error bars = SD + pH electrode accuracy)

5.3.3.4.2 Predictability of anti-*E. coli* activity of sodium fusidate based on solubility in nutrient broth with metal sulphates

The equation derived in Section 5.3.3.3.2 from Figure 5.19C was applied to the data for 1280 μM FNa solubility in the presence of metal sulphates in order to test the modelling accuracy. The resulting predictions for *E. coli* inhibition by 20 μM FNa are referred to as

“predicted (i)”. A modified model, including addition of the inhibitory effect of each metal concentration alone, was also applied and its outputs referred to as “predicted (ii)”.

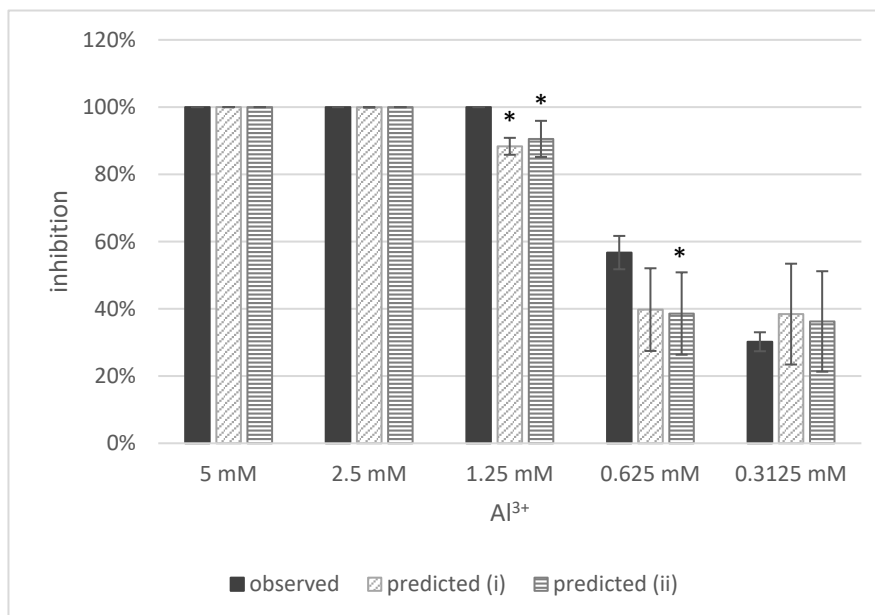


Figure 5.22 - Comparison of observed inhibition with two methods of predicting inhibition of *E. coli* NCTC 10418 by 20 μ M sodium fusidate in the presence of aluminium as sulphate in nutrient broth

(n = 3, error bars = 95 % CI, * = $p < 0.05$)

Four of the five predictions for the combined anti-*E. coli* activity of Al³⁺ and FNa using model (i) were not significantly different to the observed values ($p > 0.05$, Figure 5.22). Predicted inhibition by 1.25 mM Al³⁺ combined with 20 μ M FNa was 88.3 % whereas the observed value was 100 %. In addition, while not statistically different, mean predicted inhibition by FNa with 0.625 mM was 39.8 % while the observed inhibition was 16.9 % more at 56.7 %. When the activity of Al³⁺ alone was accounted for using model (ii) there was no improvement to the accuracy and predictions for both 1.25 and 0.625 mM were significantly different to those observed.

E. coli inhibition by 20 μ M FNa with Co²⁺ predicted by (i) was significantly different to that observed for all but the lowest tested concentration ($p < 0.05$, Figure 5.23). This was because pH, and therefore solubility of FNa, varied very little between the Co²⁺ concentrations in nutrient broth. When the activity of Co²⁺ alone was added, resulting predicted (ii) values more closely tracked the observed inhibition. However, there were still significant differences between observed and predicted inhibition with two Co²⁺ concentrations. Predicted (ii) inhibition with 0.078 mM Co²⁺ was 100 % whereas the observed inhibition was 94.2 % and with 0.039 mM predicted was 84.7 and observed 35.1 %.

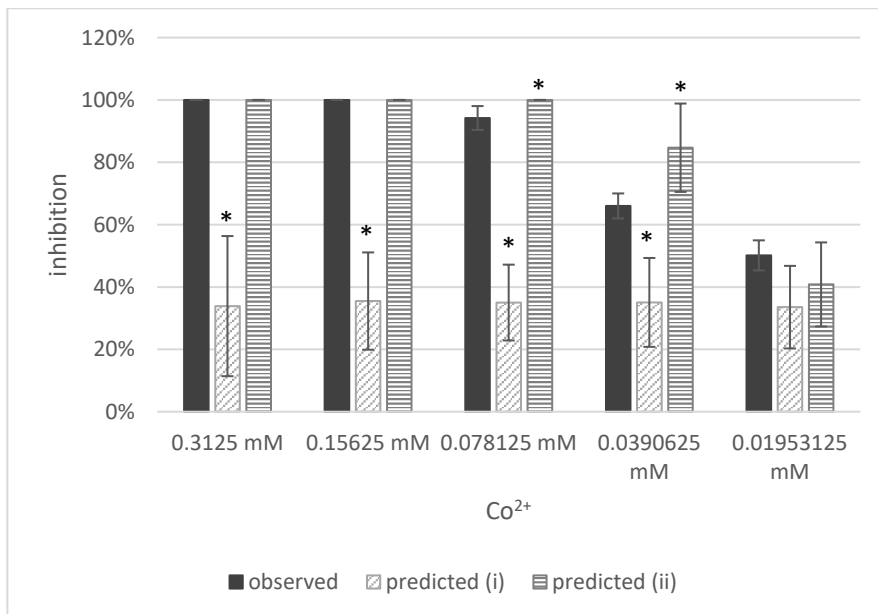


Figure 5.23 - Comparison of observed inhibition with two methods of predicting inhibition of *E. coli* NCTC 10418 by 20 µM sodium fusidate in the presence of cobalt(II) sulphate in nutrient broth

(n = 3, error bars = 95 % CI, * = p < 0.05)

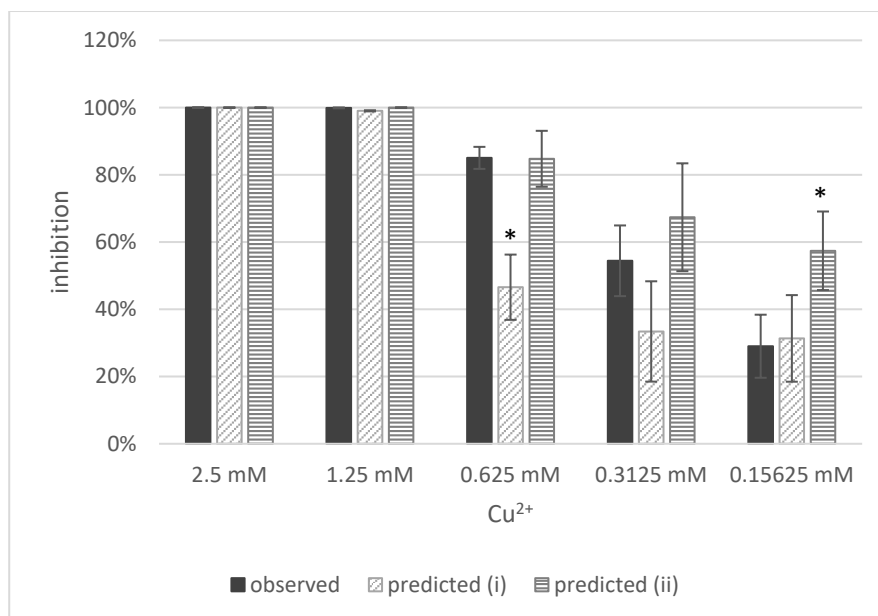


Figure 5.24 - Comparison of observed inhibition with two methods of predicting inhibition of *E. coli* NCTC 10418 by 20 µM sodium fusidate in the presence of copper(II) sulphate in nutrient broth

(n = 3, error bars = 95 % CI, * = p < 0.05)

Both models accurately predicted four of the five inhibition values for FNa and Cu²⁺ (Figure 5.24). Interestingly, inclusion of activity of Cu²⁺ alone using method (ii) gave the most accurate prediction for activity of 20 µM with 0.625 mM Cu²⁺ at 84.8 % inhibition compared to 85.0 % observed, while method (i) based on FNa solubility alone gave the

most accurate prediction for activity with 0.156 mM Cu^{2+} at 31.3 % compared to 29.0 % observed. In addition, the observed inhibition produced by FNa with 0.313 mM Cu^{2+} was 54.4 %, falling between the predictions made by each model (33.4 % by (i) and 67.4 % by (ii)). It therefore appears that the activity of 20 μM FNa in the presence of Cu^{2+} can be described differently depending on the concentration of metal present.

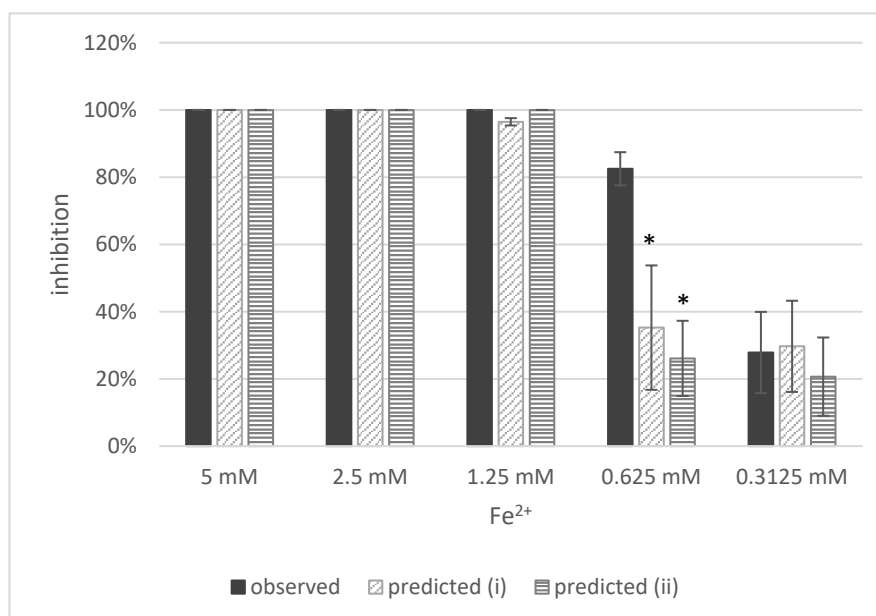


Figure 5.25 - Comparison of observed inhibition with two methods of predicting inhibition of *E. coli* NCTC 10418 by 20 μM sodium fusidate in the presence of iron(II) sulphate in nutrient broth

(n = 3, error bars = 95 % CI, * = $p < 0.05$)

Predicted inhibition of *E. coli* by FNa in the presence of Fe^{2+} calculated by either method was not significantly different to that observed ($p > 0.05$, Figure 5.25) at all concentrations other than 0.625 mM. However, both methods significantly underestimated the inhibition produced by 20 μM FNa with 0.625 mM Fe^{2+} ($p < 0.05$). Observed inhibition was 82.5 % whereas predicted values were 35.3 and 29.1 % by method (i) and (ii), respectively.

Values for predicted *E. coli* inhibition by 20 μM FNa in the presence of Mn^{2+} were closer to observed values when the activity of the metal alone was included in the calculations (predicted (ii), Figure 5.26). Without inclusion of metal activity, inhibition predicted by method (i) was significantly different to observed ($p < 0.05$) except with 1.25 mM Mn^{2+} . Conversely, using method (ii) only the prediction for 20 μM FNa with 0.313 mM Mn^{2+} was significantly different to that observed.

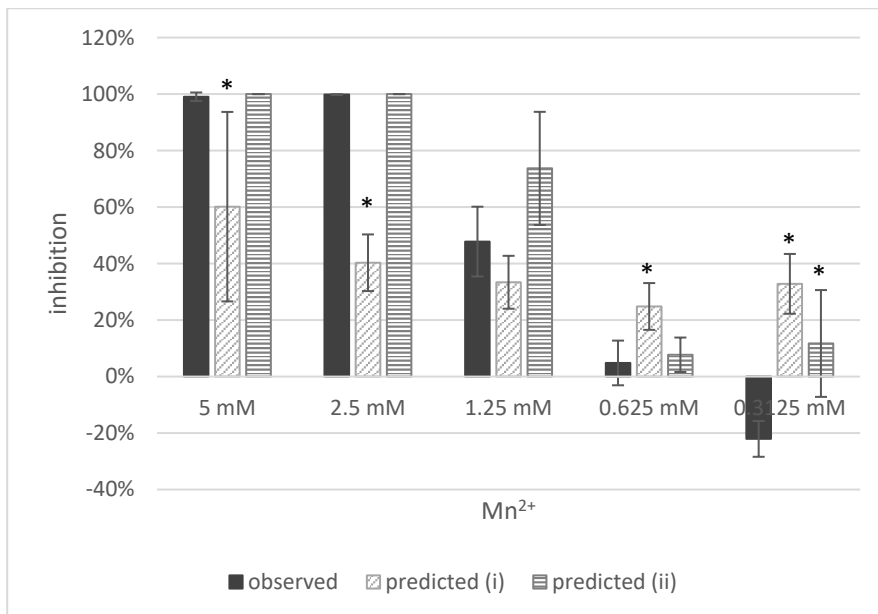


Figure 5.26 - Comparison of observed inhibition with two methods of predicting inhibition of *E. coli* NCTC 10418 by 20 µM sodium fusidate in the presence of manganese(II) sulphate in nutrient broth

(n = 3, error bars = 95 % CI, * = p < 0.05)

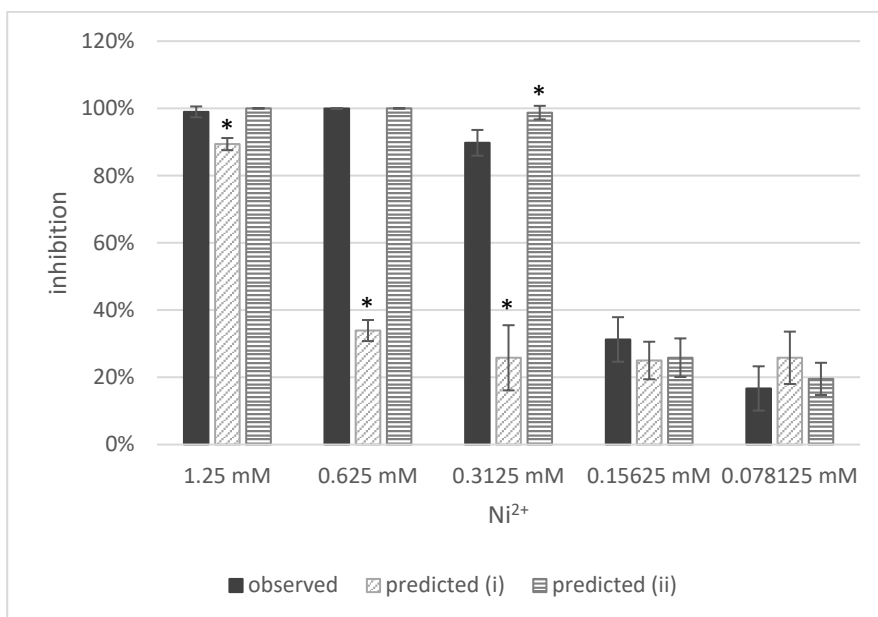


Figure 5.27 - Comparison of observed inhibition with two methods of predicting inhibition of *E. coli* NCTC 10418 by 20 µM sodium fusidate in the presence of nickel(II) sulphate in nutrient broth

(n = 3, error bars = 95 % CI, * = p < 0.05)

E. coli inhibition by 20 µM FNa in the presence of Ni²⁺ was also more accurately predicted when the activity of the metal alone was accounted for using method (ii) (Figure 5.27). The only significant difference between inhibition observed and that predicted by model (ii) was with 0.313 mM Ni²⁺ with values of 89.8 and 98.7 %, respectively.

Predictions of FNa activity when combined with Pd²⁺ were not accurate with either method (Figure 5.28). The predicted values were significantly greater than observed activity of 20 μM FNa with 0.313, 0.156 and 0.078 mM Pd²⁺. This may be explained by the tendency of Pd²⁺ to spontaneously form complexes which could reduce antimicrobial activity of FNa without proportionately effecting its solubility.

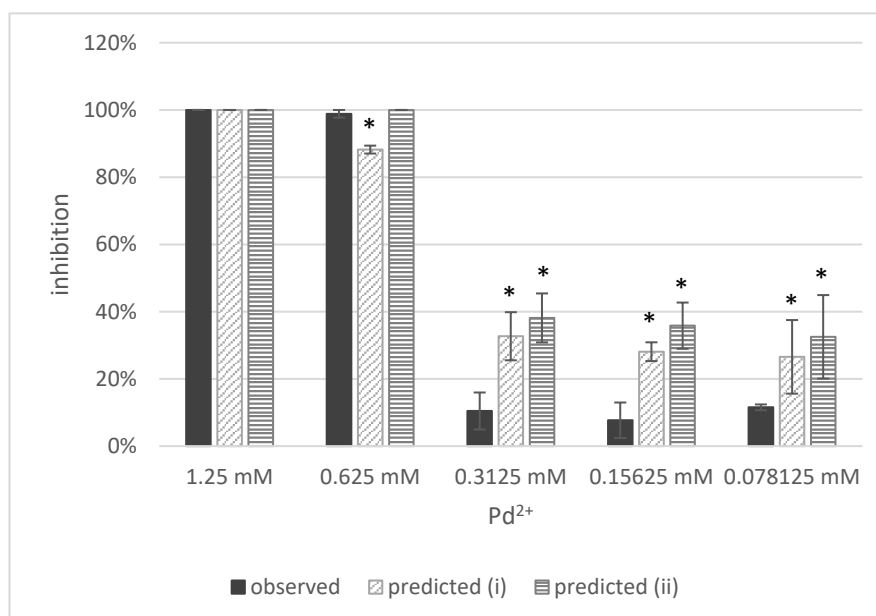


Figure 5.28 - Comparison of observed inhibition with two methods of predicting inhibition of *E. coli* NCTC 10418 by 20 μM sodium fusidate in the presence of palladium(II) sulphate in nutrient broth
(n = 3, error bars = 95 % CI, * = p < 0.05)

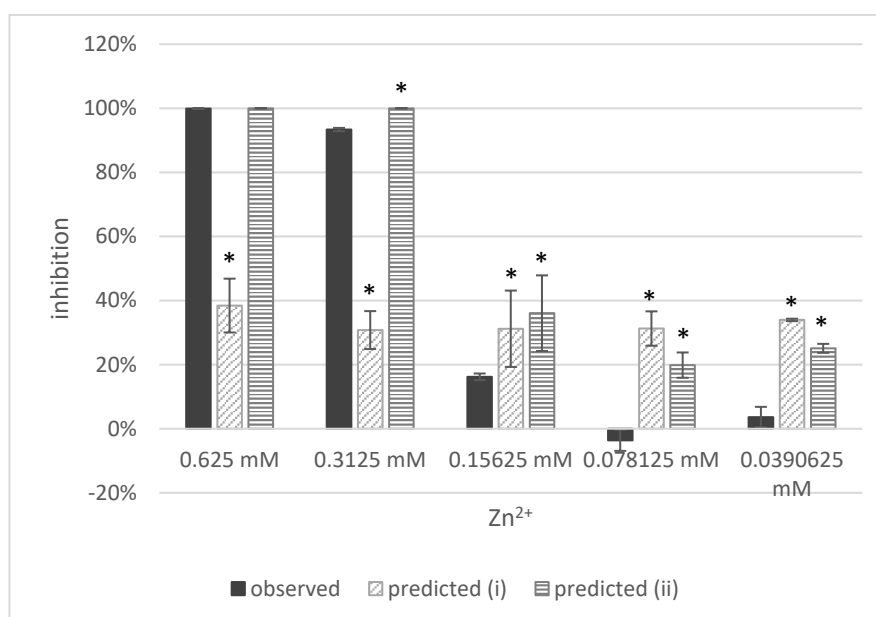


Figure 5.29 - Comparison of observed inhibition with two methods of predicting inhibition of *E. coli* NCTC 10418 by 20 μM sodium fusidate in the presence of zinc(II) sulphate in nutrient broth
(n = 3, error bars = 95 % CI, * = p < 0.05)

The combined activity of FNa and Zn²⁺ was also poorly predicted by both models (Figure 5.29). None of the values produced by model (i) accurately described the observed inhibition ($p < 0.05$). While model (ii) yielded predictions closer to the observed values, there was only no significant difference between observed and predicted activity for 20 µM FNa with 0.625 mM Zn²⁺ ($p > 0.05$).

The absolute differences between the mean observed and mean predicted inhibition of *E. coli* are summarised for model (i) and (ii) in Table 5.4 and Table 5.5, respectively. Overall, model (ii) was found to yield greater predictive accuracy than (i), with a mean of total differences of 10.1 compared to 25.5 %. However, while model (ii) more accurately predicted the activity of FNa with metal sulphates at their MIC₉₀ and above, some metals were better described by model (i) when below these concentrations. For example, the difference between model (i) predictions for FNa activity with 12.5 % MIC₉₀ of Cu²⁺ and Fe²⁺ and observed inhibition were only 2.3 and 1.8 %, respectively. However, when the observed effect of the same concentration of metal alone was included in the calculations as model (ii), the differences increased to 28.4 and 7.2 %. In contrast, predictions of activity with 12.5 % MIC₉₀ Co²⁺ or Ni²⁺ were closer to the observed values when the effect of the metal alone was included.

Table 5.4 - Difference between observed *E. coli* NCTC 10418 inhibition by 20 µM sodium fusidate in the presence of metal sulphates and that predicted by model (i)

Metal concentration (% MIC ₉₀)	Al ³⁺	Co ²⁺	Cu ²⁺	Fe ²⁺	Mn ²⁺	Ni ²⁺	Pd ²⁺	Zn ²⁺	mean
200	0.0%	66.1%	0.0%	0.0%	38.9%	9.6%	0.0%	61.5%	22.0%
100	0.1%	64.5%	0.9%	0.0%	59.5%	66.0%	10.6%	62.6%	33.0%
50	11.7%	59.2%	38.5%	3.5%	14.4%	64.0%	22.2%	15.0%	28.6%
25	17.0%	30.9%	21.0%	47.2%	20.0%	6.3%	20.4%	34.9%	24.7%
12.5	8.2%	16.6%	2.3%	1.8%	54.9%	9.1%	15.0%	30.3%	17.3%
mean	7.4%	47.5%	12.5%	10.5%	37.6%	31.0%	13.7%	40.9%	25.1%

Table 5.5 - Difference between observed *E. coli* NCTC 10418 inhibition by 20 µM sodium fusidate in the presence of metal sulphates and that predicted by model (ii)

Metal concentration (% MIC ₉₀)	Al ³⁺	Co ²⁺	Cu ²⁺	Fe ²⁺	Mn ²⁺	Ni ²⁺	Pd ²⁺	Zn ²⁺	mean
200	0.0%	0.0%	0.0%	0.0%	0.9%	1.0%	0.0%	0.1%	0.3%
100	0.0%	0.0%	0.1%	0.0%	0.2%	0.1%	1.2%	6.6%	1.0%
50	9.5%	5.8%	0.3%	0.0%	25.9%	9.0%	27.7%	19.9%	12.2%
25	18.1%	18.7%	13.0%	56.4%	2.9%	5.4%	28.1%	23.5%	20.8%
12.5	6.0%	9.3%	28.4%	7.2%	33.8%	2.8%	21.0%	21.5%	16.3%
mean	6.7%	6.8%	8.3%	12.7%	12.7%	3.7%	15.6%	14.3%	10.1%

The reduced solubility of FNa clearly plays a major role in its increased activity against *E. coli* when in combination with metal sulphates. However, these comparisons indicate that FNa solubility is not the sole determinant of activity of the combinations. In fact, while the independent antimicrobial activity of the metal generally contributes to combination efficacy, there are nuances with each metal suggesting the influence of other factors such as interplay between the various metabolic processes and survival mechanisms induced by each agent.

5.3.3.5 Predictability of anti-*E. coli* activity of sodium fusidate based on solubility in with other copper(II) salts and in other broths

The solubility of 1280 μM FNa (data not shown) in NB with Cu D-glu at unadjusted pH, NB with Cu D-glu adjusted to pH 7.2, LB with CuSO_4 and CAMHB with CuSO_4 was used to predict anti-*E. coli* activity of 20 μM FNa in the same conditions with models (i) and (ii).

5.3.3.5.1 Copper(II) D-gluconate in nutrient broth at native and neutral pH

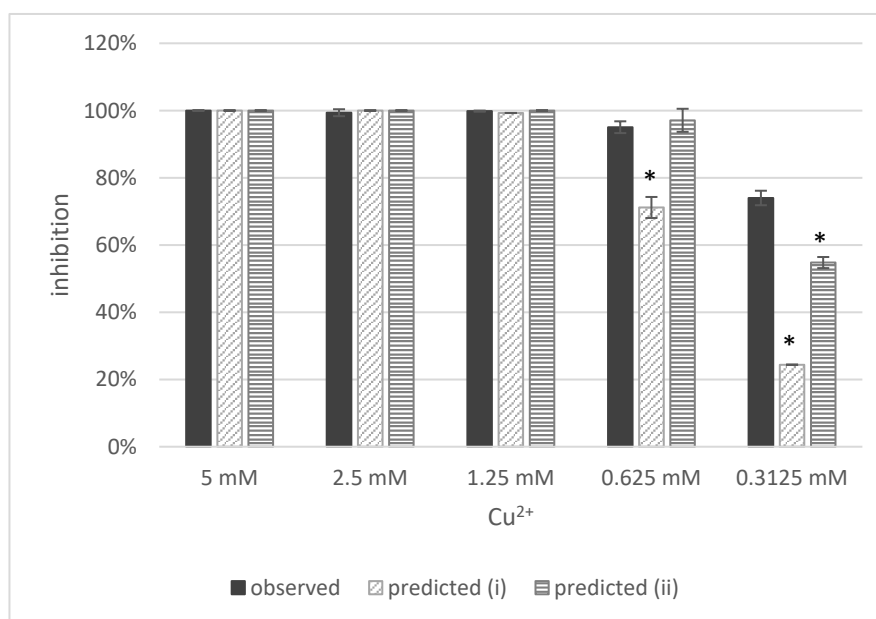


Figure 5.30 - Comparison of observed inhibition with two methods of predicting inhibition of *E. coli* NCTC 10418 by 20 μM sodium fusidate in the presence of copper(II) D-gluconate in nutrient broth at unadjusted native pH
(n = 3, error bars = 95 % CI, * = $p < 0.05$)

The activity of 20 μM FNa with Cu D-glu against *E. coli* was accurately predicted by model (ii) for four of the five Cu^{2+} concentrations investigated ($p > 0.05$, Figure 5.30). However, an additional 19.2 % inhibition was observed with 0.313 mM Cu^{2+} compared

to the (ii) prediction ($p < 0.05$). The difference between observed inhibition and that predicted by model (i) was statistically significant with both 0.625 and 0.313 mM Cu^{2+} ($p < 0.05$) at 23.9 and 49.6 %, respectively.

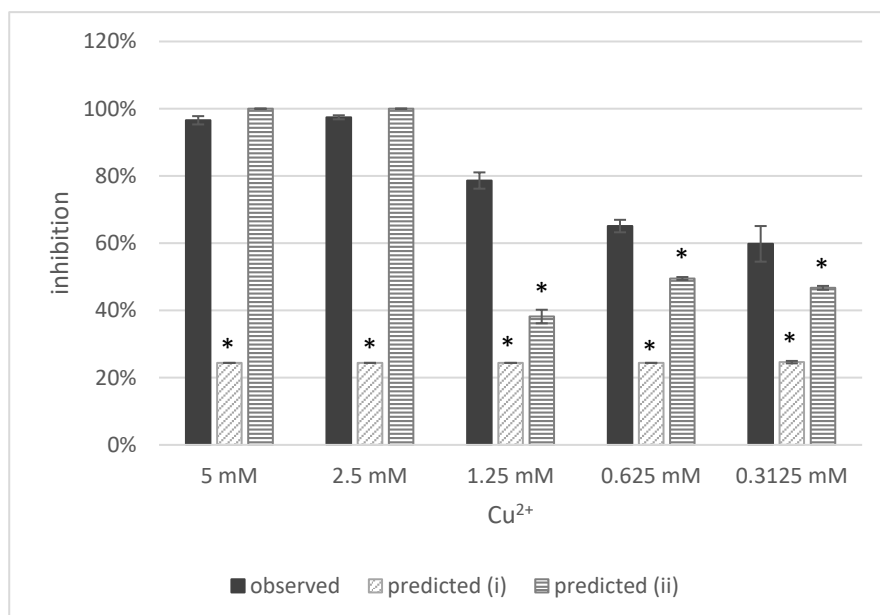


Figure 5.31 - Comparison of observed inhibition with two methods of predicting inhibition of *E. coli* NCTC 10418 by 20 μM sodium fusidate in the presence of copper(II) D-gluconate in nutrient broth adjusted to pH 7.2

($n = 3$, error bars = 95 % CI, * = $p < 0.05$)

Model (i) was unable to predict the anti-*E. coli* activity of 20 μM FNa combined with any concentration of Cu D-glu tested when the pH was adjusted to 7.2 ($p < 0.05$, Figure 5.31). This was because solubility of 1280 μM FNa was 100 % in all pH 7.2 NB solutions of Cu D-glu corresponding to a prediction of 24.4 % inhibition by 20 μM FNa in the same conditions. Inclusion of the activity of Cu D-glu alone at pH 7.2 increased the accuracy, reducing the mean difference between observed and predicted to 15.0 % with model (ii) compared to 55.1 % with (i). However, there were large and significant differences between the observed and predicted values with 1.25, 0.625, and 0.313 mM, with the actual inhibition being 40.5, 15.6 and 13.1 % higher than predicted by model (ii), respectively. While the activity of FNa combined with Cu D-glu in NB without pH adjustment correlated well with the additive effects of reduced FNa solubility and the activity of Cu D-glu alone, the results with the same combinations at pH 7.2 suggest a more complex mode of combined activity as the presence of Cu^{2+} enhances FNa activity beyond the effect of reduced solubility with independent metal activity.

5.3.3.5.2 Copper(II) sulphate in LB and cation adjusted Müller-Hinton broth

The models for solubility-based anti-*E. coli* activity of FNa were derived from observations in NB. Since bacterial growth and metabolism varies between media, predictions for activity in other broths using the same models can be expected to be limited. Indeed, while models (i) and (ii) both accurately predicted concentrations of CuSO_4 that would produce 100 % inhibition of *E. coli* growth when combined with 20 μM FNa in LB ($p > 0.05$, Figure 5.32), neither was successful at other concentrations. The mean difference between predicted and observed inhibition at the three lowest concentrations were 47.4 % with model (i) and 30.1 % with model (ii).

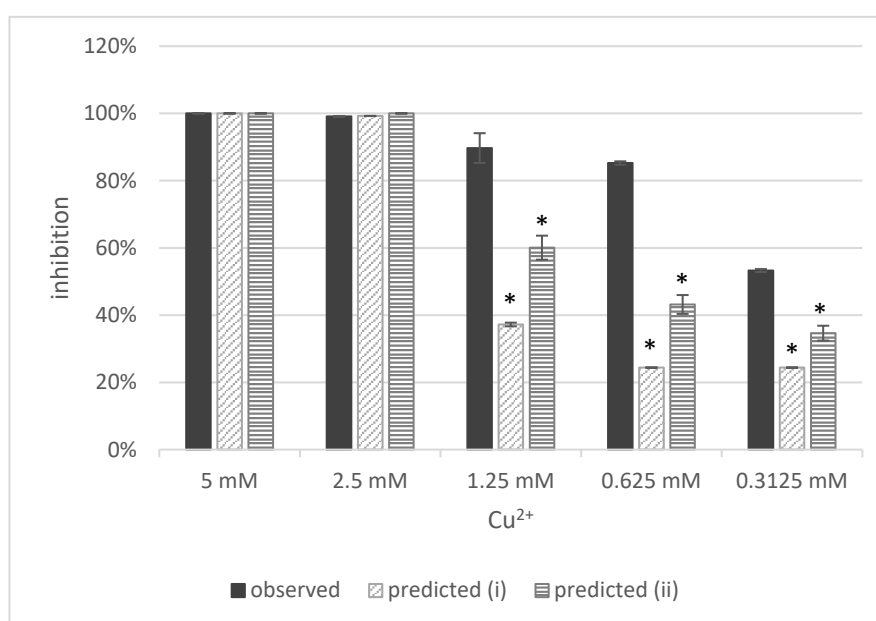


Figure 5.32 - Comparison of observed inhibition with two methods of predicting inhibition of *E. coli* NCTC 10418 by 20 μM sodium fusidate in the presence of copper(II) sulphate in Miller's lysogeny broth
($n = 3$, error bars = 95 % CI, * = $p < 0.05$)

Interestingly, predictions in CAMHB were closer to observed values than those for LB (Figure 5.33). The total mean difference between observed and predicted values was 11.2 % with model (i) and 8.7 % with model (ii), despite nearly all predictions being significantly different to the observed inhibition ($p < 0.05$). In particular, the pattern of predicted inhibition using (ii) was similar to that observed. CAMHB is supplemented with additional Ca^{2+} and Mg^{2+} to support increased bacterial growth which may be the cause of the observed inhibition being consistently lower than that predicted by model (ii).

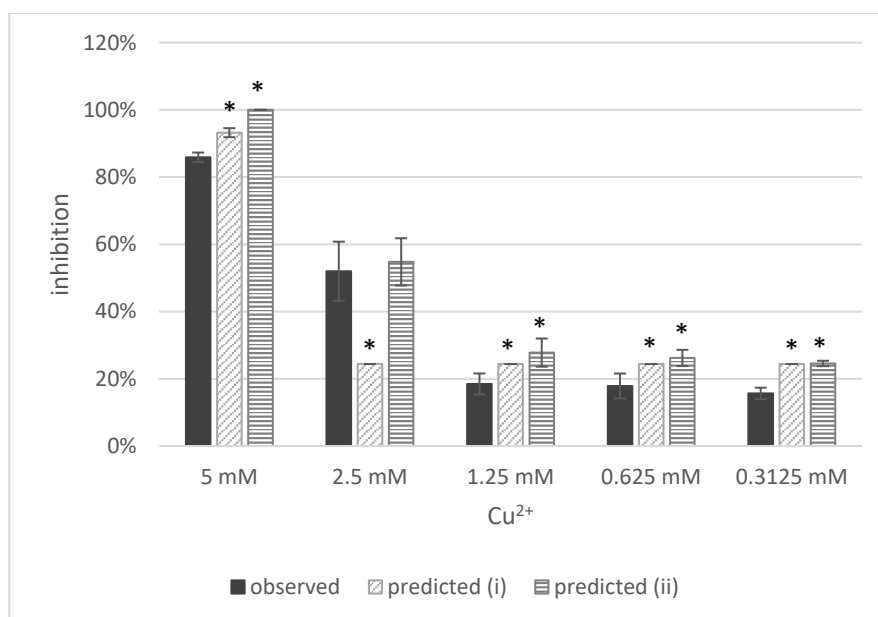


Figure 5.33 - Comparison of observed inhibition with two methods of predicting inhibition of *E. coli* NCTC 10418 by 20 µM sodium fusidate in the presence of copper(II) sulphate in cation adjusted Müller-Hinton broth
(n = 3, error bars = 95 % CI, * = $p < 0.05$)

5.3.4 Association of sodium fusidate with *E. coli* cells

The number of viable bacteria present at the end of the exposure period was selected for calculation of FNa per 10^6 cells since no significant difference was found between this and the number of viable *E. coli* NCTC 10418 initially exposed or recovered from the bacterial pellets ($p > 0.05$).

After exposure to 160 µM, 206.8 pg FNa was associated with *E. coli* NCTC 10418 per 10^6 cells (Figure 5.34). In the presence of CuSO₄, this value was greater at 278.6 ng FNa per 10^6 cells and with MnSO₄ it was lower at 143.8 ng per 10^6 cells. However, there was no statistically significant difference between the amount of FNa recovered from *E. coli* exposed to FNa in the presence of CuSO₄, MnSO₄ or the control due to variability between replicates ($p > 0.05$). In contrast, 1197.4 pg FNa per 10^6 cells was recovered from *E. coli* exposed to FNa in pH 6 broth (mean pH 5.94 ± 0.20 SD) which was significantly more than all other conditions ($p < 0.05$).

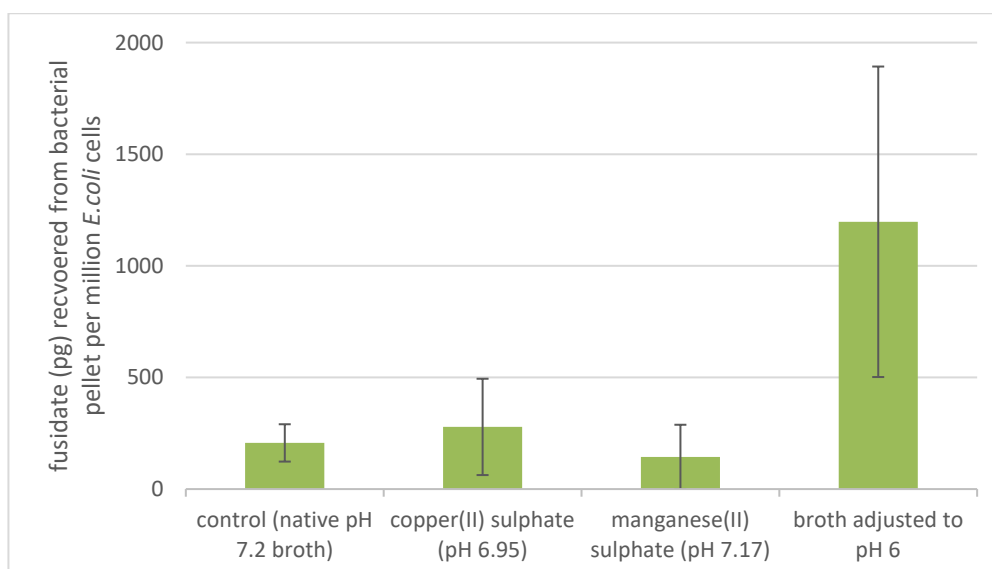


Figure 5.34 – Sodium fusidate per million *E. coli* NCTC 10418 cells recovered from bacterial pellet after exposure to 160 μM in nutrient broth in the presence of metal ions or reduced pH for 30 min at 35 °C and 120 rpm
(n = 3, error bars = 95 % CI)

Table 5.6 lists the activity and solubility of FNa compared to the amount recovered under the same conditions. While a relationship could not be described mathematically using only 4 data points, it was apparent that FNa activity against *E. coli* increased with increasing FNa recovery. This suggests that the greater activity of FNa at lower pH is at least in part due to more FNa being associated with the *E. coli* cells under these conditions. Interestingly, while a relationship between solubility or pH and FNa recovered was apparent for the control, Cu^{2+} and pH 6.0 broth, the Mn^{2+} appeared to be inconsistent. This could simply have been because of limitations in the sensitivity of the assay. However, as Mn^{2+} enhanced *E. coli* growth and was suppressive to FNa activity, an alternative explanation may involve induction of increased efflux by the metal, reducing total associated FNa disproportionately to its solubility.

Table 5.6 - Comparison of sodium fusidate recovered from *E. coli* NCTC 1014 to its activity and solubility under the same conditions, ordered by mass recovered

	Sodium fusidate (pg) recovered per 10^6 cells	<i>E. coli</i> inhibition by 160 μM sodium fusidate	Solubility of 1280 μM sodium fusidate	Solution pH
625 μM MnSO_4	143.8	54.1 %	99.9 %	7.17
control (pH 7.2)	206.8	88.7 %	100 %	7.20
312.5 μM CuSO_4	278.6	95.2 %	98.2 %	6.95
pH 6.0 broth	1197.4	99.6 %	71.6 %	6.00

5.4 Discussion

5.4.1 Precipitation (and not complexation) of sodium fusidate in the presence of copper(II) ions

UV-Vis analysis demonstrated decreased absorbance at the FA lambda max as increasing concentrations of CuSO₄ were mixed with FNa (Figure 5.2, page 119). This correlated with common titration spectra findings for complex formation – the free drug absorbance reduces as it is coordinated by metal ions^[451]. However, ITC did not indicate a complexation interaction. An example of the ITC profile generated by complexation is shown in Figure 5.1, page 107, illustrating a sigmoidal relationship between molar ratio and enthalpy per mole of injectant^[432]. ITC thermograms of CuSO₄ or Cu D-glu at their native pH titrated against FNa corresponded to precipitation (Figure 5.4A&B, page 121), with tailed enthalpy peaks of progressively decreasing size. Further, evidence of an enthalpy change is almost entirely eradicated when there is no pH drop on Cu²⁺ addition (Figure 5.4C, page 121) indicating that the precipitation is pH- rather than metal ion-mediated. The absorbance reduction in the UV-Vis spectrum at approximately FNa λ_{max} on titration with CuSO₄ can therefore be determined to be due to precipitation lowering the dissolved FNa concentration rather than complexation. This is supported by the observed elimination of absorbance change with adjustment of the Cu D-glu solution to neutral (Figure 5.3, page 120). If Cu²⁺ was complexing FNa it would be more likely to occur at higher, less acidic pH since this would encourage deprotonation of FNa and increased interaction with Cu²⁺ ^[429], but this is not the case. In addition, visual precipitate of FNa was filtered out of broth adjusted to pH 5 which lowered the effectiveness against *S. aureus* by 75 % (Figure 5.10, page 128) and this was not due to breakdown of FNa (Figure 5.13, page 131). These findings confirm lack of Cu²⁺ complexation and illustrate FNa precipitation at reduced pH. While this does not directly confirm other synergistic metals do not exert their efficacy by complexation, the trends in activity with pH and solubility discussed below indicate this is the most likely scenario.

5.4.2 Relationship between broth pH and sodium fusidate solubility

Figure 5.8 (page 125) illustrates the apparent relationship between broth pH and the activity of FNa against *E. coli*. While the pattern was consistent for synergistic metals, those that are additive or suppressive to FNa activity did not correlate, despite also

changing pH in some cases. In addition, the inhibition produced by FNa in pH-adjusted broth was consistently lower than when with metal ions at the same pH. Since the pH reduction produced by CuSO_4 had already been found to cause FNa precipitation in water (Section 5.3.1), it was hypothesised that this apparent relationship may have been due to changes in FNa solubility. Indeed, the solubility of FNa was found to strongly correlate with broth pH, both with and without metal ions after 1.5 ± 0.5 h at 20°C and 18 ± 2 h at 35°C (Section 5.3.3.3). As the pK_a of FA is 5.35^[443], the lower pHs will result in a higher proportion of the molecules being fully protonated and therefore insoluble. At lower pHs, % solubility is also seen to decrease as FNa concentration increases. FNa is known to aggregate in aqueous solutions by forming dimers with hydrophobic regions turned inwards which subsequently coalesce into much larger structures. The degree of aggregation is known to be related to at least the total concentration of FNa, presence of excess counter ions, temperature and the activity of buffers^{[443],[446],[452],[453]}. In addition, the Schulze-Hardy rule describes increased aggregation with increased counter ion valency^[454], which supports the particularly low FNa solubility observed with Al^{3+} (Figure 5.21, page 140). When the initial concentration of FNa is sufficient to result in aggregation, a large proportion of the undissolved fraction will be shielded and therefore stabilised in the precipitated form as only the surface area of aggregates would readily be able to be re-dissolved. Conversely, at lower concentrations where aggregation is not significant, all of the drug present can be readily accessed by the surrounding solvent and continuously de-protonated/protonated, even during and after high speed centrifugation to remove any precipitate. The duration of the fully protonated state is likely too short to result in any precipitation of drug when the initial concentration is low, consequently preventing removal of any undissolved fraction despite its presence.

The lower solubility after equilibration at 35°C for 18 ± 2 h than 20°C for 1.5 ± 0.5 h at pHs 4.4 to 6.0 (Figure 5.18, page 136) may be due to greater loss of EtOH from the incubated samples. The rate of EtOH evaporation has also been shown to be higher for low concentration aqueous solutions due to the preferential adsorption of EtOH to the air-liquid interface^[455]. In fact, the evaporation rate increases in rapidity inversely to the EtOH concentration remaining in solution, with the mass transfer coefficient increasing from 26.1, 47.8 to 71.2 m h^{-1} as concentration decreases from 5.38, 2.01 to 0.64 % v/v. The combination of this phenomenon with increased temperature and/or different equilibration durations could result in less EtOH in solution in the incubated samples than those at 20°C . As it acts to increase sodium fusidate solubility, this reduction in EtOH in solution would result in increased precipitation of sodium fusidate. Conversely, at pHs 6.4 and 6.8, solubility at 35 is greater than at 20°C which reflects the usually expected trend due to greater kinetic energy at higher temperature. It appears that at these pHs the increased kinetic energy sufficiently overcomes the effects of EtOH loss

allowing greater solubility than seen at lower pHs. Finally, there was no significant difference between solubility of the various initial concentrations in control broth – it seems that the effects of excess hydrogen ions, EtOH loss and increased energy are in balance to produce the same % solubility at both temperatures.

5.4.3 Predicting anti-*E. coli* activity of sodium fusidate based on its solubility

As complex aqueous solutions can often take a considerable period of time to reach equilibration and all antimicrobial activity studies were performed at 35 °C for 18±2 h, it can be reasoned that solubility data for solutions equilibrated in these conditions are likely to be more reliable and representative of the antimicrobial assay than data from 1.5±0.5 h equilibration at 20 °C. In addition, the longer equilibration period yielded more consistent pH and solubility results, particularly for unstable Fe²⁺ (Figure 5.20, page 139). When the calculated activity of reduced solubility FNa and known activity of metal ions alone were summed using model (ii) (Table 5.5, page 146), predictions were more similar to observed activity against *E. coli* than if independent metal ion activity was omitted (model (i), Table 5.4, page 146). The mean difference between predicted and observed inhibition was 25.1 %, range 0 – 66.1 % with 17/40 differences being >20 %, when metal activity was not included (model (i)). This reduced to 10.1 %, range 0 – 56.4 % with 9/40 differences being >20 % when the effect of the metal alone was accounted for with model (ii). This suggests that the combined activity of FNa and metal ions against *E. coli* is primarily a product of the additive effects of reduced FNa solubility and metal ion antimicrobial action. However, other factors such as synergising effects of pH stress (Section 5.1.2.1, page 108) and the change in pH and consequent FNa solubility during the course of incubation observed with some metals (Figure 5.20, page 139) may both contribute to explaining the inconsistencies in predictions and complicate formulation of a more accurate model.

5.4.3.1 Metal sulphates in nutrient broth

5.4.3.1.1 Sodium fusidate with synergistic aluminium, copper(II) or iron(II)

Agreement between the observed inhibition of *E. coli* NCTC 10418 and that predicted by model (ii) was higher than model (i) for both Al³⁺ (Figure 5.22, page 141) and Cu²⁺ (Figure 5.24, page 142) with 20 µM FNa. However, since sub-MIC₉₀ Al³⁺ alone had only a small impact on bacterial growth (± ≤2.2 % compared to the agent-free control), there was no

significant differences between the predicted combination activities from the two models ($p > 0.05$). While the observed activity of 0.313 and ≥ 2.5 mM Al^{3+} combined with 20 μM FNa was as predicted, observed *E. coli* inhibition by 0.625 and 1.25 mM was significantly more than that predicted. This implies some additional factor may be involved in the combined activity, perhaps the effects of pH stress. Since Al^{3+} and low pH both cause membrane damage (see Sections 4.1.1.1 and 5.1.2.1), their combined effects at these concentrations may synergise with 20 μM FNa by increasing intracellular access. Interestingly, observed activity of 20 μM FNa with ≥ 0.313 mM Cu^{2+} was best described by the sum of reduced solubility FNa activity and Cu^{2+} (model (ii), $p > 0.05$). Conversely, prediction based on the relationship between solubility FNa without accounting for metal ion activity (model (i)) was more accurate for 20 μM FNa and 0.156 mM Cu^{2+} ($p > 0.05$, Figure 5.24, page 142). This pattern suggests that the proposed additive activity of FNa at reduced solubility and metal ions against *E. coli* occurs with Cu^{2+} concentrations of ≥ 0.313 mM. Below this Cu^{2+} concentration, *E. coli* appears to be impervious to the effects of Cu^{2+} when in the presence of 20 μM FNa. Previous observations indicated that higher concentrations of ≥ 1 mM FNa stabilised the bacterial membrane and reduced sensitivity to Cu^{2+} in water (Chapter 4, Section 4.3.3.2). The lower FNa concentration investigated here may be able to aid *E. coli* in resisting the effects of lower concentrations of Cu^{2+} in NB in the same way, which could account for activity of the combination being lower than that predicted by model (ii). Alternatively, exposure to either agent at very low sub-MIC₉₀ may induce processes providing cross-resistance or enhancing overall viability and growth. In either case the similarity between predicted anti-*E. coli* activity of FNa at equivalent solubility alone and that observed in response to the combination of 20 μM FNa and 0.156 mM Cu^{2+} is likely to be coincidental.

Models (i) and (ii) gave similarly accurate predictions for the activity of Fe^{2+} with 20 μM FNa ($p > 0.05$, Figure 5.25, page 143). Only the observed activity of 0.625 mM Fe^{2+} combined with 20 μM FNa was significantly greater than predicted inhibition ($p < 0.05$), exhibiting an extra 47.2 and 56.4 % than predicted by model (i) and (ii), respectively. This concentration may represent the tipping point between manageable levels of Fe-mediated ROS generation, membrane disruption and other redox damage while still being able to simultaneously efflux 20 μM FNa when only 0.313 mM Fe^{2+} is present, and *E. coli* homeostasis mechanisms being overwhelmed by 0.625 mM Fe^{2+} .

5.4.3.1.2 Sodium fusidate with indifferent cobalt(II), nickel(II) or palladium(II)

The combined activity of 20 μM FNa and Co^{2+} (Figure 5.23, page 142) or Ni^{2+} (Figure 5.27, page 144) could not be accurately predicted using model (i). Since the pH of the tested concentrations of each metal had very little effect on the pH of nutrient broth, FNa

solubility was similar for all (except 1.25 mM Ni²⁺ which produced pH 5.97). However, when the activity of the metal ions alone was also included in the calculations, the predicted inhibition closely corresponded to that observed. The predictions for *E. coli* inhibition by 20 µM FNa with 0.078 or 0.039 mM Co²⁺ were higher than that observed ($p < 0.05$). This may be due to the micronutrient role of Co²⁺ as discussed in Section 4.4.1.2. Only the prediction for 0.313 mM Ni²⁺ with 20 µM FNa was higher than that observed, likely due to similar reasons (see Section 4.4.1.2). Conversely, the predicted *E. coli* inhibition by the three lowest concentrations of Pd²⁺, 0.313, 0.156 and 0.078 mM, combined with 20 µM FNa by both models was significantly higher than that observed ($p < 0.05$, Figure 5.28, page 145). This finding may support complexation between Pd²⁺ and FNa, as hypothesised in Chapter 4. At the lower concentrations of Pd²⁺, coordination of FNa may remove enough free metal ions from solution that the detectable antimicrobial effect attributable to them is reduced, while no FNa can penetrate the bacterial cell to exert its effect either. At higher Pd²⁺ concentrations, all FNa is again complexed and cannot enter the cells, however, there is enough free Pd²⁺ to cause considerable bacterial damage. In addition, 100 % inhibition is observed with the higher Pd²⁺ concentrations due to the additional pH stress exerted rather than free, active FNa.

5.4.3.1.3 Sodium fusidate with antagonistic manganese(II) or zinc(II)

The anti-*E. coli* activity of 20 µM FNa with both Mn²⁺ (Figure 5.26, page 144) and Zn²⁺ (Figure 5.29, page 145) was more accurately predicted with inclusion of the effects of metal ions alone by model (ii). The only significant difference between observed activity of 20 µM FNa in the presence of Mn²⁺ and that predicted was with 0.313 mM Mn²⁺. The growth of *E. coli* was enhanced by 20 % by 0.313 mM Mn²⁺ when alone and by the combination of 0.313 mM Mn²⁺ and 20 µM FNa. As discussed in Section 4.4.1.1, Mn²⁺ is a micronutrient for *E. coli* and may enhance AcrAB-TolC expression and function, which explains the growth enhancement in the presence of the combination. In addition, while NB can support growth of most non-fastidious bacteria, it is notoriously lacking in certain areas of "nutrition", including Mn²⁺ with concentrations of less than 1 µM^[456]. Therefore, an additional low concentration of 0.313 mM Mn²⁺ alone enhances *E. coli* growth as a micronutrient while higher concentrations are inhibitory. The anti-*E. coli* activity of 20 µM FNa with Zn²⁺ predicted by both models was quite different to that observed (Figure 5.29, page 145). While the inclusion of activity of Zn²⁺ when alone improved accuracy for 0.625 and 0.313 mM Zn²⁺, both models overestimated combined activity with ≤ 0.156 mM Zn²⁺. This is likely to be for similar reasons as with Mn²⁺ and discussed for Zn²⁺ in Section 4.4.1.1, namely increased AcrAB-TolC activity, MdtABC-TolC induction and greater ribosomal turnover.

5.4.3.2 Copper(II) D-gluconate in nutrient broth at native and neutral pH

The observed activity of 20 μM FNa combined with Cu D-glu at native pH against *E. coli* was very similar to that predicted by model (ii) (Figure 5.30, page 147). Interestingly, however, and in contrast to CuSO_4 , the observed inhibition with 0.313 mM Cu D-glu was significantly higher than that predicted ($p < 0.05$). As discussed in Section 4.4.2, this may be because *E. coli* can utilise gluconate as a carbon source^[457] and the resulting increase in bacterial metabolism allows greater FNa-mediated inhibition. At neutral pH, there is more disparity between the observed combined activity of 20 μM FNa with Cu D-glu and that predicted by model (ii) (Figure 5.31, page 148). The model (ii) predictions – which include the activity of the metal salt alone under the same conditions – were closer to observed inhibition than the model (i) predictions. However, the inhibition predicted by model (ii) for 20 μM FNa with ≤ 1.25 mM Cu D-glu at pH 7.2 was significantly lower than that observed. This is likely to be due to the same gluconate-metabolism and FNa activity combination as hypothesised for 20 μM FNa with 0.313 mM Cu D-glu at native pH. In addition, the phenomenon was observed at higher Cu^{2+} concentrations when adjusted to pH 7.2, presumably because neutralisation reduced pH stress, thereby allowing additional growth and its subsequent inhibition by FNa.

5.4.3.3 Copper(II) sulphate in LB and cation adjusted Müller-Hinton broth

Prediction of the anti-*E. coli* activity of FNa and Cu^{2+} in other broths using the models based on growth in NB was attempted. Accuracy was not anticipated since differences in nutritional composition of growth media alter bacterial growth characteristics and therefore the degree of inhibition. However, in some cases the activity of 20 μM FNa and Cu^{2+} could be predicted based on the solubility of 1280 μM FNa and activity of Cu^{2+} alone in LB and CAMHB. In LB (Figure 5.32, page 149), 5 and 2.5 mM CuSO_4 was observed to produce 100 % inhibition and this was accurately predicted by both models. At lower CuSO_4 concentrations, the predictions were consistently lower than observed inhibition, however, they followed a similar downward trend with Cu^{2+} concentration. In CAMHB (Figure 5.33, page 150), model (ii) predictions followed the same trend as observed inhibition but were approximately 10-15 % higher for all Cu^{2+} concentrations except 2.5 mM. Since Ca^{2+} and Mg^{2+} with which CAMHB is supplemented both play a role in membrane structure and fluidity, the lower observed inhibition may be due to additional permeability to FNa afforded by cation adjustment compared to NB. Alternatively, the differences could also simply be due to different growth and metabolism exhibited by *E. coli* in each medium composition. However, the results in LB and CAMHB do indicate that the combined activity of FNa and metal ions in other bacteriological media also correlated with FNa solubility and the independent activity of the metal ions. More

accurate models of prediction could therefore be arrived at by studying the solubility : activity relationship of FNa in these broths over a range of pHs.

5.4.4 Association of sodium fusidate with *E. coli* cells in the presence of metal ions or reduced pH

Reduction of NB pH to 6.0 significantly increased the amount of FNa that associated with *E. coli* NCTC 10418 cells after exposure to 160 μM for 30 min at 35 °C and 120 rpm ($p < 0.05$, Figure 5.34, page 151). No significant differences were detected between FNa association with *E. coli* in standard control NB, NB with 625 μM Mn^{2+} or NB with 312.5 μM Cu^{2+} ($p > 0.05$). However, there was a correlation between *E. coli* inhibition by FNa after 18 ± 2 h at 35 °C and 120 rpm and the amount of FNa associated with cells after 30 min under the same conditions. While Cu^{2+} could have been expected to have a greater effect on FNa association with *E. coli* due to synergy between the agents, the 312.5 μM selected for use did not have a dramatic impact on NB pH, reducing it only to 6.95. This concentration, 25 % MIC_{90} , was selected to avoid viability loss during exposure. In addition, the overall assay may not have been sensitive enough to detect significant differences. A longer exposure period may increase sensitivity but also introduces additional variables due to differences in inhibition and consequent bacterial growth rate between conditions, leading to greater disparity between the final number of bacteria present. Alternatively, greater starting cell numbers in a larger volume of broth could increase sensitivity by resulting in higher yield of total FNa.

5.5 Conclusions

The conclusions drawn from the work in this Chapter can be summarised as follows:

- 1) Cu^{2+} does not spontaneously complex FNa in order to enhance its activity against *E. coli* NCTC 10418.
- 2) Reduced pH decreases FNa solubility and increases activity against *E. coli* NCTC 10418.
- 3) The anti-*E. coli* synergy of Al^{3+} , Cu^{2+} and Fe^{2+} with FNa are primarily due to the additive effects of pH-mediated reduction in FNa solubility and metal ion antimicrobial activity.
- 4) Reduced pH and FNa solubility increases the association of FNa with *E. coli* NCTC 10418 cells.

**Chapter 6: Activity of sodium fusidate
 and metal ion combinations
against Gram-negative multi-
drug resistant isolates**

6.1 Introduction

E. coli serves as a valuable model GN organism for early antimicrobial activity studies; however, as discussed in Chapter 1, the most common cause of GN bacterial keratitis is *Pseudomonas aeruginosa*. Several other GN species have also been reported to infect the cornea with geographically variable frequency, including *Klebsiella pneumoniae*^{[31],[78]}. In addition, while reference strains used in the laboratory generally do not harbour multiple drug resistance mechanisms, multi-drug resistance (MDR) is becoming increasingly common in both environmental and clinical *P. aeruginosa* and *K. pneumoniae* isolates^{[70],[74],[75],[78]}. In contrast to laboratory reference strains, novel GN isolates frequently harbour plasmids carrying many MDR genes and also exhibit additional genetic and phenotypic changes to aid their survival and virulence. Such isolates can, therefore, be more representative of the possible resistance profiles and metabolic abilities of organisms likely to be involved in spontaneous clinical cases than standard reference strains. In addition, clinical and environmental MDR isolates can be used to check for cross-resistance with other antimicrobial classes and provide an indication of overall susceptibility of the wider bacterial population.

Like *E. coli*, *K. pneumoniae* is a member of the *Enterobacteriaceae* family and both species are facultative anaerobic residents of the mammalian gastrointestinal tract. Conversely, *P. aeruginosa* is an obligate aerobe found in water and the soil and belongs to the *Pseudomonadaceae* family. However, all three species are opportunistic human pathogens and intrinsically resistant to FNa. *K. pneumoniae* achieves FNa resistance by expressing AcrAB-TolC^[142], the same efflux pump utilised by *E. coli*, while *P. aeruginosa* produces an homologous RND family pump: MexAB-OprM^[143]. As for other GN species, resistance to FNa lies in preventing intracellular accumulation by efficient expulsion of the drug rather than absence of the EF-G target.

The known mechanisms of metal ion activities against GN organisms were discussed in Chapter 4. While phenotypic and metabolic differences between species may alter metal ion susceptibility and MIC values, high-level resistance is most commonly conferred by acquired genetic material. Metal resistance genes are frequently found in MDR bacterial strains and this could result in lower efficacy of the metal ion and FNa combinations compared to the comparatively sensitive *E. coli* reference strain. Nonetheless, since metal ion damage to the OM appears to be a key to the combined activity, metal resistance mechanisms which protect internal targets may be ineffectual in preventing

FNa entry and accumulation. On the other hand, there are known differences between the structure of *Enterobacteriaceae* and *Pseudomonadaceae* membranes which may manifest differences in sensitivity to FNa combined with metal ions. For example, the *P. aeruginosa* OM is devoid of the large general porins found in *Enterobacteriaceae* but instead contains only small substrate-specific membrane channels^[458]. Since the smaller membrane channels both exclude large molecules and contribute to greater OM stability, this difference is thought to account for the very low permeability of the *P. aeruginosa* OM at only 8 % that of *E. coli*^[458].

In this Chapter the sensitivities of several MDR isolates of *K. pneumoniae*, *P. aeruginosa* and *E. coli* to metal ions, FNa and combinations was investigated and compared to their reference strains in order to determine whether metal ions can also enhance FNa activity against highly resistant GN organisms capable of causing keratitis.

6.1.1 Aim and objectives

Aim: to determine if metal ions can enhance FNa activity against MDR isolates of GN organisms which cause keratitis.

Objectives:

- 1) To determine sensitivity of *E. coli*, *K. pneumoniae* and *P. aeruginosa* MDR isolates to antimicrobial metal ions.
- 2) To investigate the effects of metal ions on FNa activity against *E. coli*, *K. pneumoniae* and *P. aeruginosa* MDR isolates.
- 3) To identify the metal ion(s) which are most effective at enhancing FNa activity against *E. coli*, *K. pneumoniae* and *P. aeruginosa* MDR isolates.

6.2 Methods

6.2.1 Sources and maintenance of bacterial strains

Standard reference strains *K. pneumoniae* NCTC 9633 and *P. aeruginosa* NCTC 13359 were obtained from glycerol stocks of NCTC-sourced samples and frozen at -80 °C as described in Section 2.2.

Four MDR plasmid-harboring clinical isolates each of *E. coli*, *K. pneumoniae* and *P. aeruginosa* were kindly gifted by Dr Jonathan Tyrrell, selected at random from the Prof Timothy Walsh collection held at Cardiff University School of Medicine (Table 6.1). Glycerol stocks and working agar cultures were prepared and maintained for all strains as described in Section 2.2.

Table 6.1 – Multi-drug resistant Gram-negative isolates provided by Prof Walsh laboratories

Species	Isolate reference	Source location	Number of genes conferring resistance to:								
			aminoglycosides	β -lactams	fluoroquinolones	macrolides	sulphonamides	tetracyclines	chloramphenicol	fosfomycin	trimethoprim
<i>E. coli</i>	TWE1	India	11	8	-	-	1	1	2	-	2
	TWE2	India	10	5	-	-	1	1	2	-	2
	TWE3	India	4	4	1	-	1	1	2	-	1
	TWE4	India	7	5	1	-	1	1	3	-	1
<i>K. pneumoniae</i>	TWK1	UK	3	4	3	1	1	1	2	1	1
	TWK2	UK	*								
	TWK3	Egypt	8	4	4	-	-	-	1	1	1
	TWK4	Egypt	7	5	3	-	2	1	1	1	1
<i>P. aeruginosa</i>	TWP1	UK	3	3	1	-	1	-	2	1	-
	TWP2	Egypt	13	4	2	-	3	1	2	1	-
	TWP3	Egypt	11	4	1	1	1	-	2	1	1
	TWP4	Egypt	5	3	1	-	1	-	1	-	-

*sequencing data unavailable; multi-drug resistance phenotype identified experimentally.

6.2.2 Susceptibility testing

The MIC_{90s} of FNa and sulphates of Al³⁺, Co²⁺, Cu²⁺, Fe²⁺, Mn²⁺, Ni²⁺, Pd²⁺ and Zn²⁺ against *E. coli*, *K. pneumoniae* and *P. aeruginosa* MDR isolates and *K. pneumoniae* and *P. aeruginosa* reference strains were determined by microdilution, as described in

Section 2.4. MBCs of metal ions (as sulphates) were also measured, as described in Section 2.4.

As previous experimentation yielded significant enhancement of FNa activity against *E. coli* NCTC 10418 in the presence of synergistic and additive metal ions at ¼ their MIC₉₀ (see Section 4.3.1), microdilution was subsequently used to characterise the activity of FNa in combination with ¼ the modal MIC₉₀ of Al³⁺, Co²⁺, Cu²⁺, Fe²⁺ and Ni²⁺ (as sulphates) against the MDR and reference strains. Where appropriate, results previously generated for *E. coli* NCTC 10418 and *S. aureus* NCTC 12973 (presented in Section 4.3.1) were included in the comparison and analysis.

6.2.3 Data analysis

In both sets of experiments, the absorbance at 595 nm was used to calculate percentage inhibition and MIC₉₀s as previously described (see Section 2.4). Modal MIC₉₀s of metal ions were calculated for each species and across all species. In diagnostic microbiology, an MIC difference of one two-fold dilution difference is considered acceptable margin of error^[282]. However, data in this study were subjected to statistical analysis and differences observed between 95 % CIs considered significant ($p < 0.05$).

Since FNa and each of the metal ions affected the growth of individual bacterial strains differently, the absorbance data was also used to calculate the AUC for bacterial growth with FNa in the presence of each metal ion as a percentage of the AUC for growth with FNa alone. This analysis allowed direct comparison between strains, accounting for differences in individual agent susceptibility and was calculated as follows: Growth density in each well was calculated as a percentage of that with the corresponding FNa-free control, the metal ion alone thereby being assigned maximal or 100 % growth. The AUC for percentage maximal growth from 5 to 1280 µM FNa was determined for each metal ion and paired metal-free control of FNa alone. The AUCs with metal ions were then converted to percentage of the paired AUC for FNa alone. Mean percentage FNa AUCs were calculated from the triplicate experiments and the 95 % CI used to determine statistically significant differences ($p < 0.05$).

FIC₉₀s were calculated for each organism and metal ion combination by dividing the FNa MIC₉₀ in the presence of metal sulphate by the MIC₉₀ of FNa alone. Fold reductions in FNa MIC₉₀ were used for graphical comparison and calculated by dividing the MIC₉₀ of FNa alone by the MIC₉₀ of FNa in the presence of each metal ion.

6.3 Results

6.3.1 Metal ion activity against Gram-negative MDR isolates

The MIC₉₀s and MBCs of metal ions as sulphates against all tested strains are provided in Table 6.2. The MIC₉₀s of each metal ion across the bacterial strains varied no more than four-fold. While there were some exceptions, detailed below, each metal ion MBC against a strain was generally no more than four-fold greater than the MIC₉₀.

All but two Al³⁺ MIC₉₀s were 2.5 mM ($p > 0.05$). The exceptions were an MDR isolate of *K. pneumoniae*, TWK4, and the *P. aeruginosa* reference strain, NCTC 13359 which were two-fold higher and lower at 5 and 1.25 mM, respectively ($p < 0.05$). MBCs of Al³⁺ varied between 2.5 and >10 mM. The modal MBCs against *E. coli* and *K. pneumoniae* strains were both 5 mM, whereas the modal MBC against *P. aeruginosa* was 10 mM. *S. aureus* was also particularly resistant to killing by Al³⁺, and survived in the presence of 10 mM, the highest concentration tested.

Co²⁺ susceptibility was more variable than that of Al³⁺, however, species-specific patterns were apparent. *K. pneumoniae* strains were particularly susceptible to growth inhibition by Co²⁺, with a modal MIC₉₀ of 0.078 mM ($p < 0.05$). However, the MBC against reference strain NCTC 9633 was 0.625 mM and all MDR *K. pneumoniae* isolates were able to survive in the presence of this concentration. In contrast, the modal MIC₉₀ of Co²⁺ against *E. coli*, also a member of the *Enterobacteriaceae* family, was four times greater at 0.313 mM ($p < 0.05$) while the modal MBC was 0.625 mM. Susceptibility of *P. aeruginosa* fell between the other species with a modal MIC₉₀ of 0.156 mM which was significantly greater than *K. pneumoniae* ($p < 0.05$) but no different to *E. coli* ($p > 0.05$), and MBC of 0.625 mM.

MIC₉₀s for Cu²⁺ were lowest against *E. coli*, with a modal value of 1.25 mM. In opposition to their relative responses to Co²⁺, *K. pneumoniae* were more resistant to inhibition by Cu²⁺ than *E. coli* ($p < 0.05$), with a modal MIC₉₀ of 2.5 mM Cu²⁺. Similarly, the modal MBCs against *E. coli* and *K. pneumoniae* were 2.5 and 5 mM, respectively. *P. aeruginosa* susceptibility again lay between the two *Enterobacteriaceae*, with a higher modal MIC₉₀ than *E. coli* at 2.5 mM Cu²⁺ ($p < 0.05$) which was not significantly to the MIC₉₀ against *K. pneumoniae* isolates ($p > 0.05$).

Table 6.2 – MIC_{90S} and MBCs (in parentheses) of metal ions against MDR bacterial isolates and their reference strains (mM)

		Al ³⁺	Co ²⁺	Cu ²⁺	Fe ²⁺	Mn ²⁺	Ni ²⁺	Pd ²⁺	Zn ²⁺
<i>E. coli</i>	NCTC 10418	2.5 (2.5)	0.156 (0.313)	1.25 (2.5)	2.5 (2.5)	2.5 (>10)	0.625 (1.25)	0.625 (1.25)	0.3125 (0.625)
	TWE1	2.5 (2.5)	0.313 (>0.625)	1.25 (2.5)	2.5 (2.5)	5 (5)	1.25 (2.5)	0.625 (0.625)	0.625 (0.625)
	TWE2	2.5 (2.5)	0.313 (>0.625)	1.25 (1.25)	2.5 (2.5)	5 (5)	0.625 (2.5)	0.625 (0.625)	0.3125 (0.625)
	TWE3	2.5 (5)	0.156 (0.625)	1.25 (2.5)	2.5 (2.5)	2.5 (5)	0.625 (2.5)	0.625 (0.625)	0.3125 (0.625)
	TWE4	2.5 (5)	0.625 (0.625)	2.5 (2.5)	2.5 (2.5)	5 (5)	2.5 (2.5)	0.625 (1.25)	0.3125 (0.625)
	<i>E. coli</i> mode	2.5 (2.5)	0.313 (0.625)	1.25 (2.5)	2.5 (2.5)	5 (5)	0.625 (2.5)	0.625 (0.625)	0.3125 (0.625)
<i>K. pneumoniae</i>	NCTC 9633	2.5 (5)	0.0781 (0.625)	5 (5)	2.5 (2.5)	2.5 (5)	0.625 (1.25)	0.625 (0.625)	0.3125 (0.625)
	TWK1	2.5 (5)	0.0781 (>0.625)	2.5 (5)	2.5 (2.5)	2.5 (5)	0.625 (1.25)	0.625 (0.625)	0.625 (0.625)
	TWK2	2.5 (2.5)	0.0781 (>0.625)	2.5 (5)	2.5 (2.5)	2.5 (5)	0.625 (2.5)	0.625 (1.25)	0.625 (0.625)
	TWK3	2.5 (2.5)	0.0781 (>0.625)	5 (5)	2.5 (2.5)	2.5 (5)	0.625 (1.25)	1.25 (1.25)	0.3125 (0.625)
	TWK4	5 (5)	0.156 (>0.625)	2.5 (5)	2.5 (2.5)	2.5 (5)	1.25 (2.5)	1.25 (1.25)	0.3125 (0.625)
	<i>K. pneumoniae</i> mode	2.5 (5)	0.0781 (>0.625)	2.5 (5)	2.5 (2.5)	2.5 (5)	0.625 (1.25)	0.625 (1.25)	0.3125 (0.625)
<i>P. aeruginosa</i>	NCTC 13359	1.25 (2.5)	0.156 (>0.625)	2.5 (2.5)	1.25 (1.25)	2.5 (5)	1.25 (>2.5)	1.25 (1.25)	1.25 (1.25)
	TWP1	2.5 (10)	0.156 (0.625)	2.5 (5)	1.25 (5)	2.5 (10)	1.25 (>2.5)	1.25 (>1.25)	1.25 (10)
	TWP2	2.5 (>10)	0.156 (0.625)	2.5 (2.5)	1.25 (2.5)	2.5 (10)	0.625 (>2.5)	1.25 (>1.25)	1.25 (5)
	TWP3	2.5 (10)	0.313 (0.625)	2.5 (5)	1.25 (1.25)	2.5 (10)	0.625 (>2.5)	1.25 (>1.25)	1.25 (10)
	TWP4	2.5 (5)	0.156 (0.625)	2.5 (2.5)	0.625 (1.25)	1.25 (>10)	0.625 (>2.5)	1.25 (1.25)	1.25 (10)
	<i>P. aeruginosa</i> mode	2.5 (10)	0.156 (0.625)	2.5 (2.5)	1.25 (1.25)	2.5 (10)	0.625 (>2.5)	1.25 (>1.25)	1.25 (10)
<i>S. aureus</i>	NCTC 12973	2.5 (>10)	0.0781 (0.625)	2.5 (2.5)	2.5 (2.5)	1.25 (>10)	0.313 (2.5)	1.25 (1.25)	0.156 (>0.625)
OVERALL MODE		<u>2.5 (5)</u>	<u>0.156 (0.625)</u>	<u>2.5 (2.5)</u>	<u>2.5 (2.5)</u>	<u>2.5 (5)</u>	<u>0.625 (2.5)</u>	<u>0.625* (1.25)</u>	<u>0.3125 (0.625)</u>

Modal values for each species are given in bold. Modal values across all species are given in bold and underlined. Data for Gram-positive *S. aureus* NCTC 12973 is also included. *Modal value across all species could not be determined, the mode for Gram-negatives only is given. (n = 3)

Fe²⁺ activity was consistent against *E. coli* and *K. pneumoniae* with the modal MIC₉₀s and MBCs both being 2.5 mM against every strain ($p > 0.05$) and no variation between replicates. *S. aureus* NCTC 12973 was also susceptible to the same concentration. However, the modal MIC₉₀ and MBC of Fe²⁺ against *P. aeruginosa* were both statistically significantly lower at 1.25 mM ($p < 0.05$), and there was some variation in susceptibility between isolates. In particular, the small colony variant (SCV) MDR isolate TWP1 was able to survive in higher concentrations of Fe²⁺ than all other bacterial strains tested, resulting in an MBC 5 mM ($p < 0.05$) despite an MIC₉₀ of 1.25 mM. The growth of TWP4 – another MDR isolate but with normal colony phenotype – was also inhibited by only 0.625 mM Fe²⁺ ($p < 0.05$) but the MBC was only one two-fold dilution greater at 1.25 mM.

There was no variation between the response of *K. pneumoniae* to Mn²⁺ with MIC₉₀s and MBCs of 2.5 and 5 mM, respectively, for all five strains tested ($p > 0.05$). *E. coli* strains were less susceptible to growth inhibition and the modal MIC₉₀ and MBC were both 5 mM Mn²⁺ but there was no significant difference between isolates or to *K. pneumoniae* ($p > 0.05$). However, interestingly, the *E. coli* reference strain exhibited greater resistance to cidal action than the MDR isolates, resulting in an MIC₉₀ of 2.5 mM but MBC of >10 mM ($p < 0.05$). The modal MIC₉₀ and MBC of Mn²⁺ against *P. aeruginosa* were 2.5 and 10 mM, respectively, indicating this species were less susceptible to killing by Mn²⁺ than the others tested.

P. aeruginosa was also less susceptible to the bactericidal effect of Ni²⁺ than both *E. coli* and *K. pneumoniae* ($p < 0.05$). Modal MBCs of Ni²⁺ were 2.5 and 1.25 mM against *E. coli* and *K. pneumoniae*, respectively, and >2.5 mM against *P. aeruginosa*. However, all species were similarly susceptible to growth inhibition with modal MIC₉₀s of 0.625 mM with no statistically significant difference between them ($p > 0.05$).

Ten of the 16 bacterial strains tested were found to be killed by the same concentration of Pd²⁺ that produced apparent 90 % inhibition. All MIC₉₀s of Pd²⁺ against *E. coli* were 0.625 mM and modal MBC was also 0.625 mM ($p > 0.05$). *K. pneumoniae* strains were overall slightly less susceptible than *E. coli*, with the MIC₉₀ against two MDR isolates being 1.25 mM and a modal MBC of 1.25 mM. The MIC₉₀ against all *P. aeruginosa* strains was 1.25 mM and three MDR isolates were able to survive in the presence of this concentration making the MBC >1.25 mM.

The modal MIC₉₀ and MBC of Zn²⁺ for *E. coli* and *K. pneumoniae* strains were both 0.313 and 0.625 mM, respectively, with no statistically significant difference between strains ($p > 0.05$). *P. aeruginosa* isolates were less susceptible to Zn²⁺ compared to both of the *Enterobacteriaceae* ($p < 0.05$) with a modal MIC₉₀ and MBC of 1.25 and 10 mM, respectively.

Overall, *E. coli* strains were the most susceptible to metal ions, closely followed by *K. pneumoniae* then *P. aeruginosa*. However, there were some notable exceptions. The variations between both MIC₉₀s and MBCs against the bacterial species as a whole and the differences between strains within species likely reflects phenotypic and genetic differences which alter susceptibility.

6.3.2 Activity of sodium fusidate combined with metal ions against Gram-negative MDR isolates

Figure 6.1 illustrates the AUC for bacterial growth in the presence of metal ion and FNa combinations as a percentage of that with the same concentration range of FNa alone. Mn²⁺, Pd²⁺ and Zn²⁺ were not tested in combination with FNa against MDR isolates and their reference strains due to suppression previously identified against *E. coli* NCTC 10418 or *S. aureus* NCTC 12973 (see Section 4.3.1).

Al³⁺ and Fe²⁺ were the more effective than Co²⁺, Cu²⁺ and Ni²⁺ at reducing the AUC for bacterial growth when combined with FNa against every strain ($p < 0.05$). Co²⁺ and Ni²⁺ had the least additional antimicrobial effect, and Cu²⁺ moderately reduced growth. No growth AUCs with FNa in the presence of Co²⁺ or Ni²⁺ were significantly less than 80 % of FNa alone ($p > 0.05$). In fact, in some cases, growth was greater with the metals than without. However, the growth-reducing effects of Al³⁺, Fe²⁺ and Cu²⁺ were significant.

In all but one case, AUCs for growth in the presence of FNa and Al³⁺ were <20 % those of FNa alone ($p < 0.05$). The exception was the *E. coli* reference strain NCTC 10418 with a growth AUC for with Al³⁺ of 21.8 % of FNa alone. There was no significant difference between FNa alone-standardised growth AUCs for FNa with Al³⁺ against the MDR isolates of *E. coli* ($p > 0.05$) except between the upper and lower values for TWE3 at 8.3 % and TWE4 at 2.0 %. FNa with Al³⁺ growth AUCs for *K. pneumoniae* were all within a range of 8.2 to 16.8 % FNa alone. There was no significant difference between the MDR isolates, however, growth of the reference strain NCTC 9633 was significantly less reduced than three of them ($p < 0.05$). There was no significant difference between *P. aeruginosa* strains ($p > 0.05$) and all FNa with Al³⁺ growth AUCs were between 0.1 and 1.0 % FNa alone.

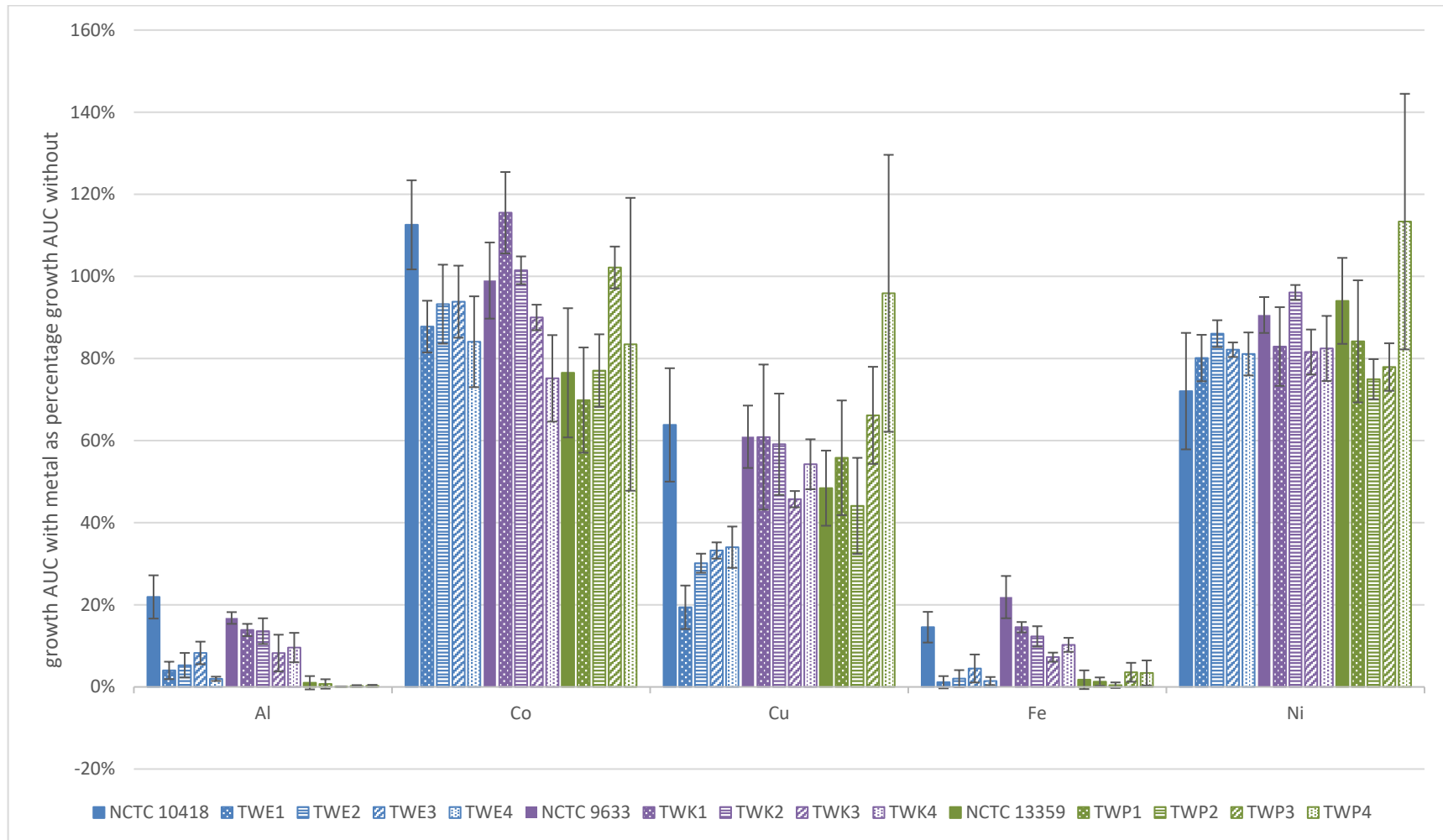


Figure 6.1 – AUCs of metal ion-normalised bacterial growth with sodium fusidate in the presence of metal ions

Data is presented as percentage paired AUC of growth with sodium fusidate alone to allow direct comparison between organisms with variable sodium fusidate susceptibility. Metal ion concentrations are 0.25 x modal MIC₉₀: 0.625 mM Al³⁺, 0.0391 mM Co²⁺, 0.625 mM Cu²⁺, 0.625 mM Fe²⁺ and 0.156 mM Ni²⁺.

(n = 3, error bars = 95 % CI)

A similar pattern was observed for Fe²⁺. *P. aeruginosa* growth AUCs for Fe²⁺ with FNa were the overall smallest percentage of growth AUCs with FNa alone, ranging from 0.4 to 3.4 %. The only significant difference between *P. aeruginosa* strains was that TWP2 growth was reduced more than TWP3 ($p < 0.05$). *E. coli* MDR isolates were similarly affected, exhibiting FNa with Fe²⁺ growth AUCs of 1.1 to 4.5 % FNa alone and no significant difference between them ($p > 0.05$). *E. coli* reference strain NCTC 10418 was again less dramatically impacted by the presence of metal than the MDR isolates ($p < 0.05$), which may indicate that this isolate is not a good model for population behaviour. Interestingly, growth of *K. pneumoniae* was significantly less reduced by the presence of Fe²⁺ with FNa compared to *E. coli* and *P. aeruginosa* ($p < 0.05$). However, the growth AUC for FNa with Fe²⁺ for all MDR isolates was less than 15 % the corresponding AUC for FNa alone while that of the reference strain, NCTC 9633, was 21.9 %.

While Cu²⁺ was effective at reducing the FNa growth AUCs for almost all strains, its impact was less than that of Al³⁺ or Fe²⁺. The growth of *E. coli* MDR isolates was reduced more than almost all the other bacterial strains. FNa with Cu²⁺ growth AUCs were between 30.1 and 34.0 % of FNa alone for TWE2, TWE3 and TWE4 with no significant difference between them ($p > 0.05$). TWE1 had an AUC with Cu²⁺ of 19.4 % and NCTC 10418 was 63.8 % FNa alone, both of which were significantly different to the other strains and each other ($p < 0.05$). Cu²⁺ had less influence on *K. pneumoniae* growth with FNa with all AUCs being between 45.7 and 60.9 % FNa alone. Four of the five *P. aeruginosa* strains exhibited similar susceptibility with AUCs of 44.1 to 66.1 % FNa alone, except TWP4 which was 95.8 % and not significantly different to FNa alone ($p > 0.05$).

6.3.3 The effect of metal ions on sodium fusidate MIC₉₀s

The MIC₉₀ of FNa alone and with each metal ion (as sulphate) against all strains tested is listed in Table 6.3 along with the FNa FIC₉₀s for the combinations. MDR isolates were significantly less susceptible to FNa than the originally tested GN model organism, *E. coli* NCTC 10418, with the modal MIC₉₀ against all being 1280 or 2560 µM ($p < 0.05$).

In the presence of 0.625 mM Al³⁺, the MIC₉₀ of FNa against *E. coli* NCTC 10418 was reduced from 320 to 40 µM ($p < 0.05$). The FNa MIC₉₀s against MDR isolates of *E. coli* were reduced from 2560 or 1280 µM to 40 to 160 µM by the inclusion of Al³⁺ ($p < 0.05$). The mean FNa FIC₉₀ against *E. coli* was 0.0688. While the MIC₉₀ of FNa against

K. pneumoniae ranged from 320-2560 μM , the presence of Al^{3+} reduced it to one eighth against every strain tested ($p < 0.05$). Addition of 0.625 mM Al^{3+} , had the largest effect on the MIC_{90} of FNa against *P. aeruginosa* compared to other species ($p < 0.05$). Alone, the MIC_{90} of FNa was 2560 μM against all strains but in the presence of Al^{3+} , every strain of *P. aeruginosa* was $\geq 90\%$ inhibited by 5 μM FNa, the lowest concentration tested. The FNa FIC_{90} was therefore ≤ 0.00195 against *P. aeruginosa*. The mean FIC_{90} of FNa with 0.625 mM Al^{3+} against all GN organisms tested was 0.0652.

Table 6.3 – Sodium fusidate MIC_{90} s (μM) and FIC_{90} s (in parentheses) with metal ions

Species	Strain	MIC_{90} (FIC_{90})					
		control	with Al	with Co	with Cu	with Fe	with Ni
<i>S. aureus</i>	NCTC 12973	0.3125	0.3125 (1)	0.15625 (0.5)	0.3125 (1)	0.15625 (0.5)	0.3125 (1)
<i>E. coli</i>	NCTC 10418	320	40 (0.125)	160 (0.5)	40 (0.125)	40 (0.125)	160 (0.5)
	TWE1	2560	80 (0.0313)	2560 (1)	320 (0.125)	10 (0.0039)	2560 (1)
	TWE2	2560	80 (0.0313)	2560 (1)	320 (0.125)	5 (0.0020)	2560 (1)
	TWE3	1280	160 (0.125)	1280 (1)	320 (0.25)	40 (0.0313)	1280 (1)
	TWE4	1280	40 (0.0313)	1280 (1)	640 (0.5)	20 (0.0156)	1280 (1)
	Species FIC_{90} mean			0.0688	0.900	0.225	0.0355
<i>K. pneumoniae</i>	NCTC 9633	640	80 (0.125)	640 (1)	320 (0.5)	80 (0.125)	640 (1)
	TWK1	1280	160 (0.125)	1280 (1)	640 (0.5)	160 (0.125)	1280 (1)
	TWK2	1280	160 (0.125)	2560 (2)	640 (0.5)	160 (0.125)	1280 (1)
	TWK3	2560	320 (0.125)	2560 (1)	1280 (0.5)	160 (0.0625)	2560 (1)
	TWK4	2560	320 (0.125)	2560 (1)	1280 (0.5)	160 (0.0625)	2560 (1)
	Species FIC_{90} mean			0.125	1.20	0.500	0.100
<i>P. aeruginosa</i>	NCTC 13359	2560	5 (0.0020)	1280 (0.5)	640 (0.25)	5 (0.0020)	1280 (0.5)
	TWP1	2560	5 (0.0020)	2560 (1)	1280 (0.5)	0 (N/A)	2560 (1)
	TWP2	2560	5 (0.0020)	2560 (1)	1280 (0.5)	5 (0.0020)	1280 (0.5)
	TWP3	2560	5 (0.0020)	2560 (1)	1280 (0.5)	5 (0.0020)	1280 (0.5)
	TWP4	2560	5 (0.0020)	2560 (1)	1280 (0.5)	0 (N/A)	2560 (1)
	Species FIC_{90} mean			0.00195	0.900	0.450	0.00195
Mean Gram-negative FIC_{90}			0.0652	1.00	0.392	0.0526	0.867

Metal ion concentrations are 0.25 x modal MIC_{90} : 0.625 mM Al^{3+} , 0.0391 mM Co^{2+} , 0.625 mM Cu^{2+} , 0.625 mM Fe^{2+} and 0.156 mM Ni^{2+} . (n = 3)

Overall, Co^{2+} did not reduce the FNa MIC_{90} against GN organisms ($p > 0.05$). The exceptions were the model organism *E. coli* NCTC 10418 and *P. aeruginosa* reference strain NCTC 13359 – the presence of 0.039 mM Co^{2+} halved the modal FNa MIC_{90} against both. Conversely, the MIC_{90} of FNa against *K. pneumoniae* TWK2 was doubled by the presence of Co^{2+} . However, these effects were not statistically significant ($p > 0.05$). The mean FIC_{90} s of FNa with Co^{2+} were 0.9, 1.2 and 0.9 against *E. coli*, *K. pneumoniae* and *P. aeruginosa*, respectively.

FNa MIC_{90} s against *E. coli* in the presence of 0.625 mM Cu^{2+} were reduced to between 40 and 320 μM , with corresponding FIC_{90} s ranging from 0.125 to 0.5. The most resistant *E. coli* strain was the MDR isolate TWE4 with an FIC_{90} of 0.5 which was significantly different to the reference strain ($p < 0.05$), while the FIC_{90} against TWE3 was 0.25 and 0.125 against all other strains. The MIC_{90} of FNa was halved against MDR isolates of *K. pneumoniae* and *P. aeruginosa* by Cu^{2+} . The FNa FIC_{90} against *K. pneumoniae* reference strain NCTC 9633 was also halved, however, while not statistically significant, the *P. aeruginosa* reference strain NCTC 13359 was slightly more susceptible to the combination with an FIC_{90} of 0.25 ($p > 0.05$). The susceptibility of *E. coli* isolates to FNa was increased more by the presence of Cu^{2+} than against either *K. pneumoniae* or *P. aeruginosa* ($p > 0.05$). The mean GN FNa FIC_{90} with Cu^{2+} was 0.392.

Fe^{2+} was also very effective at reducing the FNa MIC_{90} against *P. aeruginosa*, producing a mean FIC_{90} of ≤ 0.00195 , the same as Al^{3+} . However, two strains of *P. aeruginosa* were omitted from the analysis as the 0.625 mM Fe^{2+} used was $\geq 90\%$ inhibitory to them. The mean FNa FIC_{90} against both *E. coli* and *K. pneumoniae* with Fe^{2+} were both lower than for any other metal at 0.0355 and 0.100, respectively ($p < 0.05$), however, these were significantly greater than the FIC_{90} against *P. aeruginosa* ($p < 0.05$). Interestingly, the MIC_{90} of FNa against *E. coli* reference strain NCTC 10418 was significantly less affected by the presence of Fe^{2+} compared to the MDR *E. coli* isolates ($p < 0.05$). The overall mean FNa FIC_{90} with 0.625 mM Fe^{2+} against GNs was 0.0526.

The presence of 0.156 mM Ni^{2+} did not have a significant impact on the FNa MIC_{90} against GN organisms ($p > 0.05$). While the modal MIC_{90} of FNa against the model organism *E. coli* NCTC 10418 and three *P. aeruginosa* strains: NCTC 13359, TWP2 and TWP3 were halved by its presence, these were not statistically significant ($p > 0.05$) and there was no change against any other strain tested. The mean FIC_{90} s in the presence of Ni^{2+} were 0.9, 1.0 and 0.7 against *E. coli*, *K. pneumoniae* and *P. aeruginosa*, respectively.

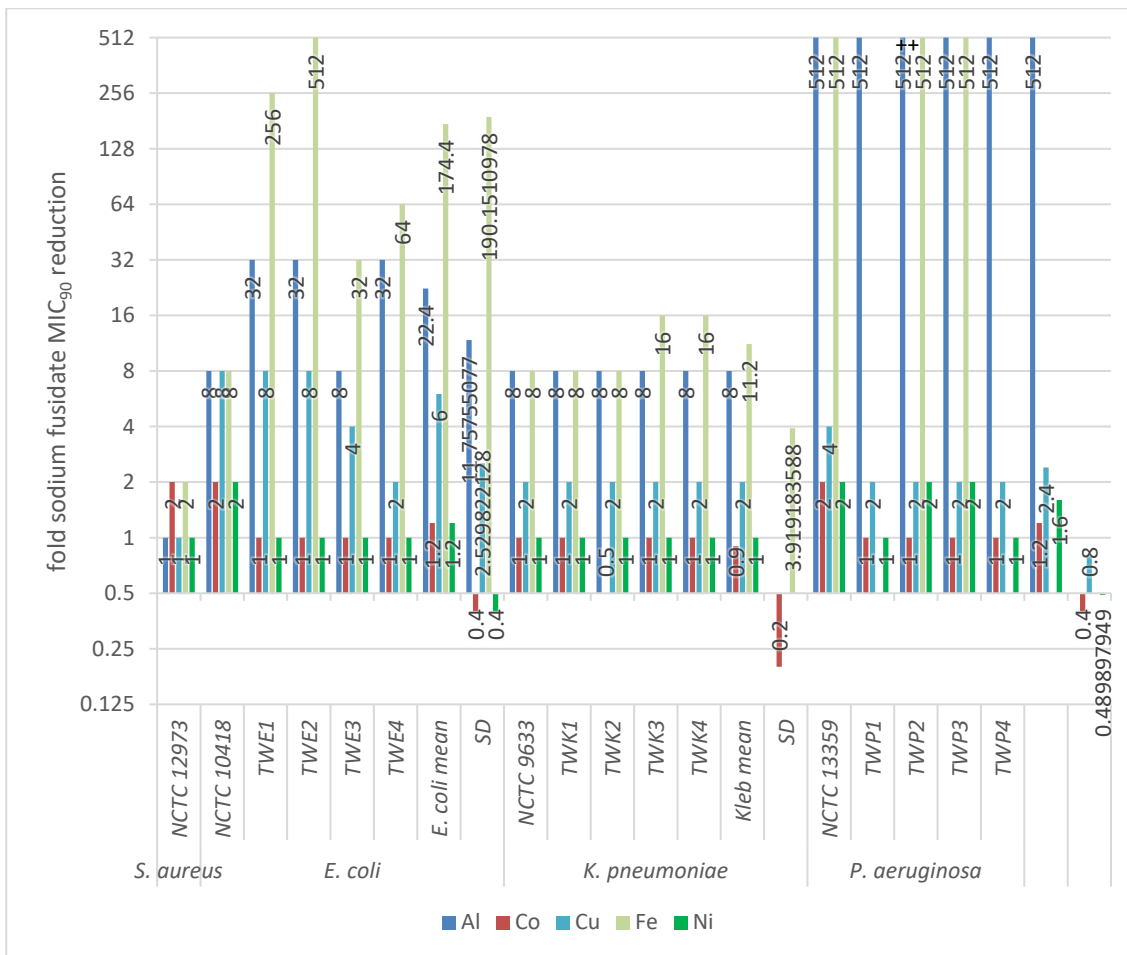


Figure 6.2 – Fold reduction in sodium fusidate MIC₉₀ when in the presence of metal ions

Metal ion were each present at 0.25 x their modal MIC₉₀: 0.625 mM Al³⁺, 0.039 mM Co²⁺, 0.625 mM Cu²⁺, 0.625 mM Fe²⁺ and 0.156 mM Ni²⁺. Greater fold reduction in sodium fusidate MIC₉₀ indicates increased inhibition when combined with metal ion.

(n = 3, y axis = log₂ scale)

Figure 6.2 illustrates the fold reduction in FNa MIC₉₀ when combined with metal ions against each bacterial strain for visual comparison. Al³⁺ reduced the FNa MIC₉₀ by ≥8-fold against all GN strains, while having no negative impact on *S. aureus* FNa susceptibility. Fe²⁺ also reduced the FNa MIC₉₀ against GNs by ≥8-fold while the MIC₉₀ against *S. aureus* was halved by its presence. While Cu²⁺ was not as effective as Al³⁺ or Fe²⁺, it consistently reduced the MIC₉₀ of FNa by 2 to 8-fold against all GNs tested and had no negative effect on activity of FNa against *S. aureus*. Co²⁺ and Ni²⁺ had no impact on the FNa MIC₉₀ against the majority of bacterial strains. There was a two-fold reduction in FNa MIC₉₀ against *E. coli* NCTC 10418, and three *P. aeruginosa* strains: NCTC 13359, TWP2 and TWP3 when in the presence of Ni²⁺. The same reduction was found against *E. coli* NCTC 10418 and *P. aeruginosa* NCTC 13359 with Co²⁺. However, the presence of Co²⁺ also doubled the FNa MIC₉₀ against *K. pneumoniae* TWK2.

6.4 Discussion

6.4.1 Activity of metal ions alone

While literature values for other species could not be found, reported Al^{3+} MICs against *E. coli* varied from 0.5 mM in minimal media to 3 mM in Lennox lysogeny broth (LLB)^[300]. The latter agreed quite well with the MIC_{90} of 2.5 mM Al^{3+} found in NB against all but two bacterial strains tested in this work (Table 6.2, page 167). Despite little variation in Al^{3+} MIC_{90} between species and isolates, the MBC ranged from 2.5 to 5 mM against the *Enterobacteriaceae* but 2.5 to >10 mM against *P. aeruginosa*. While all within one two-fold dilution of one another, the observed MBCs against *E. coli* and *K. pneumoniae* in NB were lower than the reported values of both 7 and 11 mM against *E. coli* in minimal media and LLB, respectively^[300]. As previously discussed, the composition of bacteriological growth media can have a substantial impact on antimicrobial activity due to factors such as bacterial metabolism or phenotypic changes (Chapter 3) and agent solubility (Chapter 5). The inconsistencies between employed growth medium may, therefore, explain the difference between reported and observed MBC values.

Conversely, the differences in Al^{3+} MBC against *P. aeruginosa* cannot be attributed to differences in culture medium and may be a result of phenotypic or genetic variation between strains. As mentioned in Section 6.1, *P. aeruginosa* lacks large general porins in its OM and instead relies on small substrate-specific membrane channels which increase membrane stability and reduce permeability compared to the *Enterobacteriaceae*. It is conceivable that differences in the number or type of membrane channels between *P. aeruginosa* strains would result in differences in OM stability and consequently Al^{3+} susceptibility. In addition, the structure of lipid A – a known Al^{3+} target^{[318],[319]} – differs between the *Enterobacteriaceae* and *P. aeruginosa*. While the majority of lipid A of both *E. coli*^[459] and *K. pneumoniae*^[460] is acylated with six fatty acids of C12-C14, a penta-acylated form with shorter C10-C12 fatty acids generally predominates alongside both hexa- and hepta-acylated lipid A in *P. aeruginosa*^[461]. However, all three bacterial species possess the ability to add positively charged residues such as 4-aminoarabinose to their lipid A in order to decrease their susceptibility to cations which would otherwise displace Ca^{2+} and Mg^{2+} from between LPS molecules and compromise membrane structure^[71]. The PmrA/PmrB pathway responsible for this modification has been shown to be induced by and mediate resistance to Al^{3+} exposure in *Salmonella*^[462]. The observed variation in survival of these few *P. aeruginosa* strains

may be due differences in combinations of lipid A forms and the consequent differences in the charge-modification effects of aminoarabinose addition.

The MIC₉₀ of Co²⁺ determined in NB against *E. coli* was 0.156 or 0.313 mM for all five strains investigated (Table 6.2, page 167) which was considerably lower than reported values of 1^[301] and >134.5^[463] mM in various rich media. Again, since the experimental values were within one two-fold dilution of one another, the difference to those reported is likely due to the different metabolic and solution chemistry effects of the varied growth media. Similarly, Co²⁺ MIC₉₀s against the five *K. pneumoniae* strains were found to be 0.078 or 0.156 mM in NB while an MIC of >134.5^[463] mM has been reported in a variety of rich media. Interestingly, the same authors^[463] also found a Co²⁺ MIC of >134.5 mM against *P. aeruginosa* in the various media employed, while 0.2 mM was demonstrated to produce approximately 85 % growth inhibition in NB^[464], illustrating the effects of growth medium on antimicrobial activity. In addition, this value^[464] is almost identical to the modal Co²⁺ MIC₉₀ of 0.156 mM found against *P. aeruginosa* in NB in this work.

Reported Cu²⁺ MICs against *E. coli* ranged from 4^[301] or 5^[271] mM in LB to 10 mM in MHB^[307]. These values agree closely with Cu²⁺ MIC₉₀s determined in LB and CAMHB during chequerboard incubation (see Chapter 3, Section 3.3.1, page 63). The present tests in NB yielded a modal MIC₉₀ of 1.25 mM (Table 6.2, page 167), however, no reports of MIC determination in the same broth could be identified in the literature. Interestingly, Vaidya and colleagues^[380] found a Cu²⁺ MIC of 0.25 mM against *K. pneumoniae* NCTC 9633 in NB which was only one twentieth of the 5 mM MIC₉₀ found against the same strain in the same broth in this work. However, this difference may be due to differing assay techniques. Vaidya *et al.*^[380] employed triphenyl tetrazolium chloride (TTC) as a colorimetric indicator of bacterial growth by adding 0.15 % w/v (1.5 mg mL⁻¹) to the assay plate prior to the initiation of incubation. However, the early authors of this method^[465] determined that 0.09 and 0.10 mg mL⁻¹ TTC inhibited the growth of *E. coli* and *S. aureus*, respectively, when used in this way. Therefore, it is likely that *K. pneumoniae* growth was partially inhibited by the presence of 1.5 mg mL⁻¹ TTC and, while the assay employed by Vaidya *et al.*^[380] enabled comparison between metal ion activities in the same system, the results do not appear to be comparable to TTC-free conditions. Finally, a reported Cu²⁺ MIC of 1.2 mM against *P. aeruginosa* in NB^[464] was approximately one two-fold dilution lower than the 2.5 mM MIC₉₀ found against all five of the strains tested in this work.

No Fe²⁺ MICs against *K. pneumoniae* or *P. aeruginosa* were identified in the literature. However, the reported MICs of Fe²⁺ against *E. coli* in minimal medium and LLB were 2 and 5 mM, respectively^[300]. While a different growth medium was employed, the Fe²⁺

MIC₉₀ in NB determined against all *E. coli* and *K. pneumoniae* strains in this work agreed with reported values at 2.5 mM (Table 6.2, page 167). Fe²⁺ exhibited a lower MIC₉₀ against *P. aeruginosa* strains of 0.625 or 1.25 mM, likely due to differences in the *P. aeruginosa* membrane structure compared to the *Enterobacteriaceae*. However, in contrast to the apparently protective effect of these differences on Al³⁺ exposure, *P. aeruginosa* was more vulnerable to inhibition by Fe²⁺ than *E. coli* or *K. pneumoniae*. As discussed in Chapter 4 (see Section 4.1.1.478, page 78), one of the major mechanisms of Fe antimicrobial activity is ROS generation *via* Fenton reactivity^[336]. This is also a mechanism not associated with Al³⁺ due to its single oxidation state. In addition, *P. aeruginosa* may be more sensitive to ROS DNA damage due to its comparatively high guanine-cytosine (GC) content. Guanine has the lowest oxidation potential of the nucleotides, making it particularly susceptible to ROS attack^[466]. Example genomes for *P. aeruginosa*, *K. pneumoniae* and *E. coli* indicate 66^[467], 57^[468] and 51^[469] %, respectively, of these organisms' DNA is GC. Furthermore, the presence of large general porins in the *Enterobacteriaceae* may serve as a sink for some Fe-generated ROS in the periplasm, thereby delaying the onset of membrane damage compared to *P. aeruginosa*. Finally, direct oxidative damage by Fe²⁺ may compromise the structure and function of *P. aeruginosa*'s small substrate-specific OM channels which are relied upon for both nutrient uptake and membrane stability. Compared to the *Enterobacteriaceae* which can internalise a wide variety of nutrients *via* their large general porins, this could more readily result in starvation as well as loss of OM integrity.

The only reported MIC of Mn²⁺ was 20 mM against *E. coli* in a TRIS-buffered minimal salts medium with gluconate as carbon source^[306]. While, Mn²⁺ exerted similar inhibitory activity across all bacterial strains tested in this work (Table 6.2, page 167), the modal MIC₉₀ found was only 2.5 mM, further illustrating the impact of growth medium on responses to antimicrobial substances. Three of the *E. coli* isolates were slightly less susceptible than the other bacterial strains by a difference of one two-fold dilution with MIC₉₀s of 2.5 and 5 mM. These variations could be due to genetic factors such as additional copies of genes encoding proteins targeted by Mn²⁺ or phenotypic differences in Mn²⁺ uptake, altering the rate of internalisation.

The modal Ni²⁺ MIC₉₀ across all strains was 0.625 mM. *E. coli* MDR isolates were the most variable in their susceptibility, with values of 1.25 and 2.5 mM against TWE1 and TWE4, respectively. The latter agreed closely with the reported Ni²⁺ MIC of 2 mM in LB^[301]. Interestingly, the MIC of Ni²⁺ was reported to be 0.60 mM in a minimal medium and 17 mM in LB against *P. aeruginosa*^[470]. While the value in LB is more than 25 times the Ni²⁺ MIC₉₀ observed against *P. aeruginosa* in NB, the reported activity in minimal media was very similar.

Reported values for the MIC of Pd²⁺ against *E. coli* varied from 0.015 mM in minimal medium^[304] to 2.82 mM in LB^[305]. However, the Pd²⁺ MIC₉₀ in NB was determined to fall between these values at 0.625 mM (Table 6.2, page 167). The MIC of Pd²⁺ against *P. aeruginosa* in LB from the literature was only marginally higher than that found in NB at 1.94^[305] compared to 1.25 mM, respectively. Finally, Vaidya and colleagues^[380] found an MIC of 0.055 mM against *K. pneumoniae* using the TTC-based assay described above. This value was less than one tenth the modal Pd²⁺ MIC₉₀ against *K. pneumoniae* strains, likely due to the same limitations discussed previously.

Literature values for the MIC of Zn²⁺ against *E. coli* in LB and CAMHB were 6 and 12 times the modal MIC₉₀ in NB at 2^[301] and 3.73^[303] mM, respectively. No Zn²⁺ MICs against *K. pneumoniae* were identified in the literature, however, the modal MIC₉₀ in NB was the same as against *E. coli* at 0.313 mM (Table 6.2, page 167). The reported MICs of Zn²⁺ against *P. aeruginosa* in LB and CAMHB were both ~60 times that determined in NB at 78^[470] and 73.74^[303] mM, respectively. However, the Zn²⁺ MIC₉₀ of 1.25 mM found in this work corresponded closely to the MIC of 1.5 mM reported against *P. aeruginosa* in NB elsewhere^[464].

Overall, metal ions were similarly effective against MDR isolates and reference strains. There was no correlation between antimicrobial resistance and metal ion susceptibility, despite previous reports of co-localisation of metal and drug resistance determinants^{[307],[471]}. While there were some differences in response to metal ions between species, individual strain MIC₉₀s were never more than two two-fold dilutions apart, and modal species MIC₉₀s differed by no more than one two-fold dilution. Only metals that had not been found to antagonise the activity of FNa against *E. coli* NCTC 10418 or *S. aureus* NCTC 12973 (Chapter 4) – Al³⁺, Co²⁺, Cu²⁺, Fe²⁺ and Ni²⁺ – were tested against the additional GN strains in combination with FNa.

6.4.2 Combined activity of sodium fusidate and metal ions

As with metal ions alone, there was also no correlation between resistance to any antimicrobial class and susceptibility to FNa combined with various metal ions. At a concentration of 0.25 x their respective modal MIC₉₀, Co²⁺ and Ni²⁺ were largely ineffective at increasing FNa activity against GN bacteria. The presence of neither metal reduced the growth AUC by more than 20 % (Figure 6.1, page 170) or the FNa MIC₉₀ by more than two-fold (Figure 6.2, page 174). As discussed in Chapter 4, both metals have similar antimicrobial targets and are micronutrients managed by the same homeostasis

systems (see Section 4.4.1.2, page 97), and their antimicrobial effects do not appear to enhance bacterial susceptibility to FNa.

The presence of 0.625 mM Cu^{2+} significantly enhanced FNa activity against all strains, however, the fold changes in FNa MIC_{90} s were significantly less than with Fe^{2+} or Al^{3+} . *E. coli* MDR isolates were the most susceptible to the combination of FNa and Cu^{2+} , which was most likely because the concentration of Cu^{2+} employed was 50 % the modal MIC_{90} compared to 25 % for other species. There was no significant difference between the response of *K. pneumoniae* and *P. aeruginosa* strains to FNa in the presence of Cu^{2+} ($p > 0.05$, Figure 6.1 and Figure 6.2). A difference might have been expected since increased membrane permeation due to reduced FNa solubility has been identified as a probable mediator of combined antimicrobial efficacy against *E. coli* (Chapter 5), and the difference in structure of the *P. aeruginosa* and *Enterobacteriaceae* OM is known to impact permeability. This may indicate that, despite decreased permeability to a wide range of substances, the *P. aeruginosa* OM presents no more of a barrier to low solubility FNa than that of *E. coli* or *K. pneumoniae*. While the presence of Fe^{2+} enhanced FNa activity against *P. aeruginosa* strains more than *E. coli* or *K. pneumoniae*, this was likely due to the metal ions concentration being 50-100 % the MIC_{90} compared to 25 % against both the other species. However, *P. aeruginosa* strains were significantly more susceptible to FNa in the presence of Al^{3+} than either *E. coli* or *K. pneumoniae*. All five *P. aeruginosa* strains were completely inhibited by 5 mM FNa when combined with 0.625 mM Al^{3+} . This was unexpected. A possible explanation could lie in the structure of *P. aeruginosa* LPS. Al^{3+} alone was not enough to perturb *P. aeruginosa* growth any more than that of the *Enterobacteriaceae*. However, Al^{3+} interaction with *P. aeruginosa* LPS may result in specific structural changes that more readily allow FNa entry than compared to Al-bound *E. coli* or *K. pneumoniae* LPS. Alternatively, Al^{3+} may act on an unidentified target present in *P. aeruginosa* but not the *Enterobacteriaceae*. The antimicrobial activity and mechanism of Al^{3+} has not been extensively studied and was beyond the scope of this work, however, investigation into this combined activity would be worthy of further study.

6.5 Conclusions

Conclusions drawn from the work in this Chapter can be summarised as follows:

- 1) Antimicrobial metal ions Al^{3+} , Co^{2+} , Cu^{2+} , Fe^{2+} , Mn^{2+} , Ni^{2+} , Pd^{2+} and Zn^{2+} exhibit similar activity against *E. coli*, *K. pneumoniae* and *P. aeruginosa* reference strains and MDR isolates.
- 2) Co^{2+} and Ni^{2+} do not enhance the activity of FNa against intrinsically resistant *E. coli*, *K. pneumoniae* and *P. aeruginosa* reference strains and MDR isolates.
- 3) Al^{3+} , Cu^{2+} and Fe^{2+} enhanced the activity of FNa against intrinsically resistant *E. coli*, *K. pneumoniae* and *P. aeruginosa* reference strains and MDR isolates.
- 4) The combination of FNa and Al^{3+} proved to be particularly effective against strains of *P. aeruginosa*.

**Chapter 7: Effect of sodium fusidate and
 metal ions on human corneal
epithelial cell survival and
proliferation**

7.1 Introduction

In vitro testing of novel drugs, excipients and formulations against cultured mammalian cells can enable early detection of potential toxicity, even before initiation of pre-clinical animal studies^[472]. Selection of the cell type to be employed depends on the intended application site and route of administration. For example, since the liver is a major site of toxicological effects after systemic administration due to first pass metabolism, hepatocyte cell lines such as HepG2^[473] are challenged with drugs in development for oral use. On the other hand, agents intended for topical use on the skin are commonly tested against an established spontaneously transformed immortal human keratinocyte cell line known as HaCaT^[474]. The response of appropriately selected cell lines to potential topical therapies while grown *in vitro* can be used to determine indicative locally tolerable drug concentrations and those likely to cause toxicity^{[475],[476]}. Tests for cytotoxicity and proliferation are used to determine whether the applied agent kills or modifies growth of mammalian cells, respectively. Cytotoxicity tests include the lactate dehydrogenase (LDH) assay which quantifies the proportion of a treated cell population that have died based on the release of usually intracellular LDH^[477]. Conversely, cell proliferation tests such as those employing 3-(4,5-dimethylthiazol-2-yl)-2,5-diphenyltetrazolium bromide (MTT)^[472] or neutral red^[478] quantify numbers of still metabolically active cells by measuring production of coloured degradation products in the mitochondria or internalisation of dye into lysosomes, respectively.

Table 7.1 – Mammalian cell proliferation inhibition data from the literature

Agent	Cell type	Exposure duration (h)	IC ₅₀ (mM)
FNa	primary human hepatocytes	48	0.236 ^[479]
Al ³⁺	primary rat astrocytes	72	0.343 ^[480]
Cu ²⁺	human skin-derived cells	24	0.29 ^[481]
	rat skin derived-cells	24	0.25 ^[481]
	primary rat hepatocytes	24	0.268 ^[482]
	mouse embryo fibroblasts (3T3)	24	0.444 ^[482]
	primary human hepatocytes	24	0.969 ^[482]
	human hepatocytes (HepG2)	24	1.716 ^[482]
Fe ²⁺	mouse embryo fibroblasts (3T3)	24	6.13 ^[483]
	primary human hepatocytes	24	6.40 ^[483]
	primary rat hepatocytes	24	8.81 ^[483]

In this work, the LDH and MTT assays were chosen for use in combination in order to generate a more detailed understanding of the nature and degree of any negative effects

on cell viability. Based on the antimicrobial activity presented in Chapter 6, Al^{3+} , Cu^{2+} and Fe^{2+} were selected for testing against an immortalised human corneal epithelial cell line with and without FNa. Published data for the effects of Al^{3+} , Cu^{2+} , Fe^{2+} and FNa on mammalian cell proliferation are listed in Table 7.1.

It is apparent that the degree of proliferation inhibition can vary between species and cell type. For example, the IC_{50} of Cu^{2+} against primary rat and human hepatocytes is 0.268 and 0.969 mM, respectively^[482], while it is 0.29 mM against human skin-derived cells^[481]. No published data on the effects of these metal ions or FNa on any eye-derived cell lines was identified. Therefore, the effects of Al^{3+} , Cu^{2+} , Fe^{2+} and FNa alone and in combination on the proliferation and survival of human corneal epithelial cells was investigated.

7.1.1 Aim and objectives

Aim: to determine whether FNa combined with metal ions may be suitable for further investigation as a treatment option in clinical bacterial keratitis based on the susceptibility of human corneal epithelial cells.

Objectives:

- 1) To determine inhibitory and cytotoxic activity of Al^{3+} , Cu^{2+} , Fe^{2+} and FNa individually against human corneal epithelial cells.
- 2) To determine inhibitory and cytotoxic activity of FNa combined with Al^{3+} , Cu^{2+} or Fe^{2+} against human corneal epithelial cells.
- 3) To compare activity of Al^{3+} , Cu^{2+} and Fe^{2+} each combined with FNa against human corneal epithelial cells and GN bacterial reference strains.
- 4) To identify the FNa and metal ion combination with highest selectivity index and therefore best potential for clinical use.

7.2 Methods

7.2.1 Cell line and standard culture conditions

Human corneal epithelial cells immortalised with an Adenovirus 12-SV40 hybrid virus (HCE-2 [50.B1] ATCC® CRL-11135) were purchased from the American Type Culture Collection (ATCC) *via* LGC Standards (Teddington, UK) and received at passage number 26. Culture conditions for HCE-2 were per the manufacturer's instructions, as follows.

A mixture of 0.01 mg mL⁻¹ BSA, 0.01 mg mL⁻¹ fibronectin and 0.03 mg mL⁻¹ collagen was prepared in sterile PBS and used to coat Nunclon™ Delta treated polystyrene flasks and plates (Nunc/Thermo Scientific, Roskilde, Denmark). A stock solution of 1 mg mL⁻¹ bovine serum albumin (BSA) (Fisher Scientific, Loughborough, UK) was prepared in HPLC grade water and filter sterilised. Human fibronectin purchased from Roche Diagnostics (Mannheim, Germany) had been 0.2 µm filtered prior to lyophilisation and was suspended in sterile HPLC to make a 1 mg mL⁻¹ stock solution. Aliquots of BSA and fibronectin were frozen at -20 °C for later use. Bovine collagen type I 5 mg mL⁻¹ stock solution (Gibco, Paisley, UK) was stored at 4 °C and used as received. A minimal volume of 1.5 mL for 25 cm² culture flasks and 30 µL per well for flat-bottomed 96 well plates was added to plasticware which was gently rocked to ensure surface coverage, sealed with plastic to prevent evaporation and incubated at 37 °C for 2 to 24 h. Coated flasks and plates were stored at 4 °C for up to 1 month and the coating mixture aspirated 15 min prior to use.

Cells were grown on the coated polystyrene in keratinocyte serum-free medium (KSFM) (Gibco, Paisley, UK) supplemented with 0.05 mg mL⁻¹ bovine pituitary extract (BPE) and 5 ng mL⁻¹ epidermal growth factor (EGF) as supplied, along with 0.005 mg mL⁻¹ recombinant human insulin (4 mg mL⁻¹ stock solution, Gibco, Paisley, UK) and 500 ng mL⁻¹ hydrocortisone (96 µg mL⁻¹ stock solution, Stemcell Technologies, Cambridge, UK) at 37 °C in humidified air with 5 % CO₂. Growth medium was replaced twice per week and always warmed and equilibrated to 37 °C and 5 % CO₂ for at least 30 min prior to use to ensure correct pH and temperature was reached. Under these conditions, HCE-2 grew to 80-90 % confluence in 3-5 days, totalling approximately 1 x 10⁶ cells per 25 cm² culture flask, at which point subcultivation was performed at a ratio of 1:3. The medium was removed and the cell layer rinsed twice with sterile PBS before adding 2 mL TrypLE™ Express dissociation reagent (Gibco, Paisley, UK).

TrypLE™ Express is a recombinant fungal trypsin-like protease and was selected in place of the more traditionally used animal trypsin due to its increased specificity, room temperature stability and inactivation by dilution rather than addition of an enzyme inhibitor^[484]. Cells were incubated with TrypLE™ Express at room temperature for 15 min until detachment could be confirmed using a light microscope. The dissociation enzyme was neutralised using two volumes of warmed supplemented KSFM and the resulting cell suspension centrifuged for 8 min at 130 x *g* in a VWR Mega Star 600 centrifuge. After discarding the supernatant, cells were resuspended in 15 mL fresh warmed supplemented KSFM and seeded into 3 coated 25 cm² culture flasks, 5 mL per flask.

7.2.2 Preparation, storage and recovery of frozen cell stocks

HCE-2 cells at 80-90 % confluence in 25 cm² culture flasks were harvested using TrypLE™ Express, rinsed in supplemented KSFM and pelleted as described above. The whole population from one 25 cm² culture flask (approximately 1 x 10⁶ cells) was resuspended in 1 mL freezing medium composed of 85 % supplemented KSFM, 10 % foetal bovine serum (Gibco, Paisley, UK) and 5 % dimethyl sulfoxide (DMSO), ≥99% (MP Biomedicals, Solon, OH, USA) and transferred to a labelled cryovial. Cryovial stocks were cooled to -80 °C at a rate of 1 °C min⁻¹ using a Mr Frosty™ Freezing Container (Fisher Scientific, Loughborough, UK) then transferred to the vapour phase of liquid nitrogen.

Frozen stocks were thawed rapidly, rinsed with 15 mL warmed supplemented KSFM and centrifuged for 8 min at 130 x *g*. The collected cells were resuspended in fresh warmed supplemented KSFM, enumerated and seeded into coated culture vessels at approximately 1 x 10⁴ cells per cm². Post-freeze viability was approximately 60 %.

7.2.3 Combined LDH and MTT assay procedure

LDH and MTT assays were co-optimised to enable performance of both tests simultaneously using the same cell populations (see Appendix E).

Coated flat-bottomed polystyrene 96 well plates were seeded with 8,000 HCE-2 in 100 µL supplemented KSFM in wells B2 to D10. Supplemented KSFM was added to wells E2 to G10 and KSFM without bovine pituitary extract (BPE) was added to B11 to G11 serve as cell free controls (Figure 7.1A). Since tissue extracts can contain LDH^[485],

a BPE-free control was included in order to determine any background activity attributable to its presence. Finally, wells in rows A and H and columns 1 and 12 were filled with 100 μ L sterile PBS to maintain humidity and prevent evaporation. Prepared plates were incubated at 37 °C and 5 % CO₂ in humidified air for 24 h.

Exposure to test agents was initiated by adding 10 μ L stock solution to three wells containing HCE-2 and three cell-free wells per concentration. The same volume of sterile HPLC grade water was added to the treatment-free control wells B8-G8 (Figure 7.1B). Lysis buffer from a Pierce™ LDH Cytotoxicity Assay Kit (Thermo Scientific, Loughborough, UK) x 10 μ L was also added to wells B9 to G9 as a positive control for complete cytotoxicity to total cells at the point of exposure initiation. Plates were returned to the incubator for the 18 h exposure period.

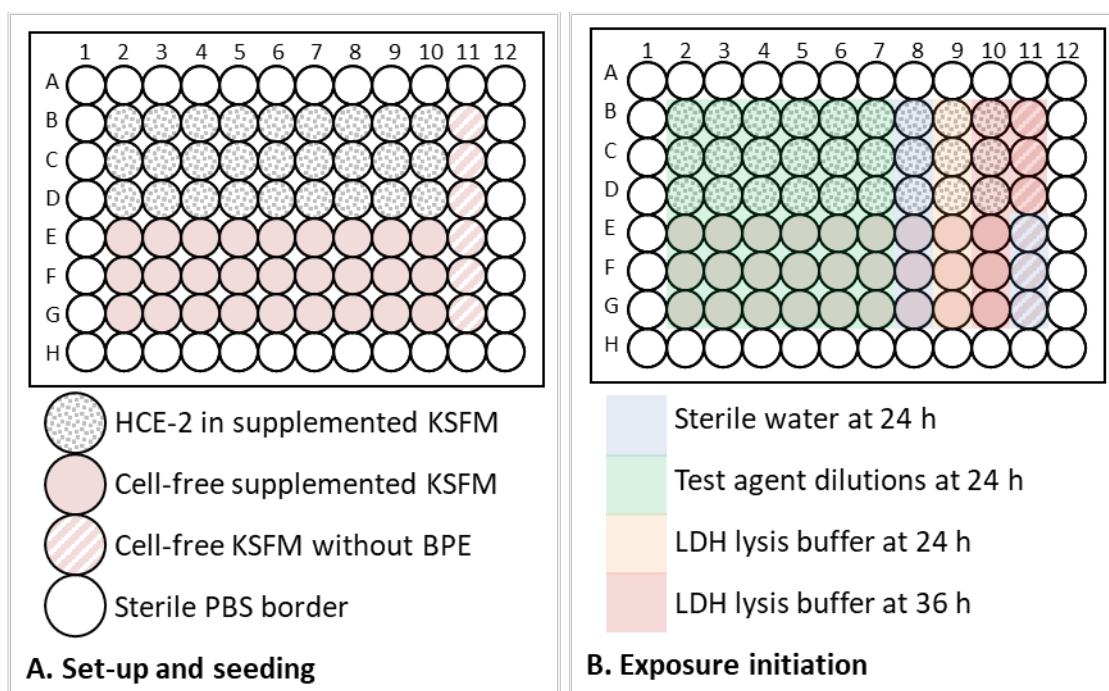


Figure 7.1 - Layout of 96 well plates for LDH and MTT assays

An individual 96 well plate served as one replicate for 6 test agent concentrations or combinations with controls and internal technical triplication.

The LDH assay was carried out per the manufacturer's instructions with minor modifications using the Pierce™ LDH Cytotoxicity Assay Kit and the MTT assay procedure was optimised based on reported protocols (see Appendix E). Both assays were carried out simultaneously, as follows:

Aliquots of 3-(4,5-dimethylthiazol-2-yl)-2,5-diphenyltetrazolium bromide (MTT) (Tocris Bioscience Bio-Techne, Bristol, UK) stock solution previously prepared in PBS and

frozen at -20 °C were thawed while protected from light. MTT stock solution was diluted in an uncoated 25 cm² culture flask (with a filter lid) 1/5 with supplemented KSFM to a final concentration of 1 mg mL⁻¹ and placed in the incubator to warm and equilibrate with 5 % CO₂ for 30-45 min before use. The LDH reaction mixture was prepared by dissolving one vial of Pierce™ substrate mix in 11.4 mL sterile HPLC grade water and adding one vial of Pierce™ assay buffer. Unused reaction mixture was stored at -20 °C for up to 4 weeks with a maximum of 3 freeze/thaw cycles.

After the 18 h test agent exposure duration, 10 µL Pierce™ lysis buffer was added to the maximum LDH activity (B10-D10), supplemented medium LDH activity (E10-G10) and BPE-free medium LDH activity (B11-D11) controls and the plate incubated at 37 °C and 5 % CO₂ for 45 min. A 50 µL aliquot of medium was transferred from each well to a fresh, uncoated, flat-bottomed 96 well plate for onward LDH assay processing. The remaining medium was aspirated from wells B2 to G9, carefully avoiding disturbance of the cell layer, and replaced with 100 µL warmed MTT dilution in supplemented KSFM. Following addition of the MTT reagent, plates were wrapped in aluminium foil to protect from light and returned to 37 °C and 5 % CO₂ for 2 h^{[486],[487]}.

Meanwhile, Pierce™ LDH reaction mixture (50 µL) was added to and gently mixed with the contents of each well in the LDH assay plate, followed by incubation at room temperature for 30 min, protected from light. At the end of the reaction period, 50 µL Pierce™ stop solution was gently mixed into each well. LDH assay plates were centrifuged at 4000 rpm for 15 min at 25 °C in a Thermo Scientific Heraeus Megafuge 40R fitted with well plate carriers in order to disperse bubbles. Any remaining bubbles were removed using a hot syringe needle. Plates were shaken orbitally for 10 s at 6 mm and the absorbance in each well was read at a measurement wavelength of 490 nm and reference wavelength of 680 nm with a Tecan Infinite M200 PRO microplate reader (wavelength accuracy ±1.5 nm^[283]).

After the 2 h incubation period, MTT-containing medium was removed from each well of the MTT assay plate and replaced with 100 µL DMSO, with gentle mixing. Plates were incubated at room temperature for 30 min, protected from light. The Tecan Infinite M200 PRO microplate reader was used to measure absorbance in each well at 506 nm, the λ_{\max} for MTT formazan product solubilised in 100 % DMSO^[472], preceded by 10 s orbital shaking at 6 mm.

7.2.4 Test concentrations and combinations

LDH and MTT assays were initially performed with twofold serial dilutions of $\text{Al}_2(\text{SO}_4)_3$, CuSO_4 , FeSO_4 or FNa. The equivalent concentrations of EtOH to those present in the FNa dilutions were also tested to determine any background activity attributable to its presence. Concentration ranges were selected to reflect those previously used against bacteria (see Section 4.2.1, page 84) and are summarised in Table 7.2.

Table 7.2 – Concentration range of each agent tested alone for cytotoxicity and proliferation effects on HCE-2

Test agent	Minimum concentration	Maximum concentration
Aluminium (as sulphate)	312.5 μM	10 mM
Copper(II) sulphate	156.25 μM	5 mM
Iron(II) sulphate	312.5 μM	10 mM
Sodium fusidate	40 μM	1280 μM
Ethanol	0.039 % v/v	1.25 % v/v

Metal sulphates were found to interfere with the LDH reaction. The generation of coloured formazan product was not apparent despite evidence of complete cell death on direct observation using a light microscope and indicated by MTT assay results. The addition of EDTA at the end of the exposure period was investigated as a means to bind metal ions in order to prevent interaction with the LDH pathway but was found to be unsuccessful. Effects of metal sulphates on HCE-2 growth were therefore quantified only using the MTT assay.

The MTT results were compared to bacteriology data and a concentration of 0.625 mM of each metal selected for testing against HCE-2 in combination with a range of FNa concentrations. In order to perform combined agent tests, double concentration stock solutions were prepared and only 5 μL of each added to the test wells so that the total addition volume was still 10 μL and the medium dilution factor equal to that when single agents were tested. Only the MTT assay was used to quantify effects of FNa with metals.

Each individual agent and combination was tested in triplicate using three different HCE-2 passage numbers between 30 and 36.

7.2.5 Data processing

7.2.5.1 Cytotoxicity

Analysis of the LDH assay results was performed per the kit manufacturer's instructions. Raw data was background corrected before determining LDH activity by subtracting absorbance at 680 nm from absorbance at 490 nm for each well. Values were then adjusted for spontaneous LDH activity by subtracting the background corrected absorbance of the untreated control from each well. Mean values for each technical triplicate were calculated. Finally, cytotoxicity of each concentration of each test agent was calculated as percentage of maximal LDH activity from cells lysed at the point of treatment initiation using the following formula:

$$\% \text{ cytotoxicity} = \frac{[\text{LDH activity from agent treated cells}]}{[\text{LDH activity from cells lysed at exposure initiation}]} \times 100$$

Lysis at the point of exposure initiation was selected for use in the analysis because the untreated cell populations were found to increase during the 18 exposure period. This growth prevented accurate quantification of complete cell death when the maximal LDH activity from cells lysed at the point of assay was used in the calculations.

7.2.5.2 Cell proliferation

Percentage proliferation was calculated following a similar process. Raw data from the MTT assay were adjusted for baseline DMSO absorbance by subtracting the lysed cell control values from every well. Any additional background interference from residual test agent was corrected for by subtracting the adjusted cell-free values from their HCE-2 containing equivalents (i.e. E2-G2 values were subtracted from B2-D2 values and so on, Figure 7.1). Mean values for each technical triplicate were calculated and proliferation as a percentage of untreated control determined for each test agent and concentration:

$$\% \text{ proliferation} = \frac{[\text{formazan absorbance from treated cells}]}{[\text{formazan absorbance from untreated control}]} \times 100$$

Percentage inhibition of cell proliferation was calculated as:

$$\% \text{ inhibition} = 100 - (\% \text{ proliferation})$$

7.2.5.3 EC₅₀, IC₅₀ and IC₉₀ calculation

Cytotoxicity and inhibition data were used to calculate the mean agent concentrations to produce 50 % cytotoxicity (EC₅₀), 50 % inhibition (IC₅₀) and 90 % inhibition (IC₉₀). The results for each individual replicate were fit to Boltzmann sigmoidal curves using the formula:

$$P = A_{min} + \frac{A_{max} - A_{min}}{1 + e^{(i-c)/s}}$$

Where P = predicted cytotoxicity or inhibition, A_{min} = minimum observed cytotoxicity or inhibition, A_{max} = maximum observed cytotoxicity or inhibition, i = the sigmoidal inflection point, c = natural logarithm of the test agent concentration and s = the slope.

Microsoft® Excel® (MSO Professional Plus 2016, Microsoft Corporation, WA, USA) Solver add-in was used to optimise the constants i and s to fit the observed data by solving for the lowest sum of least squares between observed and predicted values. The determined constants were then used to identify the natural logarithm of the test agent concentration (c) predicted to produce 50 % or 90 % cytotoxicity or inhibition, as applicable. The resulting value was inverted to obtain the EC₅₀, IC₅₀ or IC₉₀ for the given replicate and the mean and 95 % CI ($p = 0.05$) determined for each triplicate. The selectivity indices (SI) were calculated by dividing the IC₅₀s by respective MIC₉₀s against each of the GN reference strains.

7.3 Results

7.3.1 Inhibitory and cytotoxic effects of sodium fusidate, aluminium, copper and iron ions alone on corneal epithelial cells

The inhibitory and cytotoxic effects of FNa on HCE-2 are illustrated in Figure 7.2. While FNa completely inhibited HCE-2 proliferation at concentrations of $\geq 640 \mu\text{M}$, the maximum cytotoxicity was only 66.6 % with 1280 μM . Consequently, the EC₉₀ of FNa could not be determined. The FNa EC₅₀ was 425.30 μM (95 % CI = 63.23) which was statistically significantly greater ($p < 0.05$) than both the IC₅₀ and IC₉₀ of 183.53 (95 % CI = 4.83) and 338.21 μM (95 % CI = 15.41), respectively.

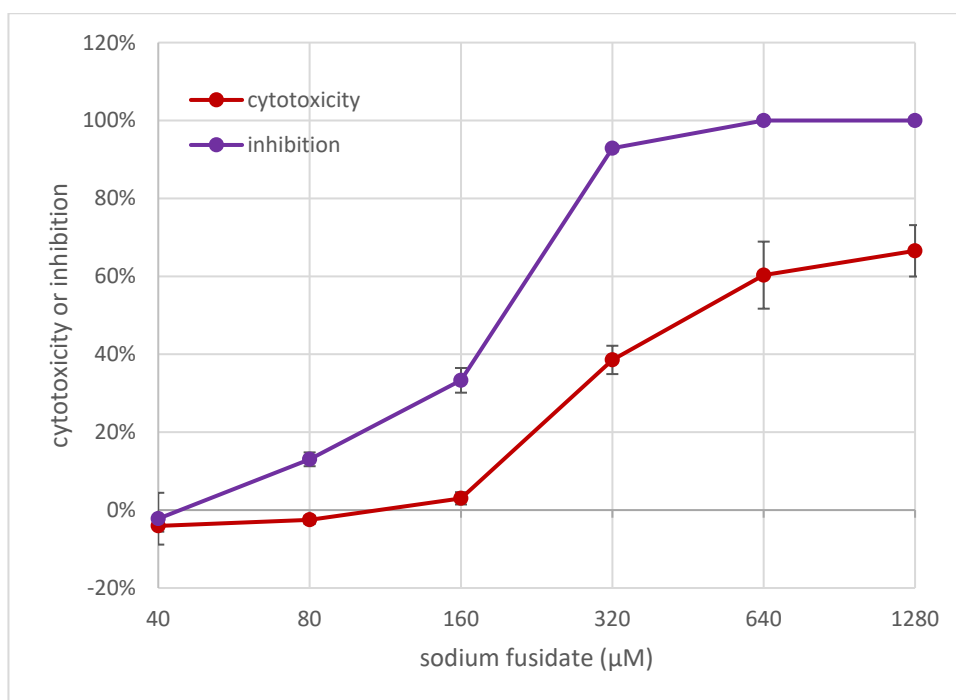


Figure 7.2 - Sodium fusidate-induced cytotoxicity and growth inhibition of human corneal epithelial cells after 18±2 h incubation at 37 °C in 5 % CO₂

A cytotoxicity or inhibition value of <0 indicates enhanced proliferation compared to untreated control.

(n = 3, error bars = 95 % CI)

The IC₅₀s of Al³⁺, Cu²⁺ and Fe²⁺ against HCE-2 were 8.27 (95 % CI = 3.03), 1.31 (95 % CI = 0.18) and 3.27 mM (95 % CI = 0.28), respectively. The proliferation inhibition profiles produced by these metal ions are illustrated in Figure 7.3. Al³⁺ at concentrations of ≤5 mM enhanced HCE-2 growth by between 12.7 and 29.6 %. Even at 10 mM, the highest concentration of Al³⁺ tested, HCE-2 proliferation was inhibited by only 68.9 %, therefore, an IC₉₀ could not be calculated. Cu²⁺ and Fe²⁺ also enhanced HCE-2 growth but at lower concentrations of ≤0.625 and ≤1.25 mM, respectively. The IC₉₀s were 2.38 mM (95 % CI = 0.93) Cu²⁺ and 4.45 mM (95 % CI = 0.83) Fe²⁺.

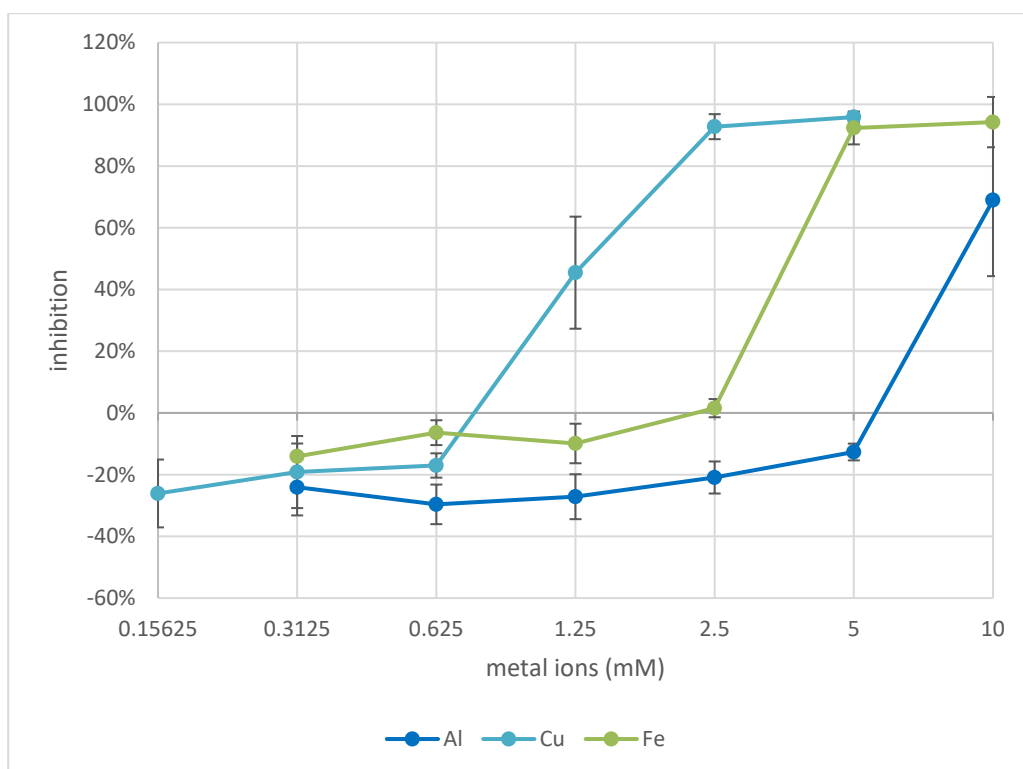


Figure 7.3 – Metal ion-induced growth inhibition of human corneal epithelial cells after 18±2 h incubation at 37 °C in 5 % CO₂

An inhibition value of <0 indicates enhanced proliferation compared to untreated control. (n = 3, error bars = 95 % CI)

7.3.2 Effects of sodium fusidate combined with metal ions on the proliferation of corneal epithelial cells

The HCE-2 inhibition profiles produced by FNa with and without 0.625 mM Al³⁺, Cu²⁺ or Fe²⁺ are illustrated in Figure 7.4. There was no significant difference between the inhibition caused by ≥160 μM FNa alone and in the presence of Al³⁺ or Fe²⁺ (*p* >0.05). However, inhibition of HCE-2 by FNa combined with Cu²⁺ was significantly greater than by FNa alone (*p* <0.05). Inhibition was 33.3 % by 160 μM FNa alone and 51.2 % in the presence of 0.625 mM Cu²⁺. While also significant, the differences between inhibition with and without Cu²⁺ were less than 3 % with 320 and 640 μM FNa. There was no significant difference (*p* >0.05) between inhibition of HCE-2 proliferation by 80 μM FNa alone and in the presence of 0.625 mM Cu²⁺ which were 13.0 and 18.6 %, respectively. With Al³⁺ and Fe²⁺ inhibition by 80 μM FNa was -1.3 and 4.4 %, respectively, and both were significantly less than FNa alone (*p* <0.05). There was no significant difference between inhibition produced by 40 μM FNa alone and in the presence of any metal ion tested (*p* >0.05).

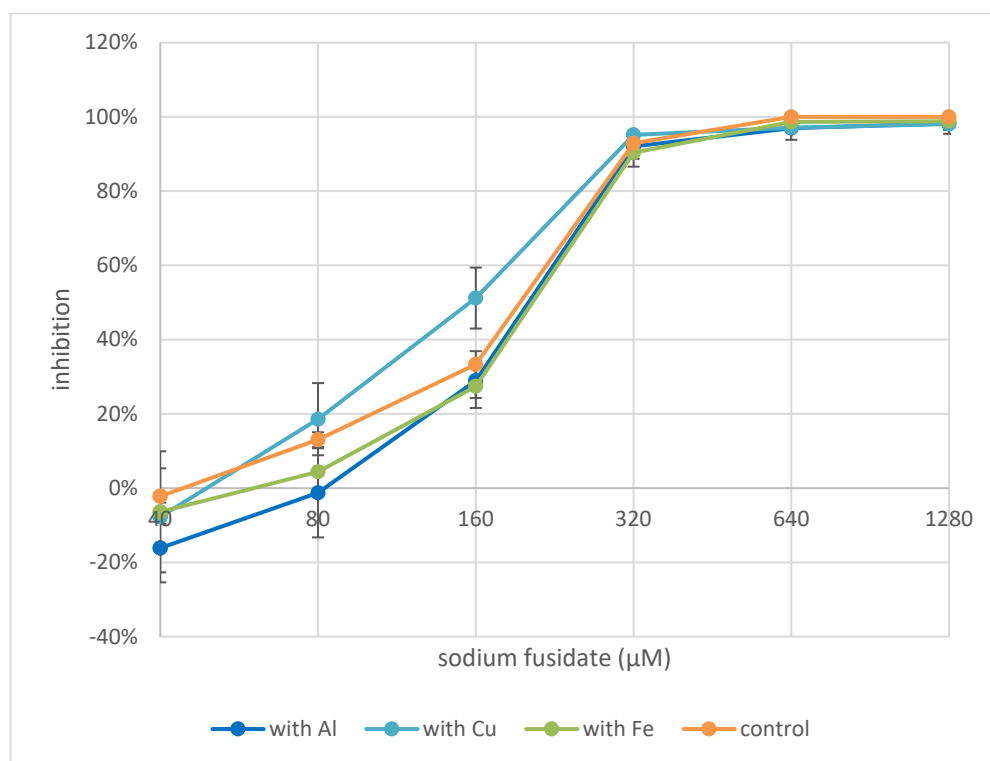


Figure 7.4 - Inhibition of human corneal epithelial cell growth by sodium fusidate combined with 0.625 mM metal ions after 18±2 h incubation at 37 °C in 5 % CO₂

An inhibition value of <0 indicates enhanced proliferation compared to untreated control. (n = 3, error bars = 95 % CI)

There was no significant difference between the IC₉₀s of FNa alone and in the presence of any of the metal ions tested ($p > 0.05$, Table 7.3). There was also no significant difference between the IC₅₀ of FNa alone and with Al³⁺ or Fe²⁺ ($p > 0.05$). However, the IC₅₀ of FNa was significantly lowered by the presence of Cu²⁺ at 146.5 μM compared to 183.5 μM FNa when alone.

Table 7.3 – Mean sodium fusidate IC₅₀s and IC₉₀s against human corneal epithelial cells, with and without 0.625 mM metal ions

	IC ₅₀ ± 95 % CI (μM)	IC ₉₀ ± 95 % CI (μM)
Al ³⁺	187.17 ± 2.66	363.03 ± 68.47
Cu ²⁺	146.53 ± 14.25	338.58 ± 43.74
Fe ²⁺	195.57 ± 11.81	340.37 ± 31.61
control	183.53 ± 4.83	338.21 ± 15.41

7.3.3 Comparison of antimicrobial activity versus corneal epithelial cell proliferation in the presence of sodium fusidate and metal ion combinations

7.3.3.1 Inhibition profiles

The inhibition profiles of HCE-2, *E. coli* NCTC 10418, *K. pneumoniae* NCTC 9633 and *P. aeruginosa* NCTC 13359 in response to FNa are illustrated in Figure 7.5. There were significant differences between the degree of inhibition of each cell type by FNa, however, HCE-2 and *K. pneumoniae* followed a similar pattern. *E. coli* was more sensitive to FNa than HCE-2 and the other bacterial species and *P. aeruginosa* was the least sensitive overall.

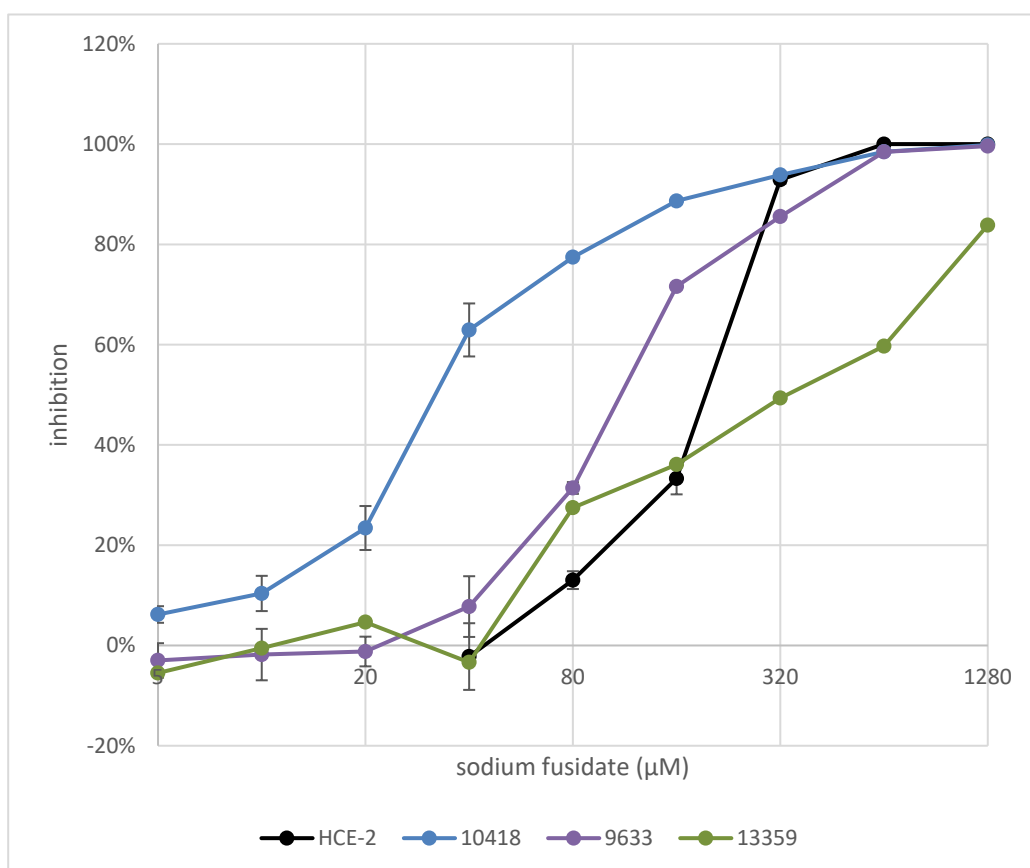


Figure 7.5 - Comparison of growth inhibition of human corneal epithelial cells and bacterial reference strains *E. coli* NCTC 10418, *K. pneumoniae* NCTC 9633 and *P. aeruginosa* NCTC 13359 by sodium fusidate alone

An inhibition value of <0 indicates enhanced proliferation compared to untreated control.
(n = 3, error bars = 95 % CI)

Conversely, *P. aeruginosa* was more inhibited by Al^{3+} than either *E. coli*, *K. pneumoniae* or HCE-2 (Figure 7.6A). In fact, all three bacterial species were 100 % inhibited by 5 mM

Al³⁺ while HCE-2 proliferation was enhanced by the same concentration with -12.7 % inhibition.

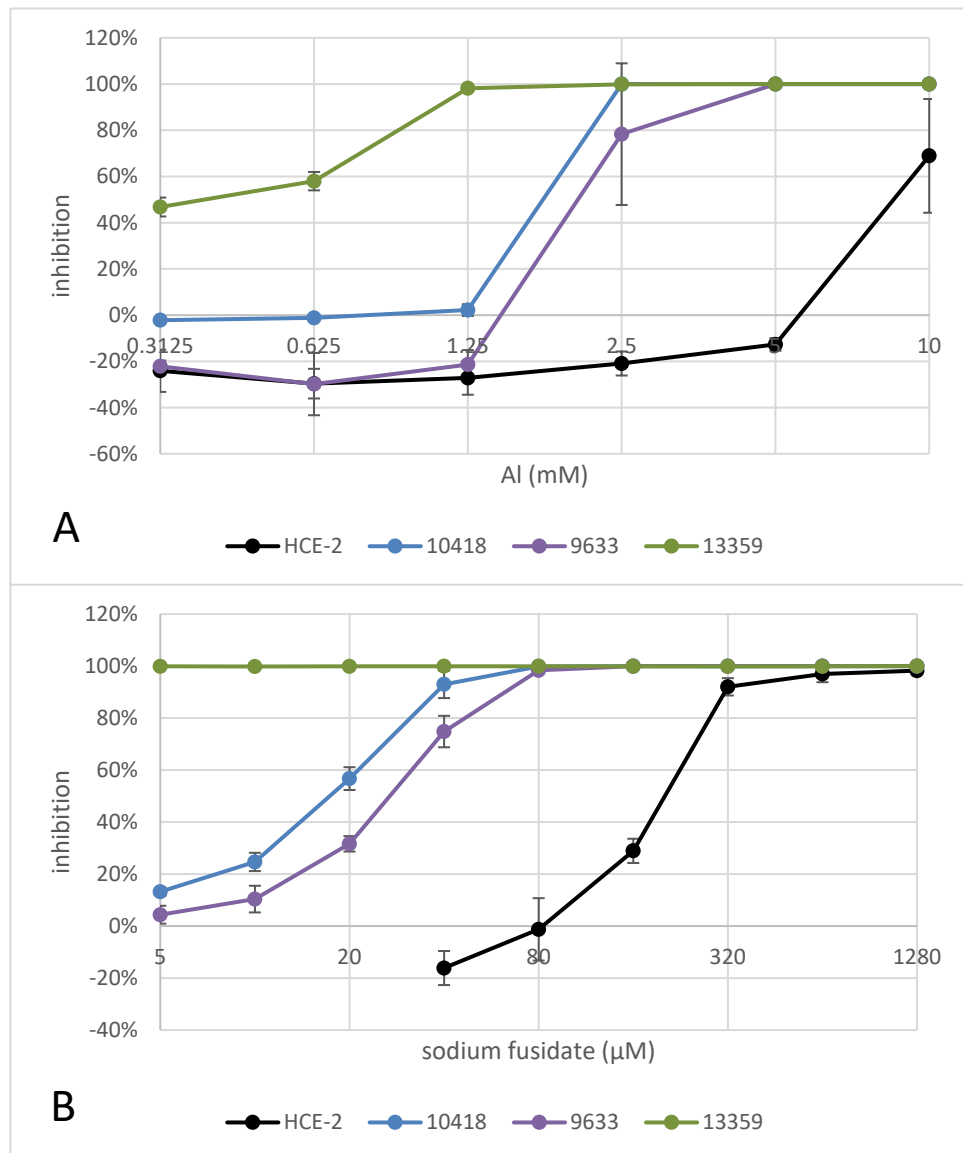


Figure 7.6 – Comparison of growth inhibition of human corneal epithelial cells and bacterial reference strains *E. coli* NCTC 10418, *K. pneumoniae* NCTC 9633 and *P. aeruginosa* NCTC 13359 by aluminium ions alone (A) and sodium fusidate in the presence of 0.625 mM aluminium ions (B)

An inhibition value of <0 indicates enhanced proliferation compared to untreated control.
(n = 3, error bars = 95 % CI)

The bacterial reference strains were also more inhibited by FNa in the presence of 0.625 mM Al³⁺ than HCE-2 (Figure 7.6B). For example, 80 μM FNa with 0.625 mM Al³⁺ produced -1.3 % HCE-2 inhibition and the same combination inhibited *E. coli* NCTC 10418, *K. pneumoniae* NCTC 9633 and *P. aeruginosa* NCTC 13359 by >98 %.

There were more similarities between inhibition of bacterial species and HCE-2 by Cu^{2+} (Figure 7.7A). At Cu^{2+} concentrations of ≤ 0.625 mM HCE-2 were the least inhibited (-26.1 to -17.0 %) followed by *K. pneumoniae* (13.0 to 17.4 %), *P. aeruginosa* (26.1 to 38.2 %) then *E. coli* (48.8 to 59.5 %). However, all cell types were >80 % inhibited by 2.5 mM Cu^{2+} .

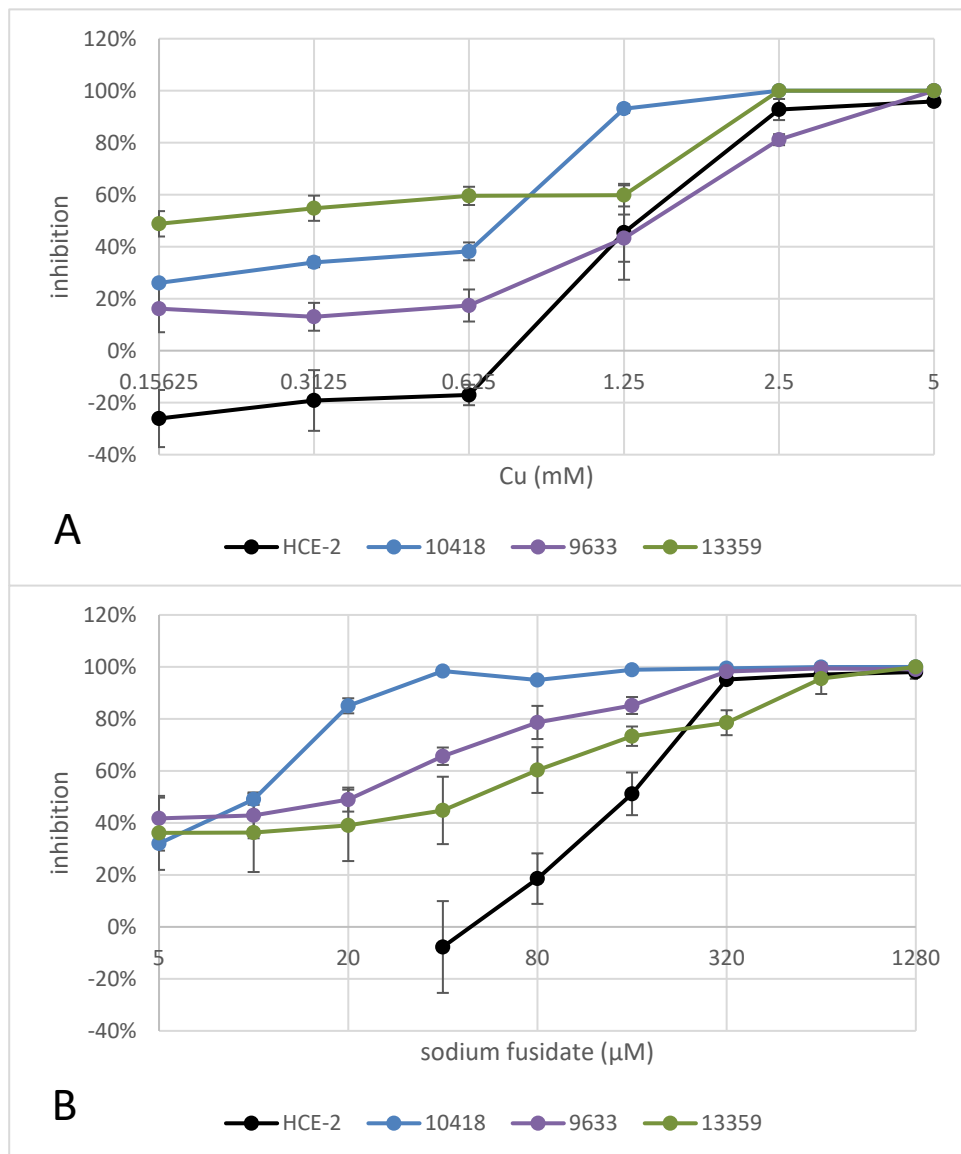


Figure 7.7 - Comparison of growth inhibition of human corneal epithelial cells and bacterial reference strains *E. coli* NCTC 10418, *K. pneumoniae* NCTC 9633 and *P. aeruginosa* NCTC 13359 by copper(II) ions alone (A) and sodium fusidate in the presence of 0.625 mM copper(II) ions (B)

An inhibition value of <0 indicates enhanced proliferation compared to untreated control.
(n = 3, error bars = 95 % CI)

The presence of 0.625 mM Cu^{2+} increased the inhibition of bacterial reference strains by FNa to a greater degree than HCE-2 (Figure 7.7B), however, the difference was not as notable as with the other metals. While 80 μM FNa with Cu^{2+} produced 18.6 % inhibition

of HCE-2, bacterial strains were inhibited by 60.3 to 95.0 % ($p < 0.05$). However, while still significant ($p < 0.05$) the difference between the effects of 160 μM FNa with Cu^{2+} on HCE-2 and bacterial strains was less with the combination inhibiting HCE-2 by 51.2 % and bacterial strains by between 73.4 and 99.0 %. Finally, 320 μM produced $>95\%$ inhibition ($p > 0.05$) of all but *P. aeruginosa*.

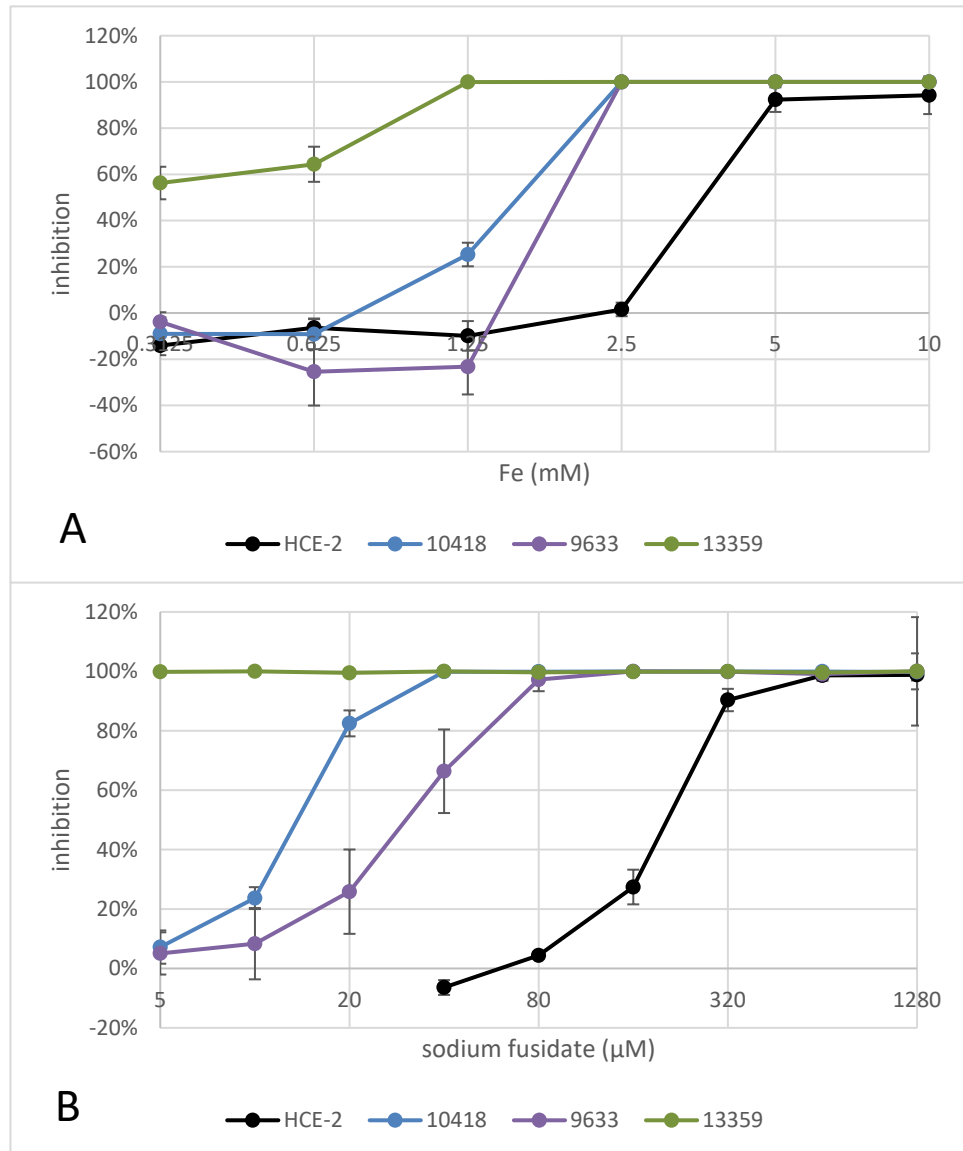


Figure 7.8 - Comparison of growth inhibition of human corneal epithelial cells and bacterial reference strains *E. coli* NCTC 10418, *K. pneumoniae* NCTC 9633 and *P. aeruginosa* NCTC 13359 by iron ions alone (A) and sodium fusidate in the presence of 0.625 mM iron ions (B)

An inhibition value of <0 indicates enhanced proliferation compared to untreated control.

($n = 3$, error bars = 95 % CI)

While Fe^{2+} (Figure 7.8A) was not as inhibitory as Al^{3+} , a similar sensitivity pattern was observed with both metals. HCE-2 proliferation was not negatively impacted by ≤ 2.5 mM

Fe²⁺, however all three bacterial strains were 100 % inhibited (*p* <0.05). *P. aeruginosa* was also more sensitive to Fe²⁺ than *E. coli* and *K. pneumoniae*.

At concentrations of ≤320 μM, FNa combined with 0.625 mM Fe²⁺ also inhibited the bacterial reference strains to a greater degree than HCE-2 (*p* <0.05, Figure 7.8B). HCE-2 proliferation was inhibited by 4.4 % by 80 μM FNa with Fe²⁺ whereas *E. coli* NCTC 10418, *K. pneumoniae* NCTC 9633 and *P. aeruginosa* NCTC 13359 were all inhibited >97 % by the same combination.

7.3.3.2 Selectivity indices

The selectivity index (SI) is a measure of the ratio of the adverse effect of an agent on mammalian cell proliferation (IC₅₀) to its antimicrobial efficacy (MIC). A value of ≥10 is used as an indicator of high clinical potential^[488]. SIs for FNa alone and in the presence of metal ions against each GN reference strain are listed in **Error! Reference source not found.** All SIs for FNa alone were <1, demonstrating its clinical ineffectiveness against GN organisms. Although the SIs for FNa with Al³⁺, Cu²⁺ and Fe²⁺ against *E. coli* NCTC 10418 – the original GN reference strain tested – were <10, all three values are similar to one another at 4.7, 3.7 and 4.9, respectively. However, against both *K. pneumoniae* NCTC 9633 and *P. aeruginosa* NCTC 13359, the SI for FNa with 0.625 mM Cu²⁺ was <1. In addition, *K. pneumoniae* NCTC 9633 was more resistant to FNa in the presence of Al³⁺ or Fe²⁺ than the other two reference stains, resulting in SIs of 2.3 and 2.4, respectively. On the contrary, the SIs for FNa in the presence of Al³⁺ or Fe²⁺ against *P. aeruginosa* NCTC 13359 were 37.4 and 39.3, respectively, indicating potential for clinical use of these combinations against *P. aeruginosa* infections.

Table 7.4 – Sodium fusidate selectivity indices against human corneal epithelial cells and Gram-negative reference strains, with and without metal ions

	<i>E. coli</i> NCTC 10418	<i>K. pneumoniae</i> NCTC 9633	<i>P. aeruginosa</i> NCTC 13359
Al ³⁺	4.679	2.340	37.434
Cu ²⁺	3.663	0.4579	0.2290
Fe ²⁺	4.879	2.445	39.306
control	0.5735	0.2868	0.07169

Selectivity index of ≥10 indicates suitability for consideration for clinical use high due to high ratio of antimicrobial activity to inhibition of mammalian cell proliferation (green, bold text).

7.4 Discussion

7.4.1 Human corneal epithelial cell proliferation in the presence of sodium fusidate, metal ions and sodium fusidate combined with metal ions

The IC_{50} of 183.53 μ M FNa determined against HCE-2 after 18 h exposure was lower than that reported against primary human hepatocytes of 235.6 μ M after 48 h^[479]. The IC_{50} would normally be expected to decrease inversely to duration of exposure. However, this difference was not surprising due to the known variability between the susceptibility of cell types to toxic agents. Interestingly, while HCE-2 proliferation was completely inhibited by ≥ 640 μ M FNa, 29.7 and 23.4 % of the cell populations were still alive after 18 h in the presence of 640 and 1280 μ M, respectively. The difference between inhibitory and cytotoxic effect was also exhibited by the statistically significantly larger EC_{50} of 425.3 μ M ($p < 0.05$), indicating that FNa more readily inhibited growth than killed HCE-2.

Due to the limitations found with the use of the LDH assay in the presence of metal ions, similar comparisons between inhibitory and cytotoxic effects could not be made for Al^{3+} , Cu^{2+} and Fe^{2+} . However, Al^{3+} was found to be substantially less inhibitory to HCE-2 than rat astrocytes, with an IC_{50} of 8.27 mM after 18 h exposure compared to 0.343 mM after 72 h^[480]. This may be explained by the similarities between astrocytes and neurons, the latter of which are known to be particularly vulnerable to Al^{3+} *via* interference with a variety of cellular functions including axonal transport and protein phosphorylation/de-phosphorylation^[489]. HCE-2 were also less susceptible to Cu^{2+} than most reported cell types with an IC_{50} of 1.31 mM falling between those reported against primary human hepatocytes and the human hepatocyte immortal cell line HepG2 (see Table 7.1, page 182). Conversely, and despite a higher IC_{50} than Cu^{2+} , HCE-2 were inhibited considerably more by Fe^{2+} (IC_{50} 3.27 mM) than the mouse fibroblasts, human hepatocytes or rat hepatocytes reported in the literature (Table 7.1). Since the effects of metal ions on mammalian cells and their proliferation appear to be even less well studied than that of bacteria, the reasons for differences between cell type susceptibilities cannot be explained. However, this data clearly demonstrates the importance of selecting an appropriate cell type for investigations into potential toxicity of novel drugs or formulations.

At a concentration of 0.625 mM, neither Al^{3+} nor Fe^{2+} had a significant impact on the inhibition profile, IC_{50} or IC_{90} of FNa against HCE-2 ($p > 0.05$). However, the presence of 0.625 mM Cu^{2+} increased inhibition when combined with 160 μ M FNa by an additional

18 % ($p < 0.05$) and reduced the IC_{50} to $146.5 \mu\text{M}$ ($p < 0.05$). This may suggest some anti-proliferative synergy between Cu^{2+} and FNa since the same concentration of Cu^{2+} alone had no impact on HCE-2 growth ($p > 0.05$). However, the mechanism is, as yet, unclear due to lack of published information on the effects of these agents on mammalian cells.

7.4.2 Comparison of human corneal epithelial cell and bacterial inhibition by sodium fusidate combined with metal ions

While the response of HCE-2 to FNa alone followed a similar pattern to that of *K. pneumoniae* and *P. aeruginosa* (Figure 7.5, page 194), the mammalian cells were significantly less inhibited than bacterial reference strains by almost all combinations of metal ions and FNa tested ($p < 0.05$). The only exceptions were in the presence of 0.625 mM Cu^{2+} and $320 \mu\text{M FNa}$ which inhibited HCE-2 significantly more than *P. aeruginosa* ($p < 0.05$, Figure 7.7B, page 196) and wherever HCE-2 and the bacterial strains were all $\geq 95\%$ inhibited ($p > 0.05$). There are several factors which could explain the comparative lack of inhibition of mammalian cells to metal ion and FNa combinations. Firstly, mammalian cells are thought to be susceptible to FNa *via* inhibition of their mitochondrial ribosomes^[490]. However, the IC_{50} of FNa against isolated mitochondrial ribosomes is $2020 \mu\text{M}$ compared to $33 \mu\text{M}$ against *E. coli* ribosomes^[491]. Therefore, while the HCE-2 cell and mitochondrial membranes are more permeable to FNa than the OM of GN bacterial strains, their resulting susceptibility is similar. Secondly, the presence of metal ions increases the amount of FNa associated with bacterial cells (see Section 5.3.4, page 150) which increases growth inhibition, while the same does not appear to occur in HCE-2. The presence of 0.625 mM Al^{3+} or Fe^{2+} had no significant impact on the activity of FNa against HCE-2 (Figure 7.4, page 193). However, these metal ions were the most effective in combination with FNa against GN isolates, reducing the FNa MIC_{90} by 8 to ≥ 512 -fold by their presence (see Chapter 6, Section 6.3.3, page 171). This may be attributable to either the comparatively low susceptibility of mitochondrial ribosomes to FNa or, possibly more likely, increased differential permeability of the LPS-containing bacterial OM to highly protonated FNa in the presence of metal ions.

The selectivity indices (SI) unfortunately indicate little clinical potential for the majority of combinations of metal ions and FNa against GN bacteria. However, the exceptions were Al^{3+} and Fe^{2+} with significantly high ratios of antimicrobial activity against *P. aeruginosa* to HCE-2 toxicity of 37.4 and 39.3, respectively. While identification of a co-formulation with a wider spectrum of antimicrobial activity was the original aim of this study, a combination active against *P. aeruginosa* is an important finding. As discussed in

Chapter 1, *P. aeruginosa* is both widely resistant to commonly used antimicrobials and the most frequent cause of GN bacterial keratitis. In addition, this bacterium is a problematic cause of many other severe, difficult to treat infections such as in burn wounds^[492] and cystic fibrosis^[493]. If similar low toxicity is found in other cell types, co-formulation of FNa with either Al³⁺ or Fe²⁺ may have potential for application in the topical treatment of eye and wound infections or as an inhaled formulation for the treatment of infections in cystic fibrosis.

7.5 Conclusions

The following conclusions can be drawn from the work presented in this Chapter:

- 1) The proliferation of human corneal epithelial cells was inhibited in the order Cu²⁺ > Fe²⁺ > Al³⁺.
- 2) The presence of Cu²⁺, Fe²⁺ or Al³⁺ did not alter human corneal epithelial cell response to FNa.
- 3) GN bacterial reference strains were more susceptible to growth inhibition by metal ion and FNa combinations than human corneal epithelial cells.
- 4) The combinations of FNa with Al³⁺ or Fe²⁺ yielded selectivity indices of >10 against *P. aeruginosa* indicating potential suitability for clinical use against this challenging opportunistic pathogen.

**Chapter 8: Anti-Gram-negative activity
 and solubility of sodium
fusidate combined with metal
ions in a novel simulated tear
fluid**

8.1 Introduction

The human tear film is a complex structure, thoroughly described in a 2012 review by Franzco^[494]. In brief, the tear film is composed of two discrete compartments (Figure 8.1). The lipid sealant film is a 100 nm layer of meibomian lipids on the outermost surface which serves to reduce evaporation. The muco-aqueous pool (MAP) is in contact with the anchored mucin and glycocalyx of the corneal epithelium and both lubricates the eye surface and provides protection from pathogens and foreign particles. The MAP is the larger compartment with a depth of 3000-9000 nm. It contains a complex mixture of electrolytes, metabolites, proteins, trace elements and mucin which creates a dense mucous layer at the cell surface to lubricate the eye and trap microbes and foreign particles.

Simulated tear fluids (STFs) are widely used in the literature with the intention to mimic *in situ* conditions at the eye surface, thereby reducing the use of animals in research. Applications include the study of drug release from ocular preparations^[495], spoilage of contact lenses^[496] and the growth of microbial pathogens^[497]. Published STF formulations range from simple solutions of electrolytes to complex mixtures of salts, proteins and lipids, with much variation in between. One of the most frequently used STF formulations is a simple electrolyte solution of sodium chloride, sodium bicarbonate and calcium chloride^{[498]–[501]}, devoid of many electrolytes and without any of the metabolites, proteins or lipids found in human tears. Other, more complex, formulations include a variety of proteins and lipids more closely resembling tear concentrations *in vivo*, but in a homogenous suspension^{[502],[503]}. Disparity between the composition and structure of tear film and reported STF formulations may mean that studies employing these STFs do not consistently produce the desired *in situ*-like setting, reducing the predictive reliability of their results.

Exposure to any individual or combination of molecules can initiate phenotypic changes in bacterial cells^[504]. Exposure to individual components or the particular molecular mixtures encountered in tear fluid may induce the switching on or off of metabolic pathways and virulence mechanisms relied upon during infection which the same bacteria do not exhibit during growth in standard bacteriological broth. In particular, mucin has been shown to induce the expression of various virulence factors and metabolic processes in *A. baumannii* which increases the bacterium's efficiency in infecting host cells^[505] and to trigger production of toxins by *Bacillus cereus*^[506].

Therefore, it was decided to investigate the efficacy of the discovered antimicrobially active FNa and metal ion combinations in an STF designed to mimic the MAP.

While the meibomian lipid layer is an important component of the tear film structure and may have an impact on a variety of ocular considerations, the aim of this investigation was to predict the solubility and activity of FNa delivered as an eyedrop to the infected cornea. Although the eyedrop will theoretically have to penetrate the exterior lipid film “sealant”, this layer is extremely thin (100 nm) and is likely considerably disrupted on addition of a 25-50 μL drop to the usual total tear volume of $\sim 7 \mu\text{L}$ ^[498]. In addition, tear production increases in keratitis resulting in an even greater proportion of the tear film volume being comprised of MAP^[507]. For these reasons, this work focussed on the rationalisation and employment of an STF representative of the physiological human MAP. Testing the identified anti-GN combinations of FNa and metal ions under these conditions may provide an indication as to efficacy *in situ* against bacteria habituated to survival and growth in tear fluid. In addition, since solubility can vary widely by solvent, investigations in STF may be particularly important to the current work due to the apparent relationship between the discovered combined antimicrobial activity and FNa solubility.

8.1.1 Aim and objectives

Aim: to investigate whether metal ion and FNa combinations found to be active against GN isolates in a bacteriological growth medium under standard laboratory conditions also exhibit anti-GN activity in a novel, rationally designed, physiologically representative STF and the relationship to solubility.

Objectives:

- 1) To rationally design a novel STF representative of the physiological human muco-aqueous pool and suitable for antimicrobial testing.
- 2) To optimise a simple assay to investigate antimicrobial efficacy in the novel STF.
- 3) To determine whether Al^{3+} , Cu^{2+} and/or Fe^{2+} increase FNa activity against *E. coli*, *K. pneumoniae* and *P. aeruginosa* reference strains in the novel STF.
- 4) To investigate whether the activity of FNa with and without metal ions in the novel STF is also related to FNa solubility.

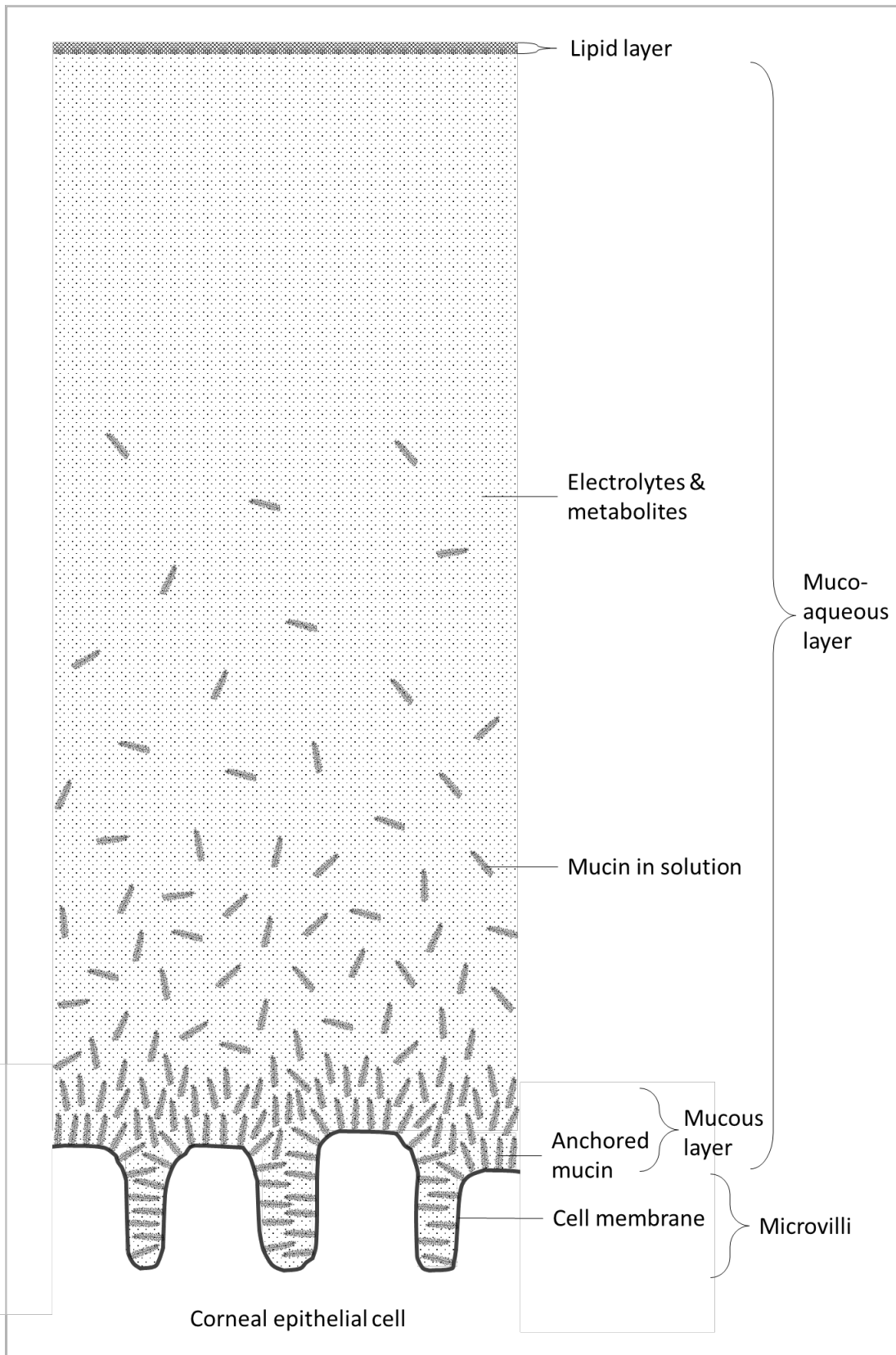


Figure 8.1 - Scale diagram of the tear film structure

The human squamous corneal epithelial cell diameter is 30-40 μm ^[508] with a microvillus surface^[509]. Approximately 1/20 of a single corneal epithelial cell diameter is shown. Anchored mucin forms part of the glycocalyx of 300-600 nm depth^[509] and covers the cell surface, increasing wettability^[510]. Additional solubilised mucin in the muco-aqueous pool (9 μm ^[511]) lubricates the cell surface to prevent damage during blinking and traps foreign particles^[512].

The outer lipid layer (100 nm) acts as a sealant to reduce evaporation^{[494],[513]}.

8.2 Methods

8.2.1 Development of a novel simulated tear fluid formulation

8.2.1.1 Collation of published data

The first task was a critical analysis of published STF formulae reported in the literature and understanding the rationale for inclusion of individual components. A literature search was undertaken for STF formulations used to mimic *in situ* conditions. For each STF formulation reported, the ingredients and concentrations were tabulated, with the units standardised (converted to mM or mg mL⁻¹, as appropriate). Electrolytes were considered as individual ions and the final concentrations of each summated. Where multiple publications employed the same formulation, only one entry was made referencing the earliest reported use. Component concentrations were compared across all identified STF formulations to determine frequency of use and the mean and range of concentrations employed.

The actual concentrations of electrolytes, metabolites and proteins measured in human tears was gathered through further literature searches. Data from the eyes of normal healthy subjects and, where available, eyes with bacterial keratitis or corneal ulceration were included. Information regarding collection method was also recorded allowing procedure-related differences in reported concentrations to be considered and rationalisation of inclusion or exclusion of each data point in the analysis. Selected literature values were tabulated, and the mean and range calculated for each component. Finally, the pH of each published STF formulation (where reported) and data for human tear fluid pH were also collated.

8.2.1.2 Design and optimisation of a novel STF

Each component as identified in 8.2.1.1 was reviewed and its inclusion in the novel STF rationalised. Where available, the reported human muco-aqueous pool component concentrations were used to deduce a formulation composed of commonly available salts and proteins. Where actual human tear fluid concentrations could not be identified, concentrations employed in published STF formulations were used as a guide.

8.2.1.2.1 Materials

Calcium chloride dihydrate, magnesium chloride hexahydrate, potassium chloride, D-glucose anhydrous, urea and BSA were purchased from Fisher Scientific (Loughborough, UK) while sodium phosphate dibasic, sodium phosphate tribasic, sodium bicarbonate, sodium chloride, sodium citrate tribasic dihydrate, sodium pyruvate, sodium DL-lactate, lysozyme from chicken egg white and mucin from porcine stomach were from Sigma Aldrich (Gillingham, UK). Sodium phosphate monobasic monohydrate was purchased from Acros Organics (Geel, Belgium). All materials were used as received.

Stock solutions were prepared in HPLC grade water and, except for mucin, sterilised by filtration through 0.22 µm PES (Sartorius, Germany). As the viscous, polymeric nature of mucin makes solutions incompatible with sterilisation by filtration, the stock solution was autoclaved for 15 min at 121 °C^[497]. STF formulations were prepared by sequential addition of stock solutions to sterile HPLC grade water and evaluated for their ability to support bacterial growth and replicate physiological pH.

8.2.1.2.2 Initial assessment of bacterial growth

The ability of test STF formulations to support quantifiable growth of GN organisms was initially assessed and compared to standard NB by generating optical density growth curves. STF formulations or NB aliquots in flat-bottomed 96 well plates were inoculated with *E. coli* NCTC 10418 to a final concentration of $5 \pm 3 \times 10^5$ CFU mL⁻¹, in triplicate. Plates were incubated in a Tecan Infinite 200 PRO plate reader at 35 °C and absorbance at 595 nm was measured every 20 min preceded by 20 s orbital shaking at 6 mm amplitude for 60 h.

8.2.1.2.3 Formulation refinement to mimic physiological pH

Based on the findings in 8.2.1.2.2 one STF formulation was selected for further refinement. Since all test STF formulations were found to exhibit more alkaline pH in normal air than that reported for human tears *in situ*, alteration of the bicarbonate concentration and modification of the included phosphate were initially investigated as a means to replicate physiological pH. Nine variations of the selected novel STF were investigated: all permutations of 100, 50 or 0 % optimised HCO₃⁻ concentration combined with the optimised phosphate concentration as PO₄³⁻, HPO₄²⁻ or H₂PO₄⁻. The STF variations were prepared in 1 mL aliquots in duplicate and left to equilibrate for 24 h in normal air at room temperature before measuring the pH.

The effects of incubation of the original selected STF formulation in 5 % CO₂ on pH were also investigated. After the 24 h normal air pH measurement was performed, the tubes were loosely covered and incubated at 37 °C in 5 % CO₂ for 48 h. To check for drift, the pH was measured after 6, 24 and 48 h of incubation. After removal from the incubator, both tubes were sealed, and the pH was measured again after cooling to room temperature for 6 h. One tube was left loosely covered for exposure to normal air while the other was resealed, and pH measured a final time after equilibration at room temperature for 18 h. A final novel STF formulation which reached physiological pH during incubation in 5 % CO₂ was selected for use.

8.2.2 Optimisation of an antimicrobial assay in novel simulated tear fluid

Growth of *E. coli* NCTC 10418 in the novel STF over 24 hours was compared to that in a range of dilute concentrations of NB in order to select an appropriate bacteriological medium comparator. A flat-bottomed 96 well plate was prepared with 90 µL aliquots of STF, standard NB, NB diluted to 50 % standard concentration (50 % NB), 20 % NB, 10 % NB and 5 % NB and equilibrated overnight in 5 % CO₂ at 37 °C. Aliquots were inoculated with approximately 2 x 10⁶ CFU mL⁻¹ bacteria grown on NA and returned to the CO₂ incubator for 24 h. After incubation, bacteria were enumerated using the Miles & Misra drop count method^[280] and the NB dilution supporting most similar growth to the novel STF selected as a comparator.

Growth curves of *E. coli* NCTC 10418, *K. pneumoniae* NCTC 9633 and *P. aeruginosa* NCTC 13359 were performed in novel STF and the selected comparator. Aliquots of 90 µL were again equilibrated overnight in 5 % CO₂ at 37 °C in duplicate before inoculation with approximately 5 x 10⁵ CFU mL⁻¹ bacteria grown on NA. Drop counts were performed immediately after inoculation and after 4, 8, 12, 16, 20, 24 and 28 h incubation in 5 % CO₂ at 37 °C. The log₁₀ CFU mL⁻¹ increase since inoculation was calculated for each timepoint, plotted against incubation time and used to select duration of bacterial acclimatisation and treatment for the antimicrobial activity assay.

8.2.3 Antimicrobial activity of sodium fusidate in novel simulated tear fluid, with and without metal ions

Aliquots of the novel STF were transferred to flat-bottomed 96 wells plates, 90 µL per well, and incubated for 12-18 h at 37 °C and 5 % CO₂ to equilibrate before use. 50 % NB

was used as a comparator. *E. coli* NCTC 10418, *K. pneumoniae* NCTC 9633 and *P. aeruginosa* NCTC 13359 were grown overnight on NA at 37 °C. Bacteria were suspended in HPLC grade water and the OD adjusted. Equilibrated STF and 50 % NB was inoculated to a final concentration of $5 \pm 3 \times 10^5$ CFU mL⁻¹ by adding 10 µL bacterial suspension. Mixing on addition was avoided in order to prevent disturbing the stratified STF structure and to ensure bacteria were presented with a similar gradient to that encountered when initiating an ocular infection. Initial concentration of bacteria was confirmed by adding 10 µL sterile HPLC grade water (the same volume of treatments to be later added to other wells), thoroughly mixing and performing a CFU count per the Miles & Misra method^[280] from wells dedicated for this purpose. Inoculated plates were incubated at 37 °C and 5 % CO₂ for 4 h to allow for acclimatisation to the new growth medium and establishment of actively growing bacterial populations.

Treatment with metal sulphates, FNa and combinations was initiated by adding a total of 10 µL to each well, comprising either 5 µL metal + 5 µL FNa, 5 µL metal + 5 µL water, 5 µL FNa + 5 µL water or 10 µL water for untreated controls, without mixing. All metal ions were added to a final concentration of 625 µM and the final FNa concentration was 80 µM. These concentrations were chosen for their combination of relatively low toxicity (see Chapter 7), considerable anti-GN activity determined previously in NB (see Chapter 6) and, for FNa, similarity to trough concentrations in the tears and cornea during standard 12-hourly treatment with 1 % FA viscous eyedrops (see Discussion, Section 8.4.2). Bacterial populations at the start of treatment were measured by CFU counting from additional dedicated wells diluted with 10 µL water. Plates were returned to 37 °C and 5 % CO₂ for a further 4 h. A 4 h exposure period was selected to ensure there would be a measurable difference between bacterial populations in wells of actively growing, uninhibited organisms and those that were inhibited or killed by the treatment, while avoiding the potential skewing effects of reaching stationary phase. Viable CFU in all treated and untreated control wells were quantified at the end of the exposure period by the Miles & Misra method^[280].

All combinations of growth medium, organism and treatment were carried out in triplicate. CFU counts were used to calculate log₁₀ change in bacterial numbers during the 4 h treatment period and the 95 % CIs compared to determine statistically significant differences ($p \leq 0.05$).

8.2.4 Solubility of sodium fusidate in novel simulated tear fluid, with and without metal ions

8.2.4.1 Sodium fusidate solubility in novel STF

Solubility of both 80 μM and 1280 μM FNa with and without 625 μM Al^{3+} , Cu^{2+} and Fe^{2+} as sulphate was determined in the novel STF and 50 % NB using a similar method to that described in Section 2.7. It was previously established that the solubility of 1280 μM FNa correlated well with bacteriostatic activity in NB (Section 5.3.3, page 127). However, the solubility of 80 μM – the concentration used in antimicrobial investigations in STF – was also investigated in the event the 1280 μM solubility : activity relationship did not follow the same pattern in this novel growth medium.

Aliquots of 900 μL STF and 50 % NB were equilibrated in loosely covered 2 mL centrifuge tubes for 12-18 h at 37 °C and 5 % CO_2 in triplicate. In order to mimic the conditions and time-course of the antimicrobial assay, 100 μL sterile HPLC grade water (in place of bacterial suspension) was added to each tube and incubation continued for 4 h. FNa and metal sulphate stock solutions were added to the test media to a total of 100 μL , comprising either 50 μL metal + 50 μL FNa or 50 μL FNa + 50 μL water and the tubes returned to 37 °C and 5 % CO_2 for 4 h equilibration.

After equilibration, tubes were removed from the incubator and immediately sealed to prevent loss of CO_2 from solution and any resulting pH change. Tubes were then centrifuged for 20 min at 37 °C in a pre-warmed Heraeus Fresco 17 (Thermo Scientific) at 17,000 $\times g$ (13,300 rpm). Samples of 500 μL each supernatant were mixed with 500 μL ethanol in HPLC vials to prevent FNa precipitation before analysis.

Solubilised FNa concentration was quantified using HPLC separation method 1 (see Section 2.6.1) and converted to % solubility of the original concentration added. The mean and 95 % CI were used to identify statistically significant differences between FNa solubility in STF and 50 % NB with and without metal ions ($p \leq 0.05$).

8.2.4.2 pH of metal sulphates in novel STF

Since previous results illustrated that pH directly influences FNa solubility, the effect of metal sulphates on the pH of the novel STF and 50 % NB was also investigated. As for solubility testing, triplicate 900 μL aliquots were equilibrated for 12-18 h at 37 °C and 5 % CO_2 before the addition of 100 μL sterile HPLC grade water and continued incubation for 4 h. Metal sulphate stock solution \times 100 μL was added to STF or 50 %NB to a final metal ion concentration of 625 μM , and 100 μL water added to the control tubes. After

equilibration at 37 °C and 5 % CO₂ for a further 4 h, tubes were sealed to prevent CO₂ loss and only re-opened immediately prior to pH measurement.

8.3 Results

8.3.1 Development of a novel simulated tear fluid formulation for bacterial studies

8.3.1.1 Collation of published data

8.3.1.1.1 Components and concentrations in published STF formulations

STF formulations described in the literature have been employed for a variety of applications including drug release, contact lens spoilage, corneal epithelial maintenance and microbial growth. Several authors used formulations previously published. The most widely used STF was found to be sodium chloride 0.67 g, sodium bicarbonate 0.2 g and calcium chloride dihydrate 0.008 g per 100 g water, originally reported by Rozier *et al* (1989)^[498]. Only the earliest report of each formulation was included in the analysis; these publications are listed in Table 8.1.

Table 8.1 - Published simulated tear fluid formulations included in the analysis

Publication	Context
Bachman & Wilson (1985) ^[514]	STF for optimal corneal epithelial surface maintenance
Rozier <i>et al</i> (1989) ^[498]	STF for sol-gel drug release assay
Mirejovsky <i>et al</i> (1991) ^[515]	STF for protein deposition on contact lenses
Cowell <i>et al</i> (1997) ^[516]	STF to study <i>in vitro</i> bacterial adhesion to contact lenses
Prager & Quintana (1997) ^[502]	STF for lipid deposition on contact lenses
Rebeix <i>et al</i> (2000) ^[496]	STF for component adsorption on/spoilage of contact lenses
Aristoteli & Wilcox (2003) ^[497]	STF to study mucin degradation by <i>P. aeruginosa</i>
Hagigit <i>et al</i> (2008) ^[495]	STF for nano-emulsion drug release assays
Lorentz <i>et al</i> (2011) ^[503]	STF for lipid deposition & stability testing of contact lenses
Ng <i>et al</i> (2013) ^[517]	STF for lysozyme deposition on contact lenses
Lee <i>et al</i> (2017) ^[518]	STF for protein deposition on contact lenses

Table 8.2 - Concentrations of electrolytes, metabolites and proteins employed in published simulated tear fluid formulations

Component	units	Deposition on contact lenses						Drug release		Bacterial behaviour		Corneal culture	Mean used	Range used
		Mirejovsky <i>et al</i> (1991) ^[515]	Prager & Quintana (1997) ^[502]	Rebeix <i>et al</i> (2000) ^[496]	Lorentz <i>et al</i> (2011) ^[503]	Ng <i>et al</i> (2013) ^[517]	Lee <i>et al</i> (2017) ^[518]	Rozier <i>et al</i> (1989) ^[498]	Hagigit <i>et al</i> (2008) ^[495]	Cowell <i>et al</i> (1997) ^[516]	Aristoteli & Wilcox (2003) ^[497]	Bachman & Wilson (1985) ^[514]		
Na ⁺	mM	130.6	144.6	147.4	166.5	143.1	165.2	138.5	138.0	145.0	150.0	143.6	146.6	130.6 - 166.5
K ⁺	mM	23.02	5.4	4.51	19.0	18.96	1.91	-	14.89	20.0	3.2	18.78	12.97	1.91 - 23.02
Ca ²⁺	mM	1.0	1.0	0.06	0.5	0.63	0.09	0.54	0.21	0.7	-	0.58	0.53	0.06 - 1.0
Mg ²⁺	mM	-	0.9	0.04	-	-	-	-	-	0.44	-	1.27	0.66	0.04 - 1.27
Cl ⁻	mM	138.4	148.0	142.8	133.0	133.0	149.2	155.7	130.4	176.5	139.7	138.8	140.5	130.4 - 176.5
CO ₃ ²⁻	mM	-	-	-	12.0	11.98	-	-	-	-	-	-	14.85	11.98 - 20.57
HCO ₃ ⁻	mM	16.38	4.0	0.21	3.0	3.0	-	23.81	22.9	-	-	25.95	12.41	0.21 - 25.95
HPO ₄ ²⁻	mM	-	0.30	5.14	24.0	24.02	8.09	-	-	-	6.5	-	11.34	0.3 - 24.02
H ₂ PO ₄ ⁻	mM	0.72	0.40	1.70	-	-	1.91	-	-	-	1.5	0.78	1.17	0.40 - 1.91
SO ₄ ²⁻	mM	-	0.4	0.02	-	-	-	-	-	0.44	-	-	0.29	0.02 - 0.44
NH ₄ ⁺	mM	-	-	-	-	-	-	-	-	10.0	-	-	10.0	n/a [†]
citrate	mM	-	-	-	1.50	1.71	-	-	-	-	-	-	1.61	1.50 - 1.71
lactate	mg L ⁻¹	270	-	-	-	-	-	-	-	-	-	-	270.0	n/a [†]
urea	mg L ⁻¹	-	-	-	72.07	72.0	-	-	-	-	-	-	72.04	72.0 – 72.07
glucose	mg L ⁻¹	-	1000	50.0	36.03	36.0	-	-	25.0	751.3*	-	-	316.4	25 - 1000
albumin	mg L ⁻¹	200	200	200	200	200	540	-	6690	-	-	-	1175.7	200 - 6690
lysozyme	mg L ⁻¹	1900	1900	2000	1900	1900	1300	-	-	2000*	-	-	1842.9	1300 - 2000
lactoferrin	mg L ⁻¹	1800	1800	1000	1800	1800	-	-	-	2000*	-	-	1700.0	1000 - 1800
α-acid glycoproteins	mg L ⁻¹	500	500	500	-	-	-	-	-	-	-	-	500.0	n/a [†]
immunoglobulins	mg L ⁻¹	100	100	300	20	20	-	-	-	100*	-	-	106.7	20 - 300
mucin	mg L ⁻¹	150	150	1000	150	150	1800	-	-	-	10,000	-	1914.3	150 - 10000

*each carbon source was used alone

†no variability between publications in concentrations employed

- = not present.

A further STF formulation was also identified which was used to investigate *P. aeruginosa* biofilm formation on contact lenses. However, the authors employed a mixture of 20 % v/v human serum and 2 g L⁻¹ lysozyme diluted in a commercial ocular irrigation solution^[519]. This prevented accurate quantification of individual electrolyte, metabolite and protein concentrations due to inter-patient variation in serum composition. This formulation was therefore omitted from the analysis.

Table 8.2 summarises the total concentration of each electrolyte, metabolite and protein incorporated into each published STF formulation, standardised to the same units, with the mean and range across all formulations. Mirejovsky *et al* (1991)^[515] also included MOPS as an additional buffer in their formulation. Of particular interest was the formulation developed by Bachman & Wilson (1985)^[514] which was derived from an investigation into the particular components required to maintain viability of the epithelial surface of *ex vivo* rabbit corneas. Their STF formula included only the electrolytes Na⁺, K⁺, Ca²⁺, Mg²⁺, Cl⁻, H₂PO₄⁻ and HCO₃⁻ at optimised concentrations. In addition, the work of Cowell *et al* (1997)^[516] showed that lysozyme, lactoferrin or IgA could be the sole carbon source for *P. aeruginosa*, *E. coli*, and two species of *Serratia* (formerly *Stenotrophomonas*), while Aristoteli & Wilcox (2003)^[497] demonstrated that *P. aeruginosa* could also utilise mucin as the sole source of both carbon and nitrogen.

8.3.1.1.2 Measurements from human tears

The mean and range of concentrations of electrolytes, metabolites and proteins in both basal (non-stimulated) and induced (stimulated) human tears reported in the literature are listed in Table 8.3 and Table 8.4. Measurements made in patients with diabetes, liver cirrhosis and other conditions were also found but only values from the healthy controls for these studies were included.

The concentration of Na⁺ ^{[520],[521]} and urea^[521] in human tear fluid has been determined to be equal to that in plasma regardless of tear secretion rate, indicating passive diffusion of these components. However, concentrations of K⁺, Ca²⁺, Mg²⁺ and Cl⁻ in tears are independent of secretion rate. K⁺ ^[520] and Cl⁻ ^[521] are both actively exported into the tear fluid, resulting in concentrations higher than those in plasma. Conversely, Ca²⁺ and Mg²⁺ are found at lower concentrations in the tears than in plasma^[520], indicating limited export or diffusion. Measured electrolyte and metabolite concentrations generally agreed well with the mean used in published STFs, particularly considering intra-patient variabilities reported. However, exceptions included citrate, urea, glucose and pyruvate. Where used in published STFs, citrate was at a mean concentration of 1.61 mM^{[503],[517]} (Table 8.2, page 213) but only 0.03 mM^[522] was found in human tears. Conversely, the range of

human tear concentrations of urea of 204.2 to 1385 mg L⁻¹ [521],[523] was considerably higher than the mean 72.04 mg L⁻¹ [503],[517] employed in published STFs. Glucose tear measurements ranged from 45 to 270.2 mg L⁻¹ [523]–[525] while published STF concentrations varied from 25 to 1000 mg L⁻¹ [495],[496],[502],[503],[516],[517] with a mean of 316.4 mg L⁻¹. Pyruvate was not included in any of the published STF formulations; however, it is present in basal tears at 4.4 - 30.8 mg L⁻¹ [523] and is an essential, immediate precursor to acetyl-CoA, utilised in bacterial synthesis of ATP^[161]. No human tear concentrations of CO₃²⁻, HPO₄²⁻, H₂PO₄⁻, SO₄²⁻ or NH₄⁺, or electrolytes or metabolites in infected eyes, were found in the literature.

Table 8.3 - Concentrations of electrolytes and metabolites measured in human tears

Electrolytes and metabolites	Healthy subjects, non-stimulated (mM)		Healthy subjects, stimulated (mM)	
	mean	range	mean	range
Na ⁺	122.9 ^[526]	n/a	144.0 ^{[521],[527]}	142 - 146 ^{[521],[522],[527]}
K ⁺	15.5 ^[528]	n/a	22.0 ^{[521],[527]}	14.9 - 29.0 ^{[521],[522],[527]}
Ca ²⁺	0.64 ^{[529],[530]}	0.33 - 2.40 ^{[529]–[531]}	-	-
Mg ²⁺	0.82 ^[530]	0.3 - 1.1 ^[520]	-	-
Cl ⁻	120 ^[532]	n/a	131.5 ^{[521],[527]}	128 - 135 ^{[521],[527]}
HCO ₃ ⁻	26 ^{[520],[522]}	n/a	-	-
citrate	0.03 ^[522]	n/a	-	-
lactate (mg L ⁻¹)	-	81.1 - 486.4 ^[523]	-	-
urea (mg L ⁻¹)	-	204.2 - 450.5 ^[523]	-	328 - 1385 ^[521]
glucose (mg L ⁻¹)	74.5 ^{[524],[525]}	45.0 - 90.1 ^[523]	-	90.1 - 270.2 ^[523]
pyruvate (mg L ⁻¹)	-	4.4 - 30.8 ^[523]	-	-

- = not found, n/a = not applicable as only one reported value identified

Three papers reported protein concentrations in infected eyes (Table 8.4). Lal *et al* (1991)^[507] compared lysozyme in the tears of patients with bacterial, viral or fungal corneal ulcers, determining that the lowest level of lysozyme was present with bacterial infection at 1700 mg L⁻¹. This value was consistent with that published by Saari *et al* (1983)^[533] who found 1770 mg L⁻¹ lysozyme in the tears of patients with keratitis and similar to the mean concentration of 1842.9 mg L⁻¹ employed in STFs (Table 8.2). Sen & Sarin (1979)^[534] determined that immunoglobulin tear concentration was decreased in cases of bacterial corneal ulcers compared to healthy controls with 204 and 260 to 288 mg L⁻¹ found, respectively (whereas concentration increased with bacterial conjunctivitis). However, Fullard & Snyder (1990)^[535] measured only 1.5 to 12.2 mg L⁻¹ immunoglobulin in non-stimulated tears and 0 to 94.8 mg L⁻¹ in stimulated tears, both considerably less than Sen & Sarin's controls. Therefore, any of the employed range of 20 to 300 mg L⁻¹ immunoglobulin in STF formulations could be considered reasonable.

Table 8.4 – Concentrations of proteins measured in human tears

Proteins	Healthy subjects, non-stimulated (mg L ⁻¹)		Healthy subjects, stimulated (mg L ⁻¹)		Ocular infections and comparators (mg L ⁻¹ : condition details)
	mean	range	mean	range	
albumin /pre-albumin	585.8 [524],[535]	38.0 – 1677.4 [524],[535]	732.6 [524],[535],[536] 36]	12.2 - 1830 [524],[535],[536]	-
lysozyme	1486.8 [524],[535],[537],[538]	650 – 3297 [524],[535],[537],[538]	2580.3 [507],[524],[535]-35]-[537],[539]	1500 – 5140 [507],[524],[535]-[537],[539]	1700: bacterial corneal ulcer ^[507] 1770: all cause keratitis ^[533] 2850: viral corneal ulcer ^[507] 3020: fungal corneal ulcer ^[507]
lactoferrin	1990.5 [524],[535],[537]	1370 – 2860 [524],[535],[537]	3071.5 [524],[535]-[537]	1587.5 – 4000 [524],[535]-[537]	-
other transferrins	0.99 ^[535]	n/a	0.50 ^[535]	n/a	-
immuno-globulins	-	1.5 - 12.2 ^[535]	-	0 - 94.8 ^[535]	204: bacterial corneal ulcer ^[534] 260 - 288: infection-free controls ^[534] 339: bacterial conjunctivitis ^[534]

- = not found, n/a = not applicable as only one reported value identified

Concentrations of α -acid glycoproteins and mucin in human tears were not identified from the literature. However, albumin or tear-specific pre-albumin concentrations have been determined as ranging between 12.2 and 1830 mg L⁻¹, with means of 585.8 and 732.6 mg L⁻¹ in non-stimulated and stimulated tears, respectively^{[524],[535],[536]}. While the mean albumin concentration incorporated in STFs was 1175.7 mg L⁻¹, it was only 200 mg L⁻¹ in five of the seven formulations in which it was employed^{[496],[502],[503],[515],[517]}. Another formulation closely reflected the mean non-stimulated tear concentration of albumin at 540 mg L⁻¹ ^[518], while the last was higher than any measured value at 6690 mg L⁻¹ ^[495]. Conversely, at 1000 to 1800 mg L⁻¹, lactoferrin concentrations in STF formulations were not overly dissimilar to the 1990.5 mg L⁻¹ mean of measurements in non-stimulated tears^{[524],[535],[537]}. Finally, other transferrins were not included in any published STF but are present in non-stimulated and stimulated human tears at 0.99 and 0.50 mg L⁻¹, respectively^[535].

8.3.1.1.3 The pH of published STFs and human tears

Where reported, the pH of reported STF formulations are listed in Table 8.5. Three of the 11 authors failed to disclose the pH of their STF formulation. Published STF pHs were between 7.4 and 7.5, however, Prager & Quintana (1997)^[502] reported only the pH of the salt solution prior to the addition of proteins and lipids and Rebeix *et al* (2000)^[496] stated only that pH 7.4 was “maintained” without further explanatory details. Four of the

formulations were adjusted manually after preparation using HCl or NaOH^{[495],[515],[516],[518]}. Bachman & Wilson (1985)^[514] purged the prepared STF with 5 % CO₂ to achieve pH 7.5, whereas Lorentz *et al* (2011)^[503] found that equilibration of their STF at room temperature for at least 3 days resulted in a pH of 7.4 which was stable for 4 weeks.

Table 8.5 - Reported pH of eight simulated tear fluid formulations

Publication	pH	Notes on pH adjustment
Bachman & Wilson (1985) ^[514]	7.5	adjusted by bubbling with 95 % air, 5 % CO ₂
Mirejovsky <i>et al</i> (1991) ^[515]	7.4	adjusted after preparation
Cowell <i>et al</i> (1997) ^[516]	7.4	adjusted after preparation
Prager & Quintana (1997) ^[502]	7.4	initial pH of Hank's buffered salts solution before protein & lipid addition
Rebeix <i>et al</i> (2000) ^[496]	7.4	listed as "maintained"
Hagigit <i>et al</i> (2008) ^[495]	7.4	adjusted after preparation
Lorentz <i>et al</i> (2011) ^[503]	7.15	initial pH after mixing of salt base solution
	7.35	pH of complete STF immediately after preparation
	7.4	pH after equilibration at room temp for 3+ days
	7.49	max pH of complete STF up to 28 days after incubation
Lee <i>et al</i> (2017) ^[518]	7.4	adjusted after preparation

Interestingly, the pH of human tear film is more variable than the consistency between published STF formulations would suggest. Figure 8.2 summarises the reported pH of the human tear film at two different locations on the ocular surface and various times after opening the lid, along with that of collected tears. While the pH of collected tears stored with a minimal volume of air was found to range from 7.14 to 7.82^{[540],[541]}, the *in vivo* human tear film was between pH 6.5^[542] and 9.3^[543]. The lowest readings were from the inferior fornix, the fold behind the lower eyelid. Abelson *et al* (1981)^[542] originally found a range of pH 6.5 to 7.6 in the inferior fornix. Coles & Jaros (1984)^[544] later determined that in the open eye, the inferior fornix tear film pH was 7.19±0.16 whereas this decreased to 7.06±0.16 when measured immediately after the eye lid had been kept closed for 1 h. However, Fischer & Wiederholt (1982)^[543] found a mean pH of 7.5 in the precorneal tear film within 2 to 4 s of opening the eye, and a maximum of pH 9.3 after 30 to 60 s. Similarly, Chen & Maurice (1990)^[545] measured a precorneal tear film pH of 7.83±0.33 1 min after opening the eye.

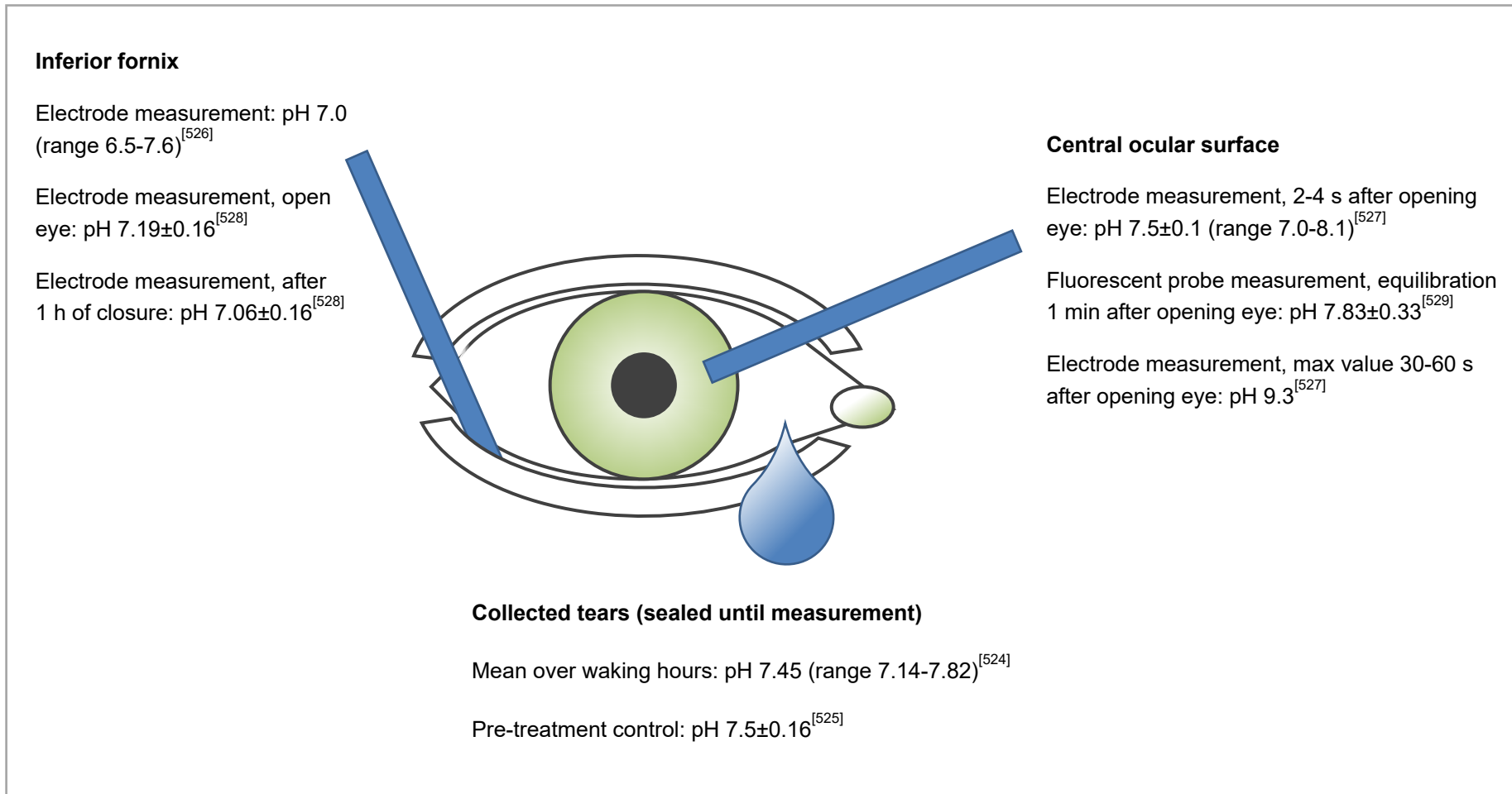


Figure 8.2 – The *in vivo* pH of human tear fluid and its variation in response to air exposure

8.3.1.2 Rational design of a novel simulated tear fluid

8.3.1.2.1 Novel STF formulation and initial evaluation

Lipid and lipid-soluble components (Appendix F) were not considered for inclusion since the focus was to develop an STF physiologically representative of the human mucocaqueous pool. Immunoglobulins, α -acid glycoprotein and transferrins were also omitted due to their potential to interfere with antimicrobial activity (see Section 8.4.1). Finally, ammonium was not considered for inclusion since its use in the single STF formulation was to ensure a nitrogen source^[516].

A base salt solution was rationally designed to reflect the electrolyte values recorded in tears. Metabolites lactate, pyruvate and urea along with BSA were also added to the base solution. Since their inclusion or concentration may impact bacterial growth, the effects of the presence or absence of mucin and lysozyme and the concentration of glucose was investigated. Table 8.6 lists the rationale for the individual component concentrations tested.

Table 8.6 - Rationalised concentrations of novel STF components

Component	Concentration (mM)	Rationale
Na ⁺	142.75	Mean of stimulated tear concentrations and published STF formulations; similar to optimal concentration for corneal epithelium maintenance
K ⁺	19.31	Mean of all reported tear concentrations; similar to optimal concentration for corneal epithelium maintenance
Ca ²⁺	0.60	Mean of reported tear concentrations and optimal concentration for corneal epithelium maintenance
Mg ²⁺	0.94	Mean of reported tear concentrations and optimal concentration for corneal epithelium maintenance
Cl ⁻	134.32	Mean of all reported tear concentrations; similar to optimal concentration for corneal epithelium maintenance
HCO ₃ ⁻	25.95	Optimal concentration for corneal epithelium maintenance
H ₂ PO ₄ ⁻	0.78	Optimal concentration for corneal epithelium maintenance
citrate	0.03	Concentration recorded in tears
lactate (mg L ⁻¹)	270.0	As used in one STF formulation and within measured concentration range
pyruvate (mg L ⁻¹)	17.60	Approximate median of reported tear concentration range
urea (mg L ⁻¹)	250.0	Approximate median of reported tear concentration range
BSA (mg L ⁻¹)	735.0	Based on mean of reported concentration in stimulated tears
glucose (mg L ⁻¹)	90.0 or 1000	90 mg L ⁻¹ = minimum concentration in stimulated tears; 1000 mg L ⁻¹ = ¼ carbon source concentration utilised in minimal bacteriological media such as M9 ^[546]
lysozyme (mg L ⁻¹)	1700.0	Reported value from eyes with bacterial corneal ulcer
mucin (mg L ⁻¹)	1500.0	No reported tear concentration; between values used in STFs

During growth curve set-up, it was observed that mixing wells containing both lysozyme and mucin on addition of *E. coli* resulted in alteration of the solution opacity. Therefore, all bacteria-free control wells were similarly mixed on addition of the same volume of sterile water and immediately after the corresponding inoculated well. This apparent interaction between lysozyme and mucin limited the accuracy of growth curve results based on optical density since opacity in all wells (including bacteria-free controls) fluctuated over time. Figure 8.3 illustrates the mean absorbance of bacteria-free control STF formulations over time. *E. coli* growth data (Figure 8.4) was therefore baseline corrected against the lowest OD observed in the corresponding bacteria-free control well to account for this equilibration.

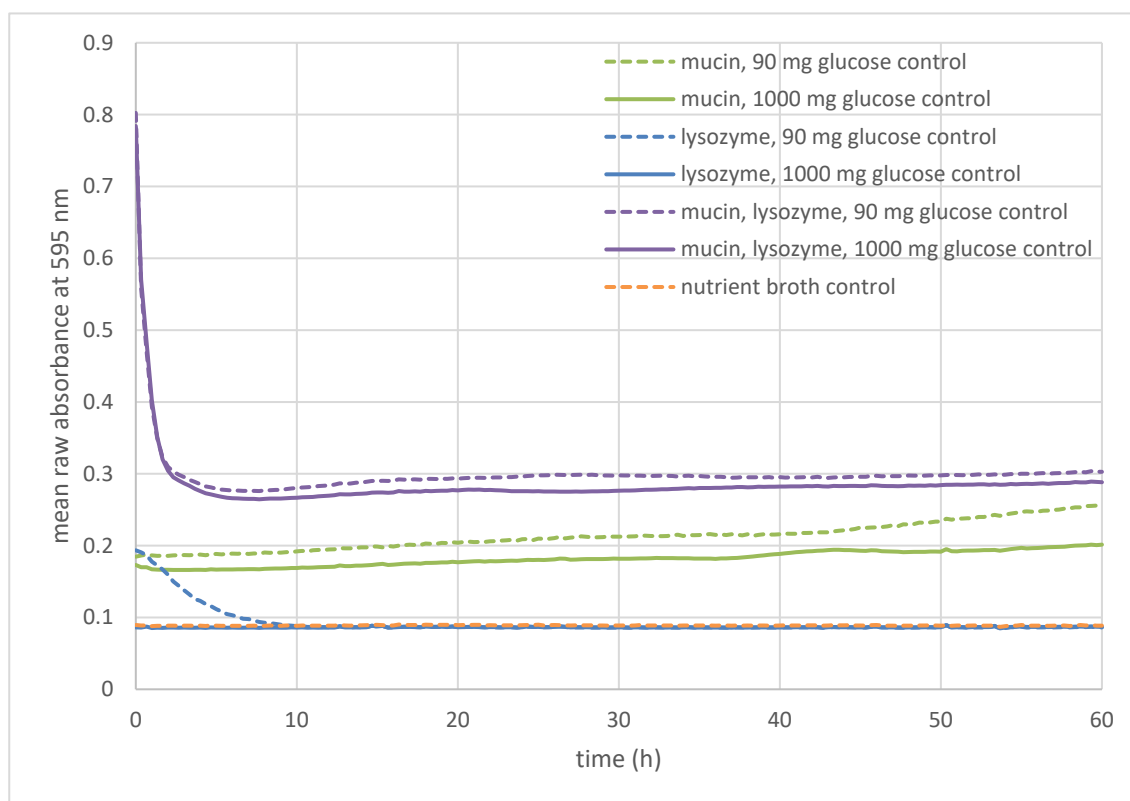


Figure 8.3 - Mean absorbance of STF formulations and nutrient broth at 595 nm over 60 h incubation at 35 °C (n=3)

Figure 8.4 illustrates *E. coli* NCTC 10418 growth curves in the STF formulations and NB comparator. While not as rapid or achieving the same density as in NB, all STF formulations were able to support *E. coli* growth, with cell numbers reaching levels detectable by the plate reader within 6 h. However, the growth curves were unusually shaped, and absorbance was found to decrease after the initial growth phase. *E. coli* OD peaked after 12-13 h in STF containing 1000 mg L⁻¹ glucose, followed by a steep decline up to 16-18 h. Growth in STF formulations with 90 mg L⁻¹ glucose was apparently slower

and steadier than in the 1000 mg L⁻¹-containing counterparts, peaking between 20 and 24 h. There was reduction in absorbance between 30 and 60 h in all formulations, however, this was least pronounced with both mucin and lysozyme combined with 90 mg L⁻¹ glucose. The formulation containing mucin, lysozyme and 90 mg L⁻¹ glucose was therefore selected for further investigation as it most closely resembled reported tear composition and supported detectable bacterial growth.

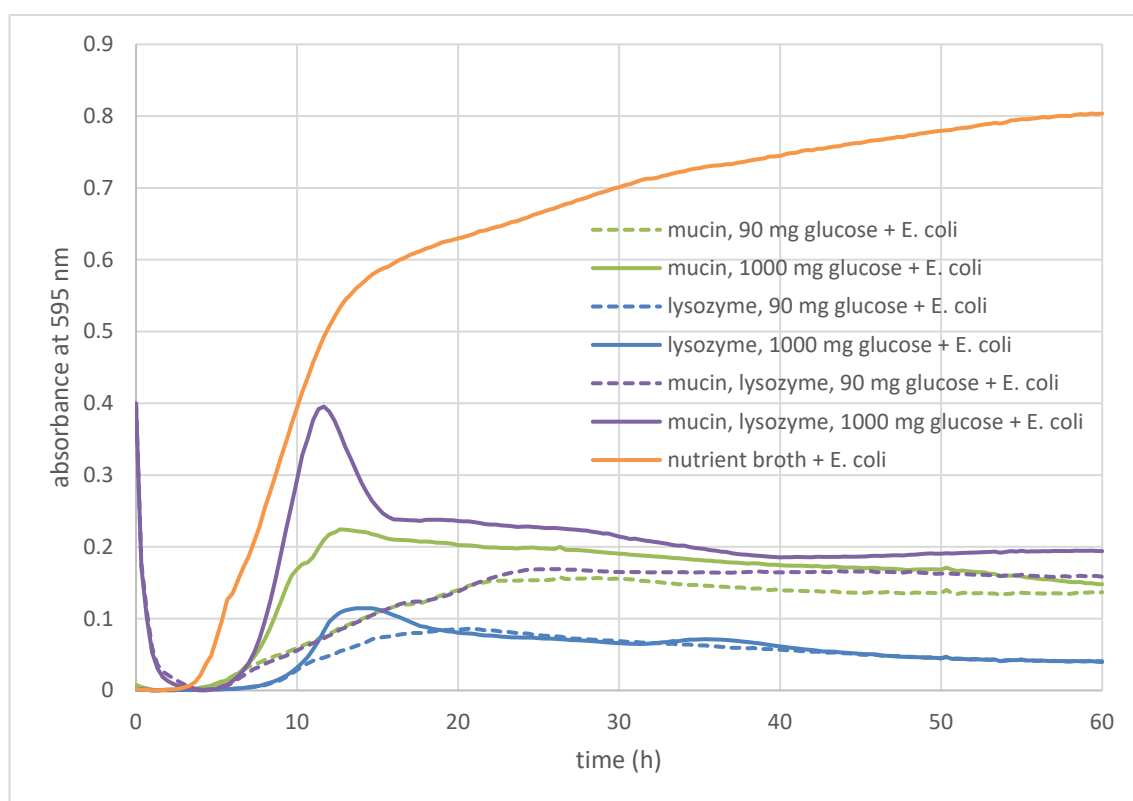


Figure 8.4 - Growth of *E. coli* NCTC 10418 in STF formulations and nutrient broth as determined by absorbance at 595 nm over 60 h incubation at 35 °C (n=3)

8.3.1.2.2 Novel STF pH issues and resolution

The pH of the novel STF formulation in normal air was 8.6. Two options for pH correction to approximate physiological conditions were investigated: 1) alteration of bicarbonate concentration combined with phosphates of different protonation states, and 2) incubation in 5 % CO₂. Table 8.7 lists the measured pH of STF formulations incorporating varying HCO₃⁻ concentrations and phosphates. Even with half the original concentration, the buffering effect of HCO₃⁻ could not be overcome by changing the phosphate anion (while using the concentration of phosphates found in tears). With complete omission of HCO₃⁻ and use of PO₄³⁻, the STF pH after 24 h at room temperature in normal air was

very similar to human tear pH at 7.58. However, inclusion of HCO_3^- was deemed preferable in order to replicate actual tear composition as closely as possible.

Table 8.7 - Effect of bicarbonate concentration and phosphate protonation state on STF pH in normal air at room temperature

Bicarbonate concentration (% rationalised value)	Phosphate anion (0.78 mM)	pH after 24 h equilibration
25.95 mM (100 %)	PO_4^{3-}	8.88
25.95 mM (100 %)	HPO_4^{2-}	8.84
25.95 mM (100 %)	H_2PO_4^-	8.82
12.975 mM (50 %)	PO_4^{3-}	8.77
12.975 mM (50 %)	HPO_4^{2-}	8.72
12.975 mM (50 %)	H_2PO_4^-	8.68
0 mM (0 %)	PO_4^{3-}	7.58
0 mM (0 %)	HPO_4^{2-}	6.75
0 mM (0 %)	H_2PO_4^-	5.90

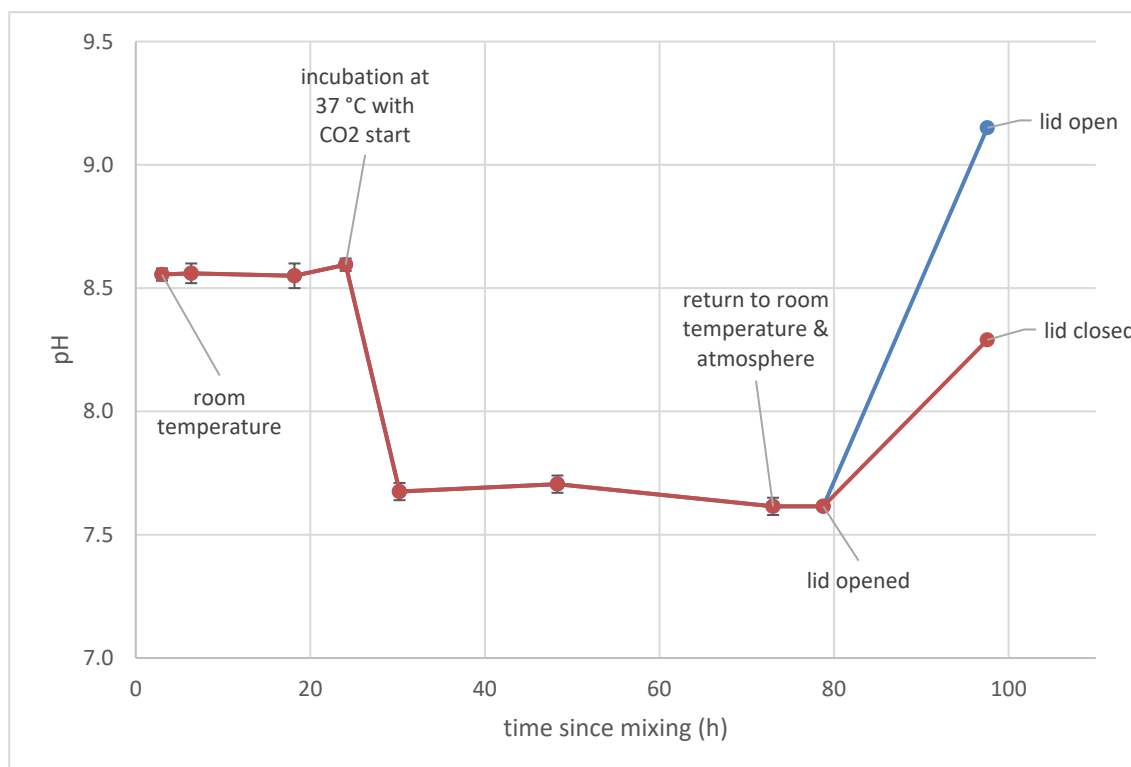


Figure 8.5 - Change in pH of novel STF before, during and after incubation at 37 °C with 5 % CO_2

Figure 8.5 illustrates the change in pH of 1 mL aliquots of the selected formulation without modification (containing 25.95 mM HCO_3^- and HPO_4^{2-}) on incubation in 5 % CO_2 . The pH substantially decreased from 8.6 to 7.6 during the incubation period, very similar to human tear pH. After removal from 5 % CO_2 , an increase in pH was observed in all samples. However, those allowed to equilibrate to normal air reached pH 9.15 compared

to 8.29 with the lid closed. In addition, during incubation at 37 °C in CO₂, the selected STF formulation developed mucin stratification similar to that reported for tear film structure *in vivo* (Figure 8.6).

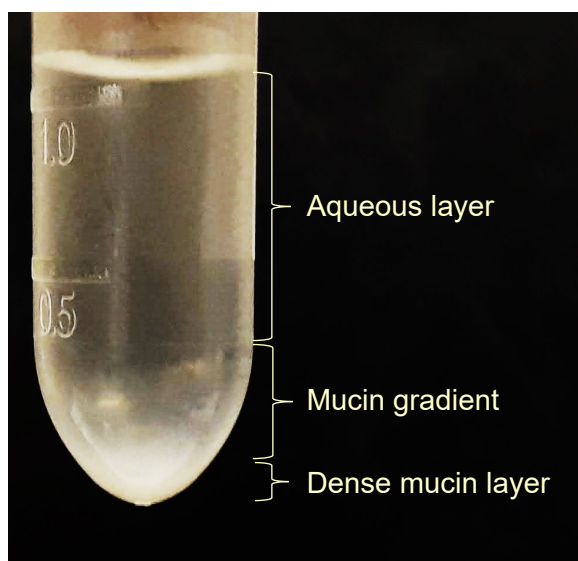


Figure 8.6 - Photograph of novel STF after overnight incubation at 37 °C and 5 % CO₂
Stratification of mucin in the optimised STF formulation after incubation after 18-24 h mimicked tear film structure (compare to Figure 8.1, page 206).

A combination of the STF containing mucin, lysozyme, 90 mg L⁻¹ glucose, 25.95 mM HCO₃⁻ and phosphate as HPO₄²⁻ along with incubation in 5 % CO₂ was, therefore, selected for further use. The composition of the optimised novel STF formulation is listed in Table 8.8.

Table 8.8 - Composition of optimised novel STF

Material	Concentration in STF
Sodium bicarbonate [#]	25.95 mM
Calcium chloride (dihydrate) [§]	0.596 mM
Magnesium chloride (hexahydrate) [§]	0.935 mM
Potassium phosphate monobasic [#]	0.775 mM
Potassium chloride [§]	18.54 mM
Sodium chloride [#]	113.20 mM
Sodium citrate tribasic (dihydrate) [#]	0.031 mM
Sodium DL-lactate [#]	270.0 mg L ⁻¹
Sodium pyruvate [#]	17.6 mg L ⁻¹
Urea [§]	250.0 mg L ⁻¹
D-glucose (anhydrous) [§]	90.0 mg L ⁻¹
BSA [§]	735.0 mg L ⁻¹
Lysozyme from hen's egg [#]	1700 mg L ⁻¹
Porcine stomach mucin [#]	1500 mg L ⁻¹

Suppliers: [#]Sigma Aldrich (Gillingham, UK), [§]Fisher Scientific (Loughborough, UK)

8.3.2 Optimisation of an antimicrobial assay in novel simulated tear fluid

After 24 h at 37 °C and 5 % CO₂, growth of *E. coli* in the novel STF was most similar to that in NB diluted to 50 % the standard concentration (Figure 8.7). The total CFU present in the novel STF was 3.4 x 10⁹ mL⁻¹ and in 50 % NB was 3.8 x 10⁹ mL⁻¹. Standard 100 % NB yielded 5.6 x 10⁹ CFU mL⁻¹, while in 20, 10 and 5 % NB *E. coli* grew to 2.2 x 10⁹, 2.3 x 10⁹ and 1.3 x 10⁹ CFU mL⁻¹, respectively. Therefore, 50 % NB was selected as an STF comparator.

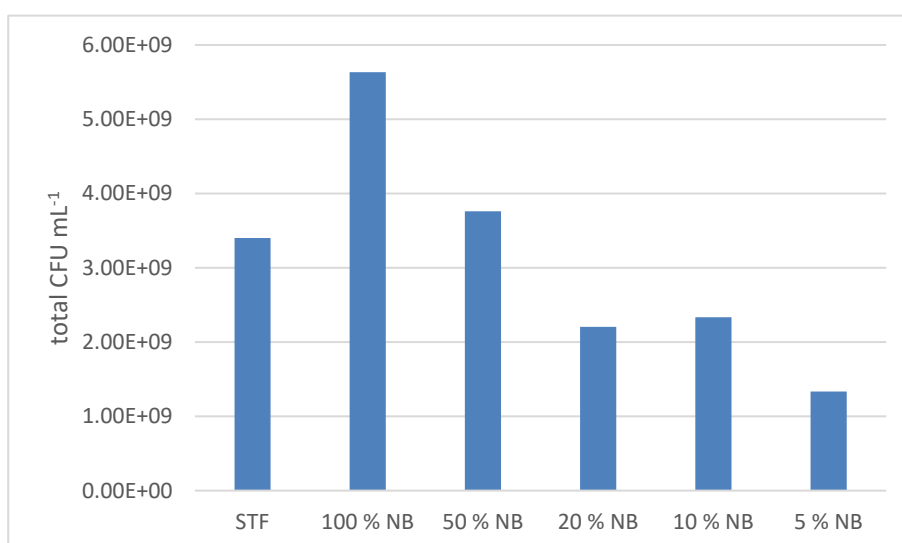


Figure 8.7 - Growth of *E. coli* NCTC 10418 after 24 h at 37 °C and 5 % CO₂ in novel STF compared to various dilutions of nutrient broth

E. coli and *K. pneumoniae* reached stationary phase in both novel STF and 50 % NB after approximately 8 h, while *P. aeruginosa* took 12 h (Figure 8.8). During the first 4 h, both *Enterobacteriaceae* populations increased by between 2.2 and 2.5 log₁₀ CFU mL⁻¹ in both media, and *P. aeruginosa* increased by 0.8 and 0.9 log₁₀ CFU mL⁻¹ in novel STF and in 50 % NB. However, between 4 and 8 h incubation, all species increased by 0.97±0.16 log₁₀ CFU mL⁻¹ in both media. Therefore, an initial acclimatisation phase of 4 h was selected, followed by an exposure period of a further 4 h.

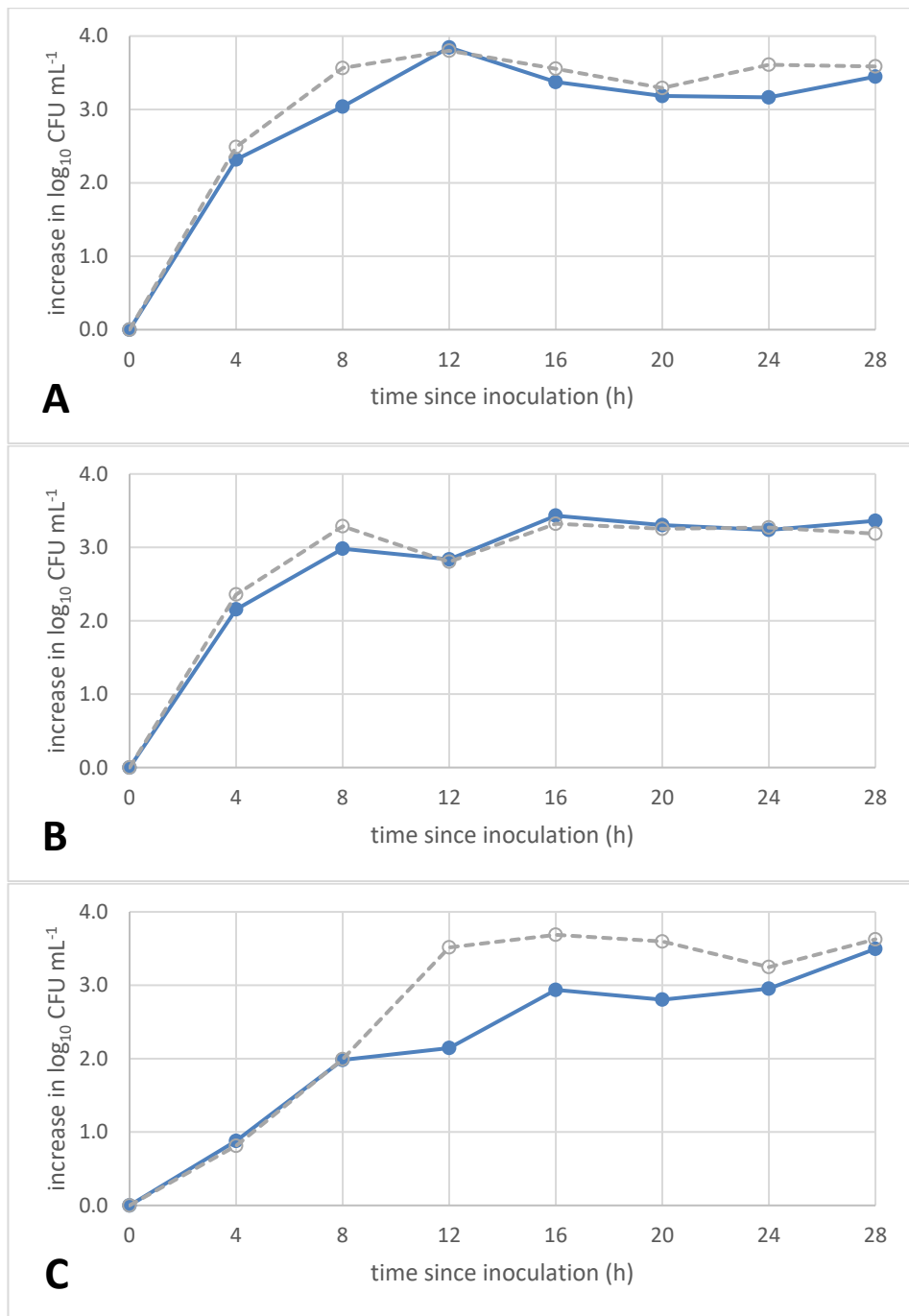


Figure 8.8 - Bacterial growth curves in novel STF and 50 % nutrient broth comparator over 28 h at 37 °C and 5 % CO₂

A: *E. coli* NCTC 10418, B: *K. pneumoniae* NCTC 9633, C: *P. aeruginosa* NCTC 13359

8.3.3 Antimicrobial activity of sodium fusidate and metal ion combinations in novel simulated tear fluid

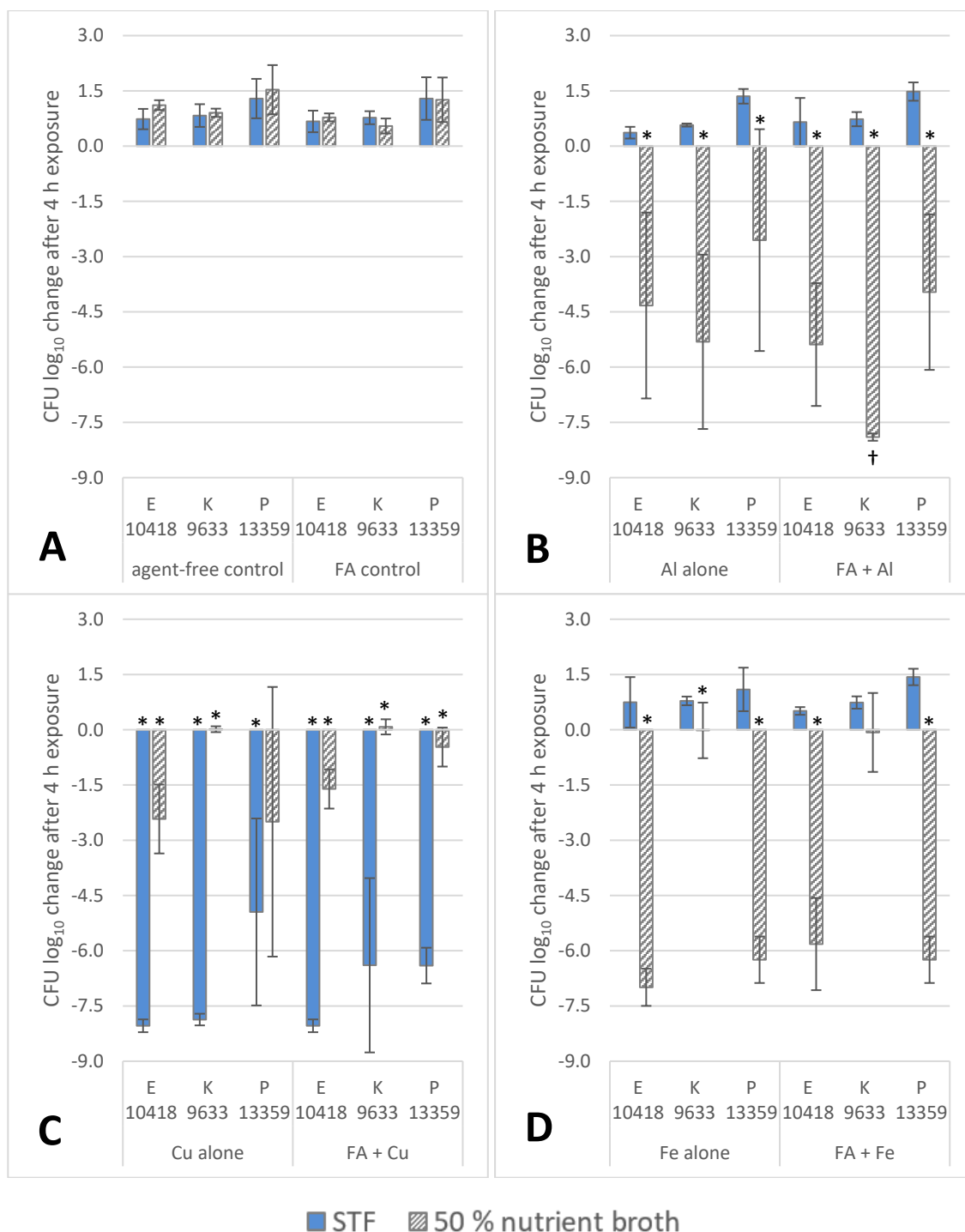


Figure 8.9 – Activity of sodium fusidate and metal sulphates against *E. coli*, *K. pneumoniae* and *P. aeruginosa* reference strains in novel STF and 50% nutrient broth

A: metal-free controls, B: 625 µM aluminium as sulphate, C: 625 µM copper(II) sulphate, D: 625 µM iron(II) sulphate.

Incubation conditions: 4 h at 37 °C and 5% CO₂. Sodium fusidate concentration: 80 µM. Positive values indicate bacterial growth during exposure period whereas negative values indicate bacterial death and a value of zero indicates bacteriostasis.

* = significant difference to metal-free control ($p \leq 0.05$);

† = significant difference to metal alone ($p \leq 0.05$).

(n = 3, error bars = 95% CI)

Without any antimicrobial agent, *E. coli*, *K. pneumoniae* and *P. aeruginosa* reference strains grew similarly in both the novel STF and 50 % NB over 4 h (Figure 8.9A). Total mean growth ranged from 0.73 to 1.59 log₁₀ CFU with *P. aeruginosa* exhibiting greater final numbers than *E. coli* and *K. pneumoniae*, however, there was no statistically significant difference between organisms or growth medium ($p > 0.05$). The presence of 80 µM FNa alone had little impact on bacterial growth in either medium: while mean growth of each organism was slightly reduced compared to the agent-free control, variation between replicates meant that there was no significant difference between any of the control conditions, with or without FNa ($p > 0.05$, Figure 8.9A).

For most metal and organism combinations, the ability of metal sulphates to inhibit bacterial growth over the 4 h exposure period differed greatly between the novel STF and 50 % NB. Al³⁺ killed all three species when 625 µM was added to 50 % NB ($p < 0.05$), however, the same concentration in STF resulted in no significant difference in growth compared to the agent-free controls ($p > 0.05$, Figure 8.9B). In a similar fashion, 625 µM Fe²⁺ had no net effect on growth of any organism in STF ($p > 0.05$) but produced ≥ 6 log₁₀ CFU reductions of both *E. coli* and *P. aeruginosa* in 50 % NB ($p < 0.05$, Figure 8.9D). Conversely, Cu²⁺ produced a significant and comprehensive reduction in bacterial numbers when added to STF ($p < 0.05$) but less dramatic reductions in 50 % NB (Figure 8.9C).

In only one case was there a statistically significant difference between log₁₀ CFU change caused by FNa with metal ions and metal ions alone. The log₁₀ reduction of *K. pneumoniae* when exposed to Al³⁺ alone in 50 % NB was 5.3, while the combination of FNa and Al³⁺ reduced bacterial numbers by 7.9 log₁₀ CFU mL⁻¹ ($p < 0.05$). There was no significant difference between activity of any other metal ion and FNa combination compared to the same metal ions alone ($p > 0.05$).

8.3.4 Effect of metal ions on sodium fusidate solubility in and pH of simulated tear fluid

There was no significant difference between the solubility of either 80 or 1280 µM FNa in STF when alone or with 625 µM Al³⁺, Cu²⁺ or Fe²⁺ ($p > 0.05$), therefore, only data for the solubility of 1280 µM FNa was used in the analysis.

FNa at a concentration of 1280 µM was freely soluble in the novel STF after 4 h at 37 °C and 5 % CO₂. While mean values varied from 91.9 to 97.3 %, there was no significant difference between FNa solubility in STF in the presence of any of the metal ions tested

and without ($p > 0.05$, Figure 8.10). In 50 % NB, on the other hand, there was significantly reduced solubility of 1280 μM FNa with all three metal ions compared to the control ($p < 0.05$). FNa solubility alone in 50 % NB was 81.4 %, whereas it was 26.5, 47.3 and 28.8 % in 50 % NB with 625 μM Al^{3+} , Cu^{2+} or Fe^{2+} , respectively.

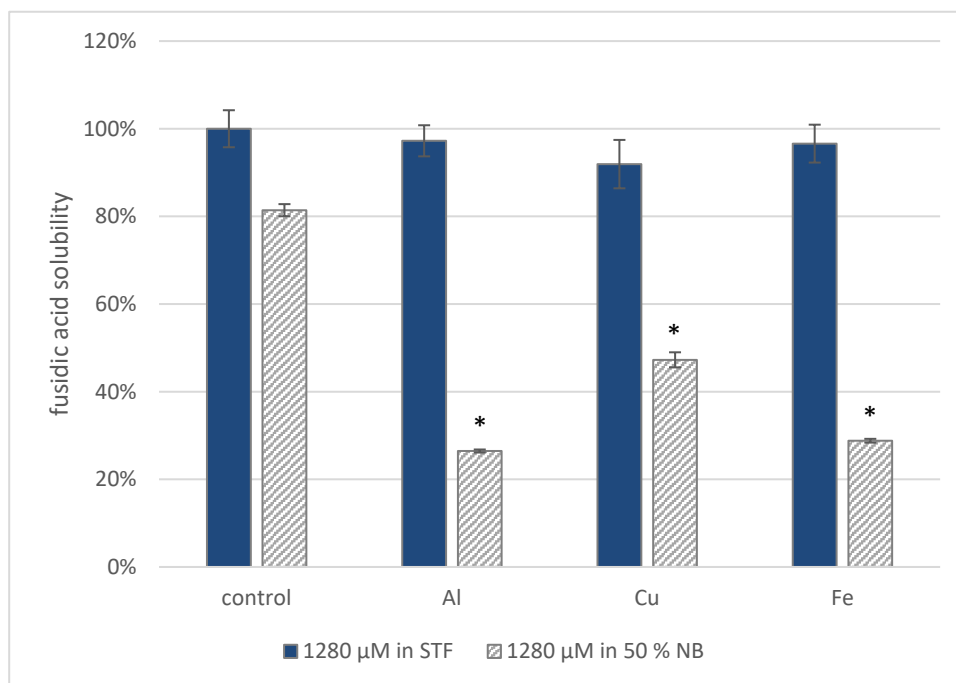


Figure 8.10 - Solubility of 1280 μM sodium fusidate in novel STF or 50 % nutrient broth with or without metal sulphates after 4 h at 37 °C and 5 % CO_2
($n = 3$, error bars = 95 % CI, * = $p \leq 0.05$ compared to solvent control)

Table 8.9 - pH of novel STF and 50 % NB with and without 625 μM metal ions after 4 h at 37 °C and 5 % CO_2

Metal sulphate	STF	50 % NB
Control	7.54 \pm 0.03	6.31 \pm 0.06
Al	7.38 \pm 0.02	4.95 \pm 0.02
Cu	7.53 \pm 0.04	5.47 \pm 0.01
Fe	7.39 \pm 0.05	5.66 \pm 0.01

Data is shown as mean of $n = 3 \pm 95\%$ CI. Apparatus accurate to ± 0.02 pH units.

As with previous investigations (see Chapter 5), FNa solubility appeared to be related to solution pH. The pH of novel STF and 50 % NB after 4 h at 37 °C and 5 % CO_2 with and without 625 μM each metal is listed in Table 8.9. Figure 8.11 illustrates the relationship between pH of the novel STF or 50 % NB and the solubility of FNa. The pH and FNa solubility in the STF was very similar across all metals and the control with differences of no more than 0.16 pH units and 8.1 % FNa solubility between them. Conversely, 50 % NB pH significantly varied with the addition of each of the metal sulphates which also

had a significant impact on FNa solubility ($p < 0.05$). Solubility of FNa compared to pH of 50 % NB containing Fe^{2+} appears to fall outside of the overall correlation between these parameters. This may be due to incomplete equilibration during the short 4 h incubation period, as observed in previous solubility studies (see Chapter 5).

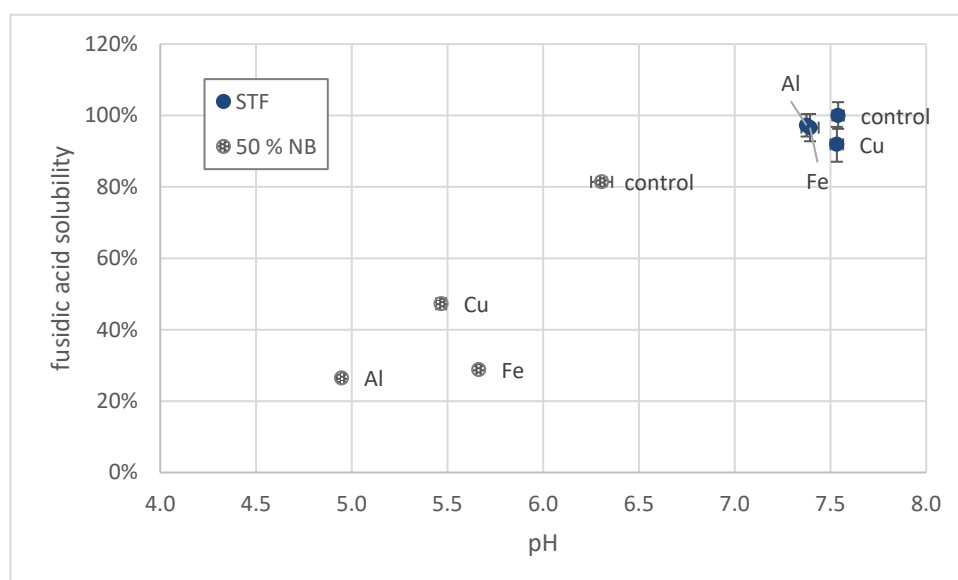


Figure 8.11 - Solubility of 1280 μM sodium fusidate sodium salt compared to pH of metal sulphates in novel STF and 50 % NB after 4 h at 37 °C and 5 % CO_2
(n = 3, error bars = SD)

8.4 Discussion

8.4.1 Novel simulated tear fluid formulation development

8.4.1.1 Omission of components found in reported formulations or human tears

The rationale for exclusion of lipid film components from the novel STF formulation is presented in Section 8.1. However, several proteins known to be present in the human muco-aqueous pool were also omitted, namely immunoglobulins, α -acid glycoproteins and transferrins. In addition, ammonium was not considered for inclusion.

The single published STF formulation found to contain ammonium in the literature^[516] included it as the only source of nitrogen, essential to bacterial growth. However, no evidence of ammonium in human tears was identified in the literature, indicating inclusion was not necessary to mimicking the human muco-aqueous pool. Since the developed

formulation included several nitrogen-containing proteins, any requirement for the addition of ammonium in order to support bacterial growth was negated.

The role of immunoglobulins *in vivo* is to adhere to foreign bodies such as bacterial cells, marking them for phagocytosis by neutrophils^[547]. While this process acts as an effective bacterial clearing mechanism in healthy eyes, an *in vitro* model involving immune cells was not the aim of this work. Therefore, the presence of immunoglobulins was not deemed as required in the STF formulation for its intended use.

While α -acid glycoproteins were used in several reported STF formulations and are known to be contributors to drug binding in the blood^{[548],[549]}, no published tear concentrations were found. Alpha-acid glycoproteins were not included in novel STF formulation development since their presence in tear fluid could not be substantiated. In addition, albumin is the most abundant drug-binding protein in both the blood^[550] and tear fluid^[551] and BSA was included in the STF formulation at a concentration equivalent to pre-albumin documented in tear fluid.

Lactoferrin, along with other transferrins, is an iron chelator and mammalian siderophore, utilised in cellular uptake, processing and storage under normal conditions as well as iron sequestration during infection^[552]. However, some bacterial species are able to acquire iron *via* human transferrins, including *P. aeruginosa*^[553]. The presence of transferrins could either reduce or enhance the activity of metal ion and FNa combinations, particularly with Fe²⁺. Sequestration of the solubilised metal ions may reduce antimicrobial activity by disrupting the mechanism of action or increase it by limiting available nutrients and therefore bacterial recovery. Alternatively, bacterial uptake of iron-loaded mammalian siderophores may reduce antimicrobial activity enabling bacteria to acquire non-toxic iron essential to cellular processes or increase it by supporting increase growth rate and therefore FNa susceptibility. While these effects may have an important impact on the activity of FNa and metal ions combinations, the transferrins were excluded in order to minimise potential complication in interpretation of bacterial growth assay results.

8.4.1.2 Novel simulated tear fluid opacity change on bacterial inoculation

The opacity of the STF test formulations after the addition of bacteria precluded microplate reader use during assessment of growth curves and antimicrobial susceptibility. This phenomenon was most apparent with the test STF formulation containing 1000 mg L⁻¹ glucose and both lysozyme and mucin (Figure 8.4, page 221). In part, this could have been due to rapid bacterial growth compared to the 90 mg L⁻¹

glucose formulations through utilisation of this easily accessible and comparatively abundant energy source. However, the reaction of mucin in response to increasing bacterial numbers was most likely to have contributed to the dramatic increase in optical density, since the opacity of solutions containing mucin were observed to dramatically increase immediately on introduction of *E. coli*. This change may have been due to bacterium-initiated adherence or aggregation of mucin, as occurs *in vivo* in order to immobilise and clear foreign particles from the eye surface^{[554],[555]}. Subsequent reduction of absorbance during growth curve investigations may, therefore, be the result of either spontaneous or *E. coli*-mediated breakdown of these aggregated structures. Interestingly, this process was not as apparent with test STF formulations containing 90 mg L⁻¹ glucose. However, comparison of microplate reader-monitored and CFU count-based growth curves revealed that while *E. coli* population increase ceased after 12 h (Figure 8.8A, page 225), absorbance continued to increase for a further 12 h in the same STF formulation (Figure 8.4, mucin, lysozyme and 90 mg L⁻¹ glucose). In addition, the absorbance curve for the STF formulation containing mucin and 90 mg L⁻¹ glucose (without lysozyme) followed a very similar trend, whereas that for STF with lysozyme and 90 mg L⁻¹ glucose (without mucin) was dissimilar, peaking around 20 h and then steadily decreasing over the remaining incubation period. This may indicate that, where present, mucin-mediated bacterial aggregation continued to increase after the *E. coli* population reached stationary phase. However, since the microplate reader-monitored growth curve cultures were incubated at 35 °C in normal air whereas the CFU count-based growth curve cultures were performed at 37 °C in 5 % CO₂, actual bacterial growth is likely to have proceeded differently under each incubation condition.

Therefore, the observed absorbance changes may have reflected bacterial numbers in test STF where only 90 mg L⁻¹ glucose was included. However, all growth curves in Figure 8.4 were performed under the same culture conditions and the differences between 90 mg L⁻¹ glucose test STF formulations demonstrate that either aggregation or bacterial population decrease when mucin is not present. Since this phenomenon was not the focus of the assay performed, an STF formulation without mucin or lysozyme was not tested, however, this would allow determination of whether absorbance reduced due to the lytic activity of lysozyme or breakdown of less stable mucin-free bacterial aggregation.

8.4.1.3 Optimisation of incubation conditions to achieve physiological pH

While tears have long been known to exert an appreciable buffering capacity^{[540],[541],[556]}, empirical pH measurements vary with exposure to air. The literature data illustrated in Figure 8.2 (page 218) clearly demonstrated a range of tear pHs which correspond to

exposure to air. This is because the tear film of closed eyes is equilibrated with the surrounding tissue, particularly the CO₂ the tissue is producing. On eye opening, the CO₂ partial pressure the tear film is exposed to reduces to that of normal atmosphere (0.2 %). This leads to alkalinisation of the tear film as solubilised CO₂ is released to equilibrate with the surrounding air.^{[511],[543],[557]} Therefore, the pH of 8.6 for the novel rationalised STF formulation in normal air was to be expected and can be primarily attributed to the alkalinising effects of bicarbonate^[544]. While elimination of sodium bicarbonate from the STF formulation proved effective in achieving physiological pH (Table 8.7, page 222), incubation in 5 % CO₂ was investigated as a means to more closely replicate *in vivo* conditions. The novel rationalised STF formulation containing the originally deduced bicarbonate concentration during and after incubation in 5 % CO₂ demonstrated very similar pH change (Figure 8.5, page 222) to those documented in *in vivo* tear film and collected tears (Figure 8.2, page 218). The pre-incubation pH of STF was 8.60 while the pH of tear film after 1 min air exposure was reported to be 7.83^[545] to 9.3^[543]. During incubation in 5 % CO₂, the STF pH dropped to 7.62, slightly higher than found in collected tears (7.45^[540] to 7.5^[541]) and *in vivo* tear film after brief air exposure (7.5^[543]). This difference was likely due to the short exposure to normal air during pH measurement. In addition, after CO₂ incubation, STF equilibrated to normal air for 24 h increased to pH 9.15, similar to the tear film after 1 min exposure to air. A pH increase was also observed in samples with closed lids post-incubation, however, this can also be explained by minimal normal air exposure during pH measurement. Therefore, incubation in 5 % CO₂ was selected to best recreate *in vivo* conditions and physiological pH of the novel STF.

8.4.2 Antimicrobial assay optimisation

8.4.2.1 Bacterial addition, acclimatisation and antimicrobial exposure duration in novel simulated tear fluid

Bacteria were carefully added to the CO₂-equilibrated novel STF without mixing in order to avoid disturbing the observed stratification (Figure 8.6, page 223) or inducing overt mucin aggregation (Figure 8.4, page 221 and Section 8.4.1.2, page 230). While mucin-mediated immobilisation is a rapid response to arriving bacteria *in vivo*, this process is overcome during the initiation of infection and bacteria are not cleared from the ocular surface. Therefore, it was desirable to avoid excessive aggregation on addition of inoculum so that bacterial growth was not overly perturbed nor cells protected from antimicrobial exposure by too much mucin coating.

All three bacterial species took at least 8 h to reach stationary phase in the novel STF and, while growth rate over the initial 4 h varied, all populations increased by approximately $1 \log_{10} \text{ CFU mL}^{-1}$ between 4 and 8 h (Figure 8.8). Therefore, an initial acclimatisation period of 4 h followed by a 4 h exposure period was selected. This allowed for bacteria to express metabolic and phenotypic characteristics induced by STF and applicable to the *in vivo* environment prior to application of the metal ion and FNa treatments. Further, while bacterial growth would not be limited by nutrient depletion *in vivo* as the tear fluid is continually replenished, limiting the exposure duration to the log period of rapid growth *in vitro* was chosen to increase sensitivity and reduce any skewing effects of the potentially limited nutrition available in STF.

8.4.2.2 Calculation of sodium fusidate test concentration

The test concentration of 80 μM FNa was determined using calculations based on pharmacokinetic literature data. The half-life of 1 % FA viscous eye drops in the tear fluid of healthy volunteers was reported to be 7.3 h by Thorn & Johansen^[558] using a single sampling protocol repeated at different post-administration timepoints on separate days. The authors used this method to prevent any washout effect of repeated tearing in response to sampling at multiple timepoints over the course of one day. However, since keratitis and other eye infections increase tear production^[507], results of earlier work by van Bijsterveld *et al*^[559] where multiple sampling was performed sequentially on the same day were determined to be more relevant to conditions in the infected eye. By this method, a half-life of 1.9 h in human tears was determined. At this elimination rate and assuming initial retention of 5 % of the applied dose^[63], the tear concentration 12 h after administration of a 50 μL drop of standard 1 % FA viscous eye drops can be expected to be 83 μM . FNa concentrations within the human cornea have not been measured, however, 24 h after a single dose to the rabbit eye, the concentration of FA in the tear fluid and cornea were found to be quite similar at 9.28^[559] and 11.95^[560] μM (as calculated based on rabbit corneal tissue comprising 77.67 % water^[561]), respectively. The corneal epithelium creates a barrier to hydrophilic drugs whereas the corneal stroma is impenetrable to lipophilic molecules^[562]. The similarity between tear and corneal FA concentrations indicates that the amphiphilic nature of FA enables it to both cross the epithelium and reside in the cornea. A 12 h trough concentration of approximately 80 μM could therefore be expected in the human cornea.

8.4.3 Antimicrobial activity of sodium fusidate and metal ions in novel simulated tear fluid and 50 % nutrient broth comparator

8.4.3.1 Sodium fusidate or metal ions alone

At 80 μM , FNa had no effect on the growth of *E. coli*, *K. pneumoniae* or *P. aeruginosa* reference strains in the novel STF or 50 % NB over 4 h ($p > 0.05$, Figure 8.9A, page 226). This was to be expected as this concentration was not found to inhibit growth of any GN organism tested using the microdilution assay (see Chapter 6) and all three species are considered clinically resistant to FNa. However, metal ions alone in 50 % NB and 5 % CO_2 for 4 h exhibited interesting antimicrobial activity, without apparent correspondence to previously determined 18 h $\text{MIC}_{90\text{s}}$ in NB and normal air. Al^{3+} exerted cidal activity on all three species (Figure 8.9B, page 226) and Fe^{2+} was cidal against *E. coli* and *P. aeruginosa* (Figure 8.9D, page 226). This may have been due to a combination of increased osmotic pressure in 50 % NB compared to standard NB and further reduced pH during incubation in 5 % CO_2 . However, *K. pneumoniae* was not killed by Fe^{2+} and populations remained static during the 4 h exposure period. In addition, Cu^{2+} was less dramatically cidal to *E. coli* and *P. aeruginosa* than the other two metals and, again, had no effect on *K. pneumoniae* numbers (Figure 8.9C, page 226). This suggests nuanced differences in bacterial metabolism or homeostatic mechanisms may be the more likely determinant of metal ion susceptibility over 4 h in 50 % NB under 5 % CO_2 .

Interestingly, bacterial responses to metal ions in STF were quite different to in 50 % NB. None of the three bacterial species were inhibited by Al^{3+} or Fe^{2+} and growth was no different to the controls ($p > 0.05$, Figure 8.9A and C, respectively, page 226). However, Cu^{2+} was cidal to all three after 4 h in STF under 5 % CO_2 (Figure 8.9B, page 226). Lack of activity of Al^{3+} or Fe^{2+} may be readily explained by sequestration of metal ions by mucin^{[563],[564]}. Mucin is known to bind metal ions, with highest affinity to harder Lewis acids such as Al^{3+} , Na^+ and Mg^{2+} ^[563]. Since Cu^{2+} is a softer Lewis acid than many of the metal ions included in the STF formulation^[565], it may have been outcompeted for mucin binding therefore producing a high thermodynamic activity of the free ions. However, other ligands, including lactate, pyruvate and bicarbonate, have been shown to be involved in metal-mucin binding in the gastrointestinal fluids^[563]. Differential binding to these components – or, indeed, lysozyme, BSA or other metabolites – may also impact the antimicrobial activity of metal ions in STF. Further investigation would be required in order to tease out these interactions.

8.4.3.2 Sodium fusidate combined with metal ions

In the novel STF, FNa combined with metal ions was no more antimicrobially active than the same metal ions alone ($p > 0.05$). A similar pattern was seen in 50 % NB, with the exception of Al^{3+} against *K pneumoniae* ($p < 0.05$). This may have been because all metal ions alone exerted either a cidal or completely bacteriostatic effect over the 4 h exposure period. Since no bacteria were growing in the presence of the metals, there was no active protein synthesis for FNa to inhibit even if it was able to more effectively access the ribosome due to the action of the metal ions. However, lack of detection of differences may have been due to the assay design and a longer exposure period may produce a different pattern. For example, during the first 4 h of exposure to metal ions alone 90 % of a bacterial population might be killed while the remaining 10 % is able to upregulate the required homeostatic processes, survive and continue to multiply. However, another population exposed to metal ions and FNa is similarly reduced during the first 4 h but regrowth of the survivors is inhibited by the combination. Alternatively, 80 μM might simply be too low a concentration of FNa to produce a combined antimicrobial effect, particularly in STF due its high level of protein binding^[566]. This concentration was modelled on the concentration of 1 % viscous eye drops and frequency of dosing used in conjunctivitis (every 12 h, Section 8.4.2.2). However, in the few reported cases of the use of FA for the treatment of bacterial keratitis, application was performed every 2 to 6 h^[567], which would produce trough values of 0.75 to 3.2 mM. Such concentrations may prove more active in combination with metal ions in STF.

8.4.4 Solubility of sodium fusidate in novel simulated tear fluid and 50 % nutrient broth comparator

FNa was significantly less soluble in 50 % NB than the novel STF after 4 h at 37 °C in 5 % CO_2 ($p < 0.05$, Figure 8.10, page 228). Solubility of 1280 μM FNa in 50 % NB with metal ions followed a similar pattern to that observed in standard NB (see Chapter 5) while there was no significant difference between with and without metal ions in STF ($p > 0.05$). However, while variation between replicates meant there was no significant difference between solubility of 1280 μM FNa in STF in any of the conditions tested and solubility of FNa alone or with Al^{3+} or Fe^{2+} was not significantly different from 100 %, the presence of Cu^{2+} reduced FNa solubility to 91.9 % which was significantly different from 100 %. This reduction in solubility may be related to the reduced mucin binding of Cu^{2+} , as hypothesised above. However, since Cu^{2+} was found to be cidal in STF, the possible increase in FNa activity due to reduced solubility was masked. Interestingly, apart from

with Fe^{2+} in 50 % NB (likely due to insufficient equilibration time), the relationship between medium pH and 1280 μM FNa solubility (Figure 8.11, page 229) appeared to follow the same pattern as presented in Chapter 5 (Figure 5.21, page 140). However, this did not correspond to the antimicrobial activities determined after 4 h exposure. As discussed above, this may be due to limitations of the present assay or an activity pattern that does not translate to other growth media or bacterial species.

8.5 Conclusions

Conclusions drawn from the work presented in this Chapter are:

- 1) A novel STF representative of the human muco-aqueous pool and suitable for antimicrobial testing was successfully developed.
- 2) The optimised novel STF was successfully utilised in simple antimicrobial efficacy assay.
- 3) Neither Al^{3+} , Cu^{2+} nor Fe^{2+} were found to increase FNa activity against *E. coli*, *K. pneumoniae* and *P. aeruginosa* reference strains in STF.
- 4) No relationship between FNa solubility and activity in STF could be defined from the data generated.

Chapter 9: General discussion



9.1 Reflections on findings and context

This thesis presents the first investigations into the combination of FNa with metal ions as a strategy to overcome intrinsic GN resistance. The primary hypothesis was that one or more antimicrobial metal ion(s) would enhance the activity of FNa against GN bacteria without reducing anti-GP efficacy. This was tested using an optimised chequerboard assay which revealed synergy between FNa and Al^{3+} , Cu^{2+} or Fe^{2+} against *E. coli* reference strain NCTC 10418 (Chapter 4). Testing against other GN species demonstrated that, while some variation in efficacy was observed, this activity was not specific only to *E. coli* or the reference strain originally employed (Chapter 6). There was also no apparent link between resistance genes harboured by MDR isolates and their susceptibility to metal ion and FNa combinations. Taken together, this is promising evidence for a potential novel antimicrobial combination. FNa combined with metal ions, particularly Al^{3+} , produced increased inhibition of all MDR and reference strains of *E. coli*, *K. pneumoniae* and *P. aeruginosa* – GN species capable of causing bacterial keratitis. In addition, the presence of metal ions did not reduce the antimicrobial efficacy of FNa against *S. aureus*, a common GP cause of keratitis. Investigations using UV-Vis spectrophotometry and ITC indicated lack of interaction between metal ions and FNa (Chapter 5). The enhanced FNa activity could be correlated with reduced solubility due to pH change and total antimicrobial effect was successfully modelled as additive between this and the independent activity of the metal ions.

This work sits at the crossroads of two antimicrobial development approaches: combinations of antimicrobial agents and adjuvants targeting resistance mechanisms. The metal ions used were, themselves, antimicrobially active, therefore combination with FNa could be considered concomitant use of two antimicrobials. However, experimental results indicated part of that the mechanism by which the metals synergised with FNa was by overcoming an intrinsic resistance mechanism – OM impermeability (Chapter 5). Due to widespread and ever-growing antimicrobial resistance, the employment of antimicrobial adjuvants to overcome resistance mechanisms is increasing in recognition. As mentioned in Chapter 1 (Section 1.4.3.2, page 34), one of the earliest adjuvants brought to market was the β -lactamase inhibitor clavulanic acid^[210]. This has led to the development of the ESBL-inhibitors which have more recently been approved, such as avibactam^[216], and ensure ongoing usability of carbapenems. While antimicrobial adjuvants as a field of research is still quite young, many more approaches to negating antimicrobial resistance mechanisms have been investigated or are in development^[568].

In fact, very recent reports include agents capable of OM permeabilisation^[569] or efflux inhibition^{[570],[571]}, the same mechanisms that were principal in guiding metal ion selection for use in this work. With regards to the antimicrobial activity investigations presented, this thesis agrees with published works in illustrating that efficacy of agents intrinsically resisted by low permeability can be enhanced. While the discovered mechanism of overcoming the OM barrier – increased protonation *via* reduced pH – may not be practical for direct translation to clinical application (see Section 9.2), other permeabilisers or formulation approaches could be employed to the same result (see Section 9.3.1.2).

It is interesting that this work also identified factors which could lead to potential topical antimicrobial agents being overlooked or undiscovered during early investigations and development. By optimising the chequerboard assay to employ NB rather than CAMHB, the synergistic anti-GN activity of a select few metal ions and FNa was discovered and determined to be related to reduced FNa solubility. If the assay had been performed in standard CAMHB, this activity would likely have been missed, particularly since acid hydrolysate of casein is known to sequester metal ions^[310]. In addition, low solubility was observed in the NB used, which is generally considered an undesirable characteristic of novel antimicrobials. In fact, this work demonstrated that, in some cases, low solubility can be advantageous to antimicrobial activity. Solubility considerations are of paramount importance when considering systemic administration, since the ingested or injected drug must reach its site of activity without precipitating. However, topical agents are usually applied directly to the infected tissue and do not need to travel far in aqueous solution in order to reach the target cells. Less soluble, more lipophilic molecules in an aqueous solution or suspension are more likely to associate with the lipids of membranes and thereby gain access the intracellular target. In addition, if insolubility becomes problematic to drug delivery the formulation may be able to be optimised, capitalising on what would otherwise have been an abandoned potential drug. An excellent example of this is the use of cyclodextrin and surfactant to solubilise and deliver a very poorly soluble antifungal (4 ng mL⁻¹) through the cornea^[572]. Other approaches are also discussed in Section 9.3.1.2. The standardised CAMHB culture conditions are excellent for producing comparable, reproducible diagnostic antimicrobial susceptibility data. However, it should be recognised that this is both 1) an artificial system which does not closely represent the conditions bacteria experience in the host, and 2) may be limiting the discovery of usual agents and mechanisms which we now have the formulation strategies to be able to employ clinically.

As with many bacterial infections, keratitis has been shown to develop as a biofilm^{[573],[574]}. These are slow-growing communities of adherent bacteria surrounded by

a polymeric extracellular matrix with very low permeability to antimicrobials^[575]. Determination of the anti-biofilm efficacy of new drugs or formulations *in vitro* may provide sensitivity data more in line with *in vivo* efficacies. While ineffective alone, FNa has been shown to synergise with vancomycin against established *S. aureus* biofilms *in vitro*^[566]. Cu^{2+} can eradicate *K. pneumoniae* biofilms^[380], however, the concentration used was equivalent to 17.25 mM which is ~7 times the IC_{90} found against HCE-2 in this work (Section 7.2.5.3). In addition, >304 mM Al^{3+} could not disperse a biofilm of *E. coli*^[576]. This may indicate that the free metal ion and FNa combinations will be ineffective against biofilms. However, formulation strategies may be able to combat this issue (see Section 9.3.1.2). In addition, due to the severity of bacterial keratitis, the FNa and metal ion combination could be included with more effective anti-biofilm agents in order to slow the growth of cells released from the biofilm.

The secondary hypothesis of this work was that the combination would exhibit low toxicity against mammalian cells and good activity in an STF mimicking the ocular environment. Indeed, metal ion IC_{90} s against HCE-2 were higher than the MIC_{90} s against GN isolates, and FNa with Al^{3+} in particular exhibited an excellent selectivity index of 37.4 against *P. aeruginosa* (Chapter 7). However, combined antimicrobial activity in a novel STF, rationally designed as physiologically representative of the human muco-aqueous pool, was not detected (Chapter 8). Lack of activity detection may have been due to the concentration of FNa and metal ions selected for testing, however, as discussed previously, protein binding in STF is likely to have been the key mediator in suppression of bacterial inhibition. This is an issue faced by many pharmacological agents. FNa is already known to be >95 % protein bound in human plasma when administered systemically^[566], however, this does not prevent *in vivo* antimicrobial activity. Metals also bind proteins, as discussed in Section 9.2, below. Despite this, there may be formulation strategies that can prevent loss of active drug to protein binding such as encapsulation in liposomes (see Section 9.3.1.2).

9.2 Limitations in application of this work

Due to the combinational nature of this system, the new activities are bimolecular events relying on FNa and metal arriving at and acting on the bacterial OM simultaneously. This excludes use systemically *in vivo*, where the likelihood of a bimolecular event is extremely unlikely, due to dilution in the bloodstream. However, topical delivery onto the surface of infection, where there is little or no such dilution, is more likely to result in the

observed potentiation. Nonetheless, there are a number of challenges to safely and effectively utilise the combination of FNa and metal ions *in vivo*.

The use of free metal ions clinically may be limited by the innate sequestration used in mammalian immune processes. Transferrins are present in human serum and secretions, including tear fluid, while activated macrophages specifically withhold iron during infection using ferritin, and recruited neutrophils release lactoferrin^[577]. In addition, and as discussed in Chapter 8 (Section 8.4.3, page 234), mucin present on the ocular surface is known to bind metal ions^{[563],[564]}. Similarly, while there is no such specifically identified sequestration process for Al³⁺, its high affinity to a variety of moieties present on glycoproteins such as mucin is likely to remove free aluminium ions from the site of application^{[563],[564]}. On the other hand, no extracellular proteins with copper sequestering function have been identified and known Lewis acid binding order^[565] combined with results presented in Chapter 8 indicate that other metal ions naturally present in tear fluid may outcompete copper for mucin binding. However, copper ions are efficiently taken up into mammalian cells by high affinity transporters^{[578],[579]}, which could reduce their local concentration. These processes may rapidly alter the free metal ion concentration in an applied dose, eliminating its antimicrobial activity. However, this may be able to be overcome through formulation strategies (Section 9.3.1.2) or further characterisation of the mechanism of combined action (Section 9.3.1.1) allowing identification of an alternative agent to metal ions.

Another factor potentially limiting the clinical use of metal ions is their undesirable effects besides discomfort on application, since their toxicity is not limited to bacteria. Although cultured human corneal epithelial cells tolerated exposure to Al³⁺, Cu²⁺ and Fe²⁺ at concentrations above those required in combination with FNa to inhibit bacterial growth, the response of other cell types and whole tissues might be quite different. For example, retinal degeneration has been observed in the rat after systemic administration of AlCl₃^[580] and intraocular injection of CuSO₄ produced inflammation and lowered intraocular pressure in the rabbit^[581]. While these routes of administration were different to the intended application, the risk of damaging ocular function must be understood prior to clinical use in order to weigh any risk against the benefits. Methods to investigate this are discussed in Section 9.3.1.3.

In addition, while solutions below pH 6 can cause discomfort, the human eye can tolerate application of preparations with pH ranging from 4 to 8^[582] and, in sight-threatening keratitis, pain on application would be far outweighed by the potential benefit. However, as discussed in Chapter 8, the tear fluid has considerable buffering capacity. Human tears have been shown to maintain pH 7.0 to 7.7 on titration with the same concentrations

of HCl or NaOH that produced pH 3.5 to 8.0 in unbuffered water^[541]. The employment of reduced solution pH as a means to increase FNa activity at the ocular surface is, therefore, likely untenable. However, other formulation approaches may be employed to increase the delivery of fusidate through the bacterial OM, as discussed in Section 9.3.1.2, below.

As discussed in Chapter 1 (Section 1.4.2), the risk of development of resistance is universal to the use of antimicrobial drugs. Rates of resistance emergence are generally lower when agents are combined due to greater efficacy and consequently shorter exposure duration^{[187],[202]–[204]}. However, only one point mutation is required to render EF-G impervious to FNa binding^[583]. Furthermore, when used systemically, FNa is always combined with at least one other agent in order to limit resistance induction^[584]. Treatment of corneal infections takes considerably longer than conjunctivitis^{[1],[585]}, the approved ocular indication of FNa, which would result in prolonged exposure of infecting bacteria to FNa. Therefore, addition of another antimicrobial agent to the formulation may be appropriate. In fact, a broad spectrum triple antibiotic formulation for the treatment of bacterial corneal ulcers combining polymyxin B, trimethoprim and rifampin has recently been proposed^[586]. The authors not only demonstrated synergy against planktonic *P. aeruginosa* and *S. aureus*, but also activity against established *in vitro* biofilms and a murine model of *S. aureus* keratitis. All additions to the antimicrobial arsenal are valuable in the face of ever-increasing resistance, however, polymyxins are still considered drugs of last resort in the treatment of MDR infections of all types^[587]. In order to limit the chances of development and spread of resistance to these important agents, the employment of the polymyxin B, trimethoprim and rifampin combination may need to be reserved only for keratitis cases of extreme severity or with resistance to other available agents. However, a formulation based on the combination of metal ions and FNa with the addition of another agent could serve as an initial first line treatment for early presenting cases with broader spectrum than current options. This could be followed by amendment to a second line combination including polymyxin B, if necessary. Such an approach would still streamline bacterial keratitis management while preserving effectiveness of precious last line antimicrobials.

9.3 Future directions

9.3.1 Further research

9.3.1.1 Mechanism of action

The evidence gathered in this thesis suggests OM damage caused by metal ions plays a role in their synergistic activity with FNa. In most circumstances, OM disruption can be detected by assaying alkaline phosphatase activity in the medium^[588]. Alkaline phosphatase is a periplasmic enzyme which can convert *p*-nitrophenyl phosphate into a coloured product, spectrophotometrically quantifiable at 410 nm. However, divalent metal ions non-competitively inhibit the enzymatic activity^[589] by inducing conformational changes and aggregation^[590] while Al³⁺ also inhibits its activity^[591] by strong but reversible binding^[592]. Modification to the assay using a metal chelation or quenching step prior to substrate addition may be able to overcome these issues providing the enzyme structure is not irreversibly denatured.

Alternatively, increased OM penetration of FNa as the mechanism of synergistic activity with metal ions could be verified by comparison to the effects of an agent known to disrupt the OM with no other antimicrobial mechanisms. For example, recently discovered B2088 specifically binds to lipid A to disrupt the LPS and has been shown to synergise with a variety of antimicrobials normally hindered by the OM^[569]. In addition, the involvement of efflux inhibition could be investigated using AcrAB-TolC inhibitors^{[570],[571]} in place of metal ions in combination with FNa. Furthermore, combinations of membrane disruptor and efflux inhibitor could be used to further characterise the involvement of each mechanism.

The work in Chapter 5, Section 5.4.4, demonstrates that the amount of FNa associated with *E. coli* cells increased as pH is reduced. Experimental parameters were selected to ensure similar numbers of live bacteria would be present across all test conditions so that results would not be skewed by passive diffusion into dead cells unable to efflux. However, the concentration of Cu²⁺ employed was not sufficient to lower pH. Therefore, the effect of metal ions and acidity could not be fully quantified by this method. An alternative method could have been to utilise fluorescent microscopy in order to quantify FNa with greater sensitivity and after a shorter exposure time^[593]. However, such an approach requires the drug of interest to fluoresce. Some antimicrobial drugs, such as quinolones^[594], contain a fluorophore which can be employed in fluorescent microscopy, however, FNa does not. Non-fluorescing drugs can be modified by chemical substitution

in order to produce fluorescence^[595]. However, production can be complex and the substitution positioning is crucial, frequently impacting the drug affinities for uptake, efflux or target, compromising the validity of such studies^[595]. Radio-labelling may be a suitable alternative since substitution with a radioactive isotope should not alter the overall properties of FNa. Microautoradiography has been used to determine the intracellular localisation of radionuclides mammalian cells^[596] and uptake of radio-labelled nutrients in environmental bacteria^[597]. The same approach may be used to explore the bacterial localisation of FNa, with and without the presence of metal ions.

Another option which would enable simultaneous 3D localisation studies of both FNa and metal ions is Time-of-Flight secondary ion mass spectrometry (TOF-SIMS). TOF-SIMS can be used to determine the 3D positioning of molecules and atoms^[598] within bacterial cells to a resolution of ~200 nm^[599]. In addition to enabling visualisation of metal ions as well as FNa and rendering information in 3D, another key advantage of this relatively new technique over microscopy-based methods is that no labelling or fluorescence of the target drug or cellular components is required^{[598],[599]}. Drugs, metal ions, important cellular components and/or mounting material can be characterised alone and resulting signal information applied to the experimental output^{[598],[599]}. The method has already been used to demonstrate the internalisation of tetracycline and ampicillin in *E. coli*^[599], localisation of quinolones in *P. aeruginosa* biofilms inside infected tissues^[600], and presence of cystic fibrosis-specific lipid markers in lung and intestinal tissue of a murine model^[601].

The mechanism of Al³⁺ in sensitising *P. aeruginosa* to FNa is a particular area of interest for future research since the combination was so unexpectedly efficacious. As discussed in Chapter 6, this may be due to increased susceptibility of the *P. aeruginosa* LPS to Al³⁺ attack compared to that of the *Enterobacteriaceae*, or increased OM permeabilisation due to different protein and porin arrangement. The aim of the investigations using MDR representatives of GN organisms capable of causing keratitis was to determine whether they were inhibited by metal ion and FNa combinations in a similar way to the *E. coli* reference strain. It was beyond the scope of the present work to characterise any differences in responses between species other than by comparison to known carriage of resistance genes. However, it may be hypothesised that, unlike against the *Enterobacteriaceae*, Al³⁺ interferes with one or more of *P. aeruginosa*'s mechanisms of FNa tolerance. This could indicate a novel drug target in an organism the US Centers for Disease Control and Prevention lists as a serious threat to public health^[602]. Wellcome Trust funding has been awarded for a project to investigate this hypothesis utilising genome-wide association studies. The MICs of FNa and Al³⁺ alone and in combination will be determined against a library of 145 genetically varied *P. aeruginosa* isolates.

Whole genome sequencing of isolates will be performed and the data used to map the degree of combination sensitivity to the presence, absence or particular allele of genes of potential targets across the isolate library. This may reveal a novel mechanism through which *P. aeruginosa* can be inhibited and a focus for future development of antimicrobial agents against this increasingly resistant organism.

9.3.1.2 Formulation

A variety of formulation strategies may be able to be employed to increase FNa delivery to bacterial cells without relying on lowering of the local pH. Two of these approaches are complexation with cyclodextrins and inclusion within liposomes, the results of both requiring less energy to successfully interact with the target membranes compared to the free drug. The lower energy requirement is due to a reduction of repulsive double layer force or increase of attractive van der Waals forces or both, as described by the Derjaguin Landau Verwey Overbeek (DLVO) theory^{[603],[604]}. Cyclodextrins are cyclic oligosaccharides composed of 6 to 8 glucose units. Their structure enables the formation of inclusion complexes with a variety of organic molecules, shielding a portion of the guest molecule and increasing its effective solubility and bioavailability^[605]. FNa can form 1:1 and 1:2 complexes with β - and γ -cyclodextrin, respectively^[606]. Complexation with cyclodextrins has been shown to enhance the permeation of a variety of drugs across mammalian corneas, including pilocarpine^[607], riboflavin^[608] and voriconazole^[609]. In addition, the highly lipophilic itraconazole has been successfully solubilised by complexation with cyclodextrins, significantly enhancing both its corneal penetration and antifungal activity^[572]. Addition of a mucoadhesive polymer can also be shown to increase the residence time and therefore corneal concentration of cyclodextrin complexed drugs by slowing elimination due to lachrymation and blinking^[610]. Liposomes are synthetic phospholipid bilayer vesicles which can be used to encapsulate drug molecules. Incorporation into liposomes can increase the drug residency time at the site of administration^[562], overcome issues of solubility^[562] and increase biofilm penetration^[611]. In particular, fusogenic liposomes are specifically designed with the inclusion of specific lipids to enhance fusion with biological membranes and more efficiently deposit the cargo into the target cells^[612]. Fusogenic liposomes containing FA have been shown to be more antimicrobially active against both GP and GN bacteria than FA encapsulated in standard liposomes *in vitro*, however, the authors did not determine MICs of free FA against the GN strains used, preventing comparison^[612]. In addition, liposomal encapsulation has been shown to increase the penetration of FA into mouse skin^[613], indicating potential for enhancing delivery into other low permeability tissues such as the cornea. Both these approaches could reduce the protein binding and

increase the bioavailability of FNa, increasing antimicrobial activity in keratitis. In addition, the incorporation of metal ions alongside FNa into liposomes could produce similar or even greater activity to that observed in NB in this work by enhancing delivery both agents directly into the bacterial periplasm.

9.3.1.3 Efficacy and toxicity

While cell culture can provide early indicative toxicity data, the effects of an agent on whole tissues has been shown to more closely correlate to *in vivo* results. An *in vitro* method to assess potential ocular irritation is to use the chorioallantoic membrane of a hen's egg as a model^{[614]–[616]}. There are several versions of the hen's egg test, all of which involve the application of the investigative substance to the exposed chorioallantoic membrane of fertilised hens' eggs and assessment of damage to the vasculature indicative of irritation^{[614]–[616]}. This model is effective due to the similarity between the vascularisation and inflammatory processes exhibited by the chorioallantoic membrane and the conjunctiva^[617]. The assay therefore enables prediction of the irritant effects of a potential ocular drug or formulation and optimisation of safe dosing ranges without the use of experimental animals. However, the hen's egg test would not be suitable for modification as a model of infectious keratitis due to gross differences in structure and tissues of the hen's egg compared to the eye.

Excised corneas from rabbit^{[618],[619]}, porcine^[620], canine^[621], caprine^[622] and human^{[623],[624]} eyes have been utilised in various *ex vivo* models of infectious keratitis. Such models enable the study of antimicrobial efficacy against microbes resident in tissue closely mimicking *in vivo* conditions. In addition, the use of eyes from slaughtered food animals such as pigs or from human donors negates the use and sacrifice of experimental animals. However, while *ex vivo* investigations may provide a good indication of *in situ* drug or formulation antimicrobial efficacy, isolation from systemic immune functions can limit the accuracy of simulated keratitis and progression. For example, *ex vivo* corneas do not develop ulceration after infection due to lack of recruitment of inflammatory and other immune cells from the circulation^[624]. This may impact the interpretation of antimicrobial efficacy since drug penetration of an ulcer presents additional challenges. For similar reasons, the infection can also progress more rapidly than often observed *in vivo*^[622]. Despite these limitations, an *ex vivo* model could be used to determine indicative spectrum of activity and, alongside the hen's egg test, used to optimise parameters such as dosing prior to *in vivo* testing, thereby limiting animal use.

Organotypic modelling of the human cornea has also been achieved using 3D culture of keratocytes embedded in a collagen gel supported by a polycarbonate filter and overlaid

with corneal epithelial cells at the air-liquid interface^[625]. A 3D culture of human corneal epithelial cells has also been shown to exhibit similar permeability and drug-metabolising enzyme expression as *ex vivo* tissue^{[626],[627]}. Such models could be used to investigate the corneal penetration and cytotoxicity of FNa and metal ion combinations to the ocular tissues without the use of experimental animals. In addition, this system could be modified to produce an *in vitro* keratitis model. While this would lack the immune response, as with *ex vivo* corneal models, it would provide a standardised, animal-free system enabling the simultaneous study of bacterial and mammalian responses to early stage developmental drugs and formulations.

Novel drugs or formulations can be tested *in vivo* using a model of bacterial keratitis. Most commonly, rabbits are employed^[628], however, a recent mouse model has also been developed^[573]. In both animals, keratitis is induced by scratching the cornea and introducing a small volume of bacterial suspension. Experimental treatment is initiated within 24 h of the infection procedure and outcomes measured by clinical scoring of the resulting ulcer and/or CFU count from homogenised excised corneas. While rabbits are the more widely accepted keratitis model, the nictitating membrane must be removed in order to more closely mimic the human eye structure which is devoid of this third eyelid^[628]. The mouse model negates this requirement, reducing some of the time, costs and animal welfare concerns associated with such investigations.

9.3.2 Additional and alternative clinical applications

Helicobacter pylori is a GN bacterium capable of colonising the acid environment of the stomach^[629]. Infection itself is often without symptoms, however, the presence of *H. pylori* is strongly correlated with gastric ulcer and gastric cancer^[630]. Current treatment regimens involve multiple antimicrobials along with suppression of stomach acid production, which can lead to secondary infections and other complications^[631]. However, the acid environment could be utilised to enhance FNa activity against *H. pylori*. In addition, several steroid-like compounds with similar structure to FNa have been isolated from a variety of gums and shown to exhibit some antimicrobial activity against *H. pylori*^[632]. Therefore, the addition of FNa and metal ions to treatment regimens could increase *H. pylori* eradication efficacy while reducing the need for long term acid suppression and associated secondary infection risk.

With appropriate formulation optimisation, the combination of FNa and Al³⁺ may be useful in other infections caused by *P. aeruginosa*. Aside from keratitis, *P. aeruginosa* can

cause severe infection secondary to other conditions including cystic fibrosis^[493] and burn^[633] or surgical^[634] wounds. These groups of vulnerable patients often suffer from long duration or refractory infections. A treatment regimen including a novel anti-*P. aeruginosa* agent from the work described in 9.3.1.1 or even combined FNa and Al³⁺ formulation could make a significant impact on early infection management and recovery.

9.4 Closing remarks

In this work, the presence of Al³⁺, Cu²⁺ or Fe²⁺ ions was found to increase the activity of FNa against a selection of intrinsically resistant *E. coli*, *K. pneumoniae* and *P. aeruginosa* reference strains and MDR isolates in NB, without interfering with anti-*S. aureus* efficacy. The mechanism of action was determined to be a combination of reduced FNa solubility enabling increased access through bacterial membranes and the independent antimicrobial activity of the metal ions. There was no apparent link between the carriage of any individual or combination of antimicrobial resistance determinants and susceptibility to the FNa and metal ion combinations in the MDR isolates tested. In addition, while exposure to metal ions can result in mammalian toxicity, human corneal epithelial cells were less inhibited by Al³⁺, Cu²⁺ or Fe²⁺ alone than GN reference strains. Of particular interest, Al³⁺ decreased FNa MIC_{90s} against *P. aeruginosa* strains by at least 512-fold and was least toxic to human corneal epithelial cells yielding a selectivity index indicative of potential suitability for clinical use. Unfortunately, the combination of FNa and Al³⁺ proved to be antimicrobially inactive against GN reference strains in a novel STF, likely due to protein binding of both agents. Further hurdles regarding penetration of the infective biofilm and development of resistance may also prove problematic. However, formulation strategies such as encapsulation of FNa and metal ion combinations in fusogenic liposomes and inclusion of an additional antimicrobial may enable direct delivery of an active drug cocktail to bacterial cells and minimise resistance induction. Furthermore, investigation into the specific mechanism of Al³⁺ in combination with FNa against *P. aeruginosa* could identify a novel antimicrobial target and guide design of a new drug to treat infections caused by this important opportunistic pathogen.

References

1. Ong, H. S. and Corbett, M. C. 2015. Corneal infections in the 21st century. *Postgraduate Medical Journal* **91**(1080): 565–571. [doi:10.1136/postgradmedj-2015-133323]
2. Fleiszig, S. M. J. and Evans, D. J. 2010. The pathogenesis of contact lens-associated microbial keratitis. *Optometry and Vision Science* **87**(4): 225–232. [doi:10.1097/OPX.0b013e3181d408ee]
3. Erie, J. C., Nevitt, M. P., Hodge, D. O. and Ballard, D. J. 1993. Incidence of ulcerative keratitis in a defined population from 1950 through 1988. *Archives of Ophthalmology* **111**: 1665–1671.
4. Whitcher, J. P., Srinivasan, M. and Upadhyay, M. P. 2001. Corneal blindness: A global perspective. *Bulletin of the World Health Organization* **79**(3): 214–221.
5. Bourkiza, R., Kaye, S., Bunce, C., Shankar, J., Neal, T. and Tuft, S. 2013. Initial treatment of *Pseudomonas aeruginosa* contact lens-associated keratitis with topical chloramphenicol, and effect on outcome. *British Journal of Ophthalmology* **97**(4): 429–432. [doi:10.1136/bjophthalmol-2012-302251]
6. Green, M., Carnt, N., Apel, A. and Stapleton, F. Queensland microbial keratitis database: 2005–2015. *British Journal of Ophthalmology* : Published Online First: 05 January 2019. [doi:10.1136/bjophthalmol-2018-312881]
7. Kruse, A., Thomsen, R. W., Hundborg, H. H., Knudsen, L. L., Sørensen, H. T. and Schønheyder, H. C. 2006. Diabetes and risk of acute infectious conjunctivitis - a population-based case-control study. *Diabetic Medicine* **23**(4): 393–397. [doi:10.1111/j.1464-5491.2006.01812.x]
8. Sheikh, A., Hurwitz, B., van Schayck, C. P., McLean, S. and Nurmatov, U. 2012. Antibiotics versus placebo for acute bacterial conjunctivitis. *Cochrane Database of Systematic Reviews* (9): Article No: CD001211. [doi:10.1002/14651858.cd001211.pub3]
9. Constantinou, M., Daniell, M., Snibson, G. R., Vu, H. T. and Taylor, H. R. 2007. Clinical efficacy of moxifloxacin in the treatment of bacterial keratitis: A randomized clinical trial. *Ophthalmology* **114**(9): 1622–1629. [doi:10.1016/j.optha.2006.12.011]
10. Lee, Y.-S., Tan, H.-Y., Yeh, L.-K., Lin, H.-C., Ma, D. H. K., Chen, H.-C., Chen, S.-Y., Chen, P. Y. F. and Hsiao, C.-H. 2014. Pediatric microbial keratitis in Taiwan: clinical and microbiological profiles, 1998-2002 versus 2008-2012. *American Journal of Ophthalmology* **157**(5): 1090–1096. [doi:10.1016/j.ajo.2014.01.013]
11. Taneja, M., Ashar, J. N., Mathur, A., Nalamada, S. and Garg, P. 2013. Microbial keratitis following vegetative matter injury. *International Ophthalmology* **33**(2): 117–123. [doi:10.1007/s10792-012-9643-0]
12. Gopinathan, U., Sharma, S., Garg, P. and Rao, G. N. 2009. Review of epidemiological features, microbiological diagnosis and treatment outcome of microbial keratitis: experience of over a decade. *Indian Journal of Ophthalmology* **57**(4): 273. [doi:10.4103/0301-4738.53051]
13. Hsu, H. Y., Ernst, B., Schmidt, E. J., Parihar, R., Horwood, C. and Edelstein, S. L. 2019. Laboratory results, epidemiologic features, and outcome analyses of microbial keratitis: a 15-year review from St. Louis. *American Journal of Ophthalmology* **198**: 54–62. [doi:10.1016/j.ajo.2018.09.032]
14. Bourcier, T., Thomas, F., Borderie, V., Chaumeil, C. and Laroche, L. 2003. Bacterial keratitis: predisposing factors, clinical and microbiological review of 300 cases. *British Journal of Ophthalmology* **87**(7): 834–838. [doi:10.1136/bjo.87.7.834]

15. Schaefer, F., Bruttin, O., Zografos, L. and Guex-Crosier, Y. 2001. Bacterial keratitis: A prospective clinical and microbiological study. *British Journal of Ophthalmology* **85**(7): 842–847.
16. Ng, A. L.-K., To, K. K.-W., Choi, C. C.-L., Yuen, L. H., Yim, S.-M., Chan, K. S.-K., Lai, J. S.-M. and Wong, I. Y.-H. 2015. Predisposing factors, microbial characteristics, and clinical outcome of microbial keratitis in a tertiary centre in Hong Kong: A 10-year experience. *Journal of Ophthalmology* : 769436. [doi:10.1155/2015/769436]
17. Keay, L., Edwards, K., Naduvilath, T., Taylor, H. R., Snibson, G. R., Forde, K. and Stapleton, F. 2006. Microbial keratitis: predisposing factors and morbidity. *Ophthalmology* **113**(1): 109–116. [doi:10.1016/j.opthta.2005.08.013]
18. Pflipsen, M., Massaquoi, M. and Wolf, S. 2016. Evaluation of the painful eye. *American Family Physician* **93**(12): 991–998.
19. Hazlett, L., Suvas, S., McClellan, S. and Ekanayaka, S. 2016. Challenges of corneal infections. *Expert Review of Ophthalmology* **11**(4): 285–297. [doi:10.1080/17469899.2016.1203254]
20. Bremond-Gignac, D., Chiambaretta, F. and Milazzo, S. 2011. A European perspective on topical ophthalmic antibiotics: Current and evolving options. *Ophthalmology and Eye Diseases* **3**: 29–43. [doi:10.4137/OED.S4866]
21. Dalmon, C., Porco, T. C., Lietman, T. M., Prajna, N. V., Prajna, L., Das, M. R., Kumar, J. A., Mascarenhas, J., Margolis, T. P., Whitcher, J. P., Jeng, B. H., Keenan, J. D., Chan, M. F., McLeod, S. D. and Acharya, N. R. 2012. The clinical differentiation of bacterial and fungal keratitis: A photographic survey. *Investigative Ophthalmology and Visual Science* **53**(4): 1787–1791. [doi:10.1167/iops.11-8478]
22. Egrilmez, S., Palamar, M., Sipahi, O. R. and Yagci, A. 2013. Extended spectrum beta-lactamase producing *Klebsiella pneumoniae*-related keratitis. *Journal of Chemotherapy* **25**(2): 123–125. [doi:10.1179/1973947812Y.0000000053]
23. Hindley, K. E., Groth, A. D., King, M., Graham, K. and Billson, F. M. 2016. Bacterial isolates, antimicrobial susceptibility, and clinical characteristics of bacterial keratitis in dogs presenting to referral practice in Australia. *Veterinary Ophthalmology* **19**(5): 418–426. [doi:10.1111/vop.12325]
24. Karsten, E., Watson, S. L. and Foster, L. J. R. 2012. Diversity of microbial species implicated in keratitis: A review. *The Open Ophthalmology Journal* **6**: 110–124. [doi:10.2174/1874364101206010110]
25. Fukuda, K., Ishida, W., Fukushima, A. and Nishida, T. 2017. Corneal fibroblasts as sentinel cells and local immune modulators in infectious keratitis. *International Journal of Molecular Sciences* **18**(9): 1831. [doi:10.3390/ijms18091831]
26. Brothers, K. M., Stella, N. A., Hunt, K. M., Romanowski, E. G., Liu, X., Klarlund, J. K. and Shanks, R. M. Q. 2015. Putting on the brakes: Bacterial impediment of wound healing. *Scientific Reports* **5**: 14003. [doi:10.1038/srep14003]
27. Teweldemedhin, M., Gebreyesus, H., Atsbaha, A. H., Asgedom, S. W. and Saravanan, M. 2017. Bacterial profile of ocular infections: A systematic review. *BMC Ophthalmology* **17**: 212. [doi:10.1186/s12886-017-0612-2]
28. Prajna, N. V., Srinivasan, M., Mascarenhas, J., Lalitha, P., Rajaraman, R., McClintic, S. M., O'Brien, K. S., Ray, K. J., Acharya, N. R., Lietman, T. M. and Keenan, J. D. 2019. Visual impairment in fungal versus bacterial corneal ulcers four years after successful antimicrobial treatment. *American Journal of Ophthalmology (in press)* [doi:10.1016/j.ajo.2019.03.010]

29. Shimizu, E., Yamaguchi, T., Yagi-Yaguchi, Y., Dogru, M., Satake, Y., Tsubota, K. and Shimazaki, J. 2017. Corneal higher-order aberrations in infectious keratitis. *American Journal of Ophthalmology* **175**: 148–158. [doi:10.1016/j.ajo.2016.12.014]
30. Sharma, S. 2012. Diagnosis of infectious diseases of the eye. *Eye* **26**(2): 177–184. [doi:10.1038/eye.2011.275]
31. Badawi, A. E., Moemen, D. and El-Tantawy, N. L. 2017. Epidemiological, clinical and laboratory findings of infectious keratitis at Mansoura Ophthalmic Center, Egypt. *International Journal of Ophthalmology* **10**(1): 61–67. [doi:10.18240/ijo.2017.01.10]
32. Cariello, A. J., Passos, R. M., Yu, M. C. Z. and Hofling-Lima, A. L. 2011. Microbial keratitis at a referral center in Brazil. *International Ophthalmology* **31**(3): 197–204. [doi:10.1007/s10792-011-9441-0]
33. Fong, C.-F., Hu, F.-R., Tseng, C.-H., Wang, I.-J., Chen, W.-L. and Hou, Y.-C. 2007. Antibiotic susceptibility of bacterial isolates from bacterial keratitis cases in a university hospital in Taiwan. *American Journal of Ophthalmology* **144**(5): 682–689. [doi:10.1016/j.ajo.2007.06.038]
34. Termote, K., Joe, A. W., Butler, A. L., McCarthy, M., Blondeau, J. M., Iovieno, A., Holland, S. P. and Yeung, S. N. 2018. Epidemiology of bacterial corneal ulcers at tertiary centres in Vancouver, B.C. *Canadian Journal of Ophthalmology* **53**(4): 330–336. [doi:10.1016/j.jcjo.2017.11.001]
35. Tam, A. L. C., Côté, E., Saldanha, M., Lichtinger, A. and Slomovic, A. R. 2017. Bacterial keratitis in Toronto: A 16-year review of the microorganisms isolated and the resistance patterns observed. *Cornea* **36**(12): 1528–1534. [doi:10.1097/ICO.0000000000001390]
36. Pakzad-Vaezi, K., Levasseur, S. D., Schendel, S., Mark, S., Mathias, R., Roscoe, D. and Holland, S. P. 2015. The corneal ulcer one-touch study: a simplified microbiological specimen collection method. *American Journal of Ophthalmology* **159**(1): 37–43. [doi:10.1016/j.ajo.2014.09.021]
37. Kaye, S., Sueke, H., Romano, V., Chen, J. Y., Carnt, N., Tuft, S. and Neal, T. 2016. Impression membrane for the diagnosis of microbial keratitis. *British Journal of Ophthalmology* **100**(5): 607–610. [doi:10.1136/bjophthalmol-2015-307091]
38. Fang, P.-C., Chien, C.-C., Yu, H.-J., Ho, R.-W., Tseng, S.-L., Lai, Y.-H. and Kuo, M.-T. 2017. A dot hybridization assay for the diagnosis of bacterial keratitis. *Molecular Vision* **23**: 306–317.
39. McLeod, S. D., Kolahdouz-Isfahani, A., Rostamian, K., Flowers, C. W., Lee, P. P. and McDonnell, P. J. 1996. The role of smears, cultures, and antibiotic sensitivity testing in the management of suspected infectious keratitis. *Ophthalmology* **103**(1): 23–28. [doi:10.1016/S0161-6420(96)30738-0]
40. Alexandrakis, G., Alfonso, E. C. and Miller, D. 2000. Shifting trends in bacterial keratitis in South Florida and emerging resistance to fluoroquinolones. *Ophthalmology* **107**(8): 1497–1502. [doi:10.1016/S0161-6420(00)00179-2]
41. Chang, V. S., Dhaliwal, D. K., Raju, L. and Kowalski, R. P. 2015. Antibiotic resistance in the treatment of *Staphylococcus aureus* keratitis. *Cornea* **34**(6): 698–703. [doi:10.1097/ICO.0000000000000431]
42. Das, S., Samantaray, R., Mallick, A., Sahu, S. K. and Sharma, S. 2019. Types of organisms and *in vitro* susceptibility of bacterial isolates from patients with microbial keratitis: A trend analysis of 8 years. *Indian Journal of Ophthalmology* **67**(1): 49–53. [doi:10.4103/ijo.IJO_500_18]

43. Begum, N. N., Al-Khattaf, A. S., Al-Mansouri, S. M., Yeboah, E. A. and Kambal, A.-M. M. 2006. A study of bacterial isolates from corneal specimens and their antibiotic resistance profile. *Saudi Medical Journal* **27**(1): 41–45.
44. Yilmaz, S., Ozturk, I. and Maden, A. 2007. Microbial keratitis in West Anatolia, Turkey: A retrospective review. *International Ophthalmology* **27**(4): 261–268. [doi:10.1007/s10792-007-9069-2]
45. Tuft, S. J. and Matheson, M. 2002. *In vitro* antibiotic resistance in bacterial keratitis in London. *British Journal of Ophthalmology* **84**(7): 687–691. [doi:10.1136/bjo.84.7.687]
46. Leibovitch, I., Lai, T. F., Senarath, L., Hsuan, J. and Selva, D. 2005. Infectious keratitis in South Australia: emerging resistance to cephazolin. *European Journal of Ophthalmology* **15**(1): 23–26.
47. Watson, S., Cabrera-Aguas, M., Khoo, P., Pratama, R., Gatus, B. J., Gulholm, T., El-Nasser, J. and Lahra, M. M. 2019. Keratitis antimicrobial resistance surveillance program, Sydney, Australia: 2016 Annual Report. *Clinical and Experimental Ophthalmology* **47**(1): 20–25. [doi:10.1111/ceo.13364]
48. Hall, R. C. and McKellar, M. J. 2004. Bacterial keratitis in Christchurch, New Zealand, 1997-2001. *Clinical and Experimental Ophthalmology* **32**(5): 478–481. [doi:10.1111/j.1442-9071.2004.00867.x]
49. Rajpal, K., Hall, R., Long, H. and Wells, A. 2007. Five-year experience of corneal scrapes at Wellington Eye Department, New Zealand. *The New Zealand Medical Journal* **120**(1260)
50. Fong, C.-F., Tseng, C.-H., Hu, F.-R., Wang, I.-J., Chen, W.-L. and Hou, Y.-C. 2004. Clinical characteristics of microbial keratitis in a university hospital in Taiwan. *American Journal of Ophthalmology* **137**(2): 329–336. [doi:10.1016/j.ajo.2003.09.001]
51. Amer Awan, M., Reeks, G., Rahman, M. Q., Butcher, I. and Ramaesh, K. 2010. The patterns of *in vitro* antimicrobial susceptibility and resistance of bacterial keratitis isolates in Glasgow, United Kingdom. *Clinical and Experimental Optometry* **93**(5): 354–359. [doi:10.1111/j.1444-0938.2010.00511.x]
52. Shalchi, Z., Gurbaxani, A., Baker, M. and Nash, J. 2011. Antibiotic resistance in microbial keratitis: Ten-year experience of corneal scrapes in the United Kingdom. *Ophthalmology* **118**(11): 2161–2165. [doi:10.1016/j.ophtha.2011.04.021]
53. Shaikh, F., Lohano, M. K. and Memon, I. 2013. Pattern of microbes associated to keratitis in patients presenting at Liaquat University Hospital. *Journal of the Liaquat University of Medical and Health Sciences* **12**(3): 145–150.
54. Hong, J., Xu, J., Hua, J. and Sun, X. 2013. Bacterial keratitis in Shanghai. *Ophthalmology* **120**(3): 647. [doi:10.1016/j.ophtha.2012.10.038]
55. Hsiao, C.-H., Sun, C.-C., Yeh, L.-K., Ma, D. H. K., Chen, P. Y. F., Lin, H.-C., Tan, H.-Y., Chen, H.-C., Chen, S.-Y. and Huang, Y.-C. 2016. Shifting trends in bacterial keratitis in Taiwan: A 10-year review in a tertiary-care hospital. *Cornea* **35**(3): 313–317. [doi:10.1097/ICO.0000000000000734]
56. Goldstein, M. H., Kowalski, R. P. and Gordon, Y. J. 1999. Emerging fluoroquinolone resistance in bacterial keratitis: A 5-year review. *Ophthalmology* **106**(7): 1313–1318.

57. Lichtinger, A., Yeung, S. N., Kim, P., Amiran, M. D., Iovieno, A., Elbaz, U., Ku, J. Y. F., Wolff, R., Rootman, D. S. and Slomovic, A. R. 2012. Shifting trends in bacterial keratitis in Toronto: An 11-year review. *Ophthalmology* **119**(9): 1785–1790. [doi:10.1016/j.optha.2012.03.031]
58. Green, M., Apel, A. and Stapleton, F. 2008. Risk factors and causative organisms in microbial keratitis. *Cornea* **27**(1): 22–27. [doi:10.1097/ICO.0b013e318156caf2]
59. Al-Dhaheri, H. S., Al-Tamimi, M. D., Khandekar, R. B., Khan, M. and Stone, D. U. 2016. Ocular pathogens and antibiotic sensitivity in bacterial keratitis isolates at King Khaled Eye Specialist Hospital, 2011 to 2014. *Cornea* **35**(6): 789–794. [doi:10.1097/ICO.0000000000000844]
60. Aung, T. and Chang, T. K. 1998. Nosocomial *Klebsiella pneumoniae* conjunctivitis resulting in infectious keratitis and bilateral corneal perforation. *Cornea* **17**(5): 558–561.
61. Pinna, A., Sechi, L. A., Zanetti, S. and Carta, F. 2005. Detection of virulence factors in a corneal isolate of *Klebsiella pneumoniae*. *Ophthalmology* **112**(5): 883–887. [doi:10.1016/j.optha.2004.12.024]
62. Kaliamurthy, J., Kalavathy, C. M., Parmar, P., Jesudasan, C. A. N. and Thomas, P. A. 2013. Spectrum of bacterial keratitis at a tertiary eye care centre in India. *BioMed Research International* : 181564. [doi:10.1155/2013/181564]
63. Järvinen, K., Järvinen, T. and Urtti, A. 1995. Ocular absorption following topical delivery. *Advanced Drug Delivery Reviews* **16**(1): 3–19. [doi:10.1016/0169-409X(95)00010-5]
64. Hooper, D. C. 2001. Mechanisms of action of antimicrobials: Focus on fluoroquinolones. *Clinical Infectious Diseases* **32**(Suppl 1): S9–S15. [doi:10.1086/319370]
65. Brook, I. 2016. Spectrum and treatment of anaerobic infections. *Journal of Infection and Chemotherapy* **22**(1): 1–13. [doi:10.1016/j.jiac.2015.10.010]
66. Gustaferra, C. A. and Steckelberg, J. M. 1991. Cephalosporin antimicrobial agents and related compounds. *Mayo Clinic Proceedings* **66**(10): 1064–1073. [doi:10.1016/S0025-6196(12)61731-5]
67. Jeng, B. H. and McLeod, S. D. 2003. Microbial keratitis. *British Journal of Ophthalmology* **87**(7): 805–806.
68. Oldenburg, C. E., Lalitha, P., Srinivasan, M., Rajaraman, R., Ravindran, M., Mascarenhas, J., Borkar, D. S., Ray, K. J., Zegans, M. E., McLeod, S. D., Porco, T. C., Lietman, T. M. and Acharya, N. R. 2013. Emerging moxifloxacin resistance in *Pseudomonas aeruginosa* keratitis isolates in South India. *Ophthalmic Epidemiology* **20**(3): 155–158. [doi:10.3109/09286586.2013.790978]
69. Garg, P., Sharma, S. and Rao, G. N. 1999. Ciprofloxacin-resistant *Pseudomonas* keratitis. *Ophthalmology* **106**(7): 1319–1323. [doi:10.1016/S0140-6736(85)91862-8]
70. Bertino Jr., J. S. 2009. Impact of antibiotic resistance in the management of ocular infections: The role of current and future antibiotics. *Clinical Ophthalmology* **3**(1): 507–521.
71. Olaitan, A. O., Morand, S. and Rolain, J.-M. 2014. Mechanisms of polymyxin resistance: Acquired and intrinsic resistance in bacteria. *Frontiers in Microbiology* **5**: Article 643. [doi:10.3389/fmicb.2014.00643]
72. Lacey, R. W. 1975. Antibiotic resistance plasmids of *Staphylococcus aureus* and their clinical importance. *Bacteriological reviews* **39**(1): 1–32.

73. Collignon, P. and McEwen, S. 2019. One Health - Its importance in helping to better control antimicrobial resistance. *Tropical Medicine and Infectious Disease* **4**(22) [doi:10.3390/tropicalmed4010022]
74. Peng, M. Y., Cevallos, V., McLeod, S. D., Lietman, T. M. and Rose-Nussbaumer, J. 2018. Bacterial keratitis: Isolated organisms and antibiotic resistance patterns in San Francisco. *Cornea* **37**(1): 84–87. [doi:10.1097/ICO.0000000000001417]
75. Pachigolla, G., Blomquist, P. and Cavanagh, H. D. 2007. Microbial keratitis pathogens and antibiotic susceptibilities: A 5-year review of cases at an urban county hospital in north Texas. *Eye and Contact Lens* **33**(1): 45–49. [doi:10.1097/01.icl.0000234002.88643.d0]
76. Song, A., McCulley, T. J., Lam, B. L., Feuer, W. J., Miller, D. and Alfonso, E. C. 2001. *Pseudomonas aeruginosa* *in vitro* corneal isolate sensitivity to ofloxacin, ciprofloxacin, and trovafloxacin: a comparative study. *American Journal of Ophthalmology* **131**(6): 795–796. [doi:10.1016/S0002-9394(00)00896-5]
77. Miller, D. and Alfonso, E. C. 2004. Comparative *in vitro* activity of levofloxacin, ofloxacin, and ciprofloxacin against ocular streptococcal isolates. *Cornea* **23**(3): 289–293.
78. Ubani, U. A. 2009. Bacteriology of external ocular infections in Aba, South Eastern Nigeria. *Clinical and Experimental Optometry* **92**(6): 482–489. [doi:10.1111/j.1444-0938.2009.00425.x]
79. Mohammad, A.-S. 2012. Etiology and antibacterial susceptibility pattern of bacterial ocular infections in a children hospital in North Jordan (2005-2009). *Biomedical and Pharmacology Journal* **5**(1): 25–31. [doi:10.13005/bpj/316]
80. Manikandan, P., Bhaskar, M., Revathy, R., John, R. K., Narendran, K. and Narendran, V. 2005. Speciation of coagulase-negative *Staphylococcus* causing bacterial keratitis. *Indian Journal of Medical Sciences* **53**(1): 59–60.
81. Reddy, A. K., Garg, P., Alam, M. R., Gopinathan, U., Sharma, S. and Krishnaiah, S. 2010. Comparison of *in vitro* susceptibilities of gram-positive cocci isolated from ocular infections against the second and fourth generation quinolones at a tertiary eye care centre in South India. *Eye* **24**(1): 170–174. [doi:10.1038/eye.2009.29]
82. Hong, J., Chen, J., Sun, X., Deng, S. X., Chen, L., Gong, L., Cao, W., Yu, X. and Xu, J. 2012. Paediatric bacterial keratitis cases in Shanghai: Microbiological profile, antibiotic susceptibility and visual outcomes. *Eye* **26**(12): 1571–1578. [doi:10.1038/eye.2012.210]
83. Butler, T. K. H., Spencer, N. A., Chan, C. C. K., Gilhotra, J. S. and McClellan, K. 2005. Infective keratitis in older patients: A 4 year review, 1998-2002. *British Journal of Ophthalmology* **89**(5): 591–596. [doi:10.1136/bjo.2004.049072]
84. Ly, C. N., Pham, J. N., Badenoch, P. R., Bell, S. M., Hawkins, G., Rafferty, D. L. and McClellan, K. A. 2006. Bacteria commonly isolated from keratitis specimens retain antibiotic susceptibility to fluoroquinolones and gentamicin plus cephalothin. *Clinical and Experimental Ophthalmology* **34**(1): 44–50. [doi:10.1111/j.1442-9071.2006.01143.x]
85. Marasini, S., Swift, S., Dean, S. J., Ormonde, S. E. and Craig, J. P. 2016. Spectrum and sensitivity of bacterial keratitis isolates in Auckland. *Journal of Ophthalmology* : 3769341. [doi:10.1155/2016/3769341]

86. Lalitha, P., Manoharan, G., Karpagam, R., Prajna, N. V., Srinivasan, M., Mascarenhas, J., Das, M., Porco, T. C., Lietman, T. M., Cevallos, V. and Keenan, J. D. 2017. Trends in antibiotic resistance in bacterial keratitis isolates from South India. *British Journal of Ophthalmology* **101**(2): 108–113. [doi:10.1136/bjophthalmol-2016-308487]
87. Iihara, H., Suzuki, T., Kawamura, Y., Ohkusu, K., Inoue, Y., Zhang, W., Shah, M. M., Katagiri, Y., Ohashi, Y. and Ezaki, T. 2006. Emerging multiple mutations and high-level fluoroquinolone resistance in methicillin-resistant *Staphylococcus aureus* isolated from ocular infections. *Diagnostic Microbiology and Infectious Disease* **56**(3): 297–303. [doi:10.1016/j.diagmicrobio.2006.04.017]
88. Samarawickrama, C., Chan, E. and Daniell, M. 2015. Rising fluoroquinolone resistance rates in corneal isolates: Implications for the wider use of antibiotics within the community. *Healthcare Infection* **20**(4): 128–133. [doi:10.1071/HI15014]
89. Yeh, D. L., Stinnett, S. S. and Afshari, N. A. 2006. Analysis of bacterial cultures in infectious keratitis, 1997 to 2004. *American Journal of Ophthalmology* **142**(6): 1066–1068. [doi:10.1016/j.ajo.2006.06.056]
90. Orlans, H. O., Hornby, S. J. and Bowler, I. C. J. W. 2011. *In vitro* antibiotic susceptibility patterns of bacterial keratitis isolates in Oxford, UK: A 10-year review. *Eye* **25**(4): 489–493. [doi:10.1038/eye.2010.231]
91. Tan, S. Z., Walkden, A., Au, L., Fullwood, C., Hamilton, A., Qamruddin, A., Armstrong, M., Brahma, A. K. and Carley, F. 2017. Twelve-year analysis of microbial keratitis trends at a UK tertiary hospital. *Eye* **31**(8): 1229–1236. [doi:10.1038/eye.2017.55]
92. Bharathi, M. J., Ramakrishnan, R., Ramesh, S. and Murugan, N. 2012. Extended-spectrum beta-lactamase-mediated resistance among bacterial isolates recovered from ocular infections. *Ophthalmic Research* **47**(1): 52–56. [doi:10.1159/000322807]
93. Rameshkumar, G., Ramakrishnan, R., Shivkumar, C., Meenakshi, R., Anitha, V., Reddy, Y. C. V. and Maneksha, V. 2016. Prevalence and antibacterial resistance patterns of extended-spectrum beta-lactamase producing gram-negative bacteria isolated from ocular infections. *Indian Journal of Ophthalmology* **64**(4): 303–311. [doi:10.4103/0301-4738.182943]
94. Hutnik, C., Mohammad, H. and Mohammad-Shahi, M. 2010. Bacterial conjunctivitis. *Clinical Ophthalmology* **4**(1): 1451–1457. [doi:10.2147/OPHTH.S10162]
95. Vazirani, J., Wurity, S. and Ali, M. H. 2015. Multidrug-resistant *Pseudomonas aeruginosa* keratitis: Risk factors, clinical characteristics, and outcomes. *Ophthalmology* **122**(10): 2110–2114. [doi:10.1016/j.ophtha.2015.06.007]
96. Tabbara, K. F., Antonios, S. and Alvarez, H. 1989. Effects of fusidic acid on staphylococcal keratitis. *The British Journal of Ophthalmology* **73**(2): 136–139. [doi:10.1136/bjo.73.2.136]
97. Wong, E. S., Chow, C. W. Y., Luk, W. K., Fung, K. S. C. and Li, K. K. W. 2017. A 10-year review of ocular methicillin-resistant *Staphylococcus aureus* infections: Epidemiology, clinical features, and treatment. *Cornea* **36**(1): 92–97. [doi:10.1097/ICO.0000000000001048]

98. Wu, P.-P., He, H., Hong, W. D., Wu, T.-R., Huang, G.-Y., Zhong, Y.-Y., Tu, B.-R., Gao, M., Zhou, J., Zhao, S.-Q., Li, D.-L., Xu, X.-T., Sheng, Z.-J., Ward, S. A., O'Neill, P. M. and Zhang, K. 2018. The biological evaluation of fusidic acid and its hydrogenation derivative as antimicrobial and anti-inflammatory agents. *Infection and Drug Resistance* **11**: 1945–1957. [doi:10.2147/idr.s176390]
99. Godtfredsen, W. O., Jahnsen, S., Lorck, H., Roholt, K. and Tybring, L. 1962. Fusidic acid: A new antibiotic. *Nature* **193**(4819): 987. [doi:10.1038/193987a0]
100. Godtfredsen, W. O., von Daehne, W., Vangedal, S., Marquet, A., Arigoni, D. and Melera, A. 1965. The stereochemistry of fusidic acid. *Tetrahedron* **21**: 3505–3530. [doi:10.1007/BF02171087]
101. Barber, M. and Waterworth, P. M. 1962. Antibacterial activity *in vitro* of fucidin. *The Lancet* **1**(7236): 931–932.
102. Taylor, G. and Bloor, K. 1962. Antistaphylococcal activity of fucidin. *The Lancet* **279**(7236): 935–937. [doi:10.1016/S0140-6736(62)91972-4]
103. Newman, R. L., Bhat, K. M., Hackney, R., Robinson, C. and Stewart, G. T. 1962. Fusidic acid: Laboratory and clinical assessment. *British Medical Journal* **2**(5320): 1645–1647.
104. Lowbury, E. J. L., Cason, J. S., Jackson, D. M. and Miller, R. W. S. 1962. Fucidin for staphylococcal infection of burns. *The Lancet* **2**(7254): 478–480.
105. Scowen, E. F. and Garrod, L. P. 1962. A case of Staphylococcal septicaemia treated with penicillin and fucidin. *The Lancet* **1**(7236): 933–935.
106. Porter, I. A. and Wilson, J. S. P. 1963. Staphylococcal infections treated with fusidic acid in nurses. *The Lancet* **282**(7309): 658–659. [doi:10.1016/S0140-6736(63)90453-7]
107. Matsaniotis, N., Messaritakis, J. and Anagnostakis, D. 1967. Fusidic acid for staphylococcal infections in children. *British Medical Journal* **1**(5539): 564.
108. Jackson, N. 1971. Fusidic acid treatment in psoriasis. *The Lancet* **2**(7726): 712.
109. Cronberg, S., Castor, B. and Thorén, A. 1984. Fusidic acid for the treatment of antibiotic-associated colitis induced by *Clostridium difficile*. *Infection* **12**(4): 276–279.
110. Dirdal, M. 1987. Fucithalamic in acute conjunctivitis: Open, randomized comparison of fusidic acid, chloramphenicol and framycetin eye drops. *Acta Ophthalmologica* **65**(2): 129–133.
111. van Bijsterveld, O. P., el Batawi, Y., Sobhi, F. S. and Nasser, M. W. 1987. Fusidic acid in infections of the external eye. *Infection* **15**(1): 16–19. [doi:10.1007/BF01646112]
112. Verbist, L. 1990. The antimicrobial activity of fusidic acid. *Journal of Antimicrobial Chemotherapy* **25**(Suppl B): 1–5.
113. Franzblau, S. G., Chan, G. P., Garcia-Ignacio, B. G., Chavez, V. E., Livelio, J. B., Jimenez, C. L., Parrilla, M. L. R., Calvo, R. F., Williams, D. L. and Gillis, T. P. 1994. Clinical trial of fusidic acid for lepromatous leprosy. *Antimicrobial Agents and Chemotherapy* **38**(7): 1651–1654. [doi:10.1128/AAC.38.7.1651]
114. Wullt, M. and Odenholt, I. 2004. A double-blind randomized controlled trial of fusidic acid and metronidazole for treatment of an initial episode of *Clostridium difficile*-associated diarrhoea. *Journal of Antimicrobial Chemotherapy* **54**(1): 211–216. [doi:10.1093/jac/dkh278]

115. Doughty, M. J. and Dutton, G. N. 2006. Fusidic acid viscous eyedrops - an evaluation of pharmacodynamics, pharmacokinetics and clinical use for UK optometrists. *Ophthalmic and Physiological Optics* **26**(4): 343–361. [doi:10.1111/j.1475-1313.2006.00416.x]
116. Jones, R. N., Biedenbach, D. J., Roblin, P. M., Kohlhoff, S. A. and Hammerschlag, M. R. 2010. Update on fusidic acid (CEM-102) tested against *Neisseria gonorrhoeae* and *Chlamydia trachomatis*. *Antimicrobial Agents and Chemotherapy* **54**(10): 4518–4519. [doi:10.1128/AAC.00235-10]
117. Still, J. G., Clark, K., Degenhardt, T. P., Scott, D., Fernandes, P. and Gutierrez, M. J. 2011. Pharmacokinetics and safety of single, multiple, and loading doses of fusidic acid in healthy subjects. *Clinical Infectious Diseases* **52**(Suppl 7): S504–S512. [doi:10.1093/cid/cir174]
118. Craft, J. C., Moriarty, S. R., Clark, K., Scott, D., Degenhardt, T. P., Still, J. G., Corey, G. R., Das, A. and Fernandes, P. 2011. A randomized, double-blind phase 2 study comparing the efficacy and safety of an oral fusidic acid loading-dose regimen to oral linezolid for the treatment of acute bacterial skin and skin structure infections. *Clinical Infectious Diseases* **52**: S520–S526. [doi:10.1093/cid/cir167]
119. Phee, L. M., Betts, J. W., Bharathan, B. and Wareham, D. W. 2015. Colistin and fusidic acid: a novel potent synergistic combination for the treatment of multidrug-resistant *Acinetobacter baumannii* infections. *Antimicrobial Agents and Chemotherapy* **59**(8): 4544–4550. [doi:10.1128/AAC.00753-15]
120. Lee, D. H., Kim, D. Y., Yoon, S. Y., Park, H. S., Yoon, H.-S. and Cho, S. 2015. Retrospective clinical trial of fusidic acid versus petrolatum in the postprocedure care of clean dermatologic procedures. *Annals of Dermatology* **27**(1): 15–20. [doi:10.5021/ad.2015.27.1.15]
121. Pushkin, R., Iglesias-Ussel, M. D., Keedy, K., MacLauchlin, C., Mould, D. R., Berkowitz, R., Kreuzer, S., Darouiche, R., Oldach, D. and Fernandes, P. 2016. A randomized study evaluating oral fusidic acid (CEM-102) in combination with oral rifampin compared with standard-of-care antibiotics for treatment of prosthetic joint infections: A newly identified drug-drug interaction. *Clinical Infectious Diseases* **63**(12): 1599–1604. [doi:10.1093/cid/ciw665]
122. Kiefer, A., Bogdan, C. and Melichar, V. O. 2018. Successful eradication of newly acquired MRSA in six of seven patients with cystic fibrosis applying a short-term local and systemic antibiotic scheme. *BMC Pulmonary Medicine* **18**: 20. [doi:10.1186/s12890-018-0588-6]
123. Portier, H. 1990. A multicentre, open, clinical trial of a new intravenous formulation of fusidic acid in severe staphylococcal infections. *Journal of Antimicrobial Chemotherapy* **25**(Suppl B): 39–44. [doi:10.1093/jac/25.suppl_B.39]
124. Burke, S. L. and Rose, W. E. 2014. New pharmacological treatments for methicillin-resistant *Staphylococcus aureus* infections. *Expert Opinion on Pharmacotherapy* **15**(4): 483–491. [doi:10.1517/14656566.2014.876991]
125. Farrell, D. J., Mendes, R. E., Castanheira, M. and Jones, R. N. 2016. Activity of fusidic acid tested against Staphylococci isolated from patients in U.S. Medical Centers in 2014. *Antimicrobial Agents and Chemotherapy* **60**(6): 3827–3831. [doi:10.1128/AAC.00238-16.Address]
126. Siala, W., Rodriguez-Villalobos, H., Fernandes, P., Tulkens, P. M. and van Bambeke, F. 2018. Activities of combinations of antistaphylococcal antibiotics with fusidic acid against Staphylococcal biofilms in *in vitro* static and dynamic models. *Antimicrobial Agents and Chemotherapy* **62**(7): e00598-18.

127. Pape, T., Wintermeyer, W. and Rodnina, M. V. 1998. Complete kinetic mechanism of elongation factor Tu-dependent binding of aminoacyl-tRNA to the A site of the *E. coli* ribosome. *The EMBO Journal* **17**(24): 7490–7497.
128. Paulsen, H. and Wintermeyer, W. 1986. tRNA topography during translocation: steady-state and kinetic fluorescence energy-transfer studies. *Biochemistry* **25**(10): 2749–2756.
129. Moazed, D. and Noller, H. F. 1989. Intermediate states in the movement of transfer RNA in the ribosome. *Nature* **342**(6246): 142–148. [doi:10.1038/342142a0]
130. Frank, J. and Agrawal, R. K. 2000. A ratchet-like inter-subunit reorganization of the ribosome during translocation. *Nature* **406**(6793): 318–322. [doi:10.1038/35018597]
131. Ermolenko, D. N., Spiegel, P. C., Majumdar, Z. K., Hickerson, R. P., Clegg, R. M. and Noller, H. F. 2007. The antibiotic viomycin traps the ribosome in an intermediate state of translocation. *Nature Structural & Molecular Biology* **14**(6): 493–497. [doi:10.1038/nsmb1243]
132. Ramrath, D. J. F., Lancaster, L., Sprink, T., Mielke, T., Loerke, J., Noller, H. F. and Spahn, C. M. T. 2013. Visualization of two transfer RNAs trapped in transit during elongation factor G-mediated translocation. *Proceedings of the National Academy of Sciences* **110**(52): 20964–20969. [doi:10.1073/pnas.1320387110]
133. Agrawal, R. K., Penczek, P., Grassucci, R. A. and Frank, J. 1998. Visualization of elongation factor G on the *Escherichia coli* 70S ribosome: The mechanism of translocation. *Proceedings of the National Academy of Sciences* **95**(11): 6134–6138. [doi:10.1073/pnas.95.11.6134]
134. Rodnina, M. V., Savelsbergh, A., Katunin, V. I. and Wintermeyer, W. 1997. Hydrolysis of GTP by elongation factor G drives tRNA movement on the ribosome. *Nature* **385**(6611): 37–41. [doi:10.1038/385037a0]
135. Spirin, A. S. 1984. Testing the classical two-tRNA-site model for the ribosomal elongation cycle. *FEBS Letters* **165**(2): 280–284. [doi:10.1016/0014-5793(84)80186-6]
136. Semenov, Y. P., Rodnina, M. V. and Wintermeyer, W. 1996. The ‘allosteric three-site model’ of elongation cannot be confirmed in a well-defined ribosome system from *Escherichia coli*. *Proceedings of the National Academy of Sciences* **93**(22): 12183–12188. [doi:10.1073/pnas.93.22.12183]
137. Borg, A., Holm, M., Shiroyama, I., Hauryliuk, V., Pavlov, M., Sanyal, S. and Ehrenberg, M. 2015. Fusidic acid targets elongation factor G in several stages of translocation on the bacterial ribosome. *The Journal of Biological Chemistry* **290**(6): 3440–3454. [doi:10.1074/jbc.M114.611608]
138. Gao, Y.-G., Selmer, M., Dunham, C. M., Weixlbaumer, A., Kelley, A. C. and Ramakrishnan, V. 2009. The structure of the ribosome with elongation factor G trapped in the post-translocational state. *Science* **326**(5953): 694–699. [doi:10.1126/science.1179709]
139. Richman, N. and Bodley, J. W. 1972. Ribosomes cannot interact simultaneously with elongation factors EF-Tu and EF-G. *Proceedings of the National Academy of Sciences* **69**(3): 686–689.
140. Hilson, G. R. F. 1962. *In vitro* studies of a new antibiotic (fucidin). *The Lancet* **1**(7236): 932–933.

141. Nikaido, H. 1998. The role of outer membrane and efflux pumps in the resistance of gram-negative bacteria. Can we improve drug access? *Drug Resistance Updates* **1**(2): 93–98.
142. Li, X.-Z., Plésiat, P. and Nikaido, H. 2015. The challenge of efflux-mediated antibiotic resistance in gram-negative bacteria. *Clinical Microbiology Reviews* **28**(2): 337–418. [doi:10.1128/CMR.00117-14]
143. Nikaido, H. 1998. Multiple antibiotic resistance and efflux. *Current Opinion in Microbiology* **1**(5): 516–523. [doi:10.1016/S1369-5274(98)80083-0]
144. Zgurskaya, H. I., López, C. A. and Gnanakaran, S. 2015. Permeability barrier of gram-negative cell envelopes and approaches to bypass it. *ACS Infectious Diseases* **1**(11): 512–522. [doi:10.1021/acsinfecdis.5b00097]
145. Nikaido, H. and Pagès, J.-M. 2012. Broad-specificity efflux pumps and their role in multidrug resistance of Gram-negative bacteria. *FEMS Microbiology Reviews* **36**(2): 340–363. [doi:10.1111/j.1574-6976.2011.00290.x]
146. Sikkema, J., de Bont, J. A. M. and Poolman, B. 1994. Interactions of cyclic hydrocarbons with biological membranes. *Journal of Biological Chemistry* **269**(11): 8022–8028.
147. Delcour, A. H. 2009. Outer membrane permeability and antibiotic resistance. *Biochimica et Biophysica Acta* **1794**(5): 808–816. [doi:10.1016/j.bbapap.2008.11.005]
148. Plésiat, P. and Nikaido, H. 1992. Outer membranes of Gram-negative bacteria are permeable to steroid probes. *Molecular Microbiology* **6**(10): 1323–1333.
149. Krishnamoorthy, G., Leus, I. V., Weeks, J. W., Wolloscheck, D., Rybenkov, V. V and Zgurskaya, H. I. 2017. Synergy between active efflux and outer membrane diffusion defines rules of antibiotic permeation into gram-negative bacteria. *mBio* **8**(5): e01172-17.
150. Sulavik, M. C., Houseweart, C., Cramer, C., Jiwani, N., Murgolo, N., Greene, J., DiDomenico, B., Shaw, K. J., Miller, G. H., Hare, R. and Shimer, G. 2001. Antibiotic susceptibility profiles of *Escherichia coli* strains lacking multidrug efflux pump genes. *Antimicrobial Agents and Chemotherapy* **45**(4): 1126–1136. [doi:10.1128/AAC.45.4.1126]
151. Anes, J., McCusker, M. P., Fanning, S. and Martins, M. 2015. The ins and outs of RND efflux pumps in *Escherichia coli*. *Frontiers in Microbiology* **6**: 587. [doi:10.3389/fmicb.2015.00587]
152. Du, D., Wang, Z., James, N. R., Voss, J. E., Klimont, E., Ohene-Agyei, T., Venter, H., Chiu, W. and Luisi, B. F. 2014. Structure of the AcrAB-TolC multidrug efflux pump. *Nature* **509**(7501): 512–515. [doi:10.1038/nature13205]
153. Wang, Z., Fan, G., Hryc, C. F., Blaza, J. N., Serysheva, I. I., Schmid, M. F., Chiu, W., Luisi, B. F. and Du, D. 2017. An allosteric transport mechanism for the AcrAB-TolC multidrug efflux pump. *eLife* **6**: e24905. [doi:10.7554/eLife.24905]
154. Du, D., van Veen, H. W. and Luisi, B. F. 2015. Assembly and operation of bacterial tripartite multidrug efflux pumps. *Trends in Microbiology* **23**(5): 311–319. [doi:10.1016/j.tim.2015.01.010]
155. Hobbs, E. C., Yin, X., Paul, B. J., Astarita, J. L. and Storz, G. 2012. Conserved small protein associates with the multidrug efflux pump AcrB and differentially affects antibiotic resistance. *Proceedings of the National Academy of Sciences* **109**(41): 16696–16701. [doi:10.1073/pnas.1210093109]

156. Nikaido, H. 2011. Structure and mechanism of RND-type multidrug efflux pumps. in *Advances in Enzymology and Related Areas of Molecular Biology* (ed. Toone, E. J.) (77): 1–60.
157. Veiga, D. F. T., Vicente, F. F. R., Nicolás, M. F. and Vasconcelos, A. T. R. 2008. Predicting transcriptional regulatory interactions with artificial neural networks applied to *E. coli* multidrug resistance efflux pumps. *BMC microbiology* **8**(101) [doi:10.1186/1471-2180-8-101]
158. Lennen, R. M., Politz, M. G., Kruziki, M. A. and Pfleger, B. F. 2013. Identification of transport proteins involved in free fatty acid efflux in *Escherichia coli*. *Journal of Bacteriology* **195**(1): 135–144. [doi:10.1128/JB.01477-12]
159. Tsukagoshi, N. and Aono, R. 2000. Entry into and release of solvents by *Escherichia coli* in an organic-aqueous two-liquid-phase system and substrate specificity of the AcrAB-TolC solvent-extruding pump. *Journal of Bacteriology* **182**(17): 4803–4810. [doi:10.1128/JB.182.17.4803-4810.2000]
160. Damier-Piolle, L., Magnet, S., Brémont, S., Lambert, T. and Courvalin, P. 2008. AdelJK, a resistance-nodulation-cell division pump effluxing multiple antibiotics in *Acinetobacter baumannii*. *Antimicrobial Agents and Chemotherapy* **52**(2): 557–562. [doi:10.1128/aac.00732-07]
161. Kim, B. H. and Gadd, G. M. 2008. *Bacterial Physiology and Metabolism*.
162. El-Zimaity, D., Kearns, A. M., Dawson, S. J., Price, S. and Harrison, G. A. J. 2004. Survey, characterization and susceptibility to fusidic acid of *Staphylococcus aureus* in the Carmarthen area. *Journal of Antimicrobial Chemotherapy* **54**(2): 441–446. [doi:10.1093/jac/dkh373]
163. Needle, J. J., Petchey, R. and Lawrenson, J. G. 2008. A survey of the scope of therapeutic practice by UK optometrists and their attitudes to an extended prescribing role. *Ophthalmic and Physiological Optics* **28**(3): 193–203. [doi:10.1111/j.1475-1313.2008.00551.x]
164. Ashburn, T. T. and Thor, K. B. 2004. Drug repositioning: Identifying and developing new uses for existing drugs. *Nature reviews. Drug discovery* **3**(8): 673–683. [doi:10.1038/nrd1468]
165. Jayasundara, K., Hollis, A., Krahn, M., Mamdani, M., Hoch, J. S. and Grootendorst, P. 2019. Estimating the clinical cost of drug development for orphan versus non-orphan drugs. *Orphanet Journal of Rare Diseases* **14**(1): 1–10. [doi:10.1186/s13023-018-0990-4]
166. Ciociola, A. A., Cohen, L. B. and Kulkarni, P. 2014. How drugs are developed and approved by the FDA: Current process and future directions. *American Journal of Gastroenterology* **109**(5): 620–623. [doi:10.1038/ajg.2013.407]
167. Rang, H. P. 2006. *Drug Discovery and Development: Technology in Transition*.
168. Breckenridge, A. and Woods, K. 2005. Medicines regulation and the pharmaceutical industry. *British Medical Journal* **331**(7520): 834–836. [doi:10.1136/bmj.331.7520.834]
169. Ventola, C. L. 2015. The antibiotic resistance crisis, Part 1: causes and threats. *Pharmacy and Therapeutics* **40**(4): 277–283.
170. Kinch, M. S. and Hoyer, D. 2015. A history of drug development in four acts. *Drug Discovery Today* **20**(10): 1163–1168. [doi:10.1016/j.drudis.2015.04.003]
171. Winship, K., Hepburn, D. and Lawson, D. 1992. The review of medicines in the United Kingdom. *British Journal of Clinical Pharmacology* **33**(6): 583–587. [doi:10.1111/j.1365-2125.1992.tb04086.x]

172. Fleming, A. 1929. On the antibacterial action of cultures of a penicillium, with special reference to their use in the isolation of *B. influenzae*. *The British Journal of Experimental Pathology* **10**(3): 226–236. [doi:10.1038/146837a0]
173. Chain, E., Florey, H. W., Gardner, A. D., Heatley, N. G., Jennings, M. a., Orr-Ewing, J. and Sanders, A. G. 1940. Penicillin as a chemotherapeutic agent. *The Lancet* **236**(6104): 226–228. [doi:10.1016/S0140-6736(01)08728-1]
174. Walsh, C. T. and Wright, G. 2005. Introduction: Antibiotic Resistance. *Chemical Reviews* **105**(2): 391–394. [doi:10.1021/cr030100y]
175. Armstrong, G. L., Conn, L. a. and Pinner, R. W. 1999. Trends in infectious disease mortality in the United States during the 20th century. *Journal of the American Medical Association* **281**(1): 61–66. [doi:10.1001/jama.281.1.61]
176. Rammelkamp, C. H. and Maxon, T. 1942. Resistance of *Staphylococcus aureus* to the action of penicillin. *Experimental Biology and Medicine* **51**(3): 386–389. [doi:10.3181/00379727-51-13986]
177. McKee, C. M. and Houck, C. L. 1943. Induced resistance to penicillin of cultures of staphylococci, pneumococci and streptococci. *Experimental Biology and Medicine* **53**(1): 33–34. [doi:10.3181/00379727-53-14172P]
178. Plough, H. H. 1945. Penicillin resistance of *Staphylococcus aureus* and its clinical implications. *American Journal of Clinical Pathology* **15**: 446–451.
179. Davies, J. & Davies, D. 2010. Origins and evolution of antibiotic resistance. *Microbiology and Molecular Biology Reviews* **74**(3): 417–433. [doi:10.1128/MMBR.00016]
180. Beović, B. 2006. The issue of antimicrobial resistance in human medicine. *International Journal of Food Microbiology* **112**(3): 280–287. [doi:10.1016/j.ijfoodmicro.2006.05.001]
181. Tängdén, T. and Giske, C. G. 2015. Global dissemination of extensively drug-resistant carbapenemase-producing *Enterobacteriaceae*: Clinical perspectives on detection, treatment and infection control. *Journal of Internal Medicine* **277**(5): 501–512. [doi:10.1111/joim.12342]
182. Howard, A., O'Donoghue, M., Feeney, A. and Sleator, R. D. 2012. *Acinetobacter baumannii*: An emerging opportunistic pathogen. *Virulence* **3**(3): 243–250. [doi:10.4161/viru.19700]
183. Gothi, D. and Joshi, J. M. 2011. Resistant TB: Newer drugs and community approach. *Recent Patents on Anti-Infective Drug Discovery* **6**(1): 27–37. [doi:10.2174/157489111794407859]
184. Toner, E., Adalja, A., Gronvall, G. K., Cicero, A. and Inglesby, T. V. 2015. Antimicrobial resistance is a global health emergency. *Health Security* **13**(3): 153–155. [doi:10.1089/hs.2014.0088]
185. Sommer, M. O. A., Munck, C., Toft-Kehler, R. V. and Andersson, D. I. 2017. Prediction of antibiotic resistance: Time for a new preclinical paradigm? *Nature Reviews Microbiology* **15**(11): 689–696. [doi:10.1038/nrmicro.2017.75]
186. Blanquart, F. 2019. Evolutionary epidemiology models to predict the dynamics of antibiotic resistance. *Evolutionary Applications* **12**(3): 365–383. [doi:10.1111/eva.12753]
187. Brooks, B. D. and Brooks, A. E. 2014. Therapeutic strategies to combat antibiotic resistance. *Advanced Drug Delivery Reviews* **78**: 14–27. [doi:10.1016/j.addr.2014.10.027]

188. Andersson, D. I. 2015. Improving predictions of the risk of resistance development against new and old antibiotics. *Clinical Microbiology and Infection* **21**(10): 894–898. [doi:10.1016/j.cmi.2015.05.012]
189. Spellberg, B., Powers, J. H., Brass, E. P., Miller, L. G. and Edwards, J. E. 2004. Trends in antimicrobial drug development: Implications for the future. *Clinical Infectious Diseases* **38**(9): 1279–1286. [doi:10.1086/420937]
190. Morgan, S., Grootendorst, P., Lexchin, J., Cunningham, C. and Greyson, D. 2011. The cost of drug development: A systematic review. *Health Policy* **100**(1): 4–17. [doi:10.1016/j.healthpol.2010.12.002]
191. Towse, A., Hoyle, C. K., Goodall, J., Hirsch, M., Mestre-Ferrandiz, J. and Rex, J. H. 2017. Time for a change in how new antibiotics are reimbursed: Development of an insurance framework for funding new antibiotics based on a policy of risk mitigation. *Health Policy* **121**(10): 1025–1030. [doi:10.1016/j.healthpol.2017.07.011]
192. Jackson, N., Czaplewski, L. and Piddock, L. J. V. 2018. Discovery and development of new antibacterial drugs: Learning from experience? *Journal of Antimicrobial Chemotherapy* **73**(6): 1452–1459. [doi:10.1093/jac/dky019]
193. Sciarretta, K., Røttingen, J.-A., Opalska, A., van Hengel, A. J. and Larsen, J. 2016. Economic incentives for antibacterial drug development: Literature review and considerations from the Transatlantic Task Force on Antimicrobial Resistance. *Clinical Infectious Diseases* **63**: 1470–1474. [doi:10.1093/cid/ciw593]
194. Daniel, G. W., Schneider, M., Lopez, M. H. and McClellan, M. B. 2018. Implementation of a Market Entry Reward within the United States. *Journal of Law, Medicine & Ethics* **46**(S1): 50–58. [doi:10.1177/1073110518782915]
195. Livermore, D. M. 2018. The 2018 Garrod Lecture: Preparing for the Black Swans of resistance. *Journal of Antimicrobial Chemotherapy* **73**: 2907–2915. [doi:10.1093/jac/dky265]
196. Chong, C. R. and Sullivan, D. J. 2007. New uses for old drugs. *Nature* **448**(7154): 645–646. [doi:10.1038/448645a]
197. Aronson, J. K. 2007. Old drugs - new uses. *British Journal of Clinical Pharmacology* **64**(5): 563–565. [doi:10.1111/j.1365-2125.2007.03058.x]
198. Savoia, D. 2016. New antimicrobial approaches: Reuse of old drugs. *Current Drug Targets* **17**(6): 731–738. [doi:10.2174/1389450116666150806124110]
199. Law, G. L., Tisoncik-Go, J., Korth, M. J. and Katze, M. G. 2013. Drug repurposing: a better approach for infectious disease drug discovery? *Current Opinion in Immunology* **25**(5): 588–592. [doi:10.1016/j.coi.2013.08.004]
200. Falagas, M. E. and Kopterides, P. 2007. Old antibiotics for infections in critically ill patients. *Current Opinion in Critical Care* **13**(5): 592–597. [doi:10.1097/MCC.0b013e32827851d7]
201. Bollenbach, T. 2015. Antimicrobial interactions: Mechanisms and implications for drug discovery and resistance evolution. *Current Opinion in Microbiology* **27**: 1–9. [doi:10.1016/j.mib.2015.05.008]
202. Cottarel, G. and Wierzbowski, J. 2007. Combination drugs, an emerging option for antibacterial therapy. *Trends in Biotechnology* **25**(12): 547–555. [doi:10.1016/j.tibtech.2007.09.004]
203. Torella, J. P., Chait, R. and Kishony, R. 2010. Optimal drug synergy in antimicrobial treatments. *PLoS Computational Biology* **6**(6): e1000796. [doi:10.1371/journal.pcbi.1000796]

204. Chait, R., Craney, A. and Kishony, R. 2007. Antibiotic interactions that select against resistance. *Nature* **446**: 668–671. [doi:10.1038/nature05685]
205. Csonka, G. W. and Knight, G. J. 1967. Therapeutic trial of trimethoprim as a potentiator of sulphonamides in gonorrhoea. *British Journal of Venereal Diseases* **43**(3): 161–165. [doi:10.1136/sti.43.3.161]
206. Reeves, D. S., Faiers, M. C., Pursell, R. E. and Brumfitt, W. 1969. Trimethoprim-sulphamethoxazole: Comparative study in urinary infection in hospital. *British Medical Journal* **1**(5643): 541–544. [doi:10.1136/bmj.1.5643.541]
207. Darrell, J. H., Garrod, L. P. and Waterworth, P. M. 1968. Trimethoprim: Laboratory and clinical studies. *Journal of Clinical Pathology* **21**(2): 202–209. [doi:10.1136/jcp.21.2.202]
208. Klugman, K. P., Capper, T. and Bryskier, A. 1996. *In vitro* susceptibility of penicillin-resistant *Streptococcus pneumoniae* to levofloxacin, selection of resistant mutants, and time-kill synergy studies of levofloxacin combined with vancomycin, teicoplanin, fusidic acid, and rifampin. *Antimicrobial Agents and Chemotherapy* **40**(12): 2802–2804.
209. Tagliaferri, T. L., Jansen, M. and Horz, H.-P. 2019. Fighting pathogenic bacteria on two fronts: Phages and antibiotics as combined strategy. *Frontiers in Cellular and Infection Microbiology* **9**: 22. [doi:10.3389/fcimb.2019.00022]
210. Howarth, T. T., Brown, A. G. and King, T. J. 1976. Clavulanic acid, a novel β -lactam isolated from *Streptomyces clavuligerus*; X-ray crystal structure analysis. *Journal of the Chemical Society, Chemical Communications* **7**: 266–267.
211. Reading, C. and Cole, M. 1977. Clavulanic acid: A beta-lactamase-inhibiting beta-lactam from *Streptomyces clavuligerus*. *Antimicrobial Agents and Chemotherapy* **11**(5): 852–857. [doi:10.1128/AAC.11.5.852.Updated]
212. Wise, R., Andrews, J. M. and Bedford, K. A. 1978. *In vitro* study of clavulanic acid in combination with penicillin, amoxycillin, and carbenicillin. *Antimicrobial Agents and Chemotherapy* **13**(3): 389–393. [doi:10.1128/AAC.13.3.389]
213. Leigh, D. A., Bradnock, K. and Marriner, J. M. 1981. Augmentin (amoxycillin and clavulanic acid) therapy in complicated infections due to β -lactamase producing bacteria. *Journal of Antimicrobial Chemotherapy* **7**(3): 229–236. [doi:10.1093/jac/7.3.229]
214. Iravani, A. and Richard, G. A. 1982. Treatment of urinary tract infections with a combination of amoxicillin and clavulanic acid. *Antimicrobial Agents and Chemotherapy* **22**(4): 672–677.
215. Zhanel, G. G., Lawrence, C. K., Adam, H., Schweizer, F., Zelenitsky, S., Zhanel, M., Lagacé-Wiens, P. R. S., Walkty, A., Denisuk, A., Golden, A., Gin, A. S., Hoban, D. J., Lynch, J. P. and Karlowsky, J. A. 2018. Imipenem-relebactam and meropenem-vaborbactam: Two novel carbapenem- β -lactamase inhibitor combinations. *Drugs* **78**(1): 65–98. [doi:10.1007/s40265-017-0851-9]
216. Liao, C.-H., Lee, N.-Y., Tang, H.-J., Shin-Jung, S., Lin, C.-F., Lu, P.-L., Wu, J.-J., Ko, W.-C., Lee, W.-S. and Hsueh, P.-R. 2019. Antimicrobial activities of ceftazidime-avibactam, ceftolozane-tazobactam, and other agents against *Escherichia coli*, *Klebsiella pneumoniae*, and *Pseudomonas aeruginosa* isolated from intensive care units in Taiwan: Results from the Surveillance of Multicenter Antimicrobial Resistance in Taiwan in 2016. *Infection and Drug Resistance* **12**: 545–552.
217. Zasloff, M. 2002. Antimicrobial peptides of multicellular organisms. *Nature* **415**(6870): 389–395. [doi:10.1038/415389a]

218. Paul, M., Carmeli, Y., Durante-Mangoni, E., Mouton, J. W., Tacconelli, E., Theuretzbacher, U., Mussini, C. and Leibovici, L. 2014. Combination therapy for carbapenem-resistant gram-negative bacteria. *Journal of Antimicrobial Chemotherapy* **69**(9): 2305–2309. [doi:10.1093/jac/dku168]
219. Feng, Q., Huang, Y., Chen, M., Li, G. and Chen, Y. 2014. Functional synergy of α -helical antimicrobial peptides and traditional antibiotics against gram-negative and gram-positive bacteria *in vitro* and *in vivo*. *European Journal of Clinical Microbiology & Infectious Diseases* **34**(1): 197–204. [doi:10.1007/s10096-014-2219-3]
220. Jammal, J., Zaknoon, F., Kaneti, G., Goldberg, K. and Mor, A. 2015. Sensitization of gram-negative bacteria to rifampin and OAK combinations. *Scientific Reports* **5**: 9216. [doi:10.1038/srep09216]
221. He, J., Starr, C. G. and Wimley, W. C. 2015. A lack of synergy between membrane-permeabilizing cationic antimicrobial peptides and conventional antibiotics. *Biochimica et Biophysica Acta* **1848**(1): 8–15. [doi:10.1016/j.bbamem.2014.09.010]
222. Hemaiswarya, S. and Doble, M. 2009. Synergistic interaction of eugenol with antibiotics against gram-negative bacteria. *Phytomedicine* **16**(11): 997–1005. [doi:10.1016/j.phymed.2009.04.006]
223. Zacchino, S. A., Butassi, E., Cordisco, E. and Svetaz, L. A. 2017. Hybrid combinations containing natural products and antimicrobial drugs that interfere with bacterial and fungal biofilms. *Phytomedicine* **37**: 14–26. [doi:10.1016/j.phymed.2017.10.021]
224. Jorge, P., Alves, D. and Pereira, M. O. 2019. Catalysing the way towards antimicrobial effectiveness: A systematic analysis and a new online resource for antimicrobial-enzyme combinations against *Pseudomonas aeruginosa* and *Staphylococcus aureus*. *International Journal of Antimicrobial Agents* **[IN PRESS]**(xxxx): 1–8. [doi:10.1016/j.ijantimicag.2019.01.001]
225. Dixon, R. A. and Chopra, I. 1986. Leakage of periplasmic proteins from *Escherichia coli* mediated by polymyxin B nonapeptide. *Antimicrobial Agents and Chemotherapy* **29**(5): 781–788.
226. Vaara, M. and Porro, M. 1996. Group of peptides that act synergistically with hydrophobic antibiotics against gram-negative enteric bacteria. *Antimicrobial Agents and Chemotherapy* **40**(8): 1801–1805.
227. Thangamani, S., Mohammad, H., Abushahba, M. F. N., Sobreira, T. J. P., Hedrick, V. E., Paul, L. N. and Seleem, M. N. 2016. Antibacterial activity and mechanism of action of auranofin against multi-drug resistant bacterial pathogens. *Scientific Reports* **6**: 22571. [doi:10.1038/srep22571]
228. Corbett, D., Wise, A., Langley, T., Skinner, K., Trimby, E., Birchall, S., Doralı, A., Sandiford, S., Williams, J., Warn, P., Vaara, M. and Lister, T. 2017. Potentiation of antibiotic activity by a novel cationic peptide: potency and spectrum of activity of SPR741. *Antimicrobial Agents and Chemotherapy* **61**(8): e00200-17. [doi:10.1128/AAC.00200-17]
229. Eckburg, P. B., Lister, T., Walpole, S., Keutzer, T., Utley, L., Tomayko, J., Kopp, E., Farinola, N. and Coleman, S. 2019. Safety, tolerability, pharmacokinetics, and drug interaction potential of SPR741, an intravenous potentiator, after single and multiple ascending doses and when combined with β -lactam antibiotics in healthy subjects. *Antimicrobial Agents and Chemotherapy* **63**(9): 1–12. [doi:10.1128/AAC.00892-19]

230. Baker, K. R., Jana, B., Franzyk, H. and Guardabassi, L. 2016. A high-throughput approach to identify compounds that impair envelope integrity in *Escherichia coli*. *Antimicrobial Agents and Chemotherapy* **60**(10): 5995–6002. [doi:10.1128/AAC.00537-16]
231. Vaara, M. and Jaakkola, J. 1989. Sodium hexametaphosphate sensitizes *Pseudomonas aeruginosa*, several other species of *Pseudomonas*, and *Escherichia coli* to hydrophobic drugs. *Antimicrobial Agents and Chemotherapy* **33**(10): 1741–1747.
232. Ayres, H. M., Furr, J. R. and Russell, A. D. 1999. Effect of permeabilizers on antibiotic sensitivity of *Pseudomonas aeruginosa*. *Letters in Applied Microbiology* **28**(1): 13–16. [doi:10.1046/j.1365-2672.1999.00486.x]
233. de Virgiliis, S., Congia, M., Turco, M. P., Frau, F., Dessi, C., Argiolu, F., Sorcinelli, R., Sitzia, A. and Cao, A. 1988. Depletion of trace elements and acute ocular toxicity induced by desferrioxamine in patients with thalassaemia. *Archives of Disease in Childhood* **63**(3): 250–255. [doi:10.1136/ad.63.3.250]
234. Nair, B. 2001. Final report of the safety assessment of sodium metaphosphate, sodium trimetaphosphate, and sodium hexametaphosphate. *International Journal of Toxicology* **20**(Suppl 3): 75–89. [doi:10.1080/10915810152630756]
235. Wang, Y., Venter, H. and Ma, S. 2015. Efflux pump inhibitors: A novel approach to combat efflux-mediated drug resistance in bacteria. *Current Drug Targets* **17**(6): 702–719. [doi:10.2174/1389450116666151001103948]
236. Cox, G., Koteva, K. and Wright, G. D. 2014. An unusual class of anthracyclines potentiate gram-positive antibiotics in intrinsically resistant gram-negative bacteria. *Journal of Antimicrobial Chemotherapy* **69**(7): 1844–1855. [doi:10.1093/jac/dku057]
237. Piña, R. G. and Cervantes, C. 1996. Microbial interactions with aluminium. *BioMetals* **9**(3): 311–316. [doi:10.1007/BF00817932]
238. Saha, R., Saha, N., Donofrio, R. S. and Bestervelt, L. L. 2013. Microbial siderophores: A mini review. *Journal of Basic Microbiology* **53**(4): 303–317. [doi:10.1002/jobm.201100552]
239. Borkow, G. and Gabbay, J. 2009. Copper, an ancient remedy returning to fight microbial, fungal and viral infections. *Current Chemical Biology* **3**(3): 272–278. [doi:10.2174/187231309789054887]
240. Alexander, J. W. 2009. History of the medical use of silver. *Surgical Infections* **10**(3): 289–292. [doi:10.1089/sur.2008.9941]
241. Sarsan, S. 2013. Effect of storage of water in different metal vessels on coliforms. *International Journal of Current Microbiology and Applied Sciences* **2**(11): 24–29.
242. Pereira, J. 1836. *Materia medica, or pharmacology, and general therapeutics*. *The London Medical Gazette* **XVIII**: 305–314.
243. Sims, J. M. 1852. Treatment of vesico-vaginal fistula. *The American Journal of the Medical Sciences* **45**: 59–82.
244. Hodges, N. D. C. 1889. The value of mercuric chloride as a disinfectant. *Science* **13**(312): 62–64.
245. Ayres, P. G. 2004. Alexis Millardet: France's forgotten mycologist. *Mycologist* **18**(1): 23–26. [doi:10.1017/S0269915X04001090]

246. Grass, G., Rensing, C. and Solioz, M. 2011. Metallic copper as an antimicrobial surface. *Applied and Environmental Microbiology* **77**(5): 1541–1547. [doi:10.1128/AEM.02766-10]
247. Vincent, M., Hartemann, P. and Engels-Deutsch, M. 2016. Antimicrobial applications of copper. *International Journal of Hygiene and Environmental Health* **219**(7): 585–591. [doi:10.1016/j.ijheh.2016.06.003]
248. Komeda, S. and Casini, A. 2012. Next-generation anticancer metallodrugs. *Current Topics in Medicinal Chemistry* **12**(3): 219–235. [doi:10.2174/156802612799078964]
249. McKee, A. S. and Marrack, P. 2017. Old and new adjuvants. *Current Opinion in Immunology* **47**(10): 44–51. [doi:10.1016/j.coi.2017.06.005]
250. Allahverdiyev, A. M., Kon, K. V., Abamor, E. S., Bagirova, M. and Rafailovich, M. 2011. Coping with antibiotic resistance: Combining nanoparticles with antibiotics and other antimicrobial agents. *Expert Review of Anti-infective Therapy* **9**(11): 1035–1052. [doi:10.1586/eri.11.121]
251. Banoe, M., Seif, S., Nazari, Z. E., Jafari-Fesharaki, P., Shahverdi, H. R., Moballeg, A., Moghaddam, K. M. and Shahverdi, A. R. 2010. ZnO nanoparticles enhanced antibacterial activity of ciprofloxacin against *Staphylococcus aureus* and *Escherichia coli*. *Journal of Biomedical Materials Research Part B: Applied Biomaterials* **93B**(2): 557–561. [doi:10.1002/jbm.b.31615]
252. Smekalova, M., Aragon, V., Panacek, A., Pucek, R., Zboril, R. and Kvitek, L. 2016. Enhanced antibacterial effect of antibiotics in combination with silver nanoparticles against animal pathogens. *The Veterinary Journal* **209**: 174–179. [doi:10.1016/j.tvjl.2015.10.032]
253. Panáček, A., Smékalová, M., Večeřová, R., Bogdanová, K., Röderová, M., Kolář, M., Kilianová, M., Hradilová, Š., Froning, J. P., Havrdová, M., Pucek, R., Zbořil, R. and Kvitek, L. 2016. Silver nanoparticles strongly enhance and restore bactericidal activity of inactive antibiotics against multiresistant *Enterobacteriaceae*. *Colloids and Surfaces B: Biointerfaces* **142**: 392–399. [doi:10.1016/j.colsurfb.2016.03.007]
254. Parada, J., Rubilar, O., Fernández-Baldo, M. A., Bertolino, F. A., Durán, N., Seabra, A. B. and Tortella, G. R. 2019. The nanotechnology among us: Are metal and metal oxides nanoparticles a nano or mega risk for soil microbial communities? *Critical Reviews in Biotechnology* **39**(2): 157–172. [doi:10.1080/07388551.2018.1523865]
255. Liu, X., Tang, J., Song, B., Zhen, M., Wang, L. and Giesy, J. P. 2019. Exposure to Al₂O₃ nanoparticles facilitates conjugative transfer of antibiotic resistance genes from *Escherichia coli* to *Streptomyces*. *Nanotoxicology* **0**(0): 1–15. [doi:10.1080/17435390.2019.1669731]
256. Uivarosi, V. 2013. Metal complexes of quinolone antibiotics and their applications: an update. *Molecules* **18**: 11153–11197. [doi:10.3390/molecules180911153]
257. Lecomte, S., Baron, M. H., Chenon, M. T., Coupry, C. and Moreau, N. J. 1994. Effect of magnesium complexation by fluoroquinolones on their antibacterial properties. *Antimicrobial Agents and Chemotherapy* **38**(12): 2810–2816. [doi:10.1128/AAC.38.12.2810]
258. Ma, H. H. M., Chiu, F. C. K. and Li, R. C. 1997. Mechanistic investigation of the reduction in antimicrobial activity of ciprofloxacin by metal cations. *Pharmaceutical Research* **14**(3): 366–370.

259. López-Gresa, M. P., Ortiz, R., Perelló, L., Latorre, J., Liu-González, M., García-Granda, S., Pérez-Priede, M. and Cantón, E. 2002. Interactions of metal ions with two quinolone antimicrobial agents (cinoxacin and ciprofloxacin): Spectroscopic and X-ray structural characterization, antibacterial studies. *Journal of Inorganic Biochemistry* **92**: 65–74. [doi:10.1016/S0162-0134(02)00487-7]
260. Vieira, L. M. M., de Almeida, M. V., Lourenço, M. C. S., Bezerra, F. A. F. M. and Fontes, A. P. S. 2009. Synthesis and antitubercular activity of palladium and platinum complexes with fluoroquinolones. *European Journal of Medicinal Chemistry* **44**(10): 4107–4111. [doi:10.1016/j.ejmech.2009.05.001]
261. Arayne, S., Sultana, N., Haroon, U. and MESAİK, M. A. 2009. Synthesis, characterization, antibacterial and anti-inflammatory activities of enoxacin metal complexes. *Bioinorganic Chemistry and Applications* **2009**: 914105. [doi:10.1155/2009/914105]
262. Živec, P., Perdih, F., Turel, I., Giester, G. and Psomas, G. 2012. Different types of copper complexes with the quinolone antimicrobial drugs ofloxacin and norfloxacin: Structure, DNA- and albumin-binding. *Journal of Inorganic Biochemistry* **117**: 35–47. [doi:10.1016/j.jinorgbio.2012.08.008]
263. Feio, M. J., Sousa, I., Ferreira, M., Cunha-Silva, L., Saraiva, R. G., Queirós, C., Alexandre, J. G., Claro, V., Mendes, A., Ortiz, R., Lopes, S., Amaral, A. L., Lino, J., Fernandes, P., Silva, A. J., Moutinho, L., de Castro, B., Pereira, E., Perelló, L. et al. 2014. Fluoroquinolone-metal complexes: A route to counteract bacterial resistance? *Journal of Inorganic Biochemistry* **138**: 129–143. [doi:10.1016/j.jinorgbio.2014.05.007]
264. Žakelj, S., Berginc, K., Uršič, D. and Kristl, A. 2007. Influence of metal cations on the solubility of fluoroquinolones. *Die Pharmazie* **62**(4): 318–320. [doi:10.1691/ph.2007.4.6242]
265. Gziut, M., MacGregor, H. J., Nevell, T. G., Mason, T., Laight, D. and Shute, J. K. 2013. Anti-inflammatory effects of tobramycin and a copper-tobramycin complex with superoxide dismutase-like activity. *British Journal of Pharmacology* **168**(5): 1165–1181. [doi:10.1111/bph.12018]
266. Giovagnoli, S., Marenzoni, M. L., Nocchetti, M., Santi, C., Blasi, P., Schoubben, A. and Ricci, M. 2013. Synthesis, characterization and *in vitro* extracellular and intracellular activity against *Mycobacterium tuberculosis* infection of new second-line antitubercular drug-palladium complexes. *Journal of Pharmacy and Pharmacology* **66**(1): 106–121. [doi:10.1111/jphp.12162]
267. Hamilton-Miller, J. M. T. and Shah, S. 1996. A microbiological assessment of silver fusidate, a novel topical antimicrobial agent. *International Journal of Antimicrobial Agents* **7**(2): 97–99. [doi:10.1016/0924-8579(96)00302-0]
268. Morones-Ramirez, J. R., Winkler, J. A., Spina, C. S. and Collins, J. J. 2013. Silver enhances antibiotic activity against gram-negative bacteria. *Science Translational Medicine* **5**(190): 190ra81. [doi:10.1126/scitranslmed.3006276]
269. Herisse, M., Duverger, Y., Martin-Verstraete, I., Barras, F. and Ezraty, B. 2017. Silver potentiates aminoglycoside toxicity by enhancing their uptake. *Molecular Microbiology* **105**(1): 115–126. [doi:10.1111/mmi.13687]
270. Kim, J., Pitts, B., Stewart, P. S., Camper, A. and Yoon, J. 2008. Comparison of the antimicrobial effects of chlorine, silver ion, and tobramycin on biofilm. *Antimicrobial Agents and Chemotherapy* **52**(4): 1446–1453. [doi:10.1128/AAC.00054-07]

271. Djoko, K. Y., Achard, M. E. S., Phan, M.-D., Lo, A. W., Miraula, M., Prombhul, S., Hancock, S. J., Peters, K. M., Sidjabet, H. E., Harris, P. N., Mitić, N., Walsh, T. R., Anderson, G. J., Shafer, W. M., Paterson, D. L., Schenk, G., McEwan, A. G. and Schembri, M. A. 2018. Copper ions and coordination complexes as novel carbapenem adjuvants. *Antimicrobial Agents and Chemotherapy* **62**(2): e02280-17. [doi:10.1128/AAC.02280-17]
272. Lemire, J. A., Harrison, J. J. and Turner, R. J. 2013. Antimicrobial activity of metals: Mechanisms, molecular targets and applications. *Nature Reviews Microbiology* **11**(6): 371–384. [doi:10.1038/nrmicro3028]
273. Andrews, J. M. 2001. Determination of minimum inhibitory concentrations. *Journal of Antimicrobial Chemotherapy* **48**(S1): 5–16. [doi:10.1093/jac/48.suppl_1.5]
274. BSAC. 2015. Methods for Antimicrobial Susceptibility Testing. (Version 14)
275. Brown, D. F. J., Wootton, M. and Howe, R. A. 2016. Antimicrobial susceptibility testing breakpoints and methods from BSAC to EUCAST. *Journal of Antimicrobial Chemotherapy* **71**(1): 3–5. [doi:10.1093/jac/dkv287]
276. EUCAST. 2015. Antimicrobial susceptibility testing EUCAST disk diffusion method. (Version 5.0)
277. Daligault, H. E., Davenport, K. W., Minogue, T. D., Bishop-Lilly, K. A., Bruce, D. C., Chain, P. S., Coyne, S. R., Frey, K. G., Jaissle, J., Koroleva, G. I., Ladner, J. T., Lo, C.-C., Meincke, L., Munk, A. C., Palacios, G. F., Redden, C. L. and Johnson, S. L. 2014. Draft genome assembly of *Klebsiella pneumoniae* Type Strain ATCC 13883. *Genome Announcements* **2**(5): e00939-14. [doi:10.1128/genomea.00973-14]
278. Wang, Y., Li, C., Gao, C., Ma, C. and Xu, P. 2014. Genome sequence of the nonpathogenic *Pseudomonas aeruginosa* strain ATCC 15442. *Genome Announcements* **2**(2): e00421-14. [doi:10.1128/genomea.00421-14]
279. Hay, R. J. 1988. The seed stock concept and quality control for cell lines. *Analytical Biochemistry* **171**(2): 225–237. [doi:10.1016/0003-2697(88)90480-0]
280. Miles, A. A. and Misra, S. S. 1938. The estimation of the bactericidal power of the blood. *Journal of Hygiene* **38**(6): 732–748. [doi:10.1017/S002217240001158X]
281. Balouiri, M., Sadiki, M. and Ibnsouda, S. K. 2016. Methods for *in vitro* evaluating antimicrobial activity: A review. *Journal of Pharmaceutical Analysis* **6**(2): 71–79. [doi:10.1016/j.jpha.2015.11.005]
282. Cockerill, F. R., Wikler, M. A., Alder, J., Dudley, M. N., Eliopoulos, G. M., Ferraro, M. J., Hardy, D. J., Hecht, D. W., Hindler, J. A., Patel, J. B., Powell, M., Swenson, J. M., Thomson, R. B., Traczewski, M. M., Turnbrighe, J. D., Weinstein, M. P. and Zimmer, B. L. 2012. *Methods for Dilution Antimicrobial Susceptibility Tests for Bacteria That Grow Aerobically. M07-A9* **32**(2)
283. Tecan Trading AG. 2016. Instructions for use for Infinite 200 PRO (Document Part No. 300527). (Revision No. 1.6)
284. Amsterdam, D. 1989. Evaluating the *in vitro* efficacy of antimicrobial combinations: Assessing synergy. *The Antimicrobial Newsletter* **6**(5): 41–43. [doi:10.1016/0738-1751(89)90043-9]
285. Bonapace, C. R., Bosso, J. A., Friedrich, L. V. and White, R. L. 2002. Comparison of methods of interpretation of checkerboard synergy testing. *Diagnostic Microbiology and Infectious Disease* **44**(4): 363–366. [doi:10.1016/S0732-8893(02)00473-X]

286. Odds, F. C. 2003. Synergy, antagonism, and what the chequerboard puts between them. *The Journal of antimicrobial chemotherapy* **52**: 1. [doi:10.1093/jac/dkg301]
287. Curbete, M. M. and Salgado, H. R. N. 2016. Stability-indicating RP-LC method for quantification of fusidic acid in cream. *Brazilian Journal of Pharmaceutical Sciences* **52**(3): 447–457. [doi:10.1590/S1984-82502016000300011]
288. Byrne, J., Velasco-Torrijos, T. and Reinhardt, R. 2015. An RP-HPLC method for the stability-indicating analysis of impurities of both fusidic acid and betamethasone-17-valerate in a semi-solid pharmaceutical dosage form. *Journal of Chromatographic Science* **53**(9): 1498–1503. [doi:10.1093/chromsci/bmv045]
289. Koeth, L. M., King, A., Knight, H., May, J., Miller, L. A., Phillips, I. and Poupard, J. A. 2000. Comparison of cation-adjusted Mueller-Hinton broth with Iso-Sensitest broth for the NCCLS broth microdilution method. *Journal of Antimicrobial Chemotherapy* **46**(3): 369–376. [doi:10.1093/jac/46.3.369]
290. Glasser, J. S., Guymon, C. H., Mende, K., Wolf, S. E., Hospenthal, D. R. and Murray, C. K. 2010. Activity of topical antimicrobial agents against multidrug-resistant bacteria recovered from burn patients. *Burns* **36**(8): 1172–1184. [doi:10.1016/j.burns.2010.05.013]
291. Dillon, N., Holland, M., Tsunemoto, H., Hancock, B., Cornax, I., Pogliano, J., Sakoulas, G. and Nizet, V. 2019. Surprising synergy of dual translation inhibition vs. *Acinetobacter baumannii* and other multidrug-resistant bacterial pathogens. *EBioMedicine* **46**: 193–201. [doi:10.1016/j.ebiom.2019.07.041]
292. Dalhoff, A., Stubbings, W. and Schubert, S. 2011. Comparative *in vitro* activities of the novel antibacterial finafloxacin against selected gram-positive and gram-negative bacteria tested in Mueller-Hinton broth and synthetic urine. *Antimicrobial Agents and Chemotherapy* **55**(4): 1814–1818. [doi:10.1128/AAC.00886-10]
293. Mead, A., Lees, P., Mitchell, J., Rycroft, A., Standing, J. F., Toutain, P.-L. and Pelligand, L. 2019. Differential susceptibility to tetracycline, oxytetracycline and doxycycline of the calf pathogens *Mannheimia haemolytica* and *Pasteurella multocida* in three growth media. *Journal of Veterinary Pharmacology and Therapeutics* **42**(1): 52–59. [doi:10.1111/jvp.12719]
294. Li, J., Li, Z., Liang, Z., Han, L., Feng, H., He, S. and Zhang, J. 2018. Fabrication of a drug delivery system that enhances antifungal drug corneal penetration. *Drug Delivery* **25**(1): 938–949. [doi:10.1080/10717544.2018.1461278]
295. Abruzzo, A., Giordani, B., Parolin, C., Vitali, B., Protti, M., Mercolini, L., Cappelletti, M., Fedi, S., Bigucci, F., Cerchiara, T. and Luppi, B. 2018. Novel mixed vesicles containing lactobacilli biosurfactant for vaginal delivery of an anti-*Candida* agent. *European Journal of Pharmaceutical Sciences* **112**: 95–101. [doi:10.1016/j.ejps.2017.11.012]
296. Luria, S. E., Adams, J. N. and Ting, R. C. 1960. Transduction of lactose-utilizing ability among strains of *E. coli* and *S. dysenteriae* and the properties of the transducing phage particles. *Virology* **12**(3): 348–390. [doi:10.1016/0042-6822(60)90161-6]
297. Bridson, E. Y. 2006. The OXOID Manual. (9th edition)
298. McDonnell, G. and Russell, A. D. 1999. Antiseptics and disinfectants: Activity, action, and resistance. *Clinical Microbiology Reviews* **12**(1): 147–179. [doi:10.1007/s13398-014-0173-7.2]

299. Cebrían, G., Arroyo, C., Mañas, P. and Condón, S. 2014. Bacterial maximum non-inhibitory and minimum inhibitory concentrations of different water activity depressing solutes. *International Journal of Food Microbiology* **188**: 67–74. [doi:10.1016/j.ijfoodmicro.2014.07.011]
300. Morrison, K. D., Misra, R. and Williams, L. B. 2016. Unearthing the antibacterial mechanism of medicinal clay: A geochemical approach to combating antibiotic resistance. *Nature Scientific Reports* **6**: 19043. [doi:10.1038/srep19043]
301. Garza-Cervantes, J. A., Chávez-Reyes, A., Castillo, E. C., García-Rivas, G., Ortega-Rivera, O. A., Salinas, E., Ortiz-Martínez, M., Gómez-Flores, S. L., Peña-Martínez, J. A., Pepi-Molina, A., Treviño-González, M. T., Cantú-Cárdenas, E. M., Escarcega-Gonzalez, C. E. and Morones-Ramírez, J. R. 2017. Synergistic antimicrobial effects of silver/transition-metal combinatorial treatments. *Scientific Reports* **7**: 903. [doi:10.1038/s41598-017-01017-7]
302. Xiong, A. and Jayaswal, R. K. 1998. Molecular characterization of a chromosomal determinant conferring resistance to zinc and cobalt ions in *Staphylococcus aureus*. *Journal of Bacteriology* **180**(16): 4024–4029.
303. Pasquet, J., Chevalier, Y., Pelletier, J., Couval, E., Bouvier, D. and Bolzinger, M.-A. 2014. The contribution of zinc ions to the antimicrobial activity of zinc oxide. *Colloids and Surfaces A: Physicochemical and Engineering Aspects* **457**(1): 263–274. [doi:10.1016/j.colsurfa.2014.05.057]
304. Bell, S. J., Friedman, S. A. and Leong, J. 1979. Antibiotic action of N-methylthioformohydroxamate metal complexes. *Antimicrobial Agents and Chemotherapy* **15**(3): 384–391. [doi:10.1128/AAC.15.3.384]
305. Patel, M. N., Dosi, P. A. and Bhatt, B. S. 2012. Nucleic acid interaction and antibacterial behaviours of a ternary palladium(II) complexes. *Spectrochimica Acta - Part A: Molecular and Biomolecular Spectroscopy* **86**: 508–514. [doi:10.1016/j.saa.2011.10.077]
306. Nies, D. H. 1999. Microbial heavy-metal resistance. *Applied Microbiology and Biotechnology* **51**(6): 730–750. [doi:10.1007/s002530051457]
307. Yang, Q. E., Agouri, S. R., Tyrrell, J. M. and Walsh, T. R. 2018. Heavy metal resistance genes are associated with bla_{NDM-1}- and bla_{CTX-M-15}-carrying *Enterobacteriaceae*. *Antimicrobial Agents and Chemotherapy* **62**(5): e02642-17. [doi:10.1128/AAC.02642-17]
308. Elguindi, J., Moffitt, S., Hasman, H., Andrade, C., Raghavan, S. and Rensing, C. 2014. Metallic copper corrosion rates, moisture content, and growth medium influence survival of copper-ion resistant bacteria. *Applied Microbiology and Biotechnology* **89**(6): 1963–1970. [doi:10.1007/s00253-010-2980-x.Metallic]
309. Booth, S. C., George, I. F. S., Zannoni, D., Cappelletti, M., Duggan, G. E., Ceri, H. and Turner, R. J. 2013. Effect of aluminium and copper on biofilm development of *Pseudomonas pseudoalcaligenes* KF707 and *P. fluorescens* as a function of different media compositions. *Metallomics* **5**(6): 723. [doi:10.1039/c3mt20240b]
310. Gugala, N., Vu, D., Parkins, M. D. and Turner, R. J. 2019. Specificity in the susceptibilities of *Escherichia coli*, *Pseudomonas aeruginosa* and *Staphylococcus aureus* clinical isolates to six metal antimicrobials. *Antibiotics* **8**(2): 51. [doi:10.3390/antibiotics8020051]
311. Williams, R. J. P. 1999. What is wrong with aluminium? The J.D. Birchall memorial lecture. *Journal of Inorganic Biochemistry* **76**(2): 81–88. [doi:10.1016/S0162-0134(99)00118-X]

312. Gugala, N., Lemire, J. A. and Turner, R. J. 2017. The efficacy of different antimicrobial metals at preventing the formation of, and eradicating bacterial biofilms of pathogenic indicator strains. *Journal of Antibiotics* **70**(6): 775–780. [doi:10.1038/ja.2017.10]
313. Mailloux, R. J., Lemire, J., Kalyuzhnyi, S. and Appanna, V. 2008. A novel metabolic network leads to enhanced citrate biogenesis in *Pseudomonas fluorescens* exposed to aluminum toxicity. *Extremophiles* **12**(3): 451–459. [doi:10.1007/s00792-008-0150-1]
314. Londono, S. C., Hartnett, H. E. and Williams, L. B. 2017. Antibacterial activity of aluminum in clay from the Colombian Amazon. *Environmental Science & Technology* **51**: 2401–2408. [doi:10.1021/acs.est.6b04670]
315. Ma, J., Kang, M., Zhang, Y., Guo, X., Tian, Z., Ding, C. and Wang, H. 2017. Self-defense of *Escherichia coli* against damages caused by nanoalumina. *Environmental Toxicology and Pharmacology* **55**: 110–117. [doi:10.1016/j.etap.2017.08.011]
316. Gutteridge, J. M. C., Quinlan, G. J., Clark, I. and Halliwell, B. 1985. Aluminium salts accelerate peroxidation of membrane lipids stimulated by iron salts. *Biochimica et Biophysica Acta* **835**(3): 441–447. [doi:10.1016/0005-2760(85)90113-4]
317. Guzzo, A., Diorio, C. and DuBow, M. S. 1991. Transcription of the *Escherichia coli* *fliC* gene is regulated by metal ions. *Applied and Environmental Microbiology* **57**(8): 2255–2259.
318. Wösten, M. M. S. M., Kox, L. F. F., Chamnongpol, S., Soncini, F. C. and Groisman, E. A. 2000. A signal transduction system that responds to extracellular iron. *Cell* **103**(1): 113–125. [doi:10.1016/S0092-8674(00)00092-1]
319. Lee, H., Hsu, F.-F., Turk, J. and Groisman, E. A. 2004. The PmrA-regulated *pmrC* gene mediates phosphoethanolamine modification of lipid A and polymyxin resistance in *Salmonella enterica*. *Journal of Bacteriology* **186**(13): 4124–4133. [doi:10.1128/JB.186.13.4124-4133.2004]
320. Hyo, Y., Yamada, S., Ishimatsu, M., Fukutsuji, K. and Harada, T. 2012. Antimicrobial effects of Burow's solution on *Staphylococcus aureus* and *Pseudomonas aeruginosa*. *Medical Molecular Morphology* **45**(2): 66–71. [doi:10.1007/s00795-011-0540-9]
321. Youn, C. K., Jang, S.-J., Jo, E.-R., Choi, J. A., Sim, J.-H. and Cho, S. II. 2016. Comparative antibacterial activity of topical antiseptic eardrops against methicillin-resistant *Staphylococcus aureus* and quinolone-resistant *Pseudomonas aeruginosa*. *International Journal of Pediatric Otorhinolaryngology* **85**: 80–83. [doi:10.1016/j.ijporl.2016.03.031]
322. Fein, J. B., Daughney, C. J., Yee, N. and Davis, T. A. 1997. A chemical equilibrium model for metal adsorption onto bacterial surfaces. *Geochimica et Cosmochimica Acta* **61**(16): 3319–3328. [doi:10.1016/S0016-7037(97)00166-X]
323. Ranquet, C., Ollagnier-de-Choudens, S., Loiseau, L., Barras, F. and Fontecave, M. 2007. Cobalt stress in *Escherichia coli*: The effect on the iron-sulfur proteins. *Journal of Biological Chemistry* **282**(42): 30442–30451. [doi:10.1074/jbc.M702519200]
324. Fantino, J. R., Py, B., Fontecave, M. and Barras, F. 2010. A genetic analysis of the response of *Escherichia coli* to cobalt stress. *Environmental Microbiology* **12**(10): 2846–2857. [doi:10.1111/j.1462-2920.2010.02265.x]

325. Valko, M., Morris, H. and Cronin, M. T. D. 2005. Metals, toxicity and oxidative stress. *Current Medicinal Chemistry* **12**(10): 1161–1208. [doi:10.2174/0929867053764635]
326. Majtan, T., Frerman, F. E. and Kraus, J. P. 2011. Effect of cobalt on *Escherichia coli* metabolism and metalloporphyrin formation. *BioMetals* **24**(2): 335–347. [doi:10.1007/s10534-010-9400-7]
327. Blériot, C., Effantin, G., Lagarde, F., Mandrand-Berthelot, M. A. and Rodrigue, A. 2011. RcnB is a periplasmic protein essential for maintaining intracellular Ni and Co concentrations in *Escherichia coli*. *Journal of Bacteriology* **193**(15): 3785–3793. [doi:10.1128/JB.05032-11]
328. Willecke, K., Gries, E.-M. and Oehr, P. 1973. Coupled transport of citrate and magnesium in *Bacillus subtilis*. *Journal of Biological Chemistry* **248**(3): 807–814.
329. Iwig, J. S., Rowe, J. L. and Chivers, P. T. 2006. Nickel homeostasis in *Escherichia coli* - The *rcnR-rcnA* efflux pathway and its linkage to NikR function. *Molecular Microbiology* **62**(1): 252–262. [doi:10.1111/j.1365-2958.2006.05369.x]
330. Thorgersen, M. P. and Downs, D. M. 2007. Cobalt targets multiple metabolic processes in *Salmonella enterica*. *Journal of Bacteriology* **189**(21): 7774–7781. [doi:10.1128/JB.00962-07]
331. van der Heijden, J., Vogt, S. L., Reynolds, L. A., Peña-Díaz, J., Tupin, A., Aussel, L. and Finlay, B. B. 2016. Exploring the redox balance inside gram-negative bacteria with redox-sensitive GFP. *Free Radical Biology and Medicine* **91**: 34–44. [doi:10.1016/j.freeradbiomed.2015.11.029]
332. Repetto, M. G., Ferrarotti, N. F. and Boveris, A. 2010. The involvement of transition metal ions on iron-dependent lipid peroxidation. *Archives of Toxicology* **84**(4): 255–262. [doi:10.1007/s00204-009-0487-y]
333. Blundell, M. R. and Wild, D. G. 1969. Inhibition of bacterial growth by metal salts: A survey of effects on the synthesis of ribonucleic acid and protein. *Biochemical Journal* **115**(2): 207–212. [doi:10.1042/bj1150207]
334. Blundell, M. R. and Wild, D. G. 1969. Inhibition of bacterial growth by metal salts: The accumulation of ribonucleic acid during inhibition of *Escherichia coli* by cobalt chloride. *Biochemical Journal* **115**(2): 213–223. [doi:10.1042/bj1150213]
335. Osman, D., Foster, A. W., Chen, J., Svedaite, K., Steed, J. W., Lurie-Luke, E., Huggins, T. G. and Robinson, N. J. 2017. Fine control of metal concentrations is necessary for cells to discern zinc from cobalt. *Nature Communications* **8**: 1884. [doi:10.1038/s41467-017-02085-z]
336. Stohs, S. J. and Bagchi, D. 1995. Oxidative mechanisms in the toxicity of metal ions. *Free Radical Biology and Medicine* **18**(2): 321–336. [doi:10.1016/0891-5849(94)00159-H]
337. Singh, K., Senadheera, D. B. and Cvitkovitch, D. G. 2014. An intimate link: Two-component signal transduction systems and metal transport systems in bacteria. *Future Microbiology* **9**(11): 1283–1293. [doi:10.2217/fmb.14.87]
338. Grass, G., Thakali, K., Klebba, P. E., Thieme, D., Müller, A., Wildner, G. F. and Rensing, C. 2004. Linkage between catecholate siderophores and the multicopper oxidase CueO in *Escherichia coli*. *Journal of Bacteriology* **186**(17): 5826–5833. [doi:10.1128/JB.186.17.5826-5833.2004]
339. Macomber, L., Rensing, C. and Imlay, J. A. 2007. Intracellular copper does not catalyze the formation of oxidative DNA damage in *Escherichia coli*. *Journal of Bacteriology* **189**(5): 1616–1626. [doi:10.1128/JB.01357-06]

340. Macomber, L. and Imlay, J. A. 2009. The iron-sulfur clusters of dehydratases are primary intracellular targets of copper toxicity. *Proceedings of the National Academy of Sciences* **106**(20): 8344–8349. [doi:10.1073/pnas.0812808106]
341. Djoko, K. Y. and McEwan, A. G. 2013. Antimicrobial action of copper is amplified *via* inhibition of heme biosynthesis. *ACS Chemical Biology* **8**(10): 2217–2223. [doi:10.1021/cb4002443]
342. Stevenson, J., Barwinska-Sendra, A., Tarrant, E. and Waldron, K. J. 2013. Mechanism of action and applications of the antimicrobial properties of copper. in *Microbial pathogens and strategies for combating them: science, technology and education* (ed. Méndez-Vilas, A.) : 468–479.
343. Nguyen, T. T. M., Park, H.-J., Kim, J. Y., Kim, H.-E., Lee, H., Yoon, J. and Lee, C. 2013. Microbial inactivation by cupric ion in combination with H₂O₂: Role of reactive oxidants. *Environmental Science & Technology* **47**: 13661–13667. [doi:10.1021/es403155a]
344. Walash, M. I. and Agarwal, S. P. 1972. Characterization of sulfonamides by TLC using metal ions. *Journal of Pharmaceutical Sciences* **61**(2): 277–278. [doi:10.1002/jps.2600610232]
345. Blasco, F., Perelló, L., Latorre, J., Borrás, J. and García-Granda, S. 1996. Cobalt(II), nickel(II), and copper(II) complexes of sulfanilamide derivatives: Synthesis, spectroscopic studies, and antibacterial activity. Crystal structure of [Co(sulfacetamide)₂(NCS)₂]. *Journal of Inorganic Biochemistry* **61**(2): 143–154.
346. Chohan, Z. H., Mahmood-UI-Hassan, Khan, K. M. and Supuran, C. T. 2005. *In vitro* antibacterial, antifungal and cytotoxic properties of sulfonamide-derived Schiff's bases and their metal complexes. *Journal of Enzyme Inhibition and Medicinal Chemistry* **20**(2): 183–188. [doi:10.1080/14756360500043257]
347. Sultana, N. and Arayne, M. S. 2007. *In vitro* activity of cefadroxil, cephalixin, cefatrizine and cefpirome in presence of essential and trace elements. *Pakistan Journal of Pharmaceutical Sciences* **20**(4): 305–310.
348. Chohan, Z. H. and Supuran, C. T. 2005. *In vitro* antibacterial and cytotoxic activity of cobalt(II), copper(II), nickel(II) and zinc(II) complexes of the antibiotic drug cephalothin (Keflin). *Journal of Enzyme Inhibition and Medicinal Chemistry* **20**(5): 463–468. [doi:10.1080/10485250500219765]
349. Sultana, N., Arayne, M. S. and Afzal, M. 2005. Synthesis and antibacterial activity of cephradine metal complexes: part II complexes with cobalt, copper, zinc and cadmium. *Pakistan Journal of Pharmaceutical Sciences* **18**(1): 36–42.
350. Jiménez-Garrido, N., Perelló, L., Ortiz, R., Alzuet, G., González-Álvarez, M., Cantón, E., Liu-González, M., García-Granda, S. and Pérez-Priede, M. 2005. Antibacterial studies, DNA oxidative cleavage, and crystal structures of Cu(II) and Co(II) complexes with two quinolone family members, ciprofloxacin and enoxacin. *Journal of Inorganic Biochemistry* **99**(3): 677–689. [doi:10.1016/j.jinorgbio.2004.11.016]
351. Chohan, Z. H., Supuran, C. T. and Scozzafava, A. 2005. Metal binding and antibacterial activity of ciprofloxacin complexes. *Journal of Enzyme Inhibition and Medicinal Chemistry* **20**(3): 303–307.
352. Saraiva, R., Lopes, S., Ferreira, M., Novais, F., Pereira, E., Feio, M. J. and Gameiro, P. 2010. Solution and biological behaviour of enrofloxacin metalloantibiotics: A route to counteract bacterial resistance? *Journal of Inorganic Biochemistry* **104**(8): 843–850. [doi:10.1016/j.jinorgbio.2010.03.017]

353. Palmer, L. D. and Skaar, E. P. 2016. Transition metals and virulence in bacteria. *Annual Review of Genetics* **50**: 67–91. [doi:10.1146/annurev-genet-120215-035146]
354. Crowley, D. E., Wang, Y. C., Reid, C. P. P. and Szaniszlo, P. J. 1991. Mechanisms of iron acquisition from siderophores by microorganisms and plants. *Plant and Soil* **130**(1–2): 179–198. [doi:10.1007/BF00011873]
355. Bokare, A. D. and Choi, W. 2014. Review of iron-free Fenton-like systems for activating H₂O₂ in advanced oxidation processes. *Journal of Hazardous Materials* **275**: 121–135. [doi:10.1016/j.jhazmat.2014.04.054]
356. Silver, S., Johnseine, P., Whitney, E. and Clark, D. 1972. Manganese-resistant mutants of *Escherichia coli*: physiological and genetic studies. *Journal of Bacteriology* **110**(1): 186–195.
357. El-Deiry, W. S., Downey, K. M. and So, A. G. 1984. Molecular mechanisms of manganese mutagenesis (DNA polymerase I/error discrimination). *Biochemistry* **81**: 7378–7382.
358. Batra, V. K., Beard, W. A., Shock, D. D., Krahn, J. M., Pedersen, L. C. and Wilson, S. H. 2006. Magnesium induced assembly of a complete DNA polymerase catalytic complex. *Structure* **14**(4): 757–766. [doi:10.1016/j.str.2006.01.011]
359. Martin, J. E., Waters, L. S., Storz, G. and Imlay, J. A. 2015. The *Escherichia coli* small protein MntS and exporter MntP optimize the intracellular concentration of manganese. *PLoS Genetics* **11**(3): e1004977. [doi:10.1371/journal.pgen.1004977]
360. Kaur, G., Kumar, V., Arora, A., Tomar, A., Ashish, Sur, R. and Dutta, D. 2017. Affected energy metabolism under manganese stress governs cellular toxicity. *Scientific Reports* **7**: 11645. [doi:10.1038/s41598-017-12004-3]
361. Sengupta, S., Mondal, A., Dutta, D. and Parrack, P. 2018. HflX protein protects *Escherichia coli* from manganese stress. *Journal of Biosciences* **43**(5): 1001–1013. [doi:10.1007/s12038-018-9807-9]
362. Macomber, L., Elsey, S. P. and Hausinger, R. P. 2011. Fructose-1,6-bisphosphate aldolase (class II) is the primary site of nickel toxicity in *Escherichia coli*. *Molecular Microbiology* **82**(5): 1291–1300. [doi:10.1111/j.1365-2958.2011.07891.x]
363. Gupta, A. D. and Karthikeyan, S. 2016. Individual and combined toxic effect of nickel and chromium on biochemical constituents in *E. coli* using FTIR spectroscopy and principle component analysis. *Ecotoxicology and Environmental Safety* **130**: 289–294. [doi:10.1016/j.ecoenv.2016.04.025]
364. Ray, S., Mohan, R., Singh, J. K., Samantaray, M. K., Shaikh, M. M., Panda, D. and Ghosh, P. 2007. Anticancer and antimicrobial metallopharmaceutical agents based on palladium, gold, and silver N-heterocyclic carbene complexes. *Journal of the American Chemical Society* **129**(48): 15042–15053. [doi:10.1021/ja075889z]
365. Fiuza, S. M., Holy, J., Batista de Carvalho, L. A. E. and Marques, M. P. M. 2011. Biologic activity of a dinuclear Pd(II)-spermine complex toward human breast cancer. *Chemical Biology and Drug Design* **77**(6): 477–488. [doi:10.1111/j.1747-0285.2011.01081.x]
366. Navarro, M., Peña, N. P., Colmenares, I., González, T., Arsenak, M. and Taylor, P. 2006. Synthesis and characterization of new palladium-clotrimazole and palladium-chloroquine complexes showing cytotoxicity for tumor cell lines *in vitro*. *Journal of Inorganic Biochemistry* **100**(1): 152–157. [doi:10.1016/j.jinorgbio.2005.10.013]

367. Kovala-Demertzi, D., Demertzis, M. A., Filiou, E., Pantazaki, A. A., Yadav, P. N., Miller, J. R., Zheng, Y. and Kyriakidis, D. A. 2003. Platinum(II) and palladium(II) complexes with 2-acetyl pyridine 4N-ethyl thiosemicarbazone able to overcome the cis-platin resistance: Structure, antibacterial activity and DNA strand breakage. *BioMetals* **16**(3): 411–418.
368. Nawrot-Modranka, J. and Nawrot, E. 2007. Synthesis, spectroscopy and alkylating properties of Pd(II) complexes of phosphorohydrazones of coumarin and chromone with potential antibacterial activity. *Acta Poloniae Pharmaceutica - Drug Research* **64**(5): 429–434.
369. Singh, R. V., Joshi, S. C., Kulshrestha, S., Nagpal, P. and Bansal, A. 2001. Antiandrogen and antimicrobial aspects of coordination compounds of palladium(II), platinum(II) and lead(II). *Metal Based Drugs* **8**(3): 149–158. [doi:10.1155/MBD.2001.149]
370. Sharma, K., Singh, R., Fahmi, N. and Singh, R. V. 2010. Microwave assisted synthesis, characterization and biological evaluation of palladium and platinum complexes with azomethines. *Spectrochimica Acta Part A: Molecular and Biomolecular Spectroscopy* **75**(1): 422–427. [doi:10.1016/j.saa.2009.10.052]
371. Singh, B. K., Jetley, U. K., Sharma, R. K. and Garg, B. S. 2007. Synthesis, characterization and biological activity of complexes of 2-hydroxy-3,5-dimethylacetophenoneoxime (HDMAOX) with copper(II), cobalt(II), nickel(II) and palladium(II). *Spectrochimica Acta Part A: Molecular and Biomolecular Spectroscopy* **68**(1): 63–73. [doi:10.1016/j.saa.2006.11.001]
372. Garoufis, A., Hadjikakou, S. K. and Hadjiliadis, N. 2009. Palladium coordination compounds as anti-viral, anti-fungal, anti-microbial and anti-tumor agents. *Coordination Chemistry Reviews* **253**(9–10): 1384–1397. [doi:10.1016/j.ccr.2008.09.011]
373. Thakor, K. P., Lunagariya, M. V., Bhatt, B. S. and Patel, M. N. 2019. Fluorescence and absorption studies of DNA-Pd(II) complex interaction: Synthesis, spectroanalytical investigations and biological activities. *Luminescence* **34**: 113–124. [doi:10.1002/bio.3587]
374. Guerra, W., de Andrade Azevedo, E., de Souza Monteiro, A. R., Bucciarelli-Rodriguez, M., Chartone-Souza, E., Nascimento, A. M. A., Fontes, A. P. S., Le Moyec, L. and Pereira-Maia, E. C. 2005. Synthesis, characterization, and antibacterial activity of three palladium(II) complexes of tetracyclines. *Journal of Inorganic Biochemistry* **99**(12): 2348–2354. [doi:10.1016/j.jinorgbio.2005.09.001]
375. Belal, F., El-Kerdawy, M. M., El-Ashry, S. M. and El-Wasseef, D. R. 2000. Kinetic spectrophotometric determination of ampicillin and amoxicillin in dosage forms. *II Farmaco* **55**(11–12): 680–686. [doi:10.1016/S0014-827X(00)00080-X]
376. Xue, J.-H., Qian, Q.-M., Wang, Y.-S., Meng, X.-L. and Liu, L. 2013. Resonance light scattering determination of metallothioneins using levofloxacin-palladium complex as a light scattering probe. *Spectrochimica Acta Part A: Molecular and Biomolecular Spectroscopy* **102**: 205–211. [doi:10.1016/j.saa.2012.10.016]
377. El Walily, A. F. M., Belal, S. F. and Bakry, R. S. 1996. Spectrophotometric and spectrofluorimetric estimation of ciprofloxacin and norfloxacin by ternary complex formation with eosin and palladium(II). *Journal of Pharmaceutical and Biomedical Analysis* **14**(5): 561–569. [doi:10.1016/0731-7085(95)01662-7]
378. Bagheri Gh., A., Yosefi Rad, A., Rezvani, M. and Roshanzamir, S. 2012. Spectrophotometric complexation of cephalosporins with palladium (II) chloride in aqueous and non-aqueous solvents. *Spectrochimica Acta Part A: Molecular and Biomolecular Spectroscopy* **89**: 317–321. [doi:10.1016/j.saa.2012.01.002]

379. El-Walily, A. F. M., Gazy, A. A., Belal, S. F. and Khamis, E. F. 2000. Quantitative determination of some thiazole cephalosporins through complexation with palladium(II) chloride. *Journal of Pharmaceutical and Biomedical Analysis* **22**(2): 385–392. [doi:10.1016/S0731-7085(99)00281-2]
380. Vaidya, M. Y., McBain, A. J., Butler, J. A., Banks, C. E. and Whitehead, K. A. 2017. Antimicrobial efficacy and synergy of metal ions against *Enterococcus faecium*, *Klebsiella pneumoniae* and *Acinetobacter baumannii* in planktonic and biofilm phenotypes. *Scientific Reports* **7**(1): 5911. [doi:10.1038/s41598-017-05976-9]
381. Gebel, T., Lantzsch, H., Pleßow, K. and Dunkelberg, H. 1997. Genotoxicity of platinum and palladium compounds in human and bacterial cells. *Mutation Research - Genetic Toxicology and Environmental Mutagenesis* **389**(2–3): 183–190. [doi:10.1016/S1383-5718(96)00145-3]
382. Ullah, S., Ahmad, A., Khan, A., Zhang, J., Raza, M., ur Rahman, A., Tariq, M., Ali khan, U., Zada, S. and Yuan, Q. 2018. Palladium nanoparticles synthesis, characterization using glucosamine as the reductant and stabilizing agent to explore their antibacterial & catalytic applications. *Microbial Pathogenesis* **125**: 150–157. [doi:10.1016/j.micpath.2018.09.020]
383. Adams, C. P., Walker, K. A., Obare, S. O. and Docherty, K. M. 2014. Size-dependent antimicrobial effects of novel palladium nanoparticles. *PLoS ONE* **9**(1): e85981. [doi:10.1371/journal.pone.0085981]
384. Spikes, J. D. and Hodgson, C. F. 1969. Enzyme inhibition by palladium chloride. *Biochemical and Biophysical Research Communications* **35**(3): 420–422. [doi:10.1016/0006-291X(69)90516-6]
385. Shultz, M. D., Lassig, J. P., Gooch, M. G., Evans, B. R. and Woodward, J. 1995. Palladium - a new inhibitor of cellulase activities. *Biochemical and Biophysical Research Communications* **209**(3): 1046–1052. [doi:10.1006/bbrc.1995.1603]
386. Liu, T. Z., Lin, T. F., Chiu, D. T. Y., Tsai, K.-J. and Stern, A. 1997. Palladium or platinum exacerbates hydroxyl radical mediated DNA damage. *Free Radical Biology and Medicine* **23**(1): 155–161. [doi:10.1016/S0891-5849(96)00553-9]
387. Liu, W., Wang, Y. and Jing, C. 2018. Transcriptome analysis of silver, palladium, and selenium stresses in *Pantoea* sp. IMH. *Chemosphere* **208**: 50–58. [doi:10.1016/j.chemosphere.2018.05.169]
388. Lee, L. J., Barrett, J. A. and Poole, R. K. 2005. Genome-wide transcriptional response of chemostat-cultured *Escherichia coli* to zinc. *Journal of Bacteriology* **187**(3): 1124–1134. [doi:10.1128/JB.187.3.1124]
389. Breazeale, S. D., Ribeiro, A. A., McClerren, A. L. and Raetz, C. R. H. 2005. A formyltransferase required for polymyxin resistance in *Escherichia coli* and the modification of lipid A with 4-amino-4-deoxy-L-arabinose: Identification and function of UDP-4-deoxy-4-formamido-L-arabinose. *Journal of Biological Chemistry* **280**(14): 14154–14167. [doi:10.1074/jbc.M414265200]
390. Subashchandrabose, S., Smith, S. N., Spurbeck, R. R., Kole, M. M. and Mobley, H. L. T. 2013. Genome-wide detection of fitness genes in uropathogenic *Escherichia coli* during systemic infection. *PLoS Pathogens* **9**(12): e1003788. [doi:10.1371/journal.ppat.1003788]
391. Inoue, T., Shingaki, R., Hirose, S., Waki, K., Mori, H. and Fukui, K. 2007. Genome-wide screening of genes required for swarming motility in *Escherichia coli* K-12. *Journal of Bacteriology* **189**(3): 950–957. [doi:10.1128/JB.01294-06]

392. El Ghachi, M., Derbise, A., Bouhss, A. and Mengin-Lecreux, D. 2005. Identification of multiple genes encoding membrane proteins with undecaprenyl pyrophosphate phosphatase (UppP) activity in *Escherichia coli*. *Journal of Biological Chemistry* **280**(19): 18689–18695. [doi:10.1074/jbc.M412277200]
393. Klein, G., Müller-Loennies, S., Lindner, B., Kobylak, N., Brade, H. and Raina, S. 2013. Molecular and structural basis of inner core lipopolysaccharide alterations in *Escherichia coli*: Incorporation of glucuronic acid and phosphoethanolamine in the heptose region. *Journal of Biological Chemistry* **288**(12): 8111–8127. [doi:10.1074/jbc.M112.445981]
394. Raivio, T. L., Leblanc, S. K. D. and Price, N. L. 2013. The *Escherichia coli* Cpx envelope stress response regulates genes of diverse function that impact antibiotic resistance and membrane integrity. *Journal of Bacteriology* **195**(12): 2755–2767. [doi:10.1128/JB.00105-13]
395. Sanders, A. N. and Pavelka, M. S. 2013. Phenotypic analysis of *Escherichia coli* mutants lacking L,D-transpeptidases. *Microbiology* **159**(9): 1842–1852. [doi:10.1099/mic.0.069211-0]
396. Xue, Y., Osborn, J., Panchal, A. and Mellies, J. L. 2015. The RpoE stress response pathway mediates reduction of the virulence of enteropathogenic *Escherichia coli* by zinc. *Applied and Environmental Microbiology* **81**(11): 3766–3774. [doi:10.1128/AEM.00507-15]
397. Li, J., Ren, X., Fan, B., Huang, Z., Wang, W., Zhou, H., Lou, Z., Ding, H., Lyu, J. and Tan, G. 2019. Zinc toxicity and iron-sulfur cluster biogenesis in *Escherichia coli*. *Applied and Environmental Microbiology* **85**: e01967-18. [doi:10.1128/AEM.01967-18]
398. Mellies, J. L., Thomas, K., Turvey, M., Evans, N. R., Crane, J., Boedeker, E. and Benison, G. C. 2012. Zinc-induced envelope stress diminishes type III secretion in enteropathogenic *Escherichia coli*. *BMC Microbiology* **12**: 123. [doi:10.1186/1471-2180-12-123]
399. Siani, H. and Maillard, J.-Y. 2015. Best practice in healthcare environment decontamination. *European Journal of Clinical Microbiology & Infectious Diseases* **34**(1): 1–11. [doi:10.1007/s10096-014-2205-9]
400. Nemeth, J., Oesch, G. and Kuster, S. P. 2015. Bacteriostatic versus bactericidal antibiotics for patients with serious bacterial infections: Systematic review and meta-analysis. *Journal of Antimicrobial Chemotherapy* **70**(2): 382–395. [doi:10.1093/jac/dku379]
401. Maillard, J. Y. 2002. Bacterial target sites for biocide action. *Journal of Applied Microbiology Symposium Supplement* **92**: 16S-27S.
402. Shoemaker, G. L., Anderson, J. B. and Kostiner, E. 1977. Copper(II) phosphate. *Acta Crystallographica Section B Structural Crystallography and Crystal Chemistry* **33**(9): 2969–2972. [doi:10.1107/S0567740877010012]
403. Grunenwald, C. M., Choby, J. E., Juttukonda, L. J., Beavers, W. N., Weiss, A., Torres, V. J. and Skaar, E. P. 2019. Manganese detoxification by MntE is critical for resistance to oxidative stress and virulence of *Staphylococcus aureus*. *mBio* **10**: e02915-18. [doi:10.1128/mBio.02915-18]
404. Sajed, T., Marcu, A., Ramirez, M., Pon, A., Guo, A. C., Knox, C., Wilson, M., Grant, J. R., Djoumbou, Y. and Wishart, D. S. 2016. ECMDB 2.0: A richer resource for understanding the biochemistry of *E. coli*. *Nucleic Acids Research* **44**(D1): D495–D501. [doi:10.1093/nar/gkv1060]

405. Meganathan, R. 2001. Ubiquinone biosynthesis in microorganisms. *FEMS Microbiology Letters* **203**(2): 131–139. [doi:10.1016/S0378-1097(01)00330-5]
406. Bekker, M., de Vries, S., Ter Beek, A., Hellingwerf, K. J. and Teixeira de Mattos, M. J. 2009. Respiration of *Escherichia coli* can be fully uncoupled via the nonelectrogenic terminal cytochrome bd-II oxidase. *Journal of Bacteriology* **191**(17): 5510–5517. [doi:10.1128/JB.00562-09]
407. Henkel, S. G., Ter Beek, A., Steinsiek, S., Stagge, S., Bettenbrock, K., Teixeira de Mattos, M. J., Sauter, T., Sawodny, O. and Ederer, M. 2014. Basic regulatory principles of *Escherichia coli*'s electron transport chain for varying oxygen conditions. *PLoS ONE* **9**(9): e107640. [doi:10.1371/journal.pone.0107640]
408. Ruggerone, P., Murakami, S., Pos, K. M. and Vargiu, A. V. 2013. RND efflux pumps: Structural information translated into function and inhibition mechanisms. *Current Topics in Medicinal Chemistry* **13**(24): 3079–3100. [doi:10.2174/15680266113136660220]
409. Ruiz, C. and Levy, S. B. 2014. Regulation of *acrAB* expression by cellular metabolites in *Escherichia coli*. *Journal of Antimicrobial Chemotherapy* **69**(2): 390–399. [doi:10.1093/jac/dkt352]
410. Pletzer, D. and Weingart, H. 2014. Characterization and regulation of the Resistance-Nodulation-Cell Division-type multidrug efflux pumps MdtABC and MdtUVW from the fire blight pathogen *Erwinia amylovora*. *BMC Microbiology* **14**: 185. [doi:10.1186/1471-2180-14-185]
411. Takahashi, H., Oshima, T., Hobman, J. L., Doherty, N., Clayton, S. R., Iqbal, M., Hill, P. J., Tobe, T., Ogasawara, N., Kanaya, S. and Stekel, D. J. 2015. The dynamic balance of import and export of zinc in *Escherichia coli* suggests a heterogeneous population response to stress. *Journal of the Royal Society Interface* **12**: 20150069. [doi:10.1098/rsif.2015.0069]
412. Moore, C. M. and Helmann, J. D. 2005. Metal ion homeostasis in *Bacillus subtilis*. *Current Opinion in Microbiology* **8**(2): 188–195. [doi:10.1016/j.mib.2005.02.007]
413. Yang, M., Mu, T., Zhong, W., Olajuyin, A. M. and Xing, J. 2017. Analysis of gluconate metabolism for pyruvate production in engineered *Escherichia coli* based on genome-wide transcriptomes. *Letters in Applied Microbiology* **65**(2): 165–172. [doi:10.1111/lam.12758]
414. Barbur, R. G. H. and Vincent, J. M. 1950. The bacteriostatic action of phenol, benzoic acid and related compounds on *Bacterium aerogenes*. *Journal of General Microbiology* **4**(2): 110–121. [doi:10.1099/00221287-4-2-110]
415. Pankey, G. A. and Sabath, L. D. 2004. Clinical relevance of bacteriostatic versus bactericidal mechanisms of action in the treatment of Gram-positive bacterial infections. *Clinical Infectious Diseases* **38**(6): 864–870. [doi:10.1086/381972]
416. Falck, E., Hautala, J. T., Karttunen, M., Kinnunen, P. K. J., Patra, M., Saaren-Seppälä, H., Vattulainen, I., Wiedmer, S. K. and Holopainen, J. M. 2006. Interaction of fusidic acid with lipid membranes: Implications to the mechanism of antibiotic activity. *Biophysical Journal* **91**(5): 1787–1799. [doi:10.1529/biophysj.106.084525]
417. Helle, A., Mäkitalo, J., Huhtanen, J., Holopainen, J. M. and Wiedmer, S. K. 2008. Antibiotic fusidic acid has strong interactions with negatively charged lipid membranes: An electrokinetic capillary chromatographic study. *Biochimica et Biophysica Acta* **1778**(11): 2640–2647. [doi:10.1016/j.bbamem.2008.06.019]

418. Muhonen, J., Vidgren, J., Helle, A., Yohannes, G., Viitala, T., Holopainen, J. M. and Wiedmer, S. K. 2008. Interactions of fusidic acid and elongation factor G with lipid membranes. *Analytical Biochemistry* **374**(1): 133–142. [doi:10.1016/j.ab.2007.10.014]
419. Dombek, K. M. and Ingram, L. O. 1984. Effects of ethanol on the *Escherichia coli* plasma membrane. *Journal of Bacteriology* **157**(1): 233–239.
420. Dyrda, G., Boniewska-Bernacka, E., Man, D., Barchiewicz, K. and Słota, R. 2019. The effect of organic solvents on selected microorganisms and model liposome membrane. *Molecular Biology Reports* **46**(3): 3225–3232. [doi:10.1007/s11033-019-04782-y]
421. Yu, Z.-W. and Quinn, P. J. 1998. Solvation effects of dimethyl sulphoxide on the structure of phospholipid bilayers. *Biophysical Chemistry* **70**(1): 35–39. [doi:10.1016/S0301-4622(97)00100-2]
422. Yamashita, Y., Kinoshita, K. and Yamazaki, M. 2000. Low concentration of DMSO stabilizes the bilayer gel phase rather than the interdigitated gel phase in dihexadecylphosphatidylcholine membrane. *Biochimica et Biophysica Acta - Biomembranes* **1467**(2): 395–405. [doi:10.1016/S0005-2736(00)00237-6]
423. Sum, A. K. and de Pablo, J. J. 2003. Molecular simulation study on the influence of dimethylsulfoxide on the structure of phospholipid bilayers. *Biophysical Journal* **85**(6): 3636–3645.
424. Zhang, L., Liu, R., Gung, B. W., Tindall, S., Gonzalez, J. M., Halvorson, J. J. and Hagerman, A. E. 2016. Polyphenol-aluminum complex formation: Implications for aluminum tolerance in plants. *Journal of Agricultural and Food Chemistry* **64**(15): 3025–3033. [doi:10.1021/acs.jafc.6b00331]
425. Kiss, T. 2013. From coordination chemistry to biological chemistry of aluminium. *Journal of Inorganic Biochemistry* **128**: 156–163. [doi:10.1016/j.jinorgbio.2013.06.013]
426. Auda, S. H., Mrestani, Y., Nies, D. H., Große, C. and Neubert, R. H. H. 2009. Preparation, physicochemical characterization and biological evaluation of cefodizime metal ion complexes. *Journal of Pharmacy and Pharmacology* **61**(6): 753–758. [doi:10.1211/jpp/61.06.0007]
427. Alovero, F. L., Olivera, M. E. and Manzo, R. H. 2003. *In vitro* pharmacodynamic properties of a fluoroquinolone pharmaceutical derivative: Hydrochloride of ciprofloxacin-aluminium complex. *International Journal of Antimicrobial Agents* **21**(5): 446–451. [doi:10.1016/S0924-8579(03)00051-7]
428. Breda, S. A., Jimenez-Kairuz, A. F., Manzo, R. H. and Olivera, M. E. 2009. Solubility behavior and biopharmaceutical classification of novel high-solubility ciprofloxacin and norfloxacin pharmaceutical derivatives. *International Journal of Pharmaceutics* **371**(1–2): 106–113. [doi:10.1016/j.ijpharm.2008.12.026]
429. Foye, W. O., Lange, W. E., Swintosky, J. V., Chamberlain, R. E. and Guarini, J. R. 1955. Metal chelates of streptomycin. *Journal of the American Pharmaceutical Association* **44**(5): 261–263. [doi:10.1002/jps.3030440503]
430. Niebergall, P. J., Hussar, D. A., Cressman, W. A., Sugita, E. T. and Doluisio, J. T. 1966. Metal binding tendencies of various antibiotics. *Journal of Pharmacy and Pharmacology* **18**(11): 729–738. [doi:10.1111/j.2042-7158.1966.tb07794.x]
431. Eze, F. I., Ajali, U. and Ukoha, P. O. 2014. Synthesis, physicochemical properties, and antimicrobial studies of iron(III) complexes of ciprofloxacin, cloxacillin, and amoxicillin. *International Journal of Medicinal Chemistry* : 735602. [doi:10.1155/2014/735602]

432. Möhler, J. S., Kolmar, T., Synnatschke, K., Hergert, M., Wilson, L. A., Ramu, S., Elliott, A. G., Blaskovich, M. A. T., Sidjabat, H. E., Paterson, D. L., Schenk, G., Cooper, M. A. and Ziora, Z. M. 2017. Enhancement of antibiotic-activity through complexation with metal ions - Combined ITC, NMR, enzymatic and biological studies. *Journal of Inorganic Biochemistry* **167**: 134–141. [doi:10.1016/j.jinorgbio.2016.11.028]
433. Niepa, T. H. R., Wang, H., Dabrowiak, J. C., Gilbert, J. L. and Ren, D. 2016. Synergy between tobramycin and trivalent chromium ion in electrochemical control of *Pseudomonas aeruginosa*. *Acta Biomaterialia* **36**: 286–295. [doi:10.1016/j.actbio.2016.03.028]
434. Baranauskienė, L., Petrikaitė, V., Matulienė, J. and Matulis, D. 2009. Titration calorimetry standards and the precision of isothermal titration calorimetry data. *International Journal of Molecular Sciences* **10**: 2752–2762. [doi:10.3390/ijms10062752]
435. Freire, E., Mayorga, O. L. and Straume, M. 1990. Isothermal titration calorimetry. *Analytical Chemistry* **62**(18): 950A-959A. [doi:10.1021/ac00217a002]
436. Quinn, C. F., Carpenter, M. C., Croteau, M. L. and Wilcox, D. E. 2016. Isothermal Titration Calorimetry Measurements of Metal Ions Binding to Proteins. in *Methods in Enzymology* **567**: 3–21. [doi:10.1016/bs.mie.2015.08.021]
437. Klebe, G. 2015. Applying thermodynamic profiling in lead finding and optimization. *Nature Reviews Drug Discovery* **14**(2): 95–110. [doi:10.1038/nrd4486]
438. Vander Meulen, K. A., Horowitz, S., Trievel, R. C. and Butcher, S. E. 2016. Measuring the Kinetics of Molecular Association by Isothermal Titration Calorimetry. in *Methods in Enzymology* **567**: 181–213. [doi:10.1016/bs.mie.2015.08.012]
439. Cuskin, F., Flint, J. E., Gloster, T. M., Morland, C., Baslé, A., Henrissat, B., Coutinho, P. M., Strazzulli, A., Solovyova, A. S., Davies, G. J. and Gilbert, H. J. 2012. How nature can exploit nonspecific catalytic and carbohydrate binding modules to create enzymatic specificity. *Proceedings of the National Academy of Sciences of the United States of America* **109**(51): 20889–20894. [doi:10.1073/pnas.1212034109]
440. Richard, H. and Foster, J. W. 2004. *Escherichia coli* glutamate- and arginine-dependent acid resistance systems increase internal pH and reverse transmembrane potential. *Journal of Bacteriology* **186**(18): 6032–6041. [doi:10.1128/JB.186.18.6032-6041.2004]
441. De Biase, D. and Lund, P. A. 2015. The *Escherichia coli* acid stress response and its significance for pathogenesis. in *Advances in Applied Microbiology* **92**: 49–88. [doi:10.1016/bs.aambs.2015.03.002]
442. Lund, P., Tramonti, A. and De Biase, D. 2014. Coping with low pH: Molecular strategies in neutralophilic bacteria. *FEMS Microbiology Reviews* **38**(6): 1091–1125. [doi:10.1111/1574-6976.12076]
443. Carey, M. C. and Small, D. M. 1971. Micellar properties of sodium fusidate, a steroid antibiotic structurally resembling the bile salts. *Journal of Lipid Research* **12**: 604–613.
444. Henderson, L. J. 1908. Concerning the relationship between the strength of acids and their capacity to preserve neutrality. *American Journal of Physiology* **21**(2): 173–179. [doi:10.1152/ajplegacy.1908.21.2.173]

445. Hasselbalch, K. A. 1917. Die Berechnung der Wasserstoffzahl des Blutes aus der freien und gebundenen Kohlensäure desselben, und die Sauerstoffbindung des Blutes als Funktion der Wasserstoffzahl. *Biochemische Zeitschrift* **78**: 112–144.
446. Carey, M. C., Montet, J.-C. and Small, D. M. 1975. Surface and solution properties of steroid antibiotics: 3-acetoxylfusidic acid, cephalosporin P1 and helvolic acid. *Biochemistry* **14**(22): 4896–4905.
447. Royce, L. A., Boggess, E., Fu, Y., Liu, P., Shanks, J. V., Dickerson, J. and Jarboe, L. R. 2014. Transcriptomic analysis of carboxylic acid challenge in *Escherichia coli*: Beyond membrane damage. *PLoS ONE* **9**(2): e89590. [doi:10.1371/journal.pone.0089580]
448. Ferreira, C. M. H., Pinto, I. S. S., Soares, E. V. and Soares, H. M. V. M. 2015. (Un)suitability of the use of pH buffers in biological, biochemical and environmental studies and their interaction with metal ions – a review. *RSC Advances* **5**(39): 30989–31003. [doi:10.1039/C4RA15453C]
449. Yu, Q., Kandegedara, A., Xu, Y. and Rorabacher, D. B. 1997. Avoiding interferences from Good's buffers: A contiguous series of noncomplexing tertiary amine buffers covering the entire range of pH 3-11. *Analytical Biochemistry* **253**: 50–56.
450. Lemaire, S., Van Bambeke, F., Pierard, D., Appelbaum, P. C. and Tulkens, P. M. 2011. Activity of fusidic acid against extracellular and intracellular *Staphylococcus aureus*: Influence of pH and comparison with linezolid and clindamycin. *Clinical Infectious Diseases* **52**(Suppl 7): S493–S503. [doi:10.1093/cid/cir165]
451. Zhang, L., Liu, Y., Wang, Y., Xu, M. and Hu, X. 2018. UV–Vis spectroscopy combined with chemometric study on the interactions of three dietary flavonoids with copper ions. *Food Chemistry* **263**: 208–215. [doi:10.1016/j.foodchem.2018.05.009]
452. Richard, A. J. 1975. Ultracentrifugal study of effect of sodium chloride on micelle size of fusidate sodium. *Journal of Pharmaceutical Sciences* **64**(5): 873–875.
453. Coello, A., Meijide, F., Rodríguez Núñez, E. and Tato, J. V. 1994. Aggregation behavior of sodium fusidate in aqueous solution. *Journal of Pharmaceutical Sciences* **83**(6): 828–832. [doi:10.1002/jps.2600830614]
454. Lyklema, J. 2013. Coagulation by multivalent counterions and the Schulze-Hardy rule. *Journal of Colloid and Interface Science* **392**(1): 102–104. [doi:10.1016/j.jcis.2012.09.066]
455. Spedding, P. L., Grimshaw, J. and O'Hare, K. D. 1993. Abnormal evaporation rate of ethanol from low concentration aqueous solutions. *Langmuir* **9**(5): 1408–1413. [doi:10.1021/la00029a040]
456. Weinberg, E. D. 1955. The effect of Mn⁺⁺ and antimicrobial drugs on sporulation of *Bacillus subtilis* in nutrient broth. *Journal of Bacteriology* **70**(3): 289–296.
457. Eisenberg, R. C. and Dobrogosz, W. J. 1967. Gluconate metabolism in *Escherichia coli*. *Journal of Bacteriology* **93**(3): 941–949.
458. Chevalier, S., Bouffartigues, E., Bodilis, J., Maillot, O., Lesouhaitier, O., Feuilloley, M. G. J., Orange, N., Dufour, A. and Cornelis, P. 2017. Structure, function and regulation of *Pseudomonas aeruginosa* porins. *FEMS Microbiology Reviews* **41**(5): 698–722. [doi:10.1093/femsre/fux020]
459. Raetz, C. R. H. and Whitfield, C. 2002. Lipopolysaccharide endotoxins. *Annual Review of Biochemistry* **71**(1): 635–700. [doi:10.1146/annurev.biochem.71.110601.135414]

460. Llobet, E., Martínez-Moliner, V., Moranta, D., Dahlström, K. M., Regueiro, V., Tomás, A., Cano, V., Pérez-Gutiérrez, C., Frank, C. G., Fernández-Carrasco, H., Insua, J. L., Salminen, T. A., Garmendia, J. and Bengoechea, J. A. 2015. Deciphering tissue-induced *Klebsiella pneumoniae* lipid A structure. *Proceedings of the National Academy of Sciences of the United States of America* **112**(46): E6369–E6378. [doi:10.1073/pnas.1508820112]
461. Pier, G. B. 2007. *Pseudomonas aeruginosa* lipopolysaccharide: A major virulence factor, initiator of inflammation and target for effective immunity. *International Journal of Medical Microbiology* **297**(5): 277–295. [doi:10.1016/j.ijmm.2007.03.012]
462. Nishino, K., Hsu, F.-F., Turk, J., Cromie, M. J., Wösten, M. M. S. M. and Groisman, E. A. 2006. Identification of the lipopolysaccharide modifications controlled by the *Salmonella* PmrA/PmrB system mediating resistance to Fe(III) and Al(III). *Molecular Microbiology* **61**(3): 645–654. [doi:10.1111/j.1365-2958.2006.05273.x]
463. Bruggaber, S. F. A., French, G., Thompson, R. P. H. and Powell, J. J. 2004. Selective and effective bactericidal activity of the cobalt(II) cation against *Helicobacter pylori*. *Helicobacter* **9**(5): 422–428. [doi:10.1111/j.1083-4389.2004.00264.x]
464. Hassen, A., Saidi, N., Cherif, M. and Boudabous, A. 1998. Effects of heavy metals on *Pseudomonas aeruginosa* and *Bacillus thuringiensis*. *Bioresource Technology* **65**: 73–82.
465. Tengerdy, R. P., Nagy, J. G. and Martin, B. 1967. Quantitative measurement of bacterial growth by the reduction of tetrazolium salts. *Applied Microbiology* **15**(4): 954–955.
466. Aslam, S., Lan, X.-R., Zhang, B.-W., Chen, Z.-L., Wang, L. and Niu, D.-K. 2019. Aerobic prokaryotes do not have higher GC contents than anaerobic prokaryotes, but obligate aerobic prokaryotes have. *BMC Evolutionary Biology* **19**: 35. [doi:10.1186/s12862-019-1365-8]
467. LaBaer, J., Qiu, Q., Anumanthan, A., Mar, W., Zuo, D., Murthy, T. V. S., Taycher, H., Halleck, A., Hainsworth, E., Lory, S. and Brizuela, L. 2004. The *Pseudomonas aeruginosa* PAO1 gene collection. *Genome Research* **14**: 2190–2200. [doi:10.1101/gr.2482804]
468. Rafiq, Z., Sam, N. and Vaidyanathan, R. 2016. Whole genome sequence of *Klebsiella pneumoniae* U25, a hypermucoviscous, multidrug resistant, biofilm producing isolate from India. *Memorias do Instituto Oswaldo Cruz* **111**(2): 144–146. [doi:10.1590/0074-02760150423]
469. Muto, A. and Osawa, S. 1987. The guanine and cytosine content of genomic DNA and bacterial evolution. *Proceedings of the National Academy of Sciences of the United States of America* **84**(1): 166–169. [doi:10.1073/pnas.84.1.166]
470. Harrison, J. J., Turner, R. J. and Ceri, H. 2005. Persister cells, the biofilm matrix and tolerance to metal cations in biofilm and planktonic *Pseudomonas aeruginosa*. *Environmental Microbiology* **7**(7): 981–994. [doi:10.1111/j.1462-2920.2005.00777.x]
471. Wales, A. D. and Davies, R. H. 2015. Co-selection of resistance to antibiotics, biocides and heavy metals, and its relevance to foodborne pathogens. *Antibiotics* **4**(4): 567–604. [doi:10.3390/antibiotics4040567]
472. Alley, M. C., Scudiero, D. A., Monks, A., Hursey, M. L., Czerwinski, M. J., Fine, D. L., Abbott, B. J., Mayo, J. G., Shoemaker, R. H. and Boyd, M. R. 1988. Feasibility of drug screening with panels of human tumor cell lines using a microculture tetrazolium assay. *Cancer Research* **48**: 589–601.

473. Diamond, L., Kruszewski, F., Aden, D. P., Knowles, B. B. and Baird, W. M. 1980. Metabolic activation of benzo[a]pyrene by a human hepatoma cell line. *Carcinogenesis* **1**(10): 871–875. [doi:10.1093/carcin/1.10.871]
474. Boukamp, P., Petrussevska, R. T., Breitkreutz, D., Hornung, J., Markham, A. and Fusenig, N. E. 1988. Normal keratinization in a spontaneously immortalized aneuploid human keratinocyte cell line. *Journal of Cell Biology* **106**(3): 761–771. [doi:10.1083/jcb.106.3.761]
475. Saarinen-Savolainen, P., Järvinen, T., Araki-Sasaki, K., Watanabe, H. and Urtti, A. 1998. Evaluation of cytotoxicity of various ophthalmic drugs, eye drop excipients and cyclodextrins in an immortalized human corneal epithelial cell line. *Pharmaceutical Research* **15**(8): 1275–1280. [doi:10.1023/a:1011956327987]
476. Arora, A. and Mitragotri, S. 2010. Novel topical microbicides through combinatorial strategies. *Pharmaceutical Research* **27**(7): 1264–1272. [doi:10.1007/s11095-010-0095-9]
477. Korzeniewski, C. and Callewaert, D. M. 1983. An enzyme-release assay for natural cytotoxicity. *Journal of Immunological Methods* **64**(3): 313–320. [doi:10.1016/0022-1759(83)90438-6]
478. Repetto, G., del Peso, A. and Zurita, J. L. 2008. Neutral red uptake assay for the estimation of cell viability/cytotoxicity. *Nature Protocols* **3**(7): 1125–1131. [doi:10.1038/nprot.2008.75]
479. Lapham, K., Novak, J., Marroquin, L. D., Swiss, R., Qin, S., Strock, C. J., Scialis, R., Aleo, M. D., Schroeter, T., Eng, H., Rodrigues, A. D. and Kalgutkar, A. S. 2016. Inhibition of hepatobiliary transport activity by the antibacterial agent fusidic acid: Insights into factors contributing to conjugated hyperbilirubinemia/cholestasis. *Chemical Research in Toxicology* **29**(10): 1778–1788. [doi:10.1021/acs.chemrestox.6b00262]
480. Struys-Ponsar, C., Guillard, O. and van den Bosch de Aguilar, P. 2000. Effects of aluminum exposure on glutamate metabolism: A possible explanation for its toxicity. *Experimental Neurology* **163**: 157–164. [doi:10.1006/exnr.2000.7355]
481. Rakers, S., Imse, F. and Gebert, M. 2014. Real-time cell analysis: Sensitivity of different vertebrate cell cultures to copper sulfate measured by xCELLigence®. *Ecotoxicology* **23**(8): 1582–1591. [doi:10.1007/s10646-014-1279-6]
482. Ponsoda, X., Jover, R., Núñez, C., Royo, M., Castell, J. V. and Gómez-Lechón, M. J. 1995. Evaluation of the cytotoxicity of 10 chemicals in human and rat hepatocytes and in cell lines: Correlation between *in vitro* data and human lethal concentration. *Toxicology in Vitro* **9**(6): 959–966.
483. Jover, R., Ponsoda, X., Castell, J. V. and Gómez-Lechón, M. J. 1992. Evaluation of the cytotoxicity of ten chemicals on human cultured hepatocytes: Predictability of human toxicity and comparison with rodent cell culture systems. *Toxicology in Vitro* **6**(1): 47–52.
484. Nestler, L., Evege, E., McLaughlin, J., Munroe, D., Tan, T., Wagner, K. and Stiles, B. 2004. TrypLE™ Express: A temperature stable replacement for animal trypsin in cell dissociation applications. *Quest* **1**(1): 42–47.
485. Latner, A. L. 1964. The dehydrogenase isoenzymes. *Proceedings of the Association of Clinical Biochemists* **3**(3): 120–129. [doi:10.1177/036985646400300311]

486. Lee, J.-B., Kim, S.-H., Lee, S.-C., Kim, H.-G., Ahn, H.-G., Li, Z. and Yoon, K. C. 2014. Blue light-induced oxidative stress in human corneal epithelial cells: Protective effects of ethanol extracts of various medicinal plant mixtures. *Investigative Ophthalmology and Visual Science* **55**(7): 4119–4127. [doi:10.1167/iov.13-13441]
487. Zheng, L. L., Myung, D., Yu, C. Q. and Ta, C. N. 2015. Comparative *in vitro* cytotoxicity of artificial tears. *JSM Ophthalmology* **3**(1): 1026.
488. Orme, I., Secrist, J., Anathan, S., Kwong, C., Maddry, J., Reynolds, R., Poffenberger, A., Michael, M., Miller, L., Krahenbuh, J., Adams, L., Biswas, A., Franzblau, S., Rouse, D., Winfield, D. and Brooks, J. 2001. Search for new drugs for treatment of tuberculosis. *Antimicrobial Agents and Chemotherapy* **45**(7): 1943–1946. [doi:10.1128/AAC.45.7.1943-1946.2001]
489. Inan-Eroglu, E. and Ayaz, A. 2018. Is aluminum exposure a risk factor for neurological disorders? *Journal of Research in Medical Sciences* **23**(1): 51. [doi:10.4103/jrms.JRMS_921_17]
490. Zhu, Y. and Weldon, J. E. 2019. Evaluating the influence of common antibiotics on the efficacy of a recombinant immunotoxin in tissue culture. *BMC Research Notes* **12**: 293. [doi:10.1186/s13104-019-4337-6]
491. Zhang, L., Ging, N. C., Komoda, T., Hanada, T., Suzuki, T. and Watanabe, K. 2005. Antibiotic susceptibility of mammalian mitochondrial translation. *FEBS Letters* **579**: 6423–6427. [doi:10.1016/j.febslet.2005.09.103]
492. Mulcahy, L. R., Isabella, V. M. and Lewis, K. 2014. *Pseudomonas aeruginosa* biofilms in disease. *Microbial Ecology* **68**(1): 1–12. [doi:10.1007/s00248-013-0297-x]
493. Stefani, S., Campana, S., Cariani, L., Carnovale, V., Colombo, C., Lleo, M. M., Iula, V. D., Minicucci, L., Morelli, P., Pizzamiglio, G. and Taccetti, G. 2017. Relevance of multidrug-resistant *Pseudomonas aeruginosa* infections in cystic fibrosis. *International Journal of Medical Microbiology* **307**(6): 353–362. [doi:10.1016/j.ijmm.2017.07.004]
494. Franzco, I. C. 2012. Fluids of the ocular surface: Concepts, functions and physics. *Clinical and Experimental Ophthalmology* **40**(6): 634–643. [doi:10.1111/j.1442-9071.2012.02758.x]
495. Hagigit, T., Nassar, T., Behar-Cohen, F., Lambert, G. and Benita, S. 2008. The influence of cationic lipid type on *in-vitro* release kinetic profiles of antisense oligonucleotide from cationic nanoemulsions. *European Journal of Pharmaceutics and Biopharmaceutics* **70**: 248–259. [doi:10.1016/j.ejpb.2008.03.005]
496. Rebeix, V., Sommer, F., Marchin, B., Baude, D. and Duc, T. M. 2000. Artificial tear adsorption on soft contact lenses: Methods to test surfactant efficacy. *Biomaterials* **21**: 1197–1205.
497. Aristoteli, L. P. and Willcox, M. D. P. 2003. Mucin degradation mechanisms by distinct *Pseudomonas aeruginosa* isolates *in vitro*. *Infection and Immunity* **71**(10): 5565–5575. [doi:10.1128/IAI.71.10.5565]
498. Rozier, A., Mazuel, C., Grove, J. and Plazonnet, B. 1989. Gelrite®: A novel, ion-activated, *in-situ* gelling polymer for ophthalmic vehicles. Effect on bioavailability of timolol. *International Journal of Pharmaceutics* **57**: 163–168.
499. Miyazaki, S., Suzuki, S., Kawasaki, N., Endo, K., Takahashi, A. and Attwood, D. 2001. *In situ* gelling xyloglucan formulations for sustained release ocular delivery of pilocarpine hydrochloride. *International Journal of Pharmaceutics* **229**: 29–36.

500. Anumolu, S. S., Singh, Y., Gao, D., Stein, S. and Sinko, P. J. 2009. Design and evaluation of novel fast forming pilocarpine-loaded ocular hydrogels for sustained pharmacological response. *Journal of Controlled Release* **137**(2): 152–159. [doi:10.1016/j.jconrel.2009.03.016]
501. Marques, M. R. C., Loebenberg, R. and Almukainzi, M. 2011. Simulated biological fluids with possible application in dissolution testing. *Dissolution Technologies* (August): 15–28. [doi:10.14227/DT180311P15]
502. Prager, M. D. and Quintana, R. P. 1997. Radiochemical studies on contact lens soiling. I. Lens uptake of ¹⁴C-lysozyme from simple and complex artificial tear solutions. *Journal of Biomedical Materials Research* **36**: 119–124.
503. Lorentz, H., Heynen, M., Kay, L. M. M., Dominici, C. Y., Khan, W., Ng, W. W. S. and Jones, L. 2011. Contact lens physical properties and lipid deposition in a novel characterized artificial tear solution. *Molecular Vision* **17**: 3392–3405.
504. Sicard, J.-F., Le Bihan, G., Vogeleer, P., Jacques, M. and Harel, J. 2017. Interactions of intestinal bacteria with components of the intestinal mucus. *Frontiers in Cellular and Infection Microbiology* **7**: 387. [doi:10.3389/fcimb.2017.00387]
505. Ohneck, E. J., Arivett, B. A., Fiester, S. E., Wood, C. R., Metz, M. L., Simeone, G. M. and Actis, L. A. 2018. Mucin acts as a nutrient source and a signal for the differential expression of genes coding for cellular processes and virulence factors in *Acinetobacter baumannii*. *PLoS ONE* **13**(1): e0190599. [doi:10.1371/journal.pone.0190599]
506. Jessberger, N., Dietrich, R., Mohr, A.-K., Da Riol, C. and Märtlbauer, E. 2019. Porcine gastric mucin triggers toxin production of enteropathogenic *Bacillus cereus*. *Infection and Immunity* **87**(4): e00765-18. [doi:10.1128/IAI.00765-18]
507. Lal, H., Ahluwalia, B. K., Khurana, A. K., Sharma, S. K. and Gupta, S. 1991. Tear lysozyme levels in bacterial, fungal and viral corneal ulcers. *Acta Ophthalmologica* **69**(4): 530–532. [doi:10.1111/j.1755-3768.1991.tb02034.x]
508. Romano, A. C., Espana, E. M., Yoo, S. H., Budak, M. T., Wolosin, J. M. and Tseng, S. C. G. 2003. Different cell sizes in human limbal and central corneal basal epithelia measured by confocal microscopy and flow cytometry. *Investigative Ophthalmology and Visual Science* **44**(12): 5125–5129. [doi:10.1167/iovs.03-0628]
509. Gipson, I. K., Spurr-Michaud, S., Tisdale, A. and Menon, B. B. 2014. Comparison of the transmembrane mucins MUC1 and MUC16 in epithelial barrier function. *PLoS ONE* **9**(6): e100393. [doi:10.1371/journal.pone.0100393]
510. Kesimer, M. and Sheehan, J. K. 2012. Mass spectrometric analysis of mucin core proteins. in *Methods in Molecular Biology* **842**: 67–79. [doi:10.1007/978-1-61779-513-8_4]
511. Baeyens, V. and Gurny, R. 1997. Chemical and physical parameters of tears relevant for the design of ocular drug delivery formulations. *Pharmaceutica Acta Helveticae* **72**(4): 191–202.
512. Davidson, H. J. and Kuonen, V. J. 2004. The tear film and ocular mucins. *Veterinary Ophthalmology* **7**(2): 71–77.
513. Wizert, A., Iskander, D. R. and Cwiklik, L. 2014. Organization of lipids in the tear film: A molecular-level view. *PLoS ONE* **9**(3): e92461. [doi:10.1371/journal.pone.0092461]

514. Bachman, W. G. and Wilson, G. 1985. Essential ions for maintenance of the corneal epithelial surface. *Investigative Ophthalmology & Visual Science* **26**(11): 1484–1488.
515. Mirejovsky, D., Patel, A. S., Rodriguez, D. D. and Hunt, T. J. 1991. Lipid adsorption onto hydrogel contact lens materials: advantages of Nile Red over Oil Red O on visualization of lipids. *Optometry and Vision Science* **68**(11): 858–865.
516. Cowell, B. A., Willcox, M. D. P. and Schneider, R. P. 1997. Growth of Gram-negative bacteria in a simulated ocular environment. *Australian and New Zealand Journal of Ophthalmology* **25**(Suppl 1): S23–S26.
517. Ng, A., Heynen, M., Luensmann, D., Subbaraman, L. N. and Jones, L. 2013. Impact of tear film components on the conformational state of lysozyme deposited on contact lenses. *Journal of Biomedical Materials Research B: Applied Biomaterials* **101B**: 1172–1181. [doi:10.1002/jbm.b.32927]
518. Lee, S. E., Kim, S. R. and Park, M. 2017. Influence of tear protein deposition on the oxygen permeability of soft contact lenses. *Journal of Ophthalmology* : 5131764. [doi:10.1155/2017/5131764]
519. Rändler, C., Matthes, R., McBain, A. J., Giese, B., Fraunholz, M., Sietmann, R., Kohlmann, T., Hübner, N.-O. and Kramer, A. 2010. A three-phase *in-vitro* system for studying *Pseudomonas aeruginosa* adhesion and biofilm formation upon hydrogel contact lenses. *BMC Microbiology* **10**: 282.
520. van Haeringen, N. J. 1981. Clinical biochemistry of tears. *Survey of Ophthalmology* **26**(2): 84–96.
521. Thaysen, J. H. and Thorn, N. A. 1954. Excretion of urea, sodium, potassium and chlorine in human tears. *American Journal of Physiology* **178**(1): 160–164.
522. Semeraro, F., Costagliola, C., Cancarini, A., Gilberti, E., Tosco, E. and Apostoli, P. 2012. Defining reference values of trace elements in the tear film: Diagnostic methods and possible applications. *Ecotoxicology and Environmental Safety* **80**: 190–194. [doi:10.1016/j.ecoenv.2012.02.021]
523. van Haeringen, N. J. and Glasius, E. 1977. Collection method dependant concentrations of some metabolites in human tear fluid, with special reference to glucose in hyperglycaemic conditions. *Albrecht von Graefes Archiv für Klinische und Experimentelle Ophthalmologie* **202**(1): 1–7. [doi:10.1007/BF00496763]
524. Farris, R. L. 1985. Tear analysis in contact lens wearers. *Transactions of the American Ophthalmological Society* **83**: 501–545.
525. Daum, K. M. and Hill, R. M. 1982. Human tear glucose. *Investigative Ophthalmology and Visual Science* **22**(4): 509–514. [doi:10.1167/iovs.10-6948]
526. Lowther, G. E., Miller, R. B. and Hill, R. M. 1970. Tear concentrations of sodium and potassium during adaptation to contact lenses - I. Sodium observations. *Optometry and Vision Science* **47**(4): 266–275.
527. di Sant'Agnes, P. A., Grossman, H., Darling, R. C. and Denning, C. R. 1958. Saliva, tears and duodenal contents in cystic fibrosis of the pancreas. *Pediatrics* **22**: 507–514.
528. Miller, R. B. 1970. Tear concentrations of sodium and potassium during adaptation to contact lenses - II. Potassium observations. *Optometry and Vision Science* **47**(10): 773–779.
529. Huth, S. W., Hirano, P. and Leopold, I. H. 1980. Calcium in tears and contact lens wear. *Archives of Ophthalmology* **98**(1): 122–125. [doi:10.1001/archophth.1980.01020030124013]

530. Savir, H., Sidi, Y. and Pinkhas, J. 1977. Tear calcium and magnesium levels of normal subjects and patients with hypocalcemia or hypercalcemia. *Investigative Ophthalmology & Visual Science* **16**(12): 1150–1151.
531. Winder, A. F., Ruben, M. and Sheraidah, G. A. K. 1977. Tear calcium levels and contact lens wear. *British Journal of Ophthalmology* **61**(8): 539–543.
532. Schmidt, P. P., Schoessler, J. P. and Hill, R. M. 1974. Effects of hard contact lenses on the chloride ion of the tears. *Optometry and Vision Science* **51**(2): 84–87.
533. Saari, K. M., Aine, E., Posz, A. and Klockars, M. 1983. Lysozyme content of tears in normal subjects and in patients with external eye infections. *Graefe's Archive for Clinical and Experimental Ophthalmology* **221**: 86–88.
534. Sen, D. K. and Sarin, G. S. 1979. Immunoglobulin concentrations in human tears in ocular diseases. *British Journal of Ophthalmology* **63**(5): 297–300. [doi:10.1136/bjo.63.5.297]
535. Fullard, R. J. and Snyder, C. 1990. Protein levels in nonstimulated and stimulated tears of normal human subjects. *Investigative Ophthalmology & Visual Science* **31**(6): 1119–1126.
536. Stuchell, R. N., Feldman, J. J., Farris, R. L. and Mandel, I. D. 1984. The effect of collection technique on tear composition. *Investigative Ophthalmology & Visual Science* **25**(3): 374–377.
537. Stuchell, R. N., Farris, R. L. and Mandel, I. D. 1981. Basal and reflex human tear analysis - II. Chemical analysis: Lactoferrin and lysozyme. *Ophthalmology* **88**(8): 858–862. [doi:10.1016/S0161-6420(81)34938-0]
538. Sen, D. K. and Sarin, G. S. 1986. Biological variations of lysozyme concentration in the tear fluids of healthy persons. *British Journal of Ophthalmology* **70**: 246–248.
539. Ronen, D., Eylan, E., Romano, A., Stein, R. and Modan, M. 1975. A spectrophotometric method for quantitative determination of lysozyme in human tears: Description and evaluation of the method and screening of 60 healthy subjects. *Investigative Ophthalmology* **14**(6): 479–484.
540. Carney, L. G. and Hill, R. M. 1979. Human tear buffering capacity. *Archives of Ophthalmology* **97**: 951–952.
541. Carney, L. G., Mauger, T. F. and Hill, R. M. 1989. Buffering in human tears: pH responses to acid and base challenge. *Investigative Ophthalmology & Visual Science* **30**(4): 747–754.
542. Abelson, M. B., Udell, I. J. and Weston, J. H. 1981. Normal human tear pH by direct measurement. *Archives of Ophthalmology* **99**: 301.
543. Fischer, F. H. and Wiederholt, M. 1982. Human precorneal tear film pH measured by microelectrodes. *Graefe's Archive for Clinical and Experimental Ophthalmology* **218**(3): 168–170. [doi:10.1007/BF02215658]
544. Coles, W. H. and Jaros, P. A. 1984. Dynamics of ocular surface pH. *British Journal of Ophthalmology* **68**(8): 549–552. [doi:10.1136/bjo.68.8.549]
545. Chen, F. S. and Maurice, D. M. 1990. The pH in the precorneal tear film and under a contact lens measured with a fluorescent probe. *Experimental Eye Research* **50**(3): 251–259. [doi:10.1016/0014-4835(90)90209-D]
546. Rédei, G. P. 2008. *Encyclopedia of Genetics, Genomics, Proteomics and Informatics*. [doi:10.1007/978-1-4020-6754-9]

547. Willcox, M. D. P. and Lan, J. 1999. Secretory immunoglobulin A in tears: Functions and changes during contact lens wear. *Clinical and Experimental Optometry* **82**(1): 1–3. [doi:10.1111/j.1444-0938.1999.tb06777.x]
548. Smith, S. A. and Waters, N. J. 2019. Pharmacokinetic and pharmacodynamic considerations for drugs binding to alpha-1-acid glycoprotein. *Pharmaceutical Research* **36**(2): 30. [doi:10.1007/s11095-018-2551-x]
549. Hassan, M. I., Waheed, A., Yadav, S., Singh, T. P. and Ahmad, F. 2008. Zinc α -glycoprotein: A multidisciplinary protein. *Molecular Cancer Research* **6**(6): 892–906. [doi:10.1158/1541-7786.MCR-07-2195]
550. Yang, F., Zhang, Y. and Liang, H. 2014. Interactive association of drugs binding to human serum albumin. *International Journal of Molecular Sciences* **15**(3): 3580–3595. [doi:10.3390/ijms15033580]
551. Mikkelsen, T. J., Chrai, S. S. and Robinson, J. R. 1973. Altered bioavailability of drugs in the eye due to drug-protein interaction. *Journal of Pharmaceutical Sciences* **62**(10): 1648–1653. [doi:10.1002/jps.2600621014]
552. Kruszewski, M. 2003. Labile iron pool: The main determinant of cellular response to oxidative stress. *Mutation Research* **531**(1–2): 81–92. [doi:10.1016/j.mrfmmm.2003.08.004]
553. Huston, W. M., Potter, A. J., Jennings, M. P., Rello, J., Hauser, A. R. and McEwan, A. G. 2004. Survey of ferroxidase expression and siderophore production in clinical isolates of *Pseudomonas aeruginosa*. *Journal of Clinical Microbiology* **42**(6): 2806–2809. [doi:10.1128/JCM.42.6.2806-2809.2004]
554. Bakshani, C. R., Morales-Garcia, A. L., Althaus, M., Wilcox, M. D., Pearson, J. P., Bythell, J. C. and Burgess, J. G. 2018. Evolutionary conservation of the antimicrobial function of mucus: A first defence against infection. *npj Biofilms and Microbiomes* **4**: 14. [doi:10.1038/s41522-018-0057-2]
555. Wei, G.-X., Campagna, A. N. and Bobek, L. A. 2006. Effect of MUC7 peptides on the growth of bacteria and on *Streptococcus mutans* biofilm. *Journal of Antimicrobial Chemotherapy* **57**(6): 1100–1109. [doi:10.1093/jac/dkl120]
556. Yamada, M., Kawai, M., Mochizuki, H., Hata, Y. and Mashima, Y. 1998. Fluorophotometric measurement of the buffering action of human tears *in vivo*. *Current Eye Research* **17**: 1005–1009.
557. Norn, M. S. 1977. Human tear pH. *Archives of Microbiology* **95**: 170.
558. Thorn, P. and Johansen, S. 1997. Pharmacokinetic investigation of fusidic acid 1% viscous eye drops in healthy volunteers. *European Journal of Ophthalmology* **7**(1): 9–12. [doi:10.1177/112067219700700102]
559. van Bijsterveld, O. P., Andriessse, H. and Nielsen, B. H. 1987. Fusidic acid in tear fluid: Pharmacokinetic study with fusidic acid viscous eye drops. *European Journal of Drug Metabolism and Pharmacokinetics* **12**(3): 215–218. [doi:10.1007/BF03189900]
560. Johansen, S., Rask-Pedersen, E. and Prause, J. U. 1996. I: A bioavailability comparison in rabbits after a single topical ocular application of prednisolone acetate formulated as a high-viscosity gel and as an aqueous suspension. *Acta Ophthalmologica Scandinavica* **74**(3): 253–258. [doi:10.1111/j.1600-0420.1996.tb00087.x]
561. Duane, T. D. 1949. The steady state of corneal hydration. *American Journal of Ophthalmology* **32**(6): 203–207. [doi:10.1016/S0002-9394(14)78373-4]

562. Duxfield, L., Sultana, R., Wang, R., Englebretsen, V., Deo, S., Rupenthal, I. D. and Al-Kassas, R. 2016. Ocular delivery systems for topical application of anti-infective agents. *Drug Development and Industrial Pharmacy* **42**(1): 1–11. [doi:10.3109/03639045.2015.1070171]
563. Powell, J. J., Jugdaohsingh, R. and Thompson, R. P. H. 1999. The regulation of mineral absorption in the gastrointestinal tract. *Proceedings of the Nutrition Society* **58**(1): 147–153. [doi:10.1079/PNS19990020]
564. Whitehead, M. W., Thompson, R. P. and Powell, J. J. 1996. Regulation of metal absorption in the gastrointestinal tract. *Gut* **39**(5): 625–628. [doi:10.1136/gut.39.5.625]
565. Hobman, J. L. and Crossman, L. C. 2015. Bacterial antimicrobial metal ion resistance. *Journal of Medical Microbiology* **64**(5): 471–497. [doi:10.1099/jmm.0.023036-0]
566. Fernandes, P. 2016. Fusidic acid: A bacterial elongation factor inhibitor for the oral treatment of acute and chronic staphylococcal infections. *Cold Spring Harbor Perspectives in Medicine* **6**(1): 1–17. [doi:10.1101/cshperspect.a025437]
567. Mayo, I., Puchades, F. and Fideliz de la Paz, M. 2008. Topical fusidic acid for treatment of *Clostridium perfringens* keratitis. *Cornea* **27**(8): 959–960. [doi:10.1097/ICO.0b013e31816f62a8]
568. Liu, Y., Li, R., Xiao, X. and Wang, Z. 2019. Antibiotic adjuvants: An alternative approach to overcome multi-drug resistant Gram-negative bacteria. *Critical Reviews in Microbiology* **45**(3): 301–314. [doi:10.1080/1040841X.2019.1599813]
569. Lakshminarayanan, R., Tan, W. X., Aung, T. T., Goh, E. T. L., Muruganatham, N., Li, J., Chang, J. Y. T., Dikshit, N., Saraswathi, P., Lim, R. R., Kang, T. S., Balamuralidhar, V., Sukumaran, B., Verma, C. S., Sivaraman, J., Chaurasia, S. S., Liu, S. and Beuerman, R. W. 2016. Branched peptide, B2088, disrupts the supramolecular organization of lipopolysaccharides and sensitizes the Gram-negative bacteria. *Scientific Reports* **6**: 25905. [doi:10.1038/srep25905]
570. Abdali, N., Parks, J. M., Haynes, K. M., Chaney, J. L., Green, A. T., Wolloscheck, D., Walker, J. K., Rybenkov, V. V., Baudry, J., Smith, J. C. and Zgurskaya, H. I. 2017. Reviving antibiotics: Efflux pump inhibitors that interact with AcrA, a membrane fusion protein of the AcrAB-TolC multidrug efflux pump. *ACS Infectious Diseases* **3**(1): 89–98. [doi:10.1021/acsinfecdis.6b00167]
571. Spengler, G., Takács, D., Horváth, Á., Szabó, Á. M., Riedl, Z., Hajós, G., Molnár, J. and Burián, K. 2014. Efflux pump inhibiting properties of racemic phenothiazine derivatives and their enantiomers on the bacterial AcrAB-TolC system. *In Vivo* **28**(6): 1071–1076.
572. Sayed, S., Elsayed, I. and Ismail, M. M. 2018. Optimization of β -cyclodextrin consolidated micellar dispersion for promoting the transcorneal permeation of a practically insoluble drug. *International Journal of Pharmaceutics* **549**(1–2): 249–260. [doi:10.1016/j.ijpharm.2018.08.001]
573. Saraswathi, P. and Beuerman, R. W. 2015. Corneal biofilms: From planktonic to microcolony formation in an experimental keratitis infection with *Pseudomonas aeruginosa*. *Ocular Surface* **13**(4): 331–345. [doi:10.1016/j.jtos.2015.07.001]
574. Bispo, P. J. M., Haas, W. and Gilmore, M. S. 2015. Biofilms in infections of the eye. *Pathogens* **4**: 111–136. [doi:10.3390/pathogens4010111]
575. Crabbé, A., Jensen, P. Ø., Bjarnsholt, T. and Coenye, T. 2019. Antimicrobial tolerance and metabolic adaptations in microbial biofilms. *Trends in Microbiology* **27**(10): 850–863. [doi:10.1016/j.tim.2019.05.003]

576. Harrison, J. J., Turner, R. J. and Ceri, H. 2005. High-throughput metal susceptibility testing of microbial biofilms. *BMC Microbiology* **5**: 53. [doi:10.1186/1471-2180-5-53]
577. Diaz-Ochoa, V. E., Jellbauer, S., Klaus, S. and Raffatellu, M. 2014. Transition metal ions at the crossroads of mucosal immunity and microbial pathogenesis. *Frontiers in Cellular and Infection Microbiology* **4**: 2. [doi:10.3389/fcimb.2014.00002]
578. Balamurugan, K. and Schaffner, W. 2006. Copper homeostasis in eukaryotes: Teetering on a tightrope. *Biochimica et Biophysica Acta - Molecular Cell Research* **1763**(7): 737–746. [doi:10.1016/j.bbamcr.2006.05.001]
579. Kaplan, J. H. and Maryon, E. B. 2016. How mammalian cells acquire copper: An essential but potentially toxic metal. *Biophysical Journal* **110**(1): 7–13. [doi:10.1016/j.bpj.2015.11.025]
580. Lu, Z., Gong, H. and Amemiya, T. 2002. Aluminum chloride induces retinal changes in the rat. *Toxicological Sciences* **66**: 253–260. [doi:10.1093/toxsci/66.2.253]
581. McGahan, M. C., Bito, L. Z. and Myers, B. M. 1986. The pathophysiology of the ocular microenvironment. II. Copper-induced ocular inflammation and hypotony. *Experimental Eye Research* **42**(6): 595–605. [doi:10.1016/0014-4835(86)90049-7]
582. Jitendra, Sharma, P. K., Banik, A. and Dixit, S. 2011. A new trend: ocular drug delivery system. *Pharma Science Monitor* **2**(3): 1–25.
583. Johanson, U. and Hughes, D. 1994. Fusidic acid-resistant mutants define three regions in elongation factor G of *Salmonella typhimurium*. *Gene* **143**(1): 55–59. [doi:10.1016/0378-1119(94)90604-1]
584. Turnidge, J. and Collignon, P. 1999. Resistance to fusidic acid. *International Journal of Antimicrobial Agents* **12**: S35–S44. [doi:10.1016/S0924-8579(98)00072-7]
585. Epling, J. 2012. Bacterial Conjunctivitis. *BMJ Clinical Evidence* **2**: 704.
586. Chojnacki, M., Philbrick, A., Wucher, B., Reed, J. N., Tomaras, A., Dunman, P. M. and Wozniak, R. A. F. 2019. Development of a broad-spectrum antimicrobial combination for the treatment of *Staphylococcus aureus* and *Pseudomonas aeruginosa* corneal infections. *Antimicrobial Agents and Chemotherapy* **63**: e01929-18. [doi:10.1128/AAC.01929-18]
587. Vaara, M. 2019. Polymyxins and their potential next generation as therapeutic antibiotics. *Frontiers in Microbiology* **10**: 1689. [doi:10.3389/fmicb.2019.01689]
588. Garen, A. and Levinthal, C. 1960. A fine-structure genetic and chemical study of the enzyme alkaline phosphatase of *E. coli* I. Purification and characterization of alkaline phosphatase. *Biochimica et Biophysica Acta* **38**: 470–483. [doi:10.1016/0006-3002(60)91282-8]
589. Chen, Q. X., Zheng, W. Z., Lin, J. Y., Shi, Y., Xie, W. Z. and Zhou, H. M. 2000. Effect of metal ions on the activity of green crab (*Scylla serrata*) alkaline phosphatase. *International Journal of Biochemistry and Cell Biology* **32**(8): 879–885. [doi:10.1016/S1357-2725(00)00026-1]
590. Wang, Z. J., Ma, W., Yang, J. M., Kang, Y. and Park, Y. D. 2018. Effects of Cu²⁺ on alkaline phosphatase from *Macrobrachium rosenbergii*. *International Journal of Biological Macromolecules* **117**: 116–123. [doi:10.1016/j.ijbiomac.2018.05.165]

591. Song, M., Huo, H., Cao, Z., Han, Y. and Gao, L. 2017. Aluminum trichloride inhibits the rat osteoblasts mineralization *in vitro*. *Biological Trace Element Research* **175**(1): 186–193. [doi:10.1007/s12011-016-0761-9]
592. Geng, F., Zou, C., Liu, J., Zhang, Q., Guo, X., Fan, Y., Yu, H., Yang, S., Liu, Z. and Li, L. 2019. Development of luminescent nanoswitch for sensing of alkaline phosphatase in human serum based on Al³⁺-PPi interaction and Cu NCs with AIE properties. *Analytica Chimica Acta* **1076**: 131–137. [doi:10.1016/j.aca.2019.05.026]
593. Masi, M., Dumont, E., Vergalli, J., Pajovic, J., Réfrégiers, M. and Pagès, J. M. 2018. Fluorescence enlightens RND pump activity and the intrabacterial concentration of antibiotics. *Research in Microbiology* **169**(7–8): 432–441. [doi:10.1016/j.resmic.2017.11.005]
594. Cama, J., Bajaj, H., Pagliara, S., Maier, T., Braun, Y., Winterhalter, M. and Keyser, U. F. 2015. Quantification of fluoroquinolone uptake through the outer membrane channel OmpF of *Escherichia coli*. *Journal of the American Chemical Society* **137**(43): 13836–13843. [doi:10.1021/jacs.5b08960]
595. Blaskovich, M. A., Phetsang, W., Stone, M. R., Lapinska, U., Pagliara, S., Bhalla, R. and Cooper, M. A. 2019. Antibiotic-derived molecular probes for bacterial imaging. in *Photonic Diagnosis and Treatment of Infections and Inflammatory Diseases II* (eds. Dai, T., Wu, M. X. & Popp, J.) : 2. [doi:10.1117/12.2507329]
596. Chéhadé, F., De Labriolle-Vaylet, C., Moins, N., Moreau, M. F., Papon, J., Labarre, P., Galle, P., Veyre, A. and Hindié, E. 2005. Secondary ion mass spectrometry as a tool for investigating radiopharmaceutical distribution at the cellular level: The example of I-BZA and ¹⁴C-I-BZA. *Journal of Nuclear Medicine* **46**(10): 1701–1706.
597. Gray, N. D., Howarth, R., Pickup, R. W., Jones, J. G. and Head, I. M. 1999. Substrate uptake by uncultured bacteria from the genus *Achromatium* determined by microautoradiography. *Applied and Environmental Microbiology* **65**(11): 5100–5106.
598. Colliver, T. L., Brummel, C. L., Pacholski, M. L., Swanek, F. D., Ewing, A. G. and Winograd, N. 1997. Atomic and molecular imaging at the single-cell level with TOF-SIMS. *Analytical Chemistry* **69**(13): 2225–2231. [doi:10.1021/ac9701748]
599. Tian, H., Six, D. A., Krucker, T., Leeds, J. A. and Winograd, N. 2017. Subcellular chemical imaging of antibiotics in single bacteria using C60-secondary ion mass spectrometry. *Analytical Chemistry* **89**(9): 5050–5057. [doi:10.1021/acs.analchem.7b00466]
600. Davies, S. K., Fearn, S., Allsopp, L. P., Harrison, F., Ware, E., Diggle, S. P., Filloux, A., McPhail, D. S. and Bundy, J. G. 2017. Visualizing antimicrobials in bacterial biofilms: Three-dimensional biochemical imaging using TOF-SIMS. *mSphere* **2**(4): e00211-17. [doi:10.1128/msphere.00211-17]
601. Desbenoit, N., Sausserieau, E., Bich, C., Bourderioux, M., Fritsch, J., Edelman, A., Brunelle, A. and Ollero, M. 2014. Localized lipidomics in cystic fibrosis: TOF-SIMS imaging of lungs from *Pseudomonas aeruginosa*-infected mice. *International Journal of Biochemistry and Cell Biology* **52**: 77–82. [doi:10.1016/j.biocel.2014.01.026]
602. Frieden, T. 2019. *Antibiotic resistance threats in the United States*. Centers for Disease Control and Prevention [doi:CS239559-B]
603. Derjaguin, B. and Landau, L. 1941. Theory of the stability of strongly charged lyophobic sols and of the adhesion of strongly charged particles in solutions of electrolytes. *Acta Physicochim* **14**: 633–662.

604. Verwey, E. J. W. and Overbeek, J. T. G. 1948. *Theory of the stability of lyophobic colloids*. [doi:10.1016/0095-8522(55)90030-1]
605. Moiseev, R. V., Morrison, P. W. J., Steele, F. and Khutoryanskiy, V. V. 2019. Penetration enhancers in ocular drug delivery. *Pharmaceutics* **11**(7): 321. [doi:10.3390/pharmaceutics11070321]
606. Jover, A., Budal, R. M., Al-Soufi, W., Mejjide, F., Vázquez Tato, J. and Yunes, R. A. 2003. Spectra and structure of complexes formed by sodium fusidate and potassium helvolate with β - and γ -cyclodextrin. *Steroids* **68**(1): 55–64. [doi:10.1016/S0039-128X(02)00115-0]
607. Aktaş, Y., Ünlü, N., Orhan, M., İrkeç, M. and Hıncal, A. A. 2003. Influence of hydroxypropyl β -cyclodextrin on the corneal permeation of pilocarpine. *Drug Development and Industrial Pharmacy* **29**(2): 223–230. [doi:10.1081/DDC-120016730]
608. Morrison, P. W. J., Connon, C. J. and Khutoryanskiy, V. V. 2013. Cyclodextrin-mediated enhancement of riboflavin solubility and corneal permeability. *Molecular Pharmaceutics* **10**(2): 756–762. [doi:10.1021/mp3005963]
609. Malhotra, S., Khare, A., Grover, K., Singh, I. and Pawar, P. 2014. Design and evaluation of voriconazole eye drops for the treatment of fungal keratitis. *Journal of Pharmaceutics* : 490595. [doi:10.1155/2014/490595]
610. Bíró, T., Horvát, G., Budai-Szűcs, M., Csányi, E., Urbán, E., Facskó, A., Szabó-Révész, P., Csóka, I. and Aigner, Z. 2018. Development of prednisolone-containing eye drop formulations by cyclodextrin complexation and antimicrobial, mucoadhesive biopolymer. *Drug Design, Development and Therapy* **12**: 2529–2537. [doi:10.2147/DDDT.S165693]
611. Martin, C., Low, W. L., Gupta, A., Amin, M. C. I. M., Radecka, I., Britland, S. T., Raj, P. and Kenward, K. 2014. Strategies for antimicrobial drug delivery to biofilm. *Current Pharmaceutical Design* **21**(1): 43–66. [doi:10.2174/1381612820666140905123529]
612. Nicolosi, D., Cupri, S., Genovese, C., Tempera, G., Mattina, R. and Pignatello, R. 2015. Nanotechnology approaches for antibacterial drug delivery: Preparation and microbiological evaluation of fusogenic liposomes carrying fusidic acid. *International Journal of Antimicrobial Agents* **45**(6): 622–626. [doi:10.1016/j.ijantimicag.2015.01.016]
613. Wadhwa, S., Singh, B., Sharma, G., Raza, K. and Katore, O. P. 2016. Liposomal fusidic acid as a potential delivery system: A new paradigm in the treatment of chronic plaque psoriasis. *Drug Delivery* **23**(4): 1204–1213. [doi:10.3109/10717544.2015.1110845]
614. Bagley, D. M., Waters, D. and Kong, B. M. 1994. Development of a 10-day chorioallantoic membrane vascular assay as an alternative to the draize rabbit eye irritation test. *Food and Chemical Toxicology* **32**(12): 1155–1160. [doi:10.1016/0278-6915(94)90131-7]
615. Kishore, A. S., Surekha, P. A., Sekhar, P. V. R., Srinivas, A. and Murthy, P. B. 2008. Hen egg chorioallantoic membrane bioassay: An *in vitro* alternative to draize eye irritation test for pesticide screening. *International Journal of Toxicology* **27**(6): 449–453. [doi:10.1080/10915810802656996]
616. Gilleron, L., Coecke, S., Sysmans, M., Hansen, E., van Oproy, S., Marzin, D., van Cauteren, H. and Vanparys, P. 1996. Evaluation of a modified HET-CAM assay as a screening test for eye irritancy. *Toxicology in Vitro* **10**(4): 431–446. [doi:10.1016/0887-2333(96)00021-5]

617. Wilson, S. L., Ahearne, M. and Hopkinson, A. 2015. An overview of current techniques for ocular toxicity testing. *Toxicology* **327**: 32–46. [doi:10.1016/j.tox.2014.11.003]
618. Zhu, H., Kochevar, I. E., Behlau, I., Zhao, J., Wang, F., Wang, Y., Sun, X., Hamblin, M. R. and Dai, T. 2017. Antimicrobial blue light therapy for infectious keratitis: *Ex vivo* and *in vivo* studies. *Investigative Ophthalmology & Visual Science* **58**(1): 586–593. [doi:10.1167/iovs.16-20272]
619. Marino, A., Blanco, A. R., Ginestra, G., Nostro, A. and Bisignano, G. 2016. *Ex vivo* efficacy of gemifloxacin in experimental keratitis induced by methicillin-resistant *Staphylococcus aureus*. *International Journal of Antimicrobial Agents* **48**(4): 395–400. [doi:10.1016/j.ijantimicag.2016.06.026]
620. Teuchner, B., Wibmer, I. D., Schaumann, P., Seifarth, C., Walochnik, J. and Nagl, M. 2019. *N*-chlorotaurine inactivates *Acanthamoeba* and *Candida albicans* in the porcine *ex vivo* corneal infection model. *Cornea* **38**(8): 1011–1016. [doi:10.1097/ico.0000000000001927]
621. Proietto, L. R., Whitley, R. D., Brooks, D. E., Schultz, G. E., Gibson, D. J., Berkowski, W. M., Salute, M. E. and Plummer, C. E. 2017. Development and assessment of a novel canine *ex vivo* corneal model. *Current Eye Research* **42**(6): 813–821. [doi:10.1080/02713683.2016.1262428]
622. Madhu, S. N., Jha, K. K., Karthyayani, A. P. and Gajjar, D. U. 2018. *Ex vivo* caprine model to study virulence factors in keratitis. *Journal of Ophthalmic and Vision Research* **13**(4): 383–391. [doi:10.4103/jovr.jovr_131_17]
623. Knickelbein, J. E., Buela, K.-A. and Hendricks, R. L. 2014. Antigen-presenting cells are stratified within normal human corneas and are rapidly mobilized during *ex vivo* viral infection. *Investigative Ophthalmology & Visual Science* **55**(2): 1118–1123. [doi:10.1167/iovs.13-13523]
624. Pinnock, A., Shivshetty, N., Roy, S., Rimmer, S., Douglas, I., MacNeil, S. and Garg, P. 2017. *Ex vivo* rabbit and human corneas as models for bacterial and fungal keratitis. *Graefe's Archive for Clinical and Experimental Ophthalmology* **255**(2): 333–342. [doi:10.1007/s00417-016-3546-0]
625. Hahne, M. and Reichl, S. 2011. Development of a serum-free human cornea construct for *in vitro* drug absorption studies: The influence of varying cultivation parameters on barrier characteristics. *International Journal of Pharmaceutics* **416**(1): 268–279. [doi:10.1016/j.ijpharm.2011.07.004]
626. Kaluzhny, Y., Kinuthia, M. W., Truong, T., Lapointe, A. M., Hayden, P. and Klausner, M. 2018. New human organotypic corneal tissue model for ophthalmic drug delivery studies. *Investigative Ophthalmology & Visual Science* **59**(7): 2880–2898. [doi:10.1167/iovs.18-23944]
627. Kölln, C. and Reichl, S. 2016. Cytochrome P450 activity in *ex vivo* cornea models and a human cornea construct. *Journal of Pharmaceutical Sciences* **105**(7): 2204–2212. [doi:10.1016/j.xphs.2016.04.010]
628. Hui, A., Willcox, M. and Jones, L. 2014. *In vitro* and *in vivo* evaluation of novel ciprofloxacin-releasing silicone hydrogel contact lenses. *Investigative Ophthalmology & Visual Science* **55**(8): 4896–4904. [doi:10.1167/iovs.14-14855]
629. Marcus, E. A., Sachs, G. and Scott, D. R. 2016. Eradication of *Helicobacter pylori* infection. *Current Gastroenterology Reports* **18**(7): 33. [doi:10.1007/s11894-016-0509-x]
630. Peek, R. M. and Crabtree, J. E. 2006. *Helicobacter* infection and gastric neoplasia. *Journal of Pathology* **208**(2): 233–248. [doi:10.1002/path.1868]

631. O'Morain, N. R., Dore, M. P., O'Connor, A. J. P., Gisbert, J. P. and O'Morain, C. A. 2018. Treatment of *Helicobacter pylori* infection in 2018. *Helicobacter* **23**(Suppl. 1): e12519. [doi:10.1111/hel.12519]
632. Sharifi, M. S. and Hazell, S. L. 2012. Isolation, analysis and antimicrobial activity of the acidic fractions of Mastic, Kurdica, Mutica and Cabolica gums from genus Pistacia. *Global Journal of Health Science* **4**(1): 217–228. [doi:10.5539/gjhs.v4n1p217]
633. Azzopardi, E. A., Azzopardi, E., Camilleri, L., Villapalos, J., Boyce, D. E., Dziewulski, P., Dickson, W. A. and Whitaker, I. S. 2014. Gram-negative wound infection in hospitalised adult burn patients - systematic review and metanalysis. *PLoS ONE* **9**(4): e95042. [doi:10.1371/journal.pone.0095042]
634. Young, P. Y. and Khadaroo, R. G. 2014. Surgical site infections. *Surgical Clinics of North America* **94**(6): 1245–1264. [doi:10.1016/j.suc.2014.08.008]
635. Oh, S., McCanna, D. J., Subbaraman, L. N. and Jones, L. W. 2018. Cytotoxic and inflammatory effects of contact lens solutions on human corneal epithelial cells *in vitro*. *Contact Lens and Anterior Eye* **41**(3): 282–289. [doi:10.1016/j.clae.2017.12.006]
636. Moon, E.-K., Lee, S., Quan, F.-S. and Kong, H.-H. 2018. Chloroquine as a possible disinfection adjunct of disinfection solutions against *Acanthamoeba*. *Experimental Parasitology* **188**: 102–106. [doi:10.1016/j.exppara.2018.04.005]
637. Datta, S., Baudouin, C., Brignole-Baudouin, F., Denoyer, A. and Cortopassi, G. A. 2017. The eye drop preservative benzalkonium chloride potently induces mitochondrial dysfunction and preferentially affects LHON mutant cells. *Investigative Ophthalmology and Visual Science* **58**(4): 2406–2412. [doi:10.1167/iovs.16-20903]
638. Araki-Saski, K., Ohashi, Y., Sasabe, T., Hayashi, K., Watanabe, H., Tano, Y. and Handa, H. 1995. An SV40-immortalized human corneal epithelial cell line and its characterization. *Investigative Ophthalmology and Visual Science* **36**(3): 614–621.
639. Liu, L., Zhang, H., Meng, X., Yin, J., Li, D. and Liu, C. 2010. Dinuclear metal(II) complexes of polybenzimidazole ligands as carriers for DNA delivery. *Biomaterials* **31**(6): 1380–1391. [doi:10.1016/j.biomaterials.2009.10.056]
640. Ning, C., Wang, X., Li, L., Zhu, Y., Li, M., Yu, P., Zhou, L., Zhou, Z., Chen, J., Tan, G., Zhang, Y., Wang, Y. and Mao, C. 2015. Concentration ranges of antibacterial cations for showing the highest antibacterial efficacy but the least cytotoxicity against mammalian cells: Implications for a new antibacterial mechanism. *Chemical Research in Toxicology* **28**(9): 1815–1822. [doi:10.1021/acs.chemrestox.5b00258]
641. Liao, X., Lu, J., Ying, P., Zhao, P., Bai, Y., Li, W. and Liu, M. 2013. DNA binding, antitumor activities, and hydroxyl radical scavenging properties of novel oxovanadium(IV) complexes with substituted isoniazid. *Journal of Biological Inorganic Chemistry* **18**(8): 975–984. [doi:10.1007/s00775-013-1046-9]
642. Huang, X., Dong, X., Li, X., Meng, X., Zhang, D. and Liu, C. 2013. Metal-polybenzimidazole complexes as a nonviral gene carrier: Effects of the DNA affinity on gene delivery. *Journal of Inorganic Biochemistry* **129**: 102–111. [doi:10.1016/j.jinorgbio.2013.09.009]
643. Dutot, M., Vincent, J., Martin-Brisac, N., Fabre, I., Grasmick, C. and Rat, P. 2013. Ocular cytotoxicity evaluation of medical devices such as contact lens solutions and benefits of a rinse step in cleaning procedure. *ALTEX* **30**(1): 41–49. [doi:10.14573/altex.2013.1.041]

644. Howl, J. and Jones, S. 2015. Protein Mimicry and the Design of Bioactive Cell-Penetrating Peptides. in *Cell-Penetrating Peptides: Methods and Protocols* (ed. Langel, Ü.) [doi:10.1007/978-1-4939-2806-4]
645. Jagadeesh, M., Rashmi, H. K., Rao, Y. S., Reddy, A. S., Prathima, B., Maheswari Devi, P. U. and Reddy, A. V. 2013. Synthesis and spectroscopic characterization of 3,4-difluoroacetophenone-thiosemicarbazone and its palladium(II) complex: Evaluation of antimicrobial and antitumour activity. *Spectrochimica Acta Part A: Molecular and Biomolecular Spectroscopy* **115**: 583–587. [doi:10.1016/j.saa.2013.06.071]
646. Kazemzadeh-Narbat, M., Kindrachuk, J., Duan, K., Jenssen, H., Hancock, R. E. W. and Wang, R. 2010. Antimicrobial peptides on calcium phosphate-coated titanium for the prevention of implant-associated infections. *Biomaterials* **31**(36): 9519–9526. [doi:10.1016/j.biomaterials.2010.08.035]
647. Mishra, A., Kaushik, N. K., Verma, A. K. and Gupta, R. 2008. Synthesis, characterization and antibacterial activity of cobalt(III) complexes with pyridine-amide ligands. *European Journal of Medicinal Chemistry* **43**(10): 2189–2196. [doi:10.1016/j.ejmech.2007.08.015]
648. Fu, Y., Yang, Y., Zhou, S., Liu, Y., Yuan, Y., Li, S. and Li, C. 2014. Ciprofloxacin containing Mannich base and its copper complex induce antitumor activity via different mechanism of action. *International Journal of Oncology* **45**(5): 2092–2100. [doi:10.3892/ijo.2014.2611]
649. 2018. Thermo Scientific Pierce LDH Cytotoxicity Assay Kit Instructions. (2503.2)
650. Paimela, T., Ryhänen, T., Kauppinen, A., Marttila, L., Salminen, A. and Kaarniranta, K. 2012. The preservative polyquaternium-1 increases cytotoxicity and NF-kappaB linked inflammation in human corneal epithelial cells. *Molecular Vision* **18**(May): 1189–1196.
651. Yu, Y., Chen, D., Li, Y., Yang, W., Tu, J. and Shen, Y. 2018. Improving the topical ocular pharmacokinetics of lyophilized cyclosporine A-loaded micelles: Formulation, *in vitro* and *in vivo* studies. *Drug Delivery* **25**(1): 888–899. [doi:10.1080/10717544.2018.1458923]
652. Song, W.-J., Lin, Q.-Y., Jiang, W.-J., Du, F.-Y., Qi, Q.-Y. and Wei, Q. 2015. Synthesis, interaction with DNA and antiproliferative activities of two novel Cu(II) complexes with norcantharidin and benzimidazole derivatives. *Spectrochimica Acta Part A: Molecular and Biomolecular Spectroscopy* **137**: 122–128. [doi:10.1016/j.saa.2014.08.069]
653. Wyrzykowski, D., Kloska, A., Pranczk, J., Szczepańska, A., Tesmar, A., Jacewicz, D., Pilarski, B. and Chmurzyński, L. 2015. Physicochemical and biological properties of oxovanadium(IV), cobalt(II) and nickel(II) complexes with oxydiacetate anions. *Biological Trace Element Research* **164**(1): 139–149. [doi:10.1007/s12011-014-0170-x]
654. Caruso, G., Distefano, D. A., Parlascino, P., Fresta, C. G., Lazzarino, G., Lunte, S. M. and Nicoletti, V. G. 2017. Receptor-mediated toxicity of human amylin fragment aggregated by short- and long-term incubations with copper ions. *Molecular and Cellular Biochemistry* **425**(1–2): 85–93. [doi:10.1007/s11010-016-2864-1]
655. Cancarini, A., Fostinelli, J., Napoli, L., Gilberti, M. E., Apostoli, P. and Semeraro, F. 2017. Trace elements and diabetes: Assessment of levels in tears and serum. *Experimental Eye Research* **154**: 47–52. [doi:10.1016/j.exer.2016.10.020]

656. Sharma, R. G., Rao, S. S. and Mathur, P. K. 1984. Estimation of tear and serum manganese in disorders of anterior segment of eye. *Indian Journal of Ophthalmology* **32**(5): 412–414.

Appendices

Appendix A: Personal and environmental safety

Safety assessments were completed prior to commencement of experimentation. All microbiology and aseptic procedures were carried out in a designated biosafety level 2 (BSL2) laboratory inside an MSC-Advantage laminar flow safety cabinet (Thermo Fisher Scientific, Loughborough, UK). All surfaces used during microbiology work were decontaminated before and after use with 70 % ethanol (EtOH) or 10 % sodium hypochlorite, as appropriate. Contaminated microbiological waste was autoclaved on-site, prior to collection for incineration, per School of Pharmacy and Pharmaceutical Sciences procedures. Cell culture work was carried out in a separate, designated BSL2 laboratory in a Heraeus HeraSafe HS12 laminar flow safety cabinet (Thermo Fisher Scientific, Loughborough, UK) with 70 % EtOH as a decontaminant. Cell culture waste was sterilised using Presept™ per local procedure. A 10x Presept™ solution, prepared by dissolving one 2.5 g tablet in 1 L water, was mixed 1:9 with liquid waste at least 30 min before disposal. All flammable, volatile and/or corrosive chemicals were stored and handled per School and labelling safety guidelines. Personal protective equipment (PPE) comprising of laboratory coat, nitrile gloves and safety glasses was employed during laboratory work, as appropriate.

Appendix B: Calibration curves for quantification of fusidate by RP-HPLC

The linear regression equations for peak area : fusidate concentration were determined for both RP-HPLC separation methods (Section 2.6, page 53) using serial twofold dilutions of FNa in 50 % v/v EtOH, in triplicate. Example chromatograms for separation methods 1 and 2 are presented in Figure 10.1 and Figure 10.2, respectively.

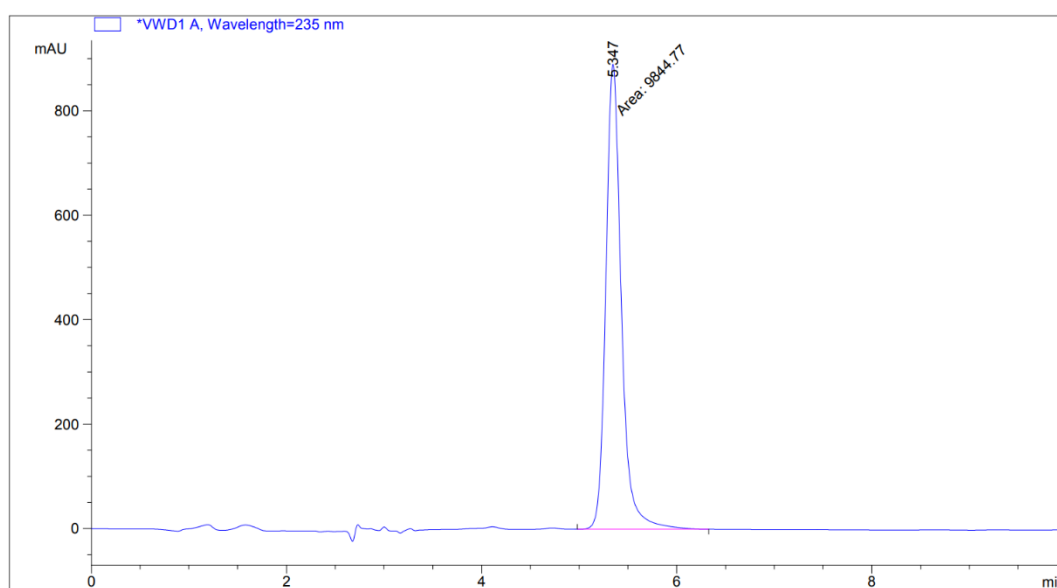


Figure 10.1 - Example chromatogram for fusidate resolved by RP-HPLC separation method 1^[287]

Sample analysed was 1280 μM sodium fusidate in 50 % EtOH

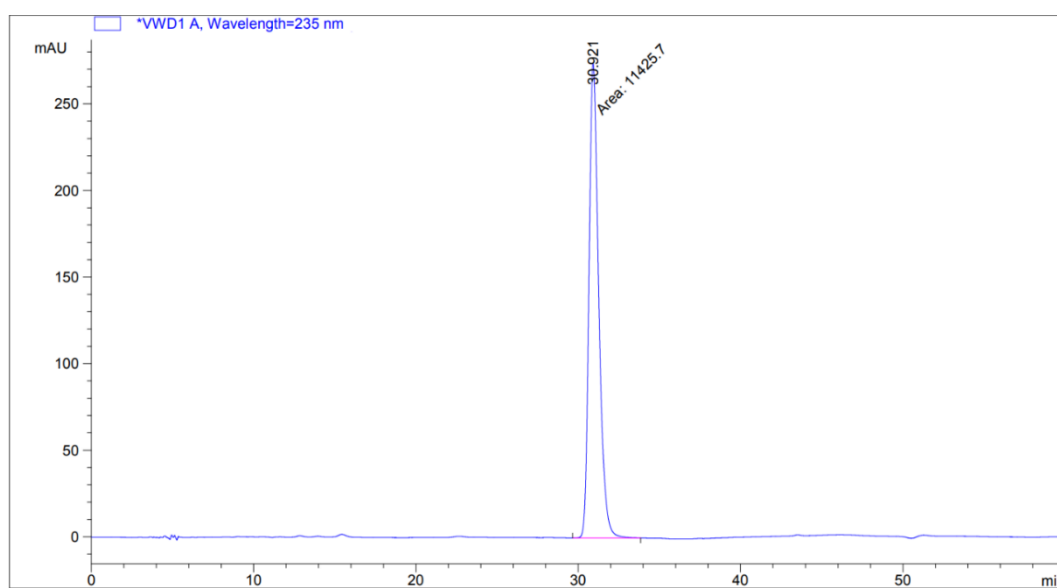


Figure 10.2 - Example chromatogram for fusidate resolved by RP-HPLC separation method 2^[288]

Sample analysed was 400 μM sodium fusidate in 50 % EtOH

Peak areas of lower LOQ and above were plotted against FNa concentration and the linearity of the relationship assessed. Accuracy of the linear regression equations was verified by using the detected peak areas and comparing the calculated fusidate concentration to that in the originally analysed samples.

The correlation between peak area produced by separation method 1 and FNa concentration was linear from 10 to 2,560 μM with an R^2 value of 0.9997 (Figure 10.3) and calculation error of $\pm 3.34\%$.

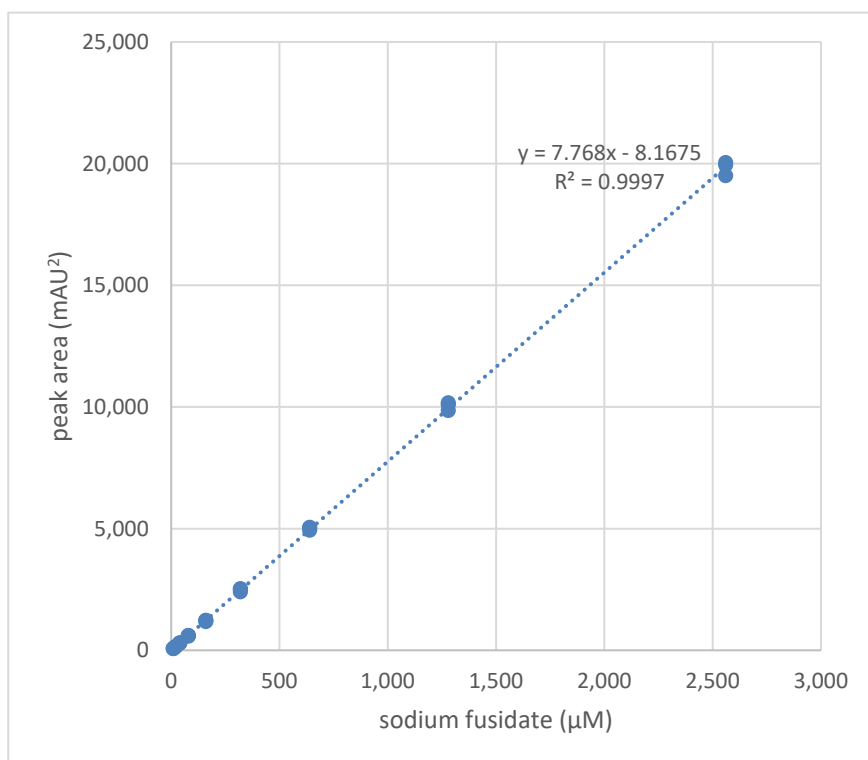


Figure 10.3 - Calibration curve for fusidate quantification by RP-HPLC separation method 1^[287]

LOD: 5 μM , LOQ: 10 μM ,
range: 10-2,560 μM (69.5-19,877.8 mAU^2), in-range error: $\pm 3.34\%$

The linear correlation was found to cover all FNa concentrations analysed by separation method 2 (1.5625 to 800 μM) and intersected at 0,0. The equation and R^2 value are shown in Figure 10.4. The calculation error across all concentrations used was $\pm 2.28\%$.

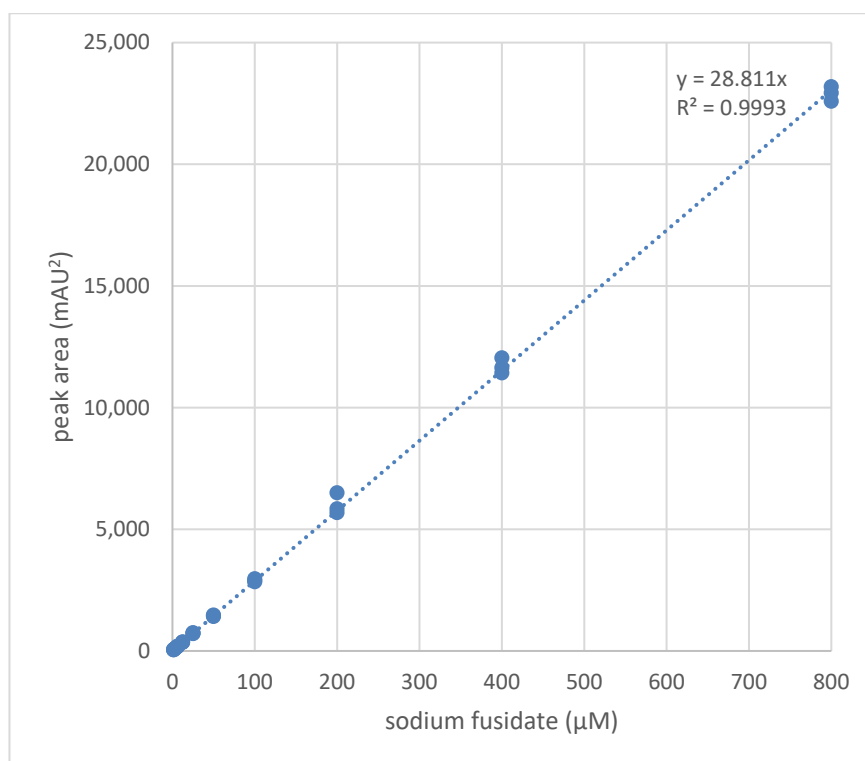


Figure 10.4 - Calibration curve for fusidate quantification by RP-HPLC separation method 2^[288]

LOD: $\leq 1.5625 \mu\text{M}$, LOQ: $\leq 1.5625 \mu\text{M}$,
 range: $1.5625\text{-}800 \mu\text{M}$ ($45.0\text{-}23,048.7 \text{ mAU}^2$), in-range error: $\pm 2.28 \%$

The inverted linear regression formula for calculation of fusidate concentration from peak areas obtained by separation method 1 was:

$$[\text{fusidate } (\mu\text{M})] = \frac{(\text{mAU}^2 + 8.1675)}{7.768}$$

While by separation method 2, the inverted linear regression formula was:

$$[\text{fusidate } (\mu\text{M})] = \frac{\text{mAU}^2}{28.811}$$

Appendix C: Optimisation of assay parameters for study of sodium fusidate association with *E. coli* cells

C(i): Verification of bacterial pellet processing and sodium fusidate extraction

E. coli NCTC 10418 was grown overnight on NA and used to inoculate six 40 mL volumes of standard NB. After incubation at 35 °C and 120 rpm for 18 to 24 h, liquid cultures were centrifuged in a Heraeus Megafuge 8R centrifuge (Thermo Scientific, Osterode am Harz, Germany) for 20 min at 3260 *g* (4500 rpm) at room temperature and the supernatants carefully decanted. Three of the six bacterial pellets were pooled and resuspended in 30 mL NB containing 160 µM FNa while the other three were pooled and resuspended 30 mL NB without FNa. Resuspended bacterial were incubated at 35 °C and 120 rpm for 30 min. After the exposure duration, the suspensions were centrifuged at 4 °C (pre-cooled) for 20 min at 4500 rpm. Post-exposure pellets were resuspended in 3 mL HPLC-grade water to which 3 mL absolute EtOH was added and thoroughly mixed.

Suspensions of *S. aureus* NCTC 12973 were prepared in sterile PBS from cultures grown overnight on NA and the optical density adjusted to 0.1±0.02 at 625 nm. Sterile cotton swabs were used to spread *S. aureus* suspension evenly over the surface of NA plates and allowed to dry for 15 min. Wells of 7.5 mm diameter were made aseptically in the centre of each inoculated plate.

Ten minutes after addition of EtOH to resuspended, FNa-exposed and control *E. coli*, 50 µL aliquots were transferred to the wells of agar diffusion plates prepared with *S. aureus*. Simultaneously, approximately 1.5 mL of the *E. coli* suspension in 50 % EtOH was syringe filtered and 50 µL filtrate also added to diffusion wells. This process was repeated 30, 60 and 120 min after EtOH addition. Control diffusion plates of 50 % EtOH without *E. coli* or FNa and 20, 40 and 80 µM FNa in 50 % EtOH without *E. coli* were also prepared. Ager plates were incubated overnight at 37 °C and the zones of inhibition measured in mm. Where confluent growth was observed up to the well edge, the zone of inhibition was recorded as 0 mm.

The growth of *S. aureus* was not inhibited by the 50 % EtOH control (Table 10.1). All three FNa concentrations produced measurable zones of inhibition and zone diameter increased FNa concentration.

Table 10.1 - Control inhibition zone diameters produced by sodium fusidate against *S. aureus* NCTC 12973 on nutrient broth

Control condition	Inhibition zone diameter (mm)
50 % EtOH	0
20 μ M FNa in 50 % EtOH	28
40 μ M FNa in 50 % EtOH	30
80 μ M FNa in 50 % EtOH	31

There was no growth of *E. coli* after exposure to 50 % EtOH for ≥ 10 min, demonstrating the bacteria were rapidly and completely killed. No inhibition was produced by lysed raw or filtered *E. coli* (Table 10.2), indicating that *S. aureus* was not perturbed by any remaining metabolites or other *E. coli* products. There was no apparent difference between zone sizes produced by filtrate or raw lysed *E. coli* after FNa exposure. This indicates FNa concentration before and after filtration is similar and FNa is not highly bound to the particulate matter remaining after *E. coli* lysis by exposure to 50 % EtOH.

Table 10.2 - Zones of inhibition of *S. aureus* NCTC 12973 on nutrient broth produced by lysate of *E. coli* NCTC 10418 exposed to sodium fusidate

Time after addition of EtOH (min)	Inhibition zone diameter (mm)			
	FNa-exposed <i>E. coli</i>		Control <i>E. coli</i>	
	unfiltered	filtered	unfiltered	filtered
10	20	19.5	0	0
30	20	20	0	0
60	20	21	0	0
120	18.5	19.5	0	0

Exposure to 50 % EtOH produces rapid killing of *E. coli* and effective solubilisation of FNa from the bacterial pellet. Filtration of the lysed, FNa-treated *E. coli* without detectable FNa loss makes this simple process amenable to employment for HPLC sample preparation.

C(ii): Selection of RP-HPLC method for quantification of fusidate

Separation method 1 did not adequately resolve fusidate when in the presence of bacterial lysate (Figure 10.5-1). However, separation method 2 was effective (Figure 10.5-2). Therefore, while the 10 min isocratic separation method 1 was employed for most fusidate quantification purposes, the 45 min gradient separation method 2 was required for the analysis of samples containing bacterial lysate.

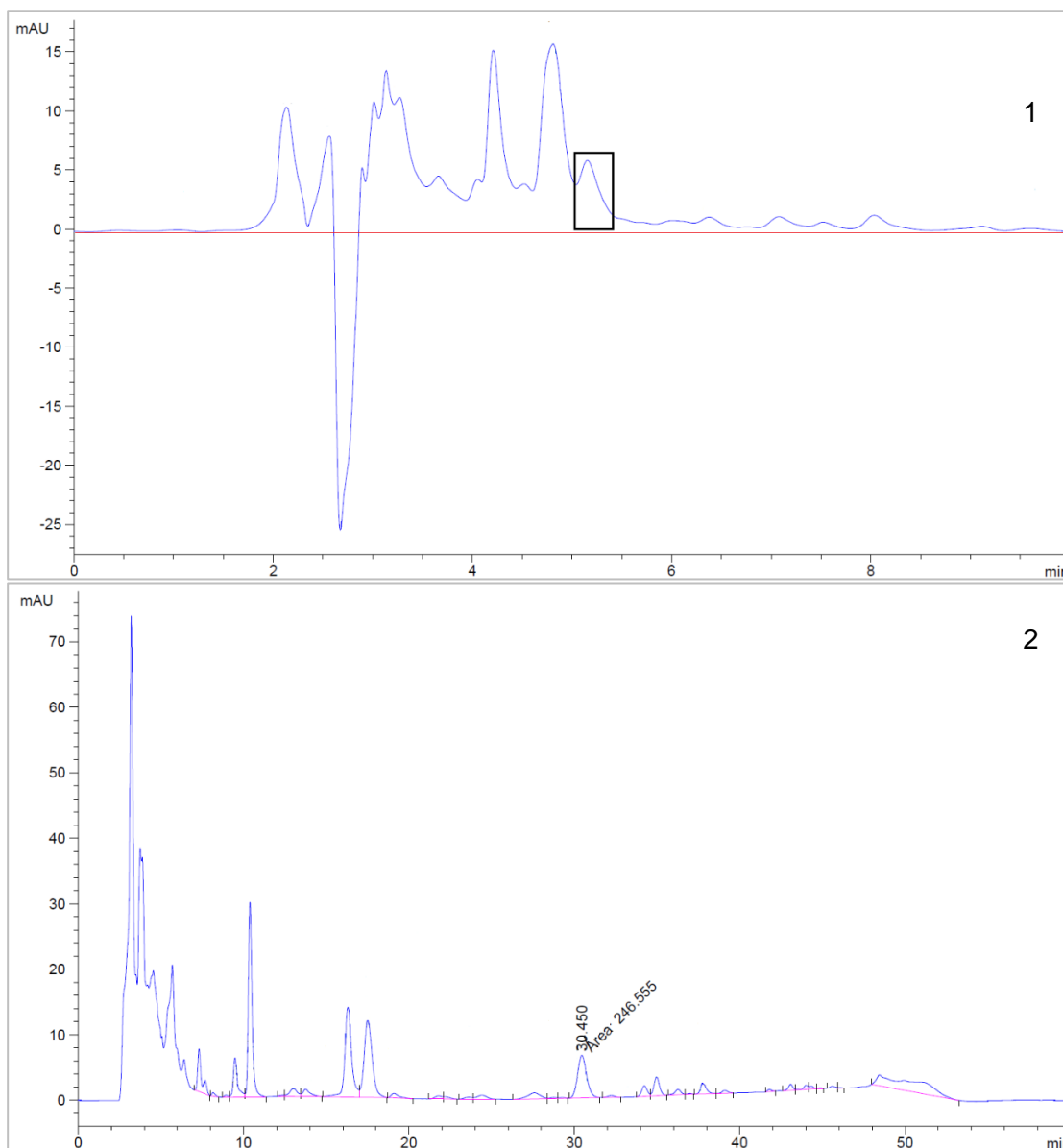


Figure 10.5 - Example chromatograms for fusidate in bacterial lysate resolved by RP-HPLC separation method 1 and separation method 2

Sample analysed by both methods was *E. coli* in 50 % v/v EtOH after exposure to 160 μ M sodium fusidate in nutrient broth for 30 min. There was insufficient separation of fusidate (black box) and the adjoining peak when using method 1 (upper panel), while fusidate (labelled peak) was well resolved and quantifiable by method 2 (lower panel).

Appendix D: Isothermal titration calorimetry (ITC) performance validation and additional replicates

D(i): EDTA-CaCl₂ performance validation standard

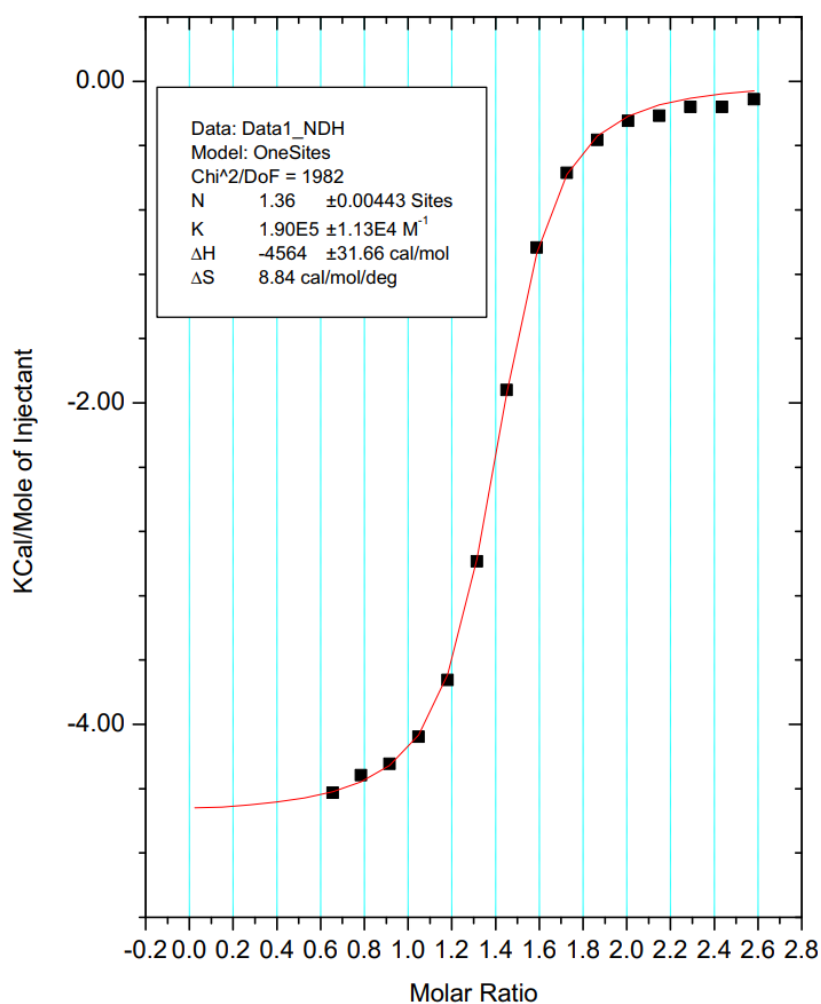


Figure 10.6 – Example of EDTA-CaCl₂ ITC performance validation data

Data generated during performance validation testing was fit to a one site interaction model using the MicroCal Origin software.

The EDTA-CaCl₂ performance validation standard was carried out at the start of each day prior to initiation of experimentation. If the results of the EDTA-CaCl₂ test did not fit the required parameters, the instrument syringe, sample cell and reference cell were thoroughly cleaned per the manufacturer's instructions and the validation run repeated until acceptable results were obtained. No more than two runs were required on any one day to achieve successful performance validation.

All solutions used in the performance validation tests were pre-made and provided by the manufacturer. The injectant was 5 mM CaCl_2 in 10 mM 2-(N-morpholino)ethanesulfonic acid (MES) at pH 5.6, the sample was 0.4 mM EDTA in 10 mM MES at pH 5.6 and 10 mM MES at pH 5.6 was used in the reference cell. The run parameters were 25 °C cell temperature, 1000 rpm stirring speed, injection interval of 150 s, and 20 injections with initial injection of 0.4 μL over 0.8 s and subsequent injections of 2 μL over 4 s. After completion of data collection, the MicroCal Origin software was used to fit the data to the one site interaction model. An example of the typical results of a successful EDTA- CaCl_2 performance validation test are shown in Figure 10.6.

D(ii): Additional experimental ITC replicates

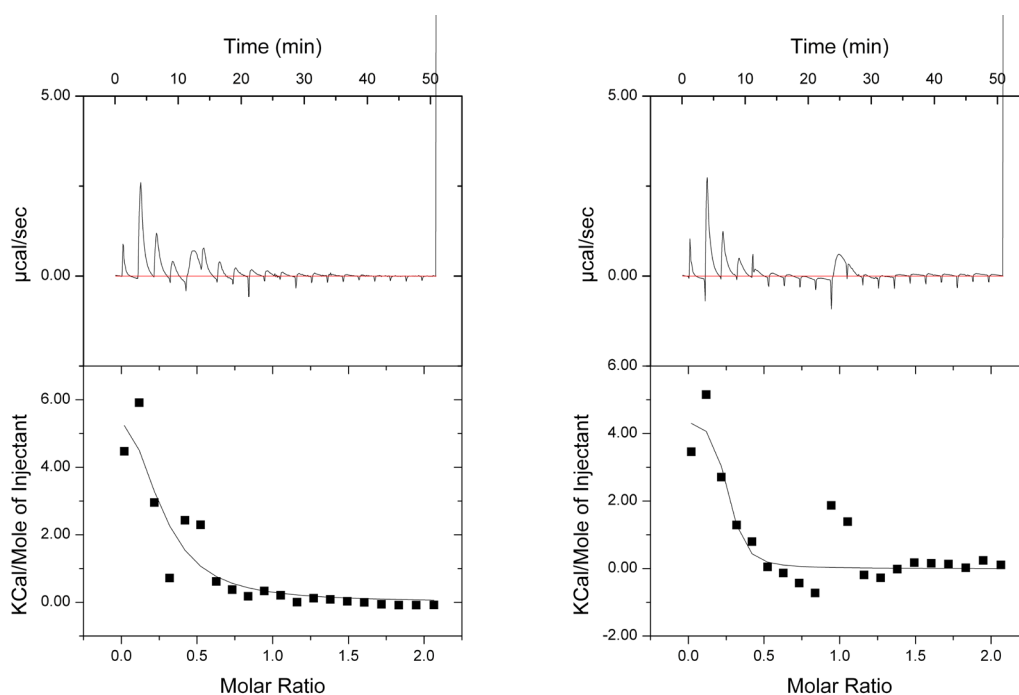


Figure 10.7 –ITC thermograms of sodium fusidate with copper(II) sulphate

Upper panels show enthalpy change at each injection over time and lower panels show the integrated enthalpy curve points normalized per mole of injectant as a function of molar ratio.

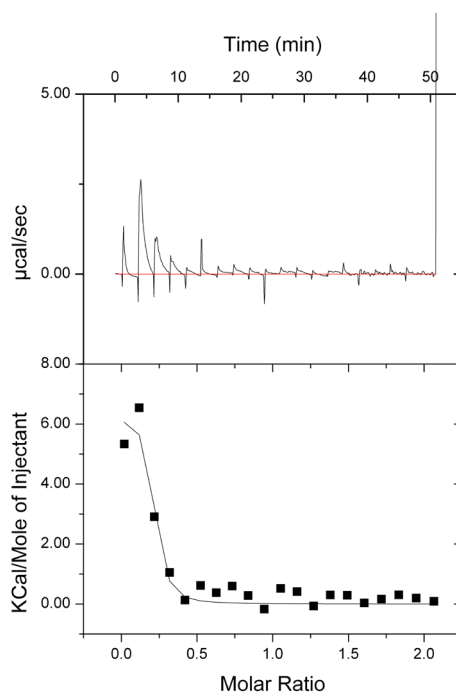


Figure 10.8 –ITC thermogram of sodium fusidate with copper(II) D-gluconate at native pH
 Upper panels show enthalpy change at each injection over time and lower panels show the integrated enthalpy curve points normalized per mole of injectant as a function of molar ratio.

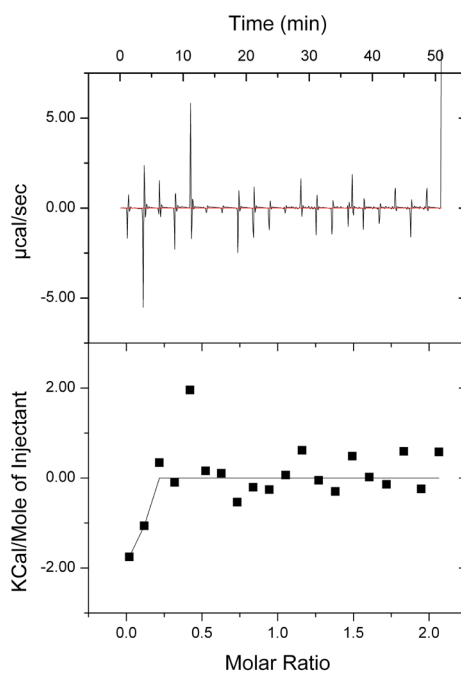


Figure 10.9 –ITC thermogram of sodium fusidate with copper(II) gluconate at pH 6.12
 Upper panels show enthalpy change at each injection over time and lower panels show the integrated enthalpy curve points normalized per mole of injectant as a function of molar ratio.

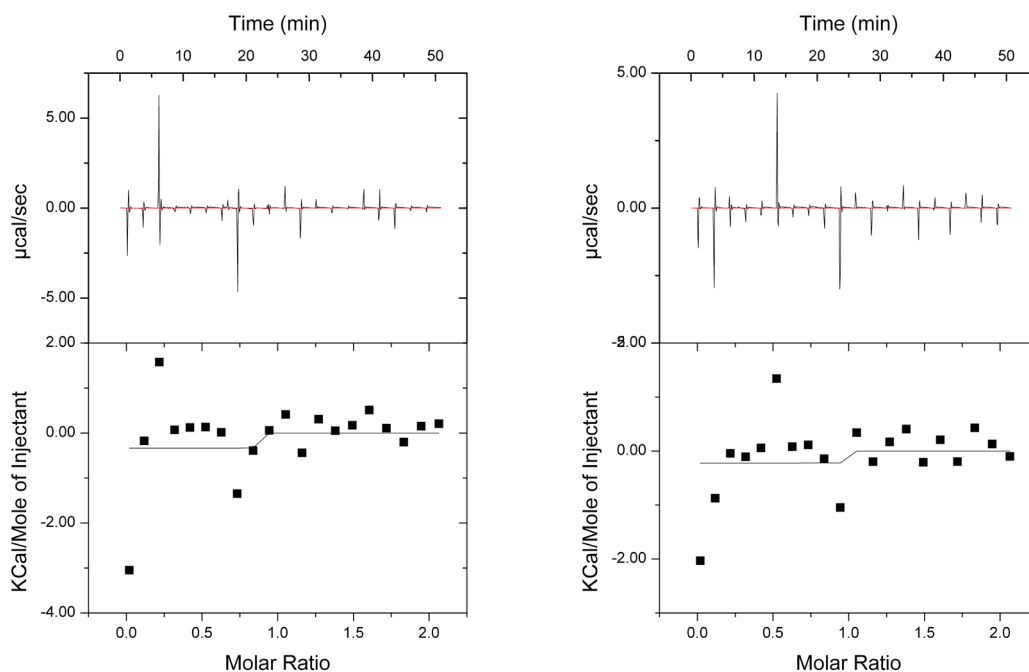


Figure 10.10 –ITC thermograms of sodium fusidate with sodium D-gluconate

Upper panels show enthalpy change at each injection over time and lower panels show the integrated enthalpy curve points normalized per mole of injectant as a function of molar ratio.

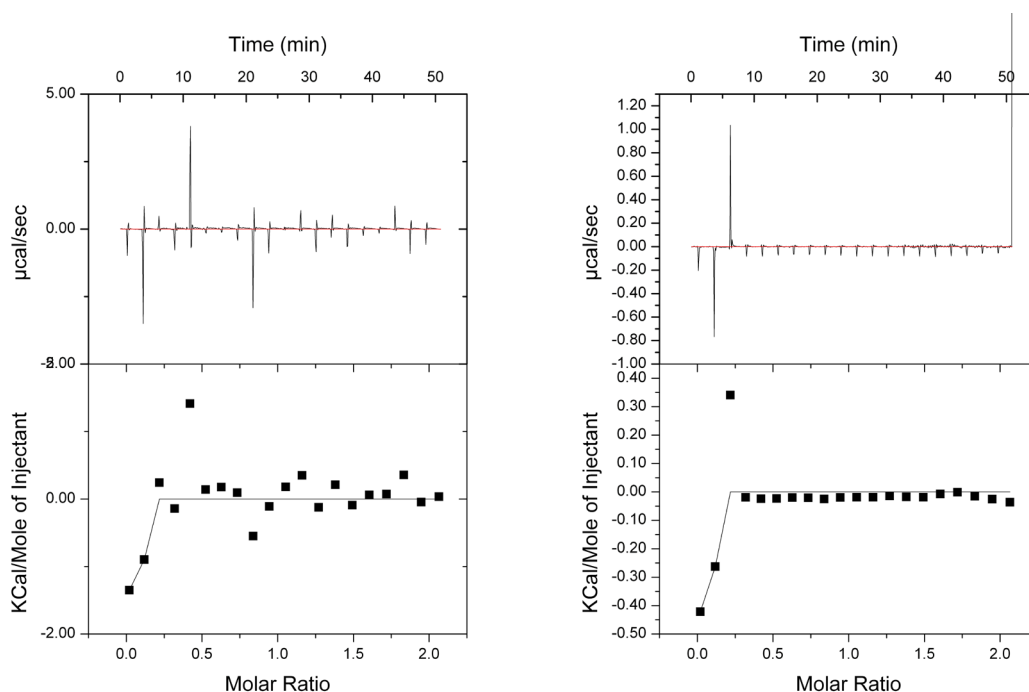


Figure 10.11 - ITC thermogram of sodium fusidate with dilute sulphuric acid

Upper panels show enthalpy change at each injection over time and lower panels show the integrated enthalpy curve points normalized per mole of injectant as a function of molar ratio.

Appendix E: Co-optimisation of LDH and MTT assays

LDH and MTT assays were co-optimised to enable performance of both tests simultaneously using the same cell populations. Human corneal epithelial cells (HCE) were selected for use as these are the most common *in vitro* model for ocular toxicity testing^{[635]–[637]}. The adenovirus-immortalised HCE-2 [50.B1] CRL-11135 from ATCC (HCE-2) cell line was chosen as opposed to primary cells. Compared to primary cells, adenovirus-immortalised HCE exhibit increased stability with normal growth and behaviour being observed for up to 400 generations rather than the one or two generations common with primary cells^[638]. In addition, employment of an established cell line negated lengthy isolation procedures and guaranteed intra-lot standardisation.

While the MTT assay is one of the most commonly used measures of *in vitro* cell proliferation, there are several parameters which lack standardisation. For example, the wavelength employed to quantify MTT formazan solubilised in DMSO has been reported as 490^{[639]–[642]}, 540^{[481],[643],[644]} and 570^{[645]–[648]} nm, however, its λ_{\max} in this solvent is 506 nm^[472]. This and other elements therefore required investigation in order to optimise the MTT assay.

The LDH assay is performed using aliquots of cell culture medium into which the enzyme is released from dying cells during exposure to the test agents. Since the collection of these aliquots does not disturb the monolayer at the bottom of the wells, surviving cells can also be used to perform the MTT assay. As such, cell seeding density was optimised to allow simultaneous performance of both the LDH and MTT assay on the same cell populations. In addition, other elements of the LDH assay were investigated and refined.

Cells used for all optimisation tests were grown and harvested as described in Section 7.2.1. All 96 well plates were coated as also described in the same section.

E(i): Pilot investigations

Eight columns of two 96 well plates were seeded with two-fold dilutions of HCE-2 ranging from 10^6 down to 781 cells per well in 100 μ L KSFM. Another column was filled with 100 μ L complete KSFM per well and a final column with 100 μ L BPE-free KSFM per well. The outer edges (columns 1 and 12 and rows A and H) were filled with 100 μ L sterile PBS to limit evaporation. Plates were incubated at 37 °C and 5 % CO₂. One plate was incubated for 18 h and the other for 42 h to mimic the planned 24 h period of cell

acclimatisation and growth followed by 18 h test agent exposure. Comparison between the two was used to confirm growth over a 24 h period.

The LDH assay was first carried out per the Pierce™ LDH Cytotoxicity Assay Kit instruction manual^[649]. Sterile HPLC grade water (10 µL) was added to each well of three rows of the 96 well plate as controls for spontaneous LDH release from the respective cell populations and medium. To the other three rows, 10 µL Pierce™ lysis buffer was added in order to quantify maximum LDH for each cell population and medium. The plate was incubated for 45 min before 50 µL aliquots from each well were transferred to a fresh, uncoated flat-bottomed 96 well plate. The LDH reaction mixture was prepared by dissolving one vial of Pierce™ substrate mix in 11.4 mL sterile HPLC grade water and adding one vial of Pierce™ assay buffer. Fifty µL LDH reaction mixture was added to each well of the reaction plate (without mixing), followed by incubation at room temperature for 30 min, protected from light. At the end of the reaction period, 50 µL Pierce™ stop solution was added to each well (without mixing). Absorbance in each well was read at 490 and 680 nm with a Tecan Infinite M200 PRO microplate reader (wavelength accuracy ± 1.5 nm^[283]) preceded by 30 s orbital shaking at 6 mm. The background corrected absorbance from spontaneous LDH release wells was subtracted from that of the lysed cell wells of the same seeding density and the mean \pm SD LDH activity calculated as an absolute absorbance value.

MTT 5 mg mL⁻¹ stock solution was prepared in PBS and filter sterilised. The stock solution was diluted 1/10 in supplemented KSFM in an uncoated 25 cm² culture flask (with a filter lid) and placed in the incubator to warm and equilibrate with 5 % CO₂ for 30-45 min before use. The final concentration of 0.5 mg mL⁻¹ MTT used in initial testing was selected based on the concentration used in several reported HCE-2 proliferation investigations^{[486],[650],[651]}. The remaining medium was aspirated from the cell culture plate, carefully avoiding disturbance of the cell layer, and replaced with 100 µL of the MTT dilution. The plates were wrapped in foil to protect from light and returned to 37 °C and 5 % CO₂ for 2 h, an incubation period previously reported for MTT on HCE-2^{[486],[487],[650]}. After the 2 h incubation, the MTT containing medium was removed and replaced with 100 µL DMSO per well (without mixing). Plates were incubated at room temperature for 20 min, protected from light. The Tecan Infinite M200 PRO microplate reader was used to measure absorbance in each well at 540 nm, a wavelength frequently used for the quantification of MTT formazan product solubilised in 100 % DMSO^{[481],[643],[644]}, with each read preceded by 30 s orbital shaking at 6 mm. The values from cell-free controls were subtracted from all other wells and the mean \pm SD absolute absorbance was calculated for each cell density.

Figure 10.12 illustrates the growth of HCE-2 over 24 h, between the 18 and 42 h post-seeding time points, as quantified by total LDH release on lysis. All cell populations were found to increase; for example, the absorbance of LDH released from cells 18 h after seeding 6,250 per well was 0.578 AU which increased to 0.977 AU after 42 h. Consequently, the LDH assay procedure was modified to include addition of the lysis buffer to a triplicate of maximal LDH release wells at the time of test agent addition in order to be able to normalise against the exposed population.

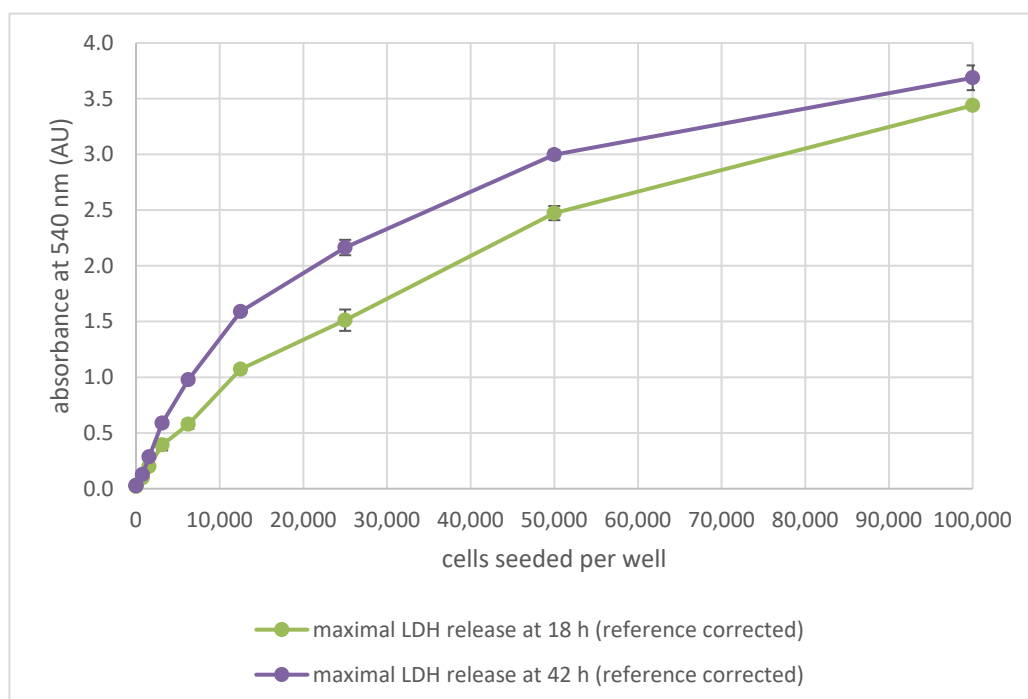


Figure 10.12 – Maximal LDH release from HCE-2 after 18 or 42 h

No linear portion in the relationship between seeded cell density and maximal LDH release absorbance was obtained with the generated data. In addition, the variance between absorbance in wells of the same technical triplicate was inconsistent and quite large in some cases, possibly indicating insufficient or varying degrees of mixing.

The quality of the MTT results were also insufficient to determine a relationship between absorbance at 540 nm and seeded cell density. In addition, variability in absorbance over time was incidentally observed while collecting readings.

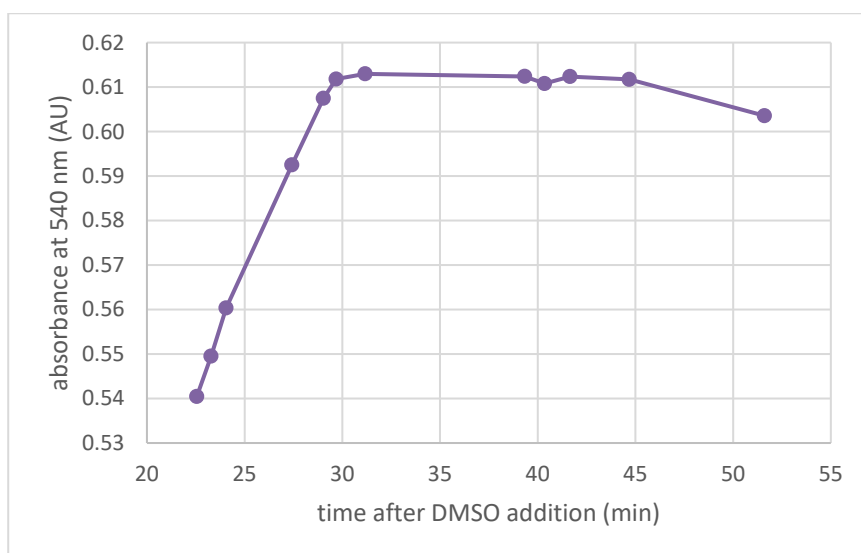


Figure 10.13 - Absorbance of MTT formazan produced by HCE-2 seeded at 12,500 cells per well over time after solubilisation in DMSO at 540 nm

Figure 10.13 illustrates the change in absorbance of MTT formazan produced by HCE-2 seeded at 12,500 cells per well over time. Observations were continued for more than 50 min, at which point absorbance started reducing. Since orbital shaking was employed before each read, the increase in absorbance could have been due to insufficient mixing prior to reading, whereas the subsequent reduction could be due to MTT formazan breakdown.

E(ii): MTT optimisation

Based on the results of the pilot test, several parameters of the MTT assay were identified as requiring optimisation: MTT concentration, whether to mix DMSO on addition, DMSO incubation duration, and the reading wavelength. While many investigators use 0.5 mg mL^{-1} MTT, others employ a concentration of 1 mg mL^{-1} [648],[652]–[654]. The higher concentration may yield greater MTT formazan production, increasing sensitivity of the assay. Since the absorbance of MTT formazan in DMSO was incidentally found to change over time during the pilot test, the incubation duration and effect of mixing the solvent on addition were selected for investigation. Finally, five read wavelengths were selected for investigation in order to identify the most appropriate in terms of sensitivity and variability.

Eight columns of two 96 well plates were seeded with two fold dilutions of HCE-2, from 37,000 down to 578 cells per well. A ninth column was filled with $100 \mu\text{L}$ complete KFSM per well as a cell-free control and the remaining columns (1, 11 and 12) and the top and

bottom rows (A and H) were filled with 100 μ L sterile PBS. Plates were incubated at 37 °C and 5 % CO₂ for 42 h.

MTT stock solution in PBS was diluted in separate volumes of supplemented KSFM to final concentrations of 0.5 and 1 mg mL⁻¹. Both were equilibrated to 37 °C with 5 % CO₂ in filter-capped tissue culture flasks for 30-45 min before use. The medium from both plates was removed, replaced with MTT dilution and the plates returned to the incubator for 2 h. After incubation, the MTT-containing medium was removed and 100 μ L DMSO added to each well, half with mixing and half without. The combination of MTT concentration and DMSO mixing status was arranged so that triplicate rows of serially diluted cells were each treated to every possible combination, as listed in Table 10.3.

Table 10.3 - Combinations of optimisation test conditions

	MTT concentration	DMSO mixing on addition
Set 1	0.5 mg mL ⁻¹	yes
Set 2	0.5 mg mL ⁻¹	no
Set 3	1.0 mg mL ⁻¹	yes
Set 4	1.0 mg mL ⁻¹	no

After DMSO addition, plates were protected from light and incubated at room temperature for 15 min. The Tecan Infinite M200 PRO microplate reader was used to measure absorbance in each well at 490, 506, 520, 553 and 570 nm. Wavelengths of 490 and 570 nm were selected based on previously reported use^{[639]–[642],[645]–[648]}; 506 nm was selected as it is the λ_{max} of MTT formazan in 100 % DMSO^[472]; 553 nm was used as it is the λ_{max} of MTT formazan in DMSO with 1 % serum which may be more appropriate to account for small volumes of medium carry-over^[472]; 520 nm was selected as it falls between 506 and 553 nm. Absorbance was read again after 30, 45, 60, 75, 90 and 120 min incubation in the dark at room temperature. Each read was preceded by 10 s orbital shaking at 6 mm. The mean \pm SD cell-free corrected absorbance was calculated for each cell seeding density, combination of assay conditions, timepoint and wavelength.

While absorbance of MTT formazan in DMSO was highest in more than 50 % of the test condition combinations at the 15 min timepoint, the variance was also the highest (mean SD 0.0189). The highest absorbance was observed after 30 min for 25 % of the test condition combinations and the variance was substantially lower with a mean SD of 0.0104. Therefore, 30 min was selected as the incubation duration for solubilising MTT formazan in DMSO and only data for the 30 min timepoint used in subsequent analyses.

The absorbance of MTT formazan in DMSO produced by cells exposed to either 0.5 or 1 mg mL⁻¹ MTT was plotted against the cell seeding density for each wavelength; mixed

and unmixed test data were assessed separately. The strength of the linear relationship between cell number and absorbance was compared between MTT concentrations. The R^2 value for 1 mg mL⁻¹ results was greater than those produced by 0.5 mg mL⁻¹ in every case (Table 10.4). An MTT exposure concentration of 1 mg mL⁻¹ was selected.

Table 10.4 - R^2 values for linear relationship between cell seeding density and absorbance of MTT formazan in DMSO produced by HCE-2 exposed to 0.5 or 1.0 mg mL⁻¹ MTT with or without mixing of DMSO on addition

Wavelength (nm)	DMSO mixed on addition		DMSO not mixed on addition	
	0.5 mg mL ⁻¹	1.0 mg mL ⁻¹	0.5 mg mL ⁻¹	1.0 mg mL ⁻¹
490	0.9895	0.9938	0.9699	0.9887
506	0.9863	0.9927	0.9728	0.9826
520	0.9825	0.9915	0.9726	0.9812
553	0.9752	0.9893	0.9708	0.9804
570	0.9759	0.9893	0.9712	0.9799

Linear relationships were calculated for cell seeding densities of for 2,000-20,000 per well.

The correlation between cell seeding density and absorbance was found to be stronger where DMSO had been mixed on addition than without mixing (Table 10.4). In addition, the variance between absorbance of individual replicates was less when DMSO had been mixed on addition with a mean SD across all cell densities and read wavelengths of 0.00681 compared to 0.0129 without mixing.

The absorbance (at each wavelength investigated) of formazan produced by HCE-2 after exposure to 1 mg mL⁻¹ MTT, mixing of DMSO on addition and 30 min DMSO incubation is plotted against seeded cell density in Figure 10.14. The R^2 for the linear portion of every curve was >0.99. However, the variance increased with wavelength with a mean SD of absorbance at 570 nm for 2,000-20,000 cells per well of 0.0131 but 0.00418 for absorbance over the same range at 490 nm. A read wavelength of 506 nm was selected due to its combination of lower variability than 520, 553 or 570 nm but higher absorbance and therefore sensitivity than 490 nm.

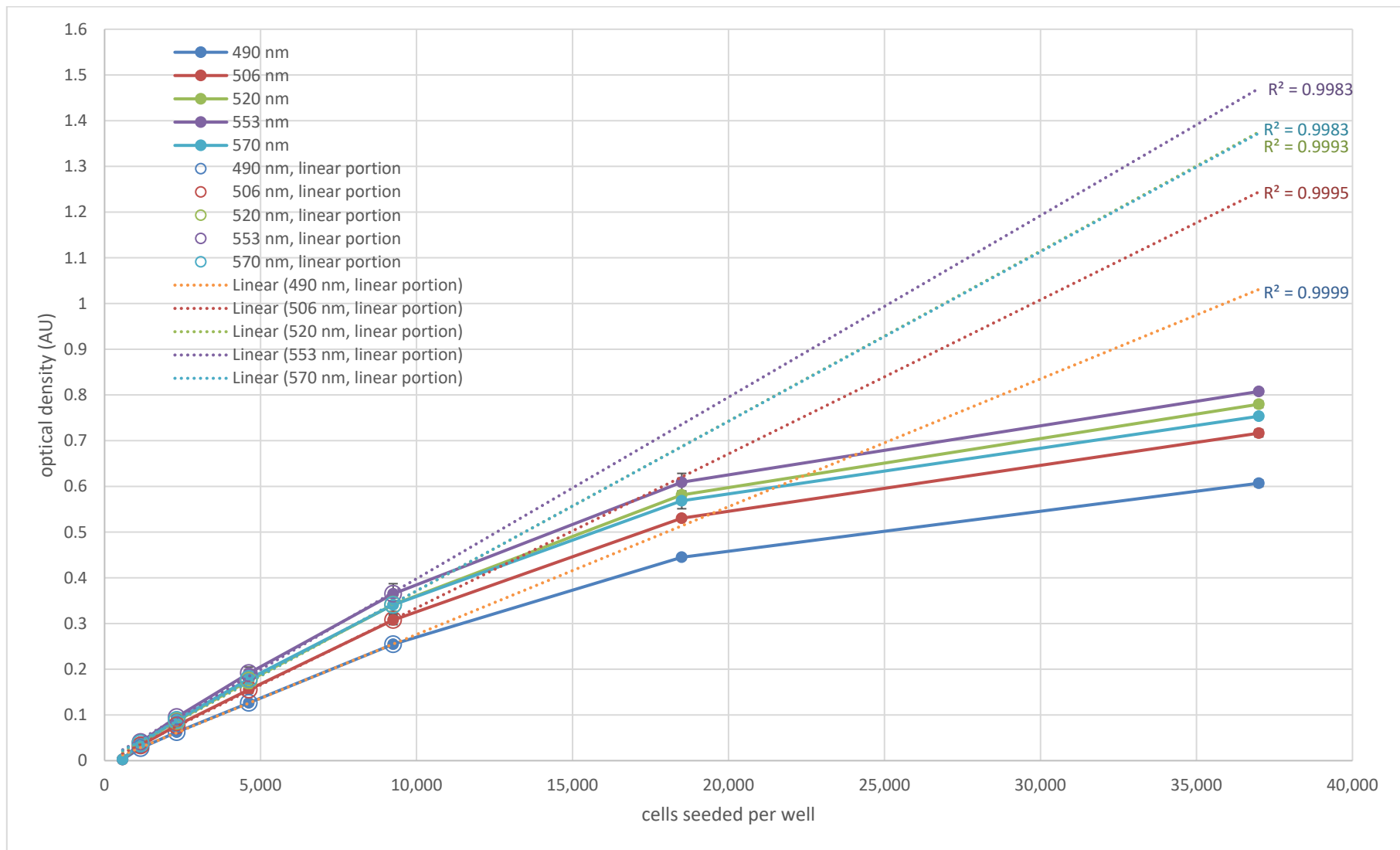


Figure 10.14 - Absorbance at a variety of wavelengths of formazan produced by HCE-2 after exposure to 1 mg mL⁻¹ MTT for 2 h and correlations with seeding density

E(iii): LDH optimisation

In response to observations during the pilot test, mixing of reaction mixture and stop solution on addition were investigated as modifications to the LDH assay. Two 96 well plates were prepared and seeded with HCE-2, as described in E(ii) above. Plates were also incubated at 37 °C and 5 % pp CO₂ for 42 h.

Sterile HPLC grade water (10 µL) was added to each well in half of each plate and 10 µL Pierce™ lysis buffer was added to the other half. After 45 min incubation at 37 °C and 5 % pp CO₂, 50 µL aliquots were transferred from every well to a fresh, uncoated flat-bottomed 96 well plate. To one reaction plate, 50 µL LDH reaction mixture was added to each well without mixing. To the second reaction plate, the same volume of LDH reaction mixture was added but with mixing on addition by gently pipetting up and down 4-5 times. Both plates were incubated at room temperature for 30 min, protected from light. At the end of the reaction period, 50 µL Pierce™ stop solution was added to each well, without mixing in the first plate and with mixing in the second. Absorbance read at 490 and 680 nm after 10 s orbital shaking at 6 mm and the mean±SD absolute LDH activity calculated as described above in Section E(i).

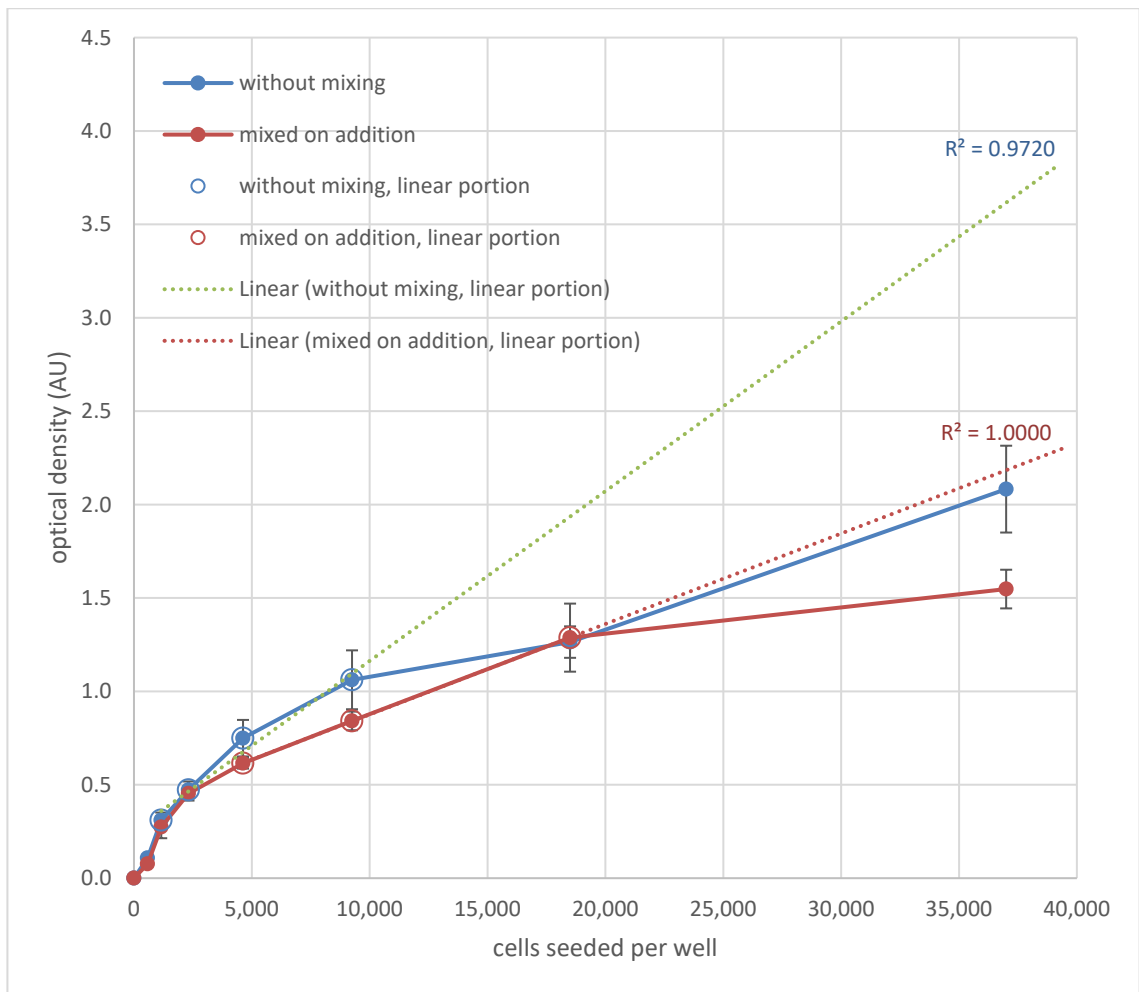


Figure 10.15 – LDH activity from HCE-2 with and without mixing on addition of assay reagents and correlations with seeding density
(n = 3, error bars = SD)

In order to disperse bubbles in the LDH reaction plate that reagents had been mixed in on addition, centrifugation for 15 min at 25 °C at 4000 rpm was found to be sufficient for the majority. The remainder were efficiently popped with a hot syringe needle.

While absorbance was generally higher when LDH reagents were not mixed on addition, the variance between technical replicates was larger and the strength of correlation of the linear portion was less than when reagents were mixed (Figure 10.15). As such, the LDH assay was modified to include mixing of reaction mixture and stop solution on addition.

E(iv): Seeding density selection

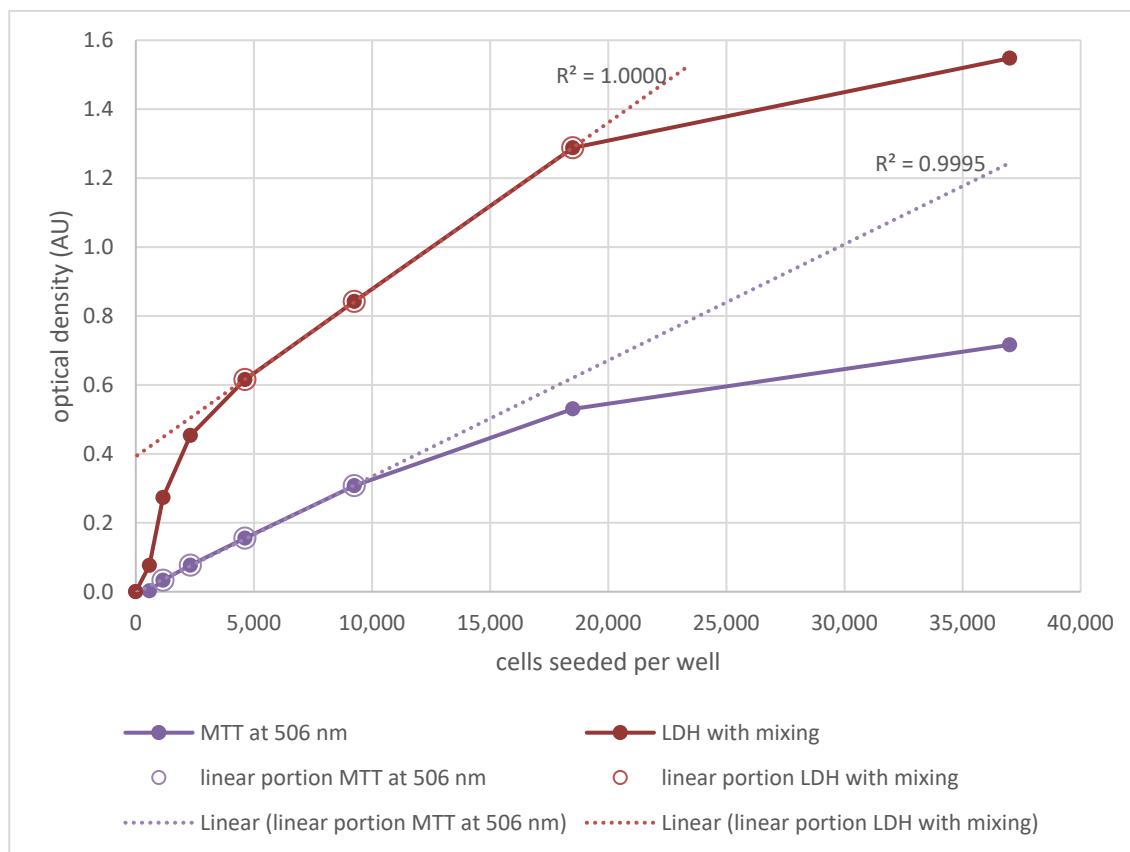


Figure 10.16 – Comparison of optimised LDH and MTT assay results and linear relationships between HCE-2 seeding density and absorbance

The absolute absorbance results from the optimised MTT and LDH assays were plotted against cell seeding density and the linear portions identified and compared (Figure 10.16). The linear portion for the LDH assay spanned 4,625 to 18,500 cells per well, while it was 1,156 to 9,250 cells per well for MTT. This corresponded well with the cell densities reported in MTT assays employing HCE-2, listed in Table 10.5. Falling within both linear portions, a cell seeding density of 8,000 per well was selected.

Table 10.5 - Published cell seeding densities used in MTT assay

Paper	Plate type	Seeding density	Pre-MTT growth time
Paimela et al, 2012 ^[650]	12 well (4 cm ²)	100,000 per well (25,000/cm ²)	48 h
Lee et al, 2014 ^[486]	35-mm dish (9 cm ²)	200,000 per plate (22,222/cm ²)	24 h
Zheng et al, 2015 ^[487]	96 well (0.32 cm ²)	5,000 per well (15,625/cm ²)	3 days
Yu et al, 2018 ^[651]	96 well (0.32 cm ²)	8,000 per well (25,000/cm ²)	24 h

E(v): Combined assay procedure

Table 10.6 lists the timing of each task, illustrating the convenience of the dual process.

Table 10.6 - Timepoints and tasks for the combined LDH and MTT assay procedure

Time	Task
0 h	addition of lysis buffer
0.75 h	removal of aliquots for LDH assay
1 h	replacement of medium with MTT dilution
1.25 h	addition of LDH reaction mixture
1.75 h	addition of LDH stop solution
2 h	centrifugation of LDH reaction plate and dispersal of bubbles
2.5 h	read LDH absorbance results
3 h	replacement of MTT dilution with DMSO
3.5 h	read MTT absorbance results

Appendix F: Concentrations of lipids and trace elements in STF formulations and human tears

Table 10.7 - Concentrations of lipids in eleven published simulated tear fluid formulations

Lipids	Concentrations in STF formulations (mg L ⁻¹)			Frequency of use (out of 11 formulations)
	mean (SD)	median	range	
cholesterol	1.68 (0.1)	1.6	1.6 - 1.8	5 ^{[496],[502],[503],[515],[517]}
cholesteryl linoleate	24 (0)	24	24 - 24	2 ^{[496],[515]}
cholesteryl oleate	24.73 (1.04)	24	24 - 26.2	3 ^{[502],[503],[517]}
dicaprin	3.2 (0)	3.2	3.2 - 3.2	2 ^{[496],[515]}
linalyl acetate	20 (0)	20	20 - 20	2 ^{[496],[515]}
oleic acid	7.2 (7.64)	1.8	1.8 - 18	3 ^{[502],[503],[517]}
oleic acid methyl ester	12 (0)	12	12 - 12	2 ^{[503],[517]}
oleic acid oleyl ester	31.1 (0)	31.1	31.1 - 31.1	1 ^[502]
oleic acid propyl ester	12 (0)	12	12 - 12	2 ^{[496],[515]}
phosphatidyl choline	5.07 (6.46)	0.5	0.5 - 14.2	3 ^{[502],[503],[517]}
triolein	13.5 (5)	16	3.5 - 16	5 ^{[496],[502],[503],[515],[517]}
undecylenic acid, sodium salt	3.1 (0.1)	3.1	3 - 3.2	2 ^{[496],[515]}

Table 10.8 - Concentrations of trace elements in eleven published simulated tear fluid formulations

Trace elements	Concentrations in STF formulations (nM)			Frequency of use (out of 11 formulations)
	mean (SD)	median	range	
Co	924.22 (0)	924.22	924.22 - 924.22	1 ^[516]
Cu	87.99 (0)	87.99	87.99 - 87.99	1 ^[516]
Fe	29.6 (0)	29.6	29.6 - 29.6	1 ^[516]
Mn	505.28 (0)	505.28	505.28 - 505.28	1 ^[516]
Ni	105.18 (0)	105.18	105.18 - 105.18	1 ^[516]
Zn	513.63 (0)	513.63	513.63 - 513.63	1 ^[516]
BO ₃	1617.34 (0)	1617.34	1617.34 - 1617.34	1 ^[516]
MoO ₄	103.33 (0)	103.33	103.33 - 103.33	1 ^[516]

Table 10.9 - Concentrations of trace elements measured in human tears

Trace elements	Concentrations measured in human tears (nM)		
	reported values (patient population and collection conditions)	mean of exact values	max range
As	0.33 (healthy, urban residents) ^[522] 3.87 (healthy, rural residents) ^[522]	2.1	0.33 to 3.87
Ba	8.0 (healthy, rural residents) ^[522] 17.6 (healthy, urban residents) ^[522] 18.9 (healthy) ^[655]	14.8	8.0 to 18.93
Co	23.8 (healthy, urban residents) ^[522] 28.0 (healthy, rural residents) ^[522] 30.0 (healthy) ^[655]	27.3	23.8 to 30.0
Cr	0.96 (healthy, urban residents) ^[522] 4.8 (healthy) ^[655] 13.2 (healthy, rural residents) ^[522]	6.3	0.96 to 13.2
Cu	97.6 (healthy) ^[655] 196.7 (healthy, rural residents) ^[522] 200.6 (healthy, urban residents) ^[522]	165.0	97.6 to 200.6
Fe	None reported	N/A	N/A
Mn	70.4 (healthy) ^[655] 344.0 (healthy, stimulated) ^[656] 347.7 (<i>Proteus</i> spp corneal ulcer, stimulated) ^[656] 349.5 (<i>S. aureus</i> corneal ulcer, stimulated) ^[656] 353.1 (<i>P. aeruginosa</i> corneal ulcer, stimulated) ^[656] 384.1 (Pneumococcal corneal ulcer, stimulated) ^[656]	308.1	70.4 to 384.1
Ni	None reported	N/A	N/A
Pb	2.4 (healthy) ^[655] 5.3 (healthy, rural residents) ^[522] 8.2 (healthy, urban residents) ^[522]	5.4	2.4 to 8.2
Rb	141.2 (healthy) ^[655] 210.6 (healthy, rural residents) ^[522] 265.0 (healthy, urban residents) ^[522]	205.6	141.2 to 265.0
Se	6.3 (healthy) ^[655] 30.4 (healthy, urban residents) ^[522] 38.0 (healthy, rural residents) ^[522]	24.9	6.3 to 38.0
Zn	270.0 (healthy, urban residents) ^[522] 321.2 (healthy, rural residents) ^[522] 508.6 (healthy) ^[655]	366.6	270.0 to 508.6
BO ₃	None reported	N/A	N/A
MoO ₄	None reported	N/A	N/A